

Geochemical Indicators of Paleoenvironmental and Paleoclimatic Change in Ancient and Recent Lake Deposits: Facies Models, Facies Distributions and Hydrocarbon Aspects

vorgelegt von
Diplom-Geologe
Andreas Fuhrmann
aus Marl

Von der Fakultät VI - Bauingenieurwesen
und Angewandte Geowissenschaften
der Technischen Universität Berlin
zur Erlangung des akademischen Grades eines
Doktors der Naturwissenschaften
- Dr. rer. nat. -

genehmigte Dissertation

Promotionsausschuss:

Vorsitzender: Prof. J. H. Schroeder, Ph. D.
Berichter: Prof. Dr. Brian Horsfield
Berichter: Prof. Dr. Ralf Littke (RWTH Aachen)

Tag der wissenschaftlichen Aussprache: 15.11.2002

Berlin 2003

D 83

Acknowledgements

This thesis was performed at the Institute for Petroleum and Organic Geochemistry (ICG-4) at the Research Centre Jülich. First of all, I would like to thank my supervisor Prof. Brian Horsfield, now head of the Institute of Organic Geochemistry and Hydrocarbon Systems at the GFZ Potsdam for his support, reviewing this thesis and for many fruitful discussions on the results of my work. I would also like to thank Prof. Ralf Littke, head of the Institute of Geology and Geochemistry of Petroleum and Coal at Aachen University of Technology for his valuable contributions to this thesis.

I wish to thank Dr. Heinz Wilkes for his constructive input and help with many chemical problems. Many discussions with Heinz were most productive for the progress of my dissertation. Scientists and Ph.D. students at the ICG-4 provided an excellent working environment. Thanks to Dr. Harald Poelchau, Dr. Rainer G. Schaefer, Thomas Oldenburg, Thomas Fischer, Herbert Volk, Antje Armstroff, Thomas Thielemann, Jochen Naeth, Ulrich Herten and Klaus Zink.

Many thanks for the pleasant co-operation are extended to my Chinese colleagues at PetroChina, formerly the Liaohe Petroleum Exploration Bureau (LPEB). I enjoyed our meeting in Panjin last year and found many new friends in China. I especially thank Liguu Hu for discussions on the geology of the Liaohe Basin and those far beyond scientific issues. The possibility to present the results at conferences and in this thesis is gratefully acknowledged. I would also like to thank Dr. Jordi Lopez who performed the structural elucidation of hydrocarbons and non-hydrocarbons within the Liaohe project.

Maar lake sediments and varve countings were provided by Dr. Achim Brauer, Dr. Jens Mingram (both GFZ Potsdam) and Dr. Bernd Zolitschka (University of Bremen). They also generously supplied computer databases and graphics. Accurate isotope measurements were performed by Andreas Lücke and his team from the Isotope and Paleoclimate Research Group of the ICG-4 at the Research Centre Jülich. I especially enjoyed our discussions regarding the research topic and several trips to the Eifel maar lakes. The study of maar lake sediments in this thesis was closely associated with the priority programme "Changes of the Geo-Biosphere during the last 15,000 years – Continental sediments as evidence for changing environmental conditions", sponsored by the Deutsche Forschungsgemeinschaft (German Research Foundation).

This work would not have been possible without the help, support and expertise of many technicians at the ICG-4, namely Franz Leistner, Werner Laumer, Ulrich Disko, Willi Benders, Helmut Willsch, Anne Richter, Wolfgang Lüdtkke and Karlheinz Nogai.

Finally I thank my parents for their support during my studies in Aachen and Jülich and Jutta for her love, help and support especially in the final stage of completing this thesis.

Abstract

Eocene lacustrine sediments (Es4 and Es3 member of the Shahejie Formation) from the Western Depression of the Liaohe Basin, NE China were examined in order to perform a systematic facies classification and to show the influence of facies variations on the source rock potential. Facies changes were reconstructed by applying a multidisciplinary approach, including mineralogy (XRD), organic petrology and organic geochemistry. The Liaohe lakes passed from alkaline to freshwater stages because of varying climatic conditions and tectonic movements. Fluorescing amorphous and lamalginite-rich organic matter (OM) was deposited in a restricted, hydrological closed-lake environment (playa and shallow lake), during Gaosheng (GS) time in the whole basin and during Dujiatai (DJT) time in the basin centre (Lei and Gao area). A high primary production dominated by cyanobacteria, low fluvial input, and paucity of terrestrial vegetation in an arid climate resulted in the deposition of type I OM. Water column stratification with anoxic, probably saline bottom waters existed which is consistent with the biomarker parameters determined in this study. Especially laminated samples from the GS sub-unit show high total organic carbon (TOC) and hydrogen-index values. They are excellent source rocks and have the potential to generate high-wax petroleum at high subsurface temperatures. The very narrow distribution of activation energies point to a mainly polymethylene kerogen structure which is supported by the pyrolysate composition. During lower DJT time intense evaporation led to the formation of magnesium and sodium rich brines with dolomite and analcime precipitation aided by evaporative pumping. In contrast, clay mineral-rich samples of the Shale I and Shale II sub-units as well as those of the Es3 member were deposited during lake-level highstands in a hydrological open freshwater environment in a more humid climate. They are mainly non-laminated and *Botryococcus* alginite predominates. Sediments in the marginal Shu-Du area were laid down in a fan-delta environment during DJT time, which is corroborated by the presence of abundant detrital minerals (feldspars, quartz) and coaly terrigenous particles.

Variations in the composition of macromolecular OM in maar lake sediments from late Quaternary deposits of the Westeifel volcanic field, Germany (Lake Holzmaar, Lake Meerfelder Maar) and South China (Lake Huguang Maar) were studied, applying analytical pyrolysis and organic petrology. Investigations on the lipid OM were carried out for comparison. The objective of this work was to find suitable parameters which mirror the local environment and climate at the time of OM incorporation into the sediment. Parameter based on methoxyphenols together with the character and the relative abundance of terrigenous

particles can be used to show variations of land plant input to the maar lakes through time. Lignin derived components increased during the amelioration of the climate, reflecting forestation of the landscape around Lake Meerfelder Maar after the last glacial retreat. A reverse trend towards the Younger Dryas cold event shows a reduction of the forest. During the Lateglacial and Younger Dryas period, high-reflecting reworked terrigenous OM from the geological substratum was introduced to the Eifel Maar lakes by soil erosion in an open, tree-less vegetation. In contrast, fresh and low-reflecting terrigenous OM predominates in the Bølling/Allerød and Holocene sequence. Beside a higher plant source, the phenols in most of the pyrolysates originate from the microbial reworking of proteinaceous tyrosine moieties or from a direct contribution of cyanobacteria.

In Lake Huguang Maar, the $\delta^{13}\text{C}_{\text{TOC}}$ parallels the isotopic enrichment of the plant-wax derived long-chain *n*-alkanes and the *botryococcene* biomarkers. This mirrors vegetation changes and specific environmental conditions which affected the algal biomass. Especially the significant transition from lithozone 4 to lithozone 3 is consistent with a rapid change from an ecosystem with relatively high primary productivity and C_3 vegetation towards a very stable ecosystem with a low primary productivity and a dominant input of C_4 grasses because of drier climatic conditions and low atmospheric CO_2 levels. This is supported by the positive isotopic excursions in lithozone 3, a lower 4-methylguaiacol to *p*-vinylphenol ratio in lithozone 3 compared to lithozone 4 and microscopic as well as palynological data. One possibility for the very heavy $\delta^{13}\text{C}$ values of the botryococcenes in lithozone 3 is that *Botryococcus braunii* changed its CO_2 demand towards a bicarbonate source. The comparison with other studies implies that downcore variations in Lake Huguang Maar are largely controlled by fluctuations of the summer and winter monsoon activity.

Kurzfassung

Eozäne lakustrine Sedimente (Es4- und Es3-Stufe der Shahejie Formation) aus der westlichen Depression des Liaohe Beckens, NO China wurden untersucht, um eine systematische Faziesklassifikation durchzuführen. Hierzu kam ein integrierter Ansatz aus mineralogischen (XRD), organisch-petrologischen sowie organisch-geochemischen Methoden zur Anwendung. Die Entwicklung der Seen war geprägt durch den Wechsel von alkalinen und höher salinaren Phasen hin zu Perioden mit reichlich Oberflächenzufluss und relativ hohen Seespiegelständen. Diese Entwicklung wurde im Wesentlichen durch die klimatischen Verhältnisse sowie die tektonische Entwicklung des Riftbeckens gesteuert. Amorphes fluoreszierendes und Lamalginit reiches organisches Material (OM) wurde in einem hydrologisch geschlossenen Seebecken (flacher bzw. Playa-See) in einem ariden Klima abgelagert, das während der Gaosheng (GS) Unterstufe im gesamten und während der Dujiatai (DJT) Unterstufe im zentralen Teil des Beckens (Lei Gebiet) vorherrschte. Diese Zeiten waren geprägt durch eine hohe Primärproduktion, eine Schichtung der Wassersäule mit anoxischem Tiefenwasser sowie dem weitgehenden Fehlen einer Vegetation im Umland der Seen. Dies führte zur Bildung eines Typ I Kerogens. Die fein-laminierten Sedimente der GS-Unterstufe mit hohen organischen Kohlenstoffgehalten (TOC) und Wasserstoffindexwerten sind die besten Muttergesteine in der westlichen Depression und in der Lage, bei hohen Temperaturen wax-reiche Erdöle zu generieren. Die sehr schmale Aktivierungsenergieverteilung deutet auf eine überwiegend aus aliphatischen Ketten aufgebaute Kero-genstruktur hin, was durch die Zusammensetzung der Pyrolyseprodukte bestätigt wird. Zu Beginn der DJT-Unterstufe führte intensive Eindampfung der Wässer im zentralen Teil der Depression zur Bildung von Magnesium- und Natrium-reichen Laugen. Unterstützt durch das sogenannte "Evaporative Pumpen" kam es zur Ausfällung von Dolomit und Analcim. Im Gegensatz dazu wurden die tonreichen Sedimente der Shale I- und Shale II-Unterstufe sowie die der Es3-Stufe in einem hydrologisch offenen Seebecken in einem humiden Klima abgelagert. Sie sind nicht laminiert und *Botryococcus* Alginit dominiert das OM. Die Sandsteine der DJT-Unterstufe im randlichen Shu-Du Gebiet wurden im Bereich eines Schwemmfächers sedimentiert.

Die Charakterisierung des OM in Spätquartären Maarseesedimenten der Westeifel, Deutschland (Holzmaar, Meerfelder Maar) sowie aus S China (Huguang Maar) bildete den zweiten Schwerpunkt dieser Arbeit. Methoxyphenole aus Pyrolyseexperimenten können zusammen mit den mikroskopisch identifizierbaren terrigenen organischen Partikeln benutzt

werden, um Variationen des Landpflanzen-eintrags in die Seen aufzuzeigen. Die Klimaerwärmung nach dem letzten Gletscherrückzug und die damit verbundene Zunahme der Vegetationsdichte im Umfeld des Meerfelder Maars schlagen sich in einem relativen Anstieg der Ligninkomponenten nieder. Der Klimarückschlag während der Jüngerer Dryas ist durch einen gegenläufigen Trend dokumentiert. Während des Spätglazials und der Jüngerer Dryas wurden überwiegend hoch-reflektierende terrigene organische Partikel in die Maarseen eingetragen, die auf eine verstärkte Lieferung über Bodenerosion in einem weitgehend waldfreien Umland hindeuten. Dagegen dominiert frisches Pflanzenmaterial und gering-reflektierende Huminit-partikel während des Bølling/Allerød und im Holozän. Die Phenole in den Pyrolysaten stammen sowohl von höheren Pflanzen als auch von der bakteriellen Überarbeitung von Proteinen (Tyrosin) bzw. von deren direktem Eintrag durch Cyanobakterien.

Stabile Kohlenstoffisotope, gemessen am Gesamtkohlenstoff ($\delta^{13}\text{C}_{\text{TOC}}$), den langkettigen *n*-Alkanen (Pflanzenwachse), sowie algenspezifischen Biomarkern (Botryococcene), zeigen einen parallelen Verlauf. Insbesondere der Übergang von Lithozone 4 zu Lithozone 3 markiert den schnellen Wechsel von einem Ökosystem mit relativ hoher Primärproduktion und C_3 -Pflanzeneintrag zu einem Ökosystem mit geringer Primärproduktion und Eintrag von C_4 -Gräsern als Ergebnis trockener klimatischer Bedingungen und geringeren CO_2 -Konzentrationen der Atmosphäre. Dies wird belegt durch die positiveren $\delta^{13}\text{C}$ -Werte und ein geringeres 4-methylguaiacol zu *p*-vinylphenol Verhältnis in Lithozone 3 sowie die mikroskopischen Ergebnisse und Pollenanalysen. Die extrem positiven $\delta^{13}\text{C}$ -Werte der Botryococcene in Lithozone 3 zeigen, dass die Alge *Botryococcus braunii* Bicarbonat assimiliert hat. Ein Vergleich mit anderen Studien ergab, dass die zeitlichen Veränderungen in den geochemischen Parametern auf Schwankungen der Intensität des Winter- und Sommermonsuns zurückzuführen sind.

Contents

Acknowledgements

Abstract

Kurzfassung

Contents

1	Introduction	1
1.1	Lake Waters and Lake Sediments	1
1.1.1	Hydrology and Lake Dynamics	1
1.1.2	Clastic, Chemical and Biochemical Sedimentation	3
1.1.3	Laminations and Cycles	4
1.1.4	Lake Types	4
1.2	Organic Matter in Lake Waters and Lake Sediments	5
1.2.1	Organic Sedimentation	5
1.2.2	Organic Matter Source and Environmental Indicators	8
1.2.3	Fossil Fuel Resources	13
2	Goals and Approach	16
3	Analytical Program	18
3.1	Elemental Analyses	19
3.2	Rock-Eval Pyrolysis	19
3.3	Mineralogy	20
3.4	Kerogen Isolation	21
3.5	Organic Petrology	21
3.6	Stable Carbon Isotopes	22
3.7	Thermal Analysis Techniques	23
3.8	Bulk Kinetics of HC-Generation	24
3.9	Solvent Extraction and Liquid Chromatographic Separation	24
3.10	Gas chromatography (GC) and Gas Chromatography-Mass Spectrometry (GC-MS)	25
4	Liaohé Basin, Peoples Republic of China	28
4.1	Geological Background	28
4.1.1	Location and Morphology	28
4.1.2	Tectonic Evolution	29
4.1.3	General Stratigraphy of the Western Depression	30
4.1.4	Hydrocarbon Sources, Accumulations and Trap Styles	34
4.2	Sample Selection	35

4.3 Mineralogy	38
4.3.1 Bulk Mineralogical Composition	38
4.3.2 Mineralogical Results of Selected Wells	40
4.3.3 Occurrence and Origin of Minerals	42
4.3.3.1 Carbonates	42
4.3.3.2 Clay Minerals	48
4.3.3.3 Quartz and Feldspars	52
4.3.3.4 Analcime [$\text{Na}_{16}(\text{Al}_{16}\text{Si}_{32}\text{O}_{96}) \cdot 16\text{H}_2\text{O}$]	55
4.3.3.5 Opal-C and Opal-CT (SiO_2)	56
4.3.3.6 Gypsum [$\text{CaSO}_4 \cdot 2\text{H}_2\text{O}$]	57
4.3.3.7 Pyrite [FeS_2]	57
4.3.3.8 Amphibole [$\text{Ca}_2\text{Na}(\text{Mg},\text{Fe})_4(\text{Al},\text{Fe})((\text{Si},\text{Al})_4\text{O}_{11})_2(\text{OH})_2$]	58
4.3.3.9 Natrojarosite $\text{NaFe}_3(\text{SO}_4)_2(\text{OH})_6$	58
4.4 Organic Petrology	60
4.4.1 Terminology	60
4.4.2 Classification	61
4.4.3 Non-laminated Samples	62
4.4.4 Laminated Samples	63
4.4.5 Additional Observations	64
4.5 Source Rock Screening	67
4.5.1 Whole Rock Samples	67
4.5.2 Kerogen Concentrates	71
4.5.3 Stable Carbon Isotopes of Kerogens	73
4.6 Kerogen Characterisation	75
4.6.1 Structural Moieties	75
4.6.2 Thermal Lability	82
4.7 Characterisation of the Soluble Organic Matter	85
4.7.1 Extract Yields and Compound Class Composition	86
4.7.2 Facies Parameters of Key Wells	87
4.7.3 Saturated Hydrocarbons	89
4.7.4 Triterpanes, Steranes and Carotenoids	92
4.7.4.1 Facies Parameters	94
4.7.4.2 Maturity Parameters	96
4.7.5 Aromatic Hydrocarbons	98
4.7.5.1 Facies Assessment	98
4.7.5.2 Maturity Assessment	101
4.7.6 Heterocompounds	104
4.7.6.1 Free Fatty Acids	104
4.7.6.2 Neutral NSO compounds	106
4.8 Paleoenvironment of Deposition	112
4.8.1 Marginal Fan-Delta Environment	113
4.8.2 Freshwater Environment	114
4.8.3 Playa and Shallow Lake Facies	118

5	Maar Lakes	124
5.1	Paleoclimatic Framework and Geological Background	124
5.1.1	Eifel Maar Lakes	124
5.3.1	Lake Huguang Maar	128
5.2	Sample Selection	130
5.3	Eifel Maar Lakes	132
5.3.1	Screening Analysis	132
5.3.2	Chemical Composition of the Kerogens	136
5.3.3	Thermal Analysis (Py-GC-FID and Py-GC-MS)	136
5.3.4	Organic Petrology	147
5.3.5	Stable Carbon Isotopes	155
5.3.6	Paleoenvironment of Deposition	159
5.4	Lake Huguang Maar	162
5.4.1	Screening Analysis	162
5.4.2	Chemical Composition of the Kerogens	167
5.4.3	Thermal Analysis (Py-GC-FID and Py-GC-MS)	167
5.4.4	Organic Petrology	173
5.4.5	Soluble Organic Matter	177
5.4.5.1	Saturated Hydrocarbons	178
5.4.5.2	Botryococenes	180
5.4.5.3	Fatty Acids	181
5.4.5.4	Compound Specific Isotope Analysis	182
5.4.6	Paleoenvironment of Deposition	184
6	Summary and Conclusions	192
7	References	195

Appendix A to P

1 Introduction

Climate and tectonics are critical factors which are responsible for the occurrence, distribution and character of ancient and modern lake deposits (Carroll & Bohacs, 1999). These factors dictate sediment delivery and dispersal, and, of paramount importance to the current study the relative supply of aquatic and terrigenous organic matter (OM) as well as redox conditions governing OM preservation. Two aspects of lake deposits dominated the study of modern and ancient lacustrine settings in the recent past. Firstly, the sediments provide detailed records and thence new insights into past climates such as several Quaternary glacial/interglacial cycles (e.g. Brauer *et al.*, 1999; Meyers & Lallier-Vergès, 1999). Secondly, many ancient lake basins are of important economic importance because they bear hydrocarbons and oil shale deposits (for review see Powell, 1986). Several studies have shown, that paleoclimate-based models are important in interpreting lacustrine petroleum source rock sequences (e.g. Carroll, 1998; Gonçalves, 2002). To evaluate the large differences between individual lake systems it is necessary to integrate physical, chemical and biological processes and their responses to climate-induced fluctuations.

In this thesis, organic petrological, organic geochemical and mineralogical data are used to define and illustrate the depositional environments and climates of Eocene lacustrine sediments from the Western Depression of the Liaohe Basin and Holocene maar lake deposits. This section describes the main factors that control inorganic, organic lake sedimentation, and the occurrence of fossil fuel resources in lake basins.

1.1 Lake Waters and Lake Sediments

1.1.1 Hydrology and Lake Dynamics

Sedimentation in lakes is affected by the properties and the chemistry of the lake waters, lake level fluctuations and the relative abundance of land-derived clastics and autochthonous sediment. Lakes can be classified as hydrological open or closed. In the water budget of **hydrological open** lakes precipitation, inflow and groundwater recharge are balanced by evaporation, outflow and infiltration to the subsurface (Eugster & Kelts, 1983). The lake chemistry is dilute and dominated by meteoric waters. In contrast, **hydrological closed** lakes lack a permanent outlet and loose water only by evaporation and infiltration. They may be perennial or ephemeral, depending upon evaporation and inflow.

The typical temperature layering of lakes includes a warm oxygenated and circulating **epilimnion**, which overlies the cooler **hypolimnion** that is anoxic and undisturbed by circulation of the water masses (Fig. 1.1). The intervening zone, characterised by a

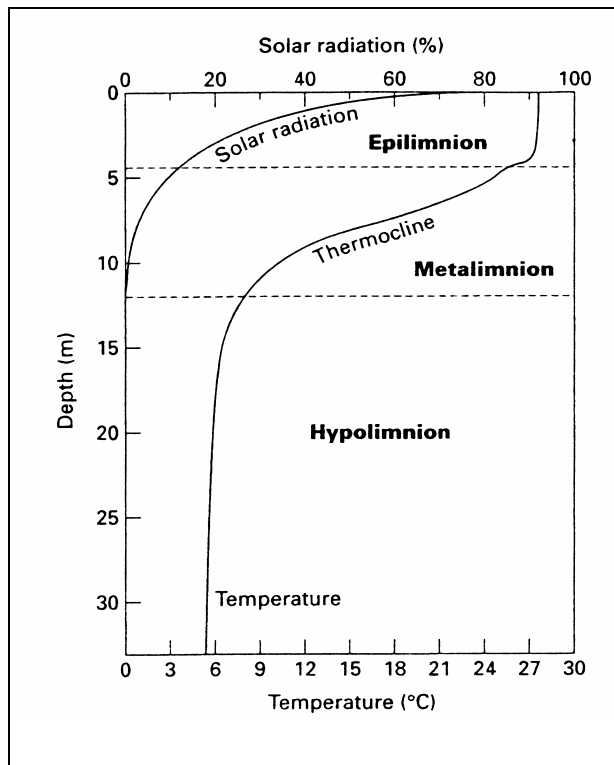


Fig. 1.1. Temperature profile and penetration of solar radiation in a lake. The thermocline marks the zone of maximum temperature change; after Wetzel (1983).

temperature gradient, the **thermocline**, has been termed the **metalimnion** (Wetzel, 1983). The near surface temperature of a lake is a direct response to the penetration of solar radiation. In temperate regions with pronounced winter and summer seasons, changes in air temperature and turbulence induced by wind disturbance can cause a breakdown of the stratification (Schwoerbel, 1993). This may lead to a complete turnover (**holomixis**) of the water column. These seasonal variations lack in deep tropical lakes because of the higher and uniform water temperatures, which favour a stratification of the water column. Lakes with permanent stagnant and anoxic bottom waters are termed **meromictic**. The oil shales of the Laney

Member in the Washakie Basin (Boyer, 1982; Dean & Anders, 1991) and those of the Eocene Lake Messel (Goth, 1990) are ancient examples of sediments thought to have been deposited in permanently stratified water columns.

A change from open to closed conditions because of climatic changes and drainage patterns with time may result in the formation of an alkaline, hypersaline **playa-lake system**. Extensive mudflats are particularly characteristic of playa lakes where desiccation destroys primary sedimentary textures. Such an evolution with subsequent refreshing periods was reported for Lake Kivu and Tanganyika since the Last Glacial Maximum (LGM) (Stoffers & Hecky, 1978). The Wilkins Peak Member of the Eocene Green River Formation is an ancient example (Eugster & Hardie, 1975; Surdam & Wolfbauer, 1975). As a result of drier conditions lakes can become periodically completely desiccated such as the giant Lake Victoria in East Africa (70,000 km²) during the LGM (Talbot & Laerdal, 2000). In open lakes pH conditions range between 6 and 9, whereas pH values as high as 12 were found in some closed lakes such as the soda lakes in East Africa (Talbot & Allen, 1996).

1.1.2 Clastic, Chemical and Biochemical Sedimentation

Changes in the mineralogy may indicate a change from open to closed conditions. Sediments in open lakes include siliciclastic particles derived from fluvial transport, either in suspension or as bed load. Lake margin coarse-grained deposits are attributed to deltaic and marginal lacustrine settings as **alluvial fan deposits**, distributary fluvial channels and channel-mouth bar deposits, which pass rapidly basinward into fine-grained deep water and sometimes-calcareous facies. Diatoms are the major source of opaline silica. Salinity and Mg^{2+}/Ca^{2+} ratios are low in open lakes and calcium carbonate is the dominant chemical and biochemical precipitation. The appearance of carbonates in lake sediments is mainly caused by benthic algal and microbial photosynthetic activity (Talbot & Allen, 1996). Removal of CO_2 raises the pH and promotes carbonate precipitation.

The chemical composition of rocks in the catchment area of a lake has an important impact on the sediment composition and the lake water chemistry. Eugster (1980) showed that silica-rich magmatic, metamorphic and carbonate rocks deliver mainly Na^+ and HCO_3^- waters, whereas basic and ultrabasic rocks provide alkaline Ca^{2+}, Mg^{2+} and HCO_3^- rich waters to the lake basin. Exposed volcanic rocks can influence the clay mineral composition. High smectite percentages in the Messel oil shale are a result of weathering of volcanic particles (Goth, 1990). Thus, the study of clay assemblages in open lake sediments may be used as an important tool to reconstruct the depositional environment because they are thought to preserve the original signature of the continental climate (Keller, 1970).

The sedimentary deposits in closed-basin lake deposits represent a mixture of material derived from runoff, reworked intrabasinal sediments, OM, biogenic silica, carbonate and chemical deposits. Wind-driven material might be of local importance. They may contain evaporites such as gypsum and halite, which precipitate from the water column due to salinity increases caused by intense evaporation. A salt concentration of approx. 5‰ is the upper limit for the existence of typical freshwater organisms (Beadle, 1981). However, in lakes where infiltration rates are greater than evaporation rates, salinities do not increase significantly (Osterkamp & Wood, 1987). Calcium-magnesium carbonates may form in closed lakes because the Mg^{2+}/Ca^{2+} ratio of the lake waters increases due to removal of Ca^{2+} ions through calcite precipitation (Eugster & Kelts, 1983). Authigenic minerals, such as zeolites can provide important environmental informations. These minerals were often reported from hypersaline lake deposits such as the Ries crater in southern Germany (Jankowski, 1981).

1.1.3 Laminations and Cycles

Laminated sediments are an ideal indicator for paleoclimatic reconstructions and an unique archive of climatic variations and result from a periodic variation in the nature of the sediment and/or OM reaching the lake floor (Kelts & Hsü, 1978). Typical examples for annually laminated sediments are the mixed clastic/diatomaceous **varves** identified in Pleistocene and Holocene sediment sequences of the Eifel Maar Lakes (Zolitschka, 1990; Brauer *et al.*, 1999). A dark allochthonous, clastic clay-rich layer was deposited during winter, when runoff increased due to the lack in vegetation. A light organic diatom rich layer formed during spring and summer. Rhythmic variations were also identified in many ancient lake deposits. Laminations of the Messel oil shale are characterised by a regular interlayering of algal-rich laminae and clay-rich laminae which indicate an episodic probably seasonal deposition, typical for a stratified lake in a warm and humid climate (Jankowski & Littke, 1986). The varve-like laminated oil shales of the Green River Formation which consist of carbonate-rich and lamalginitite-rich layers revealed several long-term cycles such as the 3-5 year rhythm, comparable to the El Nino-Southern Oscillation, an 11-year sunspot cycle and 50 cycles at a frequency of 20,000 years (Fischer & Roberts, 1991). Other large-scale lithological variations in ancient lake sequences are thought to reflect alternations of arid and humid climates. For example, lake deposits in the Jiangnan Basin, China contain 1800 to 2200 m thick cyclothems which are thought to reflect changes from fresh to saline lake waters (Powell, 1986).

1.1.4 Lake Types

The controls on lake sedimentation are very dependant on tectonics, size and morphology. A primary prerequisite for the formation of a large lake with a thick sedimentary fill is subsidence related to rifting, strike-slip movements or subsiding sags in cratonic areas (Talbot & Allen, 1996). The development of several **extensional-rift valleys** in East and West Africa as well as China during the Meso- and Cenozoic provide an ideal location that is necessary for the accumulation of thick lacustrine sediments. Several studies in the rift-valley lakes of East Africa have verified that such basins are uniquely positioned to record paleodepositional and paleoclimatic fluctuations in their sedimentary successions (e.g. Johnson, 1996). The generally high subsidence rates ensure the establishment and long persistence of the lake system. In the Songliao Basin (NE China) and Lake Tanganyika more than 4000 m of sediments were deposited (Yang, 1985; Rosendahl, 1987). Lake Baikal

in Siberia is 50 to 75 million years old and formed in a rift-valley in which perhaps as much as 7500 m of strata have been accumulated (Hutchinson *et al.*, 1992).

Many present-day lakes are found in fluvial and shoreline environments (e.g. ox-bows and coastal lagoons), but are dominated by locations related to the last Pleistocene glaciation. **Glacial lakes** are of variable size and formed by processes such as ice-damming, freeze-thaw or repeated glaciation (Talbot & Allen, 1996 and references therein). Other lakes are situated in **volcanic** or **impact structures** such as the Ries crater in southern Germany. **Maar craters** formed by phreatomagmatic eruptions, where a hot melt (lava) effectively interacts with cool water. They are surrounded by a tephra ring and cut into pre-eruptive rocks. If the crater was filled with water (precipitation and/or groundwater), a maar lake can originate. Maars commonly have diameters of about a few hundred meters and depths of several tens of meters (Lorenz, 2000). Maar lakes are favoured settings for paleoclimatic reconstructions because they have a restricted catchment area, a mainly locally dominated signature of OM contribution and very often neither inlet nor outlet. Especially the small and deep maar lakes are thought to react very sensitively to variations in environmental conditions. For example, Lake Holzmaar is an ideal climate archive because it exhibits a trap efficiency of 93 to 98%, meaning that only 2 to 7% of the sediment that enters the maar is lost through the outlet (Negendank & Zolitschka, 1993).

1.2 Organic Matter in Lake Waters and Lake Sediments

1.2.1 Organic Sedimentation

As reviewed by Meyers & Ishiwatari (1993) photosynthetic fixation of CO₂ by phytoplankton and particulate detritus from higher land plants, surrounding the lake are the major sources of OM to lake sediments (Fig. 1.2). These inputs are termed **autochthonous** and **allochthonous**, respectively. The autochthonous OM may be composed of littoral and benthic higher plants (submerged and emerged macrophytes), planktonic and benthic algae and bacteria. Cyanobacteria are other important primary producers in many lakes (e.g. Eckartz-Nolden, 1992; Trichet *et al.*, 2001). They often form cyanobacterial (microbial) mats with stromatolitic structures related to carbonate precipitation on and within the organically formed part. Algal debris in ancient lacustrine oil shales is often derived from the green algae *Botryococcus* or *Pediastrum* (e.g. Hutton, 1984; Sherwood *et al.*, 1984). Scanning electron microscopy revealed an important contribution of the coccal green-alga *Tetraedron minimum* to the Messel oil shale (Goth *et al.*, 1988). If algal productivity is sufficiently high, a pure algal type I, oil-prone kerogen or torbanite may be deposited

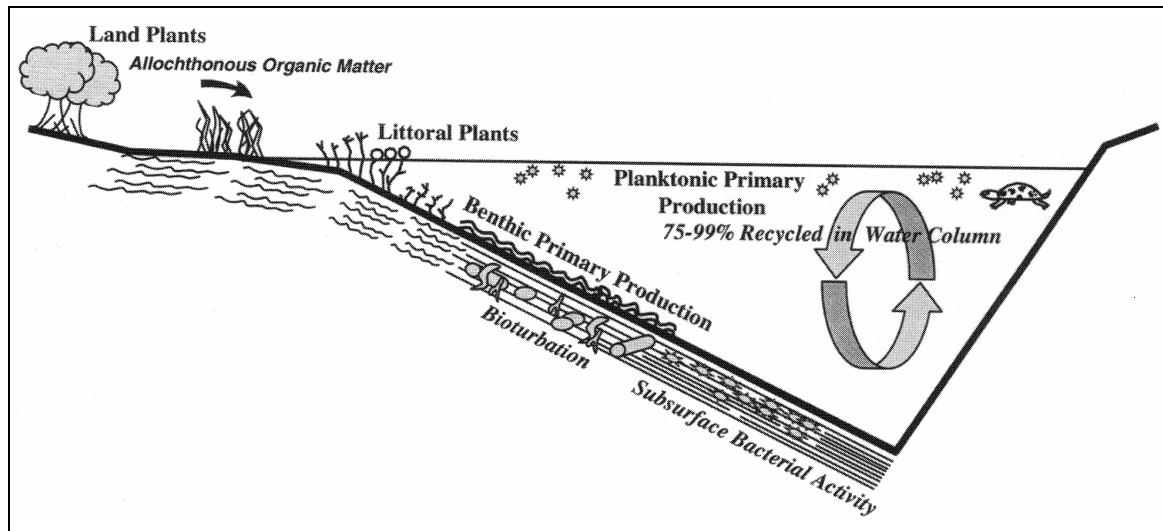


Fig. 1.2. Organic matter sources in lake environments; after Bohacs et al. (2000).

(e.g. Cook *et al.*, 1981). Although some bacteria can carry out photosynthesis (e.g. photosynthetic sulphide-oxidising bacteria), their dominant role is the heterotrophic decomposition of OM. Primary productivity is largely controlled by the availability of key nutrients, notably phosphorous, nitrogen and silica (Talbot & Allen, 1996). The abundance of nutrients serves as a basis for classifying lakes according to their trophic state. Lake waters that are deficient in nutrients are **oligotrophic** associated with low productivity. Lakes with a moderate supply of nutrients are **mesotrophic**, and lakes with high nutrient levels associated with high organic productivity are called **eutrophic**. Consumed nutrients may be renewed by surface runoff, rainfall, and eolian transport or recycling of from below the thermocline during lake overturn. However, the primary production of OM in a lake is also a function of many other variables from which solar input and water chemistry are the most important (Katz, 1990). Solar input controls the energy available for photosynthesis, which in turn supplies dissolved oxygen, essential to the metabolism of all aerobic aquatic organisms. Alkaline waters support primary production due to the availability of CO_3^{2-} ions for incorporation in addition to CO_2 (Kelts, 1988). Thus, the highest natural primary productivity is found in modern tropical alkaline lakes (Likens, 1975).

The allochthonous OM originates mainly from higher land plants. Recycled OM is another allochthonous component, derived from weathering of outcropping OM-rich rocks. Material such as pollen can be transported by wind from outside the watershed, although this fraction of the total OM is generally small.

The optimum organic enrichment in lacustrine sediments occurs where primary production is at a maximum and destruction and dilution are minimised (Bohacs, 1998). Destruction is largely controlled by the availability of oxygen. Dilution by minerals decreases the proportion of OM relative to the inorganic matrix. In oxygenated lake waters a large part of the primary OM is remineralised during transport through the water column and after resuspension by respiration, converting the OM back to CO₂ (Fig. 1.2). In the sediment below the zone of aerobic respiration, bacterial degradation continues but the OM is much more slowly altered. Thus, anoxic bottom waters are crucial for the accumulation of carbon-rich sediments because they enhance preservation by limiting bioturbation and bacterial respiration (e.g. Demaison & Moore, 1980). Oxygen deficiency will result from biological and inorganic oxidation and when the supply of reactive OM exceeds the rate at which oxygen can be renewed.

In meromictic lakes, a large fraction of the OM is preserved whereas in many temperate lakes with seasonally oxic bottom waters only highly resistant OM can prevail. Less reactive forms, such as lipids and humic substances become more dominant than the reactive forms. Thus, as a result of microbial reworking carbohydrates and proteins are enzymatically depolymerised and mineralised, but a part may also contribute to kerogen *via* the classical “**degradation-recondensation**” pathway (Tissot & Welte, 1984; Largeau & Derenne, 1993). In the water column and/or in subaquatic sediments polymeric products of sugars/amino acids or proteins (melanoidins) may form by random condensation and polymerisation of mostly plankton derived material through the Maillard reaction (Maillard, 1912). These gel-like materials can bind functionalised lipids and are thought to represent an important precursor in the formation of amorphous kerogens on diagenesis (Larter & Douglas, 1980). However, the presence of structured OM on a microscopic level points to preservation rather than precipitation of gels. Therefore, the **selective preservation** of certain macromolecular constituents (Hatcher *et al.*, 1983; Tegelaar *et al.*, 1989a), may play an important role, particularly those of outer cell walls from some algae, termed **algaenans** or exines from pollen, termed **sporopollenins**. These insoluble substances are highly aliphatic and resistant to biodegradation and chemical transformations. The review of de Leeuw & Largeau (1993) reveals an inventory of biomacromolecules, their occurrences and their preservation potential. In this perspective, humic substances or kerogens represent mixtures of both, resistant and partially transformed less resistant and degradable macromolecular biomolecules.

1.2.2 Organic Matter Source and Environmental Indicators

The amount, type and molecular composition of OM in lacustrine sediments provide important information for reconstructing the lake depositional environment as reviewed by Powell (1986) and Meyers & Ishiwatari (1993). In this chapter examples of bulk, macromolecular and lipid organic geochemical indicators that record paleolimnological changes in lakes are presented.

Bulk Organic Matter

Source and paleoproductivity information can be obtained from carbon and nitrogen stable isotopic compositions and C/N ratios as reviewed by Meyers & Lallier-Vergès (1999). Rock-Eval pyrolysis was developed as a method for rapid screening of OM quality in potential petroleum source rocks. During the past decade, it has been applied in numerous paleolimnological studies. Hydrogen Index (HI) and Oxygen Index (OI) values from Rock-Eval pyrolysis were frequently used as a first estimation of the allochthonous *versus* autochthonous contribution. In this way high HI values between 600 and 900 HC/g TOC in combination with very low OI values (< 30 mg CO₂/g TOC) in lacustrine shales of the Congo basin rift sequence indicate a type I kerogen, derived from algal and bacterial sources (Harris *et al.*, 1999). Lacustrine oil source rocks from the early Jurassic to early Cretaceous sequence of the Eromanga Basin, Australia were classified as type II/III kerogen with abundant OM derived from higher plants (Powell, 1986). The kerogen type can even vary within a single basin. The lacustrine Songliao Basin in NE China is a good example for a strong relationship between source rock quality and lake facies, which is presented in Fig. 1.3. The Upper Cretaceous oil shales and major source rocks of type I kerogen were deposited in a large eutrophic lake during maximum lake transgression in a deep water facies (Yang *et al.*, 1985). Towards the lake margin the source rock quality decreases, caused by a higher contribution of terrigenous OM (type II and III kerogen). However, other approaches have to be used complementary to Rock-Eval because oxidised aquatic OM is also associated with lower HI values and thence can bias source determinations (cf. Meyers & Lallier-Vergès, 1999). It was also suggested that different types of primary producers in a lake might lead to different HI and OI signatures of lake sediments. Sediments with elevated HI values from Lago di Albano, Italy are associated with periods dominated by cyanobacteria production, whereas diatom production was dominant in sediments with lower HI values (Ariztegui *et al.*, 1996).

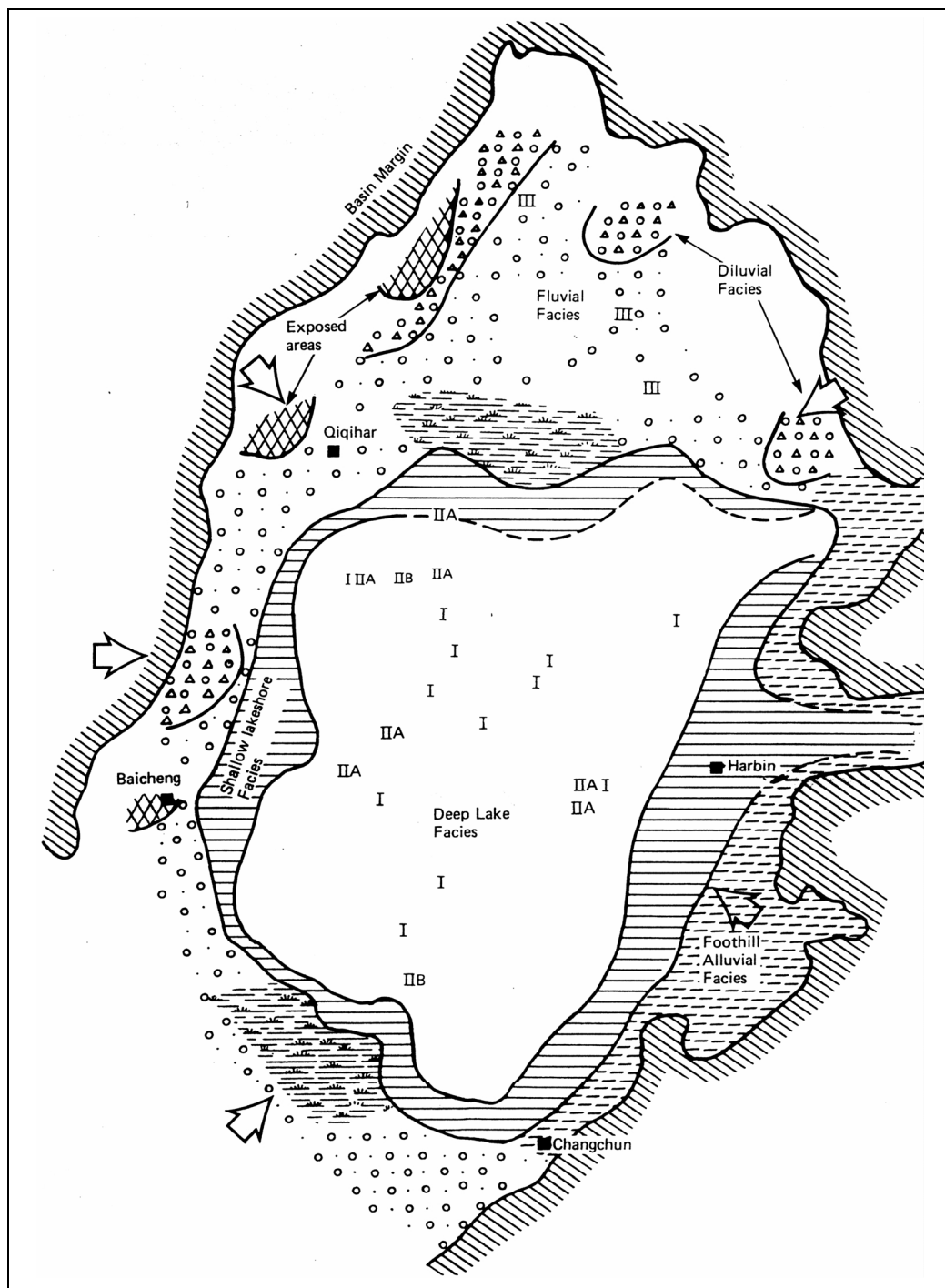


Fig. 1.3. Kerogen type (numbers) and facies relationship in the Quingshankou Formation, Songliao Basin. The arrows indicate the direction of source material; after Yang et al. (1985), modified by Powell (1986).

Macromolecular Organic Matter

More than 85% of the OM in recent sediments is neither soluble in aqueous alkaline solvents nor in organic solvents. While a large amount of information is available on the soluble OM composition, relatively few studies were devoted to the macromolecular insoluble OM in lake sediments and the informations they could furnish on the paleoclimate and depositional

environment. In contrast to lake environments the insoluble OM fraction was intensively studied in modern marine, estuarine and river sediments as well as peat-bogs and soils using organic petrology, analytical pyrolysis and spectroscopy (e.g. Schnitzer, 1977; Sigleo *et al.*, 1982; Lallier-Vergès *et al.*, 1998; Zegouagh *et al.*, 1999; Boucsein & Stein, 2000; Faure & Landais, 2001).

Organic petrology describes the visible organic particles in sediments and kerogens. Microscopic analyses are useful to determine OM origins and the degree of preservation. Three main groups of organic constituents have been identified in lake sediments (Meyers & Lallier-Vergès, 1999). “Autochthonous” or “aquatic” organic particles comprise algal debris and zooclasts. The OM in many lacustrine sediments (e.g. torbanites and coorongites) is derived from remains of the freshwater alga *Botryococcus braunii* (e.g. Largeau *et al.*, 1986). Ultrastructural studies revealed that a large part of the amorphous unstructured OM originates from microbial degradation of primary algal OM (e.g. Derenne *et al.*, 1992). “Allochthonous” or “terrestrial” particles include ligno-cellulosic debris derived from vascular plants. In lakes with abundant emergent vegetation, a large part of the OM consist of terrigenous particles (e.g. Lake Tritrivakely, Madagascar; Bourdon *et al.*, 2000). Finally, a third type of particles is brought to the lake by wind and rivers that include pollen, primary oxidised and recycled OM. Point-counting of organic particles in sediments and in kerogens after acid treatment can be used to determine the aquatic *versus* terrigenous input. On the basis of such a maceral analysis Jankowski & Littke (1986) concluded that the Messel oil shale consist of 20% terrigenous higher plant material (vitrinite and inertinite) and 80% autochthonous algal material (lamalginite). The algal/higher plant ratio was used to interpret glacial/interglacial transitions in sediments of Lac du Bouchet, France (Bertrand *et al.*, 1992). In the same lake, observations at the transition to the Holocene revealed that the aquatic production gave an earlier response *versus* warming than the pollen and the total organic flux (Sifeddine *et al.*, 1996). The same approach, extended by vitrinite reflectance measurements was applied to study the human impact to lacustrine sedimentary OM and the degree of OM oxidation in sediments of Lac d’Annecy in the French Alps (Noël *et al.*, 2001). The presence of coke and semi-coke residues in the near-surface bottom sediments of Lake Ontario was related to ship debris contamination (Lewis *et al.*, 2000).

The degradation of macromolecules into small fragments with thermolytical techniques is one important method to obtain molecular structural informations of complex organic materials (Horsfield, 1989). **Pyrolysis** of lake kerogens and plant biomass can help to identify selectively preserved biochemical and newly generated biochemical structures as well as secondary processes such as microbial reworking. The pyrolysates of many lacustrine

kerogens (e.g. Green River Shale) contain a high proportion of long-chain *n*-alk-1-enes and *n*-alkanes (Horsfield, 1989). The outer cell walls of some algae and extant plant structures contain resistant, highly aliphatic biopolymers, which are considered the precursors for a major fraction of the *n*-alkyl moieties in lacustrine kerogens. Such selectively preserved cell wall remains of the green microalgae *Tetraedron minimum* have been encountered in a facies of the Messel oil shale (Goth et al., 1988). Pyrolysis of the isolated cutan from *Agave americana* (Tegelaar et al., 1989b) and higher plant suberans (Tegelaar et al., 1995) also yielded homologous series of normal hydrocarbons. However, it must be noted that some of the *n*-alk-1-enes and *n*-alkanes are produced by random scission of polymethylene chains during pyrolysis of hydrogen-rich type I kerogens (Larter & Horsfield, 1993).

Other plant parts contain phenolic macromolecules (e.g. lignin, tannin, sporopollenin) which produce aromatic pyrolysis products such as alkylbenzenes, alkylphenols and methoxyphenols upon pyrolysis (e.g. Stout & Boon, 1994; van Bergen et al., 1994). Similarities between phenolic compounds in the pyrolysate and results from lignin composition, derived from CuO oxidation (C/V and S/V ratios), may record vegetation changes resulting from climatic and atmospheric changes in the lake catchment (Huang et al., 1999). The occurrence of alkylthiophenes in the kerogen structure may allow specific environmental interpretations. Sulphur moieties are incorporated during syndepositional reactions of reduced inorganic sulphur species with functionalised lipids, a process termed sulphurisation (for review see Sinninghe Damsté & de Leeuw, 1990). However, in lacustrine environments sulphate reduction is often limited by the low amounts of sulphate (Berner, 1984). The sulphur-rich Tertiary lacustrine Ribesalbe kerogen is an example for a type I-S kerogen, deposited in an environment where additional sulphate was provided by eroding of gypsum rocks (Sinninghe Damsté et al., 1993).

The previous examples have shown that the key to the study of macromolecules in lacustrine sediments is the combined application of microscopy and thermal degradation. However, only very few sets of data exist that provide a combined approach in a single lake archive. An evaluation of macromolecular compounds in modern lake sediments was presented by Krugé et al. (1998). The authors used analytical pyrolysis and organic petrology to assess anthropogenic organic contaminants in western Lake Ontario. Talbot & Livingstone (1989) used the petrographic composition of lacustrine OM from Late Quaternary sediments of Lake Victoria in combination with Rock-Eval pyrolysis and stable carbon isotopes to identify periods of low water tables or subaerial exposure.

Lipid Organic Matter

Lipid compounds can be isolated by solvent extraction of lake sediments that yields for example hydrocarbons, carboxylic acids, alcohols, ketones and aldehydes. **Biomarkers** are lipid compounds whose basic carbon skeleton is derived from once-living organisms (Peters & Moldowan, 1993). Specific biomarker assemblages are especially useful for typing OM and were already assigned to particular types of depositional environments. Relative contributions of terrigenous and aquatic sources in Pleistocene and Holocene lake sediments were determined by the analyses of *n*-alkanes or *n*-fatty acids (e.g. Wilkes *et al.*, 1999; Brincat *et al.*, 2000). Long-chain *n*-alkanes and *n*-fatty acids in lacustrine sediments are attributed to terrestrial higher land plant sources (Eglinton & Hamilton, 1967). In contrast to those of land-plant origin, compounds produced by planktonic microorganisms are mostly characterised by short-chain homologues. However, it is impossible to discriminate between plant species using different metabolic pathways (C_3 , C_4 , CAM plants) based on *n*-alkane and *n*-fatty lipid distributions. Carbon isotope analyses on long-chain *n*-alkanes allow specifying the types of land plants, which reflect carbon dioxide and moisture changes in the atmosphere. Rieley *et al.* (1991) analysed $\delta^{13}C$ values of individual *n*- C_{25} to *n*- C_{29} hydrocarbons from Ellesmere Lake sediments. The authors showed that willow leaves are the major source of the sedimentary *n*-alkanes.

The ratio of pristane to phytane has been widely used as an indicator of the redox conditions at the time of deposition (e.g. Didyk *et al.*, 1978). The isoprenoids pristane and phytane formed diagenetically from the phytol sidechain of chlorophyll *a*, depending on the environmental conditions. In an anoxic environment, phytol is converted to dihydrophytol and phytane. Under oxic conditions it is oxidised to phytenic acid, which is further transformed into pristane by decarboxylation and hydrogenation (Tissot & Welte, 1984). The presence of pentacyclic triterpenoids with a hopane skeleton point to the activity of bacteria in the water column or at the sediment surface (e.g. Innes *et al.*, 1997). Sterol compositions may provide important information on OM sources, diagenesis and certain environmental conditions. 24-ethylcholesterol is the dominant sterol in many macrophytes and land plants from Lake Suwa (Japan), whereas cholesterol is the major algal sterol (Nishimura & Koyama, 1977). Microbial processes are responsible for the rapid diagenetic alteration of biological sterols, including the conversion from stenols to stanols (Robinson *et al.*, 1984). In surficial sediments of Lake Lemman, Switzerland, epicolestanol is a specific sterol which is believed to be derived from anaerobic bacteria (Mermoud *et al.*, 1985). Dinosteroids and tricyclic terpanoids were only recognised in saline/alkaline lacustrine sediments (Laney Shale) from

the Eocene Green River Formation (Wang, 1998). The C₃₀ triterpane gammacerane and β -carotane are very specific for highly saline and stressed lake environments (Mello *et al.*, 1988; Peters & Moldowan, 1993). They are also usually associated with arid or semiarid lacustrine settings where the OM is primarily derived from algae and bacteria (e.g. Hills & Whitehead, 1966; Brassell *et al.*, 1988). Gammacerane has also been linked to water-column stratification (Sinninghe Damsté *et al.*, 1995). The presence of oleanane, a biomarker which is thought to derive from angiosperms, can be used to estimate the terrigenous input to ancient lake sediments (e.g. Fu & Sheng, 1989).

One major problem in paleolimnological studies is temperature determination of paleo-lake waters. Kawamura & Ishiwatari (1981) reported an increase of the proportion of polyunsaturated acids in algae with decreasing water temperatures as a biochemical response to maintain fluidity of cell membranes. They ascribed variations of the *n*-C_{18:2} to *n*-C_{18:0} fatty acid ratio in Lake Biwa (Japan) sediments with depth to paleoclimatic changes in the lake environment. Distribution patterns of C₃₇ and C₃₈ polyunsaturated long-chain alkenones were widely used as proxies for the determination of paleotemperatures in marine surface waters (e.g. Goni *et al.*, 2001; Ishiwatari *et al.*, 2001; Kienast *et al.*, 2001). Alkenones were also identified in lake sediments (Li *et al.*, 1996; Innes *et al.*, 1998; Sheng *et al.*, 1999), however their biological source is still unknown and their only episodic occurrence impedes their utility as paleotemperature "proxy-data" in the lacustrine environment (Zink *et al.*, 2001). The presence or absence of these compounds in sediments from three English lakes was interpreted to reflect different algal populations in response to varying environmental conditions (Cranwell, 1985).

1.2.3 Fossil Fuel Resources

Two fossil fuel resources are associated with lacustrine basins, namely oil shales and petroleum. Any shallow rock yielding oil in commercial amount upon pyrolysis is considered to be an **oil shale** (Tissot & Welte, 1984, p. 254). Organic richness and OM type are major requirements, which determine the assay. A lower limit of 5% organic content is necessary for shales to be of economic interest, which corresponds to an oil yield of 25 l per metric t or 6 gal. per short t (Tissot & Welte, 1984, p. 255). The average pyrolysis temperature is 500°C. A high degree of oil prone OM delivery (organic productivity), preservation (oxygen deficiency) and a lack of clastic sediment supply have favoured their accumulation in many lacustrine settings world-wide (Talbot & Allen, 1996). A number of well-known lacustrine oil shales (e.g. Green River shale, U.S.; Autun boghead, France and torbanites from different

locations) contain type I kerogen with high H/C and low O/C ratios (Tissot & Welte, 1984). They consist very often of pure algal OM (e.g. *Botryococcus*) or represent a mixture of algal and amorphous OM (e.g. Cane, 1969; Sherwood *et al.*, 1984). However, elemental data indicate that type II kerogens are often present as well (e.g. Messel shale, Germany; Irati shales, Brazil; Lower Toarcian shales of the Paris Basin, France). The richest oil shales were deposited in tropical to subtropical climates without pronounced seasonalities and profundal settings such as those of the Laney member in the Green River Formation (Dean & Anders, 1991). Results of a combined pyrolysis and biomarker study indicated that water column stratification during deposition of the Laney member was stabilised by the presence of highly saline bottom waters (Horsfield *et al.*, 1994). The Green River shales constitute the largest oil shale reserves in the world, which are evaluated to be more than 250 billion t of potential oil.

High quality lacustrine organic-rich sediments are responsible for 20% of the current worldwide hydrocarbon production (Kulke, 1995). Although lacustrine derived oils often display a large compositional variability they tend to be more paraffinic, waxier and with a few exceptions exhibit a low sulphur content (Powell, 1986). Ancient lacustrine sequences contain important sources and reservoirs of petroleum. Along the entire Brazilian margin synrift, lacustrine sedimentation took place in response to the Neocomian break-up of Gondwana. These sediments account today for over 95% of the Brazilian petroleum reserves (Mello & Maxwell, 1990). The Marlim field in the Campos basin, offshore Brazil contains approx. 14 billion bbl. of lacustrine derived oils in deep-sea reservoirs. In the North Falkland Basin, Neocomian organic-rich lacustrine mudstones which are dominated by type I amorphous kerogen are the principal source rocks (Durham *et al.*, 1999). The Kwanza, Congo and Gabon rift basins are tectonic analogous on the west coast of Africa with undiscovered resources. Paraffinic oils in the Gabon sub-salt are sourced from lacustrine shales of the Neocomian to Barremian Melania Formation, containing type I and II kerogen (Brink, 1974). Lacustrine petroleum was also discovered in pre-salt sequences of Cabinda, Angola (Brice & Pardo, 1980). Hydrocarbons in the Cenozoic South Sumatra Basin (Indonesia) are derived from both, lacustrine source rocks of the Lahat Formation and terrestrial coal and coaly shale source rocks of the Talang Akar Formation (ten Haven & Schiefelbein, 1995). The Lahat Formation (Eocene and Early Oligocene) contains oil prone type I and II kerogen (Hutchison, 1996). Known petroleum reserves of this basin are estimated at 4.3 billion bbl. of oil (Klett *et al.*, 1997). The Minas and Duri fields of central Sumatra still contain 9 and 5 billion bbl. of lacustrine derived oils (Katz, 1999).

More than 95% of China's petroleum reserve base is considered to originate from lacustrine source rocks, deposited in different lake settings including freshwater, brackish and hypersaline lakes. Based on biomarker criteria, crude oils from the north-eastern Qaidam Basin correlate with open lacustrine fresh and deep-water Middle Jurassic source rocks of the Chaishiling or Dameigou Formation (Ritts *et al.*, 1999). The giant Daqing field of China's most important oil-productive Songliao Basin has produced over 7 billion bbl. of lacustrine-derived oil from turbidite reservoirs (Katz, 1999). The oils were sourced from Upper Cretaceous rocks which were laid down in a giant fresh to brackish water lake (e.g. Hou *et al.*, 2000). In contrast to the Songliao Basin, the geochemical character of lacustrine oils from the Jiangnan Basin (Hubei Province, eastern China) is consistent with an origin from Eocene to Palaeocene, anoxic evaporitic source rock rich in algal and fluorescing amorphous type I and II kerogen (Peters *et al.*, 1996). A few shales from the Qianjiang Formation (Eocene) contain sulphur rich type I-S OM. They are possible source rocks for oils characterised by high asphaltene and sulphur contents (Powell, 1986 and references therein).

The Liaohe oil field (Bohai Bay), located in NE China's Liaoning province is the third largest oil producer of the country and one of the major heavy oil producers in the world (Li, 1991). It was controversially discussed whether these oils were formed by alteration processes such as biodegradation or are so called "immature oils" (e.g. Huang *et al.*, 1990; Lu *et al.*, 1990). Exploration for additional sources has become more difficult because found accumulations have become smaller, deeper and less economic. The Western Depression of the Liaohe Basin is an important part of the exploration effort according to the strategy of the Liaohe Oil Company. To make exploration more efficient a comprehensive understanding of the lacustrine facies is necessary, that controls the distribution of oil prone source rocks. The Eocene Shahejie Formation is of great significance because it contains both, the principal oil source rocks and reservoirs.

2 Goals and Approach

This thesis aims to show how environmental and climatic changes affected the inorganic and organic fraction in Tertiary and Recent lake sediments. To evaluate lateral and vertical changes of the depositional conditions, sediments are described and interpreted in terms of their mineralogy and organic facies. After the definition of Jones (1987) the term organic facies describes “a mappable subdivision of a designated stratigraphic unit, distinguished from the adjacent subdivisions on the basis of the character of its organic constituents, without regard to the inorganic aspects of the sediment”. It can be defined by using a combination of geochemical and microscopic data such as kerogen, maceral and lipid analysis (Jones, 1987; Tyson, 1995). These methods offer the opportunity **(1)** to determine the occurrence and type of kerogen and thence predict petroleum compositions as a function of the paleoenvironment and **(2)** to relate short-and long-term OM variations or cycles in recent or ancient sediments to paleoecology and paleoclimate.

In the **first part** of this work source rock samples from the Es4 and Es3 members of the Shahejie Formation (Eocene) in the Western Depression of the Liaohe Basin, China were studied using organic petrographic, mineralogical and various organic geochemical methods. This was performed to characterise the source rock facies, determine their source rock potential and depict depositional processes for the ancient lake deposits. To achieve these goals the following working plan was carried out:

- Quantitative whole-rock mineralogy, bulk pyrolysis and organic petrology were employed to define a depositional and facies framework.
- Analytical pyrolysis experiments (Py-GC-FID and Py-GC-MS) on kerogen concentrates were conducted for a detailed insight into structural moieties of the kerogen. Kinetic data were determined to characterise their thermal lability.
- The composition of the soluble OM was determined for facies and maturity assessment.

The study was part of a large research project conducted at the FZ Juelich (ICG-4), in cooperation with PetroChina concerning developing exploration strategies based on quantitative geochemistry and basin modelling.

In the **second part** of this thesis, a detailed investigation of macromolecular OM in maar lake sediments was performed and their utility as paleoclimatic and paleoenvironmental indicators in the late Pleistocene and Holocene was studied. The goals were as follows:

- To identify sources of macromolecular organic compounds and biogenic particles in maar lake sediments. Analytical pyrolysis (Py-GC-FID and Py-GC-MS), organic petrological methods and carbon isotopic measurements on sediments and kerogen concentrates were carried out for this purpose.
- To test their sensitivity as proxy parameters in Late Pleistocene and Holocene sediment sequences from different climatic regions.
- To establish molecular and petrological parameters characterising the paleoenvironment and paleoclimate.
- To investigate a selected stratigraphic interval by high-time resolution studies.

For a limited number of samples an investigation of selected bitumen fractions was also carried out to provide a data basis and for comparison. In this regard, it should be noted that a detailed investigation on the soluble OM in maar lake sediments is currently being performed by Thomas Fischer (Fischer, 2002, in prep.), within the priority programme “Changes of the Geo-Biosphere during the last 15,000 years – Continental sediments as evidence for changing environmental conditions”, sponsored by the Deutsche Forschungsgemeinschaft (German Research Foundation).

3 Analytical Program

A listing of analyses performed on the Liaohe source rocks and maar lake sediments is given in Tab. 3.1. Details concerning sample selection are presented in chapters 4 and 5. The Liaohe samples were cut and pieces, orientated perpendicular to the bedding were chosen for organic petrological analyses. The rest was ground in a disc mill for 30 s for further analysis.

Maar lake sediments were kept at 4°C before subsampling. Afterwards, two third of each sample were ground with pestle and mortar and subjected to organic geochemical analyses. The remaining segment was used for microscopy.

Analysis	LSR	HZM	MFM	HM	Acknowledgements
Elemental and Rock-Eval	90	38	44	77	-
X-ray diffraction	49	-	-	-	S. Franks (RockFluid Systems, U.S.)
Kerogen concentration	16	13	12	7	HARC (U.S.)
Organic petrology (1) whole rock (2) concentrates	42 -	20 12	20 12	15 7	-
Stable carbon isotopes (1) sediment (2) concentrates	16 16	13 13	12 12	45 7	A. Lücke & G. H. Schleser (ICG-4, FZ Jülich)
GC-irmMS	-	-	-	10	N. Mills (APT, Norway)
Py-GC-FID (1) sediment (2) concentrates	7 16	- 13	- 12	32 7	-
Py-GC-MS	8	8	8	12	-
Thermovaporisation	27	-	-	-	-
Bulk kinetics of HC-generation	11	-	-	-	R. di Primio (Saga Petroleum, Norway)
Solvent extraction and liquid chromatography	27	-	-	10	-
GC and GC-MS	27	-	-	10	J. Lopez (Postdoc, ICG-4, FZ Jülich)

Tab. 3.1. Methods employed to Liaohe source rocks (LSR) and maar lake sediments and acknowledgements. HZM, Lake Holzmaar 4a core; MFM, Lake Meerfelder Maar cores; HM, Lake Huguang Maar cores D, E and F; HARC, Houston Advanced Research Centre.

3.1 Elemental Analyses

Carbon and sulphur concentrations in whole rock samples as well as on kerogen concentrates were measured in duplicate by combustion in an induction furnace in a flow of oxygen, using a LECO carbon-analyser IR 112. Detection of the carbon oxides by an infrared detector allowed the calculation of carbon as weight-percent (wt.-%) of the rock sample. Total carbon (TC) was determined directly. Total organic carbon (TOC) was measured using samples that had been treated with hydrochloric acid to remove carbonate. Carbonate values were calculated from TC and TOC assuming all carbonate was CaCO₃ (calcite) using the following equation:

$$\text{CaCO}_3 \text{ (wt.-%)} = [(TC-TOC)*101]/12$$

For comparison with already established data all carbonate values are presented here according to this standard equation. It should however be noted that this is only a semi quantitative guide to carbonate mineralogy. A detailed evaluation based on XRD is presented in this thesis.

The Central Department of Analytical Chemistry (ZCH, FZ Jülich) measured nitrogen- and hydrogen values. Hydrogen was determined by sample oxidation (1100°C) and infrared (IR) detection of H₂O. The nitrogen content was obtained by thermal conductivity detection (TCD) of N₂. Oxygen was analysed separately by transformation of all oxygenated molecules into CO followed by oxidation over copper to CO₂, which was measured directly by IR detection. Elemental and Rock-Eval data of Lake Holzmaar (HZM) and Lake Meerfelder Maar (MFM) sediments were analysed in co-operation with Thomas Fischer (ICG-4, FZ Jülich).

3.2 Rock-Eval Pyrolysis

Analyses were performed using a Rock-Eval II instrument. This method has been described in detail by Espitalié *et al.* (1977) and Espitalié *et al.* (1985). Sample weights (up to 100 mg) were chosen according to TOC content to avoid detector saturation. An external standard (IFP 55000; S1 = 0.25 mg HC/g rock; S2 = 8.62 mg HC/g rock; S3 = 1.0 mg CO₂/g rock; T_{max} = 419°C) was used for calibration. Whole rock samples and kerogen concentrates were heated at 300°C for 3 min, and the released thermally distilled products were quantified by flame ionisation detector (FID) as the S1 peak. This step was followed by temperature-programmed pyrolysis at 25°C/per min up to 550°C. Generated products resulting from the

thermal breakdown of the kerogen were quantified as the S2 peak. The temperature at which the maximum amount of hydrocarbons is liberated from the kerogen is called T_{\max} . A third peak (S3) represents the amount of generated carbon dioxide up to a temperature of 390°C. CO_2 was collected in a molecular sieve trap during pyrolysis, then released by ballistic heating and analysed by TCD. The Hydrogen Index (HI) which is S2 normalised to the TOC (mg HC/g TOC) corresponds to the yield of pyrolysable hydrocarbons, and is controlled essentially by the availability of organic hydrogen in the sample. The Oxygen Index (OI) corresponds to the quantity of carbon dioxide normalised to the TOC (mg CO_2 /g TOC).

3.3 Mineralogy

X-ray diffraction was performed on the Liaohe samples by Steve Franks (RockFluid Systems, Inc., Plano, U.S.) under sub-contract. His procedure involved the following steps: Samples were disaggregated in mortar and pestle, and about 5 g were transferred to water or alcohol and pulverised using a McCrone micronizing mill. The powders were dried and pressure-packed into aluminium sample holders to produce random whole-rock mounts. XRD-analyses were performed with a Rigaku automated powder diffractometer equipped with a copper source (40 kV, 35 mA) and a solid-state scintillation detector. The samples were scanned over a two-theta range of 2-60 degrees at a scan rate of one degree per minute using a sample spinner to reduce the effects of preferred orientation.

Mineralogical identification was aided by a commercial search-match software package marketed by Material Data, Inc. Quantitative determinations of whole-rock mineral mounts utilise integrated peak areas (derived from peak decomposition/profile fitting methods) and empirical Reference Intensity Ratio (RIR) factors determined specifically for the diffractometer used in the data collection. The total layer silicate (clay and mica) abundance is determined on the whole rock XRD patterns using combined clay mineral reflections and suitable empirical RIR factors. Steve Franks performed a cluster analysis for carbonate mineral analysis. Six carbonate groups or “facies” were detected and a seventh cluster of shales classified as “low carbonate”, as described later in the thesis. The data are reported as weight percent of the whole rock sample.

The term “expandable clay” is used to describe discrete smectite and random or ordered mixed-layer illite/smectite. The term “illite & mica” is used to describe 10-angstrom material regardless of crystallinity. The term “kaolinite & chlorite” is used to describe total 7-angstrom clay material and may include one or both of these clay minerals.

3.4 Kerogen Isolation

Kerogen concentrates were prepared under sub-contract by the Houston Advanced Research Centre (HARC) - Geotechnology Research Institute (GTRI) according to the patented automated kerogen isolation method of Colling & Nolte (1992). The crushed rock was previously solvent extracted using a flow blending technique (see below for details). After that it was placed in custom designed Teflon vessels and subjected to sequential acid digestion procedures (HCl and a mixture of HCl and HF) to remove carbonates and silicates. Digestion times are in between 2 and 3 days, depending on the sample behaviour. Reaction was conducted with mild heat near 45°C. Pyrite was removed using CrCl₂. After kerogen concentration the samples were extracted once again using the flow blending technique.

3.5 Organic Petrology

Microscopical investigations were carried out on 42 **Liaohe** whole rock samples from 16 different wells to establish facies types. For microscopic studies, source rock samples were embedded in epoxy resin. For the impregnation, a mixture of an epoxy-resin (Scandiplex A) and a hardener (Scandiplex B) was used. The resultant block, orientated perpendicular to the bedding was ground flat and polished. Qualitative observations were performed in reflected white and fluorescence light (blue light excitation at 365 nm) using a Zeiss Axiophot microscope and oil immersion objectives with 25x, 50x and 100x and oculars with 10x magnifying power.

One third of each freeze-dried **maar lake** sample was used for qualitative microscopical analyses in incident light. To enable the impregnation of the soft sediment without destroying internal structures a special two component epoxy mounting system was used (SpeciFix-20; Struers). This system includes a low-density resin and a curing agent (mixing ratio 7:1 by weight). The kerogen concentrates were mounted with a special wax (Logitech) on glass slides, which were heated on a heating block to 70°C. Cooling to room temperature hardens the wax. Strew mounts were quantitatively analysed with a point counter using a method

from Senftle *et al.* (1987), whereby macerals were determined in reflected white, fluorescence and transmitted light observations. The means of illumination was changed repeatedly during analysis. Seven maceral groups or individual macerals were counted: (1) huminites/vitrinites, (2) inertinites, (3) sporinite, (4) alginite, (5) other liptinites (incl. cutinite, liptodetrinite, suberinite, resinite and chlorophyllinite), (6) fluoramorphinite and (7) hebamorphinite. All results are reported in vol.-%, on a mineral free basis. Minerals were counted as a separate category in white light mode. The reflectance of organic particles was measured with a 40x oil immersion objective using monochromatic light (546 nm) over a measuring area of 0.16 μm i.d. A minimum of 20 huminite, vitrinite and inertinite particles were measured for each sample.

3.6 Stable Carbon Isotopes

Stable carbon isotope ratios of total OM in kerogen concentrates and whole rocks were determined on samples (0.5 to 1.5 g) which had been treated with 0.5 N HCl for 24 hours to remove carbonate. The residue was centrifuged, decanted, washed several times with deionised water and freeze-dried. According to their TOC contents, a certain amount of sample, representing approx. 150 μg of organic carbon, was weighed into tin foil boats. It was combusted with excess oxygen (1050°C) in a Carlo Erba elemental analyser. After removal of water, the CO_2 was carried into an isotope-ratio mass spectrometer (Optima IRMS) using helium as carrier gas. CO_2 , whose isotopic composition was known, relative to the Pee Dee Belemnite standard, was used as a reference gas. Results are reported in the usual delta notation:

$$\delta^{13}\text{C} (\text{‰}) = [(R_{\text{sample}}/R_{\text{reference}}) - 1] * 10^3$$

where R is the ratio $^{13}\text{C}:^{12}\text{C}$.

Compound-specific carbon-isotopic measurements (GC-irmMS) on fractions were carried out under sub-contract by Nigel Mills (Applied Petroleum Technology A/S, Norway). Isotopic analysis were performed using a HP 5890 series GC (50 m HP-ultra 2, i.d. 0.20 mm, 0.25 μm film thickness) coupled to a Isochrom 3/Optima from Micromass, England. The heating program was 90°C isothermal for 4 min, up to 120°C at 50°C min^{-1} , isothermal for 1 min at 120°C, 120 to 310°C at 4°C min^{-1} , isothermal for 51 min. All values are expressed relative to the Pee Dee Belemnite standard.

3.7 Thermal Analysis Techniques

Open-system one step pyrolysis-gas chromatography (Py-GC-FID) was performed using a system described by Muscio & Horsfield (1996). A glass capillary tube with both ends open and glass wool plugs was used to hold the sample. Up to 10 mg of each kerogen and 50 mg of each whole rock sample was heated in a flow of helium. Samples were thermally extracted at a temperature of 300°C for 5 min. During this step, released hydrocarbons were vented. Then pyrolysis was carried out in a temperature range between 300°C and 600°C at 50°C/per min. The final temperature was maintained for 2 min. The generated products were collected in a cryogenic trap (liquid nitrogen cooling) from which they were liberated by ballistic heating into a Hewlett Packard 5890 gas chromatograph equipped with fused silica columns of either 25 m or 50 m length, 0.32 mm i.d., HP-1 coating of 0.5 µm thickness. The GC oven temperature was programmed from 40°C to 300°C at 5°C per min. Helium was used as a carrier gas with a flow rate of 30 ml/per min. Compounds listed in Tab. 3.2 were identified by relative retention times and Py-GC-MS and quantified by external standardisation with *n*-butane. The same analytical configuration was employed for **thermovapori-sation-GC**, whereby volatile freely occurring organic compounds were released from whole rocks at 300°C.

Group	Compounds
Aliphatic hydrocarbons	C ₆ -C ₃₂ <i>n</i> -alkanes
	C ₆ -C ₃₂ <i>n</i> -alk-1-enes
Isoprenoids	C ₁₃ -C ₂₀ saturated and mono-unsaturated
Benzenes	C ₀ -C ₄ alkylbenzenes
Phenols	C ₀ -C ₂ alkylphenols, methoxy-substituted phenols
Pyrroles	C ₀ -C ₂ alkylpyrroles
Pyridines	C ₀ -C ₂ alkylpyridines
Sulphur containing compounds	C ₀ -C ₂ alkylthiophenes
Naphthalenes	C ₀ -C ₂ alkyl-naphthalenes
Indoles	C ₀ -C ₁ alkylindoles
Furans	C ₀ -C ₁ alkylfurans
Carbonyl compounds	e.g. cyclopenten-1-ones, 2,3-butanedione, 2-propanone, furan-2-one
Polycyclic aromatic compounds	phenanthrene, fluorene

Tab. 3.2. List of identified and quantified pyrolysis products.

Pyrolysis-gas chromatography-mass spectrometry (Py-GC-MS) was carried out with a Fisons Quadrupole MD 800 mass spectrometer. Full scan mass spectra were recorded over the mass range 10-420 amu with 2.5 scans/s. The mass spectrometer was coupled to a Fisons GC 8000 equipped with a HP-1 fused silica capillary column of 50 m length, 0.32 mm i.d., and 0.5 μm film thickness. Helium was used as the carrier gas.

3.8 Bulk Kinetics of HC-Generation

For kinetic modelling of petroleum generation 10 whole rock samples were subjected to programmed-temperature open-system non-isothermal pyrolysis (e.g. Burnham *et al.*, 1988; Jarvie, 1991) at four different heating rates (1, 15, 25 and 50°C/min). Experiments were performed in co-operation with R. di Primio (Saga Petroleum, Norway) with a Rock Eval 6 system and evaluated using Optkin software (Beicip, France). Kinetic parameters were derived using a parallel reaction model. The reactions of this kinetic scheme are considered to follow first-order kinetics and the Arrhenius law. Hydrocarbon generation kinetic parameters consist of a series of activation energies and a single frequency factor.

3.9 Solvent Extraction and Liquid Chromatographic Separation

The Liaohe ground source rock samples and the Lake Huguang Maar sediments were extracted with an azeotropic mixture of methanol, chloroform and acetone (36:29:35 vol.-%) using a flow blending system (Radke *et al.*, 1978). Lake Holzmaar and Lake Meerfelder maar sediments were extracted with a mixture of dichloromethane and 1% methanol using the same device (Fischer, 2002 in prep). The residue was collected for kerogen concentration and further analytical thermal analysis. The extracts were combined and concentrated in a Zymark (Hopkinton, U.S.) Turbovap sample concentrator.

Source rock bitumens were separated into seven lipid classes: Saturates, aromatics, acids, bases, low-, medium- and high-polarity nitrogen, sulphur and oxygen (NSO) compound fractions using the liquid chromatographic procedure (Fig. 3.1) described by Willsch *et al.* (1997). Briefly, the extracts were passed through silica gel, HCl treated and KOH treated silica gel to remove high-polarity NSO compounds, bases and acids respectively. Liquid chromatography of the eluting fraction on the main silica gel column separated the medium-polarity NSO compounds (containing alcohols and sterols) from the low-polarity fraction. The latter was then separated via medium pressure liquid chromatography (MPLC) on silica gel

(Radke *et al.*, 1980) into the saturates, aromatics and low-polarity NSO compounds (containing esters and ketones).

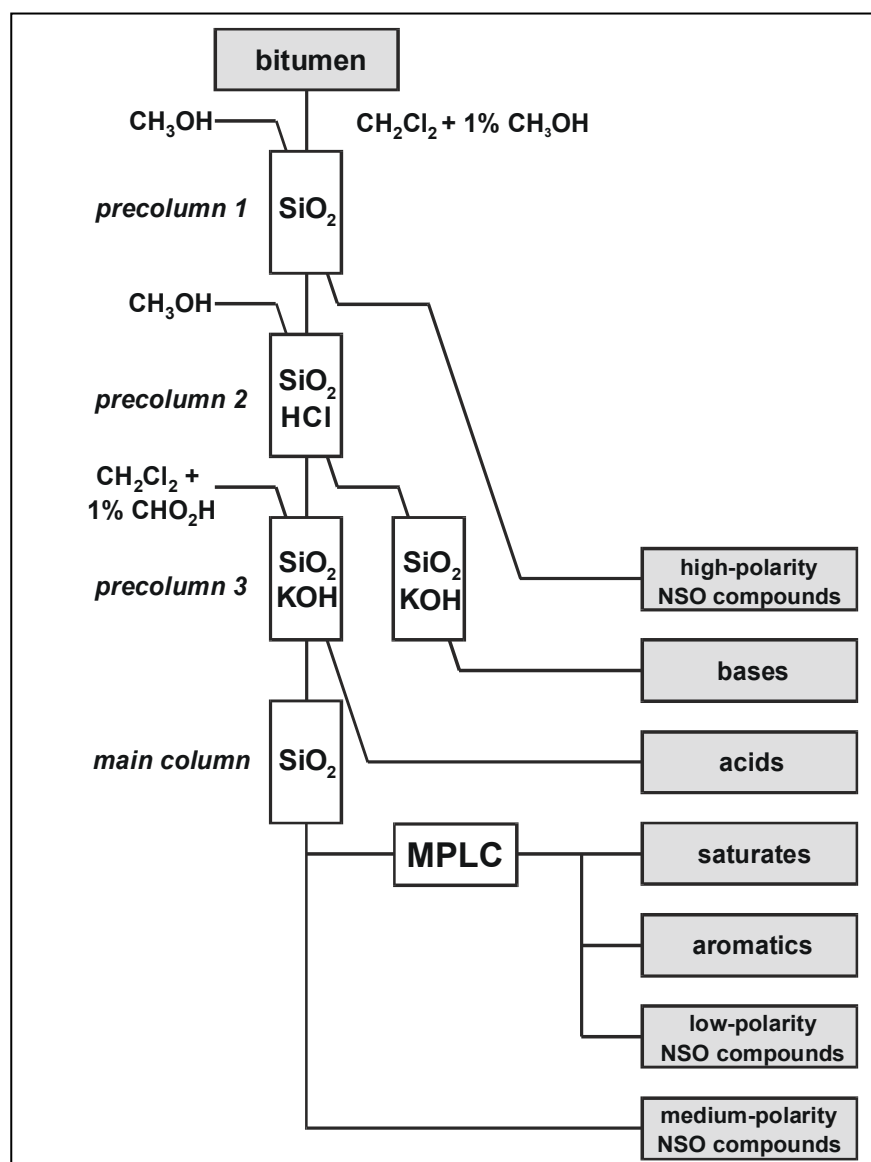


*Fig. 3.1. Schematic sketch of the liquid chromatographic separation; modified after Willsch *et al.* (1997).*

3.10 Gas chromatography (GC) and Gas Chromatography-Mass Spectrometry (GC-MS)

The **aliphatic fractions** were analysed on a HP 5890 Series II Gas Chromatograph, equipped with an on-column injector and a FID detector. The column was a HP Ultra-1, 50 m length, 0.2 mm i.d. with a methylpolysiloxane stationary phase of 0.33 μ m thickness (Hewlett Packard, U.S.). The temperature program for the aliphatic fractions started by on-column injection at 90°C (duration 2 min), followed by temperature programming at a rate of 4°C/min

to 310°C, where it was maintained for 63 min. Hydrogen was used as carrier gas with a pressure of 1.6 bar (1 ml/min) at starting temperature.

The analysis of **aromatic fractions** was performed on a HP 5890 Series II Gas Chromatograph, equipped with an on-column injector, a FID detector and a HALL Electrolytic Conductivity detector operated in the sulphur mode. The column used was 50 m in length, 0.22 mm i.d. with a 5% phenyl polysilphenylene-siloxane non-polar stationary phase (BPX-5) of 0.25 µm film thickness (SGE International Pty. Ltd., Australia). The temperature program used was as follows: Injection at 90°C (maintained for 2 min), then to 120°C at 50°C/min, hold for 1 min and finally at 3°C/min to 310°C, and kept for 52 min. For a better peak identification of the botryococenes in the aliphatic and aromatic fractions of Lake Huguang Maar bitumens the temperature program was changed. Injection at 90°C (maintained for 4 min), then to 120°C at 50°C/min, hold for 1 min at 120°C and finally at 4°C/min to 310°C and kept for 51 min. Helium (4.4 bar at starting temperature) was used as the carrier gas with a flow rate of 0.76 ml/min.

Fatty acids were subjected to a methylation procedure using diazomethane prior to analysis to produce fatty acid methyl esters. This analysis was performed using a HP 5890 Series II Gas Chromatograph, equipped with a temperature-programmable injection system KAS 3 (Gerstel, U.S.) and a FID detector. The column was a BPX-5, 50m length, 0.22 mm i.d. with 0.25 µm thickness (SGE International Pty. Ltd., Australia). The temperature program for the acid fractions started by injection at -40°C (maintained for 2 min), then heating at 12°C/s to 40°C and kept for 10 min. The oven temperature was then increased at 4°C/min to 310°C, where it was hold for 63 min.

GC-MS measurements were performed on a Finnigan MAT 95SQ mass spectrometer coupled to a Hewlett Packard 5890 B gas chromatograph. The GC was equipped with a temperature-programmable injection system (Gerstel KAS 3) and a BPX-5 fused silica capillary column of 50 m length, 0.22 mm i.d. and 0.25 µm film thickness. Helium was used as the carrier gas (EPC 1ml/min). The oven temperature was programmed from 60°C to 340°C (final hold time 23 min) at 3°C/min. In electron impact (EI) mode, the MS was operated at an electron energy of 70 eV and a source temperature of 260°C. EI mass spectra were recorded over the mass range of 50-600 Da at a scan rate of 0.7413 s/decade, an inter scan time of 0.2 s. and a scan cycle time of 1.0 s.

For the analysis of **biomarkers**, metastable ion transitions were recorded by the Metastable Reaction Monitoring mode (MRM) at a dwell time of 15 ms and a cycle time of 0.5 s. The parent → daughter ion transitions monitored were the following, for each structural family of compounds: steranes (C_{26} - C_{30} : m/z 356, 372, 386, 400, 414 → 217), methylsteranes (C_{27} - C_{31} : m/z 372, 386, 400, 414, 428 → 231), dinosteranes (C_{29} - C_{30} : m/z 400, 414 → 98), hopanoids (C_{27} - C_{35} : m/z 370, 384, 398, 412, 426, 440, 454, 468, 482 → 191) and oleanane+gammacerane (m/z 412 → 397, 369). The identification of carbazoles (m/z in EI-mode: 167, 181, 195, for carbazole, C_1 and C_2 carbazoles; m/z 217 for benzocarbazoles) and fluoren-9-ones (m/z in EI-mode: 180, 194, 208, for fluoren-9-one, C_1 and C_2 fluoren-9-ones; m/z 230 for benzofluoren-9-ones) was performed using GC-MS under EI conditions. The data obtained were processed with the ICIS-I software package (ThermoQuest Finnigan, Bremen).

Derivatisation of alcohols in the medium-polar NSO fraction was carried out using a 99:1 mixture of BSTFA (N,O-bistrifluoroacetamide) and TMCS (trimethylchlorosilane) at a temperature of 60°C over 30 min with a surplus of agent 10:1. Internal standards were added to the aliphatic (5α -androstande), aromatic (mixture of 1-phenylhexane, 1-phenylheptane, 1,8-dimethylnaphthalene, 1-phenylnaphthalene, 1-ethylpyrene and 1-butylpyrene), fatty acid (perdeuterated methyl stearate) and low-polarity NSO (9-phenylcarbazole) fraction for quantification.

4 Liaohe Basin, Peoples Republic of China

As stated in the section Goals and Approach, the Western Depression of the Liaohe Basin was investigated to relate source rock potential to depositional processes. The chapter begins with a detailed description of the regional geology. Sample selection is then documented, followed by the presentation of results.

4.1 Geological Background

4.1.1 Location and Morphology

The Liaohe Basin is the third largest oil province in China (Chen *et al.*, 1999) and is located in Liaoning Province, approx. 600 km NE of China's capital, Beijing. The provincial capital Shenyang lies at the north-eastern end of the basin (Fig. 4.1). The total basin spans ca. 450 km in length and 65 km in width. Morphologically, the area is a broad, flat alluvial basin, which is traversed by the Liao River ending into the Liaohe delta and the Bohai Sea. Two mountain ranges, the Yan-Shan Mountains, and the Jiao-Liao Mountains border the Liaohe Basin to the north-west and south-east, respectively.

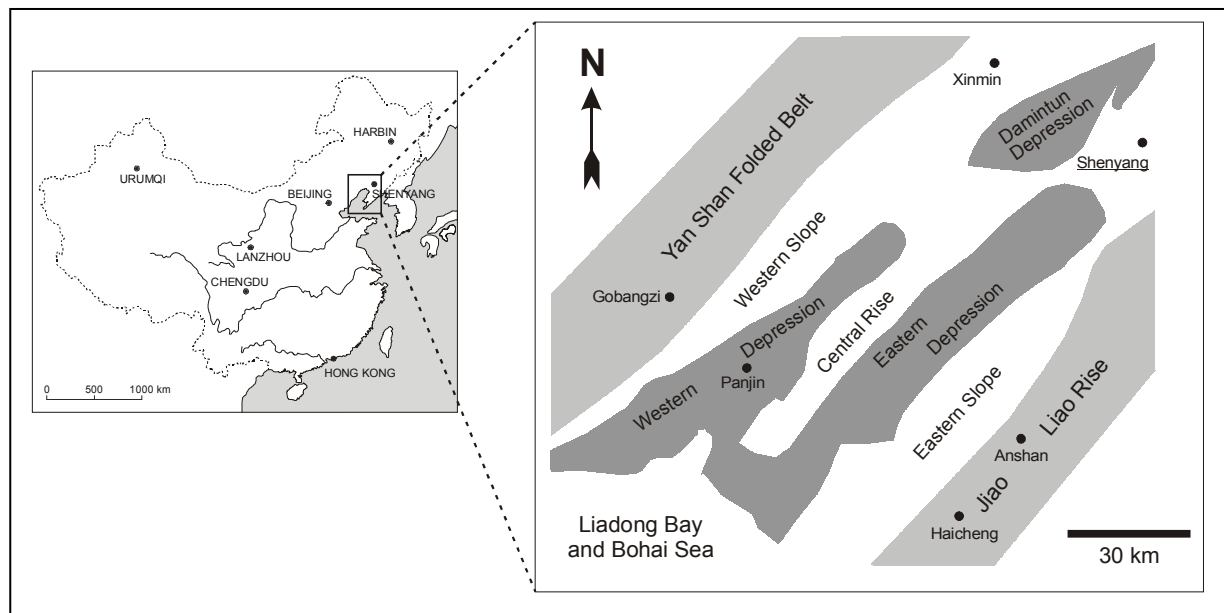


Fig. 4.1. Location and structural subdivision of the Liaohe Basin.

4.1.2 Tectonic Evolution

As a part of the Bohaiwan Basin the Liaohe Basin is a Meso-Cenozoic basin of fault-depression origin (Wang & Wang, 1988). The Bohaiwan Basin formed on the North China craton. The basement is composed of Achaean and Lower Proterozoic schists. Before the Mesozoic, this part of China was an area of east-west trending platforms, upon which marine sediments were deposited. The Bohaiwan Basin developed as a back-arc basin during the Mesozoic evolving into an intracratonic rift basin during the Cenozoic. Extensional stress along mantle uplift belts caused rifting and subsidence leading to the development of grabens and half-grabens along major NW- and NE-trending faults. During Palaeogene time the basin was divided into several fault-bounded depressions, which became one large basin during the Late Oligocene (Tian, 1990).

The Liaohe Basin is a wedge-shaped rift depression with a central horst situated between two NE trending grabens (Wang & Wang, 1988). It is bordered on the east by the Tan-Lu wrench fault zone and can be divided into several depressions, each of which contains several sub-basins or "sags" (Fig. 4.1). The Western Depression can be subdivided into four production areas (Liu, 1986; Tian, 1990) based on the structural position and the discovered accumulations of oil and gas (Fig. 4.2). The West Slope is a shallow area on the western side of the depression. The Slipping Zone connects the West Slope and the Central Depression. The latter is the deepest part of the depression with a sediment filling up to 6000 m and is characterised by the presence of major growth faults. It is separated from the East Rise by the eastern main fault. The Liaohe Basin is underlain by a Paleozoic carbonate platform

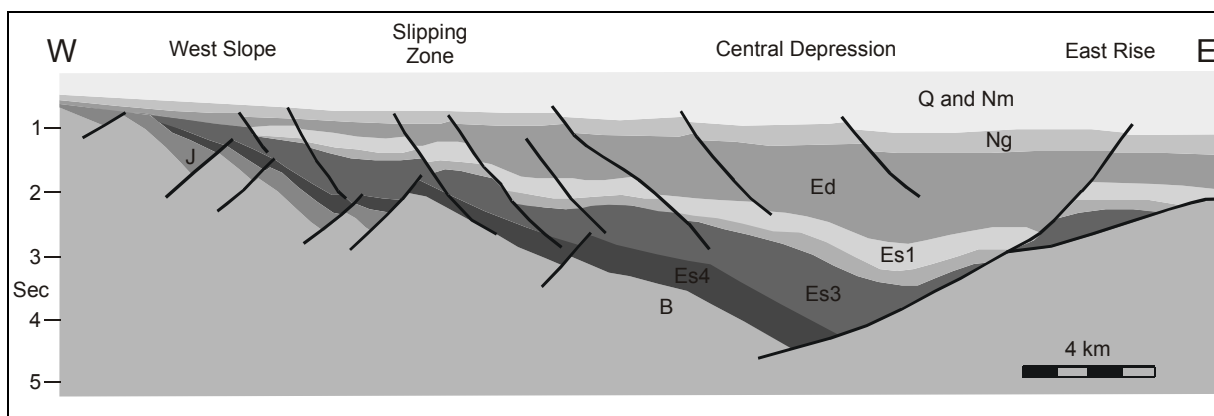


Fig. 4.2. Cross section showing the different structural and producing areas of the Western Depression; after Liu (1986) and Tian (1990). B, pre-Tertiary basement; J-Jurassic; Es-Shahejie Formation; Ed-Dongying Formation; Ng-Guantao Formation; Nm-Minghuazhen Formation; Q-Quaternary.

which is situated on Upper Proterozoic limestones and Achaean metamorphic rocks. It formed during three cycles of rifting and subsiding stages starting in the Lower Jurassic (Li, 1980). During a second cycle of rifting in Cretaceous time volcanic rocks and sediments were deposited in depressions with thicknesses of 2000 to 4360 m (Wang & Wang, 1988). The third and most important cycle of rifting was related to significant changes in the tectonic regime of the West Pacific area. At the end of the Mesozoic, extending into the early Tertiary the Kula-Pacific plate was subducted underneath the Asian margin (Uyeda & Miyashiro, 1974; Hilde *et al.*, 1977). This caused the appearance of an extensional stress field and finally formed the present morphology of the Liaohe Basin. Crustal thinning during rift development led to mantle uplift and in consequence to high heat flows. Additionally, magma and hydrothermal fluids were brought to the surface along faults or fracture zones. In the study area the *Moho* is located at approx. 30 to 38 km depth which was shown in several studies (Li, 1980; Tang, 1982; Wang & Wang, 1988).

During the Tertiary, three major tectonic phases took place (Fig. 4.3). First, the extension and rifting continued during deposition of the Es4 formation. This was followed by cooling and a rapid subsidence during early Es3 time and the development of extensional grabens and growth faults during late Es3 time. Very large offsets of these growth faults caused differences in sedimentation between basin margin and centre. Finally, a renewed rifting with reorientation of the stress field in Es2, Es1 and Ed time produced minor faulting in E-W direction. At the end of the Oligocene the direction of motion of the Pacific Plate changed, which led to a compressional stress field and the termination of the rift development stage in the Liaohe Basin (Wang & Wang, 1988).

4.1.3 General Stratigraphy of the Western Depression

The Western Depression accumulated lacustrine sediments from the early Tertiary. The Eocene Shahejie Formation (Es) is the main source of hydrocarbons in the Liaohe Basin (Chen *et al.*, 1999). Based on lithology and fossil assemblages it can be subdivided into four members (Es4, Es3, Es2, and Es1). The Es4 member is of prime importance in this study. The geological informations given in this section rely strongly on unpublished data from PetroChina and personal communications from Liguó Hu (also PetroChina).

The thickness of the Es4 member varies depending on the basin location. It is high in the northern TUO area (716 m in well TUO 16) compared to approx. 180 m in the Gao and Shu-Du area. The reason for this difference is higher clastic sedimentation rates during

Es4 time in the northern part of the depression. The Es4 member was the beginning of a transgressive cycle. In the south shales and sandstones were deposited in shallow lakes, whereas in the north oil shales, calcareous shales and sandstones were laid down in restricted lakes that are more saline. The Es4 is underlain by the volcanic rocks of the Fangshenpao Formation in the northern part of the depression. In the southern part the equivalent rocks comprise dark mudstones with intercalated coarse sandstones.

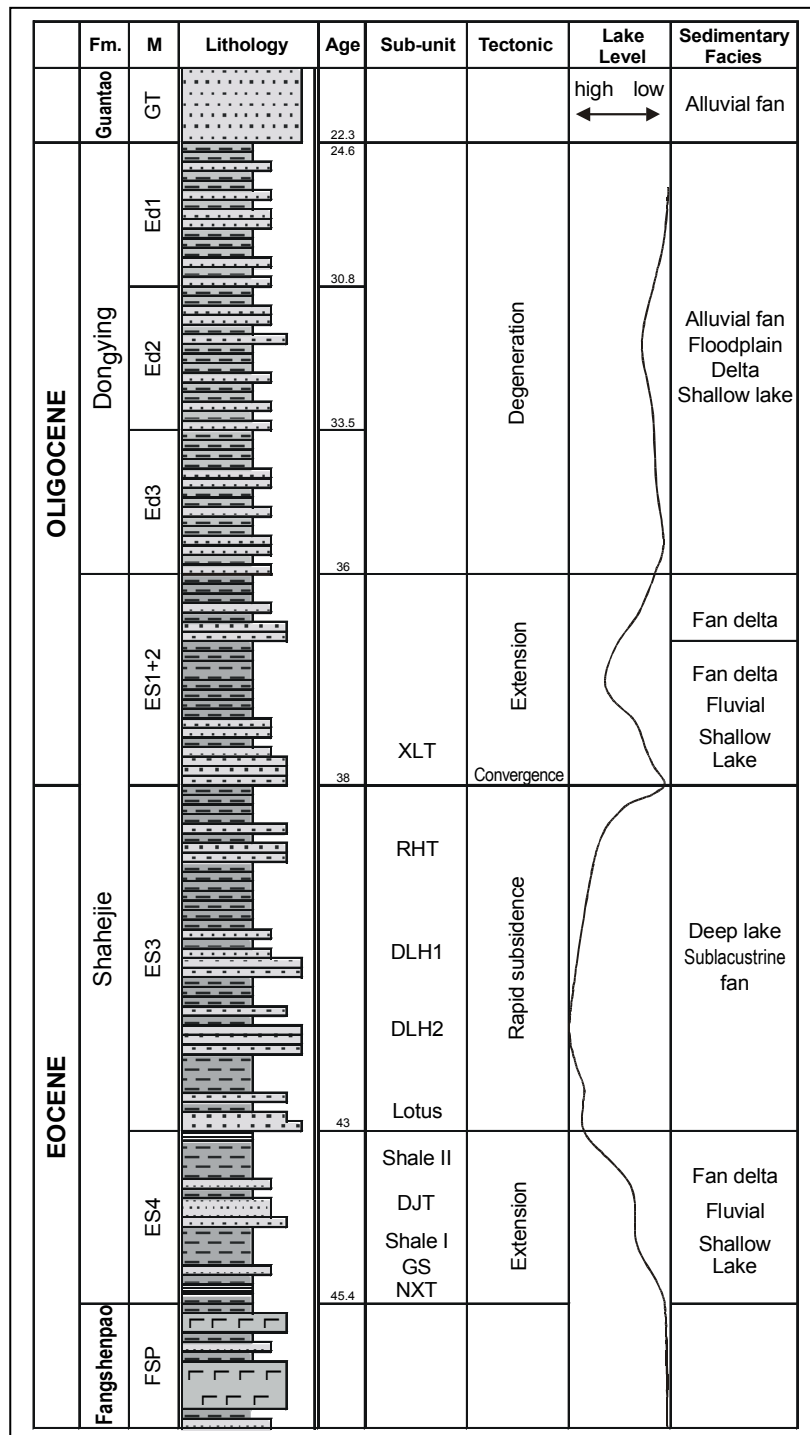


Fig. 4.3. Generalised stratigraphic column showing lithology, tectonic history, lake level and environment of the study area (PetroChina, unpublished).

Five major sub-units of the **ES4 member** can be distinguished (Fig. 4.3). **(1)** The Niuxintuo (NXT) sub-unit is mainly present the Tuo area, **(2)** the Gaosheng (GS) consists of dolomites, shaly dolomites, carbonates and few evaporites, **(3)** the Shale I represents an almost pure shale unit in the Shu-Du area. In the Lei area also some dolomitic shales are present, **(4)** the Dujiatai (DJT) contains abundant dolomites, especially in the Lei and Gao area; **(5)** the Shale II sub-unit consists of shales or dolomitic shales.

Subsidence and sedimentation started during early Es4 time (NXT sub-unit) in the Tuo area, where the first lakes formed in the Western Depression. It is the main source bed in this area. The Shale I sub-unit with abundant fine clastic sediments provide a good seal. This part of the basin received high amounts of clastic during this early phase of sedimentation. Therefore, some sub-units (e.g. DJT) are characterised by the presence of thick sandstone layers. The depocenter shifted from north to south and was located south of the Shu-Du area during early Es3 time. Sedimentary rocks in the Lei and Gao area were deposited in a restricted basin with no significant clastic input. Abundant dolomites and other carbonate rocks in both areas reflect a dominant chemical precipitation and sedimentation. The Gao area is located in a more marginal position, whereas the Lei area is in the centre of the basin. Some red shales and sandstones, older than the GS sub-unit, represent an equivalent to the NXT sub-unit of the Tuo area. In the Shu-Du area abundant siliciclastic rocks were deposited during DJT time. This point to the presence of a marginal basin environment with high clastic input from the surrounding mountain areas. Sandstones which act as important reservoirs, representing a fan-delta depositional environment. Today, they are the most productive beds in the Liaohe Basin. During Es4 time coarse sediments were sourced from the western uplift and carried mainly by rivers into the lakes.

The **Es3 member** is less than 500 m thick at the basin margin and more than 2000 m in the centre. A transgressive event which started in late Es4 time continued in the lower part of the Es3 member followed by a regression in the upper part. The lake depth and size increased notably to approx. 80% of the sag area (Chang, 1991). Shales and oil shales are abundant in the lower part of the section which were deposited in a deep-lake environment of the rift (Yan, 1990). They act as an important regional seal. The other members consist of mudstones intercalated with sandy conglomerates and feldspathic sandstones. The Lotus, the Dalinghe (DLH) and the Rehetai (RHT) sub-units represent important carrier beds and were deposited in a sub-lacustrine fan environment (Yan, 1990).

Sedimentation during **Es1+2 time** started with the deposition of the Xinglongtai (XLT) sandstone which is an important carrier and reservoir rock. Sedimentation was restricted to the centre of the basin. The lake area was reduced and accounted only for 10 to 20% of the sag area (Chang, 1991). The surrounding areas were eroded, and fluvial clastic sediments were deposited. Thickness can reach up to 450 m (Yan, 1990). During early Es1 time, shales were laid down at the culmination of a transgressive lake phase. Their deposition during a marine incursion was proposed by Chen *et al.* (1998). They serve as an important regional seal. During a regression in the upper part of the Es1 member coarse grained sediments were transported into the basin. The maximum thickness of the Es1 member is 440 m (Yan, 1990).

Due to the subsidence of the central rise during deposition of the **Dongying (Ed) Formation** the Eastern and Western Depression merged and sedimentation became more uniform in the whole basin. Sandstones, siltstones and shales were deposited in a shallow water environment. In the upper part (Ed1) some carbonaceous floodplain shales are present. The thickness can reach 1095 m (Yan, 1990). At the end of Dongying time the whole area was uplifted and erosion cut into the Oligocene and Eocene sediments.

Sedimentation started again in the Miocene with the deposition of the Guantao Formation, (Ng) followed by the Minghuazhen (Nm) and the Quaternary Pingyuan Formation (Qp). This sequence consists of coarse clastics of alluvial fan and fluvial origin, unconformable overlying the Palaeogene strata. The sedimentary facies evolves from a fluvial dominated system with small, shallow lakes to a permanent deep lake, and finally back to a fluvial dominated system.

One of the most notable features of the Liaohe rift basin is the **volcanic activity** which occurred in multiple phases during the Tertiary (Chen *et al.*, 1999). The first episode of magmatism took place during the pre-rift stage in the early Paleogene and extended from Fangshenpao time to the deposition of the early stage of the Es4 member. The section consists of nearly 1000 m of tholeiitic basalt. The second main eruption occurred during Es3 time followed by magmatic events in the middle and late Paleogene and in the early Neogene. This magmatism was accompanied with an outflow of alkali basalts and a strong tectonic activity along NE-SW trended faults. In the areas where volcanic rocks occur, the geothermal gradient had been increased significantly. Chen *et al.* (1999) reported a rise from an average gradient of 3.5°C/100 m up to 4.25°C/100 m. It was suggested that this high geothermal flow accelerated the maturation of OM and thus hydrocarbon generation from source rocks in the Eastern Depression of the Liaohe Basin (Sun *et al.*, 1995). Volcanic eruptions may have influenced the environment of the biological communities living in the

lake by promoting biomass production *via* nutrient supply, terminating life by input of toxic substances or changing the alkalinity. A drastic shift towards high pH conditions may support the use of HCO_3^- by organisms, because the amount of dissolved CO_2 available for photosynthesis is limited where the pH exceeds 8.7 (Talbot & Allen, 1996). Furthermore, floating ash layers on the water surface may restrict photosynthesis (Schwark *et al.*, 1996). The alkaline composition of lake waters in volcanic regions may also affect the mineralogy. For example, the assemblage of minerals in volcanic lakes include authigenic growth of various types of zeolites which result from the reaction of unstable volcanic glass in tuffs with interstitial waters (e.g. Surdam & Sheppard, 1978).

4.1.4 Hydrocarbon Sources, Accumulations and Trap Styles

The Western Depression is a typical half-graben shaped depression, where **petroleum migration** occurred westward and eastward from the Central Depression to the West Slope and East Rise, respectively. The most significant accumulation zone is the West Slope, where the Huanxiling and the Shuguang oilfield (Shu-Du area) are located. The Es4 and Es3 members of the Shahejie Formation are the main **hydrocarbon sources** (Chen *et al.*, 1999). While the Es4 is recognised as a co-source of petroleum in the south, the overlying Es3 member is considered the main source in this area. The northern part of the Western Depression is a region where heavy, so-called “immature oils” form a large part of the total reserves. They are thought to have been generated during late diagenesis of shallow water saline Es4 rocks and migrated into neighbouring reservoirs before exposure to further thermal cracking. The immaturity of these oils was suggested by their biomarker composition (Huang *et al.*, 1990; Huang, 1999).

Major **reservoir rocks** are sandstones in the Es4 and Es3 members (e.g. DJT sandstones), fractured dolomites and oolitic limestones as well as basement rock buried hill oil fields. Major regional seals are the thick shale layers of the Shahejie Formation. Volcanic rocks acted as caps for the Shuguang buried-hill pool in the Western Depression (Sun *et al.*, 1995). The term buried-hill refers to pre-Tertiary basement rocks which have undergone weathering and erosion for at least several hundreds of million years. These processes resulted in the development of an eroded surface and thence created secondary pores and fissures. The main reservoir of the Shuguang buried hill oilfield is a dolomite of Middle Proterozoic age but accumulations were also found in weathered granites of Achaean age. The top of the buried hill is directly overlain by the source rocks of the Es3 and Es4 member (Zheng, 1988). As a typical fault block oil field vertical migration distances are short in the Liaohe Basin

(Tang, 1982). Lithological variation and fault development facilitated good vertical and poor horizontal migration. According to statistical data the distance of horizontal migration in the Bohaiwan Basin is usually about 10 km (Chang, 1991).

4.2 Sample Selection

The Liaohe source rock samples originate from 24 exploration wells situated in the Western Depression. The main producing areas and the location of the investigated wells are illustrated in Fig. 4.4. Beside rock samples, well logs and assorted other geological information were made available by PetroChina, formerly the Liaohe Petroleum Exploration Bureau (LPEB). Only core samples, not cuttings were utilised. Altogether 90 source rocks were collected and analysed for TOC, TS and Rock-Eval parameters. Most of the samples are from the Es4 member, 14 are located in the Es3 member.

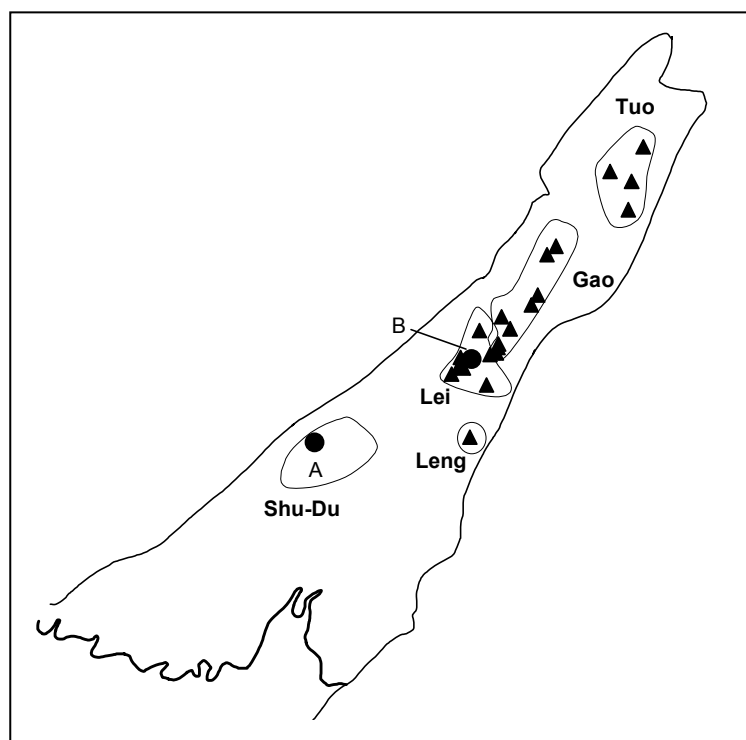


Fig. 4.4. Sketch map of the Western Depression with location of the studied wells and major producing areas. Key wells A & B are indicated.

Although always a lacustrine environment, the Shahejie Formation was deposited under highly variable conditions of salinity, and alkalinity (e.g. Yan, 1990). Thus, samples were selected to cover a broad spectrum of different lithofacies from different locations within the basin. Especially samples with dark lithologies were collected which contain sufficient OM for organic geochemical analyses. However, the rock sampling was mainly biased towards areas and wells where core sections were longest to study stratigraphic variations.

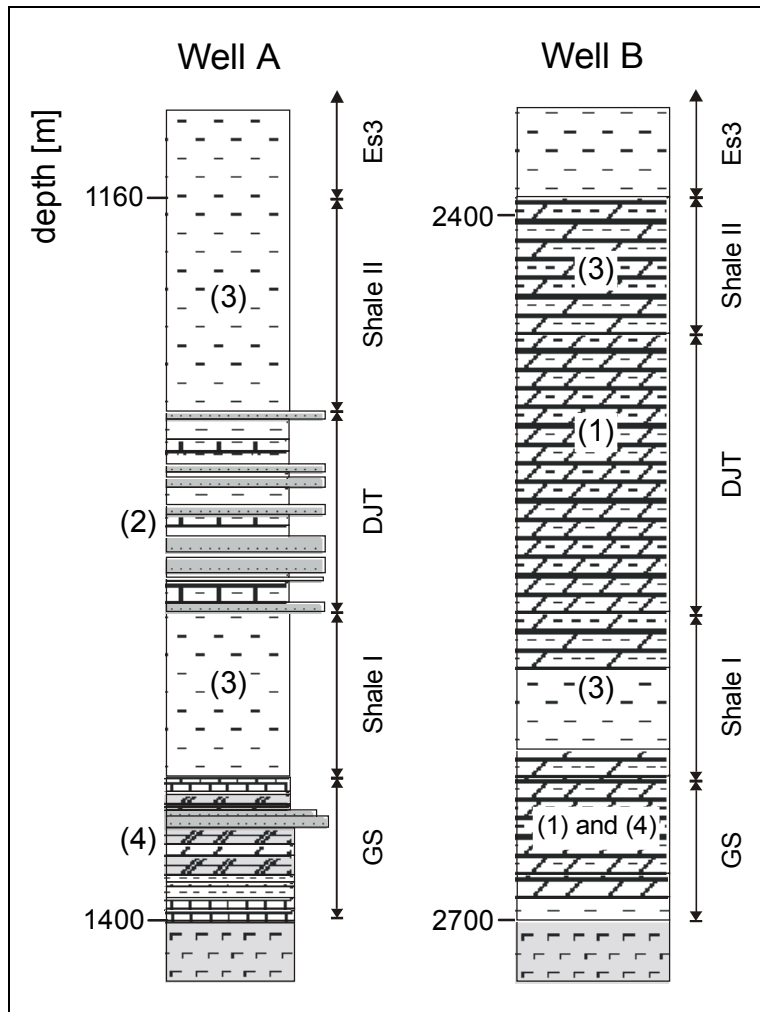


Fig. 4.5. Lithology and related lithostratigraphic subdivision of two representative key wells in the Western Depression. Well A is located in the Shu-Du area, well B in the Lei area (see Fig. 4.4). Numbers in brackets indicate the different lithofacies as presented in the text. The depth of the collected samples is given in Tab. 4.1.

In this regard, the investigations focus on the Shu-Du and the Lei area. Long sections were available from well A (Shu-Du area) where 23 samples are located within a 153 m depth interval. This well is situated in a marginal basin position in the West Slope (Fig. 4.1 and 4.2). Well B (14 samples) is the longest profile in the Lei area. Compared to Shu-Du the source rocks in the Lei area were buried deeper and closer to the depositional centre in the Western Depression. Both wells are also important because the sediment sequences were not influenced by major tectonic movements. The stratigraphy and lithology of the samples from these two key wells is presented in Fig. 4.5. The sample set is representative of the different lithofacies encountered in the studied cores whereby significant differences between the two areas exist (Fig. 4.5): (1) Massive fine to medium grained dolomites and shaly dolomites (Lei area), (2) mainly beds of massive Lei medium to coarse feldspathic sandstones and few conglomerates (DJT, Shu-Du), (3) massive beds of shales or dolomitic shales and grey or dark grey mudstones (4) laminated oil shales, calcareous shales with few carbonates (GS). The lithostratigraphic subdivision of the Es4 member as presented in Fig. 4.5 is based on these varying lithologies. In contrast, only very few samples are available from the Tuo, Leng

and Gao area, meaning that they are not necessarily typical of the stratigraphic column. A detailed listing showing depth, stratigraphy, area of the samples and analyses performed is given in Tab. 4.1.

E.nr.	Analyses	Well	Area	Fm.	Sub-unit	Depth [m]	E.nr.	Analyses	Well	Area	Fm.	Sub-unit	Depth [m]
48448		D	Lei	Es4	DJT	2571	48493		K	Gao	Es3	?	1600
48449	OP	D	Lei	Es4	DJT	2579	48494	OP,MK,EC	K	Gao	Es3	?	1455
48450		D	Lei	Es4	DJT	2589	48495		K	Gao	Es3	?	1550
48451	M	D	Lei	Es4	DJT	2591	48496		V	Gao	Es3	?	1757
48452	M	D	Lei	Es4	DJT	2594	48497	OP	U	Gao	Es3	?	1882
48453	M	D	Lei	Es4	DJT	2595	48498	M	H	Lei	Es4	?	2722
48454		D	Lei	Es4	DJT	2610	48499		F	Lei	Es3	?	2060
48455	M,OP,EC	D	Lei	Es4	DJT	2638	48500		F	Lei	Es4	?	2414
48456		B	Lei	Es3	?	1932	48501	M	I	Lei	Es4	?	2186
48457		B	Lei	Es3	?	1933	48502	M,OP,MK,EC	L	Gao	Es4	?	1357
48458		B	Lei	Es3	?	1933	48503		L	Gao	Es4	?	2533
48459	M	B	Lei	Es4	Shale II	2424	48504	M	P	Shu-Du	Es4	?	2116
48460		B	Lei	Es4	Shale II	2426	48505	M,OP,MK,EC	N	Gao	Es4	GS	1847
48461		B	Lei	Es4	Shale II	2431	48506	M,OP	N	Gao	Es4	?	2301
48462	M	B	Lei	Es4	Shale II	2446	48507	M	N	Gao	Es4	?	2512
48463	M,OP,EC	B	Lei	Es4	DJT	2512	48508		W	Lei	Es3	?	2248
48464	M,OP,EC	B	Lei	Es4	DJT	2524	48509	M	T	Tuo	Es4	?	2570
48465	M,OP,MK,EC	B	Lei	Es4	DJT	2526	48511	M	R	Tuo	Es4	?	1818
48466	M,OP,EC	B	Lei	Es4	DJT	2580	48512		S	Tuo	Es4	?	2209
48467	M,OP,MK,EC	B	Lei	Es4	GS	2688	48513	M	S	Tuo	Es4	NXT	2490
48468		B	Lei	Es4	GS	2692	48514	M,OP,MK,EC	S	Tuo	Es4	GS	2312
48469	M	B	Lei	Es4	DJT	2580	48515	M	Q	Tuo	Es4	?	1160
48470		J	Gao	Es4	Shale I	1462	48517	M,OP,MK,EC	A	Shu-Du	Es4	DJT	1252
48471		J	Gao	Es4	Shale I	1476	48518	M	A	Shu-Du	Es4	DJT	1288
48472		J	Gao	Es4	Shale I	1481	48519	M,OP,MK,EC	A	Shu-Du	Es4	Shale I	1306
48473	M	J	Gao	Es4	Shale I	1488	48520	M,OP,MK,EC	A	Shu-Du	Es4	Shale I	1309
48474		J	Gao	Es4	Shale I	1490	48521	OP	A	Shu-Du	Es4	Shale I	1314
48475	M,OP,EC	J	Gao	Es4	Shale I	1492	48522	M,OP	A	Shu-Du	Es4	Shale I	1318
48476		J	Gao	Es4	Shale I	1498	48523	OP	A	Shu-Du	Es4	Shale I	1322
48477		O	Leng	Es3	?	2471	48524		A	Shu-Du	Es4	Shale I	1325
48478		O	Leng	Es3	?	2555	48525	M,OP,MK,EC	A	Shu-Du	Es4	Shale I	1329
48479	M,OP	O	Leng	Es3	?	2556	48526	OP	A	Shu-Du	Es4	Shale I	1333
48480	M,OP,MK,EC	E	Lei	Es4	DJT	2735	48527	M,OP,MK,EC	A	Shu-Du	Es4	Shale I	1340
48481	M,OP,EC	E	Lei	Es4	DJT	2796	48528	OP	A	Shu-Du	Es4	GS	1346
48482	M,OP,EC	E	Lei	Es4	DJT	2792	48529	M,OP,MK,EC	A	Shu-Du	Es4	GS	1346
48483		C	Lei	Es4	DJT	2332	48530	OP	A	Shu-Du	Es4	GS	1347
48484	M,OP,EC	C	Lei	Es4	DJT	2335	48531	OP	A	Shu-Du	Es4	GS	1348
48485	M,OP,MK,EC	C	Lei	Es4	DJT	2342	48532	M,OP,MK,EC	A	Shu-Du	Es4	GS	1348
48486	M	C	Lei	Es4	DJT	2360	48533	OP	A	Shu-Du	Es4	GS	1351
48487	M,OP	C	Lei	Es4	DJT	2385	48534	OP	A	Shu-Du	Es4	GS	1358
48488	M	C	Lei	Es4	DJT	2392	48535	OP	A	Shu-Du	Es4	GS	1359
48489		C	Lei	Es4	DJT	2396	48536		A	Shu-Du	Es4	GS	1372
48490		G	Lei	Es3	?	2165	48537	M,OP,MK,EC	A	Shu-Du	Es4	GS	1375
48491	OP	G	Lei	Es4	?	2665	48538		A	Shu-Du	Es4	basement	1394
48492	M	G	Lei	Es4	?	2818	48539	M	A	Shu-Du	Es4	basement	1405

Tab. 4.1. Sample set for the Liaohe project. Fm., Formation; M, Mineralogy; OP, Organic Petrology; MK, kerogen concentrate; EC, extraction and bitumen analysis.

4.3 Mineralogy

The goal of this section is to characterise the lacustrine source rock sequences in the Western Depression laterally and vertically in terms of their mineral assemblages and to elucidate the conditions under which certain minerals have formed in the paleolacustrine sediments. However, the mineralogy does not reflect certain paleoenvironmental conditions alone. Diagenesis can also cause significant alterations, such as illitisation and chloritisation of smectite and kaolinite as reviewed by Morad *et al.* (2000). As stated in section 4.1.3, volcanic activity may control authigenic mineral formation, and interestingly, an important episode of magmatism was reported from some parts of the Western Depression during Es4 time (Chen *et al.*, 1999).

4.3.1 Bulk Mineralogical Composition

Tab. 4.2 lists the bulk mineralogy of rock samples from the investigated areas as determined by XRD analysis. The detailed mineralogical composition is given in Appx. A. Altogether 49 samples covering all stratigraphic units and producing areas were selected. However, the investigations focused mainly on the Shu-Du and Lei area. Samples from the Gao, Leng and Tuo area are underrepresented.

The bulk mineralogy of the Es4 source rocks is characterised by highly variable proportions of the mineral groups clay, detrital (quartz and feldspars) and carbonates (Tab. 4.2). It is defined here that sandstones contain more than 60% quartz and feldspar. Shales are fine-grained and contain not more than 60% quartz and feldspars. Carbonate rich shales are rocks containing more than 50% carbonate minerals. In wells from the centre of the basin (Lei wells) higher percentages of carbonate minerals were observed. Shales from the Es3, Shale I and Shale II generally contain high percentages of clay and low percentages of carbonate minerals. Samples from the DJT sub-unit have generally more detrital minerals than those from the GS sub-unit.

E. nr.	Depth [m]	Well	Area	Member	Sub-unit	Clay Minerals [%]	Detrital Minerals [%]	Carbonates [%]	Carbonate Facies
48479	2556	O	Leng	Es3	?	41.8	42.6	9.8	Rhodochrosite
48494	1455	K	Gao	Es3	?	47.5	33.3	12.4	Calcite
48499	2060	F	Lei	Es3	?	40.2	49.4	9.1	Siderite
48451	2591	D	Lei	Es4	DJT	29.4	46.5	20.5	Siderite
48452	2594	D	Lei	Es4	DJT	28.2	34.5	35.0	Arag./Sid.
48453	2595	D	Lei	Es4	DJT	37.8	48.5	12.1	Siderite
48455	2638	D	Lei	Es4	DJT	4.8	36.3	36.7	Kutnahorite
48459	2424	B	Lei	Es4	Shale II	37.8	56.4	2.8	Low-Carbonate
48462	2446	B	Lei	Es4	Shale II	35.8	48.9	8.0	Low-Carbonate
48463	2512	B	Lei	Es4	DJT	27.6	44.4	26.4	Siderite
48464	2524	B	Lei	Es4	DJT	32.4	35.7	29.3	Aragonite
48465	2526	B	Lei	Es4	DJT	27.1	29.2	39.6	Dolomite
48466	2580	B	Lei	Es4	DJT	2.4	19.5	52.8	Dol./Sid.
48467	2688	B	Lei	Es4	GS	9.0	36.7	51.4	Kut./Dol./Calc.
48469	2580	B	Lei	Es4	DJT	2.0	66.5	30.3	Dolomite
48473	1488	J	Gao	Es4	Shale I	64.0	33.4	0.6	Low-Carbonate
48475	1492	J	Gao	Es4	Shale I	45.5	20.4	33.4	Kutnahorite
48480	2735	E	Lei	Es4	Shale II	32.0	44.5	17.9	Calcite
48481	2796	E	Lei	Es4	DJT	22.3	46.3	28.2	Calcite/Dol.
48482	2792	E	Lei	Es4	DJT	20.2	44.3	34.0	Kutnahorite
48484	2335	C	Lei	Es4	DJT	15.5	72.4	10.3	Calc./Sid./Arag.
48485	2342	C	Lei	Es4	DJT	16.3	33.3	43.9	Aragonite
48486	2360	C	Lei	Es4	DJT	27.6	28.1	37.0	Aragonite
48487	2385	C	Lei	Es4	DJT	8.2	21.0	44.9	Dolomite
48488	2392	C	Lei	Es4	DJT	38.0	27.2	14.3	Siderite
48492	2818	G	Lei	Es4	?	26.7	31.6	36.4	Kutnahorite
48498	2722	H	Lei	Es4	?	29.9	25.8	40.5	Kutnahorite
48501	2186	I	Lei	Es4	?	9.2	33.2	34.2	Dol./Sid.
48502	1357	L	Gao	Es4	?	59.0	31.8	0.6	Low-Carbonate
48504	2116	P	Shu-Du	Es4	?	24.8	42.9	30.7	Dolomite
48505	1847	M	Gao	Es4	GS	35.7	16.7	46.4	Aragonite
48506	2301	N	Gao	Es4	?	41.1	25.5	31.8	Aragonite
48507	2512	N	Gao	Es4	?	24.3	31.3	43.6	Dol./Calc.
48509	2570	T	Tuo	Es4	?	52.7	44.3	2.4	Low-Carbonate
48511	1818	R	Tuo	Es4	?	28.7	26.5	15.8	Dolomite
48513	2490	S	Tuo	Es4	NXT	24.2	33.6	23.7	Dolomite
48514	2312	S	Tuo	Es4	GS	61.8	32.8	3.3	Low-Carbonate
48515	1160	Q	Tuo	Es4	?	54.7	43.1	2.2	Low-Carbonate
48517	1252	A	Shu-Du	Es4	DJT	15.5	72.4	10.3	Dolomite
48518	1288	A	Shu-Du	Es4	DJT	3.6	93.3	3.1	Low-Carbonate
48519	1306	A	Shu-Du	Es4	Shale I	49.0	25.7	23.1	Siderite
48520	1309	A	Shu-Du	Es4	Shale I	53.9	22.4	15.7	Siderite
48522	1318	A	Shu-Du	Es4	Shale I	63.7	29.9	0.0	Low-Carbonate
48525	1329	A	Shu-Du	Es4	Shale I	61.4	21.1	1.3	Low-Carbonate
48527	1340	A	Shu-Du	Es4	Shale I	18.6	19.3	1.1	Low-Carbonate
48529	1346	A	Shu-Du	Es4	GS	21.9	17.5	59.7	Kutnahorite
48532	1348	A	Shu-Du	Es4	GS	30.1	28.3	37.2	Calcite
48537	1375	A	Shu-Du	Es4	GS	43.8	30.5	21.5	Calcite
48539	1405	A	Shu-Du	Es4	basement	43.5	33.7	18.8	Calcite

Tab. 4.2. Bulk mineralogy and carbonate facies of samples from the Liaohe Basin determined by XRD analysis. Detrital minerals are quartz and feldspars.

4.3.2 Mineralogical Results of Selected Wells

Mineralogical variations in the two key wells A and B provide important insights into the depositional environment of the Shu-Du and Lei area, respectively. The mineral composition is very unusual. Many samples contain the rare minerals kutnahorite (manganese carbonate) and buddingtonite (ammonium feldspar). Their occurrence and possible origin is discussed in detail in the next paragraphs.

The mineralogy and stratigraphic subdivision of well A (Shu-Du area) is illustrated in Fig. 4.6. This well contains a large number of samples with more than 40% expandable clays, with highest proportions of 54.1% in the Shale I sub-unit. The percentage of illite & mica is also high in the Shale I sub-unit but reaches a maximum with 10.4% at 1375 m (E 48537). Chlorite & kaolinite range between 0 and 2.5% with maximum percentages within the Shale I sub-unit (E 48520, E 48522). No chlorite & kaolinite was detected in the GS. The amount of quartz ranges between 0.5 and 58.1%, with highest percentages in two selected sandstone samples from the DJT sub-unit. Highest plagioclase proportions (33.2%) were found in the deepest sample (E 48439) closed to the volcanic rocks of the Fangshenpao member, which

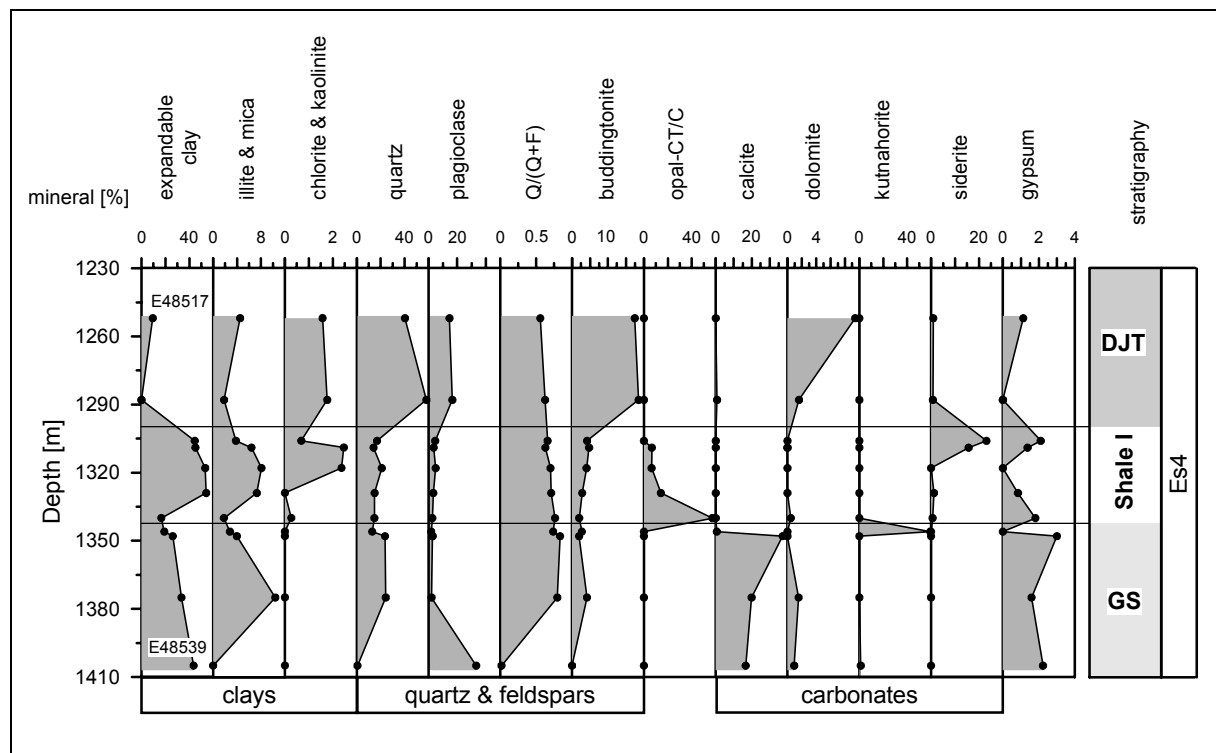


Fig. 4.6. Detailed mineralogy of the Es4 member in well A (Shu-Du area).

are underlying the lacustrine sequence. This sandstone contains abundant calcic plagioclase as well as analcime and shows a very low quartz-feldspar ratio ($Q/(Q+F)$). With the exception of the deepest sample this ratio gradually decreases during progressive sedimentation (Fig. 4.6). Buddingtonite percentages are generally low in the GS- and Shale I sub-unit but a sharp increase to the sandstone samples of the DJT (18.5%) was observed. As another variety of silica present in the Liaohe rocks opal-CT and C was found. This mineral is especially abundant in sample E 48527 from 1340 m depth (57.1%). The GS sub-unit is rich in carbonate minerals, whereas lower proportions were observed in the Shale I and DJT. Significant proportions of calcite are only present in the GS sub-unit with a maximum of 37.2% in sample E 48432. Dolomite is of minor importance in the GS but its proportions are high in the DJT (9.4%; E 48517). Sample E 48529 contains the calcium-magnesium-manganese carbonate mineral, kutnahorite, in high percentages (59.1%). Siderite is relative abundant in the samples E 48519 and E 48520 from the Shale I sub-unit. Gypsum is present in the laminated samples of the GS sub-unit with highest percentages in sample E 48537 with 2.6%. Aragonite, amphibole and natrojarosite were not detected in well A.

The mineralogical data for well B (Lei area) are presented in Fig. 4.7. The percentage of expandable clays ranges between 0 and 26.3% and is especially high in the Shale II and in the upper DJT sub-unit. Illite & mica and kaolinite & chlorite show maximum percentages of 7.9 and 6.9%, respectively within the Shale II sub-unit. Quartz proportions maximise in sample E 48462 from the Shale II sub-unit (39.3%). Generally, the Shale II and upper DJT

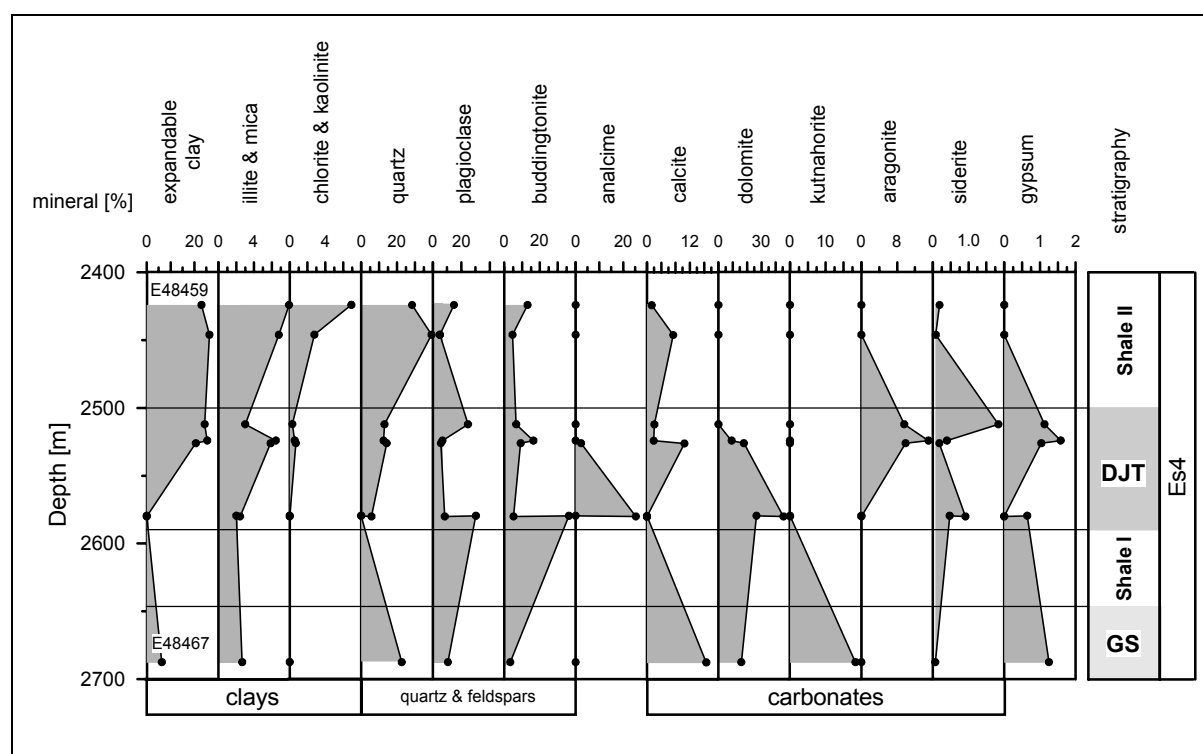


Fig. 4.7. Detailed mineralogy of the Es4 member in well B (Lei area).

sub-units are rich in clays and quartz. For example, sample E 48459 from the DJT consists of quartz, feldspars and clays whereas almost no carbonate minerals were detected.

In contrast, the feldspars plagioclase and buddingtonite are relatively abundant in the lower DJT sub-unit. This was also observed for analcime, which was determined in high amounts in sample E 48466 (25.3%). Notably, almost no expandable clay was detected in this sample, but high percentages of dolomite were found. Dolomite percentages are high in well B especially in the DJT sub-unit with a maximum of 45.5% (E 48466). Aragonite, calcite, gypsum and kutnahorite have highest percentages of 15.0% (E 48464), 16.6% (E 48467), 1.8% (E 48467) and 18.3% (E 48467), respectively. In all samples, except the two shallowest, dolomite is more abundant than calcite. Interestingly, aragonite percentages are high in the upper DJT section. Kutnahorite is only present in the GS sub-unit. Gypsum and siderite show a maximum in the upper part of the DJT sub-unit.

4.3.3 Occurrence and Origin of Minerals

4.3.3.1 Carbonates

A complex association of carbonate minerals is present in the Liaohe rocks. Calcium, magnesium, manganese and iron carbonates are major constituents. All rocks can be subdivided into seven carbonate facies types (Fig. 4.8). Additionally, a **low-carbonate** facies group was specified for samples with a general low carbonate content of maximal 8%.

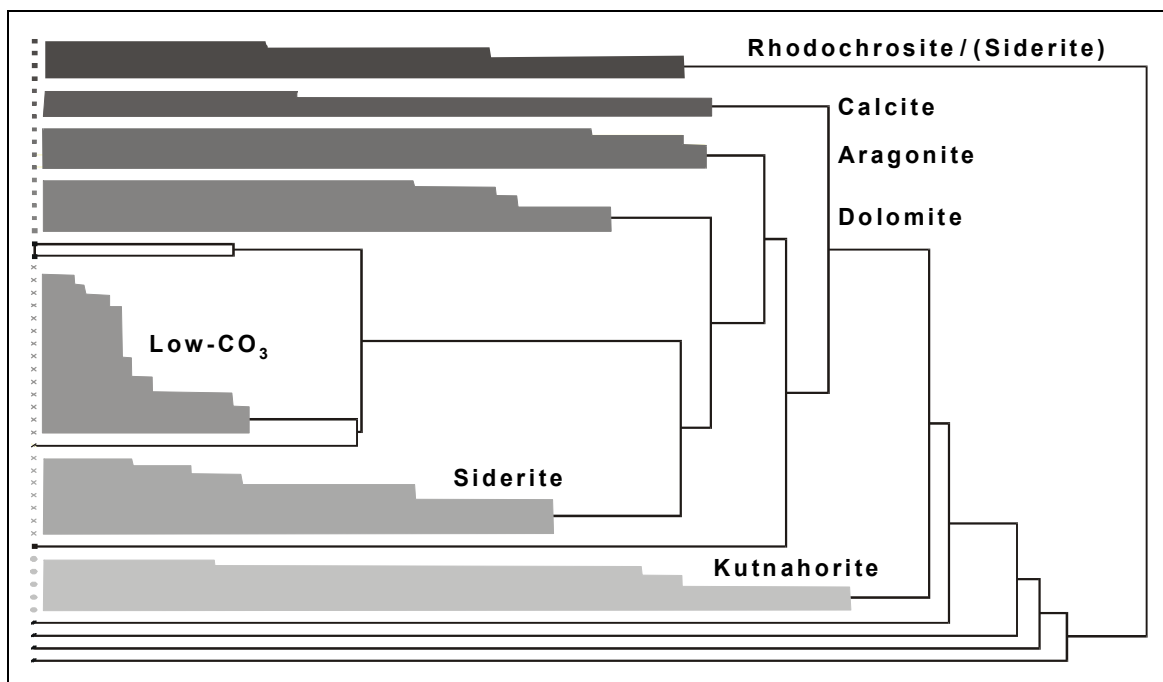


Fig. 4.8. Cluster analysis of samples based on carbonate mineralogy; after Franks (1999).

This subdivision is based on results of a cluster analysis which was performed by Franks (1999). The carbonate facies classification for all samples is provided in Tab. 4.2. The carbonate mineralogy in lake sediments depends mainly on salinity and Mg^{2+}/Ca^{2+} variations in the lake water (Kelts & Hsü, 1978; Eugster & Kelts, 1983).

Calcite [CaCO₃]

In all studied Liaohe source rocks calcite percentages vary between 0 and 37.2%. The calcite carbonate facies group consists of samples where aragonite is absent, and other carbonate minerals are present in small amounts or are absent. According to Jones & Bowser (1978) calcium carbonate in lake sediments can have four major sources: **(1)** Detrital carbonate can be derived from fluvial input and by shoreline erosion, **(2)** biogenic carbonate originates from the skeletal remains of various organisms such as molluscs, charophytes and phytoplankton, **(3)** inorganically-precipitated carbonates are biogenically induced, **(4)** diagenetic carbonate is produced by post-depositional alteration of other carbonate minerals. It was observed that calcite is very often the first carbonate precipitated from relatively diluted alkaline lake waters with a low Mg^{2+}/Ca^{2+} ratio during freshening periods and overall higher lake water levels (Dutkiewicz & von der Borch, 1995). These periods are often associated with an increased biological activity.

Dolomite [Ca,Mg (CO₃)₂]

This mineral is present from 0 to 45.5 wt.-%. The dolomite carbonate facies group contains only samples where dolomite formed more than 50% of the total carbonate fraction. Bulk chemical studies and quantitative electron-microprobe analysis of carbonates in oil shales demonstrated, that $FeCO_3$ is commonly present in dolomite as ankerite $[(Ca(Mg,Fe_{>0.2})(CO_3)_2)]$ and Fe-dolomite $[(Ca(Mg,Fe_{<0.2})(CO_3)_2)]$ (Desborough & Pitman, 1974). In this work the term dolomite is used for a dolomite type carbonate giving a 100% peak at or above 30.75 degrees. This mineral is very abundant in samples from the DJT sub-unit, especially in the Lei and Gao area. A large number of possible origins was reported for dolomite and is discussed herein: **(1)** Detrital, **(2)** primary dolomite **(3)** evaporative concentration of groundwater, **(4)** late diagenetic burial and hydrothermal dolomites, and **(5)** microbial dolomites.

(1) Erosional processes may account for the dolomite associated with the deposits of the Liaohe lakes. However, this mechanism was unlikely to occur, because metamorphic rocks are predominant in the vicinity of the Liaohe Basin where dolomite is absent.

(2) Formation of primary dolomite involves direct precipitation from the evaporating lake waters. This indicates that waters had high Mg^{2+}/Ca^{2+} ratios, high alkalinities and only small quantities of sulphate in solution (Hsü, 1967; Last & de Deckker, 1990). The high alkalinities in some stratigraphic units are supported by other typical minerals, e.g. analcime (see chapter 4.3.3.4). Folk & Land (1975) reported that Mg^{2+}/Ca^{2+} ratios for many lakes with salinities below 3.5‰ range between 0.1 and 3.0. As these waters become concentrated by evaporation the ratio is increasing and Mg-calcite and protodolomite are the dominant phase (Skinner, 1963). Modern lacustrine dolomite is forming in concentrated waters with Mg^{2+}/Ca^{2+} ratios ranging from 4.7 to 22 (Alderman & Skinner, 1957; von der Borch, 1965). A recent example where such a primary dolomite formation occurs are the Coorong lakes in south-eastern Australia (von der Borch, 1976). However, there are many kinetic inhibitions against the formation of massive dolomite sequences by primary precipitation because laboratory experiments did not support this pathway. For example, evaporation of ephemeral lake waters under laboratory conditions produced aragonite and not dolomite (Wright, 1999 and references cited within).

(3) Many similarities between the playa-lake deposits of the Green River Formation and the dolomites of the Es4 member exist. The playa-lake model consist of a vast alkaline-earth playa with an alkaline lake (Eugster & Surdam, 1973). Wolfbauer & Surdam (1974) proposed that the dolomite of the Green River Formation was formed in broad mud flats during regressive and arid phases adjacent to the lake. This process was mainly aided by the evaporative concentration of groundwater and not from the evaporation of the lake waters itself. In this case, a hydraulic concentration gradient from the groundwater table to concentrated brines with high Mg^{2+}/Ca^{2+} ratios near the surface of the mud flats existed. This mechanism can lead to the precipitation of enormous amounts of dolomite and is strongly supported by other minerals present in the Liaohe source rocks (see below).

(4) Late diagenetic and hydrothermal dolomites are subsurface cements and replacements that form below the active phreatic zone in permeable intervals, flushed by warm to hot magnesium-enriched waters as reviewed by Hardie (1987). Volcanic activity was of local importance in the Western Depression during Es4 time (Chen *et al.*, 1999). Thus, the higher gradient in these areas might cause hot saline and highly pressurised waters moved laterally out of these parts of the basin through porous and permeable horizons and vertically through

faults and fractures (cf. Oliver, 1986). The DJT sandstones served as such important conduits and acted as hydrocarbon carrier beds. Thus, they probably reflect such a permeability path where dolomite cementation took place. Interestingly, dolomite of up to 10% was found in these sandstones in well A (Fig. 4.6).

(5) Bacterial metabolism may have aided the process of dolomite precipitation in some parts of the Western Depression, where microbial action controlled primary precipitation in especially hypersaline anoxic lake settings. Recently, some authors suggested that direct mediation of bacteria can play an important role in the formation of dolomite (Vasconcelos *et al.*, 1995; Vasconcelos & McKenzie, 1997). Sulphate reducing bacteria metabolise sulphate ions and use the magnesium ions inside their cells for many vital physiological functions. Magnesium can make up to 0.5% of the cell dry weight and is released in excess with other by-products of sulphate reduction. Some authors proposed that cyanobacteria and bacteria can concentrate magnesium on their cell surface, initialising carbonate precipitation around their body (Gebelein & Hoffman, 1973; Folk, 1993). For example, cyanobacteria can concentrate magnesium in their sheets by up to four times than in seawater. Wright (1999) used these arguments to explain dolomite precipitation in the Coorong lakes, Australia. He suggested that the magnesium that is concentrated in cyanobacterial cells and sheets is released into the alkaline lake brines during desiccation. Interestingly, abundant cyanobacterial OM was recorded in all studied wells of the Western Depression by organic petrological observations and bacterial reworking was suggested by fluorescence microscopy (see section 4.4). Although the only origin of thick dolomite sequences *via* this pathway seems unlikely, it could be an additional source for dolomite present in the Liaohe source rocks.

Kutnahorite [Ca,Mn (CO₃)₂]

Some samples contain this relatively rare manganese dolomite. In this thesis, the term kutnahorite refers to a series of (Mn,Ca)-carbonates with changing stoichiometric compositions, giving a primary peak at or below 30.75 degrees 2-theta. Maximum percentages with 59.1% were observed in well A. All other rock samples with contain this mineral in significant amounts were found in wells from the Lei and Gao area with a maximum percentage of 38.8% for a carbonate rich shale from well H (E 48498). The other manganese carbonate **rhodochrosite [MnCO₃]** is only present in a shale sample from well O (E 48479; Es3 member) with 2.8%.

Kutnahorite was first described from a quarry in Kutna Hora, Czech Republic by Burkowsky (1903). This mineral was reported from hydrothermal ore deposits (Fronde! & Bauer, 1955; Tsusue, 1967) and from a number of manganese carbonates associated with black shales (Bolton & Frakes, 1985; Delian *et al.*, 1992; Roy, 1992).

(Mn,Ca)-carbonates are of great interest for paleoenvironmental reconstruction because anoxic sediments are often depleted in manganese due to a low Eh favouring the stability of manganese (Mn^{2+}) ions in aqueous solutions (Force & Cannon, 1988). This results in a leach of manganese from the sediment. Huckriede & Meischner (1996) found that the formation of manganese-rich sediments in the Baltic Sea was related to intense microbial activity at the sediment-water interface and restricted to the deepest parts of the basin. The Baltic Sea contains brackish waters with salinities in the range between 6.0 and 9.0‰, which is less than one third of seawater. The proposed pathway is presented in Fig. 4.9 and a similar origin for the manganese-rich sediments in the Liaohe source rocks is suggested. After oxidation and formation of manganese oxides, anoxic conditions were re-established. This is in agreement with observations by Calvert & Pedersen (1996). The authors found (Mn,Ca)-carbonates only in anoxic sediments beneath surface oxic horizons and concluded that their presence signifies that the host sediment must have accumulated in oxygenated bottom waters. Microbial processes may also play an important role (Aller & Rude, 1988; Thamdrup *et al.*, 1993; Böttcher, 1998). Manganese oxides (Mn^{4+}) are directly reduced by biochemical processes, creating favourable conditions for manganese carbonate precipitation. Another important prerequisite is that dissolved manganese concentrations are in the range between 10 and 100 ppb to allow carbonate precipitation (Hartmann, 1964). One possible source for manganese is terrestrial OM input as proposed by Suess (1979). However, this would require an unrealistic high input of terrigenous OM, which was not observed in the Liaohe sediments. Therefore, it is more likely that the manganese was delivered by fluvial transport and dissolved manganese from the surrounding watershed (cf. Pontér *et al.*, 1990). Relatively alkaline lake waters can be assumed because kutnahorite was found to precipitate in solutions with a pH between 8.5 and 9.0 (Hem & Lind, 1994).

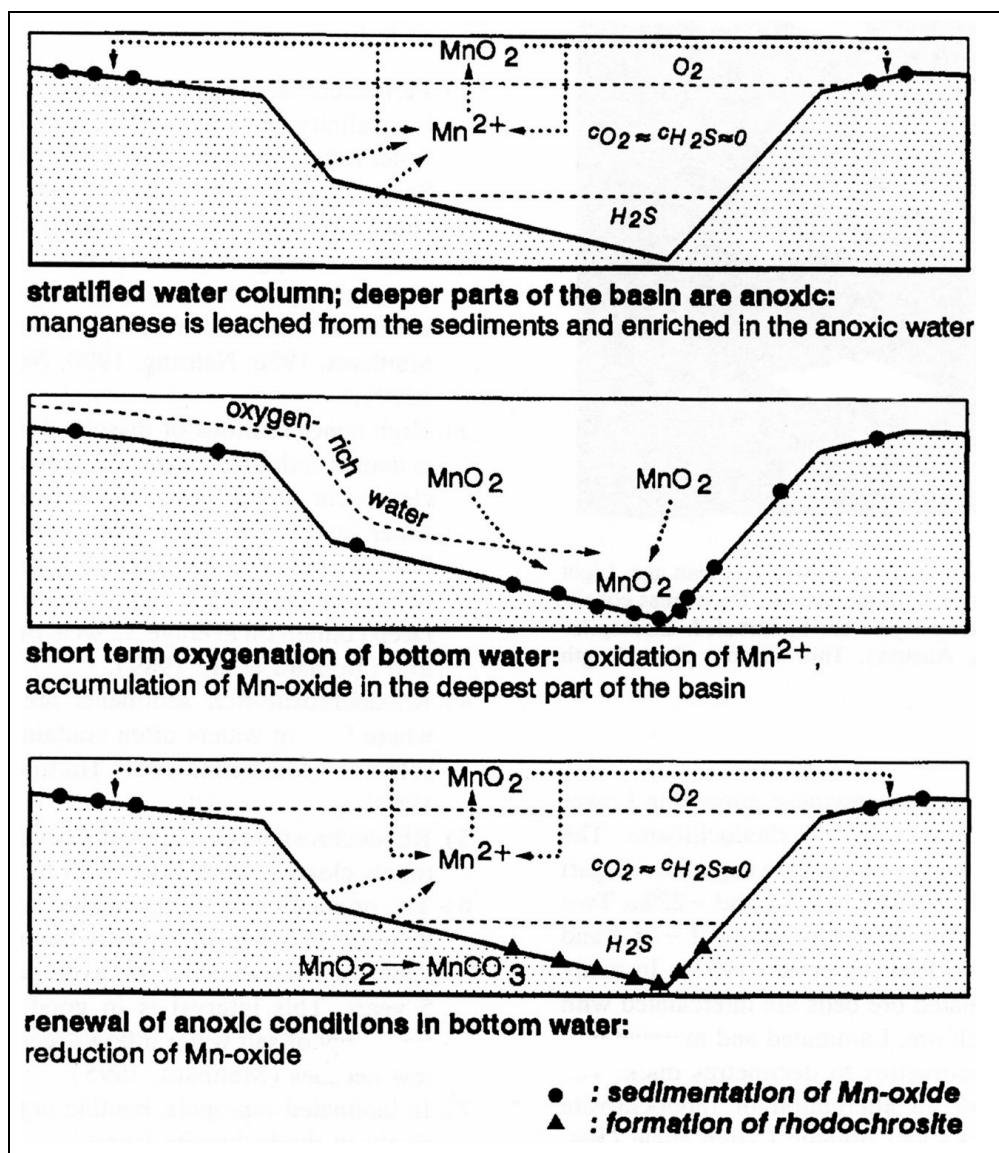


Fig. 4.9. Formation of manganese-rich sediments; after Huckriede & Meischner (1996). This example describes the reduction of Mn-oxide to rhodochrosite ($MnCO_3$).

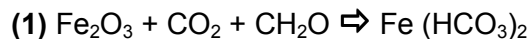
Aragonite [rhombohedral $CaCO_3$]

Mineral contents range up to 34.1% and comprise more than 50% of the total carbonates in the aragonite facies group. Ideal pH values for aragonite precipitation are 8.5 to 9.0. Kitano (1962) found that the temperature is also crucial. At temperatures below 25°C inorganic calcite forms, at higher temperatures aragonite precipitates. Some authors reported that high rates of CO_2 degassing, due to evaporation in warm, littoral high-energy environments with strong waves and currents favour aragonite precipitation (Given & Wilkinson, 1985; Zhang *et al.*, 1996). The precipitation rate increases with increasing magnesium in solution and the more alkaline a solution is (Kitano, 1962; Kitano *et al.*, 1962).

However, it was also found that aragonite is very often absent from lakes where dolomite occurs, but can precipitate in lakes with high sulphate concentrations (Wright, 1999). This was observed for the Liaohe sediments. For example, in well B (Fig. 4.7) aragonite is relatively abundant in the upper part of the DJT sub-unit, where dolomite is absent.

Siderite [FeCO₃]

This carbonate facies contains samples with siderite percentages between 7.8 and 23.1%. The mineral was reported from reducing, deep water environments with pore waters that have a high P_{CO₂} from the microbial decay of OM (Zhang *et al.*, 1996). In siderite rich lakes the measured pH is 7.1 to 7.6. The following mechanisms were proposed for siderite formation. First, iron (Fe³⁺) -oxides and hydroxides were washed into the lakes as a colloidal suspension or bound to clay minerals. They were reduced to Fe²⁺ in an anoxic environment **(1)**, and if sulphate and Ca²⁺ are mainly absent, the reduced soluble iron became enriched in the deep pore waters of a lake **(2)**. A Ca/Fe ratio of less than 20 is necessary for the precipitation of iron carbonates (Kelts & Hsü, 1978). Siderite is therefore a very sensitive indicator of the water chemistry within a lake. Only after all of the available H₂S is incorporated into pyrite, the better soluble FeCO₃ is formed in an environment which is most likely methanogenic (Füchtbauer & Richter, 1988). The main reaction pathway can be described as follows:



4.3.3.2 Clay Minerals

Expandable clays are by far the dominant clay minerals in the Western Depression. Highest percentages were found in samples from the Shale I sub-unit (Fig. 4.6). Expandable clays contain discrete **smectite** and **mixed-layer illite/smectite (I/S)** commonly forming from the weathering of ultrabasic or very basic rocks which produce magnesium minerals (Surdam & Stanley, 1979). However discrete smectite is only present in three samples (well A, R, S). Only few carbonate and analcime rich samples from the DJT sub-unit in the Lei area have higher percentages of **illite & mica** than expandable clays (Fig. 4.7), which signals an environmental influence that will be discussed below. The amount of illite & mica varies between 0 and 10.4%. **Kaolinite & chlorite** percentages reach a maximum in sample E 48459 (well B). They are especially significant in samples from the Es3 sub-unit. Illite &

mica as well as kaolinite & chlorite show a positive correlation with quartz, which might indicate that at least some of the clay minerals are detrital. Clay minerals are especially abundant in samples from the Es3 member (on average 41.8%), Shale I/Shale II sub-units (on average 44.0%) and in the GS sub-unit (on average 35.1%), whereas lower proportions were found in the DJT sub-unit (on average 21.5%).

The overwhelming fraction of clay minerals in lake sediments is of detrital origin (Jones & Bowser, 1978; Hardy & Tucker, 1988). They were frequently used as environmental and paleoclimatic indicators since the work of Keller (1956). Climate has a strong influence on rock alteration and clay minerals are often the main product of this process. For example, the global pedogenic and climatic zonation is reflected in the latitudinal distribution of certain clay minerals (Chamley, 1989). However, other factors than climate such as lithology, topography, transport and diagenetic changes can modify the original clay assemblage (cf. Yuretich *et al.*, 1999). Four main genetic hypothesis for the origin of smectite and mixed layer I/S exist: (1) reworking of soils and enrichment by differential settling, (2) alteration of volcanic material, (3) transformation of detritals, and (4) authigenesis (Chamley, 1989; Thiry & Jaquin, 1993). The absence of any conceivable volcanic precursor, such as tuff or glass in the studied sediments indicates that the expandable clays are mainly of a detrital origin. Smectite is the predominant clay mineral in many lacustrine settings. For example, it makes up to 100% of the shale minerals in some stratigraphic units of the Messel oil shale (Weber, 1991). The author suggested a humid/warm climate with a diverse fauna and flora in the catchment area.

Especially in lakes, clays are very sensitive to diagenetic alterations such as increasing alkalinity and salinity of the lake waters (e.g. Stoffers & Hecky, 1978). Fig. 4.10 shows that the percentages of expandable clays are decreasing with increasing dolomite percentages, visible for the DJT sub-unit. Because dolomite precipitation is associated with alkaline lake waters (see above), this suggests an influence of the lake water chemistry on the clay mineralogy. It was previously reported that in saline lake deposits, smectites and mixed-layer I/S are often absent due to transformations in the saline environment (Hay & Moiola, 1963; Jankowski, 1981; Remy & Ferrell, 1989). Dyni (1976) and Hosterman & Dyni (1972) established a salinity zonation for clay minerals in the Green River Formation. They found that kaolinite, illite, mixed-layer I/S, and smectite are present in the fluvial or freshwater environment. Mudstones deposited in a nearshore moderate saline environment contain only illite and smectite. The hypersaline depocenter of the Piceance Creek basin is nearly devoid of clay minerals due to chemical reactions and dissolution in highly saline and alkaline fluids (Dyni, 1985).

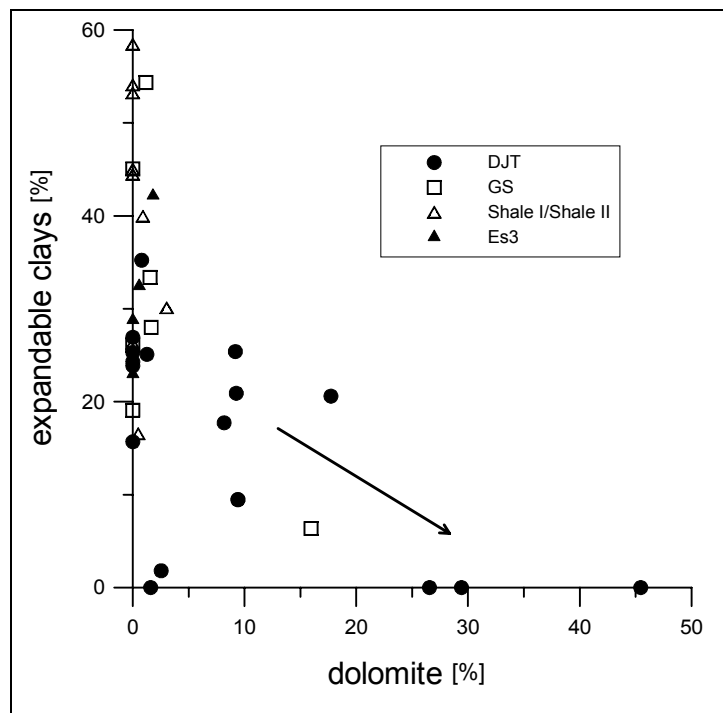


Fig. 4.10. Expandable clays versus dolomite for the different stratigraphic units in the Western Depression of the Liaohe Basin.

XRD analyses revealed that the Liaohe shales deposited during Shale I or Shale II times contain a wide variety of clay minerals (Figs. 4.6 and 4.7). The sediments deposited during early DJT time show a very restricted clay mineral suite (Fig. 4.7), where only illite & micas are present. This is in agreement with observations on dolomite and analcime rich sediments of the Nördlinger Ries, where no smectites and mixed layer clays were determined (Jankowski, 1981). Instead, these sediments are dominated by illite as in the Liaohe sediments. The author proposed that illite was formed as an authigenic mineral at the expense of expandable clays, due to reactions with the highly saline lake waters. Thus, sediments with illite and no other clay minerals, together with the presence of analcime and dolomite signify a maximum salinity of the Liaohe lake waters. These investigations were substantiated by Stoffers & Singer (1979) and Singer & Stoffers (1980). They studied clay mineral distributions in East African lakes and found diagenetic transformations of smectite into illite, induced by saline paleo-lake waters. However, if the illite in the Liaohe sediments formed at the expense of expandable clays we would expect higher than normal percentages, but this is not the case. Hay & Moiola (1963) suggested a different transformation pathway and believed that the illite in such saline sediments is of detrital origin. Expandable clays were dissolved by reactions with saline and alkaline brines and the remaining aluminium and silica was used to form analcime or feldspars (see chapter 4.3.3.4).

Smectite converts to illite during burial diagenesis *via* an intermediate mixed layer phase (Velde, 1985). In random mixed layer I/S structures the proportion of the expandable part (smectite) is higher than 20% (Perry & Hower, 1970). An ordered mixed-layer mineral is one with regularly alternating non-expanding and expandable layers. An increasing ordering of the layers results in a decreasing number of expandable clays (Velde, 1985). All samples from the Lei area contain ordered mixed layer I/S. In well A only sample E 48537 at a depth of 1375 m contain ordered mixed layer I/S, whereas the others consist of random mixed layer I/S or discrete smectite. This suggests a negligible influence of burial diagenesis in well A whereas in the Lei area a diagenetic overprinting might have occurred in response to higher thermal stress. Franks (1999; 2000) stated that the degree of ordering in the I/S clays increases and the expandability decreases with temperature and depth for the Liaohe source rocks (Fig. 4.11). This mineralogical transition typically occurs near the beginning of the oil window for source rocks originating in saline-alkaline setting and just prior to the oil-generation window in normal marine source rocks.

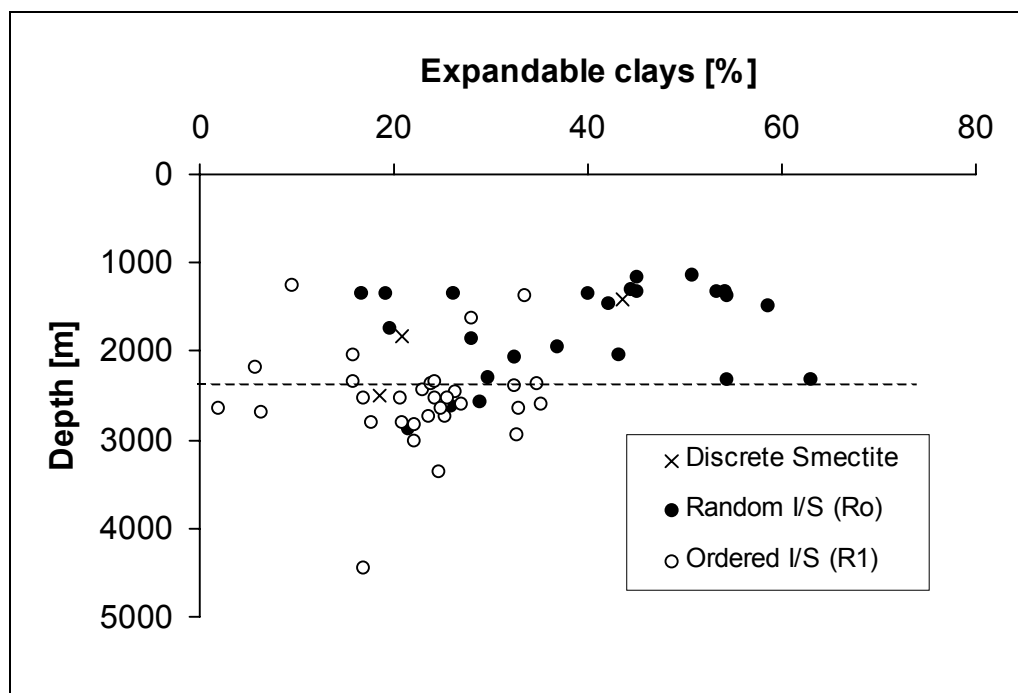


Fig. 4.11. Expandable clays versus depth for samples from the Western Depression of the Liaohe Basin; after Franks (1999).

4.3.3.3 Quartz and Feldspars

Quartz and feldspars are with 12.0% and 39.0% (plagioclase), respectively the most important minerals in the earth crust (Matthes, 1987). Feldspars are mainly formed in magmatic and metamorphic rocks. **Quartz** is highly resistant against weathering processes and a common detrital mineral in sedimentary rocks. The quartz contents in the investigated sediments vary between 0 and 58.1% (E 48518, well A). Percentages are high in samples from the Es3 member and in the Shale I/Shale II sub-units with 24.6 and 24.3% on average, respectively.

In contrast to quartz, **feldspars** are easily affected by chemical weathering processes and transformed to clay minerals. Thus, abundant feldspars in sandstones point to a predominantly physical weathering and/or is an indicator that the detritus comes from proximal provenances (Folk, 1974; Vogt, 1997). The $Q/(Q+F)$ ratio can be used as a parameter to determine the distance to the parent rocks or is related to the climate in the source area. In felsic basement rocks, $Q/(Q+F)$ is 0.3 to 0.4 and ranges between 0.9 and 1.0 for intensely weathered sands in the humid tropics (van de Kamp & Leake, 1996). Its decrease in well A might either indicate a decreasing chemical weathering intensity due to a more arid climate or reflect a closer location to the lake margin during DJT time (Fig. 4.6). With the exception of one sample all ratios are very low values in well B which points an arid climate with a predominant physical weathering in a closed lake basin (Folk, 1974).

Plagioclase feldspar occur in all samples ranging from 1.5 (E 484775, well J) to 33.2% (E 48539, well A). Although detailed investigations were not performed, the XRD results suggest that most samples contain sodic feldspar (Franks, 1999, 2000). Only sample E 48539 (well A) contains more calcic plagioclase which points to a volcanic origin. The relatively uncommon mineral **buddingtonite** represents the non-plagioclase feldspar fraction. Buddingtonite is an ammonium feldspar with zeolitic water and the stoichiometric composition $[NH_4AlSi_3O_8 \cdot 1/2 H_2O]$. It is present in 48 of the 49 samples ranging from 0.7% (E 48480, well E) to 36% (E 48469 well B). Although the feldspar was interpreted as buddingtonite, the peak position is very similar to anorthoclase which might indicate that some samples may contain a mixture of alkali feldspar types (Franks, 1999).

A large part of nitrogen in minerals is fixed as ammonium in silicates such as feldspars, micas or zeolites, in crystallographic sites usually occupied by alkali ions. Charge and radius of the NH_4^+ ion make it a logical substitute for potassium (K) ions in silicate lattices (e.g. Erd *et al.*, 1964). The author was first who described the mineral buddingtonite from Quaternary andesites (Sulphur Bank, California). The volcanic rocks had been hydrothermally altered by ammonium-rich hot-spring waters. During this reaction, albitic plagioclase was partly to completely replaced by ammonium feldspar. However, as already stated above, no direct evidence for a hydrothermal activity was found in the studied sediment sequences in the present study. Natural clay minerals and feldspars generally contain too little ammonium to produce measurable quantities of ammonium during pyrolysis (Everlien, 1990).

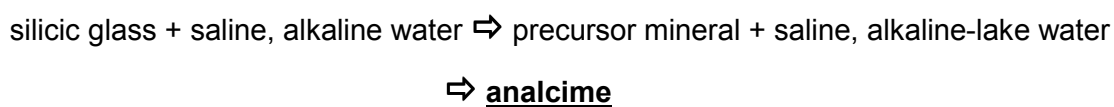
Organic nitrogen in living organisms is overwhelmingly present in amido- and amine-groups in proteins and peptides. Although a significant proportion of the nitrogen in surface sediments (possibly up to 40% of the total nitrogen) is present in the form of pyrrolic- and pyridinic-type structures (Patience *et al.*, 1992), amino acids account for more than 40% in shallow sediments (<1m) from the Peru upwelling region (Henrichs & Farrington, 1987; Patience *et al.*, 1990). As summarised by Baxby *et al.* (1994), the early diagenetic transformation of organic nitrogen involves its incorporation into kerogen; or the loss as NH_3 as a result of microbial or chemical mineralization. This may be followed by adsorption and fixation of NH_4^+ in minerals such as clays or feldspars. Ramseyer *et al.* (1993) found significant amounts of K- NH_4 -feldspar in Miocene sandstone of the San Joaquin and Los Angeles Basin. Based on petrographic and isotopic studies he concluded that bacterial decay of OM is the source of ammonium and that the feldspar precipitated during early diagenesis within the zone of methanogenesis. Loughnan & Roberts (1983) found up to 16% buddingtonite in the lacustrine Condor oil shale deposit, Australia. They proposed a diagenetic origin within the mud of a stratified lake and suggested bacterial degradation of proteins and amino acids in algal OM as the most likely ammonium sources. It has been previously shown that the amino-acid composition in lacustrine surface sediments is mainly planktonic and bacterial in character (e.g. Dungworth *et al.*, 1977). Gulbrandsen (1974) detected extremely high ammonium yields within organic-rich sediments of the Phosphoria Formation, Idaho (U.S.) and interpreted their occurrence in a similar way.

An alternative pathway for buddingtonite formation is attributed to migrating fluids in the basin. High buddingtonite percentages were determined for two sandstones from the DJT sub-unit in well A (E 48517 and E 48519). Interestingly, they have also anomalous high Production Index (PI) and S1/TOC ratios. Sample E 48517 from the DJT sub-unit (well A) shows a PI of 0.41 and a S1 normalised to TOC of 335.3 mg/g TOC. Similar data were also obtained from other parts of the Western Depression such as sample E 48466 from well B (DJT sub-unit). Organic petrologic observations revealed the occurrence of yellow fluorescing bitumen in all these samples. As already mentioned in chapter 4.2.4 the DJT sandstones act as important reservoirs and carrier beds in the Western Depression. This suggests that oil-bearing fluids that migrated through the basin may have caused the high ammonium concentrations in the feldspars. High fixed-NH₄⁺ yields in clay minerals of mudstones from the Eocene Wilcox Group (Louisiana) are also associated with increased organic-geochemical indicators for migrated hydrocarbons (Williams *et al.*, 1989; Williams *et al.*, 1992). The authors concluded that the nitrogen was released from the OM as NH₃ (ammonia) during maturation and migrated together with the pore fluids, volatile phases and crude oil through more permeable carrier beds. However, the majority of nitrogen in ancient sediments (e.g. coals) has been shown to predominate in pyrrole and to a lesser extent in pyridine structure types (e.g. Bartle *et al.*, 1987). Thus, the generation of significant amounts of NH₃ from these sediments upon maturation is unlikely. In contrast Wallace (1986) found that a high proportion of nitrogen in oil shale asphaltenes occurs in amide and amine groups (approx. 40%) which may be possible precursors for NH₃. Nitrogen loss from OM as NH₃ was supported in artificial heating experiments on immature sediments (algal mat and Staten Island peat), carried out by Rohrbach *et al.* (1983). The generation of ammonia during the catagenetic stage (70 to 150°C) from the thermolytic cracking of OM is substantiated by Hunt (1979, p. 164), Jüntgen & Klein (1975) and other references quoted therein. This NH₃ may react with H⁺ resulting in high ammonium concentrations which were previously observed in many oilfield formation waters (e.g. Collins, 1975) and finally results in additional adsorption and fixation of NH₄⁺ by clay minerals (Williams *et al.*, 1992). Thus, changes in ammonium concentrations in clay minerals and feldspars (buddingtonite) may serve as indicators for the presence of hydrocarbons or the migration pathways the crude oils followed from source rocks to reservoirs.

4.3.3.4 Analcime [$\text{Na}_{16}(\text{Al}_{16}\text{Si}_{32}\text{O}_{96}) \cdot 16\text{H}_2\text{O}$]

Analcime is the only zeolite identified in the source rocks and present in 11 of the 49 examined samples ranging from 1.5 (E 48492, well G) to 25.3% (E 48466, well B). Analcime occurs most frequently in the lower DJT sub-unit and lacks in the clay rich Es3 member and in the Shale I and Shale II sub-units (Fig. 4.7). It is mainly found in source rocks of the Lei area but is restricted to rocks where feldspar percentages are higher than 10%. The shallowest occurrence is at 1405 m in well A (E 48539). The deepest occurrence is at 2818 m in well G. Analcime co-exists with all carbonate phases, but most abundant with shales rich in dolomite.

Analcime has a wide spectrum of genetic types, from sedimentary (continental and marine), to magmatic, to low grade metamorphic and also hydrothermal as reviewed by Gottardi & Galli (1985). Analcime can form from the alteration of **pyroclastic debris** (volcanic glass) which was delivered to the lake basin (Surdam & Parker, 1972; Surdam & Eugster, 1976; Surdam & Sheppard, 1978), *via* the reaction pathway:



Although the literature indicates that volcanic activity occurred regionally in the Western Depression during Es4 time (see chapter 4.1.3), two lines strongly suggest that most of the analcime was not derived from this source. Firstly, large quantities of volcanic material are necessary to produce the analcime detected in the shales. However, no volcanic detritus, such as the minerals hornblende or augite was found in association with the studied sediments and no major volcanic influence was reported from the analcime-rich intervals, such as the lower DJT sub-unit in well B. Secondly, the XRD analyses indicated that analcime is the only zeolite in the shales.

Authigenic analcime has been widely reported from alkaline, saline lacustrine sediments that lack volcanic detritus. Typical ancient and recent examples are mudstones from the Green River Formation in the south-central Uinta Basin (Remy & Ferrell, 1989), lacustrine rocks of the Hartford and Newark rift-basin (Hubert *et al.*, 1992; van de Kamp & Leake, 1996), lacustrine sediments from the Nördlinger Ries (Jankowski, 1981) and Quaternary lacustrine sediments from Lake Bogoria, Kenya Rift Valley (Renaut, 1993). In all these cases, the analcime is thought to have formed in closed saline and alkaline lakes by reaction

of sodium rich brines reacted with silicates during dry periods. Sodium rich groundwater was concentrated by evaporative pumping and evapotranspiration. Expandable clays are very often the principle reactants which provide the silica and aluminium (Hay *et al.*, 1991 and chapter 4.3.3.2). Temperatures below 50°C were proposed for the analcime formation. An alkaline environment with a pH 9-12 is necessary for this reaction as determined by Baldar & Whittig (1968).

4.3.3.5 Opal-C and Opal-CT (SiO₂)

Opaline silica was detected in only four samples all of them located in the Shale I sub-unit (well A). Maximum percentages of 57.1% were found at a shallow depth of 1340 m (Fig. 4.6). Other minerals present in these rocks are mainly expandable clays and quartz. No analcime and only trace amounts of carbonates were found. The opal-A polymorph was not detected by XRD analyses.

The presence of opal-C and/or opal-CT suggests a high silica content of the lake waters. Silica generally precipitates from natural aqueous solutions as amorphous silica by polymerisation. Precipitation can be induced organically during periods of a high biosiliceous productivity or inorganically, as in silcretes, geyserites, and precious opal deposits (Williams & Crerar, 1985). However, it is difficult to reconstruct the depositional environment from the occurrence of this mineral due to its generally amorphous nature. For example, Noel & Rouchy (1986) found that even the biogenic origin of opal-CT rich sediments is difficult to recognise. They observed by scanning electron microscopy (SEM) that diatoms were completely replaced by massive aggregates of opal-CT lepispheres. These highly amorphous, layered structures are similar to those investigated in sample E 48527 (well A). High diatom productivity would imply an elevated availability of nutrients. However, primary production of diatoms is limited by the salinity of the lake waters. It was stated that diatoms do not survive salinities of above 130 gL⁻¹ (Rouchy *et al.*, 1995). Interestingly, the opal-A polymorph that is generally associated with biosiliceous deposits, was not detected in the Liaohé source rocks. Therefore, other sources of silica must be considered. For example, in a recent paper English (2001) argued that evaporation and evapotranspiration facilitates silica precipitation from supersaturated waters at or near the groundwater table.

4.3.3.6 Gypsum [$\text{CaSO}_4 \cdot 2\text{H}_2\text{O}$]

Gypsum was detected in 27 of the 49 investigated samples. Its percentages range from 0.1% (E 48514; well S) to 2.6% (E 48537; well A). It occurs most frequently in the GS and in the DJT sub-unit.

Gypsum is beside sodium and magnesium carbonates the main evaporative precipitate in hypersaline lakes (Müller, 1988). Several mechanisms for the formation of gypsum in lacustrine environments are possible. It precipitates mainly as tiny prismatic needles in very shallow hypersaline water bodies under arid depositional conditions, either within the water column or at the surface of the sediment (Schreiber & El Tabakh, 2000). Some deposits with deep water settings are known in the rock record, for instance from the Green River Formation (Eugster & Surdam, 1973; Fischer & Roberts, 1991) and from the Dead Sea lake system (Katz & Kolodny, 1989). Other gypsum occurrences are reworked or re-sedimented gypsum and cements as well as void fillings in non-evaporative sediments, carried in by evaporative enriched groundwater (Schreiber & El Tabakh, 2000). In addition, the oxidation of sulphides and the sulphate released by bacterial breakdown of OM can lead to the formation of gypsum (El Tabakh *et al.*, 1997). Ponds with gypsum precipitation must have a salinity of 130 to 320 gL^{-1} (Schreiber & El Tabakh, 2000).

4.3.3.7 Pyrite [FeS_2]

This mineral was detected in amounts up to 7.2% (E 48462; well B). It is relatively abundant in sediments from the Shale I and Shale II sub-unit and especially in the Es3 member. Microscopic observations revealed that pyrites found in the shales are of framboidal shape. Pyrite is an early diagenetic precipitation induced by bacterial OM degradation within the young sediment (Füchtbauer & Richter, 1988). It is formed during bacterial sulphate reduction (1) and reaction of H_2S with iron minerals to form iron monosulfides (2), and finally the reaction of iron monosulfides to form pyrite (3) (Berner, 1970; Berner, 1984). An anoxic depositional environment is a prerequisite for sulphate reduction.



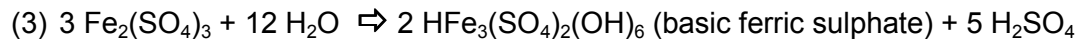
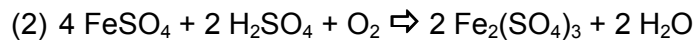
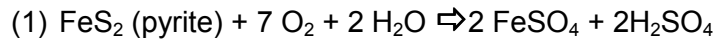
The limiting factors are the availability of labile metabolisable OM and the concentration and reactivity of iron minerals. Sulphate is very often the limiting factor in the lacustrine environment (Berner & Raiswell, 1983). In many freshwaters, sulphate is less than 1.0% of that in the marine regime. Tectonic lakes during active phases are an exception. They can contain sulphate-rich waters (Powell, 1986). Iron is supplied by detrital sources where it is often bound as an oxide to surfaces of clastic components, especially clay minerals, which provide a high internal surface area. This probably explains the high pyrite and siderite percentages in the clay rich stratigraphic units.

4.3.3.8 Amphibole $[\text{Ca}_2\text{Na}(\text{Mg,Fe})_4(\text{Al,Fe})((\text{Si,Al})_4\text{O}_{11})_2(\text{OH})_2]$

Only sample E 48511 (well R; Tuo area) contains 8.3% of this mineral. High percentages of expandable clays, analcime, plagioclase and dolomite were also found in this sample. Amphibole is a common mineral in quartz deficient mafic or ultramafic magmatic or metamorphic rocks. It can be related to a strong volcanic activity or rifting processes (Briot *et al.*, 2001). Large amphibole crystals were also found in volcanoclastic sediments of phreatomagmatic origin (Nemeth *et al.*, 1999). Another process, which might lead to amphibole enrichment, is the erosion of older amphibole containing rocks such as gneisses or schists. Because amphiboles are heavy minerals they are very often present in sediments at the lake borders a feature that can be related to particle sizes and transport processes (Bertelle *et al.*, 1998).

4.3.3.9 Natrojarosite $\text{NaFe}_3(\text{SO}_4)_2(\text{OH})_6$

Natrojarosite is a sulphate containing Fe- and Na-hydroxide which occurs only in sample E 48502 from well L in the Gao area (6.3%). Jarosite-type minerals frequently form upon oxidation of iron sulphide containing minerals at low pH of 3 to 4 in acid sulphate soils (Schwertmann, 1961). For example, the oxidation of pyrite results in extremely acidic conditions in an environment favourable for the weathering of plagioclase and micas, which in turn are the main sources of K and Na. Then natrojarosite forms under conditions where the supply of K limits jarosite formation (Öborn & Berggren, 1995). These processes are favoured in a setting, where oxidising groundwater and/or iron-oxidising bacteria are present such as *Thiobacillus ferroxidans* (Ivarson *et al.*, 1978). The main reactions can be written as follows:



Because natrojarosite is decomposed rapidly under alkaline conditions (Patino *et al.*, 1998), it can be concluded that an acidic and oxidising environment prevailed during deposition of this shale.

Points to Remember – Mineralogy

A wide variety of minerals, including clays, quartz, feldspars and carbonates were detected by XRD analysis in the Liaohe sediments. The analysed samples are mineralogically very unusual because they contain the rare carbonate mineral kutnahorite and the ammonium feldspar buddingtonite. If the ammonium is derived from crude oil related fluids, buddingtonite may serve as an indicator for the presence of fluid conduits and migration pathways. Alternatively, ammonium could be released from OM by bacterial degradation during early diagenesis and replaces alkali metal ions in feldspars. The presence of kutnahorite indicates high concentrations of manganese and is a sign for changing redox conditions in the water column during the depositional history. The DJT sub-unit in the Shu-Du area represents a coarse-grained facies with breccias, conglomerates and sandstones. Quartz, feldspar and clay minerals predominate. In the centre of the basin (Lei and Gao area) a clay-, carbonate-, gypsum- and analcime bearing facies developed with no significant clastic input and abundant chemical precipitation. The lithological sequences filling the basin represent a higher saline and alkaline lake facies in which authigenic minerals (e.g. analcime) developed through precipitation of surface and subsurface waters, especially during lower DJT time. The GS sub-unit in well A is dominated by clay minerals and calcite the latter suggesting a low $\text{Mg}^{2+}/\text{Ca}^{2+}$ ratio and relatively diluted lake waters, whereas higher dolomite percentages in the Lei and area indicate more concentrated and alkaline lake waters at the same time. The thick dolomite deposits in the Lei area formed mainly by evaporative concentration in shallow waters or on exposed mudflats. This process was probably aided by cyanobacterial and bacterial dolomite precipitation. The Es3 member and the Shale I and Shale II sub-units contain the highest percentages of clay minerals, dominated by mixed-layer I/S.

4.4 Organic Petrology

The aim of this chapter is to characterise the dispersed OM in selected rock samples from the Es4 and Es3 member of the Shahejie Formation, using reflected white and fluorescent light microscopy. As one key criterion of the organic facies concept defined by Jones (1987), organic microfacies analysis was performed which refers specifically to the maceral classification of organic constituents (cf. Stasiuk *et al.*, 1991; Stasiuk, 1999). Previous studies have demonstrated that variations of the maceral composition in lacustrine sequences can provide important informations about varying primary productivity in the lake or environmental factors such as changing water chemistries. For example, organic petrographic investigations revealed that the algal OM in sediments from the Nördlinger Ries changed in response to changes in salinity (Jankowski, 1981; Rullkötter *et al.*, 1990).

4.4.1 Terminology

Macerals were classified according to the terminology as issued by the International Committee for Coal and Organic Petrology (1998; 2001) and the definitions provided in the textbook "Organic Petrology" (Taylor *et al.*, 1998). Alginite and bituminite are the most common macerals in the Liaohe source rocks. Alginite is subdivided into telalginite and lamalginite according to Hutton (1987). **Telalginite** is alginite, derived from colonial or thick-walled unicellular algae, with strong fluorescence at low rank and with distinctive external structure, and in many cases internal botanical structures. **Lamalginite** is alginite, derived from small, unicellular or thin walled, colonial planktonic or benthic algae, with weak to moderate fluorescence at low rank and only little recognisable structure. In this study the amorphous unstructured organic matter (AOM) is subdivided into **fluoramorphinite** (yellow-fluorescing AOM) and **hebamorphinite** (non-fluorescing AOM) according to the classification of Senftle *et al.* (1987). **Vitrinite** is supposed to originate from humic substances, which are themselves alteration products of lignin and cellulose and form the basic framework of higher plant-cell walls. **Sporinite**, **cutinite**, **resinite** and **liptodetrinite** are besides alginite other important liptinites macerals in the source rock samples. They originate mainly from the hydrogen-rich plant materials sporopollenin, cutin and resins and contain higher proportions of aliphatic constituents than humic substances. **Funginite**, introduced by Lyons (2000), and **fusinite** are the most important macerals of the inertinite group. Funginite, formerly sclerotinite, is of fungal origin. Fusinite originates from the same precursors as vitrinite but received a higher degree of aromatisation and condensation that results in a higher reflectivity.

This can be related to processes such as charring, oxidation, desiccation or fungal attack. A detailed subdivision is given in Tab. 4.3.

Maceral-Group	Maceral	Maceral variety	Reflection	Fluorescence
Vitrinite	vitrite		gray	no
Inertinite	funginite fusinite		light-gray light-gray	no no
Liptinite	sporinite cutinite resinite liptodetrinite		dark brown-black dark brown-black dark brown-black dark brown-black	yes yes yes yes
	alginite	telalginite lamalginite	light brown-dark brown dark brown-black	yes yes
	bituminite (AOM)	hebamorphinite fluoramorphinite	black gray	no yes

Tab. 4.3. Maceral classification applied in this study; after Hutton (1987), Senftle et al. (1987) and Taylor et al. (1998).

4.4.2 Classification

The following criteria were used to classify the analysed samples into certain organic microfacies types: (I) lamination characteristics, (II) abundance and type of algae, (III) abundance of terrestrial particles, (IV) abundance of fluoramorphinite. Classification of all samples is presented in Tab. 4.4. An example for each organic microfacies type is illustrated in Fig. 4.12.

Type A: homogenous texture, dispersed small unicellular algae (lamalginite), almost no telalginite, only a few vitrinite particles, carbonate and/or clay rich mineral matrix (Fig. 4.12 A).

Type B: homogenous texture, abundant telalginite (remains of *B. braunii*) all orientated parallel to the bedding, only a few vitrinite particles (Fig. 4.12 B).

Type C: almost no lamination, only few lamalginite and telalginite, abundant vitrinite particles, sporinite and liptodetrinite are common macerals (Fig. 4.12 C1 and C2).

Type D: strong lamination with an alternation of fluoramorphinite containing carbonate rich (10 to 20 μm) and darker clay lamalginite containing layers (50 μm), few vitrinite particles (Fig. 4.12 D).

Type E: irregular or weak lamination (lenses), abundant fluoramorphinite, few vitrinite particles (Fig. 4.12 E).

Type A	Type B	Type C	Type D	Type E
48449	48479	48463	48467	48455
48465	48502	48485	48475	48464
48466	48521	48497	48481	48480
48491	48522	48515	48487	48482
48506	48523	48517	48527	48484
48520	48525	48519	48528	48494
	48526		48529	48505
			48530	48514
			48531	48533
			48532	
			48534	
			48535	
			48536	
			48537	

Tab. 4.4. Organic microfacies classification of the studied samples.

4.4.3 Non-laminated Samples

The OM composition of the non-laminated source rock samples from type A to C is as follows: **Type A** facies contains only small algae, which are finely disseminated in a carbonate and/or clay rich mineral matrix. The diagnostic morphology shows mainly organic longitudinal structures which points to the presence of small unicellular lacustrine algae (Fig. 4.12 A). Together with type C these samples have the lowest TOC-contents. Many of these rock samples are from stratigraphic units where dolomite and especially analcime are abundant. Thus, Type A is especially typical for the lower DJT sub-unit in the Lei area.

In **type B** telalginite is more abundant than in all other types (Fig. 4.12 B). It is dominated by *B. braunii* colonies, which are floating in a clay-rich matrix. This type was frequently found in the shale rich stratigraphic units (Shale I and Shale II, Es3 member). Vitrinite, inertinite, sporinite, liptodetrinite and funginite are present in **type C** samples (Fig. 4.12 C). With the exception of this facies type, the contribution of terrigenous particles to the total OM is low in the studied sample set which points to a complete lack of higher land-plant vegetation in the catchment area of the lake. Non-fluorescing AOM (hebamorphinite) is especially abundant in samples of type C. In reflected white light, it has a light to dark brown colour and occurs mainly as long irregular streaks or round particles (Fig. 4.12 C1). These constituents are probably a precipitate of humic acids derived from terrigenous OM (Littke, 1993). Darker rims around the boundaries of vitrinites (Fig. 4.12 C1) are reported to form during subaquatic oxidation (Bustin *et al.*, 1985, p. 74).

4.4.4 Laminated Samples

Source rock **type D and E** are laminated and contain alginite as well as abundant yellow fluorescing AOM that is concentrated in the bright layers (Fig. 4.12 D and E). The laminated samples are characteristic for the GS sub-unit in the Shu-Du area and for the GS and DJT sub-unit in the Lei area. Dolomite, calcite and aragonite are the most important minerals in the laminated shales. In some samples, especially in type E, fluorescing lamalginite in diffused filamentous organisation is visible in lenses, which points to the presence of cyanobacteria (Fig. 4.12 E). The darker layers consist of clay minerals with few lamalginite and some unicellular algal structures as in type A. The abundance of alginite and fluoramorphinite in these samples point to a type I or mixed type I/II kerogen (Tyson, 1995), and correspond to the organic facies types A and AB after the classification of Jones (1987). The fluoramorphinite is often associated with carbonate minerals. Dolomitic laminae, between 100 and 300 μm in thickness are present and the dolomite grains are frequently coated with thin lamalginite. Sometimes zones of oxidative degradation within the lamalginite were found. They have lower fluorescence intensity and emit fluorescence nearer the red region than the unaltered lamalginite. Similar observations were made by Stasiuk *et al.* (1991) in marine lamalginite rich source rocks. Pyrite nodules are often found in the lower part of the fluorescing layers which points to oxygen depleted conditions and H_2S production by certain bacterial communities.

Lacustrine source rocks often contain large amounts of amorphous OM (Tissot & Welte, 1984, p. 256). It is an important constituent of the OM in the Irati shales (Permian, Brazil) or in the Green River shale (Eocene, U.S.). Some authors speculated, that amorphous kerogens originated from organic oozes, colloidal solutions, gels, precipitates and sapropels derived from organic debris, bacteria, faecal and pellets which have putrefied near the sediment-water interface (e.g. Durand, 1980; Robert, 1981). High percentages of brightly yellow to orange fluorescing unstructured OM (fluoramorphinite), as observed in the present study were also identified in the Messel shale (Eocene, Germany) and in the Ries oil shale (Miocene, Germany) (Taylor *et al.*, 1998, pp. 245-247). This material in petroleum source rocks has been proposed to result from the degradation and microbial alteration of lipid-rich OM such as benthic and planktonic algae or cyanobacteria (e.g. Gutjahr, 1983; Stasiuk, 1993). There are strong optical-chemical relationships of different types of amorphous kerogens (Thompson & Dembicki, 1986; Senftle *et al.*, 1987). The brightly fluorescing AOM, present in the studied samples was always considered the AOM with the highest hydrocarbon potential.

4.4.5 Additional Observations

The maturity determination based on vitrinite reflectance values is extremely difficult due to the overall lack of vitrinite particles in the Liaohe sediments. In addition, the reflectance in the Es3 and Es4 member is often suppressed which is clearly indicated by measured data (Liguo Hu, pers. comm.). A possible explanation for this effect is that bitumen expelled from algal material was adsorbed by vitrinite macerals due to their very high microporosity. This process has been said to suppress the vitrinite reflectance values, especially in algal rich organic source rocks (e.g. Teichmüller, 1974; Hutton & Cook, 1980).

In sample E 48517 from a DJT sandstone, a strong yellow fluorescing fluid was detected which reflects a contamination with migrated crude oil. Interestingly, this sample has also one of the highest extract yield, S1 as well as production index (see chapter 4.5.1). Finally, in two samples from the Gao area (E 48505, E 48514) a dark grey amorphous substance was found in cracks and fissures which fulfils all requirements of solid bitumen.

Points to Remember – Organic Petrology

Five facies types were distinguished by qualitative observations in reflected white and fluorescence-inducing blue light. The types A, B and C are non-laminated and contain small alginite, *Botryococcus* telalginite and terrigenous macerals, respectively (Fig. 4.12 A-C2). The types D and E are laminated and consist of abundant algal and fluorescing AOM, the latter resulting from the microbial alteration of lipid-rich OM (Fig. 4.12 D and E). The observations show that the distinct types are restricted to certain stratigraphic members in the Western Depression and thus reflect organic facies changes: (1) Type A – lower DJT in the Lei area; (2) Type B – Shale I, Shale II, Es 3 member; (3) Type C – DJT of the Shu-Du area; (4) Type D – GS; (5) Type E – GS and DJT.

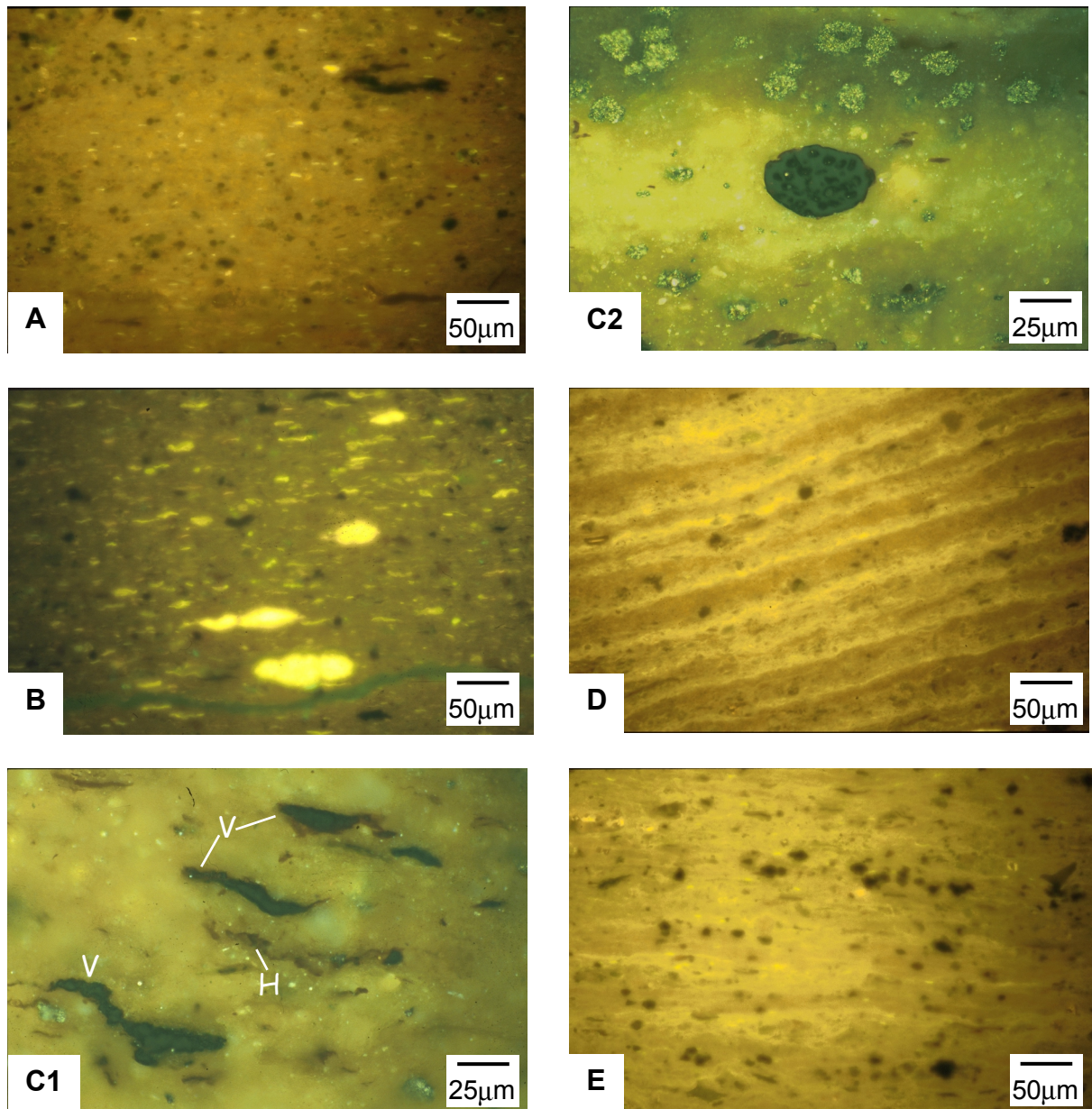


Fig. 4.12. Microscopic characteristics of non-laminated (A to C2) and laminated (D and E) source rock samples from the Western Depression of the Liaohe Basin.

- A) Sample E 48491 (well G) from 2665 m depth. Small yellow fluorescing alginite and liptodetrinite. 250x, blue light excitation.
- B) Sample E 48525 (well A) from 1329 m depth. Strong yellow fluorescing *B. braunii* telalginite and smaller alginite particles. 250x, blue light excitation.
- C) **C1**, Sample E 48497 (well U) from 1882 m depth. Vitrinites (V) with oxidation rims and non-fluorescing AOM (hebamorphinite, H). 500x, reflected white light; **C2**, Sample E 48485. Funginite. 500x, reflected white light.
- D) Sample E 48467 (well B) from 2688 m depth. Strong laminated sample with abundant lamalginite and fluoramorphinite. 250x, blue light excitation.
- E) Sample E 48455 (well D) from 2638 m depth. Irregular, weak laminations with abundant fluoramorphinite. 250x, blue light excitation.

4.5 Source Rock Screening

4.5.1 Whole Rock Samples

Screening analyses were performed in order to gain a rapid overview of organic richness, quality and maturity, and to select a smaller representative sample population for further detailed analyses. For this purpose, TOC and TS contents were determined and Rock-Eval pyrolysis experiments were performed. A tabulation of results is provided in Tab. 4.5.

The examined samples have TOC contents between 0.2 and 17.6%. The most frequent values are between 2.0 and 5.0%. The highest on average TOC values with 8.2% were determined for the GS sub-unit, the lowest with 3.3% on average for the Es3 member. Maximum TS values up to 3.5% were observed in samples from the Lei and Gao area. Stratigraphically, the highest TS contents were measured on samples from the Shale I/ Shale II sub-units and from the Es3 member. A plot of the pyrolysable hydrocarbon yield versus pyrolysable carbon dioxide yield, both normalised to TOC can be used to distinguish

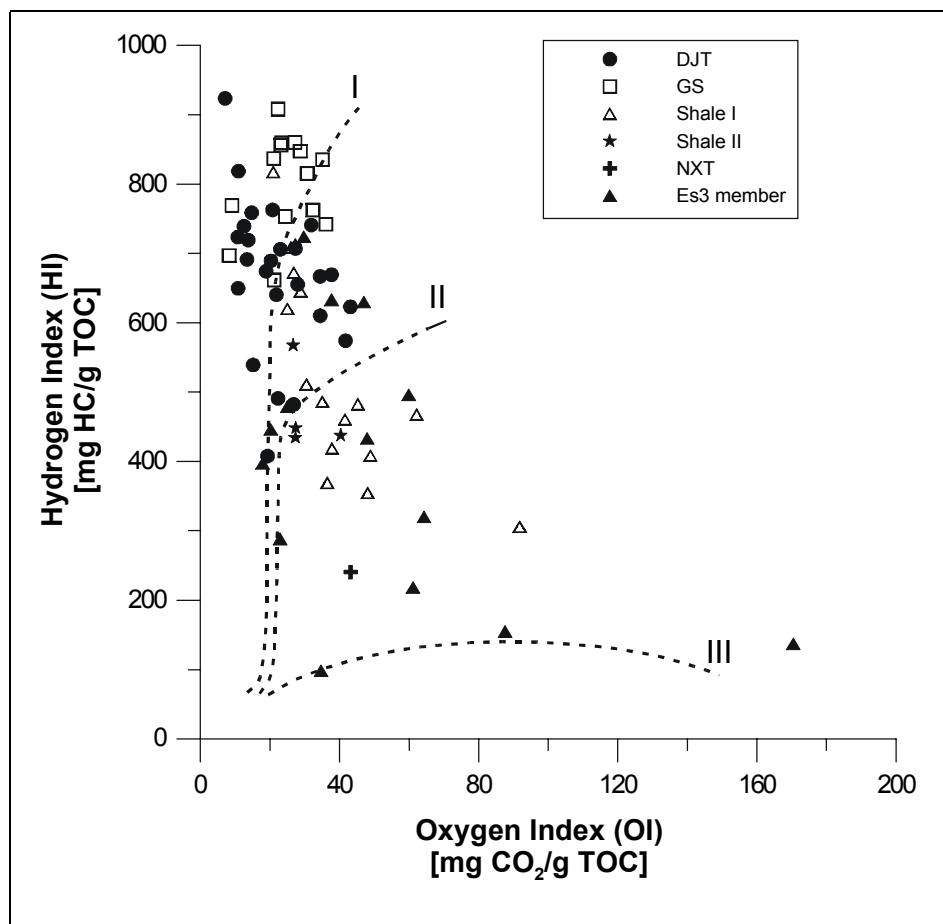


Fig. 4.13. Hydrogen Index (HI) versus Oxygen Index (OI) values for the analysed sample set.

E.nr.	Well	Member	Sub-unit	Depth [m]	TOC [%]	TS [%]	S1	S2	Tmax	PI	HI	OI
							[mg HC/g Probe]	[mg HC/g Probe]				
48456	B	Es3	?	1932	2.8	0.7	0.2	9.0	432	0.02	320	64
48457	B	Es3	?	1933	2.2	3.5	0.1	3.4	427	0.02	155	88
48458	B	Es3	?	1933	2.1	0.6	0.1	2.9	430	0.03	137	170
48477	O	Es3	?	2471	1.7	0.1	0.2	4.9	432	0.03	288	23
48478	O	Es3	?	2555	2.8	1.9	0.3	11.1	431	0.03	397	18
48479	O	Es3	?	2556	3.6	2.6	0.5	16.1	430	0.03	446	20
48490	G	Es3	?	2165	5.3	1.9	0.4	25.2	424	0.02	479	25
48493	K	Es3	?	1600	2.8	0.1	9.8	19.9	431	0.33	724	30
48494	K	Es3	?	1455	7.5	2.3	1.2	47.4	419	0.03	633	38
48495	K	Es3	?	1550	4.2	1.1	0.6	18.0	421	0.03	433	48
48496	V	Es3	?	1757	4.0	3.0	0.5	19.9	426	0.02	496	60
48497	U	Es3	?	1882	5.1	0.5	2.6	31.8	420	0.08	630	47
48499	F	Es3	?	2060	1.6	0.5	0.1	3.4	426	0.04	218	61
48508	W	Es3	?	2248	1.0	0.9	0.0	1.0	428	0.04	98	35
48448	D	Es4	DJT	2571	5.3	0.8	0.9	38.3	438	0.02	723	11
48449	D	Es4	DJT	2579	6.1	0.4	1.5	46.3	439	0.03	759	15
48450	D	Es4	DJT	2589	6.0	0.9	0.9	49.1	442	0.02	819	11
48451	D	Es4	DJT	2591	4.0	1.1	0.9	27.0	437	0.03	674	19
48452	D	Es4	DJT	2594	4.6	0.3	1.0	34.1	440	0.03	741	32
48453	D	Es4	DJT	2595	6.9	0.6	0.6	49.6	438	0.01	719	14
48454	D	Es4	DJT	2610	5.4	0.5	1.2	37.2	436	0.03	689	20
48455	D	Es4	DJT	2638	4.2	0.4	1.4	29.7	429	0.04	707	27
48459	B	Es4	Shale II	2424	2.9	1.3	0.5	12.6	432	0.04	435	27
48460	B	Es4	Shale II	2426	2.7	1.4	0.4	12.1	435	0.03	448	27
48461	B	Es4	Shale II	2431	2.7	1.5	0.6	11.8	431	0.05	438	40
48462	B	Es4	Shale II	2446	4.2	2.6	1.0	23.8	431	0.04	567	27
48463	B	Es4	DJT	2512	3.5	0.8	4.0	20.1	427	0.17	574	42
48464	B	Es4	DJT	2524	6.8	0.7	1.9	50.3	435	0.04	739	13
48465	B	Es4	DJT	2526	3.6	0.6	2.7	22.0	429	0.11	610	34
48466	B	Es4	DJT	2580	2.6	0.1	8.7	17.4	429	0.33	669	38
48469	B	Es4	DJT	2580	8.7	1.8	7.1	56.5	437	0.11	650	11
48467	B	Es4	GS	2688	8.0	0.8	2.0	61.5	442	0.03	769	9
48468	B	Es4	GS	2692	3.5	1.8	0.7	23.2	440	0.03	662	21
48470	J	Es4	Shale I	1462	2.6	1.0	0.1	9.2	433	0.01	355	48
48471	J	Es4	Shale I	1476	4.5	0.2	0.2	23.0	436	0.01	511	31
48472	J	Es4	Shale I	1481	7.4	0.6	0.5	45.9	435	0.01	620	25
48473	J	Es4	Shale I	1488	8.9	0.7	0.8	63.4	437	0.01	713	27
48474	J	Es4	Shale I	1490	5.6	1.2	1.3	39.7	428	0.03	709	26
48475	J	Es4	Shale I	1492	6.2	0.5	1.6	50.7	428	0.03	817	21
48476	J	Es4	Shale I	1498	2.2	0.2	0.2	10.3	438	0.02	468	62
48480	E	Es4	DJT	2735	4.2	2.0	1.7	20.6	431	0.08	491	22
48481	E	Es4	DJT	2796	7.2	1.1	3.3	49.8	433	0.06	691	13
48482	E	Es4	DJT	2792	6.0	0.6	3.1	38.4	436	0.07	640	22
48483	C	Es4	DJT	2332	3.5	0.3	1.0	22.9	435	0.04	655	28
48484	C	Es4	DJT	2335	3.8	1.4	1.1	25.6	434	0.04	667	34
48485	C	Es4	DJT	2342	3.7	0.7	1.5	23.1	428	0.06	623	43
48486	C	Es4	DJT	2360	5.6	0.5	0.9	39.5	430	0.02	706	23
48487	C	Es4	DJT	2385	5.3	1.0	2.7	40.4	428	0.06	763	21
48488	C	Es4	DJT	2392	2.8	2.2	0.4	15.3	433	0.03	539	15
48489	C	Es4	DJT	2396	2.5	0.5	0.2	10.0	434	0.02	408	19
48491	G	Es4	?	2665	5.5	1.6	1.8	38.5	439	0.04	704	14
48492	G	Es4	?	2818	4.1	1.0	1.0	28.0	436	0.04	681	25
48498	H	Es4	?	2722	5.0	1.3	0.9	36.2	440	0.02	719	11
48500	F	Es4	?	2414	7.3	0.0	0.8	60.7	437	0.01	836	11
48501	I	Es4	?	2186	3.4	0.5	0.7	22.2	429	0.03	661	22
48502	L	Es4	?	1357	8.8	1.5	1.5	49.9	425	0.03	566	34
48503	L	Es4	?	2533	2.0	0.7	0.2	5.4	432	0.04	274	42
48504	P	Es4	?	2116	4.5	-	2.0	34.4	437	0.05	769	19
48505	M	Es4	GS	1847	7.0	-	2.4	51.6	424	0.04	742	36
48506	N	Es4	?	2301	4.7	0.5	1.5	32.5	428	0.04	692	33
48507	N	Es4	?	2512	3.4	0.2	0.5	22.3	438	0.02	666	20
48509	T	Es4	?	2570	1.7	0.2	0.1	3.0	433	0.03	176	12

Tab. 4.5. Organic carbon, sulphur and Rock-Eval data of all samples analysed.

E.nr.	Well	Member	Sub-unit	Depth [m]	TOC [%]	TS [%]	S1	S2	Tmax	PI	HI	OI
							[mg HC/g Probe]	[mg HC/g Probe]				
48511	R	Es4	?	1818	1.2	0.1	0.2	6.0	435	0.04	494	25
48512	S	Es4	?	2209	2.6	0.5	0.2	10.6	430	0.02	408	22
48513	S	Es4	NXT	2490	0.5	1.0	0.1	1.2	429	0.05	241	43
48514	S	Es4	GS	2312	4.7	0.9	0.7	33.0	436	0.02	697	8
48515	Q	Es4	?	1160	4.0	0.4	0.3	18.8	429	0.02	469	28
48517	A	Es4	DJT	1252	3.2	0.7	10.6	15.2	422	0.41	482	27
48518	A	Es4	DJT	1288	7.7	0.1	12.5	71.1	435	0.15	924	7
48519	A	Es4	Shale I	1306	2.3	0.6	0.8	7.0	424	0.11	306	92
48520	A	Es4	Shale I	1309	3.3	0.4	0.3	13.4	428	0.02	409	49
48521	A	Es4	Shale I	1314	4.3	0.3	0.3	20.9	431	0.02	483	45
48522	A	Es4	Shale I	1318	4.3	0.3	0.4	21.1	428	0.02	486	35
48523	A	Es4	Shale I	1322	3.7	0.9	0.3	17.1	427	0.02	461	42
48524	A	Es4	Shale I	1325	3.9	0.7	0.4	16.1	424	0.02	419	38
48525	A	Es4	Shale I	1329	4.2	1.0	0.4	15.5	426	0.03	369	36
48526	A	Es4	Shale I	1333	7.6	0.9	0.9	49.3	431	0.02	645	29
48527	A	Es4	Shale I	1340	6.0	1.4	1.1	40.5	429	0.03	672	27
48528	A	Es4	GS	1346	11.5	0.7	4.5	87.7	413	0.05	763	32
48529	A	Es4	GS	1346	7.4	0.4	1.4	60.5	433	0.02	815	31
48530	A	Es4	GS	1347	9.4	0.9	2.1	78.8	431	0.03	835	35
48531	A	Es4	GS	1348	9.9	2.5	1.7	85.1	433	0.02	860	27
48532	A	Es4	GS	1348	11.7	1.6	2.4	98.7	431	0.02	847	29
48533	A	Es4	GS	1351	10.1	0.7	1.7	86.5	433	0.02	856	23
48534	A	Es4	GS	1358	17.6	1.6	4.9	150.9	433	0.03	860	23
48535	A	Es4	GS	1359	6.8	0.6	1.2	57.2	434	0.02	837	21
48536	A	Es4	GS	1372	4.3	0.8	0.8	32.2	432	0.02	753	24
48537	A	Es4	GS	1375	11.5	1.2	3.6	104.5	430	0.03	908	22
48538	A	Es4	basement	1394	0.2	0.7	0.0	0.1	420	0.13	43	203
48539	A	Es4	basement	1405	0.3	0.2	0.0	0.2	427	0.18	74	9

Tab. 4.5 (cont.). Organic carbon, sulphur and Rock-Eval data of all samples.

between the kerogen types I, II and III (Fig. 4.13). As reported by Meyers & Lallier-Vergès (1999) type I OM in lake sediments is often amorphous, hydrogen rich and originates from the microbial biomass or the waxy coatings of land plants. The intermediate type II derives from algae. Type III OM is oxygen rich and originates mainly from terrigenous OM. However, if a type I or type II OM is reworked or oxidised in the water column it can take also the characteristics of a type III kerogen. While type I OM is highly oil-prone, type III OM which contains mainly aromatic and hetero-structures is mainly gas-prone (Hunt, 1996).

The Hydrogen Index (HI) values of the whole rock samples are in the range between 43 and 908 mg HC/g TOC. The most frequent values are between 600 and 900 mg HC/g TOC. The highest on average HI values were determined for samples from the GS (800 mg HC/g TOC on average) and DJT sub-unit (666 mg HC/g TOC on average). Similar high HI values were found in other lacustrine shales. Lamalginite rich layers of the Laney Shale (Green River Formation) can reach HI values up to 900 mg HC/g TOC (Horsfield *et al.*, 1994). A high petroleum potential of oil shales from the Mae Sot Basin, Thailand is expressed by HI values between 450 and 1050 mg HC/g TOC (Curiale & Gibling, 1994). The Oxygen-Index (OI) values are generally low with most frequent values between 20 and 30 mg CO₂/g TOC (Fig. 4.13). Extremely high OI values are artefacts and result from thermal breakdown of carbonate minerals in whole rock samples. The source rocks analysed in the present study

contain mainly hydrogen-rich, oil prone kerogen, denoting the presence of predominantly aquatic (algal/bacterial) OM (Fig. 4.13). A few values are consistent with the presence of type II to III kerogen, comprising OM of mixed aquatic/terrestrial origin or reworked/oxidised OM.

The highest PI values were determined for samples impregnated with bitumen (e.g. E 48517). These samples contain high percentages of the uncommon feldspar buddingtonite, a correlation discussed in an earlier section (4.3.3.3). The other samples have most frequent PI values between 0.01 and 0.06. Maturation can be obtained from Rock-Eval pyrolysis, where Tmax is the temperature at which the maximum hydrocarbon generation occurs (Tissot & Welte, 1984, p. 510). The Tmax is both kerogen type and maturity dependant. Tmax data imply that the sample set is thermally immature (Fig. 4.14). Very high Tmax values around 442°C reflect a predominantly algal OM, rather than high maturities (Tissot *et al.*, 1987). A reliable maturity assessment based on Tmax values is very problematic because the Tmax changes very little with maturity for type I kerogens with a polymethylene structure.

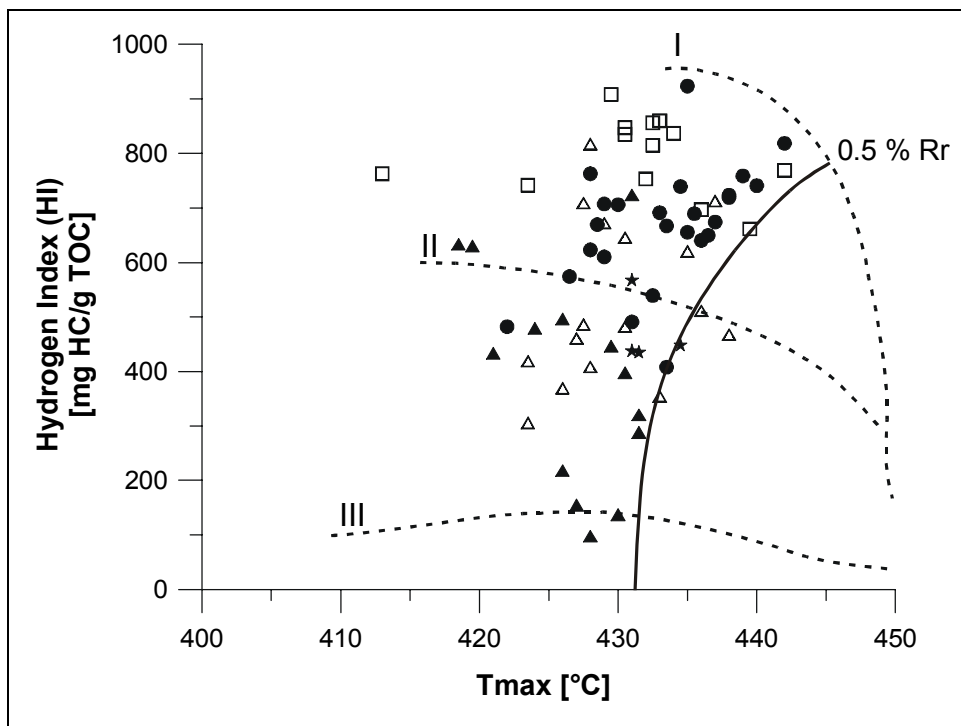


Fig. 4.14. Hydrogen Index versus Tmax. Legend as in Fig. 4.13.

4.5.2 Kerogen Concentrates

Kerogen is defined as the part of the OM that is insoluble in the most common solvents (Tissot & Welte, 1984). It is a complex function of its biochemical source-related composition and modifications depending on facies and thermal evolution. Based on whole rock sample screening and organic petrology, 16 kerogen concentrates from extracted source rocks were prepared at the Houston Advanced Research Centre, U.S. for Py-GC-FID and Py-GC-MS experiments. Prior to these analyses a screening using TOC, TS and Rock-Eval was performed. The results are listed in Tab. 4.6. The HI values of the kerogen concentrates analysed range from 642 to 998 mg HC/g TOC. Highest HI values were determined for the laminated and lowest for the non-laminated samples. All OI values are low with values between 10 and 36 mg CO₂/g TOC. Kerogen concentrates were used for analytical pyrolysis to prevent influences of the mineral matrix which can occur during laboratory pyrolysis at high temperatures because of catalytic effects of clay minerals, carbonates or pyrite (Horsfield & Douglas, 1980).

E.nr.	Depth [m]	Well	Member	Sub-unit	TOC [%]	TS [%]	Tmax °C	HI [mg HC/g TOC]	OI [mg CO ₂ /g TOC]	δ ¹³ C [‰ PDB]	H/C atomic	O/C atomic
48465	2526	B	Es4	DJT	47.2	3.1	425	770	12	-28.48	1.30	0.08
48467	2687	B	Es4	DJT	76.2	1.3	432	950	10	-28.83	1.35	0.05
48480	2735	E	Es4	DJT	46.7	1.1	425	733	36	-24.92	-	-
48485	2342	C	Es4	DJT	56.7	3.0	425	793	11	-29.79	1.31	0.08
48494	1450	K	Es3	?	52.3	6.8	414	792	24	-21.09	1.28	0.16
48502	1357	L	Es4	?	59.6	2.0	422	859	23	-24.79	1.37	0.13
48505	1847	M	Es4	GS	70.5	1.6	418	884	14	-26.59	1.46	0.09
48514	2312	S	Es4	GS	66.6	4.5	428	836	10	-29.54	1.42	0.09
48517	1252	A	Es4	DJT	50.1	13.6	425	642	19	-26.92	1.20	0.14
48519	1306	A	Es4	Shale I	50.6	10.5	423	870	23	-27.26	1.40	0.15
48520	1309	A	Es4	Shale I	58.6	6.7	425	823	24	-26.16	1.37	0.15
48525	1329	A	Es4	Shale I	63.7	5.7	420	756	23	-24.71	1.36	0.14
48527	1340	A	Es4	Shale I	63.3	5.9	424	884	17	-27.91	1.48	0.13
48529	1346	A	Es4	GS	72.5	2.2	425	959	23	-29.12	1.49	0.10
48532	1348	A	Es4	GS	65.8	6.8	426	960	27	-27.71	1.48	0.11
48537	1375	A	Es4	GS	70.0	3.8	427	998	16	-27.69	1.61	0.08

Tab. 4.6. Organic carbon, sulphur, elemental and Rock-Eval data of the Liaohe kerogen concentrates.

On the other hand it has been reported that the kerogen isolation method has a hydrolysing effect on the OM of sediments which is stronger at low levels of maturation (Durand & Nicaise, 1980). Results from Rock-Eval analysis (Tabs. 4.5 and 4.6) indicate that differences between whole rock samples and kerogen concentrates are large. HI values show an increase after kerogen concentration which is largest for the kerogens E 48519 and E 48525 of more than 100%. A possible explanation is the retention of heavier hydrocarbons in the mineral matrix as reported before by Espitalié *et al.* (1980). Especially the clay mineral illite is

very efficient to retain hydrocarbons but also others such as expandable clays or kaolinite. Notably, all of them are present in the Liaohe rocks.

Atomic H/C and O/C ratios were determined and plotted in a van Krevelen diagram (Fig. 4.15). It illustrates that the chemical composition of the OM in the different stratigraphic units is relatively heterogeneous and that major differences between the kerogens occur due to variations of the atomic O/C ratio. Especially the GS concentrates have high atomic H/C ratios up to 1.61 and low atomic O/C ratios which points to OM that is excellent to generate liquid hydrocarbons at higher stages of thermal maturity. Based on the concept by Jones (1987), which combines results from elemental data, Rock-Eval pyrolysis and microscopy they plot within the algal, amorphous and anoxic organic facies fields A and AB (Fig. 4.15). By comparison, samples from the Shale I sub-unit and Es3 member have higher O/C atomic ratios and plot within the fields B and BC typical for OM mixtures and/or more oxic depositional conditions. Samples from the DJT suggest slightly higher maturities.

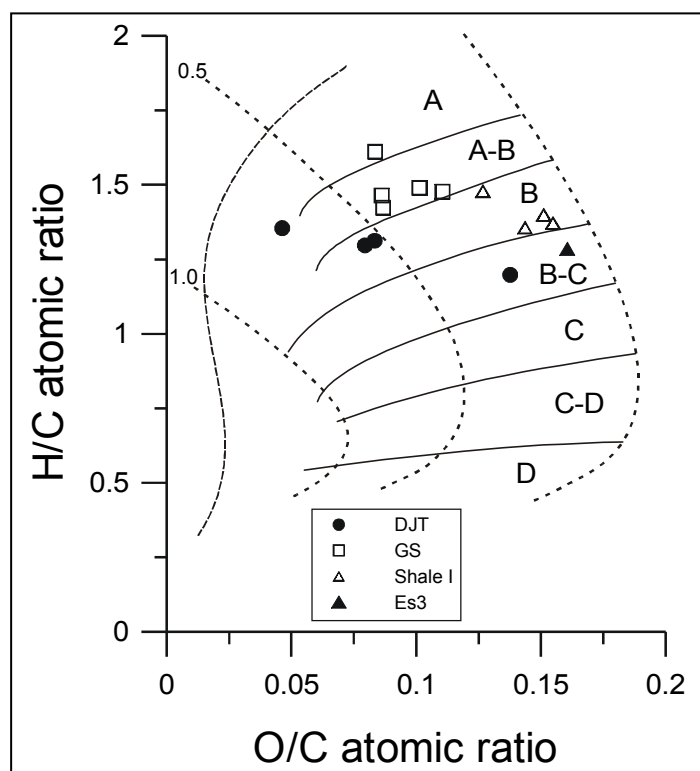


Fig. 4.15. Van Krevelen diagram for the analysed kerogen concentrates; organic facies fields (A-D) adopted from Jones (1987). Organic facies: A, anoxic, lamalginite or telalginite and AOM; AB, anoxic-dysoxic, usually telalginite-rich AOM; B, anoxic-dysoxic, AOM with minor terrestrial; B-C; some oxidation, complex mixtures; C, some oxidation, dominantly terrestrial; C-D, reworked, degraded and partially oxidised OM; D, reworked, strongly oxidised OM. Numbers indicate vitrinite reflectance values (% Rr).

4.5.3 Stable Carbon Isotopes of Kerogens

The isotopic composition of the carbon source and the dynamics of carbon assimilation during photosynthesis determine the carbon isotopic composition of OM in lake sediments. Photosynthetic uptake of CO₂ leads to fractionation of carbon isotopes. Photosynthetic plants discriminate against ¹³C and incorporate carbon into OM using the C₃, C₄ and CAM pathway. C₃ plants preferentially take up ¹²C with an isotopic discrimination that averages -20‰ (O'Leary, 1988). The C₄ pathway produces a shift of about -7‰, whereas discrimination in the CAM pathway can vary from -4 to -20‰. OM produced from atmospheric CO₂ by C₃ plants has an average δ¹³C of approx. -28‰ and by those using the C₄ pathway approx. -14‰. If phytoplankton (C₃) utilises dissolved CO₂, the OM produced is isotopically indistinguishable from OM produced by C₃ plants in the watershed. However, other factors such as the availability of CO₂ impact the carbon isotopic composition of algal OM (e.g. Hollander & McKenzie, 1991). In this regard, differences in the δ¹³C values of OM in lake sediments deposited at different times provide information about OM sources and paleoenvironmental changes.

Typical carbon isotope values of different sources are displayed in Fig. 4.16 together with the δ¹³C signatures of OM in the Liaohe and some other lacustrine kerogens. Large variations of the isotopic compositions between -29.6‰ (E 48514) and -21.1‰ (E 48494) were determined, which suggest variable environmental conditions (Tab. 4.6). Lacustrine kerogens from the Mae Sot basin exhibit similar δ¹³C signatures (Curiale & Gibling, 1994), but significantly more negative values were determined for the Green River oil shale (Dean & Anders, 1991). Based on microscopic observations, higher plants can be mainly excluded as a source to the OM in the studied sequences.

The laminated, lamalginite and fluoramorphinite containing samples from the GS sub-unit are more depleted in δ¹³C (mean value -28.3‰) relative to the other samples. Thus, samples with high HI values are characterised by more negative carbon isotope values, which is exact the opposite trend reported from the Mae Sot Basin (Curiale & Gibling, 1994), where a high primary productivity led to reduced pCO₂ in the water column. In the Western Depression, the heaviest value was measured for a partially laminated kerogen from the Es3 member in the Gao area (E 48494). *B. braunii* rich kerogens from the Shale I sub-unit have identical values as sediments rich in this algal species (Huang *et al.*, 1999 and references therein).

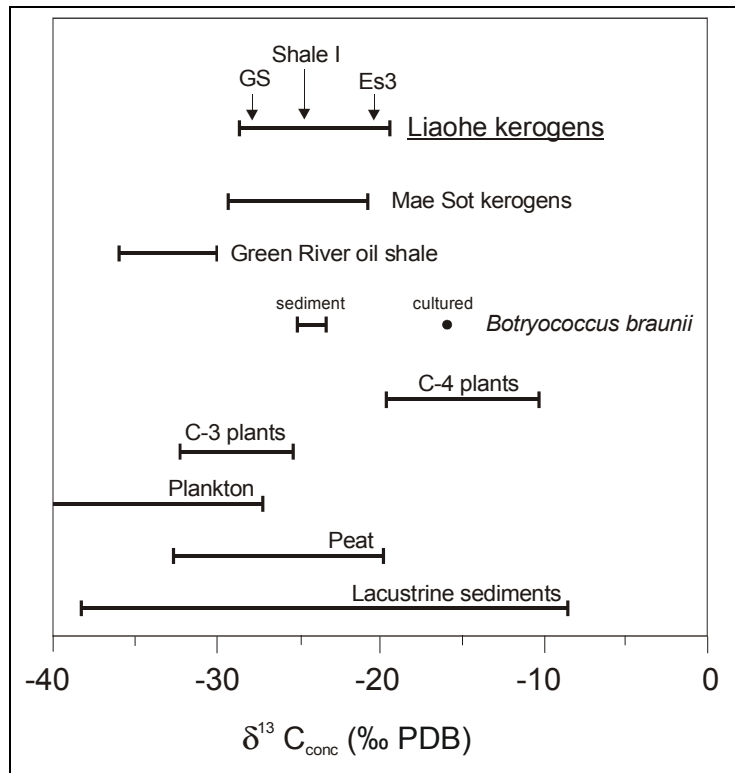


Fig. 4.16. Carbon isotope values of the Liaohe kerogens ($\delta^{13}C_{conc}$) and other lacustrine sediments and oil shales; data from Dean & Anders (1991), Curiale & Gibling (1994) and Huang et al. (1999).

Points to Remember – Source Rock Screening

Most of the source rock samples from the Western Depression of the Liaohe Basin are located along the type I and type II path which points to the presence of predominantly bacterial and algal OM. Some samples have a mixed origin or the OM was reworked/oxidised. Based on their Tmax values they can be classified as immature. The laminated source from the GS and in part those from the DJT sub-unit contain OM that is hydrogen rich and highly oil prone. The quality and quantity of the OM in the Shale I, Shale II and in the Es3 member is lower and the measured carbon isotope values are more positive than those from the GS and DJT.

4.6 Kerogen Characterisation

Geochemical screening analyses are useful to describe kerogen in a general way. However, it was demonstrated previously that parameters such as HI or the atomic H/C ratio do not uniquely describe the molecular structure of a kerogen (e.g. Horsfield, 1989; Larter & Horsfield, 1993). As reviewed by Horsfield (1997) the overall composition of the pyrolysate reflects the structure of the kerogen. The main goal of this chapter is to characterise the source rock kerogen by pyrolysis-gas chromatography (Py-GC-FID) and pyrolysis-gas chromatography-mass spectrometry (Py-GC-MS). With these techniques, it is possible to get detailed information of the kerogen structure itself and define in more detail the relationship between the sedimentary environment and organofacies. A detailed listing of the gross pyrolysate composition and individual compound yields is given in Appx. B.

4.6.1 Structural Moieties

A correlation between pyrolysates and the petroleum composition on the basis of the average chain length distributions of alkyl-moieties provides a framework to classify different forms of sedimentary OM and to obtain information about the source depositional environment (Horsfield, 1989). The large ternary diagram in Fig. 4.17 has at its apices the proportions of (1) total resolved pyrolysate in the C_1 to $n-C_5$ range, (2) summed C_6 to C_{14} n -alkanes and n -alk-1-enes, and (3) summed C_{15+} n -alkanes and n -alk-1-enes. Most of the pyrolysates, especially those from the GS sub-unit are rich in long chain n -alkanes and n -alk-1-enes (Tab. 4.7 and Fig. 4.17) and belong to the high-wax paraffinic crude oil generation facies as defined using pyrolysates of the lacustrine Green River Shale. Shorter chain lengths characterise the kerogen pyrolysates from the DJT and Shale I sub-unit. Notably, pyrolysates from the Gao area already plot in or at the border of the high-wax, paraffinic-naphthenic-aromatic crude oil facies field which usually occurs in lower delta plain and inner shelf environments (Tissot & Welte, 1984). It can be concluded from this that the depositional environment exert a major influence on the chain lengths distribution.

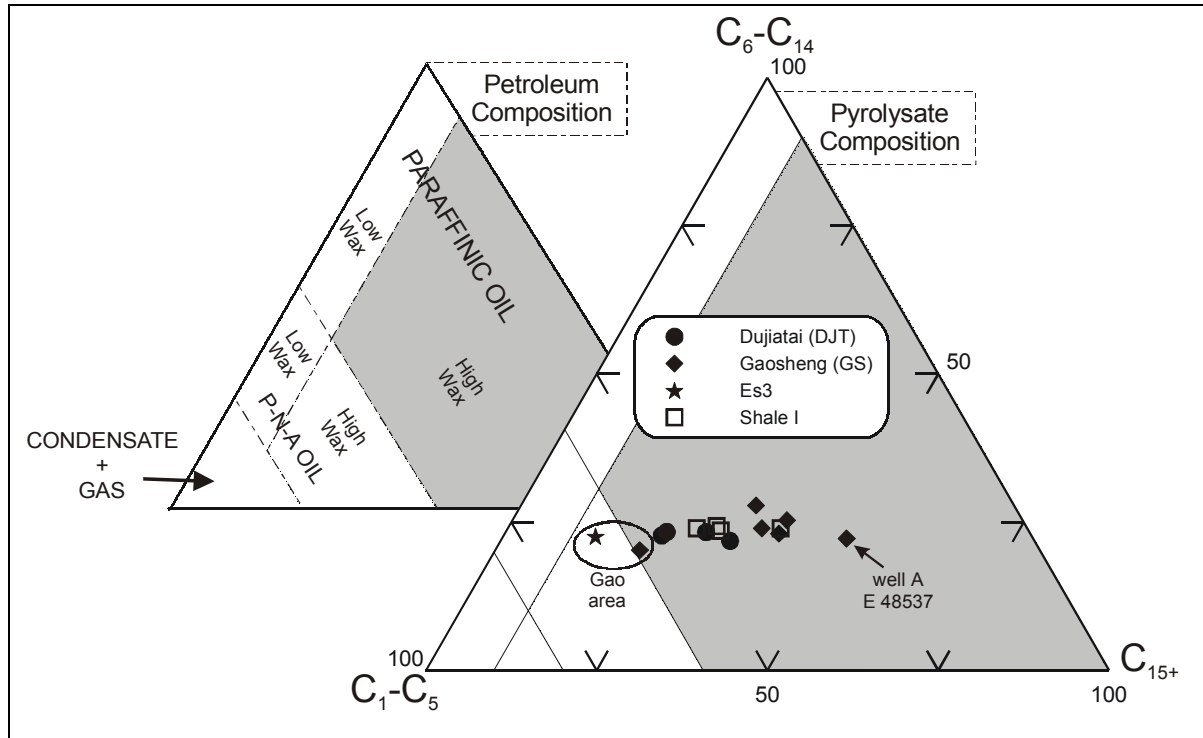


Fig. 4.17. Kerogen typing according to the chain length distribution of total C_1-C_5 resolved pyrolysate, C_6-C_{14} n -alkanes plus n -alk-1-enes and C_{15+} n -alkanes plus n -alk-1-enes derived from one-step Py-GC-FID. Petroleum compositions are shown in the background ternary diagram; modified from Horsfield (1989).

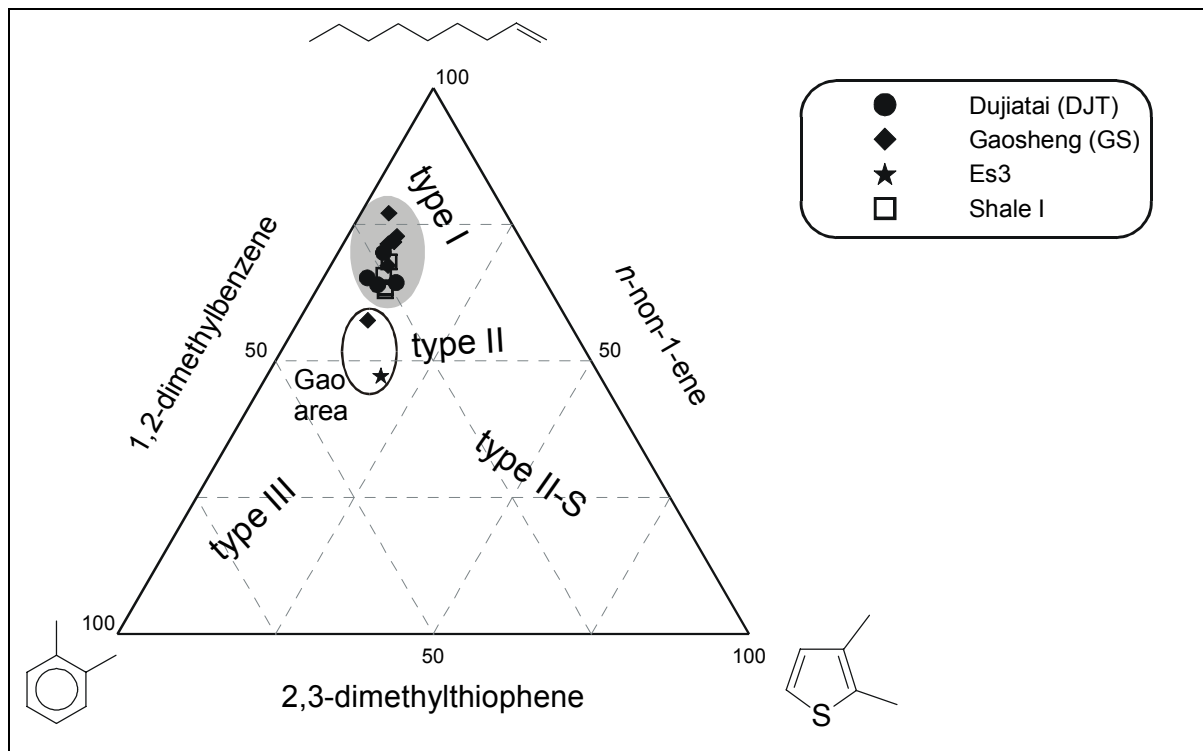


Fig. 4.18. Kerogen typing on the basis of sulphur-containing, aromatic and alkyl groups from Py-GC-FID; modified from Eglinton et al. (1990).

E.nr.	Strat.	"chain length"			"organic sulphur"		
		C ₁ -C ₅	C ₆ -C ₁₄	C ₁₅ +	<i>n</i> -non-1-ene	1,2-dimethylbenzene	2,3-dimethylthiophene
E48465	DJT	54.1	22.7	23.2	64.4	23.7	11.9
E48467	DJT	37.8	27.8	34.4	77.0	18.5	4.5
E48480	DJT	53.1	23.3	23.6	63.9	26.8	9.2
E48485	DJT	47.3	23.3	29.4	69.8	23.0	7.2
E48494	Es3	63.9	22.6	13.5	47.3	34.6	18.0
E48502	?	47.9	23.1	28.9	63.9	24.7	11.4
E48505	GS	58.6	20.3	21.2	57.4	31.7	10.9
E48514	GS	38.9	23.9	37.2	71.4	21.4	7.1
E48517	DJT	44.6	21.8	33.7	65.2	27.8	6.9
E48519	Shale I	45.3	24.3	30.4	65.7	25.0	9.3
E48520	Shale I	45.1	23.5	31.4	63.4	25.9	10.7
E48525	Shale I	48.4	24.0	27.7	62.9	26.2	10.9
E48527	Shale I	36.1	23.9	40.0	68.1	23.0	8.9
E48529	GS	34.5	25.3	40.2	71.8	20.3	7.9
E48532	GS	36.8	23.0	40.2	67.5	23.5	9.1
E48537	GS	27.3	22.2	50.5	72.9	19.4	7.8

Tab. 4.7. Kerogen typing according to chain length distribution and organic sulphur compounds. The table provides data used in Figs. 4.17 and 4.18.

Sulphur-containing groups can have a strong impact on hydrocarbon generation. If sulphur has been incorporated into the kerogen structure the thermal stability of the macromolecular OM decreases and petroleum generation can take place at lower maturities (e.g. Orr, 1986). Eglinton *et al.* (1990) established a framework to distinguish kerogen types according to the pyrolysate components *n*-non-1-ene, 1,2-dimethylbenzene and 2,3-dimethylthiophene (Fig. 4.18). The yield of organic sulphur compounds formed on pyrolysis is low in comparison to other organic-rich source rocks from marine environments. The 2,3-dimethylthiophene contribution ranges from 4.5 to 18.0% (Tab. 4.7) and is highest for a sample from the Gao area (Es3). All other pyrolysates have much higher aliphatic contributions and fall in the field typical of type I kerogens.

Using GC-fingerprints and quantitative parameters expressing bulk compositional characteristics based on *n*-alkane/*n*-alk-1-ene doublets, isoprenoids, phenols, concentrations of alkylbenzenes and the aromaticity, four families could be recognised. The following ratios were calculated to show variabilities. A tabulated listing of the calculated parameters is shown in Tab. 4.8.

- the **wax-index (WI)** of a kerogen describes the relative amount of *n*-alkanes and *n*-alk-1-enes in the non-gaseous pyrolysate ($\sum C_{20+}/\sum C_{5+}$) and was previously used by Tegelaar & Noble (1993).
- the **phenol ratio (PhR)** is defined as the ratio of phenol vs. *n*-C_{11:0} plus *n*-C_{11:1}.

- the **isoprenoid ratios (IpR 1+2)** are defined as C₁₃ to C₂₀ isoprenoids vs. *n*-alkanes and *n*-alk-1-enes ($\sum C_{5+}$) and prist-1-ene vs. *n*-C_{11:0} plus *n*-C_{11:1}, the latter was introduced by Curry & Simpler (1987).
- the **alkylbenzene ratio (AbR)** is defined as the ratio of C₀-C₃ alkylbenzenes vs. *n*-alkanes and *n*-alk-1-enes ($\sum C_{5+}$).
- The **aromaticity** is defined as the ratio of selected aromatic hydrocarbons (C₀-C₂ alkylbenzenes plus C₀-C₁ alkylphenols plus C₀-C₁ alkyl-naphthalenes) vs. *n*-alkanes and *n*-alk-1-enes ($\sum C_{5+}$).

E.nr.	Sub-unit	WI [$\sum C_{20+}/\sum C_{5+}$]	PhR	IpR 1	IpR2	AbR	Aromaticity [Ar/(Ar+Al)]
E 48465	DJT	0.24	0.16	0.10	0.55	0.12	0.13
E 48467	DJT	0.30	0.06	0.04	0.12	0.05	0.06
E 48480	DJT	0.24	0.27	0.06	0.20	0.10	0.14
E 48485	DJT	0.29	0.33	0.07	0.34	0.08	0.12
E 48494	Es3	0.16	0.58	0.10	0.35	0.17	0.29
E 48502	?	0.30	0.23	0.05	0.19	0.08	0.12
E 48505	GS	0.27	0.30	0.16	0.68	0.18	0.18
E 48514	GS	0.38	0.14	0.04	0.24	0.05	0.07
E 48517	DJT	0.35	0.70	0.06	0.25	0.09	0.18
E 48519	Shale I	0.31	0.40	0.05	0.20	0.07	0.13
E 48520	Shale I	0.34	0.32	0.06	0.24	0.07	0.12
E 48525	Shale I	0.27	0.18	0.07	0.26	0.08	0.12
E 48527	Shale I	0.42	0.22	0.04	0.27	0.05	0.08
E 48529	GS	0.36	0.11	0.04	0.21	0.04	0.07
E 48532	GS	0.39	0.21	0.05	0.28	0.05	0.08
E 48537	GS	0.48	0.10	0.04	0.28	0.03	0.05

Tab. 4.8. Parameters applied for kerogen characterisation from one-step Py-GC-FID. Their definitions are given in the text and in Appx. D.

After applying these parameters, four pyrograms, one from the Gao area (well M), one from well B and two from well A, can be considered as representative end members. They are illustrated in Fig. 4.19. All traces are characterised by the presence of doublets of *n*-alk-1-enes and *n*-alkanes up to C₃₂ and a variety of mono- and di-aromatic as well as isoprenoid hydrocarbons. Sulphur containing components, namely alkylthiophenes, represent only a small fraction of the entire kerogen.

The kerogen sample **E 48467 (well B, GS, type D microscopy)** is characterised by the overwhelming dominance of *n*-alkane/*n*-alk-1-ene doublets over aromatic and isoprenoid pyrolysis products (Fig. 4.19 A). Aromaticity and the isoprenoid ratios are extremely low (Tab. 4.8). These findings, combined with the fact found that the HI value is high (950 mg HC/g TOC) are consistent with the presence of predominantly polymethylene moieties in the kerogen structure originating either from a highly aliphatic biomacromolecule (algaenan) present in the outer cell walls of algae (e.g. Goth *et al.*, 1988; Derenne *et al.*, 1997) or from lipids grafted to the kerogen by recondensation reactions (Larter & Douglas, 1980). Curry & Simpler (1987) stated that the IpR 2 is significantly lower in pyrolysates of kerogens from highly anoxic depositional environments due to an increased preservation of aliphatic moieties.

Kerogens from the Gao area (E48494, E48505) have a higher aromaticities and isoprenoid concentrations compared with the other samples (Tab. 4.8). This points to a more heterogeneous kerogen structure (Fig. 4.19 B). A characteristic feature of the kerogen from sample **E 48505 (well M, GS, type E microscopy)**, distinguishing it from the others, is the high contribution of C₁₃ to C₂₀ saturated and mono-unsaturated isoprenoid hydrocarbons with prist-1-ene as the dominant peak. Prist-1-ene may derive from several precursors. The phytol side chain of chlorophyll (Ishiwatari *et al.*, 1991) and tocopherols (Goossens *et al.*, 1984) are possibilities. Chappe *et al.* (1982) proposed that kerogen bound diphytanyl ethers of some species of methanogens yield prist-1-ene on pyrolysis which signifies that microbial input to the sediments was probably important in the Gao area. Chromans bound into kerogens may also be a source of prist-1-ene (Li *et al.*, 1995). Interestingly, abundant chromans were detected in the soluble OM of some sample in the Gao and Lei area (see section 4.7.5.1). Other likely candidates for prist-1-ene precursors are macromolecular bound aromatic carotenoids, which were detected in the soluble OM of sample E 48505 in high concentrations (*ibid.*). Experiments performed by Koopmans *et al.* (1999) on lacustrine sediments of the Green River oil shale indicated that the precursor of prist-1-ene might occur in sulphur- or in oxygen-bound form. Höld *et al.* (2001) also stated that sulphur-bound precursors can generate prist-1-ene upon pyrolysis. However, sulphur bound moieties are not important in the investigated kerogens from the Western Depression (Fig. 4.18).

The high concentration of 1,3-dimethylbenzene, 1,4-dimethylbenzene, 1,2,4-trimethylbenzene and 1,2,3-trimethylbenzene is another characteristic of the kerogen E 48505 (Fig. 4.19 B), which is also expressed by the high AbR (Tab. 4.8). Requejo *et al.* (1992) found C₀-C₄ alkylbenzenes of carotenoid origin in kerogen pyrolysates of Paleozoic source rocks from the Western Canada Basin. Hartgers *et al.* (1994a) demonstrated, that the structure of monoaromatic moieties in kerogens is biologically controlled. They proposed that a relatively high abundance of 1,3-dimethylbenzene, 1,4-dimethylbenzene and 1,2,3-trimethylbenzene is indicative of the presence of bound carotenoids (e.g. ββ-carotene) which have undergone aromatisation. The relative enhancement of 1,2,4-trimethylbenzene may be indicative of the incorporation of plastoquinones. These compounds are widely distributed in certain algae and cyanobacteria (Ratledge & Wilkinson, 1988). In the Liaohe kerogens 1,2,3,4-tetramethylbenzene was detected in smaller amounts. Hartgers *et al.* (1994b) showed that this compound is derived from macromolecular-bound isorenieratene. This carotenoid is specific for photosynthetic green sulphur bacteria (*Chlorobiaceae*) which are common in algal bloom initiated photic zone anoxia (Koopmans *et al.*, 1996). However, a more recent study indicated that an algal origin is also possible (Hoefs *et al.*, 1995).

The pyrogram of sample **E 48525 (well A, Shale I, type B microscopy)** is dominated by *n*-alkane/*n*-alk-1-ene doublets from C₆ to C₃₂ with no odd-over even predominance and a sub-maximum at C₁₇ followed by a smooth decrease (Fig. 4.19 C). Major branched compounds are C₁₃ to C₁₉ isoprenoid alkanes and alk-1-enes. Similar results for chemical structures of *Botryococcus*-rich algaenans were previously obtained by Kadouri *et al.* (1988) and Derenne *et al.* (1994). They provide an important input to kerogens *via* the selective preservation pathway (e.g. Largeau *et al.*, 1986; Derenne *et al.*, 1991). Since *Botryococcus*, from organic petrological studies, is known to contribute to this kerogen, the alkyl-containing pyrolysis products are likely to be derived from *Botryococcus* algaenan.

The kerogen from sample **E 48537 (well A, GS, type D microscopy)** is characterised by a high WI, visible by the high contribution of long-chain alkanes and alk-1-enes with a maximum at C₂₅ (Fig. 4.19 D). Similar long-chain alkyl units with a characteristic maximum at C₂₇ were observed in flash pyrolysates of algaenans from eustigmatophytes of the *Nannochloropsis* genus (Gelin *et al.*, 1997; Gelin *et al.*, 1999). The isoprenoids are dominated by prist-1-ene and the aromatic hydrocarbons are only present as minor constituents.

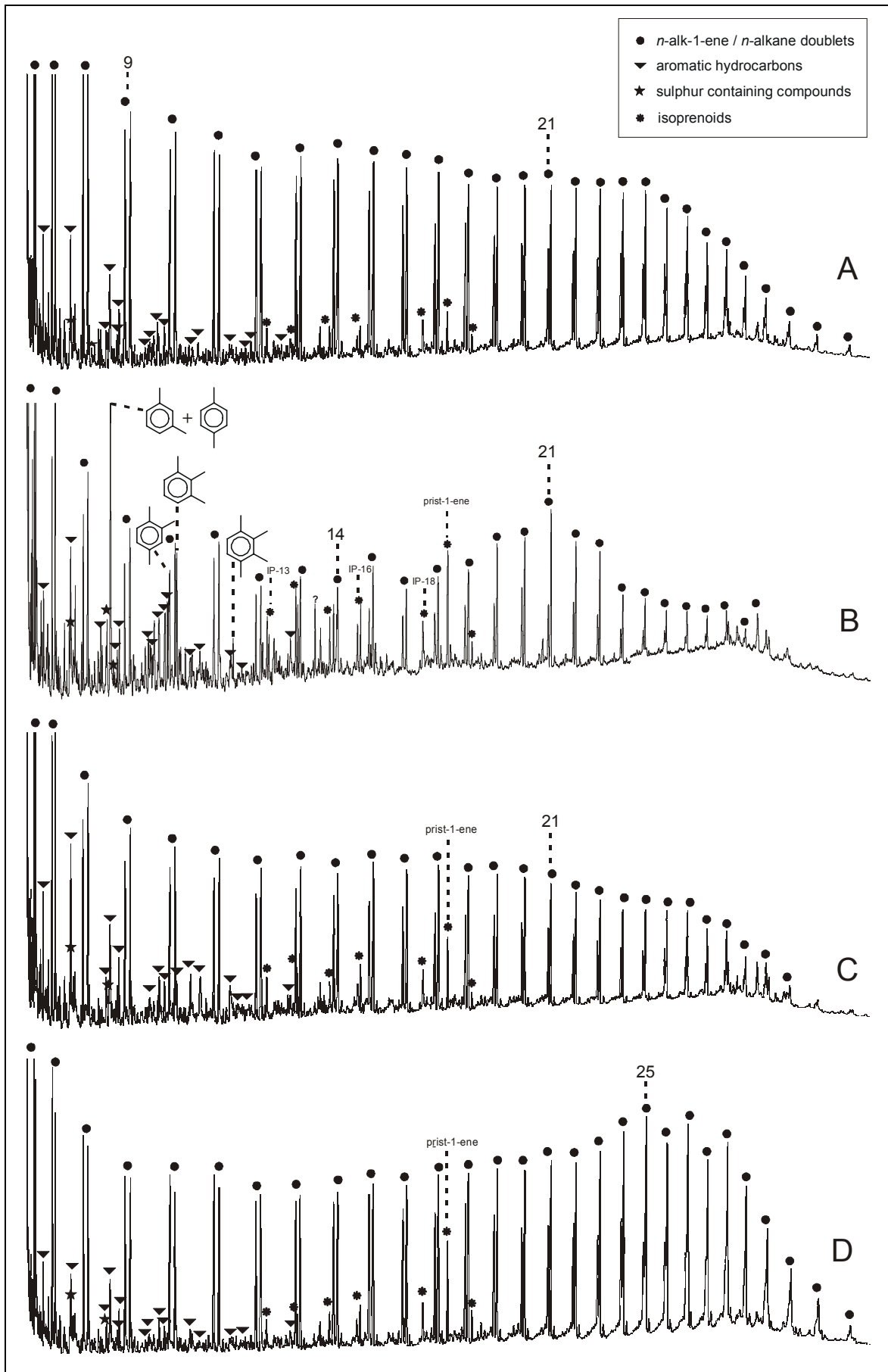


Fig. 4.19. Pyrolysis gas-chromatograms of typical representative kerogens from the Western Depression of the Liaohe Basin. Numbers indicate *n*-alkyl chain lengths. A, E 48467 (well B, GS); B, E 48505 (well M, GS); C, E 48505 (well A, Shale I); D, E 48537 (well A, GS).

4.6.2 Thermal Lability

The transformation of sedimentary OM via kerogen to oil and gas during burial is determined by reactions which are irreversible and controlled by chemical kinetics (Tissot & Welte, 1984). Many different types of chemical bonds are present in the investigated kerogens, for instance C-C, C-S, or C-O. Each of these different bonds has distinct rupture energies which vary according to neighbouring functional groups or chain length. Petroleum generation is the result of a large number of chemical reactions leading from kerogen to liquid bitumen. These reactions are governed by chemical kinetics and the formation of petroleum from a certain kerogen depends on the type, amount and distribution of bonds in its matrix. The distribution of **activation energies** and the pre-exponential factor describe the hydrocarbon generation characteristics of a given kerogen, according to the mathematical model from Schaefer *et al.* (1990). The breadth of the temperature range over which generation occurs is directly controlled by the activation energy distribution and thence kerogen heterogeneity.

Published geochemical results have indicated that the OM in most lacustrine kerogen samples contains a large proportion of aliphatic moieties, typical of polymethylene structures. A relatively narrow distribution of activation energies is typical (e.g. Tissot *et al.*, 1987; Tegelaar & Noble, 1993; Béhar *et al.*, 1997). In contrast, broader distributions have been found in type II and type III kerogens because of a wider variety of chemical bonds (e.g. Schenk *et al.*, 1997; Schenk & Horsfield, 1998). Concerning published information on the petroleum generation kinetics of lacustrine source rocks, a mean activation energy of 56 kcal/mole was found for a lacustrine kerogen from the Green River Shale of the Uinta Basin, with a single major energy (Burnham *et al.*, 1987; Tissot *et al.*, 1987). A similar, slightly lower value (54 kcal/mole) was observed in experiments by Béhar *et al.* (1997) and Tegelaar & Noble (1993). However, this is not always the case. Type I kerogens from the Green River Shale of the Washakie Basin displayed a broad distribution (Horsfield *et al.*, 1994). An extremely narrow distribution was also observed for a lacustrine Cretaceous type I kerogen from the Songliao Basin, NE China peaking between 55 and 58 kcal/mole (Zhou & Littke, 1999).

A total of 10 extracted source rock samples from the Es4 and Es3 member, from different areas and sub-units were selected for programmed-temperature pyrolysis with subsequent kinetic modelling of bulk petroleum generation. With this method the hydrocarbon generation characteristics of a given kerogen can be used to model its behaviour in geological time. Samples were pyrolysed at four different heating rates: 1, 15, 25 and 50 K/min. The best fit

between experimental and calculated formation rates were obtained with the activation energy distribution and pre-exponential factors shown in Fig. 4.20 for some selected samples.

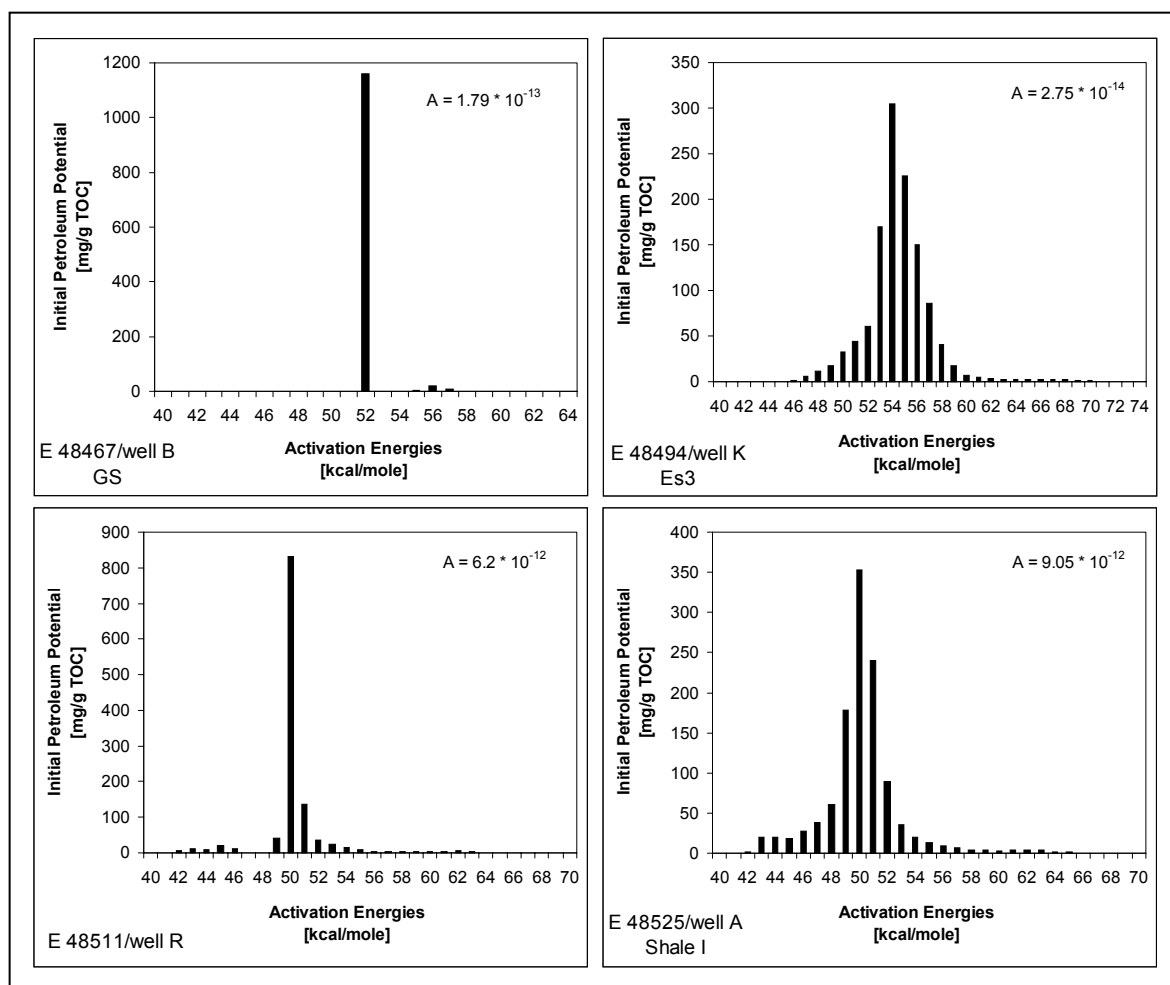


Fig. 4.20. Activation energy distributions as derived from pyrolysis experiments of selected source rock samples from the Western Depression. A is the pre-exponential factor (per second).

Concerning kerogen heterogeneity considerations, the expected narrow distribution was found in only two samples: E 48467 from well A in the Lei area and E 48511 from well R in the Tuo area (Fig. 4.20). This reflects a very homogenous mainly polymethylene kerogen structure (Béhar & Vandenbrouke, 1988). Results from Py-GC-FID support these observations (Fig. 4.19 D). Pepper & Corvi (1995) linked kinetic parameters and origin of the OM. They classified this tight activation energy distribution as a lacustrine organofacies, typical for kerogens rich in the remains of freshwater algae. Clay-rich samples from the Es3 and Shale I (E 48494, E 48525) show a very broad distribution of activation energies, which is indicative of a more heterogeneous kerogen structure with a variety of chemical bonds. Consequently, petroleum generation takes place over a wide maturity interval. For sample

E 48494, this is supported by high levels of aromatic moieties in the corresponding pyrolysate (Fig. 4.19 B). However, there is no direct link between kinetic parameters and aromatic groups in the kerogen of sample E 48525 (Fig. 4.19 C).

Geological Tmax values were calculated according to the respective bulk petroleum formation rates at 5.3 K/million years. Schenk & Horsfield (1998) concluded that petroleum generation over geological time can be reliably extrapolated from open-system pyrolysis due to the analysis of immature samples. The resulting kinetic parameters were then used to assess bulk petroleum formation rates for geological heating conditions. Geological Tmax values between 148 and 159°C were obtained indicating that the investigated samples are very stable to high levels of thermal stress. The highest stabilities were observed for samples from the GS sub-unit (E 48467) and for the analysed sample from the Es3 member. Lowest geological Tmax values were detected for samples from the Shale I and DJT sub-unit. These temperatures are in the same range as those calculated for other lacustrine kerogens such as the Green River shale (Horsfield *et al.*, 1994).

Points to Remember – Kerogen Characterisation (Structure/Lability)

Most of the kerogens analysed produce abundant long-chain aliphatic moieties upon pyrolysis and belong to the high-wax paraffinic crude oil type. This points to a very homogenous polymethylene kerogen structure (C-C bonds) which most likely originates from algaenan biomacromolecules. However, the very narrow distribution of activation energies, typical for many lacustrine kerogens was found for only two samples. Kerogen pyrolysates from the Gao area yield abundant isoprenoids and alkylbenzenes. Their occurrence can be related to specific environmental conditions. Methanogens, chromans and aromatic carotenoids are a possible source of isoprenoids, while alkylbenzenes point to organisms who initiated photic zone anoxia. A broader distribution of activation energies was found for samples from the Es3 and Shale I. High geological Tmax values indicate that the kerogens are very stable to high levels of thermal stress. Sulphur-containing groups are only minor constituents in the pyrolysates.

4.7 Characterisation of the Soluble Organic Matter

In this chapter, a look for specific *biological markers* or *biomarkers* in the soluble organic matter (SOM) was performed to trace source organisms. In addition, structures and stereochemical variations of individual organic compounds can be used to get detailed insights into the organofacies and reconstruct the environment of deposition at the molecular level as reviewed by Peters & Moldowan (1993). Simultaneously, diagenetic effects and the degree of thermal maturation can be estimated. The samples were chosen according to previous screening analysis and stratigraphic position.

The structural elucidation of hydrocarbons and non-hydrocarbons was performed exclusively by Jordi Lopez; tentative structures and mass spectra of the most significant compounds are illustrated in Appx. C. It was a task of the author of this thesis to place the occurrence of these compounds in a geochemical context, i.e. facies and maturity.

E.nr.	Well	Stratigraphy	Remarks	Extract yield [mg/g TOC]	Saturates [%]	Aromatics [%]	NSO compounds [%]
48494	K	Es3		71.54	13.7	4.5	81.8
48455	D	DJT		58.47	18.8	4.9	76.2
48463	B	DJT		329.37	42.9	6.3	50.8
48464	B	DJT		63.86	30.3	8.8	61.0
48465	B	DJT		222.15	38.8	5.7	55.6
48466	B	DJT	impregnated	804.99	40.4	8.6	51.0
48467	B	GS		61.07	40.3	19.3	40.4
48475	J	Shale I		100.81	16.4	2.0	81.6
48480	E	Shale II		176.67	37.2	3.4	59.4
48481	E	DJT		122.34	49.1	5.9	45.0
48482	E	DJT		143.70	59.9	4.0	36.1
48484	C	DJT		118.87	28.4	6.1	65.5
48485	C	DJT		163.78	33.6	5.5	60.9
48502	L	Es4/?		91.26	7.4	1.4	91.2
48505	M	GS		192.51	13.9	5.3	80.9
48514	S	GS		77.96	27.6	4.6	67.8
48517	A	DJT	impregnated	1493.62	51.5	8.7	39.9
48519	A	Shale I	impregnated	455.39	37.2	7.0	55.8
48520	A	Shale I		57.24	7.7	2.0	90.3
48525	A	Shale I		402.69	8.0	0.8	91.1
48527	A	Shale I		116.80	9.9	0.7	89.4
48529	A	GS		85.94	8.1	1.1	90.7
48532	A	GS		47.89	7.9	0.8	91.3
48537	A	GS		93.16	17.4	1.4	81.2

Tab. 4.9. Extract yields and proportions of saturates, aromatics and NSO compounds in source rock bitumens from the Es3 and Es4 member.

4.7.1 Extract Yields and Compound Class Composition

The amounts of SOM extracted from the source rocks are listed in Tab. 4.9. Some samples are impregnated with bitumen and were omitted from the environmental and maturity interpretations. Samples from the DJT sub-unit have extract yields between 58.5 and 329.4 mg/g TOC, averaging 152.8 mg/g TOC. Samples from the Shale I and Shale II sub-units yield on average 170.8 mg/g TOC with maximum concentrations of 402.7 mg/g TOC in well A at 1329 m depth. Flow-blending extraction of the GS samples gave a maximum of 192.5 mg/g TOC extract and 93.1 mg/g TOC SOM on average.

In total 24 bitumen samples were separated into seven lipid fractions using a normal- and a hetero-MPLC system. Fig. 4.21 illustrates the variations of saturates, aromatics and NSO compounds in different stratigraphic units from the Western Depression. NSO compounds and saturates dominate the source rock extracts. The proportion of heterocompounds is high and varies between 36.1% (E 48482) and 91.3% (E 48532). The saturated fraction accounts for 7.4% (E 48502) to 59.9% (E 48482) of the total extract. The contribution of aromatic hydrocarbons is generally low, only sample E 48467 (well B) contains elevated concentrations (19.3%). Samples with the highest proportions of NSO compounds and lowest of saturates are from well A (depths between 1300 and 1400 m). In contrast, samples from the Lei and Tuo area are from depths greater than 2300 m. They contain higher concentrations of saturates.

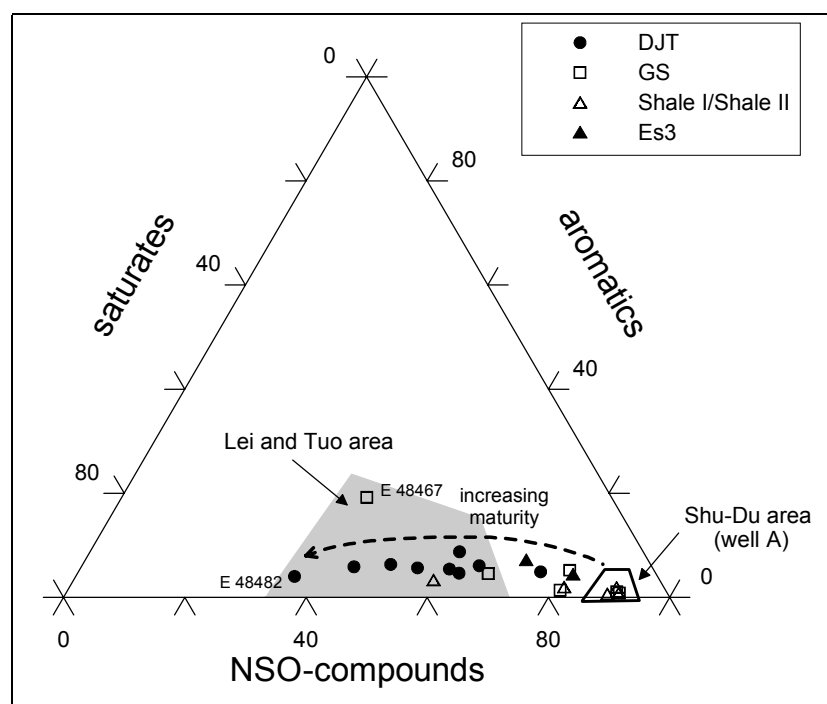


Fig. 4.21. Compound class distribution. Variation of NSO compounds, aromatics and saturates in source rock extracts from the Western Depression.

Thus, the variations in Fig. 4.21 reflect differences in maturity, with a generally low content of saturates in immature source rocks and an increase of saturated hydrocarbons as maturation progresses. Similar compositions were found in other source rock sequences from the Bohai Bay area (Wang *et al.*, 1997). In agreement with the results of the present study, the authors observed an increase of the saturate hydrocarbon fraction with increasing depth in the Shahejie Formation.

4.7.2 Facies Parameters of Key Wells

In Fig. 4.22 and 4.23 selected parameters for facies assessment are plotted *versus* depth for well A (Shu-Du area) and well B (Lei area) to analyse stratigraphic variations. Data for all samples are given in Tab. 4.10. Detailed explanations concerning the individual parameters are given in the following chapters. They are defined in Appx. D. Two samples from the DJT and Shale I in well A (E 48517, E 48519) and one sample from the DJT in well B (E 48466) were neglected because of bitumen impregnations.

E.nr.	Well	Stratigraphy	pr/ph	ph/n-C ₁₈	pr/n-C ₁₇	CPI	GI	OLI	HHI	DIAR	Chromane
48494	K	Es3	0.41	4.21	1.32	2.49	0.13	0.005	0.029	-	1.70
48455	D	DJT	0.81	0.62	0.33	1.25	0.21	0.006	0.035	0.01	0.90
48463	B	DJT	0.40	3.20	0.48	1.40	0.11	-	0.047	-	1.10
48464	B	DJT	0.39	2.24	0.30	1.39	0.14	0.003	0.019	-	1.00
48465	B	DJT	0.36	3.05	0.33	1.42	0.10	0.004	0.051	0.01	1.70
48467	B	GS	0.63	1.06	0.48	1.15	0.26	0.004	-	-	1.00
48475	J	Shale I	0.27	1.90	0.31	1.57	0.15	0.002	-	-	2.70
48480	E	Shale II	0.46	1.86	0.54	1.42	0.01	0.007	0.007	-	2.20
48481	E	DJT	0.63	1.64	0.82	1.28	0.13	0.002	-	-	3.90
48482	E	DJT	0.62	1.77	0.86	1.21	0.10	0.001	-	-	2.10
48484	C	DJT	0.57	2.76	0.45	1.37	0.19	0.002	-	0.02	0.90
48485	C	DJT	0.42	3.38	0.41	1.40	0.16	0.002	0.049	-	1.30
48502	L	Es4/?	0.60	2.10	0.80	3.10	0.01	-	0.0319	-	3.30
48505	M	GS	0.22	11.05	0.18	2.15	0.17	0.001	0.043	-	5.70
48514	S	GS	0.32	5.45	1.01	2.45	0.10	0.002	0.028	0.19	-
48520	A	Shale I	1.93	1.08	1.17	2.20	0.09	0.004	-	-	1.10
48525	A	Shale I	0.78	0.89	0.52	1.76	-	0.010	-	0.01	-
48527	A	Shale I	0.41	6.19	1.72	2.48	0.08	0.010	0.005	-	3.90
48529	A	GS	0.41	3.68	1.30	2.61	0.25	0.003	-	-	2.80
48532	A	GS	0.25	2.36	0.92	2.36	0.23	0.015	-	-	2.60
48537	A	GS	0.17	11.75	0.95	3.43	0.32	0.003	0.048	-	1.90

Tab. 4.10. Facies parameters calculated from thermovaporisation-GC and GC-MS. Pr, pristane; ph, phytane; CPI, Carbon Preference Index; GI, Gammacerane Index; OLI, Oleanane Index; HHI, Homohopane Index; Chromane, Chromane Index; dbth, dibenzothiophene; phen, phenanthrene; - denotes no data due to the absence or low concentration of a specific compound. For definition see Appx. D.

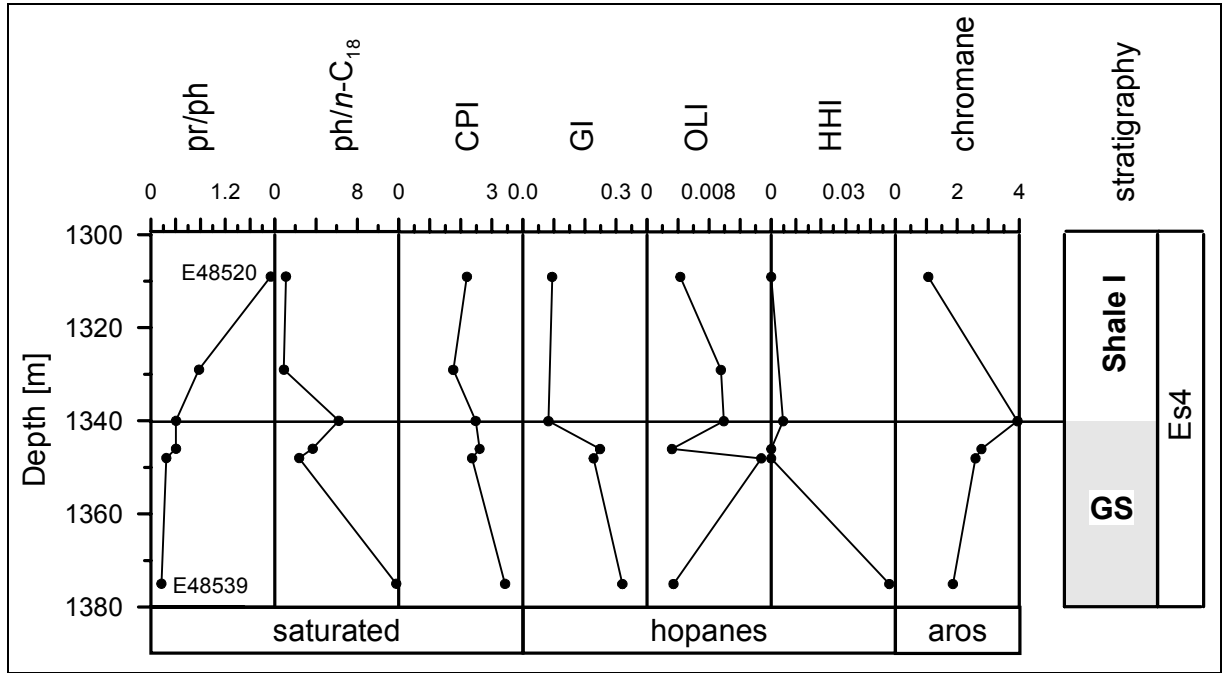


Fig. 4.22. Biomarker parameters and stratigraphy for well A (Shu-Du area). Pr, pristane; ph, phytane; CPI, Carbon Preference Index; GI, Gammacerane Index; OLI, Oleanane Index; HHI, Homohopane Index; Chromane, Chromane Index. For parameter definition see Appx. D.

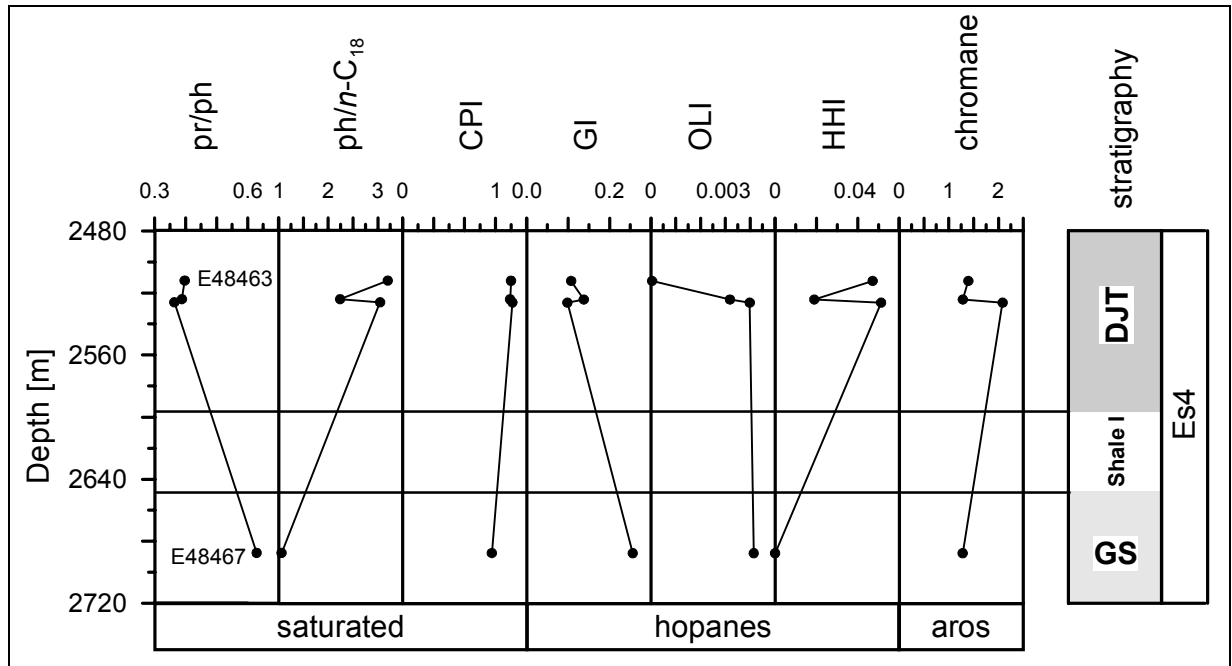


Fig. 4.23. Biomarker parameters and stratigraphy for well B (Lei area). Definition of parameters as in Fig. 4.22.

4.7.3 Saturated Hydrocarbons

The saturated hydrocarbons were analysed quantitatively by thermovaporisation-gas chromatography. The quantitative results are listed in Appx. E. Significantly compositional differences between samples from the two key wells exist (Fig. 4.24 A and B).

All source rock samples from well A are characterised by an odd over even predominance of the *n*-alkanes as well as high concentrations of steroidal and triterpenoidal hydrocarbons. An example is illustrated in Fig. 4.24 A. **Carbon Preference Index (CPI)** values for high molecular weight *n*-alkanes (C₂₅-C₃₁) significantly above 1.0 indicate that the bitumen is thermally immature. Values of 1.0 suggest that an oil or bitumen has a higher maturity. CPI values of less than 1.0 are unusual and are typically associated with extracts from carbonate and hypersaline environments (Tissot & Welte, 1984, p. 101f.). The calculated CPI values for the investigated samples are in the range between 2.20 and 3.43 (Tab. 4.10). Long-chain *n*-alkanes mainly occur in epicuticular waxes of higher land plants leading to an odd predominance of the CPI (Eglinton & Hamilton, 1967), but they may be also derived from other sources, such as planktonic algae or cyanobacteria (e.g. Gelpi *et al.*, 1970). Samples E 48529 to 48537 from the GS sub-unit show a characteristic maximum at *n*-C₂₇. However, *n*-alkanes of the samples E 48520 to E 48527 from the Shale I sub-unit maximise at *n*-C₂₃ or *n*-C₂₇. The samples E 48520 and E 48525 have a second maximum at *n*-C₁₇. A predominance of *n*-C₁₇ to *n*-C₂₀ alkanes was attributed to the contribution of specific algal

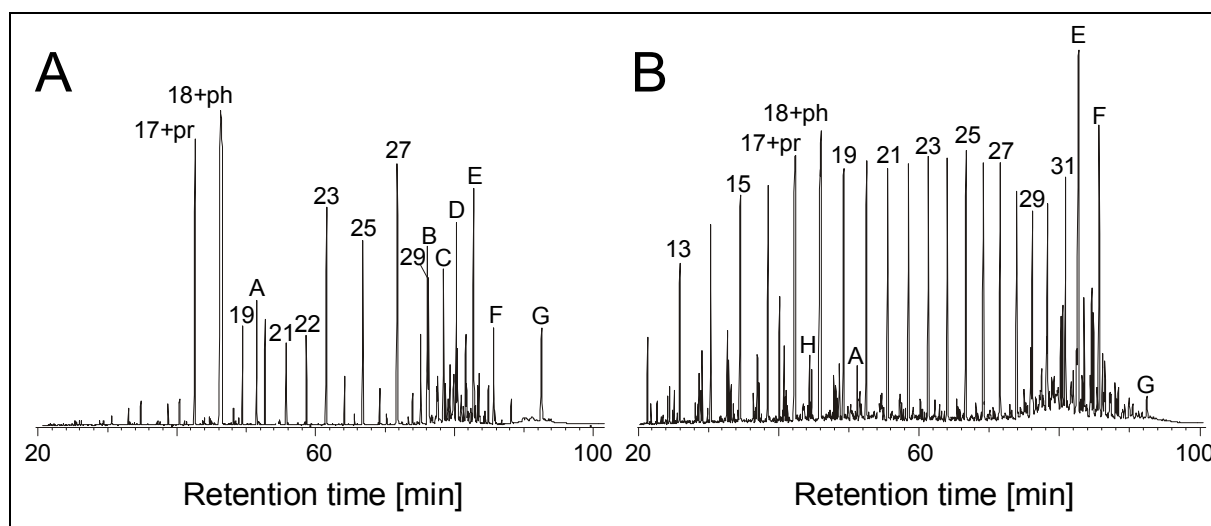


Fig. 4.24. GC-MS total ion chromatograms of the aliphatic hydrocarbons in sample E 48537 (A), well A and E 48467 (B), well B. Numbers on peaks refer to chain length of *n*-alkanes. pr, pristane; ph, phytane; A, branched alkane (2-methylnonadecane ?); B, (20*R*)-5 α (H),14 α (H),17 α (H)-cholestane; C, (20*R*)-24-Methyl-5 α (H),14 α (H),17 α (H)-cholestane; D, (20*R*)-24-Ethyl-5 α (H),14 α (H),17 α (H)-cholestane; E, 17 α (H),21 β (H)-hopane; F, γ -carotane; G, β -carotane; H, branched alkane (7-methylheptadecane ?).

OM (Han, 1969; Elias *et al.*, 2000). Enhanced abundances of mid-chain length, n -C₂₃ and n -C₂₅ n -alkanes simultaneous with low amounts of the long-chain homologues $>n$ -C₂₉ may point to an input of submerged and floating freshwater aquatic macrophytes (Ficken *et al.*, 2000). The occurrence of a branched alkane in sample E 48537 (Fig. 4.24 A), tentatively assigned as 2-methylnonadecane, might indicate the contribution of certain cyanobacteria to the OM (e.g. Köster *et al.*, 1999).

The **isoprenoids**, pristane and phytane can have different sources such as the phytol side chain of chlorophyll *a* (Powell & McKirdy, 1973), bound tocopherols and chromans (Goossens *et al.*, 1984; Li *et al.*, 1995b). A contribution of ether lipids from archaea (e.g. methanogens) to pristane and phytane was also suggested (e.g. Chappe *et al.*, 1982; Rowland, 1990; Navale, 1994). Especially the isoprenoid phytane is generally found in higher concentrations than the neighbouring n -alkanes in the investigated samples from well A. The ph/n -C₁₈ ratio follows a decreasing trend with decreasing depth for this well (Fig. 4.22). The **pristane/phytane (pr/ph)** ratio can be used to determine the redox conditions of the sediment during deposition, based on the assumption that both pristane and phytane originate from the phytol side chain of chlorophyll *a* (e.g. Didyk *et al.*, 1978; Powell, 1987). Oxidic conditions are indicated by pr/ph ratios >1 . Pr/ph ratios less than unity indicate an anoxic depositional environment. The ratio of the analysed samples from well A varies between 0.17 and 1.93 indicating considerable variations of the redox potential (Tab. 4.10).

A characteristic of the Shale I sub-unit in well A is the high concentration of **lycopane**, identified by GC-MS (Appx. C, I), especially in sample E 48525. This compound can originate from the precursor lycopa-14(E), 18(E)-diene which was isolated as the main hydrocarbon from the L race of *B. braunii* present in some tropical freshwater lakes (Metzger & Casadevall, 1987). However, it is not specific to this precursor but can also be derived from reduction of C₄₀ carotenoids (e.g. lycopene), found in a variety of micro-organisms (Schmidt, 1978 and references therein).

In source rock bitumens from the Lei area, no odd over even predominance of the n -alkanes was observed (Fig. 4.24). Instead, a weak maximum at either n -C₂₃ or n -C₂₅ was detected. **CPI values** between 1.15 and 1.42 were determined for well B, which are much lower than for well A (Tab. 4.10). CPI values from other wells in the Lei area are in the same range which shows that the bitumens have higher maturities than in the Shu-Du and also than in the Gao area, where CPI values are between 1.57 (well J) and 3.10 (well L).

The **pr/ph ratio** for the analysed samples from well B varies between 0.36 and 0.63 (Tab. 4.10). The pr/ph values from other wells in this area and for the available source rock bitumens from the Gao area are in the same range.

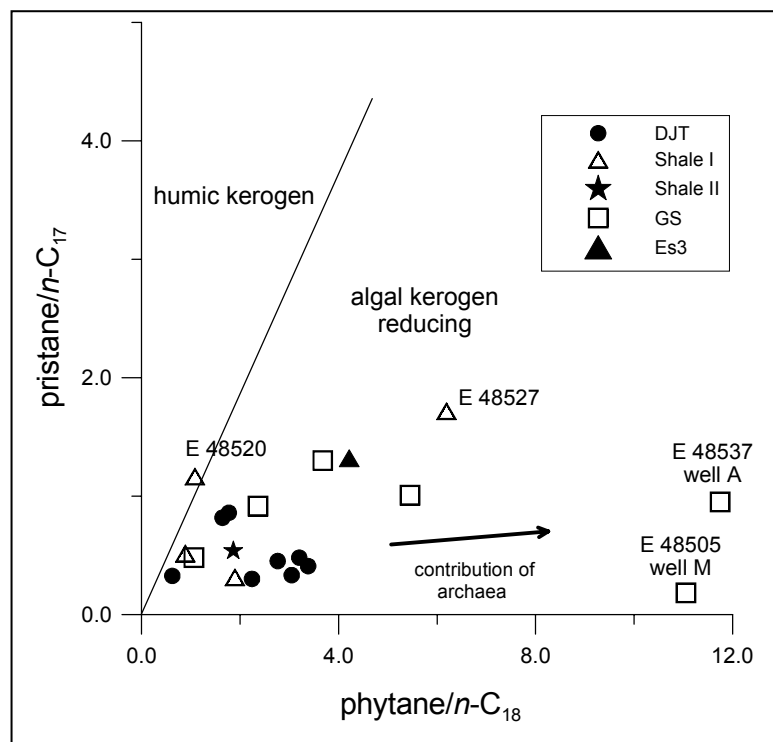


Fig. 4.25. Plot of pristane/ n -C₁₇ versus phytane/ n -C₁₈ for source rock bitumens from the Es4 and Es3 member; fields adopted from Hunt (1996).

Fig. 4.25 illustrates the pristane/ n -C₁₇ and phytane/ n -C₁₈ ratios for the studied samples from the Western Depression. This plot is frequently used to assess depositional regime, maturity and biodegradation of crude oils and bitumens from sedimentary rocks (e.g. Connan & Cassou, 1980; Peters *et al.*, 2000). Most of the samples plot in the field typical for an algal type kerogen deposited under reducing conditions. Only one samples (E 48520) from the Shale I sub-unit plot at the border of the humic kerogen field. Pristane/ n -C₁₇ values are in the range between 0.18 (E 48505; well M) and 1.72 (E 48527; well A). Phytane/ n -C₁₈, especially those from the GS sub-unit, are higher ranging between 0.62 (E 48455; well D) and 11.75 (E 48537; well A). These high ratios suggest an additional source for phytane. Especially the samples E 48537 and E 48505 have very high phytane/ n -C₁₈ and very low pr/ph ratios ($\ll 1$) which probably indicates an anoxic environment where additional phytane was available from archaea. It was also reported that a higher relative concentration of the isoprenoids pristane and phytane relative to the n -alkanes may reflect biological degradation (Connan *et al.*, 1980). However, in the present case only the phytane/ n -C₁₈ ratio increases whereas the pristane/ n -C₁₇ ratio stays relatively constant.

4.7.4 Triterpanes, Steranes and Carotenoids

Identification of these biomarkers was carried out by GC-MS analysis. Figs. 4.26 and 4.27 show representative hopane and sterane distribution patterns. The hopanes are dominated by the $17\alpha(H)$, $21\beta(H)$ -hopane (peak G). Unsaturated (hopenes; Appx. C, III) and $\beta\beta$ -epimers of hopanoids are characteristic for sample E 48532 from well A (Fig. 4.26 A), which attest to low maturity (e.g. Larcher *et al.*, 1987). They are lacking in sample E 48467 from well B (Fig. 4.26 B). In addition, sample E 48467 is characterised by a high concentration of gammacerane (peak K) and progressively decreasing homohopane concentrations in going from C_{31} to C_{35} homologues.

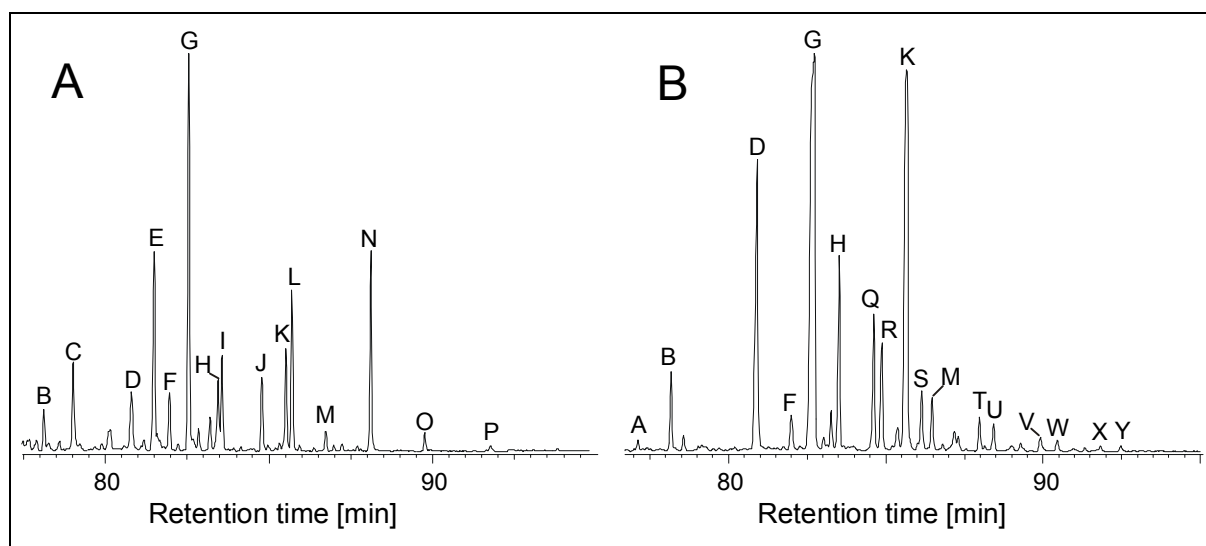


Fig. 4.26. Hopane distribution patterns (m/z 191) in samples E 48532 (A), well A and E 48467 (B), well B. A, $18\alpha(H)$ -trisnorhopane; B, $17\alpha(H)$ -trisnorhopane; C, $17\beta(H)$ -trisnorhopane; D, $17\alpha(H)$, $21\beta(H)$ -30-norhopane; E, C_{30} Hopene; F, $17\beta(H)$, $21\alpha(H)$ -30-norhopane; G, $17\alpha(H)$, $21\beta(H)$ -hopane; H, $17\beta(H)$, $21\alpha(H)$ -hopane; I, C_{31} Hopene; J, C_{30} Gammacerene (?); K, Gammacerane; L, $17\beta(H)$, $21\beta(H)$ -hopane; M, $22(R)$ - $17\alpha(H)$, $21\beta(H)$ -bishomohopane; N, $22(R)$ - $17\beta(H)$, $21\beta(H)$ -homohopane; O, $22(R)$ - $17\beta(H)$, $21\beta(H)$ -bishomohopane; P, $22(R)$ - $17\beta(H)$, $21\beta(H)$ -trishomohopane; Q, $22(S)$ - $17\alpha(H)$, $21\beta(H)$ -homohopane; R, $22(R)$ - $17\alpha(H)$, $21\beta(H)$ -homohopane; S, $22(S)$ - $17\alpha(H)$, $21\beta(H)$ -bishomohopane; T, $22(S)$ - $17\alpha(H)$, $21\beta(H)$ -trishomohopane; U, $22(R)$ - $17\alpha(H)$, $21\beta(H)$ -trishomohopane; V, $22(S)$ - $17\alpha(H)$, $21\beta(H)$ -tetrahomohopane; W, $22(R)$ - $17\alpha(H)$, $21\beta(H)$ -tetrahomohopane; X, $22(S)$ - $17\alpha(H)$, $21\beta(H)$ -pentahomohopane; Y, $22(R)$ - $17\alpha(H)$, $21\beta(H)$ -pentahomohopane.

The m/z 217 chromatogram for two source rock bitumens (Shale I and GS sub-unit) from well A show the dominance of the $20R$ (biological) epimers relative to the $20S$ (geological) epimers (Fig. 4.27). This indicates, together with the dominance of the $5\alpha(H)$, $14\alpha(H)$, $17\alpha(H)$ -steranes, that these samples are immature based on sterane maturity parameters. Interestingly, the thermodynamically unstable $5\beta(H)$, $14\alpha(H)$, $17\alpha(H)$ -steranes are present in relatively high concentrations. This has been previously reported

from lacustrine sediments of the Green River Shale (Gallegos, 1971; Horsfield *et al.*, 1994) and immature lacustrine source rocks of the Mae Sot Basin (Curiale & Gibling, 1994).

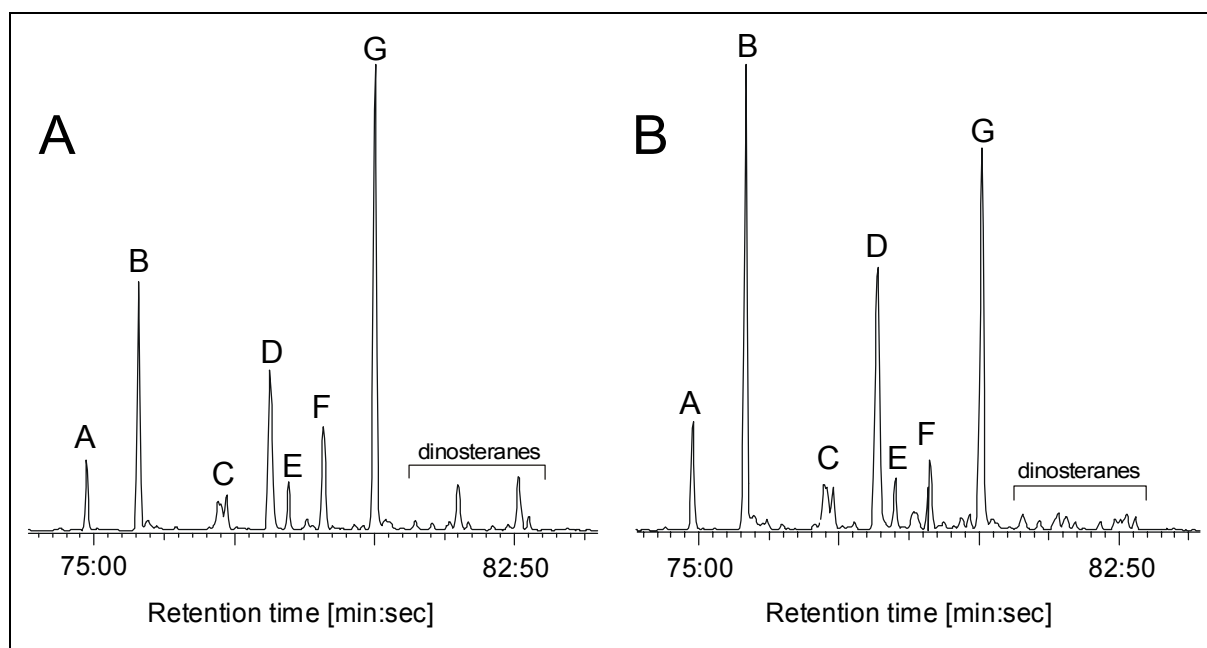


Fig. 4.27. Different sterane distribution patterns (m/z : 217) in well A. Samples E 48525 (A), Shale I sub-unit and E 48529 (B), GS sub-unit. A, (20R)-5 β (H),14 α (H),17 α (H)-cholestane; B, (20R)-5 α (H),14 α (H),17 α (H)-cholestane; C, (20R)-24-Methyl-5 β (H),14 α (H),17 α (H)-cholestane; D, (20R)-24-Methyl-5 α (H),14 α (H),17 α (H)-cholestane; E, (20S)-24-Ethyl-5 α (H),14 α (H),17 α (H)-cholestane; F, (20R)-24-Ethyl-5 β (H),14 α (H),17 α (H)-cholestane; G, (20R)-24-Ethyl-5 α (H),14 α (H),17 α (H)-cholestane.

The $\alpha\alpha\alpha$ C₂₉-20R-sterane occurs in high concentrations (20-65%) in the source rock bitumens (Fig. 4.28). According to the interpretation of Huang & Meinschein (1979) high concentrations of C₂₉ compared to C₂₇ and C₂₈-steranes may indicate a land plant source. However, previous results in this study show that land plant input was minor. Other sources, such as diatoms (Volkman *et al.*, 1981), certain alga (Grantham, 1986) and cyanobacteria (Matsumoto *et al.*, 1982) are possible. Based on a correlation between the sterane abundance and the algal content of other lacustrine source rocks from Chinese basins, it was proposed that C₂₇ to C₂₉ steranes are unique products of algal OM (Wang *et al.*, 1997). With one exception (E 48482), the bitumens from the DJT sub-unit plot in a distinct field in Fig. 4.28. This suggests a uniform composition of the OM and thence a similar depositional environment. Generally, source rock extracts from the DJT and GS sub-unit contain higher concentrations of $\alpha\alpha\alpha$ C₂₈-sterane than those from the Shale I and Shale II sub-units and from the Es3 member. Interestingly, Ritts *et al.* (1999) determined higher concentrations of $\alpha\alpha\alpha$ C₂₈-steranes in source rock extracts and lacustrine crude oils from hypersaline settings. Dinosteranes which are most probably derived from dinoflagellates (e.g. Robinson *et al.*,

1986; Moldowan *et al.*, 1996) are present in almost all samples, but they are more abundant in samples from the Shale I subunit. Dinoflagellates can be important primary producers in lake waters and thus provide OM to lacustrine source rocks (e.g. Köhler & Clausing, 2000).

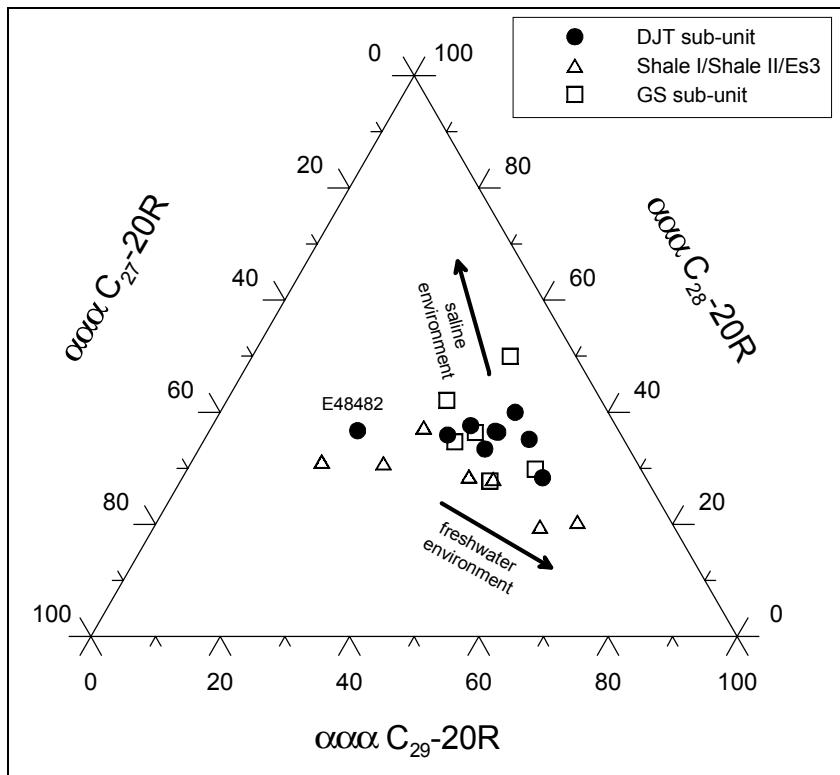


Fig. 4.28. Ternary distribution of $\alpha\alpha\alpha$ -20R steranes in bitumens from the Es4 and Es3 member. Interpretation after Ritts *et al.* (1999) on the basis of investigations on Tertiary and Jurassic lacustrine source rocks and crude oils from the Qaidam Basin, China.

The carotenoids β - (Appx. C, II) and γ -carotane were found in the laminated shale samples from the GS sub-unit in high concentrations. Their presence has been attributed to an anoxic and arid lacustrine depositional environment with a higher salinity and abundant deposition of algal OM (e.g. Fu *et al.*, 1986; Fu *et al.*, 1990). Hanson *et al.* (2001) found abundant β - and γ -carotane in oils and extracts derived from Tertiary hypersaline lacustrine source rocks in the Qaidam basin (NE China).

4.7.4.1 Facies Parameters

The relative abundance of **gammacerane** has been widely used as an indication of increased water salinity during deposition of source rocks (Moldowan *et al.*, 1985). Hypersaline conditions result in high **gammacerane indices (GI)**. Gammacerane is derived from the reduction of tetrahymanol, a lipid thought to replace steroids in the membranes of certain protozoa or phototrophic bacteria (ten Haven *et al.*, 1989; Venkatesan, 1989). Several authors found an association with hypersalinity (e.g. Fu *et al.*, 1986). However, Sinnighe Damsté *et al.* (1995) argued that gammacerane is not restricted to hypersaline conditions

and that the principal control is water column stratification creating anoxic conditions. The authors showed that anaerobic bacterivorous ciliates living at or near the chemocline produce tetrahymanol and are thus important sources of gammacerane. The association of very low pr/ph ratios with hypersaline environments was reported by ten Haven *et al.* (1988). The investigated source rock bitumens have GI values between 0.01 (wells E, L) and 0.32 (well A). Hanson *et al.* (2001) found that oils, sourced from hypersaline lacustrine settings of the Qaidam Basin (NE China), have GI values up to 0.57. Other source rocks from the Bohai Bay Basin, associated with hypersalinity show similar or even higher values (Huang & Pearson, 1999). Although the values obtained here are generally low, higher GI values were observed for the GS than for the other stratigraphic units (Tab. 4.10). Interestingly, samples from the GS have also the lowest pr/ph ratios. A similar association of gammacerane with generally low pr/ph ratios was noted by Peters & Moldowan (1993) in Angolan lacustrine-sourced oils.

The triterpane oleanane is a diagenetic product of β -amyrin, which is widely distributed in angiosperms (ten Haven & Rullkötter, 1988). It is commonly found in Cretaceous through Cenozoic sediments and related oils (e.g. Fu & Sheng, 1989; Alberdi & López, 2000) and is a very sensitive age-specific environmental indicator of terrestrial OM in source rocks. Its absence precludes the contribution of flowering plants to the Es4 lake sediments (Moldowan *et al.*, 1994; Moldowan *et al.*, 2001). The **oleanane index (OLI)** of all investigated source rock samples is very low, indicating that terrigenous input to the lakes was minor (Tab. 4.10).

The **homohopane index (HHI)** is used as an indicator of redox conditions (Peters & Moldowan, 1991). High concentrations of C₃₅-homohopanes indicate a highly reducing environment. The homohopanes are believed to be derived from bacteriohopanetetrol in prokaryotic microorganisms (Ourisson *et al.*, 1984). The ratio is low in most of the studied source rock bitumens with values ranging between 0.005 and 0.049. Hanson *et al.* (2001) determined HHI values between 0.10 and 0.34 for source rocks deposited in an anoxic, strongly reducing hypersaline environment. The values obtained here are more consistent with a freshwater source rock. In well A only sample E 48537 contains significant amounts of homohopanes suggesting a higher reducing depositional environment for the GS sub-unit (Fig. 4.22). However, other authors found that this ratio is also influenced by other parameters such as the lithology (Fu *et al.*, 1986) and sulphur availability (Huang & Pearson, 1999).

The **diasterane ratio (DIAR)** is commonly used to distinguish petroleum from carbonate versus those from clastic rocks (Mello *et al.*, 1988; Peters & Moldowan, 1993). The conversion of steranes to diasteranes may be catalysed by acidic sites on clays. Therefore, a low DIAR indicates anoxic carbonate rich source rocks whereas a high DIAR is typical for clay rich source rocks. In consequence, the concentrations of diasteranes are low in most of the investigated samples, reflecting the carbonate rich lithology. Interestingly, a relatively high ratio of 0.19 was obtained for the clay rich shale sample E 48514 (Tab. 4.10).

4.7.4.2 Maturity Parameters

Source rock and petroleum maturity can be estimated by ratios of biomarker compounds with a different thermodynamic stability (Seifert & Moldowan, 1978). These indicators result from isomerisations at certain carbon atoms or cracking reactions including aromatisation. To minimise source facies effects, which can cause a large data scattering the different stratigraphic units have been considered separately in this chapter. Samples which are stained with oil were omitted from the interpretations. Calculated maturity parameters are given in Tab. 4.11.

Hopane maturity determinations were calculated from the C_{31} -hopanes. According to (Peters & Moldowan, 1993) the **homohopane isomerisation (HISO)** is highly specific for early oil generation, because isomerisation at the C-22 position in the C_{31} $17\alpha(H)$ -hopanes

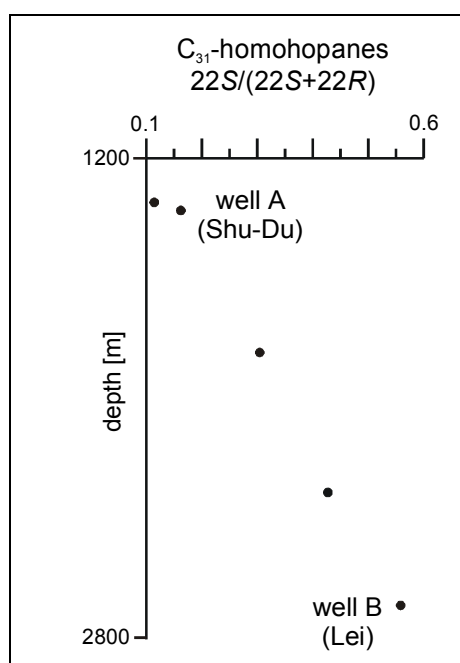


Fig. 4.29. HISO versus depth for bitumens from the GS sub-unit.

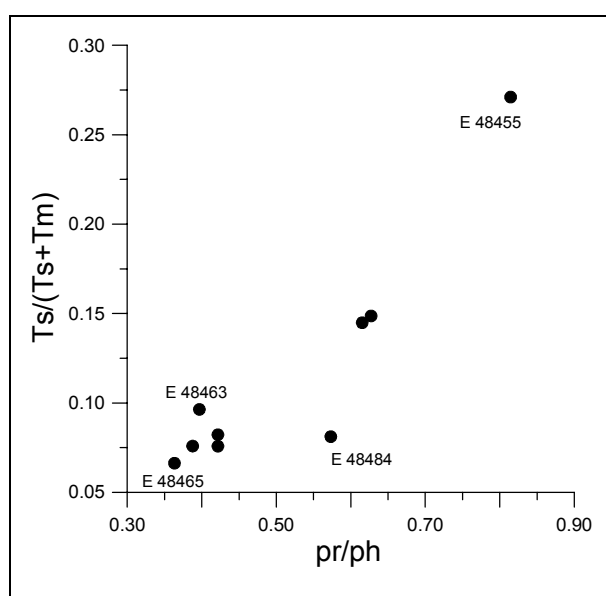


Fig. 4.30. Pr/ph versus Ts/(Ts+Tm) for bitumens from the DJT sub-unit.

occurs early during maturation. The equilibrium values fall between 0.57 and 0.62 and correspond to a vitrinite reflectance of approx. 0.5% Ro (Schoell *et al.*, 1983). The trend for GS is well defined (Fig. 4.29). Samples from well A have the lowest maturity, the sample from well B (E 48467) has the highest maturity. For the DJT sub-unit this parameter shows no discernible relationship with depth and hence maturity. Overall low values were noted for the **Ts/(Ts+Tm)** ratio which is strongly influenced by the source rock mineralogy. It was reported that samples rich in clay minerals shows enhanced values due to clay having catalysed the Tm to Ts transition (Philp & Fan, 1987; Waples & Machihara, 1991). Low values in the GS might be due to the higher carbonate percentages (Rullkötter *et al.*, 1985). The positive correlation with the pr/ph ratio for the DJT samples in Fig. 4.30 illustrates a facies dependence of this ratio. The hopane to moretane **H/(M+H)** ratio is higher than 0.95 in mature source rock and oils (Peters & Moldowan, 1993). For the investigated samples, ratios between 0.86 and 0.96 were observed (Tab. 4.11). However, no discernible depth relationship was seen within the stratigraphic units.

E.nr.	Well	Stratigraphy	hopanes			C ₂₉ -steranes	
			HISO	Ts/(Ts+Tm)	H/(M+H)	ββ/ββ+αα	20S/(20S+20R)
48494	K	Es3	0.49	0.81	0.93	0.29	0.17
48455	D	DJT	0.59	0.27	0.88	0.28	0.27
48463	B	DJT	0.51	0.10	0.92	0.21	0.12
48464	B	DJT	0.52	0.08	0.90	0.25	0.14
48465	B	DJT	0.52	0.07	0.94	0.19	0.12
48467	B	GS	0.56	0.13	0.95	0.16	0.25
48475	J	Shale I	0.24	0.10	0.93	0.25	0.08
48480	E	Shale II	0.53	0.11	0.94	0.30	0.18
48481	E	DJT	0.59	0.15	0.91	0.11	0.11
48482	E	DJT	0.46	0.14	0.96	0.35	0.10
48484	C	DJT	0.52	0.08	0.95	0.15	0.10
48485	C	DJT	0.46	0.08	0.88	0.24	0.12
48502	L	Es4/?	0.11	0.03	0.95	0.20	0.03
48505	M	GS	0.30	0.05	0.94	0.28	0.09
48514	S	GS	0.43	0.25	0.94	0.29	0.06
48520	A	Shale I	0.34	0.14	0.86	0.18	0.03
48525	A	Shale I	-	0.04	-	0.24	0.02
48527	A	Shale I	0.34	0.02	0.90	0.32	0.04
48529	A	GS	-	0.03	-	0.28	0.08
48532	A	GS	0.11	0.04	0.88	0.29	0.08
48537	A	GS	0.16	0.02	0.84	0.29	0.15

Tab. 4.11. Hopane and sterane maturity parameters calculated from GC-MS; - denotes no data due to the absence or low concentration of a specific compound. Detailed explanations and definitions are given in the text and Appx. D.

Maturity indicators based on **sterane isomerisation** reactions generally indicate low maturities. The C₂₉ sterane $\beta\beta/(\beta\beta+\alpha\alpha)$ ratio ranges between 0.11 and 0.35 without any depth related trend and indicate vitrinite reflectance values of approx. 0.50 to 0.60% Ro. It usually increases during maturation from zero to an equilibrium value of about 0.70 (Seifert & Moldowan, 1986). Rullkötter & Marzi (1988) and ten Haven *et al.* (1986) noted higher values for bitumens from hypersaline rocks compared to shales. There is also no well-defined depth trend for the C₂₉ sterane **20S/(20S+20R)** ratio within the different stratigraphic units. The values range between 0.03 and 0.27 and show a high variability. Seifert *et al.* (1983) observed low-maturity oils with ratios in the range 0.23 to 0.29 which might indicate the onset of immature oil generation. Li *et al.* (1994) studied lacustrine freshwater shales from the Leng Area in the Western Depression. They found that around 0.3% Ro a relative early generation of 5 α (H),14 β (H),17 β (H)-steranes and 5 α (H),14 α (H),17 α (H)-steranes occurred which probably indicates an influence of the depositional environment (e.g. Peakman *et al.*, 1989). This might explain the wide variability of the sterane maturity indicators in the present study.

4.7.5 Aromatic Hydrocarbons

Several recent studies have substantiated the usefulness of aromatic compounds for an interpretation of the depositional environment (e.g. Fan *et al.*, 1991; Hughes *et al.*, 1995; Requejo *et al.*, 1996; Marynowski *et al.*, 2000). In addition, different aromatic compounds have been employed as important tools for determining the level of maturation in source rocks and crude oils (e.g. Radke & Welte, 1981; Radke *et al.*, 1982; Radke & Willsch, 1993; Santamaría-Orozco *et al.*, 1998). Tentative structures are given in Appx. C.

4.7.5.1 Facies Assessment

Several **aromatic terpenoids** (Appx. C, IV) are important constituents of the aromatic fraction. These tri-, tetra- and pentacyclic aromatics with an oleanane or ursane skeleton are probably indicative of higher plant input originating from triterpenoids which are widespread in lacustrine ancient sediments (Loureiro & Cardoso, 1990). They are derived from the diagenesis or combustion of natural precursors such as amyryns (Wakeham *et al.*, 1980). These compounds are abundant in bitumens from the GS and Shale I sub-unit, whereas they are minor constituents or lack in rocks from the DJT sub-unit. **Aromatised lycopenes** (Appx. C, V) are present in the samples E 48520 and E48525 from well A. They can be

related to the L-race of the alga *B. braunii* (e.g. Béhar *et al.*, 1995), which was identified in these samples from the Shale I sub-unit by organic petrology.

Mono-aromatised carotenoids (Appx. C, VI) are important in the laminated oil shale samples from well A (GS sub-unit). Together with chromans they are the major compounds in the aromatic fraction of many source rock bitumens in the Lei and Gao area and often form a characteristic “hump” in the chromatograms (Fig. 4.31). Very high concentrations were found in well B (E 48463). These compounds have a prominent fragment ion at m/z 119 or 133 depending on the number of methyl-substituents on the aromatic ring, and a molecular ion of M^+ 550 or 552 (Lopez, pers. comm.). Carotenoids and transformation products can serve as biomarkers to determine the presence of anoxic conditions in the paleo-water column extending up to the photic zone (e.g. Koopmans *et al.*, 1996). The reduced counterparts of the corresponding intact diaromatic carotenoids isorenieratene, renieratene and reniera-purpurin occur in a wide range of organic rich sediments (e.g. Keely *et al.*, 1995; Grice *et al.*, 1996; Sinninghe Damsté *et al.*, 2001). Schaeffer *et al.* (1997) found similar monoaromatic carotenoid structures in recent sediments of Lake Cadagno, Switzerland. Based on compound specific stable carbon isotopic compositions they suggested a biological origin from *Chlorobiaceae* and *Chromatiaceae* which live at or below the oxic/anoxic boundary layer.

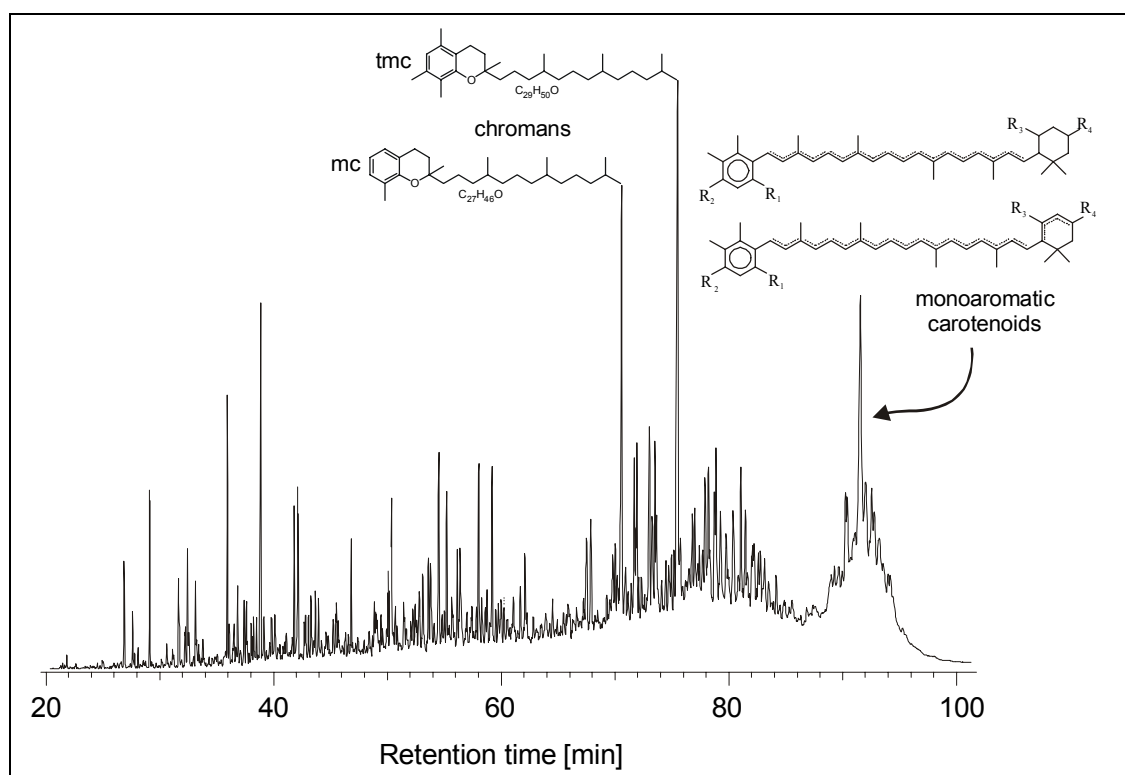


Fig. 4.31. GC-MS total ion chromatogram of the aromatic fraction from sample E 48463. Tentative structures of monoaromatic carotenoids and chromans are indicated. mc, methylchromans; tmc, trimethylchromans

The abundance of **methylated chromans** (Appx. C, VII) in sediments and oils can be used as a paleoenvironmental indicator to assess the occurrence of palaeohypersalinity (Sinninghe Damsté *et al.*, 1987; Sinninghe Damsté *et al.*, 1993). The authors found that sediments from non-hypersaline environments show a dominance of trimethylchromans (tmc) whereas a typical feature of samples from hypersaline environments is the presence of methylchromans (mc). Therefore, a very low **chromane index** should indicate a hypersaline environment. In all investigated samples the tmc dominate the distribution pattern (e.g. Fig. 4.31). The chroman index shows a large variability in the investigated source rock samples (Tab. 4.10). The values range between 0.90 (E 48455; well D) and 5.70 (E 48505; well M). The absolute concentration of the chromans is generally higher in the Lei and Gao than in the Shu-Du area. Chroman index values are lower in well B than in well A (Figs. 4.23 and 4.24) and values from the Gao area are significantly higher than those from the Lei area. All source rock values for the chroman index are far from those (<0.5) which are considered to originate in highly saline environments (Sinninghe Damsté *et al.*, 1987). Values around 0.63 were reported from mesohaline paleoenvironments such as the Darawish oil shale in Jordan (Sinninghe Damsté *et al.*, 1989). Similar values were calculated for samples from the Nördlinger Ries (Barakat & Rullkötter, 1997). This suggests brackish to fresh lacustrine conditions during sediment deposition in the Liaohe lakes.

The **dibenzothiophene/phenanthrene (dbt/phen) ratio** was used before as an indicator of water washing for crude oils (Dahl & Spears, 1986), and to elucidate the organic input to a carbonate-anhydrite source rock sequence from Guatemala (Connan *et al.*, 1986). Hughes *et al.* (1995) used this ratio to discriminate the crude oil depositional environment and lithology of source rocks. According to their interpretation the pr/ph ratio reflects the redox conditions and the dbt/phen ratio the availability of reactive sulphur for interaction with OM. Fig. 4.32 illustrates that most of the investigated samples contain an excess of phytane over pristane (pr/ph < 1) and are sulphur poor (dbt/phen < 1). Thus, the sediments were deposited in an anoxic environment with low sulphate ion concentrations, where fermentation rather than sulphate reduction was the dominant process. The authors proposed, that this typical for brackish water lakes with a slightly enhanced salinity. In zone 3 sulphate reduction occurs but the supply of reactive iron is large and thence pyrite formation is the major process.

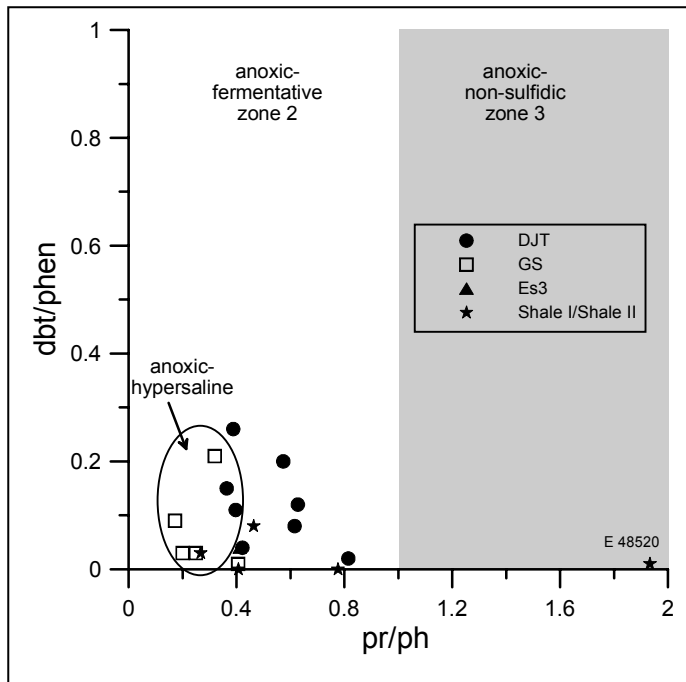


Fig. 4.32. *Pr/phen* versus *dbt/phen* ratio for bitumens from the Es3 and Es4 member; modified after Hughes *et al.* (1995).

4.7.5.2 Maturity Assessment

Changes in the relative distribution of alkylated homologues of phenanthrene and sulphur-related compounds (e.g. Radke *et al.*, 1991; Santamaría-Orozco *et al.*, 1998) have been shown to be closely maturity-related. The aromatic maturity parameters mpi 1 and mpr 2

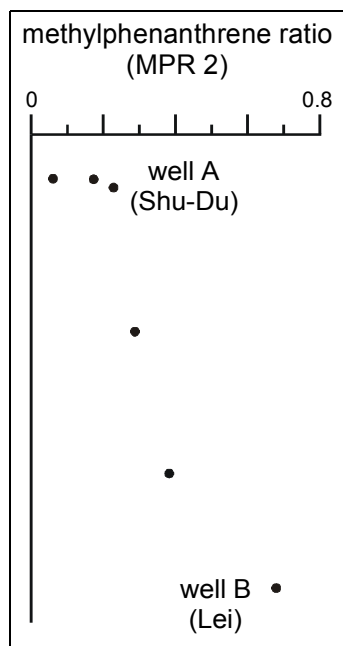


Fig. 4.33. *Mpr 2* versus depth for samples from the GS sub-unit.

show an increase with depth for the GS but no clear trend with depth was observed for the DJT sub-unit. The mpr 2 shows the least scatter with a relative maturity increases from well A to well B for the GS (Fig. 4.33). Reflectance data were calculated from the mpi 1 (Tab. 4.12). The values determined are in the range between 0.45 (E 48525) and 0.88 %Rc (E 48455).

It was reported, that selected alkyldibenzothiophenes and dibenzothiophenes are very sensitive in the low maturity range (Radke *et al.*, 1982; Radke & Willsch, 1994). However, the results in Tab. 4.12 show that the ratios mdr 1 (1-methyldibenzothiophene to dibenzothiophene), mdr 4 (4-methyldibenzothiophene to dibenzothiophene) and edr (4,6-dimethyldibenzothiophene to ethyldibenzothiophene), are not defined indicating their very limited utility as maturation parameters for this immature source rock sequence. They are

possibly affected by the depositional environment. For example, Huang & Pearson (1999) analysed Bohai Bay crude oils and found other controls than maturity on the methyl-dibenzo-thiophene isomerism. They observed that high mdr 4 ratios are associated with fresh water source rock deposition, while high mdr 1 ratios are found in oils from hypersaline lacustrine sources.

E.nr.	Well	Sub-unit	mpi 1	%Rc	mpr 1	mpr 2	mdr 1	mdr 4	edr	mah	bhp
48494	K	Es3	0.44	0.66	0.25	0.25	-	-	-	0.51	0.44
48455	D	DJT	0.79	0.88	0.61	0.72	1.94	1.80	5.69	0.85	1.00
48463	B	DJT	0.46	0.68	0.24	0.25	0.92	0.36	0.51	0.55	0.69
48464	B	DJT	0.71	0.83	0.54	0.54	1.03	0.47	0.48	0.45	0.74
48465	B	DJT	0.54	0.73	0.30	0.31	1.00	0.60	0.62	0.46	0.72
48467	B	GS	0.79	0.87	0.69	0.68	0.57	-	-	0.46	-
48475	J	Shale I	0.17	0.50	0.08	0.08	-	-	-	0.16	0.51
48480	E	Shale II	0.59	0.75	0.36	0.39	0.85	0.36	1.33	0.85	0.86
48481	E	DJT	0.57	0.74	0.69	0.43	0.77	-	-	0.83	0.91
48482	E	DJT	0.53	0.72	0.62	0.38	0.81	-	-	0.87	0.94
48484	C	DJT	0.53	0.72	0.45	0.33	0.99	-	-	0.30	0.65
48485	C	DJT	0.29	0.58	0.11	0.13	0.91	-	-	0.26	0.62
48502	L	Es4/?	0.34	0.61	0.26	0.18	-	-	-	0.07	0.27
48505	M	GS	0.42	0.65	0.41	0.29	0.99	0.60	0.27	0.20	0.30
48514	S	GS	0.45	0.67	0.74	0.38	0.77	-	-	0.77	0.61
48520	A	Shale I	0.15	0.49	0.05	0.06	-	-	-	0.15	0.24
48525	A	Shale I	0.08	0.45	0.03	0.03	-	-	-	-	-
48527	A	Shale I	0.08	0.45	0.02	0.03	-	-	-	0.03	0.42
48529	A	GS	0.14	0.49	0.03	0.06	-	-	-	0.10	0.22
48532	A	GS	0.28	0.57	0.14	0.17	-	-	-	-	0.28
48537	A	GS	0.37	0.62	0.28	0.23	0.05	0.10	3.59	-	0.33

Tab. 4.12. Aromatic maturity parameters calculated from GC-MS; - denotes no data due to the absence or low concentration of a specific compound. Detailed explanations and definitions are given in the text and Appx. D. Vitrinite reflectance (%Rc) was calculated from mpi 1.

Two parameters based on **aromatic hopanoids** show very sensitive changes with increasing depth for the GS as well as for the DJT sub-unit (Fig. 4.34). Ring D aromatised 8,14-secohopanoids and benzohopanoids (Appx. C, VIII & IX-X) were first identified in carbonate source rocks and related crude oils (Hussler *et al.*, 1984a; Hussler *et al.*, 1984b). The ratio of the aromatic secohopanoids relative to the benzohopanoids (**mah**) was observed to increase with increasing burial depth for mudstone extracts and crude oils from the Shahejie Formation in the Western Depression of the Liaohe Basin (He & Lu, 1990). The authors reported, that a **mah** ratio of 0.3 is equivalent to the threshold of oil generation. Ratios of 0.8 are typical for mature source rock bitumens and crude oils generated during peak oil generation. The **mah** of the studied samples varies between 0.03 (well A) and 0.87 (well E; Tab. 4.12). Highest ratios and are observed for samples from the Lei area. Benzo-

hopanoids were identified, arising by cyclisation-aromatisation of the side-chain with nucleus carbon atom C-20 and C-16, respectively. It was found that the abundance of the $C_{32}H_{48}$ benzohopanooid (C20-series) increases relative to the abundance of the $C_{31}H_{46}$ analogue from the C-16 series with increasing depth (**bhp**; Fig. 4.34 B). It has been said that compounds from the C-20 series are thermodynamically more stable than those of the C-16 series (Schaeffer *et al.*, 1995). Fig. 4.34 B shows, that this ratio increases very rapidly over a relative small depth interval (2400 to 2800 m) for samples from the DJT sub-unit. A progressively increase was also observed for the GS sub-unit.

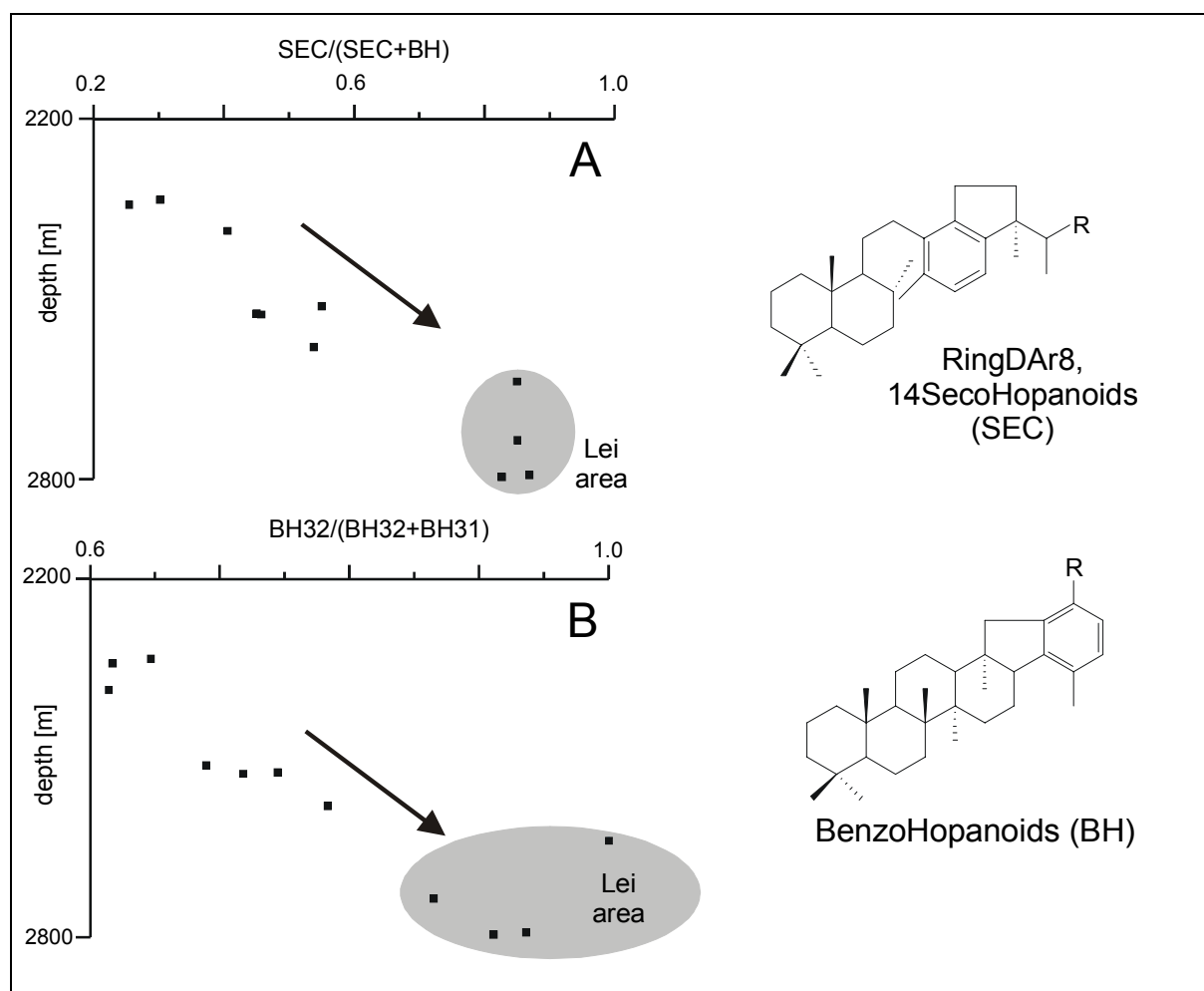


Fig. 4.34. Aromatic hopanoids ratio vs. depth for bitumens from the DJT sub-unit. A, Aromatic seco-hopanooids (SEC) relative to benzohopanooids (BH), termed **mah ratio** after He & Lu (1990). B, Benzohopane ratio (**bhp**). In both cases samples from the Lei area are indicated by highest maturity levels.

4.7.6 Heterocompounds

The primary objective of this chapter is to show the influence of the depositional environment on the heterocompound composition in the Liaohe source rocks. Beside this, the impact of thermal maturity on the geochemical source rock characteristics was studied. Molecules with the heteroatoms nitrogen, sulphur and oxygen (NSO-compounds) were previously used as indicators for migration effects, maturity determinations and source rock facies (e.g. Larter *et al.*, 1996; Clegg *et al.*, 1998; Horsfield *et al.*, 1998).

E.nr.	Well	Stratigraphy	fatty acids	<i>n</i> -alkan-1-ols	
			CPI C ₂₂ -C ₂₈	$\Sigma(9-20)/\Sigma(21-28)$	CPI C ₂₂ -C ₂₈
48494	K	Es3	4.11	1.20	2.31
48455	D	DJT	1.52	1.16	7.08
48463	B	DJT	1.30	0.71	1.62
48464	B	DJT	1.35	1.17	4.34
48465	B	DJT	1.22	0.94	2.47
48467	B	GS	1.11	0.97	2.62
48475	J	Shale I	1.58	1.27	1.34
48480	E	Shale II	1.25	0.02	2.48
48481	E	DJT	1.19	0.52	2.32
48482	E	DJT	1.18	0.53	1.67
48484	C	DJT	1.55	0.40	2.64
48485	C	DJT	1.14	0.59	2.26
48502	L	Es4/?	3.96	1.53	1.15
48505	M	GS	1.55	-	-
48514	S	GS	3.41	0.95	0.78
48520	A	Shale I	3.57	0.67	1.35
48525	A	Shale I	6.23	1.66	1.49
48527	A	Shale I	2.13	1.15	1.03
48529	A	GS	2.33	0.59	1.24
48532	A	GS	2.17	0.25	1.21
48537	A	GS	3.95	0.16	1.02

Tab. 4.13. Facies parameters based on heterocompounds. Detailed explanations and definitions are given in the text and Appx. D.

4.7.6.1 Free Fatty Acids

Major compounds detected from the fatty acid fraction are straight-chain acids (*n*-fatty acids), isoprenoid fatty acids, 2-methyl straight-chain acids (*iso*-acids), 3-methyl straight-chain acids (*anteiso*-acids) and hopanoic acids. The carbon preference index (CPI_{FA}) for the long chain *n*-fatty acids (C₂₂-C₂₈) is high for bitumens from well A with a maximum of 6.23 (E 48525, Shale I sub-unit) indicating a strong even over odd-predominance (Tab. 4.13). Most samples have a bimodal distribution with C₁₄ to C₁₈ *n*-fatty acids with varying maxima in the short-

chain range and a dominant peak at n -C₂₈ (Fig. 4.35 A). The latter might be indicative for the input of terrigenous OM (Eglinton & Hamilton, 1967; Matsuda & Koyama, 1977). Short chain fatty acids (C₁₄ to C₁₈) were synthesised from many algae, cyanobacteria and different microbes (Cranwell *et al.*, 1987; Heras *et al.*, 1989; Merritt *et al.*, 1991; Lichtfouse *et al.*, 1995). It was also observed, that diatoms can produce short-chain compounds (Colombo *et al.*, 1996). The presence of *iso*- and *anteiso*-acids in many samples indicates an important bacterial input to the OM. Some of them (*iso*-tetradecanoic and hexadecanoic) are commonly found in *gram-positive* eubacteria (Cho & Salton, 1966). This indicates that a considerable degree of microbial reworking took place. The occurrence of phytanic acid points to the presence of methanogenic archaea which live in very severe reducing environments (de Rosa & Gambacorta, 1988). Especially in sample E 48537 (well A) from the GS sub-unit (Fig. 4.35 A), the concentration of phytanic acid is extremely high (1593 µg/g bitumen).

Hopanoic acids are diagenetic products, derived from the bacteriohopanepolyols (e.g. Innes *et al.*, 1998) which are present in the cell membrane of a wide range of bacterial and cyanobacterial organisms (Rohmer *et al.*, 1984; Rohmer, 1993). The thermodynamically less stable C₃₁-, C₃₂- and C₃₃-17β(H), 21β(H) hopanoic acids are abundant in all of the source rock bitumens from well A, which is a sign of source rock immaturity (Seifert & Moldowan, 1980). Hopanoic acids are less important in the Lei wells but occur in high concentrations in samples from the Gao area. Most of the sample are dominated by the C₃₂-hopanoic acids which were reported from a large number of Recent and ancient sediments and result from a

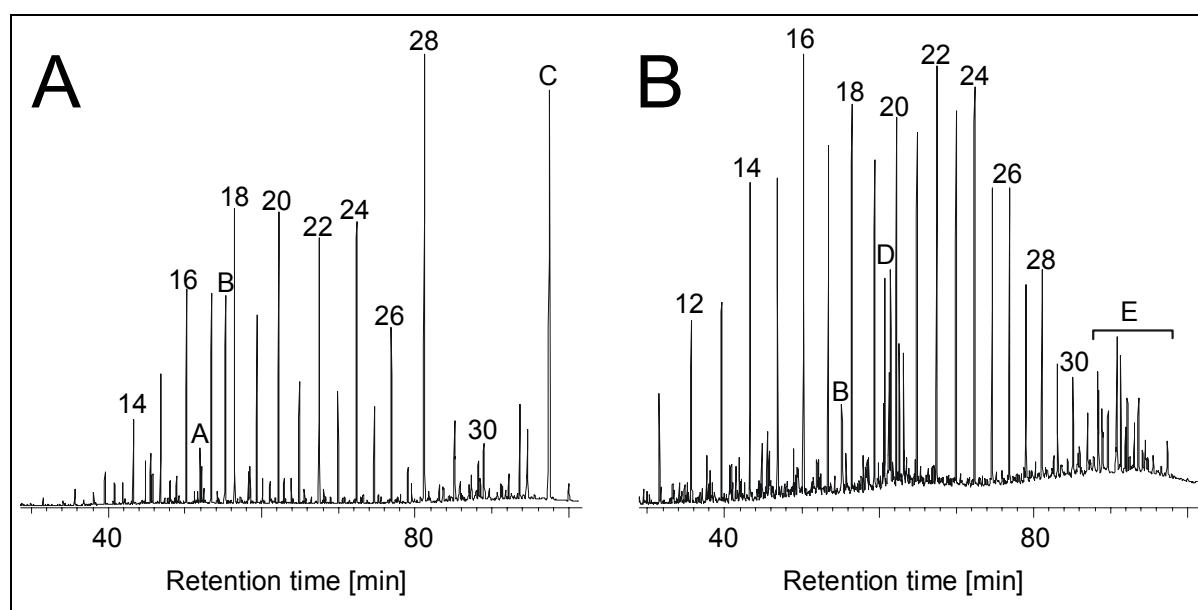


Fig. 4.35. GC-MS total ion chromatograms of the carboxylic acid fraction in sample E 48537 (A), well A and E 48480 (B), well E. Numbers on peaks refer to chain length of n -fatty acids. A, pristanic acid; B, phytanic acid; C, 17β(H), 21β(H)-bishomohopanoic acid; D, various isoprenoid fatty acids; E, various hopanoic acids.

very high bacterial productivity and conditions favourable for the preservation of OM in sediments (e.g. Buchholz *et al.*, 1993). Only in sample E 48532 (well A) the C₃₃-17β(H), 21β(H) is predominant.

Even-numbered *n*-fatty acids, especially *n*-C₁₆, *n*-C₂₂ and *n*-C₂₄ are the dominant compounds in the fatty acid fraction of well B (Fig. 4.35 B). A maximum at *n*-C₂₂ was observed in most of the bitumens from the Gao area. With the exception of the sample E 48480 (*n*-C₁₆) the fatty acids in well E maximise at *n*-C₂₆ or *n*-C₂₈, which might suggest higher terrigenous input to the lake. The CPI values for the long-chain fatty acids in the Lei area are much lower compared to the Shu-Du area. The highest value of 1.55 was observed for sample E 48484 from well E. This is an indication of the higher maturity level. Source rock bitumens from the Gao area show higher CPI values with up to 4.11 (well K).

4.7.6.2 Neutral NSO compounds

N-Alcohols

The *n*-alcohols are the major alcohols detected, although they have very low concentrations. Bitumens of the laminated shales in well A (E 48529 to 48537, GS sub-unit) show a bimodal distribution of the *n*-alkan-1-ols, maximising at *n*-C₁₅, *n*-C₁₆ or *n*-C₁₈ and *n*-C₂₀, *n*-C₂₂ or *n*-C₂₄, respectively. The short to long chain ratio ($\sum n\text{-C}_{9-20} / \sum n\text{-C}_{21-28}$) ranges from 0.16 to 1.66 indicating that the short-chain *n*-alkan-1-ols are predominant (Tab. 4.13). Robinson *et al.* (1984) found that short-chain *n*-alcohols are degraded much faster than their longer-chain homologues. Thus, variations of this ratio result from diagenetic processes. The CPI of the long-chain *n*-alkan-1-ols (C₂₂ to C₂₈) ranges between 0.78 (E 48514) and 7.08 (E 48455; Tab. 4.13). The even-carbon-number predominance of the *n*-alcohols in most of the samples arises from their biosynthetic formation by the enzymatic reduction of *n*-fatty acids. The non-laminated samples (E 48525 and E 48520, Shale I sub-unit) show a characteristic maximum at *n*-C₁₈. A maximum in the short-chain range is thought to be associated with algal (Weete, 1976) or bacterial (Albro, 1976) input. The second maximum in the long-chain range (24-28) was attributed to higher plant input (Eglinton & Hamilton, 1967) whereas *n*-alkan-1-ols in the mid-chain-range (20-24) might be typical for macrophytes (Ogura *et al.*, 1989; Ficken *et al.*, 1998). However, this very simplistic interpretation is questionable because bacteria and phytoplankton can also produce long-chain *n*-alcohols (McCaffrey *et al.*, 1991; Duan, 2000). The distribution of the *n*-alkan-1-ols in the Lei area is characterised by a

predominance of the short-chain and medium-chain compounds (18-22). A lack of long-chain *n*-alkan-1-ols was observed which might be a sign of the higher maturity level in this area.

Sterols and Hopanols

Sterols are present in all eukaryotes as rigidifies of cell membranes. They are important constituents of the alcohol fraction. Samples from the DJT sub-unit in the Lei area contain abundant stanols. 24-Ethylcholestan-3-ol (Appx. C, XI), with minor amounts or its nor-homologue, 24-methylcholestan-3-ol are abundant in the wells B, C and E. The stenols, Cholest-5-en-3 β -ol, 24-methylcholest-5-en-ol and 24-ethylcholest-5-en-3 β -ol (Appx. C, XII) were identified in all of the source rock samples with two exceptions (E 48480 and E 48494). The distribution is usually dominated by the C₂₉-stenol. Volkman (1986) concluded a higher plant origin for the occurrence of 24-ethyl sterols in the marine environment. Edmunds & Eglinton (1984) as well as Kohlhase & Pohl (1988) found high concentrations of 24-ethyl sterols in cyanobacteria and cyanobacterial mats in lake deposits. The generally large proportions of stanols might be due to direct biogenic input (Nishimura, 1977), including cyanobacteria (Kohlhase & Pohl, 1988) and/or to *in situ* hydrogenation processes by intense microbial reprocessing of stenols (e.g. Nishimura, 1977; Rieley *et al.*, 1991). The stenol/stanol conversion starts in the water column, with the consequence that both compounds are present in surficial sediments (Robinson *et al.*, 1984; Robinson *et al.*, 1986). It continues after burial in the lake sediments (Nishimura & Koyama, 1976). Hydrogenation in oxygenated environments is expected to favour the 5 α (H)-stanol form, whereas the 5 β (H)-stanol form is dominant in strongly anoxic sediments (Reed, 1977; Nishimura, 1982). Interestingly, the 5 α (H)-stanol form is dominant in the investigated source rock bitumens from the Lei and Leng areas.

In the samples E 48502 and E 48525 from well B the hopanoid alcohols 22,29,30-trisnorhop-21-ol and 30-norhopan-22-ol (Appx. C, XIII) were identified which are important products of many bacteria (Rohmer *et al.*, 1984). They are diagenetic products of bacteriohopanepolyols and may originate from cyanobacteria.

Steran-3-ones

A series of steroid ketones (steran-3-ones) with the keto-group in the A ring were detected and the structures tentatively assigned (e.g. Appx. C, XIV). Two distribution types were detected. The first shows a dominance of $\alpha\alpha\alpha$ 20R isomers and was observed in most of the source rock samples within the Western Depression, while a higher degree of rearrangements and isomerisation was observed for the second type (Jordi Lopez, pers. comm.). The latter was only found in source rock bitumens from well A and from the Gao area. Steroid ketones are most likely indicative of a microbial alteration of sterols at an very early diagenetic stage (de Leeuw & Baas, 1986), although a direct biogenic origin can not be excluded (Kokke *et al.*, 1982).

Carbazoles and Fluoren-9-ones

Beside their usefulness in reservoir geochemical studies (e.g. Larter & Aplin, 1995) and as primary and secondary petroleum migration markers (e.g. Li *et al.*, 1995a), it was also demonstrated that maturity changes influence the amount and distribution of certain carbazoles (Clegg *et al.*, 1998; Horsfield *et al.*, 1998). The influence of source characteristics on polar organic nitrogen and oxygen compounds and lithology was discussed in several recent studies (Clegg *et al.*, 1997; Li *et al.*, 1999; Bakr & Wilkes, 2002). Li *et al.* (1995a) studied crude oils from the Liaohe Basin but found no facies relationships. The knowledge of the sources of polar nitrogen and oxygen compounds is still limited. Nitrogen precursors may be derived from alkaloids with an indole nucleus, often found in higher plants (Snyder, 1965) but also in blue-green algae (Cardellina *et al.*, 1979).

The low polar fraction of all bitumens comprises carbazole, benzocarbazole and their alkyl derivatives (Appx. C, XV to XVII). Total carbazole concentrations (Appx. G) range from 1.5 (E 48517, well A) to 1239 $\mu\text{g/g}$ bitumen (E 48455, well D). The maximum concentrations of total methylcarbazoles, total C₂-carbazoles and total benzocarbazoles are 4119, 3713 and 1059 $\mu\text{g/g}$ bitumen (E 48455, well D), respectively. The 1-methylcarbazole is the most abundant isomer, the 3-methylcarbazole is the least abundant. Remarkable differences between the sub-units exist. The concentrations of total methylcarbazoles in the GS ranges from 77 to 599 $\mu\text{g/g}$ bitumen. Similar trends are seen for the carbazole, C₂-carbazoles and benzocarbazoles. The amounts in the source rock extracts were found to depend on maturity.

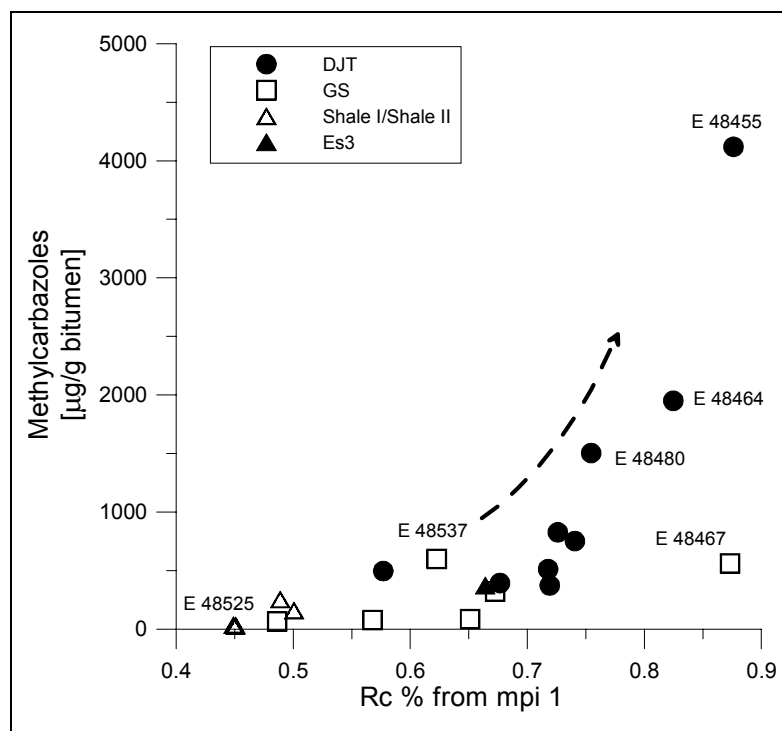


Fig. 4.36. Concentration of methylcarbazoles ($\mu\text{g/g}$ bitumen) vs. calculated vitrinite reflectance from mpi 1 for source rock bitumens from the Es4 and Es3 member.

A plot of total methylcarbazoles concentrations *versus* vitrinite reflectance calculated from mpi 1 is shown in Fig. 4.36. This plot shows an intense generation of methylcarbazoles at a vitrinite reflectance of 0.7% Rc. This would mean that generation occurs earlier than in other source rock sequences. Clegg *et al.* (1998) found an intense generation and between 0.9 and 1.09% Rr. Clegg *et al.* (1997) described a systematic change of the benzo[a]carbazole/(benzo[a]carbazole+benzo[c]carbazole) and other ratios based on alkylcarbazoles with increasing maturity. However, only the 1,8-dimethylcarbazole/(1,8-dimethylcarbazole+1-ethylcarbazole) ratio displays an increasing trend with increasing maturity for the DJT. Most noteworthy are the very high concentrations in some samples of the DJT in the Lei area (E 48455, E 48464 and E 48480) and the unusual high concentrations in sample E 48537 from well A (Appx. G). They are a full order of magnitude higher than in the GS sub-unit and up to three times that reported in the literature. Clegg *et al.* (1998) studied Mexican source rock bitumens from the Sonda de Campeche and found highest concentrations of 333 $\mu\text{g/g}$ bitumen for the total methylcarbazoles at 1.09% Rr. Maximum recovered concentrations for the total methylcarbazoles from clastic source rocks of the Posidonia shale are below 100 $\mu\text{g/g}$ bitumen (Horsfield *et al.*, 1998). These high concentrations are mainly affected by maturity, however an additional facies influence is likely because such high concentrations were not observed previously. One possibility is the contribution of certain algae, rich in organic nitrogen compounds (e.g. Cardellina *et al.*, 1979).

Fluoren-9-ones are common in diesel engine combustion products and burning woods (Ramdahl & Becher, 1982; Jensen & Hites, 1983). In geological setting, they were first identified in the Willington petroleum (Latham *et al.*, 1962). Reports on their utility to characterise the depositional environment are rare. Mojelsky & Strausz (1986) concluded that they might be used as redox potential indicators in reservoirs.

Fluoren-9-one and its alkylated homologues (Appx. C, XVIII & XIX) are the quantitatively most important compounds in the low-polarity NSO compound fraction of the investigated source rock bitumen. The maximum concentrations for the fluoren-9-one is 968 $\mu\text{g/g}$ bitumen and for the 1-methylfluoren-9-one 1643 $\mu\text{g/g}$ bitumen (E 48455, well D). By comparing the Lei area with well A (Shu-Du area), significant differences were recognised concerning the distribution and abundances of fluoren-9-ones. In all samples from well A with the exception

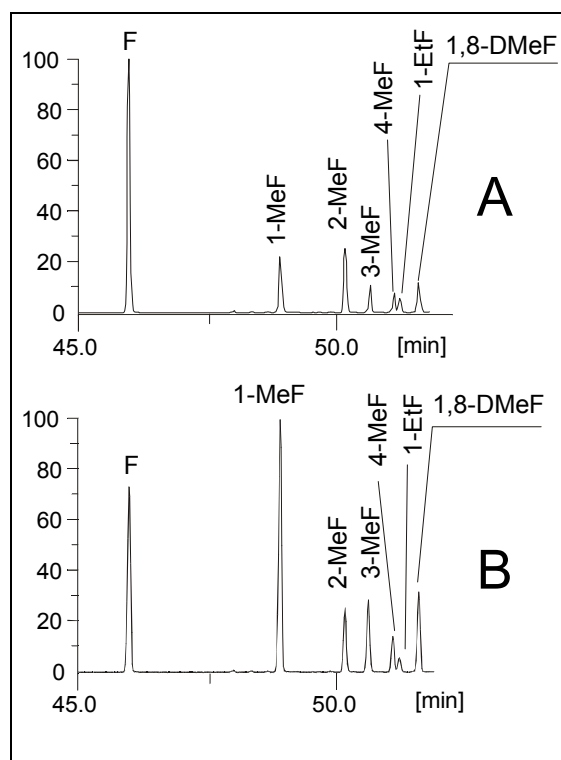


Fig. 4.37. Distribution patterns of fluoren-9-ones and alkylated derivatives. GC-MS measurements (m/z : 180, 194, 208); A, group 1; B, group 2.

of the deepest, the unsubstituted fluoren-9-one (F) is more abundant than the alkylated fluoren-9-ones (group 1, Fig. 4.37 A). The four methylfluoren-9-one isomers are dominated by 1-methylfluoren-9-one (1-MeF) or 2-methylfluoren-9-one (2-MeF). In many samples from the Lei area the fluoren-9-one concentration is lower compared with that of the methylated homologues. A dominance of 1-methylfluoren-9-one was observed in these samples (group 2, Fig. 4.37 B). For example, all analysed samples from well C belong to the second group. Although this distribution pattern may express different stages of maturity, strong source related differences were also found. Interestingly, all samples from the shale rich Shale I/II sub-units and Es3 member belong to group 1. Concentrations of the fluoren-9-ones within the GS

are also controlled by maturity. Concentrations of fluoren-9-one and 1-methylfluoren-9-one show an increasing trend with increasing depth (Appx. G). Wilkes *et al.* (1998) observed an increasing trend with increasing maturity for the Posidonia Shale. The ratio of 1-ethylfluoren-9-one/(1-ethylfluoren-9-one+1,8-dimethylfluoren-9-one) shows an increase with increasing depth for the GS as well as for the DJT (Appx. G) and is therefore the exact opposite of the trend reported for the Posidonia Shale maturity sequence (Wilkes *et al.*, 1998).

Points to Remember – Soluble Organic Matter

Liquid chromatographic separation of the extracted source rock samples revealed, that the bitumens are rich in NSO compounds. The lower CPI values of the *n*-alkanes in the Lei than in the other areas indicate higher maturity for the deeper buried samples. Conventional maturity parameters such as the $T_s/(T_s+T_m)$ are strongly influenced by the depositional environment. Good trends with depth were observed for the non-aromatic and aromatic hopanoids as well as for parameters based on methylphenanthrenes. Pr/ph ratios show considerable variations within the sample set. Generally, low ratios for the GS and DJT were observed, reflecting the carbonate rich anoxic environment. The carotenoids β - and γ -carotane as well as higher concentrations of $\alpha\alpha\alpha$ -C₂₈-sterane point to a more anoxic, higher saline depositional environment within the GS and DJT. The gammacerane index values are generally low, but higher values were found for the laminated samples from the GS, indicating higher salinities and/or an at least partly stratified water column. Branched alkanes as well as specific sterols and stanols can be related to the presence of cyanobacteria and cyanobacterial mats. The occurrence of mono-aromatic carotenoids in the aromatic fraction points to the presence of photic zone anoxia in the paleo-water column. Very high ph/*n*-C₁₈ ratios suggest an additional source for phytane, derived from chlorophyll *a*, chromans or archaeal lipids. An origin from archaea is consistent with the occurrence of high concentrations of phytanic acid. The oleanane indices are generally low, indicating that angiosperm input to the lake basin was minor. A high abundance of lycopane and its aromatised diagenetic analogs, which are thought to derive from the L-race of *B. braunii*, were found in bitumens from the Shale I. Abundant hopanoids, high concentrations of steran-3-ones as well as the presence of iso- and anteiso fatty acids, especially within the GS and DJT laminated source rock samples indicate an important bacterial contribution to the OM or that a considerable degree of microbial reworking took place. Variations in the concentration and distribution of carbazoles and fluoren-9-ones depend mainly on maturity.

4.8 Paleoenvironment of Deposition

A subdivision of lake basins was established by Carroll & Bohacs (1999) and Bohacs *et al.* (2000). This classification utilises three end-member facies associations in lake strata based on physical, chemical and biological factors. These facies associations correspond to distinct lake-basin types. Each type is characterised by typical litho- and organofacies associations. **(1)** The overfilled lake-basin with a fluvial-lacustrine facies association (open-lake hydrology) which contain a freshwater fauna and mixtures of aquatic and terrigenous OM (type I to III kerogen). **(2)** The balanced-fill lake-basin with a fluctuating-profundal facies association contain a fresh- to saline water biota and is dominated by aquatic OM (algal-bacterial type I kerogen). The lake hydrology can be open or closed and **(3)** the underfilled lake basin with an evaporative facies association exists in a closed lake and contains a wide variety of litho-facies with evaporites and a mainly low-diversity, salinity tolerant flora (type I kerogen). The terms overfilled, balanced fill and underfilled are linked to basin tectonics and describe a system where the accommodation rate is lower, in balance or much larger than water plus sediment supply. Bohacs *et al.* (2000) has proposed that the Es4 member of the Shahejie Formation belongs to the third lake-basin type. However, the results presented in this thesis allow a much more detailed subdivision based on lithofacies and organofacies variations. This subdivision recognises carbonate dominated systems with playas and mud flats during lake level lowstands in DJT and GS time, while clastic dominated freshwater conditions prevailed during highstands in Shale I, Shale II and Es3- time. The DJT sub-unit in the marginal Shu-Du area is characterised by litho- and organofacies successions typical for a fan-delta depositional environment. The evolutionary changes in the lake through time (Es4, Es3) and space (well A, well B) are presented in Tab. 4.14.

time space	Environment		Source Potential
	Well A (Shu-Du)	Well B (Lei)	
Es3 member	open lake, freshwater		moderate (type II/III)
Shale II	open lake, freshwater		moderate (type II/III)
DJT	fan-delta	upper: playa/shallow lakes	moderate to excellent (type I/II)
	fan-delta	lower: broad mudflats	poor (oxidation)
Shale I	open lake, freshwater		moderate (type II/III)
GS	shallow lakes	playa/shallow lakes	excellent (type I)

Tab. 4.14. Development of the Liaohé lake through time and space.

4.8.1 Marginal Fan-Delta Environment

Abundant quartz and feldspar containing sandstone layers of the DJT sub-unit in well A reflect abundant clastic input to the lake basin (Tab. 4.2). Especially at the margins of ancient lake basins coarse clastic facies developed, while axial areas are dominated by the accumulation of laminated muds (e.g. Renaut & Tiercelin, 1994). This suggests that the sediments during DJT time in the marginal Shu-Du area were deposited in areas of relatively high topographic relief on large alluvial fans and deltas, where a slope favours rapid transfer of sediment to the basin floor. Other lake margin facies associations have been previously

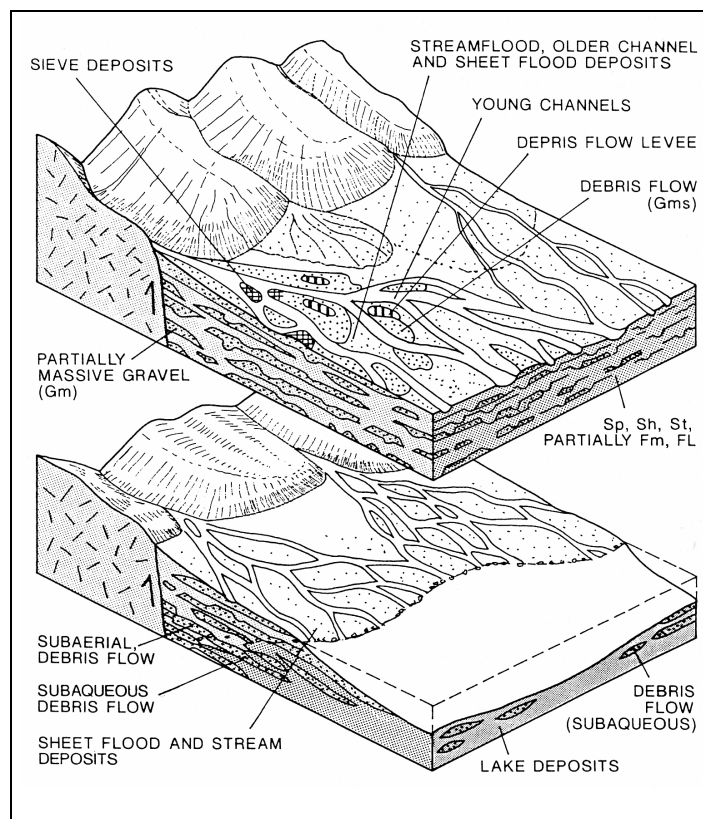


Fig. 4.38. Fan-delta depositional environment with facies associations; after Einsele (2000).

interpreted as fan-delta deposits such as the coarse grained alluvial sediments of the Colton and Wasatch Formations within the Uinta Basin (Ryder *et al.*, 1976). After McPherson *et al.* (1987) the term fan-delta describes small, coarse-grained deltas which formed where an alluvial fan at the foot of a mountain source area progrades into a standing body of water. Gravel and sand accumulate at the mouth of streams but can and move as subaqueous debris flows into deeper water and can thence alternate with muddy lake deposits. Fig. 4.38 shows a typical alluvial fan entering an active tectonic graben occupied by

a lake. Erosion and transport occurred during the more humid parts of climatic cycles when rivers were able to carry a high sediment load (Einsele, 2000). The detritus was not reworked extensively during transport and derived from proximal provenances, namely the marginal mountain areas of the Jiao-Liao Rise and the Yan-Shan folded belt. A similar environment has been proposed for the Tuo area in the northern part of the Western Depression (Liguo Hu, pers. comm.).

TOC contents are overall low (Tab. 4.5). Lower HI values and H/C ratios of a kerogen from well A at 1252 m depth (E 48517) reflect a predominantly mixed to terrestrial OM source (type II to III kerogen; Tab. 4.6). The aromaticity and the phenol ratio (PhR) from Py-GC-FID are high (Tab. 4.8) which points to an increasing terrigenous input (e.g. Horsfield, 1989). Microscopic examinations revealed the presence of huminite, vitrinite, sporinite and liptodetrinite (Figs. 4.12 C1 and C2). This is supported by Sun *et al.* (1995) who studied facies variations in the Shahejie Formation of the Eastern Depression. The authors observed that marginal fan-delta areas always contain abundant huminite and vitrinite particles. The higher proportions of liptodetrinite within this facies type may result from an OM deposition in waters with periodically influence of energetic flows (e.g. Smith & Gibling, 1987).

4.8.2 Freshwater Environment

This facies is typical for the Shale I and Shale II sub-unit as well as for the shales from the Es3 member. Samples contain the highest percentages of clay minerals and siderite (Fig. 4.6 and Fig. 4.7). The thick shale packages represent transgressive cycles with lake-level high-stands and were deposited during extensional phases of the rift development mainly in greater water depth in the lake centre (Liguo Hu, pers. comm.). The abundance of smectites and mixed-layer clay minerals was related to weathering of volcanic particles in a warm and humid climate in the drainage area (Deconinck & Chamley, 1995; Gingele, 1996).

The shales in this environment are mainly non-laminated (see section 4.4). One important prerequisite for the formation of laminated sediments are seasonal changes, such as algal bloom periods during warm periods (e.g. Anderson & Dean, 1988). This indicates the absence of any important annually or seasonal climatic oscillations. TOC contents and HI values can give an indication of the amount and type of OM deposited and its degree of preservation. The TOC contents within this facies type range between 3.6 and 8.8% and HI values vary between 370 and 645 mg HC/g TOC, indicating type II to III kerogen. While the TOC is directly related to lake productivity and the degree of dilution by clastic material, the HI is more connected to preservation which in turn depends on the persistence of anoxic conditions and lake circulation patterns (cf. Dean, 1981; Curiale & Gibling, 1994). Because the OM composition is very unique (*Botryococcus* alginite), the varying HI values within this facies type (Fig. 4.13) may indicate different degrees of oxidation due to sediment deposition in different lake environments. For example, Picard & High (1981) observed a strong offshore increase of organic carbon in modern lakes and proposed a better preservation in a deep

anoxic lake facies. However, a greater oxidation of the OM may also result from an intense water column circulation or from lower lake levels and desiccation.

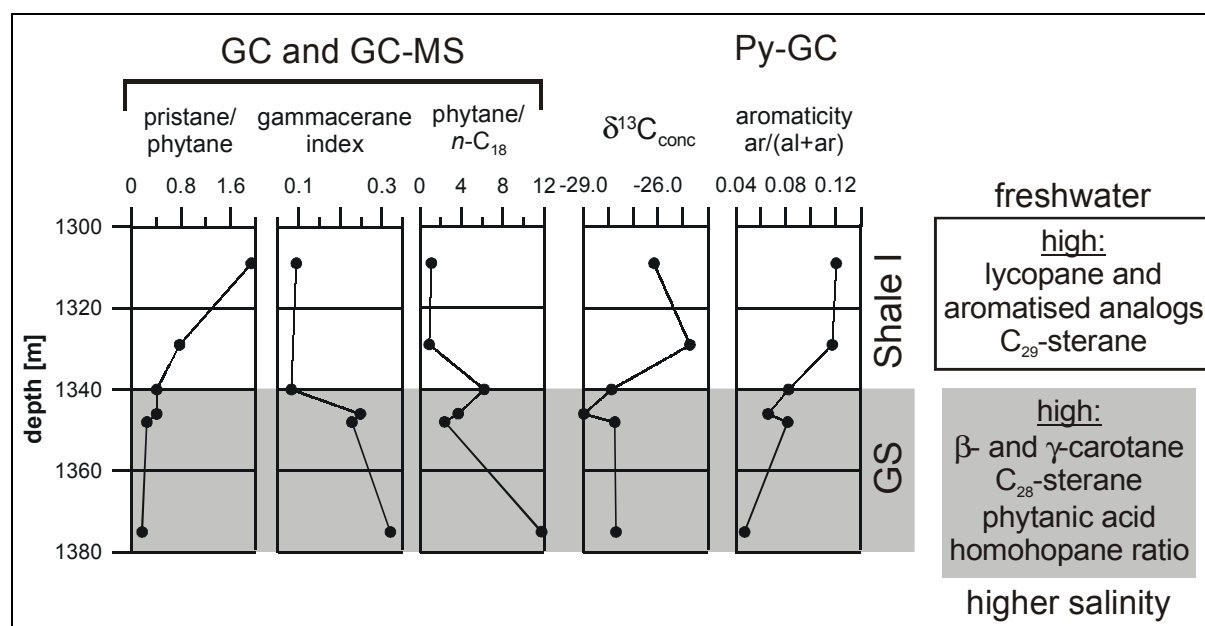


Fig. 4.39. Facies summary for well A. Organic geochemical parameters for well A in the Western Depression of the Liaohe Basin. The aromaticity is based on the aromatic (ar) versus aliphatic (al) nature of the kerogen from Py-GC-FID.

Deposition in an anoxic, deep-water facies is strongly supported by the presence of siderite with proportions up to 23.1% (Fig. 4.6). Siderite is restricted to environments with low sulphate waters and thus very common in low salinity open lake basins (Hsü & Kelts, 1978). Zhang *et al.* (1996) found abundant FeCO_3 in open areas of Chinese deep lakes (depth above 10 meters), while the mineral was absent in shallow lakes, delta-front and prodelta settings. Siderite generally forms under strongly reducing conditions in the methanic zone (Berner, 1981). Goth (1990) interpreted the occurrence of siderite as an indicator of meromixis within the ancient Lake Messel, which was stabilised by the oversaturation of Fe^{2+} and HCO_3^- ions in the lake body.

The OM, as observed under the microscope is mainly composed of telalginite (*Botryococcus*) with minor contributions of vitrinite and sporinite (Fig. 4.12 B). The planktonic, predominantly fresh or brackish-water green alga *B. braunii* belongs to the *Chlorophyceae* and forms polymorphous colonies of 0.1 to 0.6 mm in size (Guy-Ohlson, 1992, 1998). The alga is known to bloom and because of its buoyancy to form floating mats of several hundred square meters. Similar $\delta^{13}\text{C}$ values, around -25 as for the Liaohe kerogens (Fig. 4.39; Tab. 4.6) were reported from other Recent lake sediments with abundant remains of the alga *B. braunii* (Huang *et al.*, 1999).

Because of the overall lack of macerals derived from land plants, the odd over even predominance in the *n*-alkane distribution (Tab. 4.10) are related to terrigenous OM that is submicroscopic or to other sources than terrigenous OM. Similar distributions, maximising at *n*-C₂₃ or *n*-C₂₇ were previously observed in maar-type oil shale deposits of Gércse and Pula located in Hungary (Lichtfouse *et al.*, 1994; Derenne *et al.*, 2000). Based on $\delta^{13}\text{C}$ measurements it was interpreted, that the long-chain *n*-alkanes (*n*-C₂₇ to *n*-C₃₃) result from the diagenetic reduction of odd-numbered *B. braunii* alkadienes. Based on this similarity, it is possible that the *n*-alkane distribution reflect a significant contribution of *Botryococcus* to the OM, although an input of OM from macrophytes cannot be excluded. Especially submerged and floating species were reported to cause high concentrations of mid-chain length, C₂₃ and C₂₅ *n*-alkanes (Ficken *et al.*, 2000).

Three different chemical races, termed A, B and L can be distinguished in extant *B. braunii*, based on the type of hydrocarbons biosynthesised. Race A produces long-chain *n*-alkadienes and *n*-alkatrienes in the C₂₅ to C₃₁ range (Metzger *et al.*, 1986), race B produces *botryococcene* hydrocarbons and race L lycopa-14(*E*),18(*E*)-diene (Metzger & Casadevall, 1987). The high concentration of lycopane and its aromatised homologues (Appx. C, I and V) in the aliphatic and aromatic fractions from the Shale I sub-unit point to the presence of the L-race of this algal species. The chemical structure of the algaenans from the A and B races is based on long polymethylenic chains (e.g. Kadouri *et al.*, 1988). In addition, the L race comprises C₄₀ isoprenoid chains with a lycopane skeleton yielding a number of isoprenoid compounds upon pyrolysis (Derenne *et al.*, 1989; Derenne *et al.*, 1990). Thus, the presence of the isoprenoid alkanes and alk-1-enes in the Shale I pyrolysates (Tab. 4.8; Fig. 4.19 C) may reflect a significant contribution of the L race of *B. braunii* in agreement to that what was observed by microscopical analysis.

Pr/ph ratios range between 0.8 and 1.9 within the Shale I in well A and are generally higher than those of the GS sub-unit (Fig. 4.39). Source rocks deposited in a freshwater environment are characterised by pr/ph ratios between 1.2 to 2.2 as observed in a number of other Chinese basins (Wang *et al.*, 1997), while ratios less than unity indicate a brackish-saline depositional environment. Li *et al.* (1995) found pr/ph ratios between 0.9 and 2.0 in source rock extracts of the Es3 member from the Western Depression. The carotenoids β - and γ -carotane are only minor constituents of the aliphatic fraction, whereas the $\alpha\alpha\alpha$ C₂₉-sterane is more abundant than its C₂₈-homologue, both reflecting a greater freshwater influence (Ritts *et al.*, 1999). This is also supported by lower gammacerane indices between 0.04 and 0.08 in the Shale I compared with the GS (Fig. 4.39; Tab. 4.10). The schematic diagram in Fig. 4.40 illustrate the open lacustrine depositional environment of a broad and deep lake with its fine clastic lithologies in the basin centre that lack of evaporites.

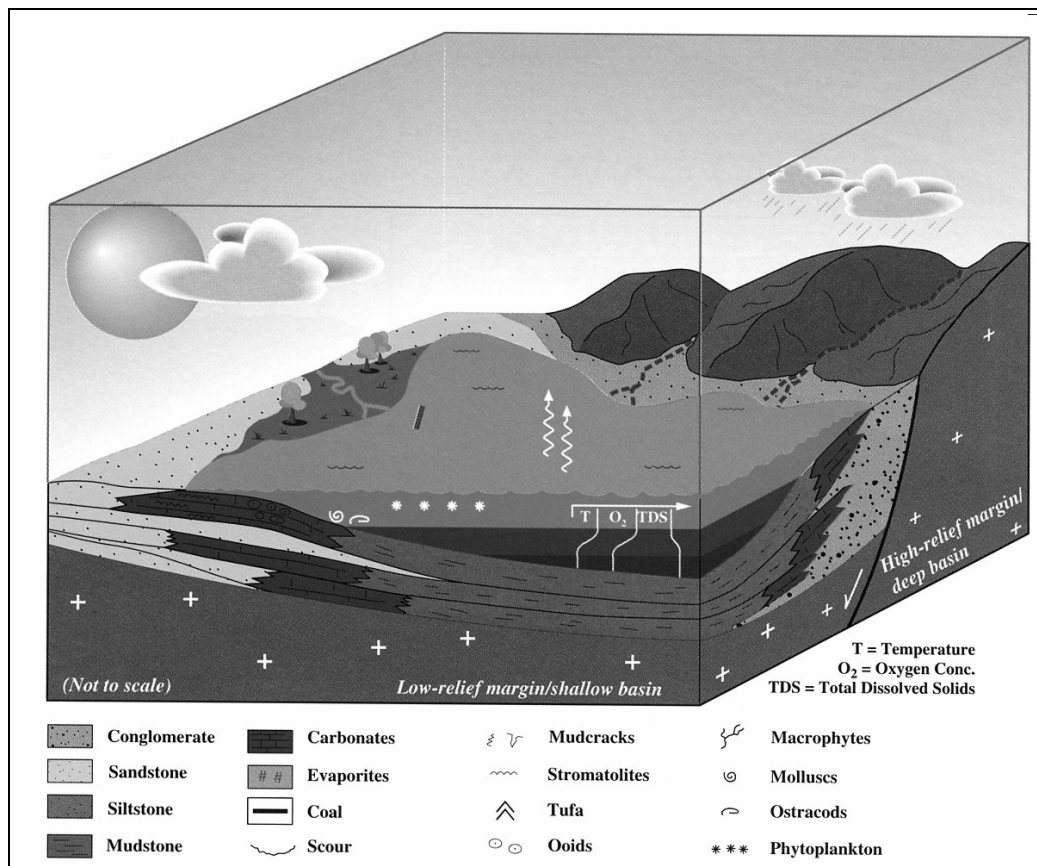


Fig. 4.40. Fluctuating-profundal facies association, typical for the freshwater facies in the Western Depression of the Liaohe Basin; from Bohacs *et al.* (2000).

4.8.3 Playa and Shallow Lake Facies

The variability of the Liaohe lakes from an expanded form (Shale I, Shale II, and Es3) to a shallow lake system (GS, DJT) occurred in response to increased aridity. Typical for this lacustrine stage are hydrologic closure of the lake basin and increasing importance of groundwater influence.

The mineral assemblages in the playa-lake facies (chapter 4.3) are a direct response to precipitation-evaporation cycles. The lakes had low water tables, higher saline waters and high Mg^{2+}/Ca^{2+} ratios. In such an environment lake-levels can fall and rise drastically from small playa lakes at lowstands to perennial lakes at highstands. Broad saline mudflats existed during dry seasons. Frostick *et al.* (1986) observed that in the modern rift-basins of Africa only a few meters of lake-level rise and drop are necessary to flood or to expose large areas. Carbonates, gypsum and analcime are the characteristic minerals. The following precipitation sequence can be applied to the sediments deposited:

low-Mg calcite \Rightarrow high-Mg calcite \Rightarrow aragonite \Rightarrow gypsum \Rightarrow dolomite \Rightarrow analcime

Abundant dolomite is present (Fig. 4.7) which generally forms in alkaline environments and do not precipitate in freshwater lakes (Jones & Bowser, 1978). As stated in section 4.3.3.1 this process occurred in very shallow waters and was aided by evaporitic pumping and probably mediated by cyanobacterial release of magnesium. Gypsum has to be removed prior to dolomite formation by the precipitation of gypsum and/or activity of sulphate reducing bacteria.

Analcime which is especially abundant in the lower DJT sub-unit (Fig. 4.7) in the central Lei area, formed as an authigenic mineral in muds with the sodium supplied from brines in a dry climate. It is a very late diagenetic product of a brine evolution which suggests that the evaporating waters had already very high concentrations. No volcanic rocks or pyroclastic sediments are involved in this process. Analcime cementation occurred early diagenetic at near surface or shallow-depth, prior to significant compaction of the sediments, and is controlled by the chemistry of pore waters inherited from the lacustrine environment (Renaut, 1993). Aluminium and silica were delivered by solution of detrital silicates such as expandable clays in high alkaline residual sodium brines (ph 9-12). The evaporative pumping mechanism played an important role in the reaction with silicates to form analcime (Fig. 4.41). Water and dissolved salts moved from the phreatic zone toward the surface so

that the salts were concentrated into brines (Hsü & Siegenthaler, 1969). The brines probably evolved from rainwater that eroded the metamorphic rocks in the surrounding mountain areas of the Liaohe Basin. The waters moved into the lakes and underlying sediments while they took up ions in solution. Finally, they were concentrated by evaporation and precipitated or the brines reacted with silicates. Such a saline fluid development was described for Recent Lake Megadi, Kenya (Eugster, 1970; Jones *et al.*, 1977).

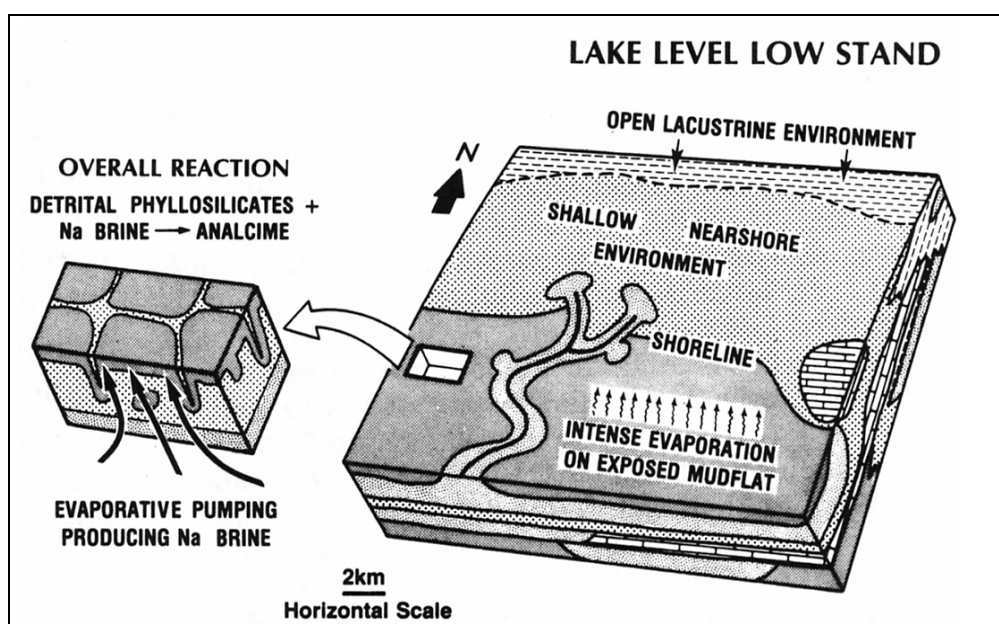


Fig. 4.41. Mineral precipitation in a playa-lake/mudflat environment; from Remy & Ferrell (1989).

The organic petrology type A (Fig. 4.12 A) is characteristic for the lower DJT sub-unit. Only very small unicellular algae were found, reflecting a hypersaline and evaporitic environment with a low-diversity biota (Carroll & Bohacs, 1999). Exposure, frequent desiccation, oxidation and destruction of the OM lead to relatively low TOC (2.5 to 5.3%) and HI values (408 to 650 mg HC/g TOC), indicating that ultimate preservation was low.

The deposition of abundant calcite in the upper DJT sub-unit in well B marks the onset of a freshwater influence with lower Mg^{2+}/Ca^{2+} ratios and higher lake-levels than in the lower DJT sub-unit. No analcime and only minor dolomite were found in this section but siderite is relatively abundant (Fig. 4.7). This is supported by XRD data from other wells in the Lei area. Calcite precipitation is indicative for lowest salinity and highest lake level and often formed during refreshment periods of lakes. Aragonite is precipitated mainly during warm climates. In the Dead Sea this happens only when water temperatures exceed 35°C (Neev & Emry, 1967). Finally, during deposition of the Shale II sub-unit only calcite persisted. This evolution

points to a stepwise establishment of full lacustrine conditions which is part of a major transgressional cycle that started at the end of the Es4 member (Fig. 4.3).

During GS-time, shallow lakes were a preferential setting for the accumulation of an organic-rich facies. The alkaline lake waters supported a high level of primary production because of the abundance of CO₃ ions available for incorporation by diverse organisms (Kelts, 1988). A lamination is typical for sediments from this facies type (Figs. 4.12 D and E). Fluoramorphinite and fluorescing lamalginite are concentrated in bright layers, separated from darker layers. The lamination reflects a cyclic, probably seasonal sedimentation pattern. Most likely the fluorescing AOM result from the microbial alteration of lipid-rich OM such as cyanobacteria and benthic and planktonic algae (Teichmüller & Ottenjann, 1977; Mukhopadhyay *et al.*, 1985; Stasiuk, 1993). Based on TEM observations Largeau *et al.* (1990) suggested, that fossil cyanobacterial OM in microbial mats is generally amorphous. In the investigated samples lateral transitions from fluoramorphinite to lamalginite and the occurrence of lamalginite structures within fluoramorphinite layers were observed. These observations strongly suggest that the fluoramorphinite is a residue of microbial altered algae and cyanobacteria, which lived in a “cyanobacterial mat” or microbial mat. Such microbial mats are major sources of OM in a shallow playa lake environment (e.g. Bauld, 1981). Different primary producers are incorporated in the formation of a microbial mat, including filamentous cyanobacteria, filamentous algae, pink filamentous bacteria, purple sulphur bacteria or heterotrophic bacteria living on microbial mat OM (Kenig *et al.*, 1990; Kenig, 2000; Riding, 2000). Microbial mats are layered communities with phototrophic organisms in the upper layers and chemoorganotrophic bacteria with H₂S production in the lower layers (Madigan *et al.*, 1997, p. 546). As reviewed by Riding (2000) the irregular surface morphology of such mats can easily trap micritic sediment which was transported by eolian processes. These grains become the substrate for further microbial growth which occurs during pauses in sedimentation and act as a stabilisation. This process may lead to the observed laminations. However, an alternating deposition of lacustrine sediments (flooding) and microbial growth is also possible (Kendall & Skipwith, 1969).

Organic geochemical analysis revealed, that with the exception of type A (Fig. 4.12 A), HI values are generally high and vary between 763 and 908 mg HC/g TOC for type D and 493 and 856 for type E. TOC contents are in the range between 6.0 to 11.5% and 3.8 to 10.1%, respectively (Tab. 4.5). This reflects an excellent source rock potential and an oil prone type I kerogen. These values are higher than those from the literature for analysed cyanobacterial mats (e.g. Kenig, 2000), but this also depends strongly on environmental factors such as desiccation and preservation.

Pyrolysates of laminated samples from the GS sub-unit are especially rich in long-chain *n*-alk-1-enes and *n*-alkanes as expressed by a low aromaticity (Fig. 4.39) and belong to the high-wax paraffinic crude oil generation facies. Changes in autochthonous *versus* allochthonous contribution can be responsible for variable aliphatic proportions of the kerogens. However, it was previously shown that terrigenous input to the sediments was not important. Recent investigations revealed that different microalgal species can produce very specific algaenans with varying alkyl chain lengths (e.g. Gelin *et al.*, 1999). Thus, differences between the chromatograms in Fig. 4.19 probably reflect specific algal OM input. The *n*-alk-1-ene/*n*-alkane distribution of sample E 48537 from the GS sub-unit, with a strong predominance of long-chain alkyl units could indicate a contribution of biomacromolecules from Eustigmatophytes such as the euryhaline algae *Nannochloropsis* to the kerogen. Flash pyrolysates of the algaenans from two species are very similar to the pyrolysates studied herein (Gelin *et al.*, 1997; Gelin *et al.*, 1999), although the series of mid-chain ketones were not detected. However, varying redox conditions in the lacustrine environment may also lead to changes in the chain length distribution. It was reported that higher-wax contents can be related to hydrogen-rich OM which was deposited under more anoxic conditions (Sachsenhofer *et al.*, 1995). This is substantiated by the lower pr/ph ratios in the GS than in the Shale I sub-unit of well A (Fig. 4.39). The alkalinity and salinity of the lake waters may also play an important role. Fig. 4.17 shows that the laminated samples from the more saline and alkaline GS sub-unit plot in a different part of the diagram than the samples from the freshwater influenced Shale I and Es3 member. This contradicts results from Horsfield *et al.* (1994) who indicated that deposition in a saline or freshwater has no measurable effect on the petroleum composition. High concentrations of alkylbenzenes (Tab. 4.8; Fig. 4.19 B) are especially abundant in pyrolysates from the Gao area and suggest the presence of macromolecular bound carotenoids (Requejo *et al.*, 1992; Hartgers *et al.*, 1994). Possible precursors are green and purple sulphur bacteria, which are possibly associated with the microbial mats.

Two authors analysed the pyrolysate composition of cyanobacterial mats. Chalansonnet *et al.* (1988) found a resistant nonhydrolysable biopolymer in cyanobacteria which is matching those isolated from *B. braunii*. However, generally shorter chain lengths were observed showing no similarity to the laminated Liaohe kerogens. It was recently reported that the macromolecule described in this study might represent an artefact resulting from the isolation process (Allard *et al.*, 1997). Remains of cyanobacteria in microbial mats consist largely of carbohydrate sheets (Boon *et al.*, 1983). The authors detected furans, benzenes and phenols, but these are only minor compounds in the pyrograms investigated here, probably

suggesting that the sheets are no major contributors to the OM or were preferentially destroyed during early diagenesis.

Many carbonate or evaporitic source rocks, as well as oils from hypersaline lacustrine settings are characterised by low pr/ph ratios and an even carbon number predominance of the *n*-alkanes (e.g. Powell & McKirdy, 1973; Mello *et al.*, 1988). This is supposed to result from the reduction of even fatty acids or alcohols in strongly reducing carbonate evaporitic environments. CPI values less than 1.0 were commonly reported from carbonate rich source sequences (Tissot & Welte, 1984). Samples from the GS sub-unit in well A have high carbonate percentages up to 59% but still display a strong odd over even predominance (CPI between 2.6 to 3.4) with a characteristic maximum at *n*-C₂₇. Gelpi *et al.* (1970) observed C₂₁-C₂₇ odd numbered *n*-alkanes in the cyanobacterium *Anacystis montana*. Kenig *et al.* (1990) found an odd over even predominance of long-chain *n*-alkanes in the saturated fraction of buried microbial mats. In contrast, Boon *et al.* (1983) and Merritt *et al.* (1991) studied cyanobacterial OM and found *n*-alkanes maximising predominantly in the short-chain range (<*n*-C₂₀).

According to the interpretation of Hughes *et al.* (1995) very low pr/ph ratios together with low concentrations of aromatic sulphur compounds reflect an anoxic and fermentative carbonate rich environment. Very low pr/ph ratios (<0.4) and high ph/*n*-C₁₈ were found where phytane is available from archaea (Figs. 4.32 and 4.40). Such a source of phytane is a characteristic of higher saline lacustrine environments, which are deficient in sulphate and thus incorporation of sulphur into OM is minimal (ten Haven *et al.*, 1988). This is consistent with the occurrence of high concentrations of phytanic acid (Fig. 4.39). Interestingly, it was reported previously that methanogenic archaea often inhabit dead cyanobacterial assemblages (Kenig, 2000). Abundant gammacerane and β- and γ-carotane suggest a higher saline stratified and anoxic environment. Higher C₂₈-sterane concentrations in the GS can be related to an anoxic hypersaline environment (Ritts *et al.*, 1999). Salinity stratification in shallow lake waters, redox interfaces and thus chemically reducing conditions in the bottom muds are responsible for the good preservation of the OM. However, the chromane indices are far from those typical for hypersaline environments. Mono-aromatised carotenoids which are widespread in source rock bitumens from the GS and DJT sub-units are an indicator for the presence of green- and purple sulphur bacteria, which were frequently found in the lower part of microbial mats (Kenig *et al.*, 1990). In addition, the presence of these compounds provides evidence for euxinic conditions within the photic zone. The exclusion of oxygen might be induced by the formation of the cyanobacterial mat (Palmisano *et al.*, 1989). Iso- and anteiso-acids in many samples indicate an important bacterial input to the OM or that a considerable degree of

microbial reworking took place. Additional signs of an important bacterial contribution are the presence of abundant hopanoids and steroid ketones. The abundant 24-ethylsterols in the investigated bitumens most likely originate from cyanobacteria which is supported by observations Kohlhasse & Pohl (1988).

5 Maar Lakes

In the following chapters, a detailed analysis of the macromolecular OM in maar lake sediments is presented, using analytical thermal techniques (Py-GC-FID and Py-GC-MS) and microscopy. Other proxy data, such as pollen and inorganic geochemical analysis are available from other working groups and can be used for correlation. The chapter begins with a detailed description of the paleoclimate and regional geology of the study area. Sample selection is then documented, followed by the presentation of results. The studied maar lake sediments were provided by the “Sedimentation and Basin Analysis Group (PB 3.3)” of the GFZ Potsdam (Head: Prof. Jörg F. W. Negendank). The lakes are located in different climatic settings. Lake Holzmaar (HZM) and Lake Meerfelder Maar (MFM) are found at midlatitudes in central Europe and Lake Huguang Maar (China) in the subtropical to tropical belt of Asia.

5.1 Paleoclimatic Framework and Geological Background

5.1.1 Eifel Maar Lakes

Lake Holzmaar and Lake Meerfelder Maar are located in the Westeifel volcanic field, Germany (Fig. 5.1). Various high resolution paleoclimatic records show that abrupt climatic oscillations followed the last deglaciation in **Europe** and around the North Atlantic (e.g.

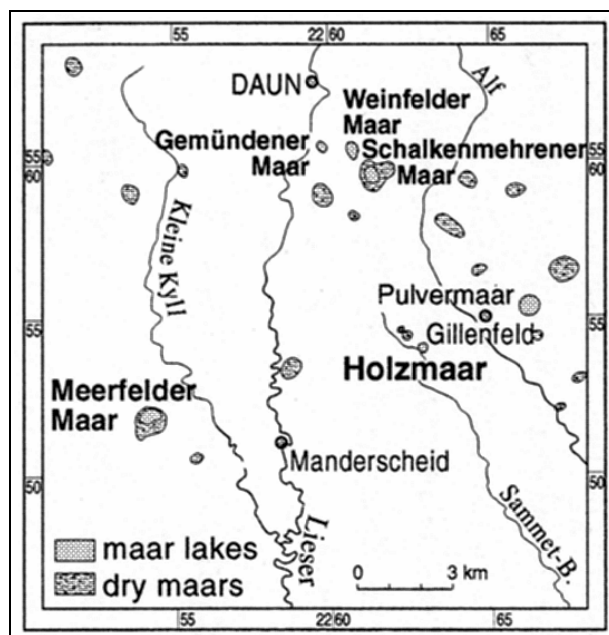


Fig. 5.1. Lake Holzmaar and Lake Meerfelder Maar in the Westeifel volcanic field; after Negendank & Zolitschka (1993)

Björck *et al.*, 1996; Goslar *et al.*, 1999; Merkt & Müller, 1999; Severinghaus & Brook, 1999). The driving forces for these events are still unclear and a matter of debate. Cold events such as the Younger Dryas were explained by the input of low-density glacial melt water with a consequent decrease of surface water salinities and breakdown of the Atlantic thermohaline circulation and associated poleward heat fluxes (e.g. Lehman & Keigwin, 1992; Broecker, 1994). This hypothesis was supported by high atmospheric ^{14}C concentrations (e.g. Goslar *et al.*, 1995; Hughen *et al.*, 2000), but also questioned, because proxy records from other deep

marine and lake sediments gave conflicting results (e.g. Charles & Fairbanks, 1992; Goslar *et al.*, 2000). Oxygen isotope records from Greenland ice cores provided evidence for dramatic and rapid changes in air temperature. They show a prominent warming from 10 to 18°C at the Late Pleniglacial/Bølling transition (Fig. 5.2). This was followed by a change to near glacial conditions, the Younger Dryas period before entering the warm Holocene which is subdivided into Preboreal, Boreal, Atlantic, Subboreal and Subatlantic. Even in the Holocene climatic shifts were large as reported in several studies (e.g. Keigwin, 1996; Alley *et al.*, 1997; Zhao *et al.*, 2000; Watanabe *et al.*, 2001).

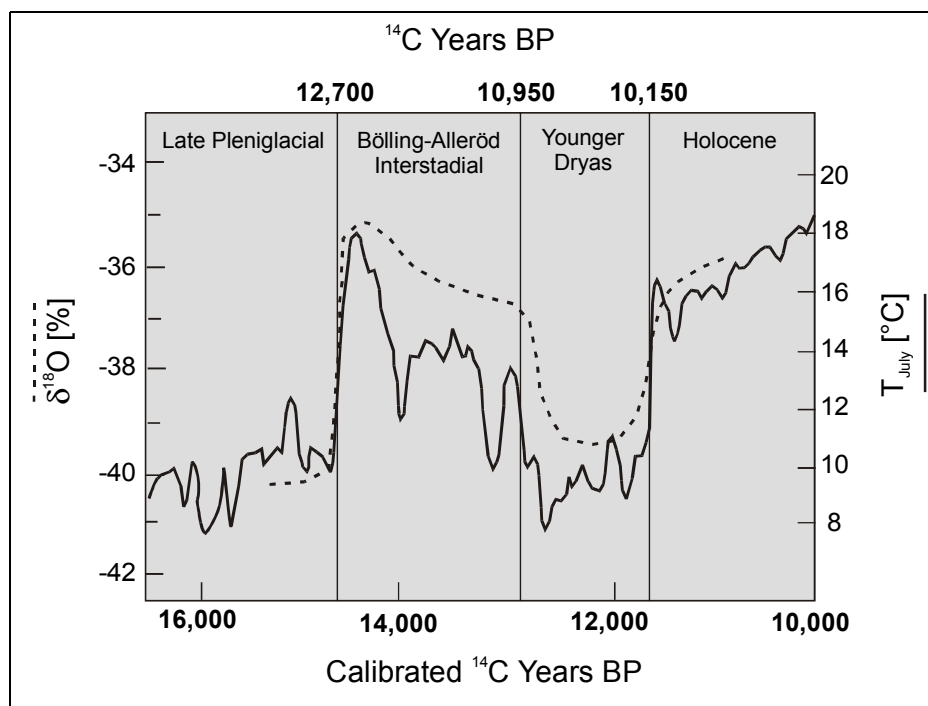


Fig. 5.2. Stratigraphy of the Lateglacial. The lines show $\delta^{18}\text{O}$ as measured in the GRIP ice-core and corresponding calculated temperatures; after Dansgaard *et al.* (1993).

The present climate in the Eifel is characterised by a pronounced precipitation maximum during winter (November to March). The mean annual precipitation is 846 mm and the mean annual temperature 7.5°C. January is the coldest month with an average temperature of -1.0°C, whereas during July 16.0°C were recorded (DVD, 1978; Müller, 1980).

Lake Meerfelder Maar (50°06'N; 6°45' E) and **Lake Holzmaar** (50°07'N; 6°53' E) are situated in the Westeifel volcanic field (Fig. 5.1), approx. 45 km north-east of the city of Trier and 95 km south of the city of Cologne. They have minimum ages of 40,000 and 35,000 years, respectively and occur in craters created by phreatomagmatic eruptions (Büchel, 1993).

The volcanism in this part of the Rhenish Massif started around 1.0 Mio to 0.6 Mio years and lasted until approx. 10,000 years BP (Büchel & Mertes, 1982).

Lake Meerfelder Maar (336.5 m a.s.l.) has a maximum depth of 17 m and is located in the largest maar crater of the Westeifel. Pyroclastic deposits, Devonian schists and Triassic rocks of the Middle Bunter Sandstone can be found in the catchment area (Schettler & Romer, 1998). The modern lake is holomictic, eutrophic and extends approx. 700 m in the E-W direction and 500 m in the N-S direction, filling 1/3 of the crater while 2/3 represent a shallow delta plain. The modern catchment area is 1.53 km², however, the catchment of the paleo-lake was much larger than today (Scharf & Menn, 1992; 2000). A small stream, the Meerbach passes through the lake and exits the crater in the south-east. More than 40 sediment cores have been taken from all parts of the lake basin (Negendank & Zolitschka, 1993). Lake Meerfelder Maar sedimentary history provides an annually laminated varve chronology for the last 14,500 years BP (Brauer *et al.*, 1999b). The top of the sequence consists of partly varved organic rich deposits with clastic intercalations (Fig. 5.3). The deepest part of the lithological profile below 960 cm is predominantly clastic and non-laminated. Two tephra layers, the 7 cm thick Laacher See Tephra (LST) and the 0.3 mm thin Ulmener Maar Tephra (UMT), were recognised within the sequence. The varve chronology dates the Allerød/Younger Dryas transition at 12,680 and the transition to the Holocene at approx. 11,590 varve yrs BP (Brauer *et al.*, 1999a).

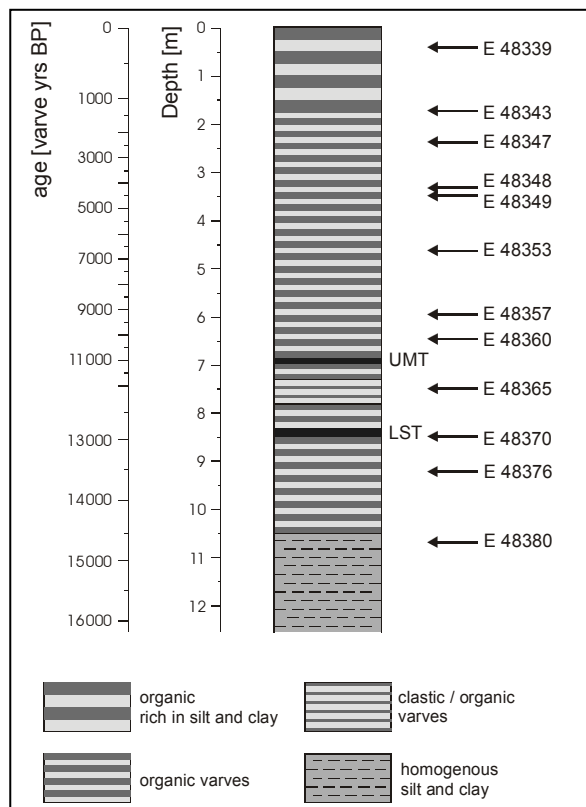


Fig. 5.3. Lithological profile of MF; after Brauer (unpublished). UMT, Ulmener Maar Tephra; LST, Laacher See Tephra). Studied kerogen concentrates are indicated.

Lake Holzmaar (HZM) is 325 m in diameter and the smallest of the Westeifel maar lakes. It is located on a peneplain at approx. 425 m a.s.l. and drained by the Sammetbach creek into the river Alf which is a tributary to the river Mosel (Zolitschka, 1998b). Lake Holzmaar is dimictic, holomictic, and mesotrophic to eutrophic today. The Sammetbach is carrying dissolved nutrients which were mainly responsible for an increasing eutrophication since the Lateglacial (Scharf & Ehlscheid, 1992; Scharf & Oehms, 1992). Seasonal related anoxic conditions below a water depth of 15 m were observed during summer (Lücke, 1998). The catchment area is made up by Lower Devonian schists, greywackes and siltstones as well as Quaternary loess and pyroclastics (Meyer, 1994). A shallow embayment evolved in the south-western corner of the lake after anthropogenic damming during the Late Middle Ages. The sediments from Lake Holzmaar are annually laminated (Zolitschka, 1990, 1991). A lamination-based chronology was established for the past 23,220 calendar years BP (Zolitschka *et al.*, 2000). The adjusted calendar-year time scale for Lake Holzmaar dated the beginning of the Holocene at 11,600 calendar years BP. The stratigraphic subdivision of the sediment cores is based on the varve chronology in combination with palynological studies (Zolitschka, 1998a; Brauer *et al.*, 1999b; Litt & Stebich, 1999; Leroy *et al.*, 2000).

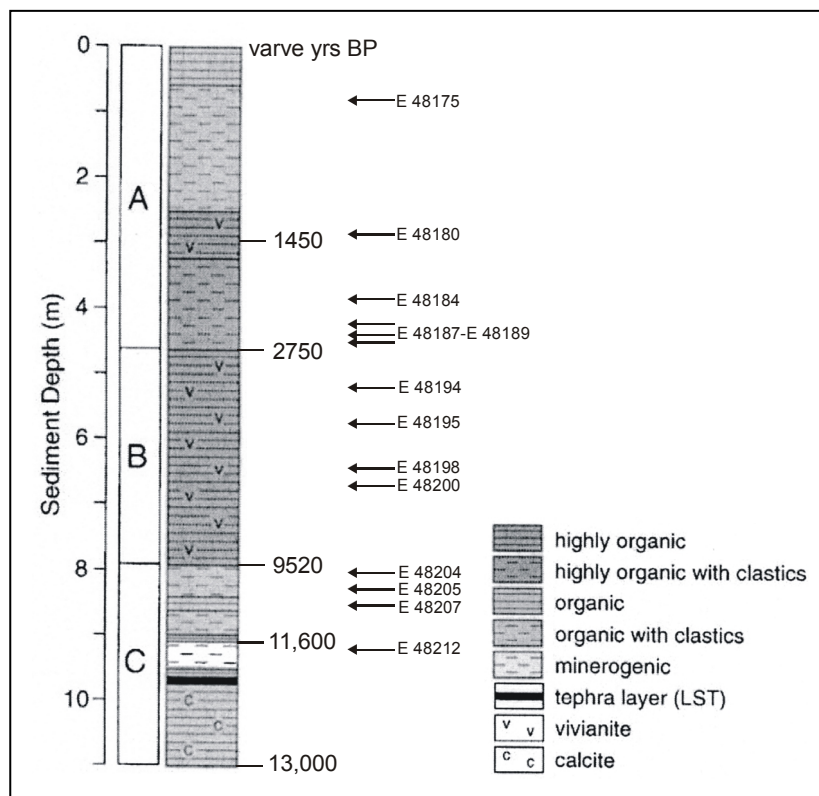


Fig. 5.4. Lithological profile of Lake Holzmaar; after Zolitschka & Negendank (1998). Studied kerogen concentrates are indicated.

The studied HZM sediment record is divided into three sections on the basis of lithological, physical and geochemical results (Zolitschka, 1998a; Zolitschka & Negendank, 1998). The sediment profile is presented in Fig. 5.4. **Section A** (460 cm depth to top; 2750 varve yrs BP to date) consists of highly organic deposits with clastic intercalations deposited during the Subatlantic. Within **section B** (780-460 cm depth; 9520-2750 varve yrs BP) the deposition of autochthonous organic laminated sediments was predominant, reflecting stable paleoenvironmental conditions with major contributions from diatoms during the middle Holocene (late Boreal to Subboreal pollen zone). **Section C** (>780 cm depth; >9520 varve yrs BP) represents the Lateglacial and early Holocene (Allerød to early Boreal pollen zone). It is characterised by organic deposits fluctuating with deposits rich in allochthonous minerogenic sedimentation. These variations can be related to the transition from glacial to interglacial conditions. This section includes the Younger Dryas period in a depth of 943-913 cm which was dated between 12,300-11,600 varve years BP (Zolitschka, 1998a).

5.3.1 Lake Huguang Maar

This maar lake is located approx. 20 km south-west of the city of Zhanjiang on the Leizhou Peninsula in south-east China (110°17'E, 21°9'N; Fig. 5.5). Sediment cores from volcanic structures in the Quaternary Lei-Qiong volcanic field provide especially extensive paleoenvironmental and paleoclimatic records.

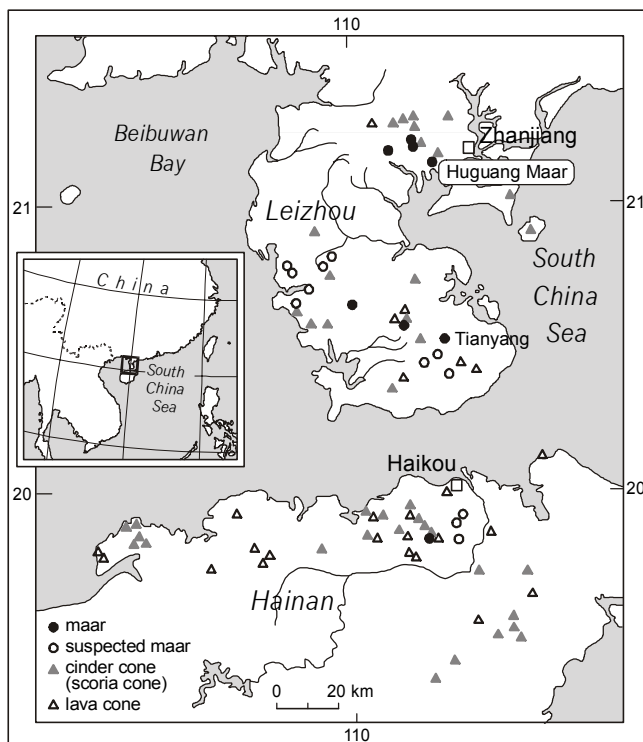


Fig. 5.5. Location of Lake Huguang Maar and the Tianyang crater.

For example, sediments from the Tianyang maar (Fig. 5.5) dating back to approximately 400,000 years (Zheng & Lei, 1999). The Huguang crater has an age of 127,000 years (Fong, 1992). Although the present lake has a maximum depth of 25 m, two thirds are less than 12 m deep. Based on physical and chemical sediment properties, the lithological profile can be subdivided into eight lithozones based on physical and chemical sediment data (Mingram *et al.*, 2000). A continuous profile containing six of the eight lithozones was available from section F. The sediment is mainly composed of a homogenous

non-laminated, greenish-black algal gyttja, only in lithozone 6 varve-like laminations were found. Abundant reworked woody material was observed in the lithozones 4 and 6. The chronological framework was established by ^{14}C -AMS-datings. All conventional ^{14}C ages were transferred into calibrated ages. A detailed description of the sedimentology and chronological framework is presented in Mingram *et al.* (2000).

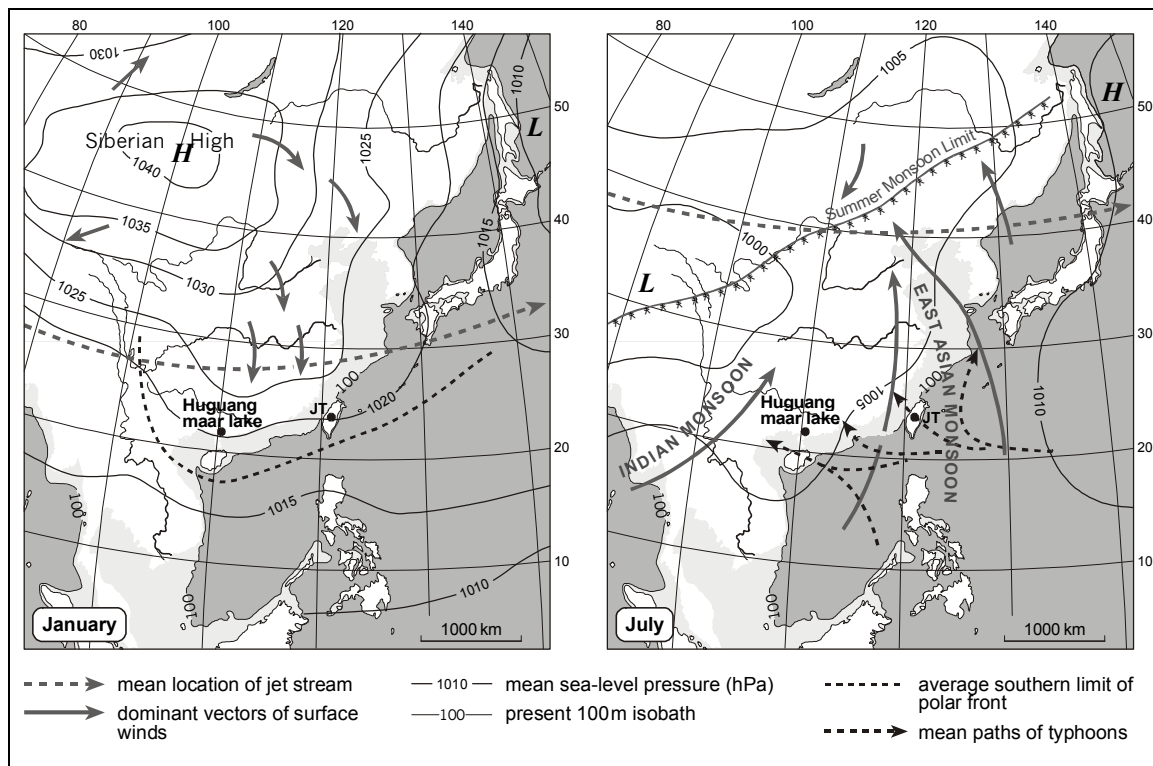


Fig. 5.6. Monsoon influence in south-east Asia.

The local climate is controlled by the East Asian monsoon system, playing a key role in south-eastern China (Winkler & Wang, 1993). Seasonal reversals of the wind direction between summer and winter drive the SW and NE monsoons (Fig. 5.6). Pronounced seasonalities exist with dry and cold periods during autumn and winter. The summer monsoon dominates the atmospheric circulation from May to September. It transports moist air masses from the West Pacific and the South China Sea and produces abundant rainfall over the Chinese mainland. The annual mean precipitation ranges between 1400 and 1700 mm. The hottest month is July and the coldest January with mean average temperatures of 29°C and 3.8°C, respectively (data from Zheng & Lei, 1999). On the Leizhou Peninsula, the present vegetation is dominated by open forests and tropical grassland, whereas most of the subtropical evergreen monsoon forest has been destroyed by human activities.

5.2 Sample Selection

Samples were obtained from cores taken by high-precision piston coring (Usinger- system). Selected pieces had a width of approx. 3 cm, whereas their length varied between 1 and 10 cm. All pieces >1 cm were combined and a representative sample was created representing a maximum age of 250 years. Samples were frozen after sub-sampling and freeze-dried. They were taken from significant stratigraphic and lithological units from Lake Holzmaar core 4a (HZM) and several Lake Meerfelder Maar (MFM) sediment cores. The sample set covers the last approx. 12,900 and 14,685 years, respectively. A calendar year time scale based on varve countings (provided by A. Brauer and B. Zolitschka) was available which enables a precise knowledge of the absolute sample ages.

Samples and microscopic sections from Lake Huguang Maar, China (HM) were provided by Jens Mingram (GFZ Potsdam). They were taken from three sediment cores drilled during a campaign in 1997 in the deepest part of the lake. The available samples from the D, E and F core cover the last approximately 68,000 years. The age model was established with help of ^{14}C -AMS-datings (Mingram *et al.*, 2000). During the time of the project, the sample set was extended continuously. During the first two years altogether 45 samples, one sample per meter, from the D and F core were analysed. Each sample was combined from 2 to 6 cm long sections of the sediment core. In the third year, a high-time resolution study was performed on 34 samples from two selected sections of the E core. One sample per 15 cm was gathered with a length of 3 to 5 cm. The final sample set is given in Tab. 5.1, a detailed listing of the analysed samples is provided in the respective result chapters. All important limnological and morphometric data of the investigated maar lakes and their catchment areas are listed in Tab. 5.2.

Maar lake	Core	Section length [cm]	Samples (E.nr.)	Max. age BP (approx.)
Lake Holzmaar (HZM)	HZM 4a	70 - 980	38 (48174 - 48212)	12,900
Lake Meerfelder Maar (MFM)	several cores (V to Z)	24 - 1092	44 (48338 - 48381)	14,685
Lake Huguang Maar	D	50 - 150	2 (47709 - 47710)	545
	E	715 - 915 and 2960 - 3313	9 (49996 - 50004) 25 (50005 - 50029)	13,019 45,000
	F	250 - 4500	43 (47711-48170)	68,000

Tab. 5.1. Maar lake sample set for the project.

	MFM	HZM	HM
Location	50°06'N; 6°45' E	50°07'N; 6°53' E	21°9'N 110°17'E,
Elevation of present lake-level [m a.s.l.]	336,5	425,1	23
Maximum depth [m]	17	19	25
Diameter [m]	700	325	n.a.
Volume [10^6 m ³]	2.31	0.51	0.70
Lake surface area [m ²]	256,000	58,000	2,250,000
Catchment area [km ²]	1.53/5.76 ⁺	2.25/0.37*	3,14
Mixing	holomictic, dimictic	holomictic, dimictic	holomictic, monomictic
Present trophic state	eutrophic	mesotrophic to eutrophic	polytrophic to eutrophic

Tab. 5.2. Morphometric and limnological data of the investigated maar lakes. HZM, Lake Holzmaar; MFM, Lake Meerfelder Maar; HM, Lake Huguang Maar; ⁺paleo-catchment area; *without Sammetbach. Data after Scharf & Menn (1992), Oehms (1995) and Brauer et al. (2000).

5.3 Eifel Maar Lakes

5.3.1 Screening Analysis

Screening data, varve ages and the stratigraphy for the two investigated sections are given in the Tabs. 5.3 and 5.4 for Lake Holzmaar (HZM) and Lake Meerfelder Maar (MFM), respectively. Downcore variations of selected elemental and Rock-Eval parameters are illustrated in Figs. 5.7 and 5.8.

The TOC contents for the HZM samples vary between 2.7 and 14.6% (Tab. 5.3), indicating a wide range of organic richness. Significant variations were observed within the three sections. The average TOC value in section A is 7.0% with a significant maximum of 11.3% at 460 cm depth (2686 varve yrs BP). TOC contents are slightly higher in section B (7.1% on average), reaching a maximum of 10.2% at 674 cm depth (7390 varve yrs BP). In the Lateglacial/early Holocene section C the TOC content is relatively low (3.4% on average) and shows a maximum of 5.1% at 821 cm depth (10,325 varve yrs BP) and a minimum of 2.6% at 910 cm depth (11,540 varve yrs BP). The TS values range between 0.1 and 2.4%, with highest percentages in section B (1.5% on average).

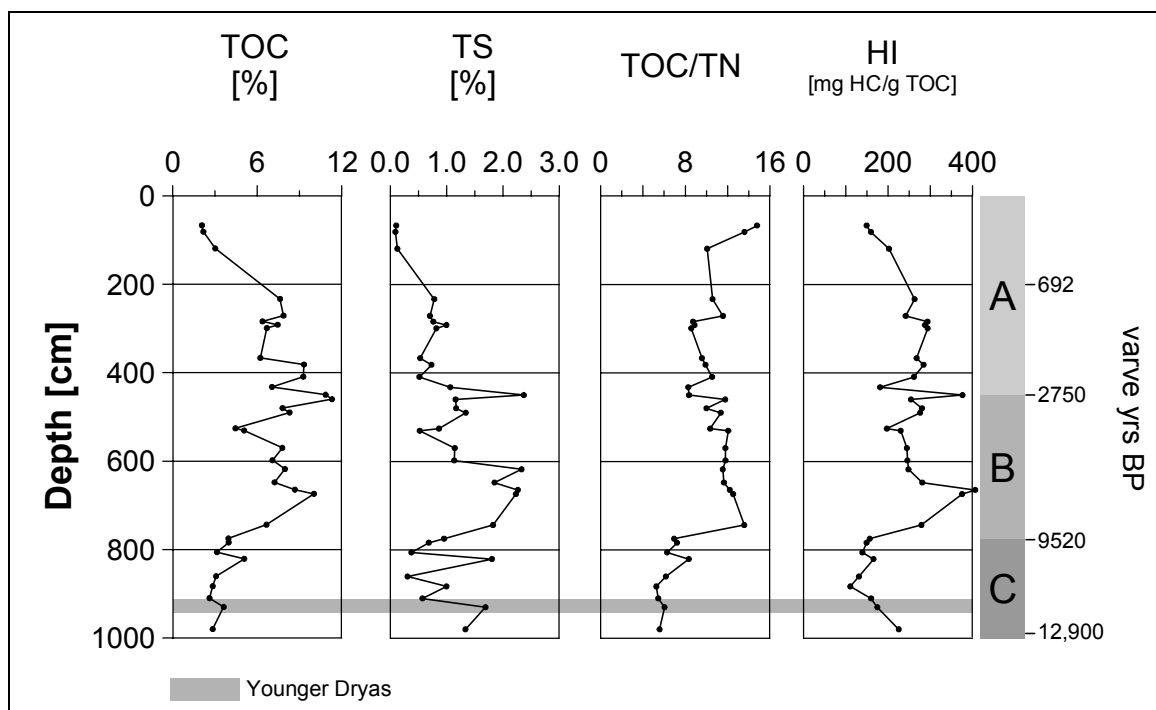


Fig. 5.7. Sample screening for the sediment profile from HZM.

E.nr	Depth [cm]	Age varve yrs BP	Section	TOC [%]	TS [%]	TN [%]	TOC/TN	S2 [mg HC/g sample]	HI [mg HC/g TOC]
48174	66.5	143	A	2.07	0.11	0.14	14.8	3.09	149
48175	81.0	184	A	2.18	0.09	0.16	13.6	3.47	160
48176	119.0	324	A	3.02	0.13	0.30	10.1	6.10	202
48178	233.0	870	A	7.62	0.78	0.72	10.6	20.01	263
48179	271.0	1170	A	7.86	0.71	0.68	11.6	18.99	242
48180	284.0	1311	A	6.38	0.77	0.73	8.7	18.69	293
48181	291.5	1374	A	7.45	1.00	0.84	8.9	21.40	287
48182	299.0	1440	A	6.68	0.82	0.78	8.6	19.61	294
48183	366.5	1952	A	6.22	0.53	0.65	9.6	16.64	268
48184	381.5	2083	A	9.32	0.73	0.94	9.9	26.47	284
48185	409.0	2334	A	9.27	0.52	0.88	10.5	24.20	261
48187	432.3	2536	A	7.04	1.07	0.85	8.3	12.76	181
48188	450.0	2608	A	10.85	2.37	1.30	8.3	40.80	376
48189	460.0	2686	A	11.30	1.16	0.96	11.8	28.74	254
48190	480.0	3330	B	7.80	1.17	0.78	10.0	21.86	280
48191	490.0	3530	B	8.29	1.34	0.73	11.4	22.87	276
48193	526.0	4858	B	4.45	0.86	0.43	10.3	8.77	197
48194	530.8	4960	B	5.07	0.52	0.42	12.1	11.65	230
48195	570.0	5690	B	7.78	1.15	0.66	11.8	19.02	244
48196	598.0	6098	B	7.08	1.14	0.60	11.8	17.40	246
48197	618.0	6340	B	7.97	2.33	0.69	11.5	19.77	248
48198	648.0	6888	B	7.23	1.85	0.62	11.7	20.29	281
48199	664.5	7220	B	8.67	2.27	0.71	12.2	35.20	406
48200	674.0	7390	B	10.02	2.23	0.80	12.5	37.59	375
48201	744.0	8775	B	6.65	1.83	0.49	13.6	18.54	279
48202	775.0	9480	B	3.96	0.96	0.57	6.9	6.19	157
48203	784.0	9610	C	3.97	0.68	0.55	7.2	5.92	149
48204	806.0	10150	C	3.14	0.38	0.50	6.3	4.37	139
48205	821.0	10325	C	5.08	1.81	0.61	8.3	8.42	166
48207	860.5	10910	C	3.08	0.31	0.50	6.2	4.03	131
48208	883.0	11220	C	2.84	1.00	0.54	5.3	3.15	111
48209	910.0	11540	C	2.61	0.57	0.48	5.4	4.17	160
48210	930.0	11970	C	3.62	1.69	0.60	6.0	6.32	175
48212	980.0	12900	C	2.84	1.34	0.51	5.6	6.40	225

Tab. 5.3. TOC, TS, TN and Rock-Eval data for the sediment profile from HZM.

The organic carbon (TOC) to total nitrogen (TN) ratio is frequently used to characterise organic matter sources in lacustrine environments as reviewed by Meyers & Ishiwatari (1993) and Meyers & Lallier-Vergès (1999). TOC/TN instead of TOC/N_{org} values can be used for source interpretations because for most sediments it can be assumed that the N_{inorg} is insignificant compared with TN and thus can be neglected (Müller & Mathesius, 1999; Schubert *et al.*, 2000). It was reported that protein rich lake phytoplankton has TOC/TN ratios between 4 and 10, while TOC/TN ratios of higher plants are commonly higher than 20 and may be higher than 200 (Hedges *et al.*, 1986; Meyers, 1990; Talbot & Johannessen, 1992; Meyers, 1994). Diatoms exhibit ratios from 5.5 to 7.5, while mean ratios of 5.0 to 6.0 and 4.0 to 5.0 were found for zooplankton and bacteria, respectively (Bordowskiy, 1965a, b). TOC/TN ratios of 10.3 and 11.3 on average were calculated for the sections A and B, respectively, but significantly lower values were found for section C (6.3 on average). Maximum ratios up to 14.8 were determined for the most recent samples maximising at

67 cm depth (143 varve yrs BP). The highest HI value of 406 mg HC/g TOC was observed for HZM at 665 cm depth (E 48199) in section B (7220 varve yrs BP).

E.nr.	Depth [cm]	Age varve yrs BP	Stratigraphy	TOC [%]	TS [%]	TN [%]	TOC/TN	S2 [mg HC/g sample]	HI [mg HC/g TOC]
48338	24.0	160	Holocene	2.15	0.20	0.47	4.6	3.62	169
48339	42.0	280	Holocene	4.69	0.59	0.77	6.1	11.13	237
48340	57.0	380	Holocene	1.64	0.11	0.04	40.9	2.20	134
48341	102.0	680	Holocene	2.34	0.21	0.18	13.0	4.92	210
48342	127.5	850	Holocene	4.24	0.57	0.50	8.5	12.38	292
48343	178.5	1240	Holocene	12.60	2.02	1.70	7.4	57.04	453
48344	201.0	1740	Holocene	13.15	1.74	1.90	6.9	63.01	479
48345	208.5	1910	Holocene	5.78	0.41	0.62	9.3	16.32	283
48347	235.5	2115	Holocene	9.91	0.79	1.10	9.0	35.26	356
48348	333.0	3765	Holocene	21.40	1.57	2.40	8.9	107.22	501
48349	347.3	4000	Holocene	11.20	0.87	1.10	10.2	46.54	416
48350	346.0	3990	Holocene	11.25	0.87	1.20	9.4	48.48	431
48350a	353.5	4205	Holocene	14.80	1.08	1.50	9.9	53.65	363
48351	410.5	5455	Holocene	12.80	1.47	1.30	9.8	43.59	341
48352	420.5	5665	Holocene	11.65	1.33	1.30	9.0	51.62	443
48353	465.8	6290	Holocene	7.46	0.79	0.76	9.8	22.27	299
48354	496.0	6735	Holocene	7.01	0.81	0.82	8.5	23.59	337
48355	549.0	7640	Holocene	8.55	0.77	1.00	8.6	25.40	297
48356	558.0	8670	Holocene	7.77	0.76	1.00	7.8	19.37	249
48357	598.0	8850	Holocene	9.25	1.62	1.00	9.3	39.23	424
48358	627.0	9325	Holocene	6.42	0.46	0.58	11.1	20.71	323
48359	637.5	9460	Holocene	5.91	0.54	0.54	10.9	18.76	317
48360	646.8	10035	Holocene	7.53	0.86	0.65	11.6	27.44	364
48361	655.5	10310	Holocene	7.50	0.74	0.70	10.7	26.67	356
48362	676.0	10755	Holocene	4.20	0.72	0.42	10.0	9.84	234
48364	731.0	11500	Holocene	3.66	0.63	0.39	9.4	8.95	244
48365	749.0	11800	YD	1.61	0.22	0.13	12.4	3.05	189
48366	766.5	12100	YD	1.61	0.17	0.15	10.7	2.99	186
48367	778.5	12250	YD	3.08	0.46	0.30	10.3	8.09	263
48368	793.5	12355	YD	4.48	0.66	0.55	8.1	15.17	339
48370	846.0	12900	Allerød	4.92	0.83	0.57	8.6	13.98	284
48371	855.0	13000	Allerød	3.33	0.83	0.36	9.2	7.21	217
48372	864.0	13240	Allerød	3.25	0.80	0.38	8.6	6.03	186
48373	875.5	13390	Allerød	2.41	0.36	0.28	8.6	4.40	183
48374	885.0	13480	Allerød	2.24	0.56	0.23	9.7	3.99	178
48375	893.8	13600	Allerød	1.82	0.28	0.11	16.5	2.79	154
48376	923.5	13865	Allerød	1.10	0.13	0.04	27.5	1.30	118
48377	982.8	14245	Allerød	1.21	0.15	0.04	30.1	1.78	147
48378	1009.8	14385	Allerød	1.14	0.20	0.05	22.7	1.60	141
48379	1044.5	14545	Allerød	0.33	0.03	0.04	8.2	0.37	113
48380	1075.5	14635	Allerød	0.46	0.04	0.04	11.5	0.37	80
48381	1091.5	14685	Allerød	0.53	0.04	0.04	13.2	0.55	104

Tab. 5.4. TOC, TS, TN and Rock-Eval data for the sediment profile from MFM. YD, Younger Dryas.

The TOC values for the Holocene MFM sediments (Tab. 5.4; Fig. 5.8) are generally higher than those for the HZM (8.3% on average). They are reaching a maximum of 21.4% at 333 cm depth (3765 varve yrs BP). In the Lateglacial the TOC content is generally low (2.1% on average) reaching a maximum of 4.9% in the Late Allerød at 846 cm (12,900 varve yrs BP). At the bottom of the profile the lowest overall TOC values are observed. The TS values vary between 0.1 and 2.0% and thus are in the same range than those obtained from HZM. TOC/TN ratios of 10.4 and 13.5 on average were observed for the Holocene and Lateglacial, respectively with a significant maximum of 40.9 at 57 cm depth (380 varve yrs BP) and of

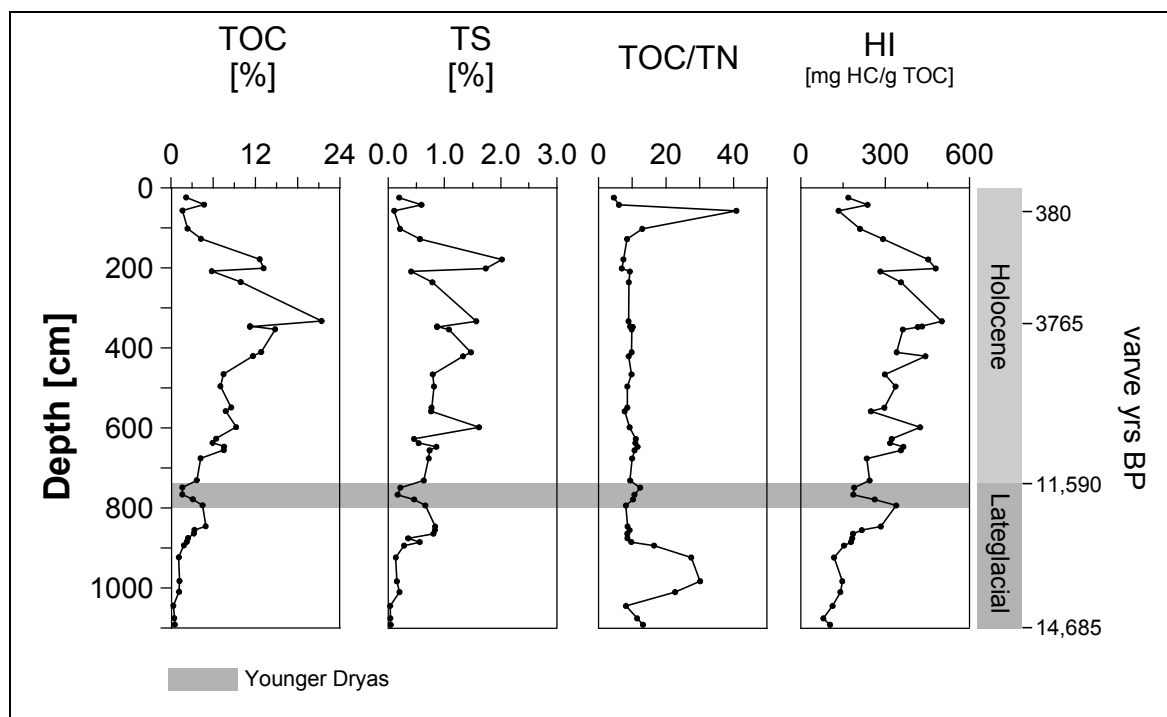


Fig. 5.8. Sample screening for the sediment profile from MFM.

30.1 at 983 cm depth (14,245 varve yrs BP) are indicative for significant allochthonous OM contributions. Higher on average HI values were found for the Holocene in MFM (329 mg HC/g TOC) compared to HZM (260 mg HC/g TOC) with a maximum of 501 mg HC/g TOC at 333 cm depth (12,900 varve yrs BP), indicating that the aquatic production was more important in MFM or that stronger oxidation of the OM occurred in HZM.

Organic source interpretations based on OI values must be carried out with caution. A contribution of carbon dioxide from the early decomposition of unstable carbonates can lead to elevated values and may cause a data scattering. Such an influence on Rock-Eval data was previously described as a mineral matrix effect (e.g. Katz, 1983; Whelan & Thompson-Rizer, 1993). An alternative way to obtain information on OM sources is to simply deconvolute the HI into its two components, S2 and TOC, as shown in Fig. 5.9 (Katz & Elrod, 1983; Langford & Blanc-Valleron, 1990). The two dashed straight lines define the three kerogen types. Each line is representative for a distinct HI value of 200 mg HC/g TOC and 700 mg HC/g TOC for the type III/II and the type II/I boundary, respectively. The slope of the regression line through a sample suite compared to the slope of the boundary lines gives the type of OM. Values from the Lateglacial, Early Holocene and the very recent sediments are separated in this plot. They contain predominantly mixed type II/III or type III OM. Although S2 values are generally higher in the Holocene between 680 and 10,900 varve yrs BP, the slope of this sample suite is only slightly steeper, indicating the presence of type II OM.

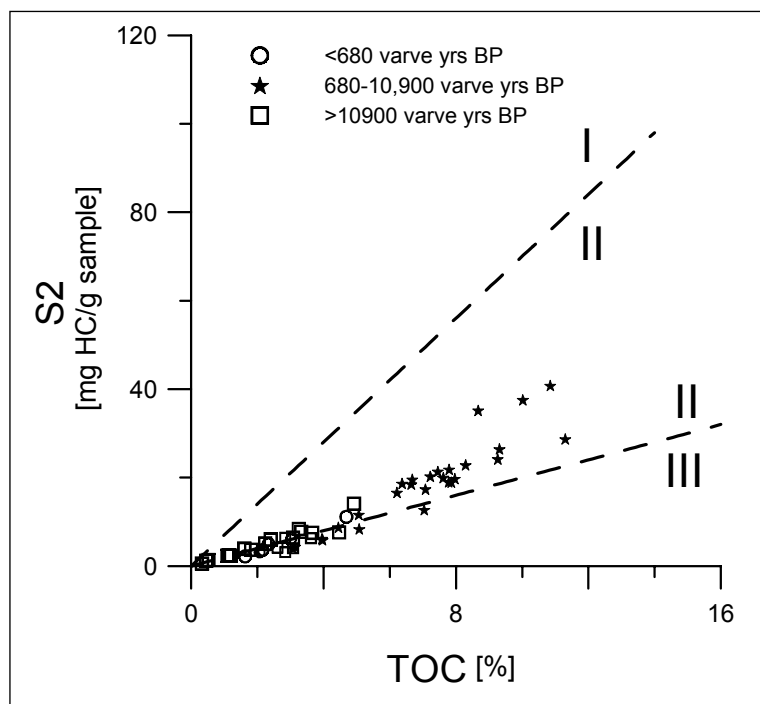


Fig. 5.9. S2 versus TOC of sedimentary OM from selected stratigraphic intervals in HZM and MFM. Interpretation lines adopted from Langford & Blanc-Valleron (1990).

5.3.2 Chemical Composition of the Kerogens

For further investigations only kerogen concentrates were used. The elemental data for the bulk kerogens from HZM and MFM are presented in Tab. 5.5. Their stratigraphic location is presented in the Figs. 5.3 and 5.4. The kerogen concentrates are hydrogen-rich with atomic H/C ratios between 1.3 and 1.7, typical for highly aliphatic material. The atomic O/C ratios range from 0.2 to 0.4 which are typical values for kerogens from young sediments rich in oxygen bearing compounds, such as carbohydrates and phenols (Tissot & Welte, 1984). Interestingly, the TOC/TN ratios of the kerogens are significantly higher than those calculated for the sediments (Tab. 5.5). This feature will be discussed in detail in chapter 5.3.5.

5.3.3 Thermal Analysis (Py-GC-FID and Py-GC-MS)

These investigations were carried out to perform a qualitative and quantitative assessment of the structural and chemical properties of various macromolecules through time. For detailed molecular characterisation, 12 samples from HZM and 11 samples from MFM were analysed. Quantitative analysis of 83 compounds was performed, which are listed in Appx. H. Compounds were identified based on mass spectra and GC retention indices with reference to the literature. Chromatograms of the pyrolysates from HZM and MFM contain variable proportions of *n*-alkane/*n*-alk-1-ene doublets, alkylbenzenes, organic nitrogen

compounds (ONC; pyrroles, pyridines, indoles), alkylphenols, methoxyphenols, naphthalenes, indenes and pyrolysis products of polysaccharides (e.g. alkylfurans). Organic sulphur compounds (OSC) such as thiophenes are virtually absent. All pyrolysates are dominated by aliphatic hydrocarbons with a mean proportion of 60% of all quantified components, followed by phenols (17% on average) and benzenes (13% on average). All other compound classes are only minor constituents.

E.nr.	Depth [cm]	Lake	Section/ Stratigraphy	TOC [%]	TS [%]	H/C atomic	O/C atomic	TOC/TN conc
48175	81.0	HZM	A	43.70	0.43	1.30	0.38	29.1
48480	284.0	HZM	A	49.10	0.92	1.53	0.37	24.6
48184	381.5	HZM	A	48.90	0.82	1.71		37.6
48187	432.3	HZM	A	49.20	0.74	1.37	0.34	21.4
48188	450.0	HZM	A	59.60	2.62	1.31	0.23	19.2
48189	460.0	HZM	A	48.95	0.10	1.38	0.45	22.3
48194	530.8	HZM	B	51.30	1.03	1.34	0.37	20.5
48195	570.0	HZM	B	52.30	1.35	1.35	-	19.4
48198	648.0	HZM	B	54.30	1.46	-	-	-
48200	674.0	HZM	B	43.00	5.68	1.55	0.38	17.2
48205	821.0	HZM	C	46.30	0.60	-	-	-
48207	860.5	HZM	C	47.35	0.79	1.31	0.40	23.7
48210	930.0	HZM	C	41.45	6.84	1.30	0.44	19.7
48339	24.0	MFM	Holocene	45.30	0.84	-	-	-
48343	178.5	MFM	Holocene	52.60	1.42	1.49	0.35	15.5
48347	235.5	MFM	Holocene	51.30	0.74	1.37	0.37	20.5
48348	333.0	MFM	Holocene	51.85	2.00	1.49	0.36	16.2
48349	347.3	MFM	Holocene	50.70	0.90	-	-	-
48353	465.8	MFM	Holocene	51.75	1.08	1.32	0.39	19.9
48357	598.0	MFM	Holocene	47.36	3.46	1.48	0.32	17.5
48360	646.8	MFM	Holocene	53.40	1.32	1.37	0.31	14.8
48365	749.0	MFM	YD	44.00	0.93	-	-	-
48370	846.0	MFM	Allerod	54.20	0.94	1.50	0.40	18.1
48376	923.5	MFM	Allerod	40.70	0.94	1.30	-	20.4
48380	1075.5	MFM	Allerod	31.00	0.72	-	-	-

Tab. 5.5. Elemental data of selected kerogen concentrates.

Selected chromatograms of the pyrolysates from HZM are presented in Fig. 5.10, which monitor specific compound class distributions. The possible origin and geochemical importance of the different compound classes is discussed below. Sample E 48188 from HZM at 450 cm depth (2608 varve yrs BP) is dominated by *n*-alkane/*n*-alk-1-ene doublets which maximise at C₂₁ (Fig. 5.10 A). By strong contrast kerogen E 48189 at 460 cm depth (2686 varve yrs BP) contains abundant aromatic compounds (incl. alkylphenols), methoxyphenols, alkylfurans, prist-1-ene and the *n*-C₁₆ fatty acid (Fig. 5.10 B). Finally, the sample from the Younger Dryas period (E 48210) in 930 cm depth (11,970 varve yrs BP) contains higher concentrations of aromatic over *n*-alkyl moieties and relatively high yields of nitrogen compounds like alkylpyrroles and alkylpyridines (Fig. 5.10 C). Relative abundances of the different compound classes were calculated and are illustrated in Fig. 5.10.

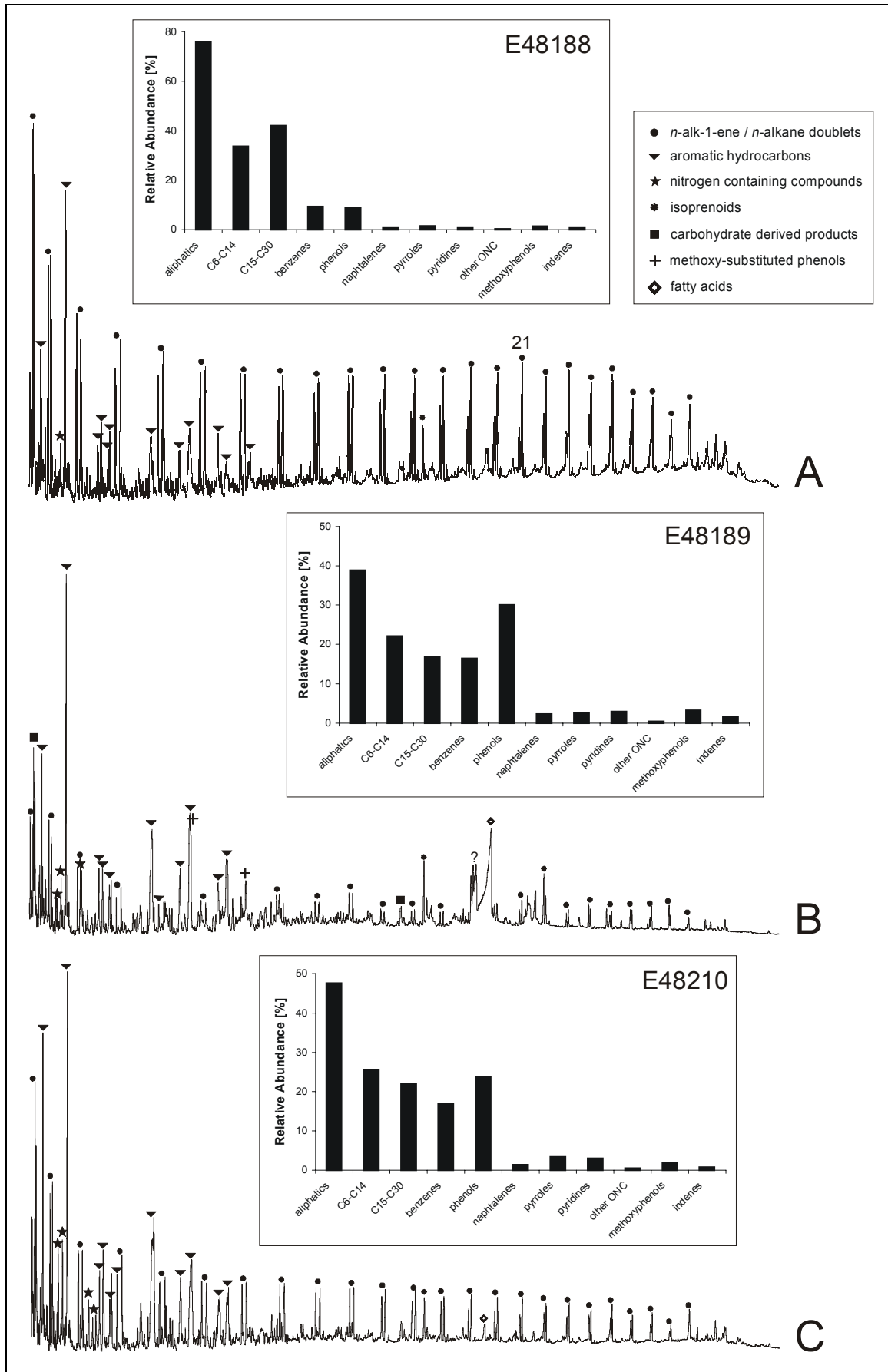


Fig. 5.10. Pyrolysis gas-chromatograms of selected representative maar lake kerogens from HZM (for identification see Tab. 5.5) and relative quantitation results, summed for the principal compound classes. Numbers indicate *n*-alkyl chain lengths.

An autochthonous and a semi-allochthonous **reference sample of specific organisms** were selected from Lake Holzmaar to help to allocate the different sources contributing to the OM. Fig. 5.11 A shows the total ion current (TIC) trace obtained from a field sample collected during a bloom period of *Oscillatoria* (*Oscillatoria agardhii/rubescens* group; Ehlscheid, 1992), which is one of the major primary producers in both maar lakes. The sample was taken in 12 m depth. The major pyrolysis compounds encountered in this sample are toluene, styrene, phenol, 3- and 4-methylphenol, and indole. Fatty acids are detected as well, especially hexadecanoic acid is abundant. Since this sample was not extracted before pyrolysis, parts of the fatty acids observed might reflect released thermal desorption products. Homologous series of aliphatic compounds were not found. Fig. 5.11 B displays the TIC trace of the emergent aquatic macrophyte species *Carex gracilis*. This reference sample is dominated by acetic acid and furans which are pyrolysis products of polysaccharides. Aromatic compounds are represented by toluene and phenols. Abundant methoxyphenols indicate that lignin is an important constituent of these water plants.

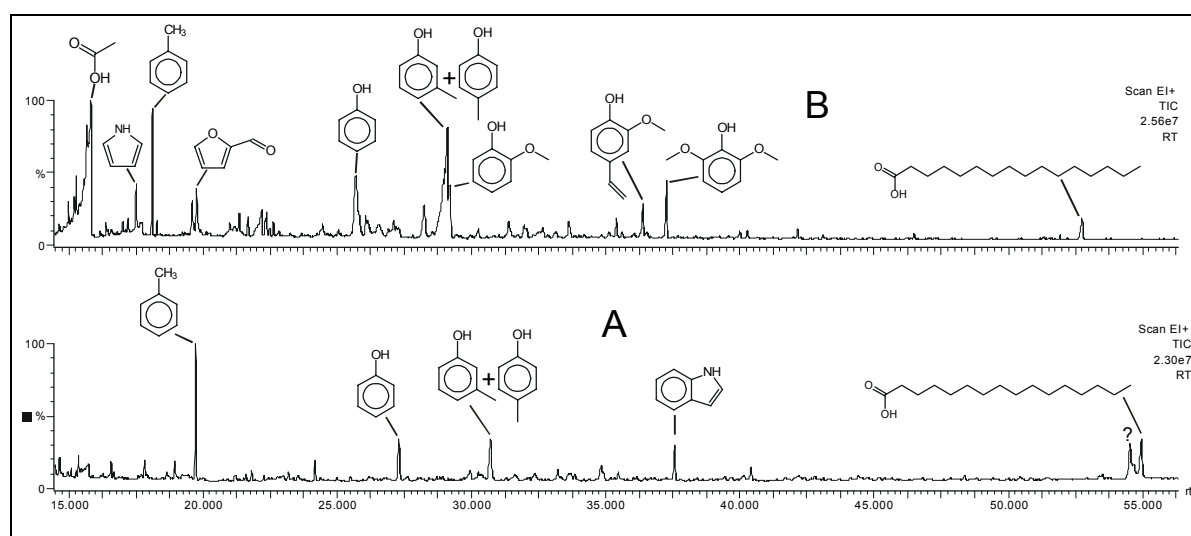


Fig. 5.11. Total ion current (TIC) traces of the pyrolysate and characteristic pyrolysis products of an (A) *Oscillatoria* and (B) aquatic macrophyte (*Carex gracilis*) reference sample.

Alkanes/alk-1-enes

In most of the investigated samples the doublets, which were identified via mass chromatography (m/z 55+57), are important constituents of the pyrolysates (60% on average) with chain lengths in the C_6 - C_{30} range and no odd or even carbon number predominance. This suggests that they are derived from the homolytic cleavage of unbranched alkyl chains. Selectively preserved highly aliphatic macromolecules are believed to consist of a network of long polymethylene chains as reviewed by de Leeuw & Largeau (1993). Previous investiga-

tions have shown that highly aliphatic algae derived biomacromolecules (*algaenans*) are especially very common in thick organic cell walled algae species such as *B. braunii* (e.g. Largeau *et al.*, 1986; Kadouri *et al.*, 1988) whereas they are absent in microalgae with a mineral exoskeleton such as diatoms (Gelin *et al.*, 1999). Chalansonnet *et al.* (1988) detected a highly resistant biopolymer in the cyanobacterium *Oscillatoria rubescens*. However, the pyrolysate was dominated by shorter saturated hydrocarbon chains and a very high *n*-alkane/*n*-alk-1-ene ratio showing no similarities to the pyrolysis-gas chromatograms in this study. Furthermore, no doublets were detected in the *Oscillatoria* reference sample (Fig. 5.11 A), indicating the absence of an aliphatic biopolymer in cell walls of this dominant phytoplankton species in HZM and MFM. Nevertheless, the *n*-alkane/*n*-alk-1-ene doublets could originate from other green microalgae such as *Pediastrum* (Blokker *et al.*, 1998). This alga was found in MFM and is especially abundant in the early Younger Dryas (Brauer *et al.*, 1999). There are, however, other possible sources for the *n*-alk-1-ene/*n*-alkane doublets in pyrolysates, namely, the aliphatic components of *sporopollenin* (e.g. Guilford *et al.*, 1988), *cutan* (e.g. Nip *et al.*, 1986a) and *suberan* (Tegelaar *et al.*, 1995). *Sporopollenin* is a structural constituent of the outer cell walls of spores and pollen and can be considered as the precursor of the maceral sporinite, comprising fossil exines of both spores and pollen. *Cutan* is a component of the cuticular membrane covering the aerial parts of plants. Suberan is present as a wall component of cork cells. All these macromolecules are highly resistant to diagenetic degradation resulting in an excellent chemical and morphological preservation. In addition, lipids that were incorporated during early diagenesis into to the macromolecular OM because of polymerisation and condensation reactions can be a source of the doublets. These lipid components originate from algae, bacteria and/or from higher plant waxes (e.g. Tulloch, 1976; Ishiwatari & Machihara, 1983).

Alkylbenzenes

All pyrolysates contain relatively large amounts of alkylbenzenes (13% on average of the resolved components) which are thought to originate from the cleavage of aromatic rings linked to the macromolecule (Hartgers *et al.*, 1994). Many papers have shown that such structures occur in all kinds of biomolecules ranging from algal aquatic (Derenne *et al.*, 1996; van Heemst *et al.*, 1996) to terrigenous (e.g. van Smeerdijk & Boon, 1987; Stankiewicz *et al.*, 1997b) implying multiple sources for the alkylbenzenes. Thus, these compounds are not very specific as environmental markers. Toluene, an ubiquitous product, predominates all studied pyrograms reflecting some similarities to pyrolysates of sediment traps from the Mediterranean sea where this is consistent with an origin from aquatic OM (Peulvé *et al.*, 1996).

However, in the present case C₁ and C₂ alkylated benzenes could at least partly originate from proteins containing phenylalanine (Tsuge & Matsubara, 1985; Stankiewicz *et al.*, 1998) which were for instance incorporated into melanoidin-type macromolecules (Fig. 5.12 A).

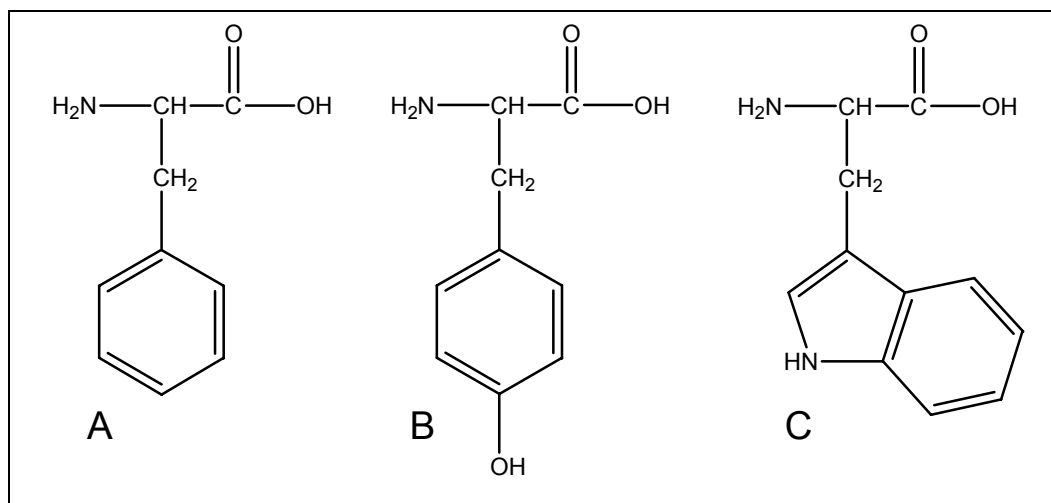


Fig. 5.12. Structures of three common amino acids. A, phenylalanine; B, tyrosine; C, tryptophan.

Phenols and Methoxyphenols

Alkylphenols in pyrolysates, occurring together with methoxyphenols are commonly considered to derive from lignins or degraded lignins (Saiz-Jimenez & de Leeuw, 1984, 1986b; van der Heijden & Boon, 1994). In the pyrolysates of HZM and MFM abundant alkylphenols as well as contributions of methoxyphenols were observed indicating the presence of intact lignin from higher plant constituents in the lake or watershed. Both compound classes are especially abundant in the HZM sample E 48189 from 460 cm depth (Fig. 5.10 B) and MFM sample E 48376 from 923 cm depth (13,865 varve yrs BP) revealing abundant terrigenous contributions. They were also detected in the aquatic macrophyte reference sample (Fig. 5.11 B). This indicates that at least parts of the phenols are derived from the lignocellulose of terrestrial higher plants in the surroundings of the maar lakes or from emergent, submerged or floating plants.

The thermal degradation of transformed proteins containing tyrosine (α -amino- β -[*p*-hydroxyphenyl]-propionic acid; Fig. 5.12 B) rich moieties can also generate phenols (Tsuge & Matsubara, 1985; van Heemst *et al.*, 1999). It was also suggested that algal derived polyphenolic biomacromolecules such as phlorotannins, fucols or phloroethols are possible

sources for phenols (Ragan & Jensen, 1978; Ragan & Glombitza, 1986; Glombitza & Koch, 1989; van Heemst *et al.*, 1996). They are widely used as defence chemicals against grazing herbivores (Boettcher & Targett, 1993). The origin of the alkylphenols can be discriminated based on their distribution patterns in the mass chromatograms (van Heemst *et al.*, 1999). The amino acid tyrosine yields intense peaks for phenol and 4-methylphenol and less intense peaks for 2- and 3-methylphenol upon pyrolysis. In contrast, thermal degradation of non-proteinaceous, polyphenolic macromolecules yield intense peaks for phenol, 2-methylphenol and C₂-phenols relative to 4-methylphenol. Mass chromatograms of alkylphenols from HZM and MFM pyrolysates are shown in Fig. 5.13.

The alkylphenol distributions of many samples are characterised by a very low abundance of 2-methylphenol and C₂-phenols which points to a proteinaceous phenol origin (e.g. Fig. 5.13 A). The relative abundance does not vary significantly with depth for both maar lakes, indicating that the phenols were generated from the same precursor. An exception is the HZM sample collected in 460 cm depth (Fig. 5.13 B) which shows high yields of C₂-phenols (4-ethylphenol, 3-ethylphenol and 3,5 dimethylphenol) and lignin pyrolysis markers and thus closely resembles a polyphenolic-like in combination with a lignin

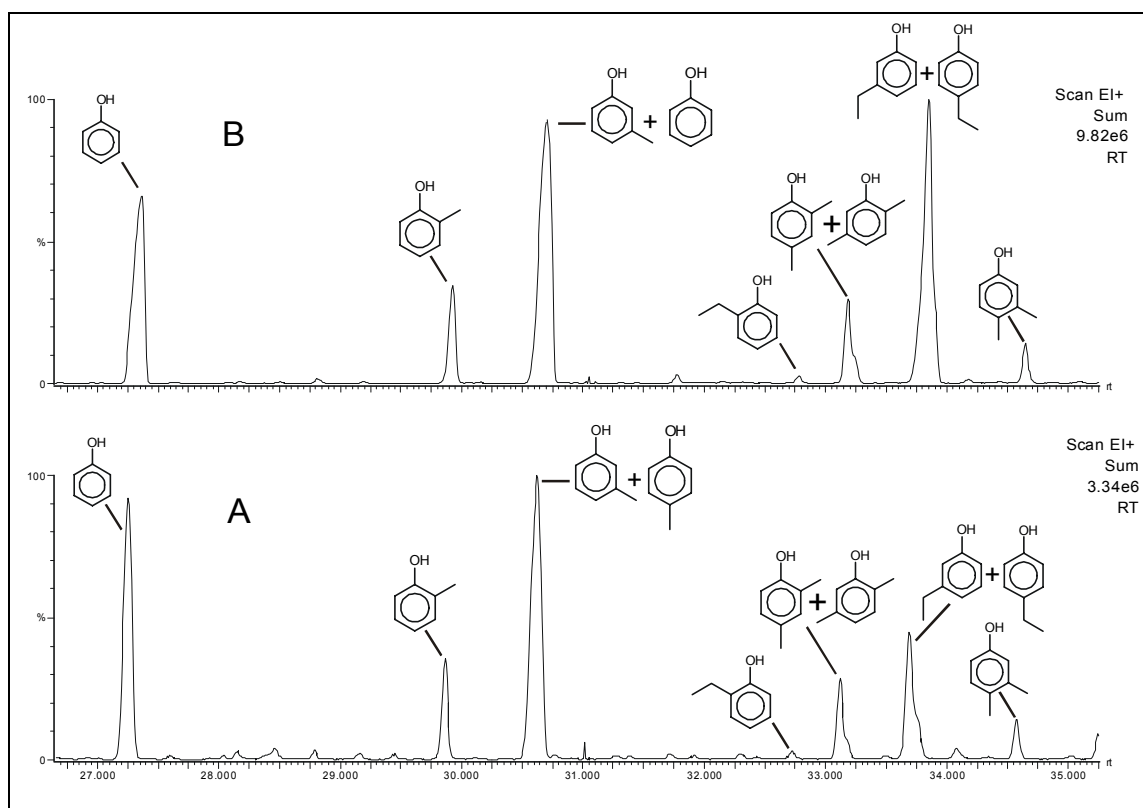


Fig. 5.13. Partial summed mass chromatograms of m/z 94+107+108+120+121+122 revealing the distributions of the C₁-C₂ alkylated phenols of the kerogens (A) E 48353 (MFM) from 465.8 cm and (B) E 48189 (HZM) from 460.0 cm depth.

derived distribution pattern (Fig. 5.13 B). Thus, beside a higher plant source the phenol distribution pattern indicate the presence of degraded protein units (tyrosine), probably resulting from hydrolytic transformation by microorganisms in the water column or sediment (van Heemst *et al.*, 1999). Gadel & Bruchet (1987) argued that such a phenol distribution can also indicate a direct contribution of phytoplankton to the OM in the form of tyrosine residues from cyanobacteria. These primary producers are very important in MFM and HZM, and the *Oscillatoria* reference sample (Fig. 5.11 A) shows a very similar phenol pattern. Stankiewicz *et al.* (1998) demonstrated that tyrosine moieties are very resistant and can survive even extensive microbial and chemical degradation. Such an origin for a part of the phenols is also very likely, because no specific phlorotannin pyrolysis products, for instance phloroglucinol, were observed.

Organic Nitrogen Compounds (ONC)

Pyridines and pyrroles as well as indoles were detected in the pyrolysates. Pyrroles are the most important ONC in the pyrolysates. Such nitrogen-containing compounds are present in pyrolysates of a large number of biomacromolecules. Pyridines were frequently observed in pyrolysates of chitin biopolymers, i.e. crustacean cuticles (e.g. Stankiewicz *et al.*, 1998). However, other prominent and specific pyrolysis products of chitin such as 2-(N-acetylamino) levoglucosan, acetamidofuran or oxazoline derivatives must be present (van der Kaaden *et al.*, 1984a; Baas *et al.*, 1995; Stankiewicz *et al.*, 1997a; Bierstedt *et al.*, 1998). They were not detected in the studied pyrolysates.

Pyrroles are considered to derive from the cleavage of tetrapyrrole structures as observed by comparison of flash pyrolysates of a kerogen from the Miocene Monterey Formation with standard mixtures (Sinninghe Damsté *et al.*, 1992). However, in this study the C₃ and C₄ alkylpyrroles are predominant and the alkylpyrrole distribution pattern shows no similarity to those of the HZM and MFM pyrolysates, where pyrrole is always more abundant than the alkylated pyrroles. Therefore, other precursors must be considered as sources for the pyrroles such as proline containing moieties from proteinaceous material (Tsuge & Matsubara, 1985). Similar pyrrole distributions as in the present case were previously observed in pyrolysates of DOM from the North Sea (van Heemst *et al.*, 1999), suspended OM from the Rhone Delta (Sicre *et al.*, 1994) and refractory OM from the African upwelling-system (Zegouagh *et al.*, 1999). It was interpreted that they derive from degraded proteinaceous OM from autochthonous sources. In addition, Peulvé *et al.* (1996) suggested that the ONC in macromolecular OM from sediment traps of the Mediterranean Sea originate

from melanoidin like precursor macromolecules. These are complex mixtures formed by condensation of monomers and alteration products of proteins and carbohydrates (e.g. Rubinsztain *et al.*, 1984).

Indole and methylindoles are typical pyrolysis products of tryptophan moieties (Fig. 5.12 C) in proteins (Danielson & Rogers, 1978). These compounds were found in small amounts, with the methylindoles always more abundant in the pyrolysates than indole. Because tryptophan is very unstable in water, their presence may indicate favourable circumstances for preservation of basic nitrogenous molecules, i.e. cold and reducing conditions in the water column (Gadel & Bruchet, 1987).

The presence of aliphatic amino acids from proteins can be monitored by using the mass chromatograms of m/z 195+209 (Saiz-Jimenez & de Leeuw, 1986a; Boon & de Leeuw, 1987). The compounds reported in these studies, for example 3,5-alkyl-3,4-dihydro-2H-pyrrole-2,4-dione, were not observed in the pyrolysates of HZM and MFM kerogens indicating their negligible contribution.

Polysaccharides

Carbohydrate derived pyrolysis products dominated by furans and furan derivatives were found, indicating the presence of partially intact and unaltered cellulose (Pouwels *et al.*, 1987; Pouwels *et al.*, 1989; Pastorova *et al.*, 1994) and storage materials such as amylose (van der Kaaden *et al.*, 1984b). An additional but minor source of the furans could be nucleic acids (Posthumus *et al.*, 1974). Normally, cellulose decomposes rapidly in sediments. Its presence might signal that post-depositional degradation was low (cf. Hatcher *et al.*, 1982; Cowie & Hedges, 1984). However, the partial preservation can also result from its linkage to lignin as hemicellulose (e.g. Stafford, 1988). Polysaccharides are not source specific, because they are ubiquitous and encountered in vascular plants, algae, fungi and bacteria as reviewed by de Leeuw & Largeau (1993).

Fatty Acids

Some of the pyrolysates contain a series of saturated fatty acids, dominated by the C₁₆ homologue (e.g. Fig. 5.10 B and Fig. 5.11). Such fatty acids were previously observed in algaenan derived pyrolysates (Kawamura *et al.*, 1986; Largeau *et al.*, 1986). They were also found in pyrolysates of kerogen concentrates from Arctic surface sediments of the Lena River delta and Laptev Sea (Zegouagh *et al.*, 1996), as well as melanoidin type macromolecules from sediments underlying the African upwelling system (Zegouagh *et al.*, 1999).

Fatty acid moieties in the macromolecular structure of kerogens can originate from the incorporation of partly altered lipids at an early diagenetic stage (e.g. Peters *et al.*, 1981; Jaffé & Gardinali, 1991), or by condensation reactions during melanoidin formation (Larter & Douglas, 1980; Allard *et al.*, 1997). They can be directly inherited from the source organism, i.e. the microalga *B. braunii*, via the formation of ester linkages to an algaenan biomacromolecule (Largeau *et al.*, 1986; Derenne *et al.*, 1991). Bound kerogen acids are very stable and can only be released by thermal stress (Jaffé & Gardinali, 1991). Fatty acids were also identified in higher plant biopolymers. The *cutin* and *suberin* macromolecules contain characteristic units of ω -hydroxy C₁₆ and C₁₈ fatty acids (Holloway, 1984; Nip *et al.*, 1986b). *Cutin* is a characteristic biopolymer of the cuticular membrane that is present as a thin extracellular layer on the surface of the epidermal cells of leaves, fruits and non-woody stems (Holloway, 1984). Interestingly, the pyrolysate of sample E 48189 (HZM, 460 cm depth) with abundant cutinite macerals (see chapter 5.3.4) shows the highest concentration of hexadecanoic acid (Fig. 5.10 B).

Other Compounds

The isoprenoid prist-1-ene is an important constituent of the kerogen pyrolysates. It is especially abundant in sample E 48189 (HZM, 460 cm depth). As already discussed in chapter 4.6.1, this compound can have multiple precursors such as chlorophyll *a* (Ishiwatari *et al.*, 1991), tocopherols (Goossens *et al.*, 1984) or diphytanyl ethers from archaea (e.g. Chappe *et al.*, 1980). Thus, the relatively high content of prist-1-ene reflects a multi-source origin. Naphthalenes are only minor constituents and were previously observed in pyrolysates of recent macromolecular OM from the north-western Mediterranean Sea (Peulvé *et al.*, 1996). They were also detected as pyrolysis products of OM in bottom sediments from western Lake Ontario (Kruge *et al.*, 1998) and a contribution from combustion residues was suggested.

Points to Remember – Screening/Pyrolysis

Bulk and molecular data from analytical pyrolysis point to variable OM sources and preservation in the HZM and MFM sequences. Higher TOC and HI values in the Holocene sediments were observed compared to the Lateglacial, excluding samples from the last approx. 500 years. The TOC/TN ratios suggest a predominantly phytoplankton or mixed source with a significant allochthonous OM contribution around 14,000 varve yrs BP and in the most recent time period (<500 yrs BP). The pyrolysates are dominated by aliphatic hydrocarbons which are derived from highly aliphatic macromolecules of algae or higher plant parts. The phenols derived from proteinaceous tyrosine units and together with methoxy-substituted phenol from the lignocellulosic material of higher plants and macrophytes. Organic nitrogen compounds originate from proteinaceous material of autochthonous sources perhaps linked to melanoidin like precursors. Fatty acids can be related to the higher plant biopolymers cutin and suberin and/or reflect lipids that were incorporated into the kerogen structure. Benzenes and carbohydrates occur in a variety of biomacromolecules and are thus not source specific.

5.3.4 Organic Petrology

These investigations were carried out to relate the abundance and textural properties of certain organic particles to specific depositional conditions and to calibrate these data with the bulk and molecular geochemical data. In the following section, detailed morphological observations of the individual samples are presented. Microphotographs are illustrated in Fig. 5.14. The detailed quantitative results of the maceral analysis and reflectance measurements are given in Appx. I. Downcore variations for the percentages of amorphous, terrigenous and aquatic OM in HZM and MFM are presented in Fig. 5.15.

E.nr.	Lake	AOM [%]	Terrigenous OM [%]	Aquatic OM (alginite) [%]	Huminite/Vitrinite and terrigenous Liptinite [%]	Inertinite and recycled Huminite/Vitrinite [%]
48175	HZM	73.3	22.7	0.0	18.7	4.0
48180	HZM	64.0	30.0	1.0	29.0	1.0
48184	HZM	71.2	21.2	7.7	21.2	0.0
48187	HZM	82.3	13.5	1.0	11.5	2.1
48188	HZM	74.7	10.8	13.3	10.8	0.0
48189	HZM	20.0	50.0	0.0	50.0	0.0
48194	HZM	77.1	16.7	2.1	15.6	1.0
48195	HZM	68.6	12.3	14.6	10.1	2.2
48198	HZM	67.4	10.2	16.3	8.2	2.0
48200	HZM	77.0	7.7	12.8	6.4	1.3
48205	HZM	59.4	35.9	1.6	34.3	1.6
48207	HZM	63.3	32.6	2.0	22.4	10.2
48210	HZM	53.8	44.3	0.0	30.8	13.5
48339	MFM	57.6	36.3	6.1	21.2	15.1
48343	MFM	88.3	10.6	1.1	8.5	2.1
48347	MFM	70.2	26.6	3.2	23.4	3.2
48348	MFM	86.9	7.9	2.6	7.9	0.0
48349	MFM	80.6	19.4	0.0	17.3	2.0
48353	MFM	79.5	17.2	0.0	12.9	4.3
48357	MFM	82.3	16.6	1.0	15.6	1.0
48360	MFM	65.5	24.1	10.3	20.7	3.4
48365	MFM	65.9	31.6	1.3	6.3	25.3
48370	MFM	68.8	25.0	1.6	20.3	4.7
48376	MFM	70.0	27.7	2.3	15.0	12.7
48380	MFM	79.5	20.5	0.0	2.3	18.2

Tab. 5.6. Petrographic composition of kerogen concentrates in vol.-% [mf]. Terrigenous OM, huminite/vitrinite+sporinite+inertinite. See text for further definitions.

Amorphous Organic Matter (AOM)

On average 69.9 vol.-% [mf] of the OM in the Eifel maar lake sediments are composed of unstructured organic aggregates. The majority (43.2 vol.-%) occurs as fluorescing AOM (fluoramorphinite) of irregular shape (Fig. 5.14 A), similar to those observed in the Liaohe source rocks. Thus, it may result from the microbial degradation of algal or cyanobacterial OM as discussed in chapter 4.4.4. Ultrastructural studies (TEM) on Recent sediments from Lac du Bouchet, France showed biological remnants which confirm an aquatic origin of the fluorescing AOM (Patience *et al.*, 1995). An early flocculation of labile OM and clay particles in the water column may have occurred (Bishop & Philp, 1994). Non-fluorescing AOM (hebamorphinite) was frequently counted (on average 26.7 vol.-%) in samples rich in terrigenous macerals, for example in section C of the HZM profile. That AOM can also be a result of the degradation of higher plant debris was recently suggested by Bourdon *et al.* (2000).

Higher Plant Sources

Within the terrigenous fraction, different states of preservation were observed. Some of the woody tissues of lignocellulosic origin still display the original cell structure. Most of this textinite is larger than 40 µm. Gelified or partly gelified particles are present as well. This type of constituent is known as the macerals ulminite or telogelinite (Taylor *et al.*, 1998, p. 182f.) which have a brown to grey colour in reflected white light and a homogenous structure where cell walls are mainly absent (Fig. 5.14 B). Sample E 48189 from HZM at 460 cm depth (2686 varve yrs BP) contains high proportions of terrigenous OM (Fig. 5.15 A; Tab. 5.6), including the figured liptinite maceral cutinite (30.0 vol.-%), which exhibit an excellent preservation of morphological features (Fig. 5.14 C). This maceral can be related to plant cuticles which act as a protective cover between the plant and its environment. However, the high amount of terrigenous OM in this sample may be related to slumping and not reflect widespread environmental changes.

Most of the huminite/vitrinite particles are smaller than 10 µm and of angular shape (humodetrinite/vitrodetrinite) (Fig. 5.14 D). Large fusinites with characteristic open cell lumina were detected only in the Lateglacial, Early Holocene or most Recent samples such as E 48175 from HZM in 81 cm depth (184 varve yrs BP; Fig. 5.14 E). Instead, the inertinite fraction is mainly represented by small particles (5-10 µm) of high reflectance. These inertodetrinites

can be related to oxidation processes such as local forest fires or they may be derived from the erosion of ancient sediments (Buillit *et al.*, 1997). Their general small size and sub-rounded shape probably indicates transport over long distances. In the HZM section C at 930 cm depth (11,970 varve yrs BP) funginites were detected. Spores and pollen are present in all of the investigated samples. They were brought to the lakes by wind and rivers. The terrigenous OM fraction ranges between 7.7 vol.-% in section B of HZM (7390 varve yrs BP) and 50.0 vol.-% in HZM at 460 cm depth (2686 varve yrs BP; Section A), with 22.9 vol.-% on average (Tab. 5.6). Only very few huminite/vitrinite compared to inertinite macerals were observed in the Younger Dryas interval of MFM (Tab. 5.6).

Aquatic OM

Filamentous alginites of approx. 10-20 μm display a green to yellow fluorescence colour and are present in almost all samples (Fig. 5.14 G). They resemble structures which were previously observed by Clausen (1998) and interpreted to originate from cyanobacteria. In a few samples from the Holocene in HZM and MFM intercalations of yellow fluorescing lamalginite containing layers and darker layers with clay and huminite detritus are visible (e.g. Fig. 5.14 F). Strongly red-fluorescing chlorophyllinite was often found in association with these algal layers (Fig. 5.14 F). In three Holocene samples from HZM at 570 cm (E 48195), 648 cm (E 48198) and 674 cm (E 48200) a small colonial alga (approx. 15 μm) was found (Fig. 5.14 H). This leads to the high proportions of aquatic OM (up to 16.3 vol.-% alginite) in section B (Fig. 5.15 A; Tab. 5.6). Liptodetrinites, which are present in all samples, represent fragments of larger liptinite macerals.

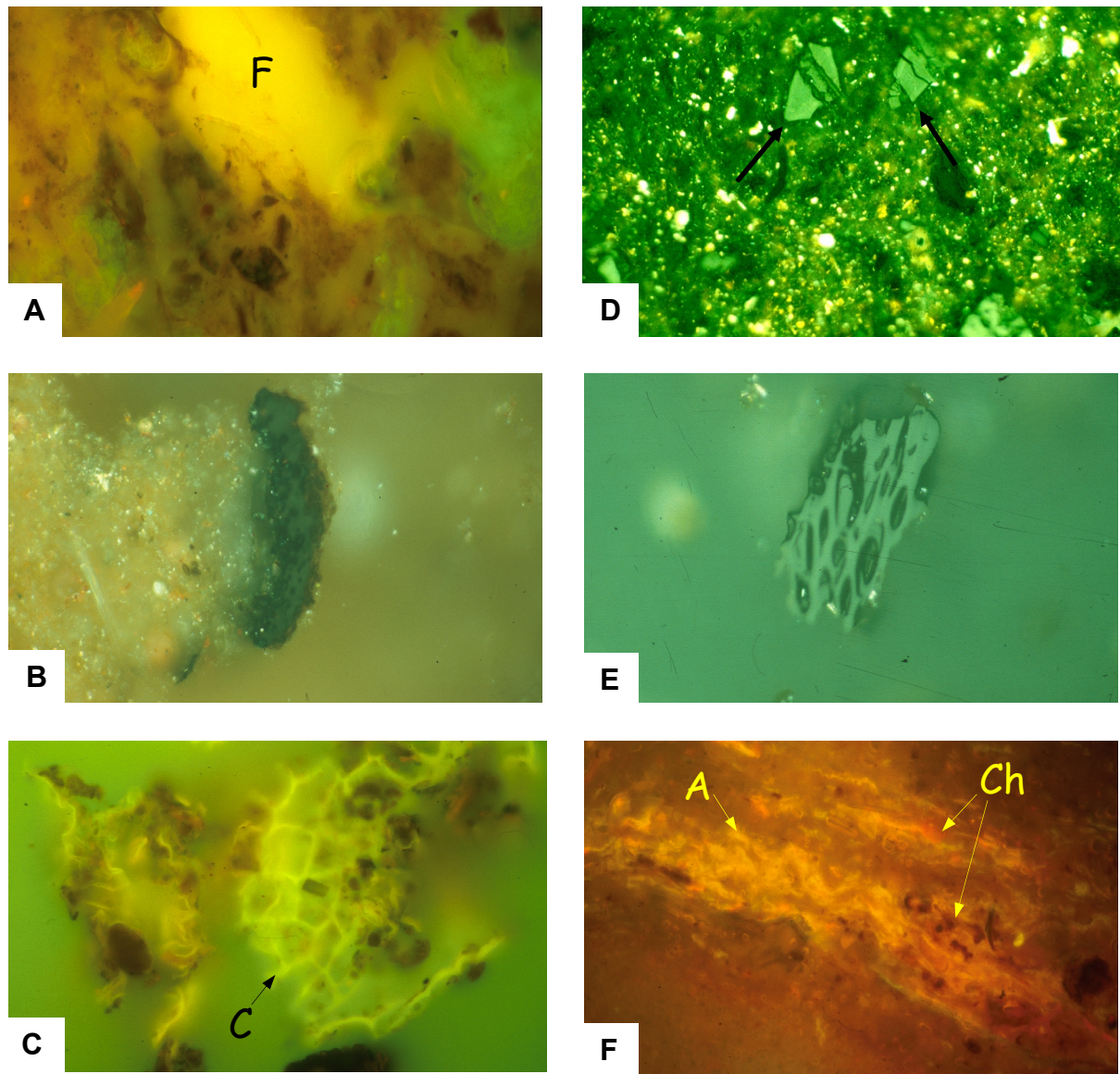


Fig. 5.14. Microphotographs of OM in sediment samples and kerogens from Lake Holzmaar (HZM) and Lake Meerfelder Maar (MFM).

- A) Sample E 48339 (MFM) from 42 cm (280 varve yrs BP). Fluorescing amorphous OM (fluoramorphinite; F). 500x, blue light excitation.
- B) Sample E 48365 (MFM) from 749 cm (11,800 varve yrs BP). Grey to dark grey vitrinite (textinite) documenting open or partly gelified cell lumina of plant tissues. 500x, reflected white light.
- C) Sample E 48189 (HZM) from 460 cm (2886 varve yrs BP). Yellow fluorescing cutinite (C) in a terrigenous dominated sample. 500x, blue light excitation.
- D) Sample E 48370 (MFM) from 846 cm (12,900 varve yrs BP). Grey vitrodetrinite particles (arrows). 500x, reflected white light.
- E) Sample E 48175 (HZM) from 81 cm (184 varve yrs BP). High reflecting fusinite with open cell lumina excitation. 500x, reflected white light.
- F) Sample E 48194 (HZM) from 530.8 cm (4960 varve yrs BP). Yellow fluorescing filamentous alginite (A) and red fluorescing chlorophyllinite (Ch). 250x, blue light excitation.

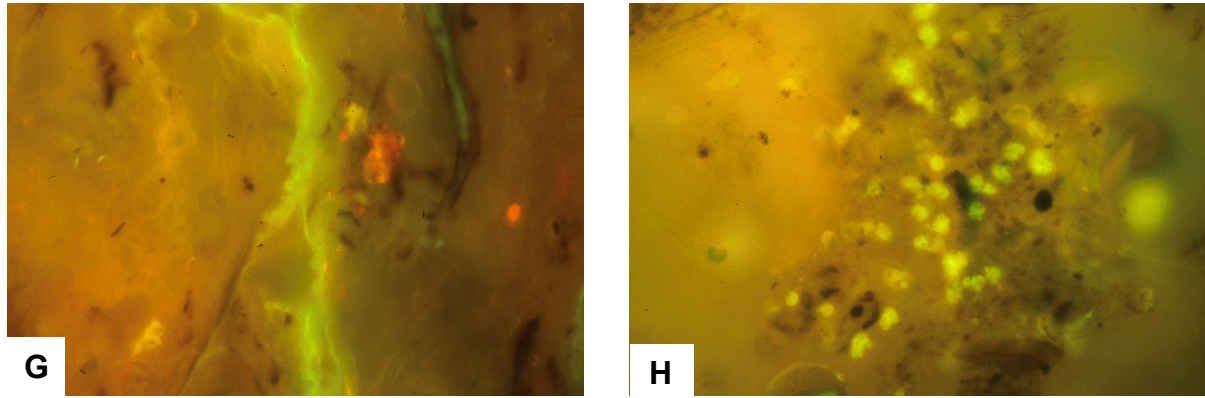


Fig. 5.14 (cont.). Microphotographs of OM in sediment samples and kerogens from Lake Holzmaar (HZM) and Lake Meerfelder Maar (MFM).

G) Sample E 48184 (HZM) from 381.5 cm (2083 varve yrs BP). Strong green to yellow fluorescing filamentous alginite probably derived from cyanobacteria. 500x, blue light excitation.

H) Sample E 48198 (HZM) from 648 cm (6888 varve yrs BP). Unknown small yellow fluorescing colonial alga. 250x, blue light excitation.

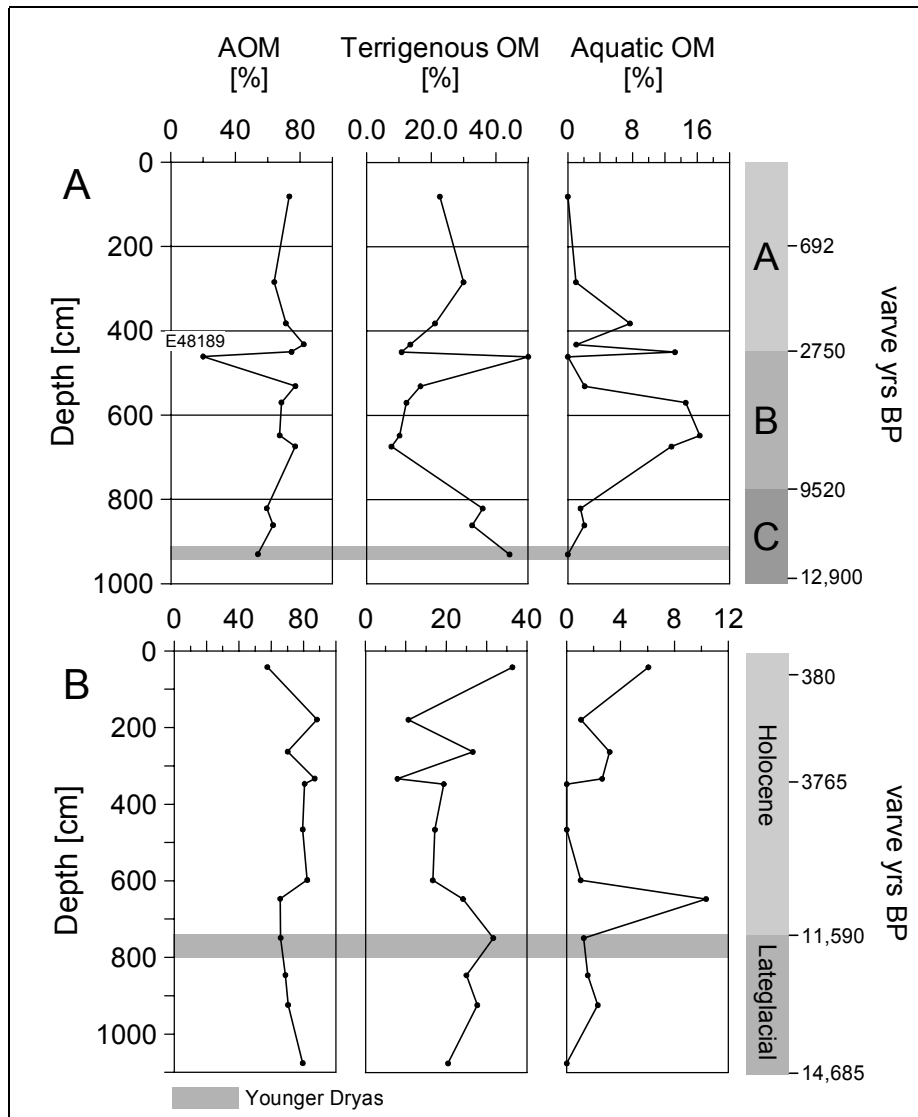


Fig. 5.15. Proportions of amorphous organic matter (AOM), terrigenous OM (huminite/vitrinite+sporinite+inertinite) and aquatic OM (alginite) versus depth for (A) HZM and (B) MFM in vol.-% [mf].

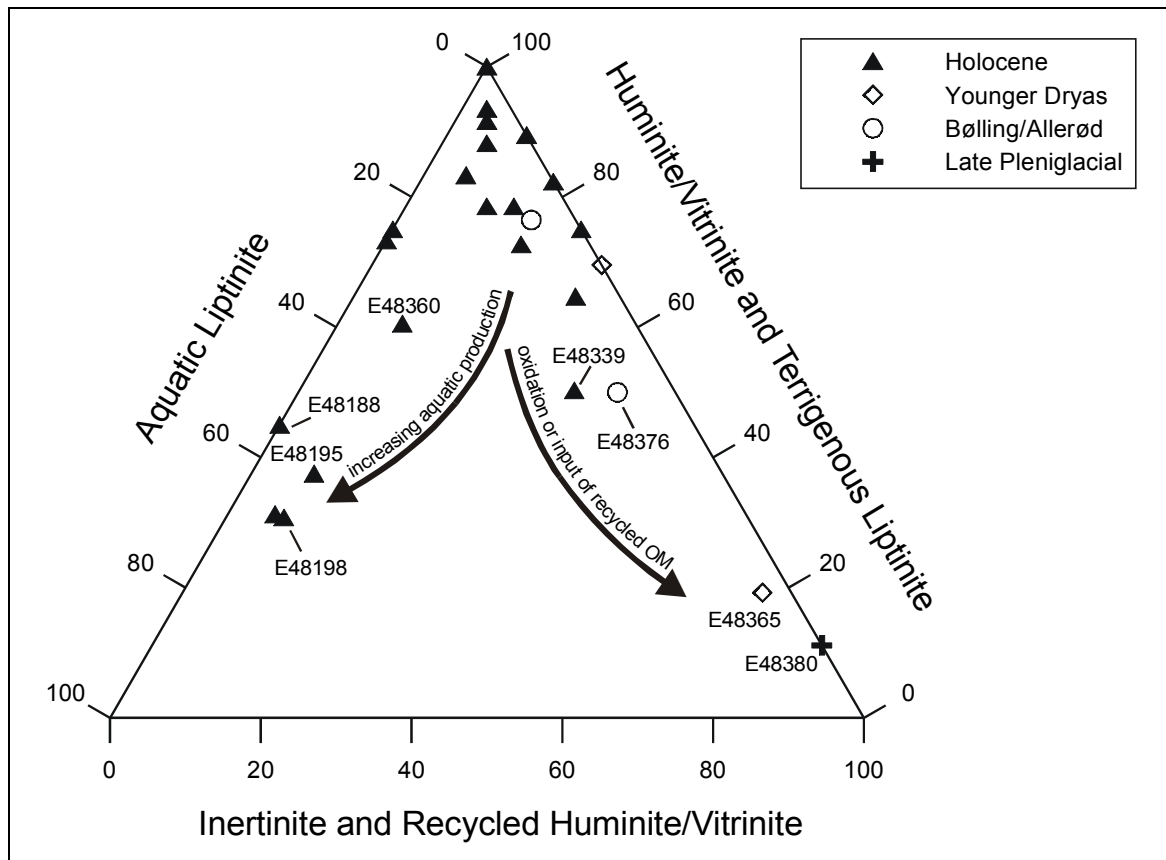


Fig. 5.16. Petrographic composition of kerogen concentrates from Lateglacial and Holocene sediments from HZM and MFM. The three classes were adopted from Littke & Sachsenhofer (1994) and determined by point-counting. If necessary, the proportion of the inertinite and recycled huminite/vitrinite class was corrected based on the results by the reflectance measurements.

The petrographic composition of the OM in the maar lake sediments is illustrated in Fig. 5.16. The three classes were previously introduced by Littke & Sachsenhofer (1994) for deep sea sediments. **(1)** A huminite/vitrinite and terrigenous liptinite class including sporinite, **(2)** an inertinite and recycled huminite/vitrinite class, representing material which underwent primary oxidation processes or is derived from the erosion of older sediments and **(3)** a lacustrine aquatic liptinite class comprising alginite were distinguished. In addition, reflectance measurements of all terrigenous particles were performed to distinguish fresh, huminite/vitrinite particles from higher-reflecting reworked/oxidised OM (Fig. 5.17). Because of the small particle size in some samples, it was difficult to differentiate between fresh and recycled material. In these samples, the point-counts used in Fig. 5.16 were corrected according to the histograms. The reflectance values for the HZM and MFM terrigenous particles range between 0.16% R_r and 3.16% R_r. Based on microscopic observations it was decided that reflectance values >0.6% R_r are used to describe components that were oxidised or reworked (inertinite and recycled huminite/vitrinite), while values <0.6% R_r reflect direct input by the local vegetation. This relatively high value was chosen because

reflectance contrasts in the peat and lignite stage can be very large and disappear with higher levels of coalification (Taylor *et al.*, 1998, p. 192f.). The same boundaries were applied to characterise the terrigenous fraction in ODP sediments (Wagner, 1999).

Figs. 5.16 and 5.17 illustrate that significant differences in the organic petrographic composition between the Lateglacial and the Holocene sedimentary OM exist. Samples from the Late Pleniglacial (only MFM) and from the Younger Dryas generally contain a large part of high-reflecting inertinites and recycled huminites/vitrinites of either primary oxidised or reworked origin (Figs. 5.16 and 5.17 C and D). In contrast, most kerogens from the Holocene and Bølling/Allerød consist of low-reflectance huminite/vitrinite particles with a pronounced reflectance maximum in the range between 0.0-0.3% R_r (Figs. 5.16 and 5.17 B). Abundant higher reflecting organic particles were also identified in the very recent samples (Fig. 5.17 A).

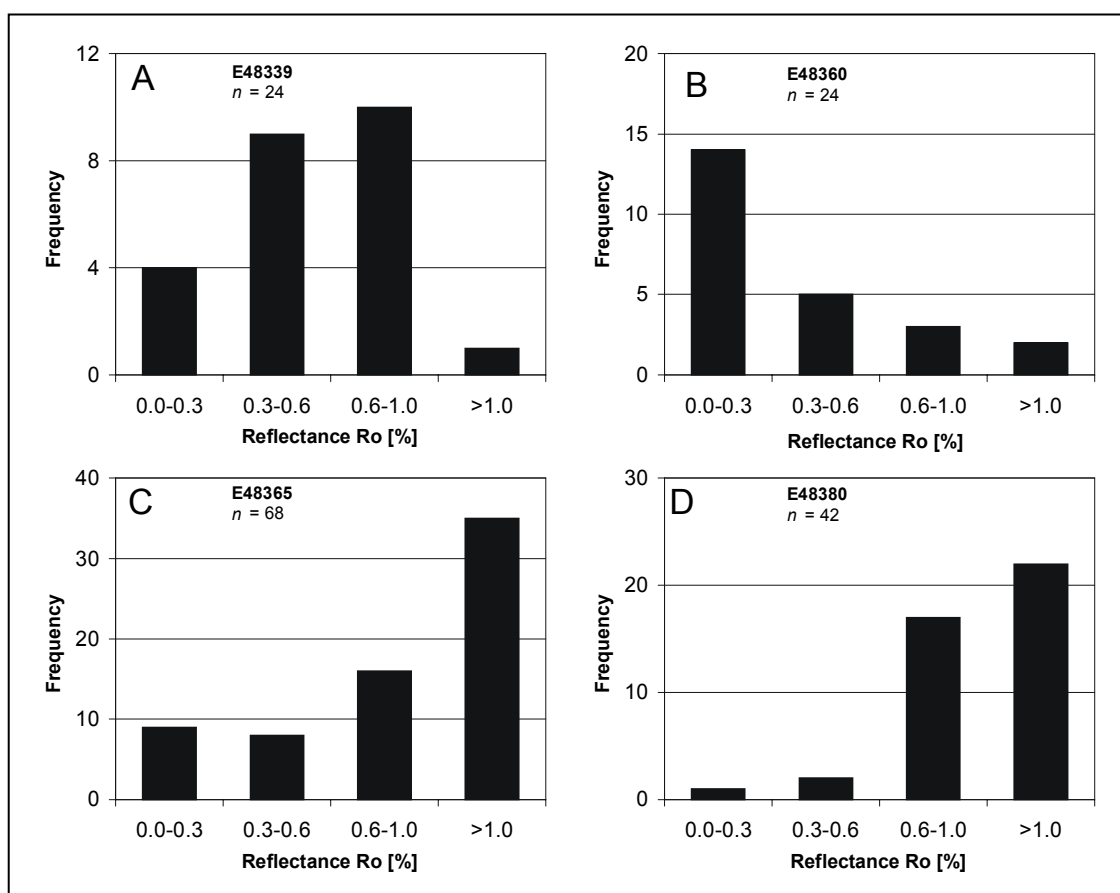


Fig. 5.17. Histograms of reflectance, measured on huminite, vitrinite and inertinite particles in sediment samples and kerogens from MFM. The occurrence of reflecting particles above 0.6% R_r indicate enhanced sedimentation of recycled and/or oxidised terrigenous particles. A, Holocene (280 varve yrs BP); B, Holocene (10,035 varve yrs BP); C, Younger Dryas (11,800 varve yrs BP); D, Late Pleniglacial (14,635 varve yrs BP).

Points to Remember – Organic Petrology

Amorphous OM (AOM) and organic remains from higher plant sources such as huminites, sporinites and inertinites are the predominant macerals in the maar lake sediments. Some samples are rich in alginite (aquatic OM), although land derived higher plant debris is more abundant. The petrographic composition and the reflectance values indicate that a large part of the plant derived OM transported to the lakes was primary oxidised or strongly reworked during the Younger Dryas, Late Pleniglacial and in recent times. In comparison, the terrigenous fraction of the Holocene and Bølling/Allerød samples is dominated by fresh non-oxidised particles.

5.3.5 Stable Carbon Isotopes

To gain specific OM source information, stable isotopic compositions of carbon were measured on carbonate free sediments, demineralised using dilute hydrochloric acid ($\delta^{13}\text{C}_{\text{TOC}}$) and on corresponding kerogen concentrates, obtained by hydrochloric (HCl) and hydrofluoric (HF) acid digestion ($\delta^{13}\text{C}_{\text{conc}}$). Stable carbon isotopes from lake sediments have been widely used to determine paleoenvironmental and paleoclimatic excursions (e.g. Meyers, 1994; Hollander & Smith, 2001). However, most of the previous studies have been focused on $\delta^{13}\text{C}_{\text{TOC}}$. Carbon isotopic variations of kerogens were determined in this study, **(1)** to compare the $\delta^{13}\text{C}_{\text{TOC}}$ and $\delta^{13}\text{C}_{\text{conc}}$ values, **(2)** to interpret these values in terms of OM sources and **(3)** to relate these results to the molecular and microscopic data obtained previously. All determined isotopic data are given in Tab. 5.7.

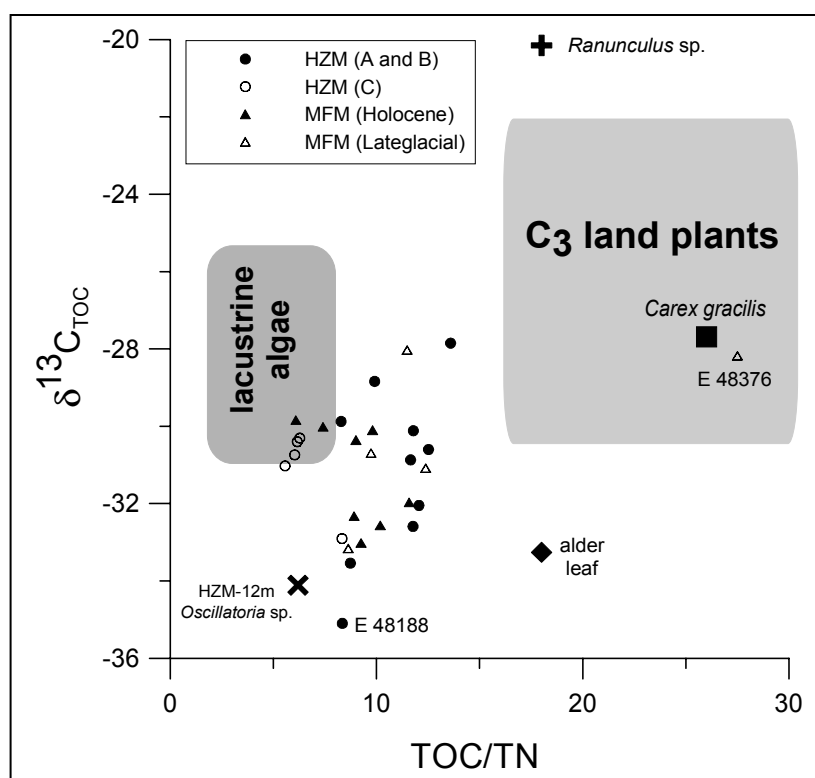


Fig. 5.18. TOC/TN versus $\delta^{13}\text{C}_{\text{TOC}}$ of sediments from HZM and MFM and collected reference samples (*Oscillatoria*, macrophytes and alder leaf). Interpreted fields adopted from Meyers (1997) and Meyers & Lallier-Vergès (1999).

Stable isotopic compositions of organic carbon ($\delta^{13}\text{C}_{\text{TOC}}$) vary between -27.9 in HZM at 81 cm depth (184 varve yrs BP) and -35.1 ‰ in HZM at 450 cm depth (2608 varve yrs BP). These values are similar to isotopic composition reported in previous studies of MFM and HZM (Brown *et al.*, 1991; Lücke *et al.*, 2000). For a general classification, the elemental and carbon isotopic data are plotted in Fig. 5.18. Most of the values fall between the two indicated fields (lacustrine algae and C₃ land plants) suggesting a mixture of these two

sources or a contribution of an additional source to the OM. Only a few samples contain organic carbon with an isotopic and elemental signature typical for lacustrine or terrigenous OM. For example, the values of sample E 48376 (MFM) from 923 cm depth (13,865 varve yrs BP) are consistent with a C₃ plant origin. This was substantiated by organic petrological observations and analytical pyrolysis. With one exception, all sediment samples from section C (HZM) plot in the lacustrine algal field. However, bulk and microscopical data contradict these results.

E.-nr.	Lake	Depth [cm]	varve yrs BP	$\delta^{13}\text{C}_{\text{conc}}$	$\delta^{13}\text{C}_{\text{TOC}}$	$\Delta^{13}\text{C}$ ($\delta^{13}\text{C}_{\text{TOC}} - \delta^{13}\text{C}_{\text{conc}}$)
48175	HZM	81.0	184	-29.18	-27.85	1.33
48180	HZM	284.0	1311	-33.54	-33.54	0.00
48184	HZM	381.5	2083	-29.66	-28.84	0.82
48187	HZM	432.3	2536	-30.91	-29.88	1.04
48188	HZM	450.0	2608	-36.68	-35.10	1.59
48189	HZM	460.0	2686	-30.60	-32.59	-1.99
48194	HZM	530.8	4960	-33.03	-32.05	0.98
48195	HZM	570.0	5690	-30.90	-30.12	0.79
48198	HZM	648.0	6888	-32.30	-30.87	1.43
48200	HZM	674.0	7390	-31.17	-30.60	0.57
48205	HZM	821.0	10325	-33.10	-32.90	0.20
48207	HZM	860.5	10910	-31.32	-30.40	0.92
48210	HZM	930.0	11970	-30.72	-30.74	-0.02
48339	MFM	42.0	280	-30.73	-29.84	0.89
48343	MFM	178.5	1240	-32.16	-30.02	2.14
48347	MFM	235.5	2115	-31.09	-30.36	0.73
48348	MFM	333.0	3765	-32.97	-32.32	0.65
48349	MFM	347.3	4000	-32.94	-32.56	0.38
48353	MFM	465.8	6290	-30.75	-30.10	0.65
48357	MFM	598.0	8850	-34.22	-33.02	1.20
48360	MFM	646.8	10035	-33.56	-31.97	1.59
48365	MFM	749.0	11800	-31.59	-31.08	0.51
48370	MFM	846.0	12900	-32.23	-33.16	-0.93
48376	MFM	923.5	13865	-28.94	-28.18	0.77
48380	MFM	1075.5	14635	-28.77	-28.02	0.75
References						
HZM-12m				-34.11	-	<i>Oscillatoria</i> sp.
48087				-27.69	-	<i>Carex gracilis</i>
48089				-33.26	-	alder leave
48092				-20.15	-	<i>Ranunculus</i> sp.

Tab. 5.7. Stable isotopic values of organic carbon measured on carbonate free sediments ($\delta^{13}\text{C}_{\text{TOC}}$), corresponding kerogen concentrates ($\delta^{13}\text{C}_{\text{conc}}$) and reference samples from HZM and MFM.

To obtain more specific source information, the elemental and isotopic values of the cyanobacterial reference sample (*Oscillatoria*) as well as typical plant materials (alder leave and two macrophytes) from HZM were determined and plotted in Fig. 5.18. The *Oscillatoria* sample has the most negative $\delta^{13}\text{C}$ value of -34.1‰ and a low TOC/TN ratio of 6.2. This is in agreement with other data from HZM for *Oscillatoria* rich samples. However, a wide range of isotopic values between approx. -22.0 and -36.0‰ were previously determined for this

cyanobacteria species which reflect seasonal fluctuations of the autochthonous population (A. Lücke, pers. comm.). Sample E 48188 from HZM at 450 cm depth (2608 varve yrs BP) contains abundant filamentous alginite confirming that high contributions of cyanobacterial OM in HZM are associated with very negative carbon isotopic values. The submerged macrophyte *Ranunculus* has the most positive $\delta^{13}\text{C}$ value of -20.2‰ (Tab. 5.7) and a TOC/TN ratio of 18.0, while the emergent macrophyte *Carex gracilis* falls in the C_3 land plant field. Finally, the alder leaf has an astonishingly negative $\delta^{13}\text{C}$ value of -33.3‰ which is not consistent with C_3 plant material. However, the carbon isotopic composition of leaves can vary significantly due to a large number of environmental influences such as light and water availability. For instance, leaf $\delta^{13}\text{C}$ decreases as observations were made deeper in the canopy. Furthermore, when measuring only outer canopy leaves, $\delta^{13}\text{C}$ was decreased with decreasing radiance (Ehleringer *et al.*, 1986; Ehleringer *et al.*, 1987).

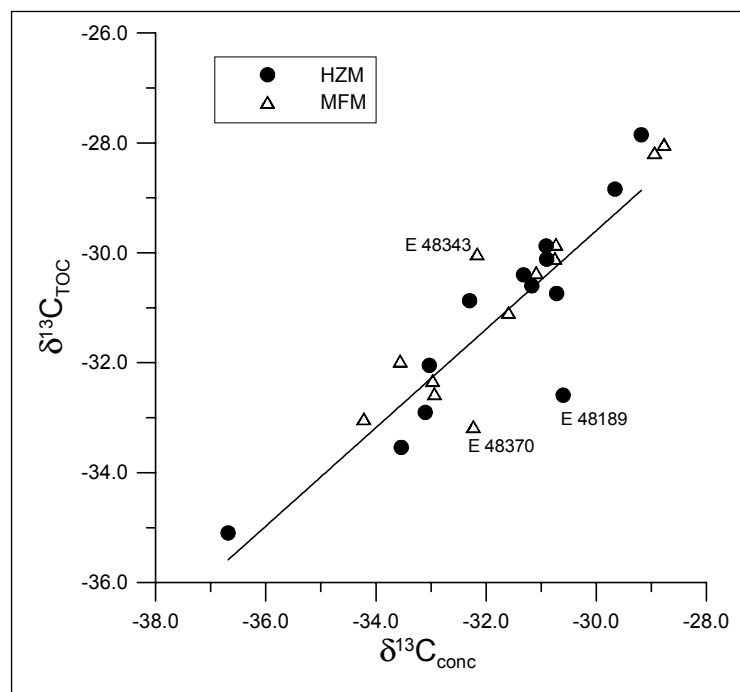


Fig. 5.19. Carbon isotopic compositions of the HCl demineralised sediments ($\delta^{13}\text{C}_{\text{TOC}}$) versus kerogen concentrates ($\delta^{13}\text{C}_{\text{conc}}$) from HZM and MFM.

The $\delta^{13}\text{C}_{\text{conc}}$ values vary between -28.8‰ (MFM) at 1075 cm depth (14,635 varve yrs BP) and -36.7‰ (HZM) at 450 cm depth (2608 varve yrs BP). A cross plot of the isotopic composition of the studied sediments and kerogen concentrates shows a high degree of correlation (Fig. 5.19), disregarding the samples E 48189 (HZM), E 48343 and E 48370 (both MFM). However, the $\delta^{13}\text{C}_{\text{conc}}$ values were found to be generally 0.7‰ lighter on average compared to the $\delta^{13}\text{C}_{\text{TOC}}$. Some samples show a large difference between the carbon isotopic composition of the kerogen concentrates and the sediments ($\Delta^{13}\text{C} = \delta^{13}\text{C}_{\text{TOC}} - \delta^{13}\text{C}_{\text{conc}}$ in Tab. 5.7). This suggests that either the extraction with dichloromethane or the kerogen concentration

process (HCl-HF digestion) has removed an isotopically heavier fraction in most of the samples. Usually the extractable bitumen is about 0.5 to 1.5‰ depleted in ^{13}C compared to the related kerogen (Peters & Moldowan, 1993). Therefore, the removal of a ^{13}C -enriched fraction by extraction is unlikely. Interestingly, the TOC/TN ratios of the kerogen concentrates are much higher than for the sediments and show a greater range of variation (cf. Tab. 5.3 to Tab. 5.5). It was reported previously that nitrogen compounds such as proteins and amino acids have isotopically heavier $\delta^{13}\text{C}$ values than for instance lignin or cellulose (Abelson & Hoering, 1961; Deines, 1980). Krishnamurthy *et al.* (1999) studied kerogen concentrates and HCl demineralised sediments from a lake in Michigan (U.S.). The authors found similar variations of the TOC/TN ratios and $\delta^{13}\text{C}$ values as determined in the present study and suggested that a considerable amount of heavier nitrogen was removed during HCl and HF digestion.

5.3.6 Paleoenvironment of Deposition

The sediments of HZM and MFM are rich in macromolecular organic remains which represent the primary production of the phytoplankton in the lakes and the local vegetation in the watershed. Temporal variations in the supply of certain macromolecular components as indicated by selected parameters from analytical pyrolysis, maceral composition and stable carbon isotopes are summarised for MFM and HZM in Figs. 5.20 and 5.21, respectively. For correlation, the TOC contents and HI values are given as well. The pyrolysis product 4-methylguaiacol is derived from the pyrolytic decomposition of lignin from land plants or macrophytes within the lakes. Thus, the 4-methylguaiacol to n -C_{11:1}+4-methylguaiacol (Ratio A) together with the aromaticity and the relative abundance of huminite/vitrinite particles can be used to show variations of higher plant input through time. Fig. 5.20 illustrates a good correlation with the already established pollen stratigraphy for Lake Meerfelder Maar (Litt & Stebich, 1999), whereas it is more difficult to interpret the organic geochemical data of HZM in terms of paleoenvironmental and paleoclimatic changes (Fig. 5.21). The increase of

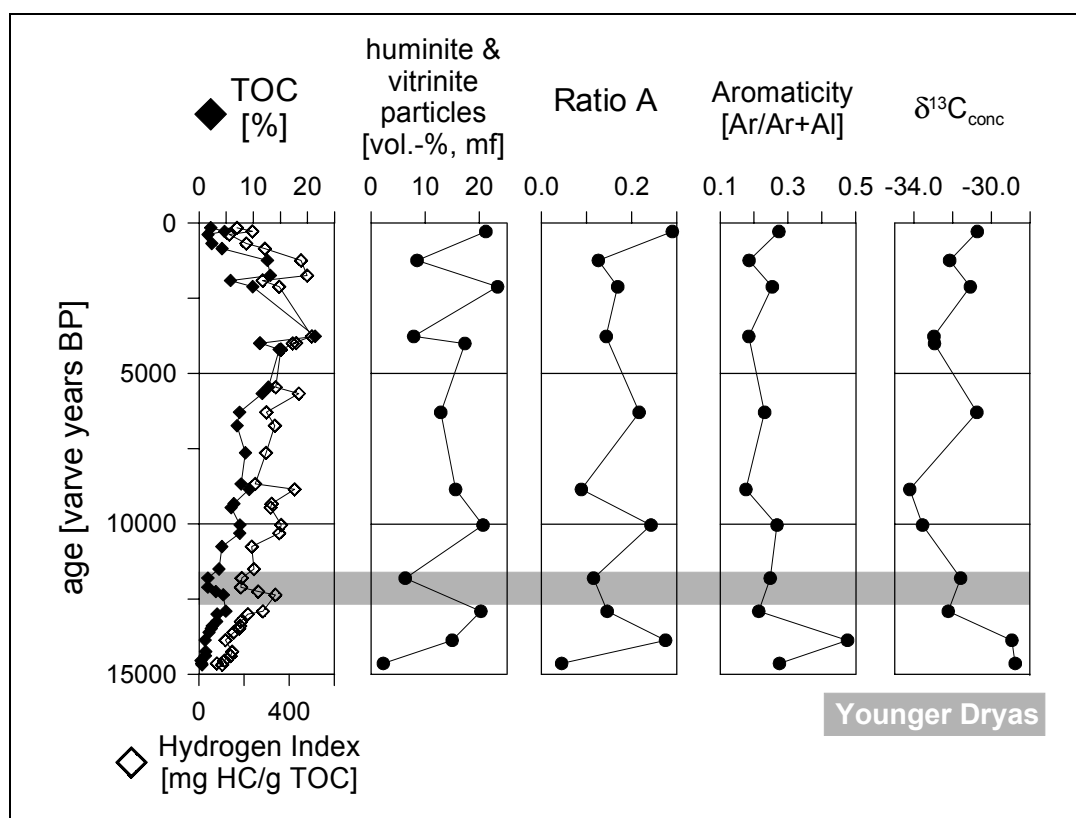


Fig. 5.20. Temporal variations of macromolecular parameters based on maceral analysis and analytical pyrolysis for MFM. Ratio A, 4-methylguaiacol/ n -C_{11:1}+4-methylguaiacol; the aromaticity is based on the aromatic (Ar) versus aliphatic (Al) nature of the kerogen.

lignin-derived components in MFM parallels the amelioration of the climate, indicating forestation of the landscape after the last glacial retreat (Fig. 5.20). This is substantiated by a significant increase of the TOC/TN ratios (Fig. 5.8) during the Lateglacial in a depth between 1045 to 885 cm (14,545 to 13,480 varve yrs BP) and abundant low reflecting huminite/vitrinite particles in kerogens from the Bølling/Allerød (Fig. 5.20). A reverse trend towards the Younger Dryas shows a reduction of the forest around the maar lake. High amounts of inertinite and recycled huminite/vitrinite particles point to a source from the geological substratum (Figs. 5.16 and 5.17 C). These allochthonous components were probably introduced by the erosion of soils during run-off periods which in turn reflect a predominantly open, tree-less vegetation. In addition, the high proportion of recycled/oxidised OM might be a good indicator of paleoaridity with a major input of wind derived dust particles within a dry glacial climate. The very low HI values in samples from the Late Pleniglacial and from the Younger Dryas (Fig. 5.20) reflect the oxidised nature of the OM rather than source variations. However, the characteristic HI maximum at the beginning of the Younger Dryas (12,355 varve yrs BP) in the MFM section (Fig. 5.20) is due to an increased primary production in the lake, which was reported previously for this period (Brauer *et al.*, 1999). The authors found thick diatom layers (e.g. *Stephanodiscus*), *Pediastrum* alginite and an increase in biogenic opal.

TOC and HI values increase relatively rapidly in the **Holocene** (Fig. 5.20). This reflects a greater increase of carbon to the lake in response to an intensified paleoproductivity during the warmer Holocene. The establishment of woodland around the lake during the Preboreal and Boreal is documented by an increasing Ratio A and a higher aromaticity. The kerogens from the Holocene consist of low-reflectance non-oxidised huminite particles (Figs. 5.16 and 5.17 A & B) with multiple leaf and woody fragments and varying contributions of alginite. Because oxidation of the OM is less important during the Holocene it can be assumed that the HI variations describe changes in the relative contributions of autochthonous and allochthonous OM. The increase of the TOC/TN ratios in HZM from section C to A (Fig. 5.7) indicates a change from an ecosystem with an overwhelming autochthonous primary production in section C to an ecosystem with allochthonous and autochthonous OM sources in the sections B and A. The higher contribution of cyanobacterial filaments and an unknown colonial alga, observed in the HZM section (Fig. 5.14 A) between 7390 and 5690 varve yrs BP, reflect the enhanced primary productivity during the Holocene optimum.

The increase of huminites and lignin derived pyrolysis products during Recent times in MFM (< 500 varve years BP) could be due to enhanced soil erosion and therefore input of land derived organic particles to the lake which is supported by high TOC/TN ratios in both sediment sections (Figs. 5.7 and 5.8). Interestingly, they appear synchronously to a period of high allochthonous input as proposed by Zolitschka (1998). It was interpreted as the results of an increased human impact due to an intensive forest clearing and thus high erosion rates during the Subatlantic. Therefore, both low reflecting fresh plant OM and high reflecting reworked OM were identified in the studied sediments (Fig. 5.17 A). The enhanced higher plant delivery to the lakes is also corroborated by the lower HI values in the uppermost part of section A (Fig. 5.21).

Stable carbon isotope values measured on kerogen concentrates indicate a dominant terrigenous source with values around -28‰ in the late Pleniglacial, typical for C_3 plants. Towards the Holocene, the primary aquatic production became relatively more important and thus lower values prevail during the Holocene, reflecting the dominant input of lacustrine organic carbon (ratios below -30‰). This is substantiated by the generally higher HI values in the Holocene sediments as well as higher amounts of filamentous alginite in the kerogen concentrates with very negative $\delta^{13}C_{\text{conc}}$ values.

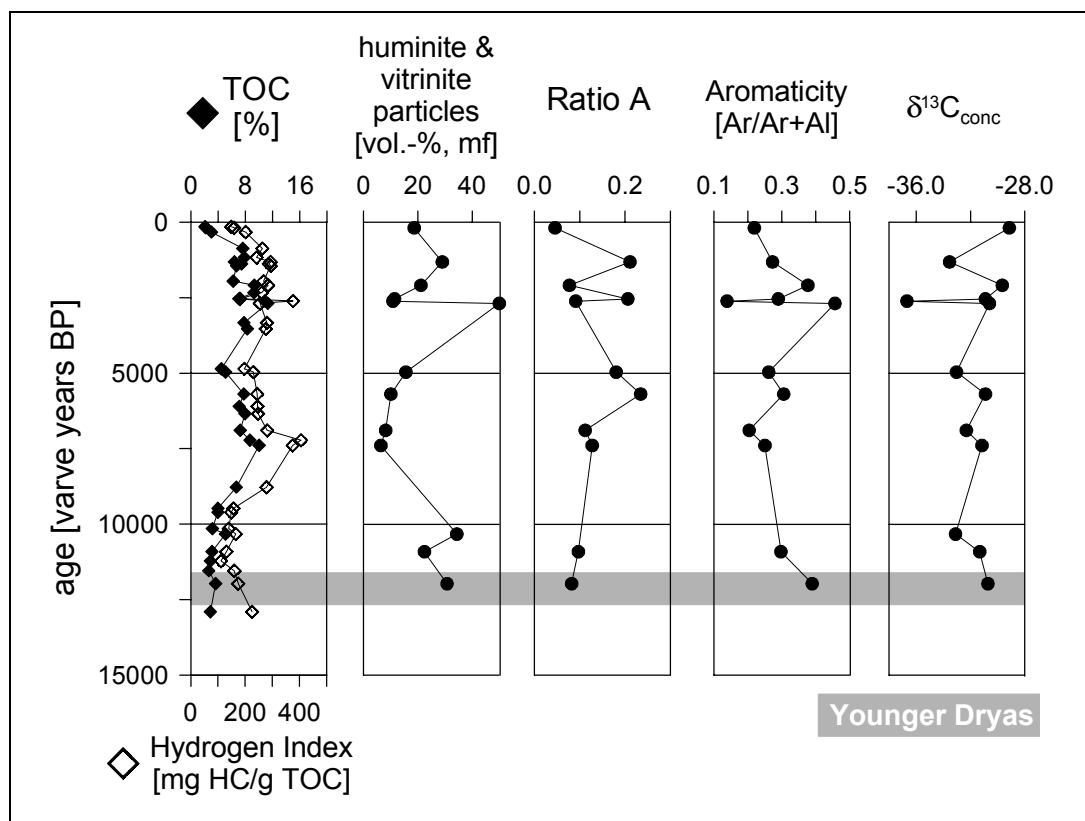


Fig. 5.21. Temporal variations of macromolecular parameters based on maceral analysis and analytical pyrolysis for HZM. Definition of parameters as in Fig. 5.20.

5.4 Lake Huguang Maar

5.4.1 Screening Analysis

Variations of TOC, TS, HI, stable carbon isotopes ($\delta^{13}\text{C}_{\text{TOC}}$) and TOC/TN ratios are presented in Fig. 5.22 A for the D and F core. In Figs. 5.22 B and C downcore variations within the selected intervals of the high-resolution study (core E) are illustrated. All depths were normalised to core F. The different lithozones, following the subdivision of Mingram *et al.* (2000), are indicated. On the right several calibrated ages from radiocarbon ^{14}C -AMS datings are given. Bulk organic geochemical parameters of the lithozones are presented in Tab. 5.8 (mean values) and Appx. J.

Lithozone	Depth [cm]	n	TOC	TS	TOC/TS	TN	TOC/TN	S2	HI	$\delta^{13}\text{C}_{\text{TOC}}$
			[%]	[%]		[%]		[mg HC/g sample]	[mg HC/g TOC]	[%]
1	0-523	5	3.10	0.08	36.2	0.30	9.7	6.20	172	-22.30
2	523-1070	15	8.40	0.28	29.5	0.79	9.9	25.57	302	-19.97
3	1070-2917	22	4.40	0.17	32.1	0.48	9.7	9.18	188	-18.28
4	2917-3243	24	12.60	0.37	33.8	0.87	14.3	42.36	337	-25.99
5	3243-3952	8	5.70	0.16	37.1	0.59	9.6	16.67	281	-22.30
6	3952-4546	6	14.10	0.67	22.1	0.47	30.3	44.77	330	-29.73

Tab. 5.8. Bulk organic geochemical parameters of the lithozones (mean values).

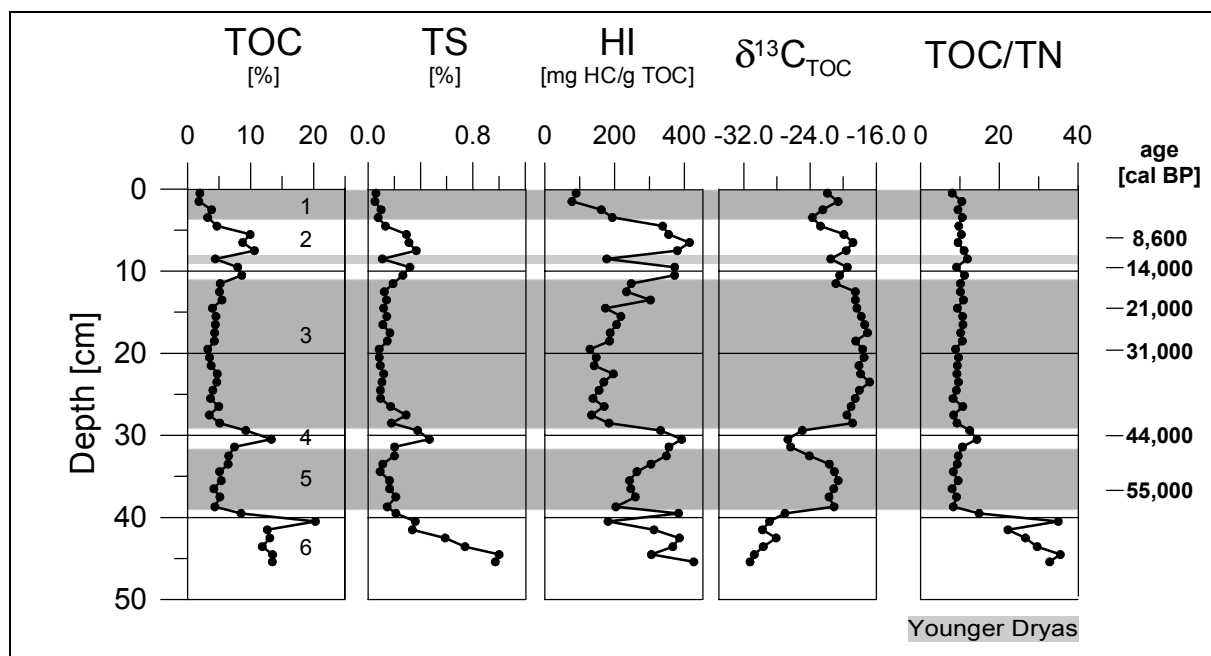


Fig. 5.22 A. Sample screening for the HM profile (core D and F); lithozones (indicated by numbers 1 to 6) and ages according to Mingram *et al.* (2000).

Overall **TOC contents** vary between 1.7 and 20.7%. The highest values were observed in the lithozones 4 and 6, where several layers with plant fragments are present. Lithozone 1 is characterised by relatively low TOC values (3.1% on average), while they increase towards lithozone 2 (8.4% on average). A significant minimum of 4.4% was found in the F-core at 850 cm depth (E 47717; Fig. 5.22 A). This minimum was also detected in the E-core (Fig. 5.22 B) and corresponds to the Younger Dryas cold period. Within lithozone 3, the TOC contents are generally low and uniform with a mean value of 4.4%. The TOC values increase towards lithozone 4 (12.6% on average) with a characteristic maximum of 20.7% at 3019 cm depth (Fig. 5.22 C), followed by a return to relatively low values in lithozone 5 (5.7% on average; Fig. 5.22 A). Finally, in lithozone 6 the highest overall TOC contents were determined (14.1% on average) with a significant maximum of 20.3% at the top of this section (4050 cm depth).

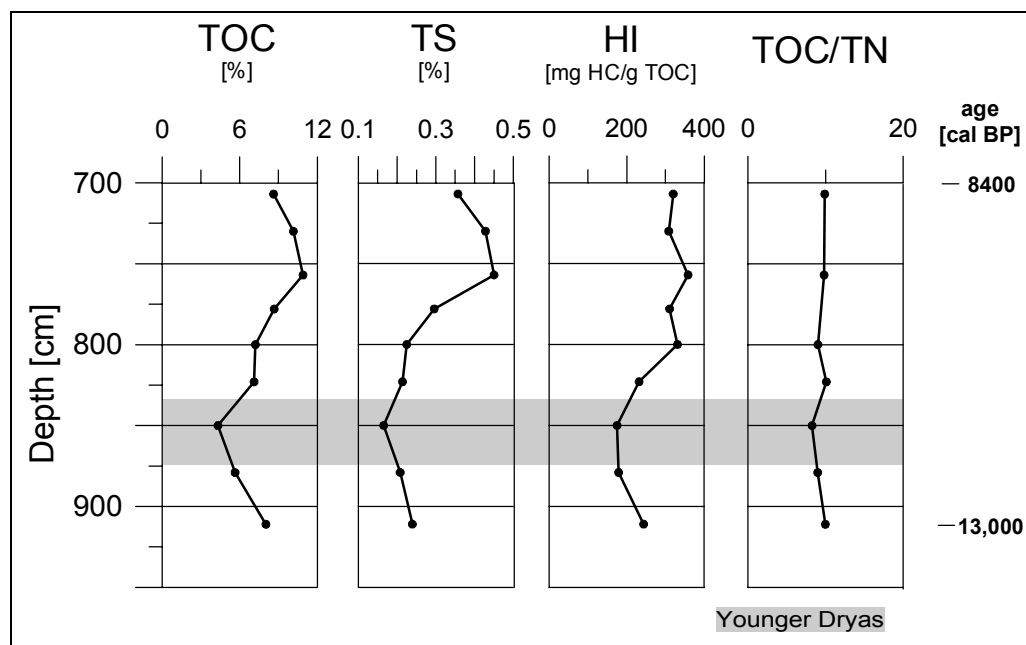


Fig. 5.22 B. Sample screening for the HM high resolution profile (core E) lithozone 2; ages according to Mingram *et al.* (2000). Depths are normalised to core F.

The **TS contents** vary between 0.1 and 1.0%. They are generally low compared to HZM and MFM. The highest TS values were observed in lithozone 6 (0.67% on average). Sulphur in lake sediments may originate from sedimenting organic particles or bacterial sulphate reduction. Nriagu & Soon (1985) and Rudd *et al.* (1986) observed that sulphate reduction is the primary source of sulphur in hypolimnetic and epilimnetic freshwater sediments. They found that organic sulphur compounds such as carbon bonded sulphur and sulphate esters are predominant because of a preferential loss of inorganic iron sulphides by re-oxidation. Thus, a lowering of the TOC/TS ratio with depth could indicate a progressive sulphur addition to the

sedimentary OM (Urban *et al.*, 1999). In contrast a dominant origin of organic sulphur derived directly from the sedimenting biomass was proposed by Guillet & Maman (1995) for sediments from Lac du Bouchet, France. A positive correlation between the TOC and TS values was observed in the present study, disregarding the three deepest samples from lithozone 6, whose TS contents are perhaps influenced by inorganic sulphur from the volcanic rocks underlying the lake sediments (Fig. 5.22 A). The TOC/TS ratio is generally high and ranges from 11.8 at 2350 cm depth to 57.6 at 3350 cm depth with a mean value of 33.2. TOC/TS ratios of autochthonous OM are generally between 15 and 30, while ratios around 100 or above were found for higher plant and macrophyte debris in littoral lake sediments (Gorham *et al.*, 1974; Nriagu & Soon, 1985). Samples with high amounts of higher plant debris such as E 48165 in lithozone 6 at 4050 cm depth show the highest TOC/TS ratios. Thus, variations of the TOC/TS ratios are linked to the varying input of OM from terrigenous sources.

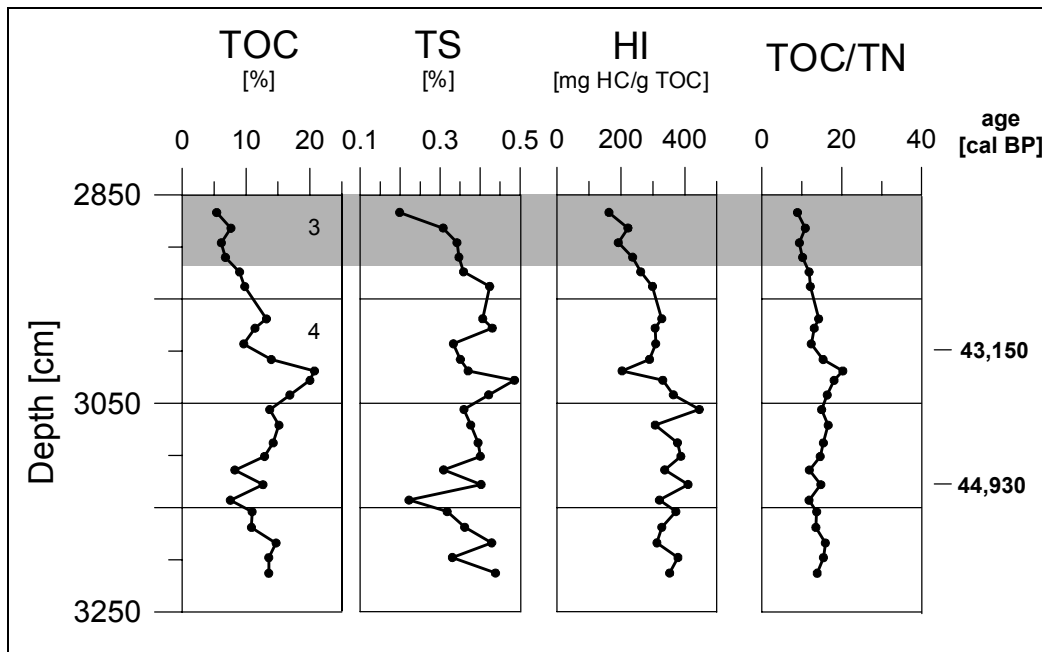


Fig. 5.22 C. Sample screening for the HM high resolution profile (core E) lithozone 3 and 4; ages according to Mingram *et al.* (2000). Depths are normalised to core F.

Carbon isotope values of bulk OM ($\delta^{13}\text{C}_{\text{TOC}}$) show large variations which range between -31.3 and -17.1 ‰ (Fig. 5.22 A). Two negative excursions were observed in the lithozones 4 and 6, reaching depleted on average values of -26.0 and -29.7 ‰, respectively. The glacial lithozone 3 is characterised by stable, relatively heavy $\delta^{13}\text{C}_{\text{TOC}}$ values (-18.3 ‰ on average). Some remarkable oscillations between the top and 10.5 m depth characterise the Lateglacial and Holocene lithozones 1 and 2 with an isotopic minimum of -23.7 ‰ at 345 cm depth (E 47712) and a maximum of -18.8 ‰ at 650 cm depth (E 47715). Interestingly, a relatively

negative value of -21.5‰ was observed for the Younger Dryas period at 850 cm depth (E 47717). This bulk isotopic signal of organic carbon in the HM lake sediments resemble the $\delta^{13}\text{C}_{\text{TOC}}$ values from other tropical sediment archives of the studied time interval (Talbot & Johannessen, 1992; Street-Perrott *et al.*, 1997; Hodell *et al.*, 1999).

The **HI values** show large fluctuations (Fig. 5.22 A to C) with three distinct maxima in lithozone 2 at 6.5 m depth (415 mg HC/g TOC), lithozone 4 at 30.6 m depth (445 mg HC/g TOC; E-core) and lithozone 6 at 45.5 m (426 mg HC/g TOC). The highest overall HI values were observed in lithozone 4 (337 mg HC/g TOC on average) while the lowest values were found in lithozone 3 (184 mg HC/g TOC on average). A significant shift to lower HI values towards recent times is characteristic for lithozone 1. As discussed previously (chapter 5.3.1) high OI values (234 mg CO_2 /g TOC) can be mainly attributed to an overprinting influence of the mineral matrix and do not permit an OM source interpretation. The S2 and TOC values for the different lithozones are plotted in Fig. 5.23. This graph illustrates that all lithozones contain OM which resembles a mixture of type II and type III OM. However, the OM in lithozone 3 comprises OM that is relatively enriched in type III OM or is more oxidised.

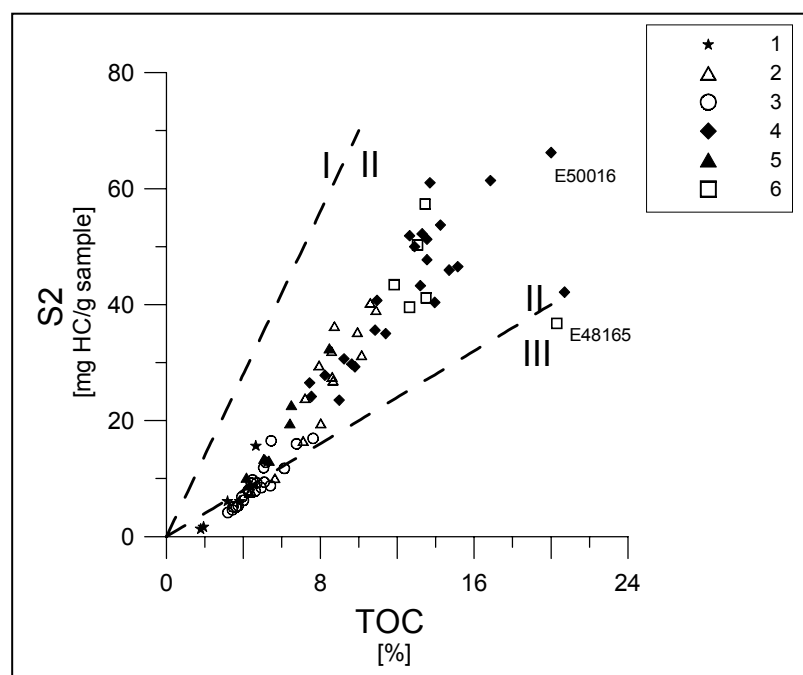


Fig. 5.23. S2 versus TOC of sedimentary OM from HM. Numbers indicate the different lithozones. Interpretation lines adopted from Langford & Blanc-Valleron (1990).

The **TOC/TN ratios** show only very little variations throughout the investigated profile. A mean ratio of 9.7 was determined for the lithozones 1, 2, 3 and 5, which suggests the contribution of predominantly aquatic OM. The ratios are slightly higher in lithozone 4 (12.9 on average) but maximum ratios of 35.5 were calculated for lithozone 6 (30.3 on average). High C/N ratios in these two lithozones were also observed in a study by Mingram *et al.* (2000) and interpreted to reflect the relatively higher contribution of terrigenous OM to the

sediments in these zones. A plot of the HI values and the TOC/TN ratios (Fig. 5.24) illustrates that the samples from the lithozones 4 and 6 are separated in the diagram, whereas samples from the other lithozones are characterised by large HI variations but relatively stable TOC/TN ratios. This shows that factors other than the composition of the OM erased the large TOC/TN differences between vascular plant and algal OM (see section 5.3.1). First, the alga *Botryococcus braunii* is relatively abundant in the lithozones 4 and 6 (see section 5.4.4). Hydrocarbon synthesis of this alga in large amounts can lead to exceptional high TOC/TN ratios of about 36.0 (Huang *et al.*, 1995). Second, the preferential retention of nitrogen in the HM sediments previously described for marine sediments by Müller (1977) and Lallier-Vergès & Albéric (1990) may have altered the TOC/TN ratio. Anaerobic destruction of organic carbon yields CO_2 and CH_4 which escape rapidly. The microbial degradation of organic nitrogen compounds produces NH_4^+ which is adsorbed to clay minerals, thus preventing a decrease of the TN content and in turn leads to relatively low TOC/TN ratios. Interestingly, the TN contents and the HI values show a positive correlation (Fig. 5.24), with the exception of the samples from lithozone 6. The highest TN contents were observed for the lithozones 2 and 4, whereas the lowest values were determined for the lithozones 1 and 3. This finding suggests that the TN content instead of the TOC/TN ratio is a more sensitive parameter to define changes in the relative contribution of aquatic *versus* terrigenous OM.

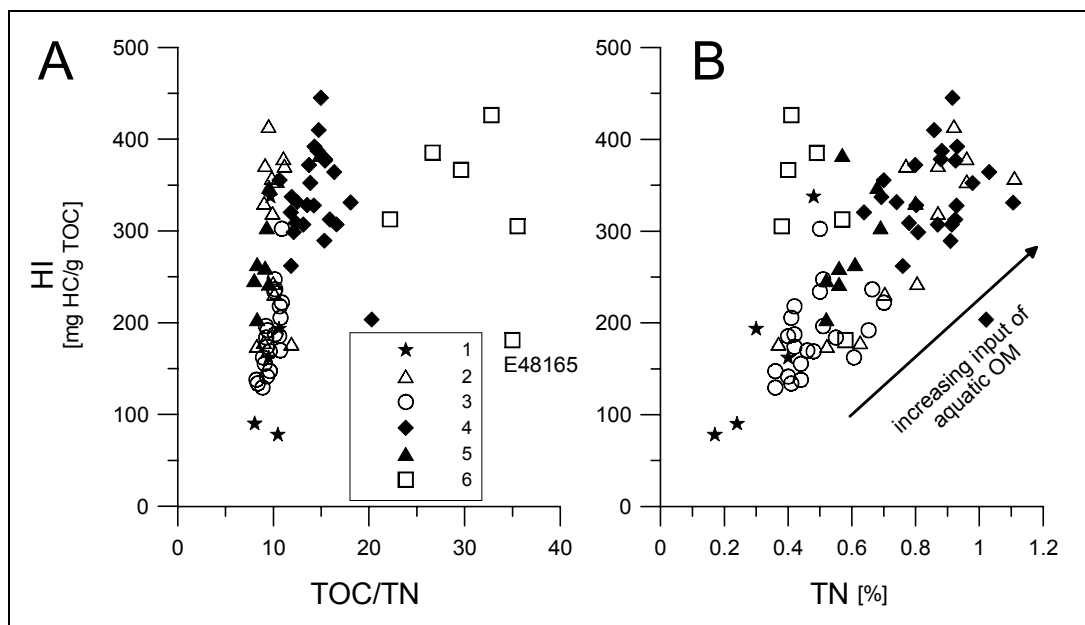


Fig. 5.24. (A) HI versus TOC/TN and (B) HI versus TN in sediment samples from HM. Numbers indicate the different lithozones.

5.4.2 Chemical Composition of the Kerogens

The elemental composition was determined for seven kerogens listed in Tab. 5.9, and their stratigraphic location is given in Fig. 5.25. The H/C ratios are relatively low (0.8 to 1.4) compared to the HZM and MFM kerogens (1.3 to 1.7). The O/C ratios are in the same range. The sulphur contents of the kerogens vary between 1.6 and 3.9%. The values show that the kerogens analysed here have low sulphur contents, compared to studies on sulphur rich marine sediments (e.g. di Primio, 1995; Lückge, 1997).

E.nr.	Depth [cm]	Lithozone	TOC [%]	TS [%]	H/C atomic	O/C atomic	TOC/TN
47716	749	2	54.00	2.60	1.16	0.30	16.4
47730	2150	3	57.10	1.04	0.82	0.29	35.7
47736	2752	3	49.40	1.79	1.00	0.35	24.7
47739	3048	4	54.10	1.64	1.21	0.41	23.5
47744	3550	5	54.40	1.66	1.06	0.35	21.8
48165	4050	6	49.95	0.52	1.19	0.42	29.4
48170	4540	6	52.40	4.70	1.42	0.30	25.0

Tab. 5.9. Elemental data of selected kerogen concentrates.

5.4.3 Thermal Analysis (Py-GC-FID and Py-GC-MS)

Seven kerogen concentrates (core F) and 32 whole rock sediments (core E) were analysed to study the macromolecular OM in HM. Their origin is illustrated in a generalised stratigraphic column (Fig. 5.25). Detailed pyrolysis quantitation results are summarised in Appx. K.

The kerogens are dominated by aliphatic compounds (*n*-alkane/*n*-alk-1-ene doublets) with a mean value of 61% of all quantified compounds. The range extended from 73% at 4540 cm depth (E 48170) to 41% at 4050 cm depth (E 48165). Although the *n*-alkane/*n*-alk-1-ene doublets are still predominant, overall lower percentages were determined for the whole rock sediments with 36% on average. Especially the long-chain *n*-alk-1-enes (>C₁₅) have lower concentrations compared to the corresponding kerogens. The alkylbenzenes make up an important fraction in the pyrolysates of the kerogens and sediments (17% on average). Selected polysaccharide derived pyrolysis products make up 17% on average of the bulk sediment pyrolysates. Other important compound classes are phenols which make up

11 and 12% in the pyrolysates of the kerogens and sediments, respectively. All other compound classes are only minor contributors to the resolved pyrolysate.

Two representative pyrograms are illustrated in Fig. 5.26. Predominance of *n*-alkane/*n*-alk-1-ene doublets up to C₃₀ points to a strong contribution of algal OM as seen for example in the deepest sample (E 48170) of core F from 4540 cm depth (Fig. 5.26 A), and has previously been said to be typical of highly aliphatic chemically resistant and insoluble biopolymers, termed *algaenans* (Tegelaar *et al.*, 1989). In chapter 5.4.4 it will be shown by organic petrological observations, that *Botryococcus* alginite is an important part of the OM. Aromatic compounds are only minor constituents of this pyrolysate. The carbon isotopic composition of this kerogen (−31.2‰) reflects its dominant lacustrine aquatic nature.

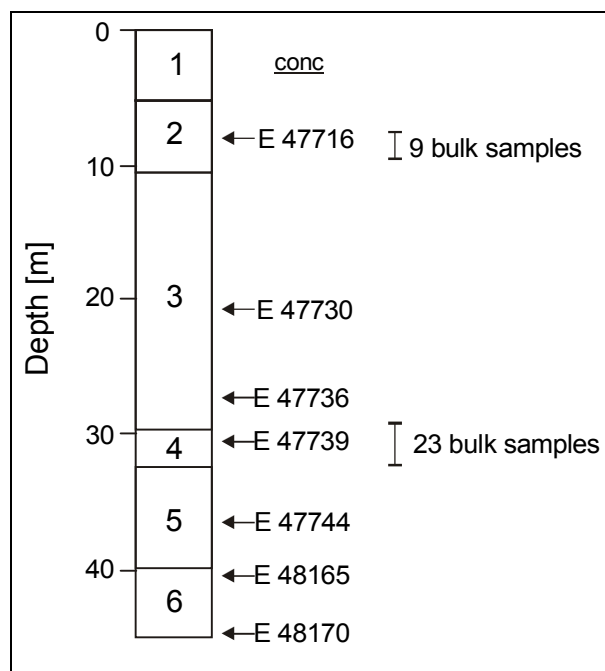


Fig. 5.25. Stratigraphic origin of the kerogen concentrates (*conc*) and bulk samples for Py-GC-FID and Py-GC-MS. Lithozones 1 to 6 are indicated by numbers.

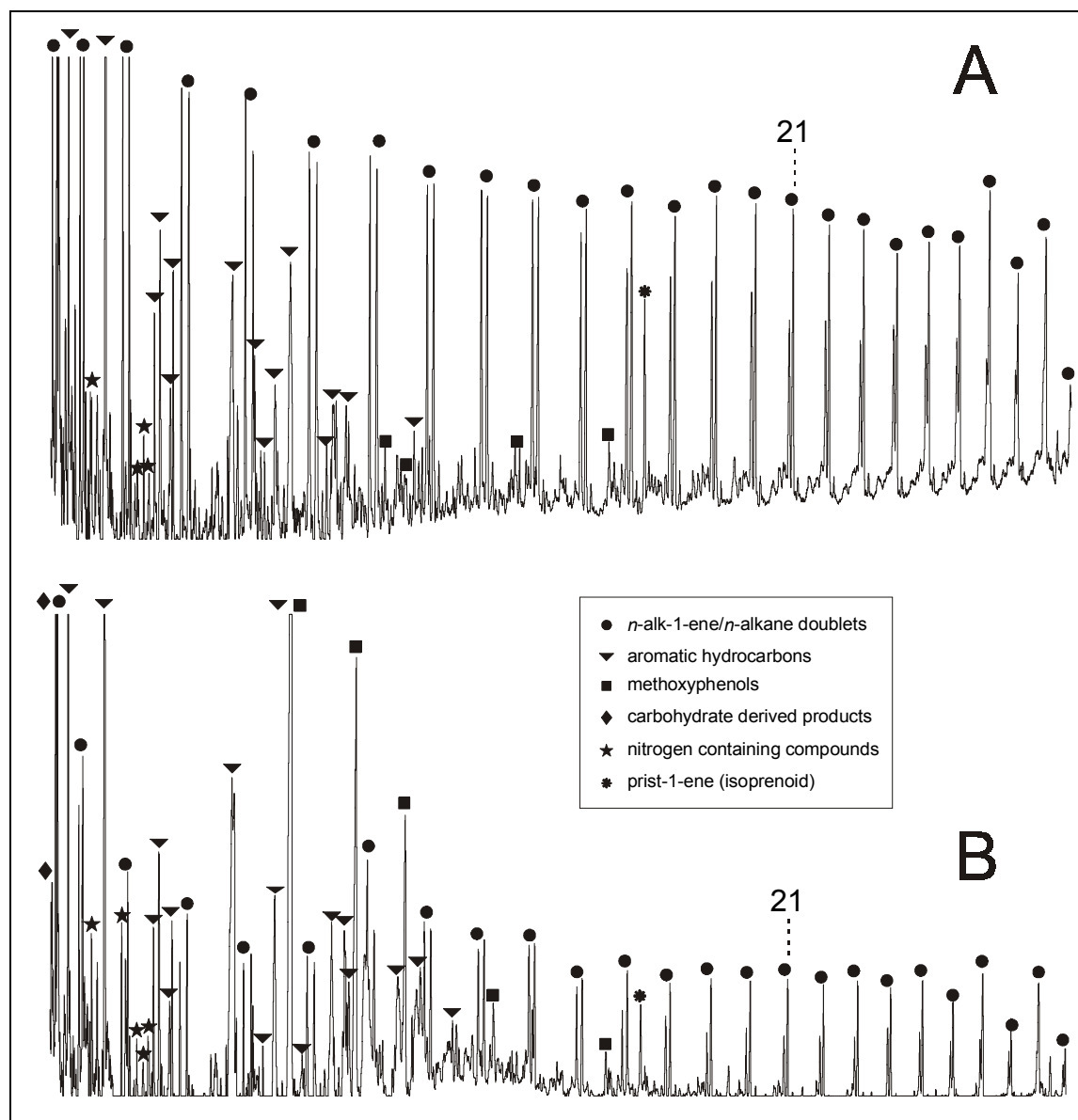


Fig. 5.26. Pyrolysis gas-chromatograms of selected representative HM kerogens. Numbers indicate *n*-alkyl chain lengths. (A) Sample E 48170 from 4540 cm depth; (B) Sample E 48165 from 4050 m depth.

The simple mono-aromatic hydrocarbons benzene, toluene, catechols and methoxyphenols, the latter originating from the thermal degradation of lignin during pyrolysis, predominate the sample from 4050 m depth (Fig. 5.26 B). This kerogen has a terrigenous origin and thus the relatively low proportions of *n*-alk-1-ene/*n*-alkane doublets in the pyrolysates must be related to aliphatic components of higher plant macromolecules such as cutan and suberan. Notably the liptinite maceral suberinite which consist mainly of this suberan biomacromolecule (Tegelaar *et al.*, 1995), was detected by microscopic observations in this sample (Fig. 5.31 E).

Lignin macromolecules are polymeric products synthesised in plants by the dehydrogenative polymerisation of three primary precursor monomers: *trans*-*p*-coumaryl, *trans*-coniferyl and *trans*-sinapyl alcohols (Fig. 5.27). Pyrolysis gas-chromatography has become an important method in the study of lignocellulosic materials because it avoids time-consuming chemical degradation (Meier & Faix, 1992). The identification of specific lignin markers by Py-GC-MS is straightforward, because of the diagnostic mass spectra, containing an intense molecular ion and characteristic fragment ions. For comparison, detailed compilations of lignin markers were made available by Meier & Faix (1992) and Galletti & Bocchini (1995). The typical lignin pyrolysis fragments identified in the HM pyrolysates are phenolic products with *p*-hydroxyphenyl (H), guaiacyl (G) and syringyl (S) basic units, with or without alkyl substituents. The quantification of these fragments is presented with the other identified compounds in Appx. K.

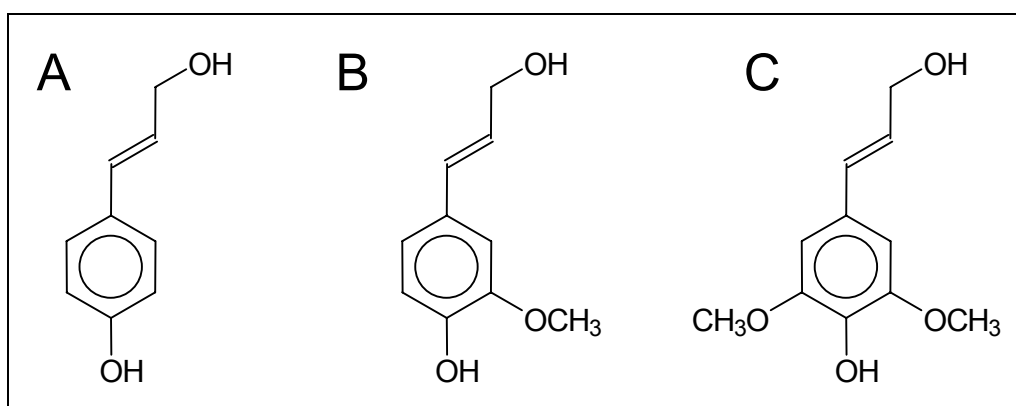


Fig. 5.27. Structures of lignin precursor alcohols. Typical lignin pyrolysis fragments detected in Py-GC-MS analyses are phenolic compounds with (A) *p*-hydroxyphenyl (*p*-coumaryl alcohol), (B) guaiacyl (coniferyl alcohol) and (C) syringyl (sinapyl alcohol) basic units.

Specific lignin fragments were used to estimate the predominant precursor monomer in pyrolysates of samples from different lithozones of core E and F as illustrated in Fig. 5.28. Samples from the lower lithozone 2 including the Younger Dryas and lithozone 3 contain higher concentrations of hydroxyphenyl related lignin products whereas pyrolysates from the lithozone 4 and 6 are dominated by pyrolysis products with guaiacyl units. The average H:G:S proportions for samples from lithozone 2 and 3 are essentially the same (78:10:12 and 70:13:17, respectively). Pyrolysates of samples from lithozone 4 contain higher amounts of guaiacyl units (on average 33:49:18 H:G:S). An overwhelming predominance of guaiacyl over syringyl and *p*-hydroxyphenyl units (2:96:2) was observed for the kerogen pyrolysate from 4050 cm depth in lithozone 6 (E 48165). However, an important early diagenetic loss of up to 30% was reported for the syringyl phenols during wood burial in sediments

(Hedges *et al.*, 1985). Consequently, the overall content of syringyl phenols is probably underestimated. A detailed environmental interpretation of the distribution in Fig. 5.28 is presented in section 5.4.7.

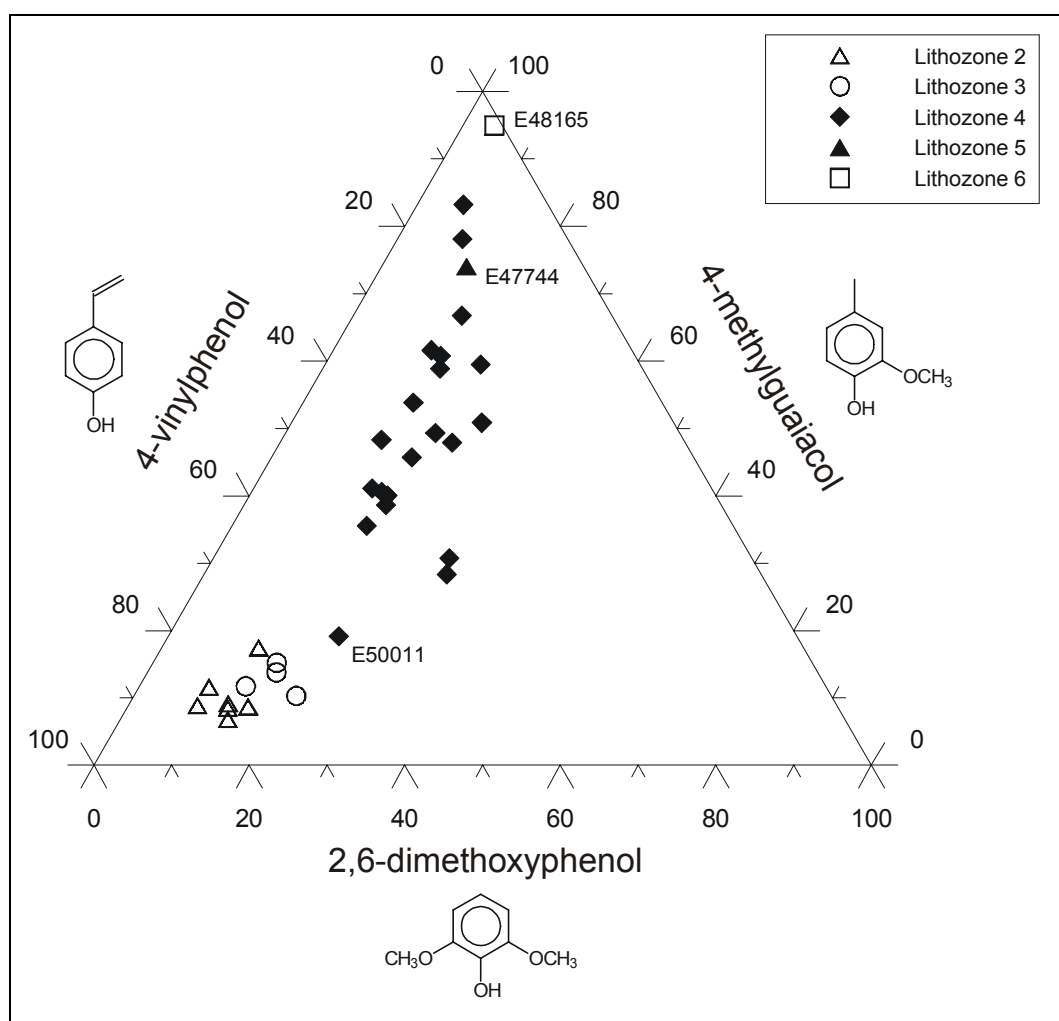


Fig. 5.28. Distribution of lignin pyrolysis products in lithozones of core E and F.

Lignin is linked with polysaccharides, primarily through arabinose, xylose, and galactose units in the hemicellulose components of higher plants (Koshijima *et al.*, 1989). Relatively high concentrations of polysaccharide derived pyrolysis products such as furans were detected especially in lithozone 6, indicating the presence of partially intact cellulosic materials (Pouwels *et al.*, 1989). Since these compounds normally decompose rapidly in sediments it can be deduced that post-depositional degradation was relatively low (Hedges *et al.*, 1985). Other major polysaccharide pyrolysis products are a series of cyclopenten-1-ones which were previously observed in pyrolysates of soil OM (Saiz-Jimenez & de Leeuw, 1986) and were also encountered in pyrolysates of amylose (van der Kaaden *et al.*, 1983) as well as recent lake sediments from Lake Ontario (Kruge *et al.*, 1998). According to van Heemst *et al.* (2000), the cyclopenten-1-ones represent the altered polysaccharide fraction.

The most probable sources for the detected catechols are condensed vegetable tannins such as catechin (Galletti & Reeves, 1992), or biodegraded lignins (Saiz-Jimenez & de Leeuw, 1984). According to Faix *et al.* (1987 and references therein) the presence of catechols could also be a result of specific pyrolysis conditions and thus may have resulted from the thermal demethylation of guaiacyl units.

5.4.4 Organic Petrology

Point counting of seven kerogen concentrates revealed that the OM in the different lithozones is dominated by yellow to orange **fluorescing or non-fluorescing AOM** (46.2 to 80.6%). Tab. 5.10 lists the proportions of the amorphous, aquatic and terrigenous fraction in the studied samples. The detailed point-counting results and vitrinite reflectance data are available in Appx. L. The percentage of fluorescing AOM ranges between 16.7 at 4050 cm depth in the top section of lithozone 6 (E 48165) and 61.1% in lithozone 2 at 749 cm depth (E 47716).

E.nr.	Lithozone	Depth [cm]	AOM [%]	Terrigenous OM [%]	Aquatic OM (alginite) [%]
47716	2	749	80.6	15.0	2.7
47730	3	2150	59.0	40.0	1.0
47736	3	2752	57.5	42.6	0.0
47739	4	3048	74.9	9.6	8.4
47744	5	3550	61.5	32.2	2.1
48165	6	4050	46.2	53.6	0.2
48170	6	4540	71.6	10.4	14.9

Tab. 5.10. Bulk petrographic composition of the HM kerogen samples.

Microscopical investigations on the kerogens as well as on prepared sediment sections showed that the **lacustrine aquatic fraction** consists mainly of the colonial green alga *Botryococcus* (Fig. 5.29 A). This floating planktonic alga is a member of *Chlorophyceae*, characterised by an organisation of colonies (between 10 to 50 μm) which are best visible when viewed in transmitted light. It displays a bright yellow fluorescence when observed in reflected light with blue filter excitation. The varying sizes most likely reflect different development stages in the life history of the algae (Guy-Ohlson, 1992). In lithozone 1 only few algal bodies were detected, whereas almost no alginite was counted in lithozone 3. Instead of this, some remains of the alga *Pediastrum* were identified in the lithozones 2 and 3. Highest proportions of *Botryococcus* alginite were determined for the kerogen samples E 48170 (14.9%) from 4540 cm in lithozone 6 and E 47739 (8.4%) from 3048 cm in lithozone 4. Well-preserved colonies dominate in the entire sample set with the exception of lithozone 4, where partly or completely degraded remnants were found. While well preserved algal remains are a result of a very rapid deposition and burial in an undisturbed environment (Glikson *et al.*, 1989), a morphological alteration of *Botryococcus* alginite might indicate evaporitic events (Derenne *et al.*, 2000).

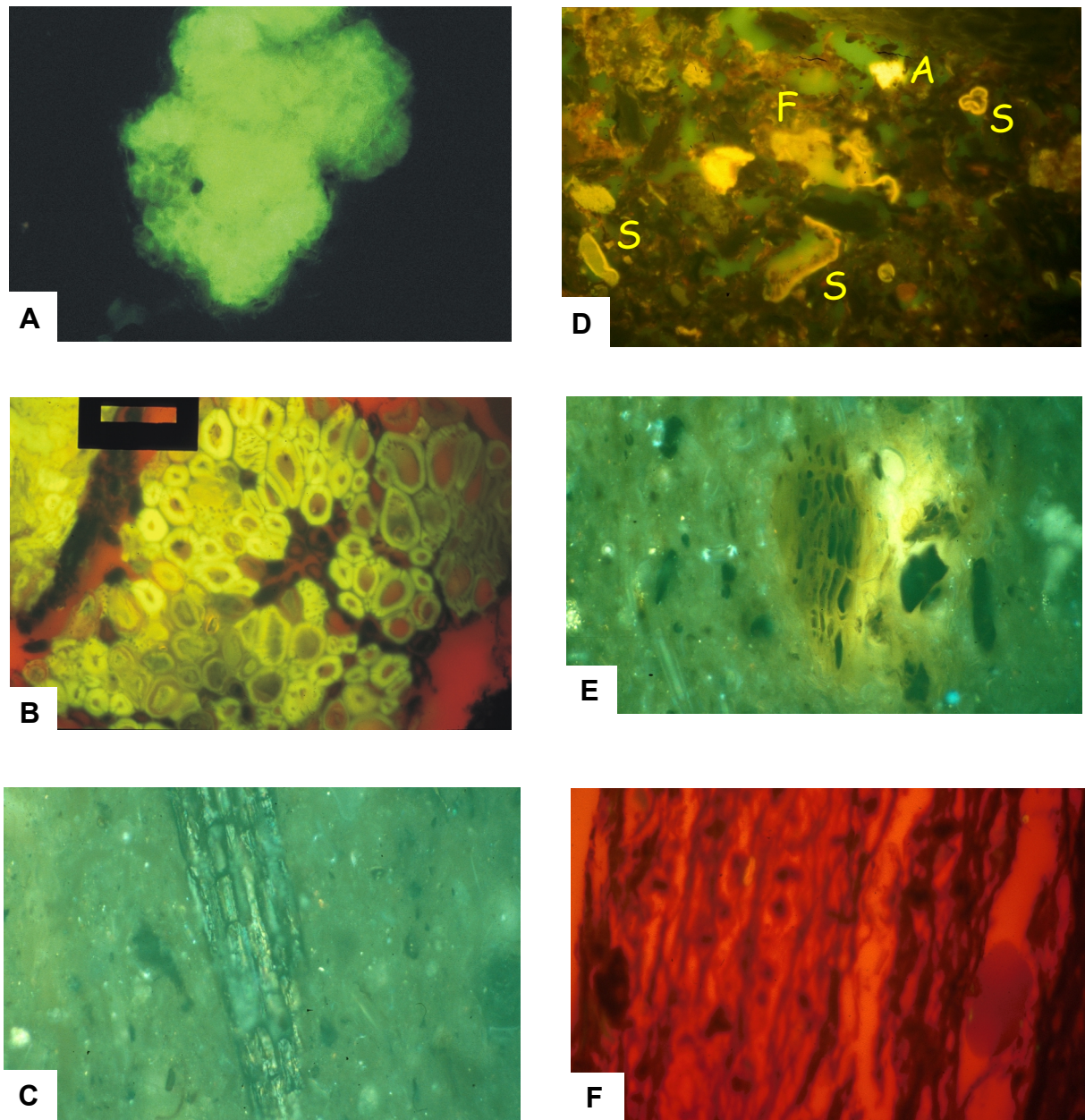


Fig. 5.29. Microphotographs of OM in sediment samples and kerogens from Lake Huguang Maar.

- A) Sample E 47739 from 3048 cm depth (lithozone 4). *Botryococcus alginite*. 1000x, blue light excitation.
- B) Sample E 48165 from 4050 cm depth (lithozone 6). Plant fragments with intact cell structures. 250x, blue light excitation.
- C) Sample E 47744 from 3550 cm depth (lithozone 5). Higher reflecting particle. 500x, reflected white light.
- D) Sample E 48170 from 4540 cm depth (lithozone 6). Sporinite (S), fluoramorphinite (F) and small alginite (A). 500x, blue light excitation.
- E) Sample E 48165 from 4050 cm depth (lithozone 6). Suberinite (cork). 500x, blue light excitation.
- F) Sample E 48165 from 4050 cm depth (lithozone 6). Strong red-fluorescing chlorophyllinite. 500x, blue light excitation.

Organic petrology reveals the presence of abundant plant fragments with intact cell structures within the lithozone 6 (Fig. 5.29 B). For example, the huminite fraction makes up to 51.0% of the total visible OM in the sample from 4050 cm depth (E 48165). In the other lithozones, the **terrigenous derived fraction** mainly consists of huminite/vitrinite particles (5 to 15 μm) with varying reflectance values. Especially within lithozone 3 higher reflecting particles make an important contribution to the total OM (Fig. 5.29 C). Additionally some highly oxidised particles were found in this section, reflecting an input of eroded older geological OM or primary oxidised fragments. The highest overall reflectance values were determined for samples from lithozone 3. Measured values are mainly in the range between

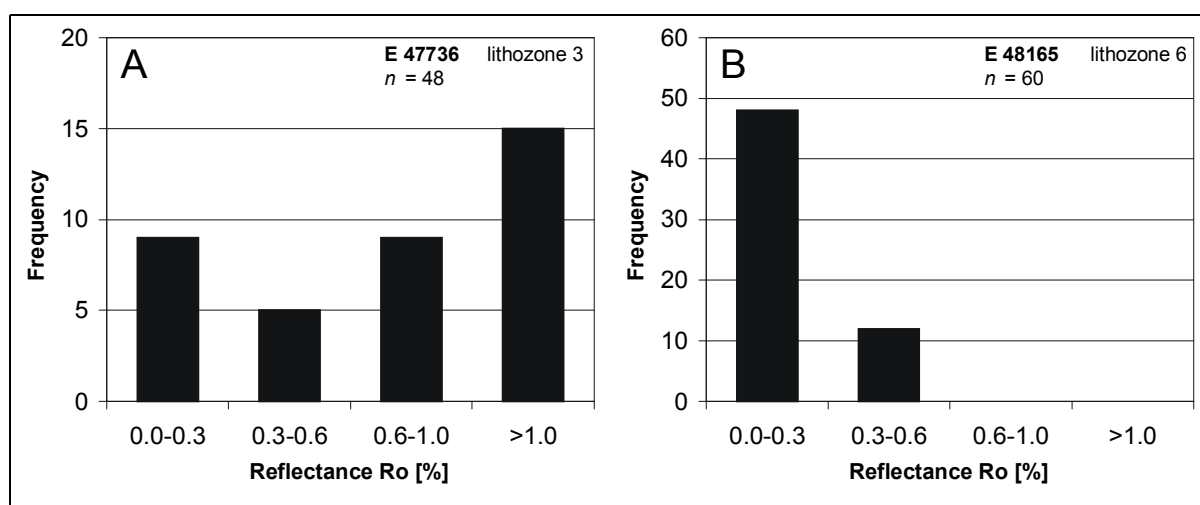


Fig. 5.30. Histograms of reflectance, measured on huminite, vitrinite and inertinite particles in two kerogens from HM. Samples are from 2752 cm (A) and 4050 cm (B) depth.

0.6 to 1.0% Rr and above 1.0% Rr. (Fig. 5.30 A). In comparison the terrigenous OM in the lithozones 4 and 6 is composed of fresh non-oxidised OM (Fig. 5.30 B) with reflectance values in the range of 0.0 to 0.3% Rr. The allochthonous liptinite macerals sporinite and suberinite (Figs. 5.29 D and E) were detected in fluorescence mode in many studied samples. Therefore, it is most likely that the doublets in the terrigenous dominated sample E 48165 originate from the aliphatic components of the plant macromolecules *sporopollenin* and *suberan*. Microscopy of terrigenous dominated samples (e.g. E 48165) from lithozone 6 revealed the presence of abundant intense red-fluorescing *chlorophyllinite* in terrigenous OM rich laminae (Fig. 5.29 F). This maceral is known to originate from the porphyrin-enriched fraction of chlorophyll from leaves or fruits of vascular plants and from green algae. It occurs mainly as small round particles of 1 to 5 μm size (Taylor *et al.*, 1998, p. 223). Recently, Stasiuk & Sanei (2001) described larger particles (50 μm size) and matrix chlorophyllinite in Holocene sediments. Normally, especially land derived-pigments are degraded very rapidly during diagenesis in lacustrine sediments (e.g. Carpenter *et al.*, 1986). Thus, the occurrence

of chlorophyllinite reflects a high degree of chlorophyll preservation as a result of specific environmental conditions such as a very rapid sedimentation (Sanger, 1988; Leavitt *et al.*, 1989).

Points to Remember – Screening/Pyrolysis/Organic Petrology

Large fluctuations of the screening parameters characterise the studied profiles. Variations are relatively small within one lithozone but rapid and sharp transitions occur. The most striking feature is that $\delta^{13}\text{C}$ values are on average 10.6‰ heavier in lithozone 3 compared to lithozone 6. The TOC/TN ratio does not describe autochthonous *versus* allochthonous contributions due to the presence of *B. braunii* and preferential retention of nitrogen in the sediments. The parallelism of TOC and TS is the result of productivity and biomass changes in the catchment area through time. Lithozone 3 comprises OM which originates from terrigenous sources and is more oxidised compared to the other lithozones. As a result, lower HI values and higher reflecting particles were found. In contrast the algae *B. braunii* is important in the lithozones 6 and 4 leading to higher TOC and HI values as well as low-reflecting terrigenous particles. Lignin macromolecules were studied in detail by Py-GC-FID and Py-GC-MS. Pyrolysates from the lithozone 2 and 3 contain mainly hydroxyphenyl related lignin products whereas those from the lithozone 4 and 6 are dominated by lignin pyrolysis products with guaiacyl units.

5.4.5 Soluble Organic Matter

The saturated and aromatic hydrocarbon fraction from ten selected samples was analysed by GC and GC-MS. Seven samples originate from core F, while three were selected from core E. In addition, the fatty acid fraction from seven of these ten samples was examined. Compound-specific isotope analyses of individual *n*-alkanes and specific *Botryococcus* derived lipid biomarkers (botryococcenes) were determined as an additional tool for OM source identification and to interpret environmental changes. The total amount of bitumen and fraction yields are given in Tab. 5.11. Concentrations of *n*-alkanes, *n*-fatty acids and selected isoprenoids are presented in Appx. M. The total extract is dominated by the high-polarity NSO fraction (8.4 to 28.6 mg/g TOC).

E.nr.	E 47716	E 50002	E 47730	E 47736	E 50006	E 47739	E 50018	E 47744	E 48165	E 48170
Depth [cm]	750	850	2150	2750	2880	3050	3060	3550	4050	4540
Core	F	E	F	F	E	F	E	F	F	F
Lithozone	2	2 (YD)	3	3	3	4	4	5	6	6
TOC [%]	10.6	4.3	3.7	3.4	7.6	13.3	13.7	5.3	20.3	13.5
$\delta^{13}\text{C}_{\text{TOC}}$ [‰]	-19.6	-	-18.1	-19.6	-	-26.7	-	-20.6	-28.9	-31.3
HI [mg HC/g TOC]	380	175	142	134	222	392	445	243	181	426.0
Extract yield [mg/g TOC]	86.1	51.6	62.4	93.2	50.8	109.7	113.7	99.7	88.4	87.3
Fraction yields [mg/g TOC]										
acids	3.30	-	1.59	5.40	-	3.56	-	4.83	3.28	6.24
bases	4.64	-	3.31	19.57	-	4.59	-	5.38	2.01	1.73
high-polar NSO	15.08	-	8.42	21.19	-	11.06	-	28.61	17.62	24.95
medium-polar NSO	4.56	-	3.41	9.85	-	4.44	-	10.43	5.38	6.23
low-polar NSO	3.41	4.36	2.05	4.87	5.23	3.05	15.34	5.13	3.39	2.98
aromatics	0.69	0.67	0.42	0.39	0.26	2.14	4.01	0.99	0.98	0.78
saturates	1.59	1.46	0.94	2.24	1.53	5.61	8.39	2.20	2.47	3.22
Parameters/Isotopes										
CPI _{HC}	2.79	2.63	3.54	3.38	2.47	3.87	4.12	4.08	7.99	3.53
ATR _{HC}	0.05	0.10	0.13	0.13	0.11	0.02	0.06	0.19	0.02	0.02
P _{aq}	0.30	0.36	0.29	0.40	0.39	0.24	0.26	0.27	0.17	0.21
CPI _{FA}	4.91	-	6.20	6.16	-	5.95	-	5.34	13.79	11.24
ATR _{FA}	0.22	-	0.12	0.29	-	0.17	-	0.39	0.03	0.03
$\delta^{13}\text{C}$ (n-C ₂₉)	-29.3	-28.1	-	-	-27.2	-	-	-28.5	-32.8	-
$\delta^{13}\text{C}$ (n-C ₃₁)	-27.0	-26.4	-	-	-26.4	-	-	-28.4	-32.9	-
$\bar{\delta}^{13}\text{C}$ (<i>n</i> -alkanes)	-27.2	-26.4	-	-	-25.8	-	-	-27.8	-32.3	-
$\bar{\delta}^{13}\text{C}$ (botryococcenes)	-14.6	-10.8	-	-	-6.2	-	-31.7	-19.4	-25.6	-

Tab. 5.11. Bulk geochemical parameters, fraction yields, biomarker parameters and compound specific carbon isotopic compositions for sediment samples from HM analysed for lipid distributions; - not analysed. For definition of biomarker parameters see Appx. D. YD, Younger Dryas.

5.4.5.1 Saturated Hydrocarbons

Relatively low concentrations of saturated hydrocarbons between 0.9 and 8.4 mg/g TOC were determined. A homologous series of *n*-alkanes was detected with carbon numbers ranging from C₁₅ to C₃₅, sometimes to C₃₇. The distribution and abundance of the analysed samples is illustrated in Fig. 5.31. They display a strong odd-over-even predominance. The CPI_{HC} in the C₂₄ to C₃₂ range varies between 2.47 in lithozone 3 and 7.99 in lithozone 6 (Tab. 5.11). For definition of biomarker parameters see Appx. D. Recent and ancient lake sediments have CPI values commonly >4 (Cranwell, 1982; Otto *et al.*, 1994) while, vascular plants typically exhibit CPI values between 2.1 and 40.3 (Collister *et al.*, 1994; Lockheart *et al.*, 2000). The long-chain *n*-alkanes maximise at *n*-C₂₉ or *n*-C₃₁ and are characteristic for epicuticular waxes derived from higher plants. However, long-chain *n*-alkanes were also reported from *Botryococcus* rich sediments where they result from the diagenetic reduction of alkadienes (Lichtfouse *et al.*, 1994). Short-chain *n*-alkanes were previously observed in many algae and bacteria. The lowest aquatic/terrestrial ratios for hydrocarbons (ATR_{HC}), adopted from Wilkes *et al.* (1999), were determined within lithozone 6. The highest ratio was observed for lithozone 5 (Tab. 5.11). The *n*-alkanes from lithozone 3 and 5 show a bimodal distribution with additional maxima in the medium-chain length range at *n*-C₂₁ or *n*-C₂₃, respectively. The P_{aq} ratio was introduced by Ficken *et al.* (2000) and expresses the relative proportion of mid-chain length (*n*-C₂₃, *n*-C₂₅) to long-chain length homologues (*n*-C₂₉, *n*-C₃₁). According to their interpretation, a high ratio between 0.4 and 1.0 is indicative for a high contribution of submersed or floating aquatic macrophytes, while a ratio between 0.1 and 0.4 corresponds to emergent macrophytes. A very low ratio <0.1 reflects terrestrial plant input. The P_{aq} ratios in the present study range between 0.17 and 0.40 with highest values in the lower lithozone 3 (Tab. 5.11).

In addition to the *n*-alkanes, triterpenoid hydrocarbons of hopanoid origin were detected. Characteristic compounds present in all studied extracts are 22*R*-17β(H),21β(H)-homo-hopane and hop-17(21)-ene which are diagenetic products of bacterial lipids (e.g. Farrimond *et al.*, 2000). The tetracyclic triterpenoid hydrocarbon de-(A)-lupane, eluting between *n*-C₂₄ and *n*-C₂₅, is another characteristic compound in the saturated hydrocarbon fraction. It is typical for sediments from a tropical climate and results from a photochemical or photo-mimetic degradation of triterpenoids (Corbet *et al.*, 1980; Schmitter *et al.*, 1981).

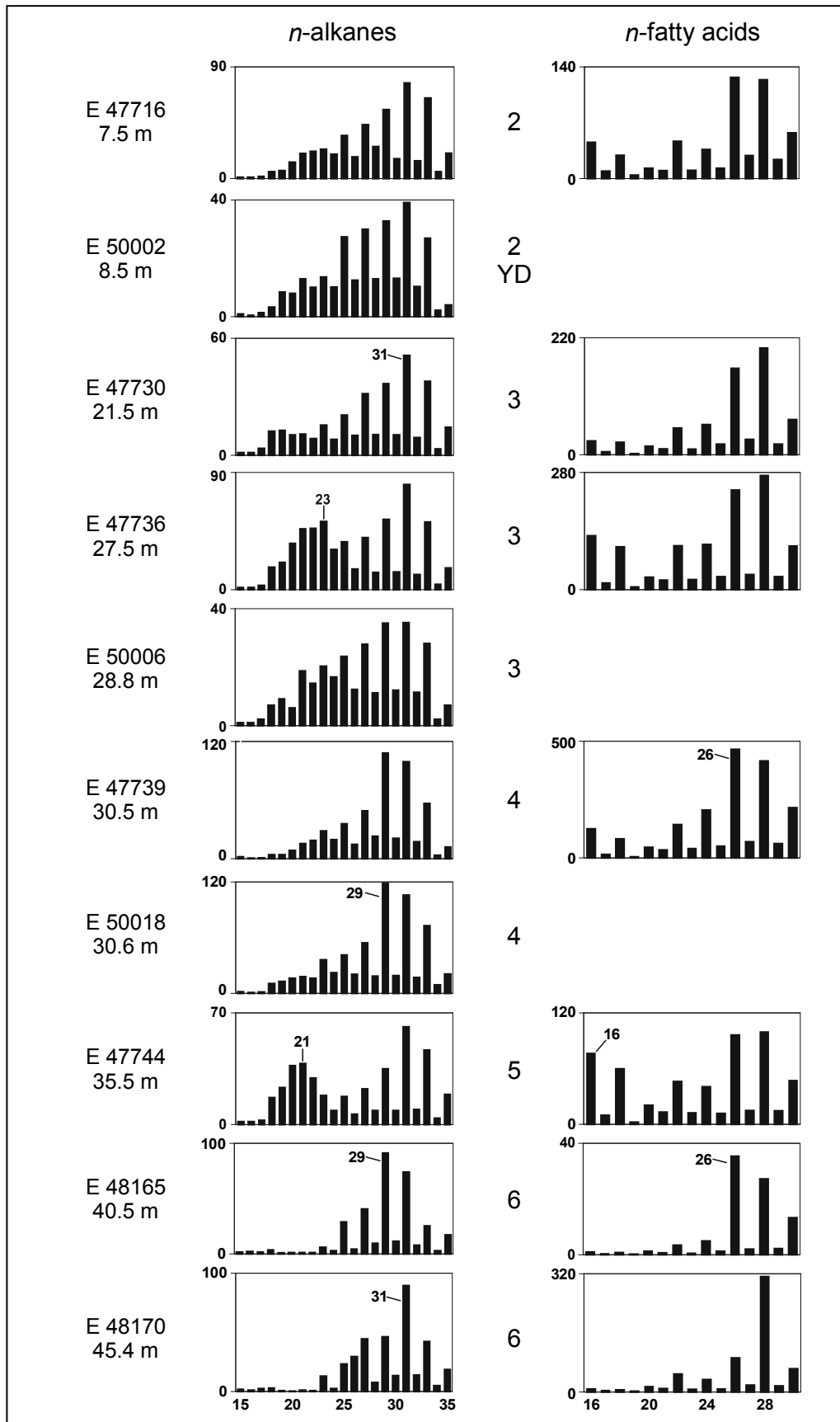


Fig. 5.31. Distributions and concentrations ($\mu\text{g/g TOC}$) of *n*-alkanes and *n*-fatty acids in the analysed samples from HM. Numbers in between the bar charts indicate the different lithozones. Peak numbers refer to chain length. YD, Younger Dryas.

5.4.5.2 Botryococenes

The aliphatic and aromatic fraction contains a series of compounds which were previously isolated from cultures of the microalgae *B. braunii* (e.g. Metzger *et al.*, 1988). More than 25 different botryococenes were detected in the sediment extracts of HM. Six significant and characteristic compounds were chosen to show stratigraphic variations in their distributions and concentrations. Several of these straight- or branched chain hydrocarbons and monocyclic derivatives were previously identified, all with the generic molecular formula C_nH_{2n-10} where n equals 30-37 (e.g. Metzger *et al.*, 1985; David *et al.*, 1988). Because *B. braunii* is widespread in the lacustrine environment, botryococenes were detected in several organic poor and organic-rich lake deposits such as the Dead Sea (Grice *et al.*, 1998), Sacred Lake, Kenya (Huang *et al.*, 1995; Huang *et al.*, 1996) and Lake Cadagno, Switzerland (Behrens *et al.*, 2000). Based on stable carbon isotopic measurements it was recently speculated that other micro-organisms such as green sulphur bacteria might be the biological precursors of cyclic polyunsaturated botryococenes (Behrens *et al.*, 2000). Nevertheless, the close association of these compounds and the alga *B. braunii* is widely accepted.

The botryococene structures (Appx. C, XX to XXIII) were assigned by interpretation of their mass spectra and subsequent comparison with literature data. Compound **1** was identified as a C_{34} botryococene (Appx. C, XX) with a structure similar to those reported by Cox *et al.* (1973) and Huang *et al.* (1999). Structures of compounds **2** to **4** have been proposed previously (Wake & Hillen, 1981; Huang & Murray, 1995; Huang *et al.*, 1999). They were identified as 1,6,17,21-octahydrobotryococene **2** (Appx. C, XXI), isobotryococene **3** (Appx. C, XXII) and a cyclic botryococene **4** (Appx. C, XXIII). Two novel botryococenes **5** and **6** were found with a characteristic molecular ion at m/z 470 and the m/z 177 (Appx. C, XXIV & XXV) which suggests the presence of a monocyclic $C_{34}H_{62}$ hydrocarbon with four degrees of unsaturation. This fragmentation is thought to derive from the short-chain side of a quaternary carbon centre in a methylene cyclohexyl ring (Huang *et al.*, 1996).

The concentrations of the compounds **1-6** and available specific carbon isotopes are presented in Tab. 5.12. Interestingly, significant changes occur between the different lithozones. Monocyclic and acyclic botryococenes are present in lithozone 2. For instance, the compounds **1**, **2** and **5** are relatively abundant in the extract of sample E 47716. In contrast, predominantly acyclic botryococenes are present in lithozone 3 (E 50006). Finally, the saturated and aromatic hydrocarbon fraction of sample E 50018 (lithozone 4) is clearly

dominated by the cyclic compounds **5** and **6**, whereas both structure types are present in the lithozones 5 and 6. A significant change from straight-chain compounds during the LGM to structures containing a cyclohexyl ring was previously reported by Huang *et al.* (1995) and Huang *et al.* (1999).

E.nr.	47716	50002	47730	47736	50006	47739	50018	47744	48165	48170						
Depth [cm]	750	850	2150	2750	2880	3050	3060	3550	4050	4540						
Lithozone	2	2 (YD)	3	3	3	4	4	5	6	6						
Concentrations in µg/g TOC and carbon isotopic ratios of botryococenes																
1 (acyclic)	55.08	-10.5	16.78	-13.7	2.65	0.00	23.65	-6.2	26.07	22.21	-	6.80	-	1.71	-	0.00
2 (acyclic)	87.41	-15.3	0.65	-20.0	1.47	0.96	0.92	-	45.06	0.75	-	32.18	-21.2	3.68	-	6.93
3 (acyclic)	4.70	-	1.64	-	0.29	0.00	0.00	-	0.00	0.00	-	1.19	-	0.00	-	0.00
4 (cyclic)	16.38	-	4.27	-	0.58	0.00	0.00	-	4.63	40.32	-	1.36	-	0.34	-	0.00
5 (cyclic)	90.10	-20.6	19.83	-	1.00	0.99	10.74	-	1533.59	4697.92	-34.6	16.35	-	4.96	-	1.64
6 (cyclic)	10.91	-	3.27	-	0.79	0.67	0.00	-	860.45	5957.07	-35.4	14.66	-22.3	10.70	-25.6	6.04
Sum	264.58		46.44		6.79	2.62	35.31		2469.80	10718.26		72.54		21.39		14.61

Tab. 5.12. Concentrations (in µg/g TOC) and carbon isotopic values of individual botryococenes from HM. Bold numbers (1-6) refer to the compound structures in Appx. C. Acyclic and cyclic compounds are indicated. YD, Younger Dryas; - denotes no data due to the absence or low concentration of a specific compound.

5.4.5.3 Fatty Acids

The fatty acid distributions and concentrations of selected samples for the individual lithozones are illustrated in Fig. 5.31. The fatty acid yields vary between 1.6 and 6.2 mg/g TOC corresponding to 2.5 to 4.8 wt.-% of the total extract. The distributions are characterised by a predominance of long-chain *n*-fatty acids with a strong even-over-odd predominance and a maximum at *n*-C_{26:0} or *n*-C_{28:0}. A second maximum at *n*-C_{16:0} was observed in lithozone 5. The CPI_{FA} in the C₂₂ to C₂₈ range varies between 4.91 (lithozone 2) and 13.79 (lithozone 3). The aquatic/terrestrial ratio for fatty acids (ATR_{FA}) proposed by Wilkes *et al.* (1999) can be used as a relative measure of the autochthonous *versus* allochthonous input. This parameter ranges between 0.03 and 0.39 with the highest ratio observed for lithozone 5 (Tab. 5.11). While long-chain fatty acids are important as cuticular wax constituents (Kolattukudy, 1980), short-chain compounds were previously identified in many algae and bacteria (e.g. Merritt *et al.*, 1991). The hopanecarboxylic acids are present in relatively high concentrations and are dominated by the 22*R*-17β(H), 21β(H)-dihomohopanecarboxylic acid.

5.4.5.4 Compound Specific Isotope Analysis

The carbon isotopic composition of individual *n*-alkanes (*n*-C₂₀ to *n*-C₃₃) ranges between –34.3 and –24.3‰. All *n*-alkane $\delta^{13}\text{C}$ values are given in Appx. M. The terrigenous

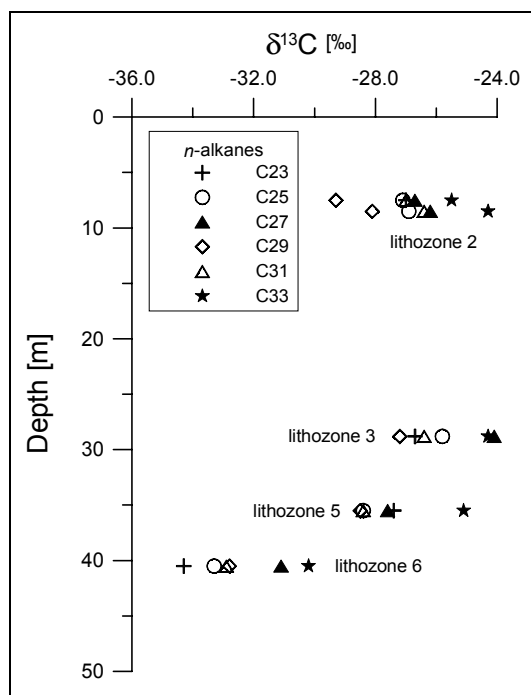


Fig. 5.32. $\delta^{13}\text{C}$ ratios of individual *n*-alkanes in HM sediment samples. Lithozones are indicated.

dominated sample E 48165 from lithozone 6 shows the most depleted on average $\delta^{13}\text{C}$ ratio with –32.3‰ while the heaviest on average $\delta^{13}\text{C}$ ratio was determined for the *n*-alkanes in sample E 50006 with –25.8‰ (lithozone 3). Several of the more positive values occur in the long-chain range at C₃₃. Generally, the isotopic differences between the individual *n*-alkanes are relatively large (Fig. 5.32). The $\delta^{13}\text{C}$ value for the *n*-C₂₉ and *n*-C₃₁ alkane shows a variation of 5.6 and 6.5‰, respectively throughout the cores (Fig. 5.32 and Tab. 5.11). The value is relatively light in lithozone 2 and increase towards the Younger Dryas (E 50002). Enriched values were determined for lithozone 3 while they decrease towards lithozone 4. The most depleted values were observed in lithozone 6 for the *n*-C₂₉ as well

as for the *n*-C₃₁ alkane which are characteristic for plant wax derived *n*-alkanes of C₃ plants (cf. Collister *et al.*, 1994). The isotopic values of the other *n*-alkanes essentially parallel this trend.

Larger shifts of the $\delta^{13}\text{C}$ values were observed for the studied **botryococcenes** than for the *n*-alkanes. The *botryococcene* peak assignment and stable carbon isotope values of three selected samples (lithozones 2, 3 and 4) are presented in Fig. 5.33. The $\delta^{13}\text{C}$ ratios of the botryococcenes vary between –6.2 and –35.4‰. Large variations of the $\delta^{13}\text{C}$ values were also determined for the different lithozones (Tab. 5.11). Isotopic ratios of all measured botryococcenes are on average –14.6‰ in lithozone 2 at 750 cm depth and become significantly heavier in the Younger Dryas period (–10.8‰ on average). The isotopic composition of the C₃₄ botryococcene 1 shows the maximum value of –6.2‰ in lithozone 3 (E 50006). Notably, this component is 19.6‰ more enriched in ¹³C than the corresponding *n*-alkanes from the same lithozone 3. The overall most depleted values were observed in lithozone 4 with a mean value of –31.7‰. The minimum value with –35.4‰ (compound 6) occurs in

30.6 m depth (E 50018). Only very low amounts of this compound were detected in the lithozones 5 and 6. Although only a few values are available from the units below, they indicate a return to heavier values (-19.4‰ on average) in lithozone 5, whereas they become again more depleted in lithozone 6. Interestingly, the cyclic compounds are very often more depleted in ^{13}C than the acyclic.

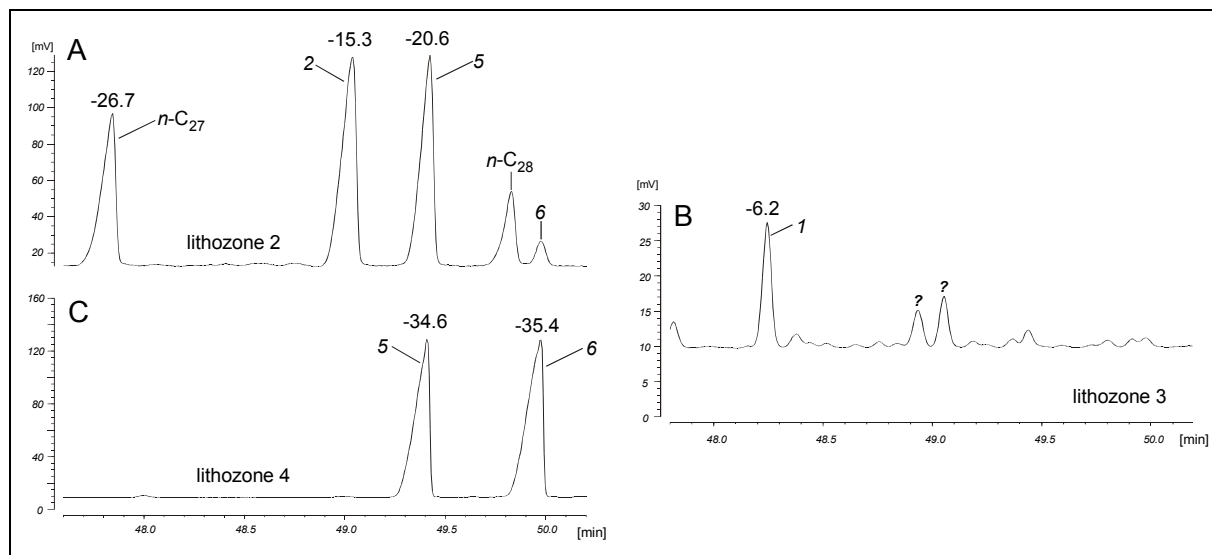


Fig. 5.33. Distributions and stable carbon isotope values ($\delta^{13}\text{C}$) of botryococenes extracted from HM sediments deposited during (A) lithozone 2 (E 47716, aliphatic fraction), (B) lithozone 3 (E 50006, aromatic fraction) and (C) lithozone 4 (E 50018, aliphatic fraction). *Italic numbers refer to the compound structures in Appx. C. Numbers on the peak top indicate the $\delta^{13}\text{C}$ value.*

Points to Remember – Soluble Organic Matter

Saturated hydrocarbons and fatty acids display a predominance of long-chain compounds indicative for OM originating from terrigenous sources. Relatively high contributions of macrophyte derived mid-chain *n*-alkanes were detected in the lower lithozone 3. Here, the heaviest *n*-alkane carbon isotopic compositions were determined whereas they are much more depleted in lithozone 6. A series of botryococenes was identified in the sediment extracts with monocyclic and acyclic structures. They exhibit varying distribution and $\delta^{13}\text{C}$ values within the different lithozones.

5.4.6 Paleoenvironment of Deposition

Organic Matter Sources

Lignin macromolecules, which occur exclusively in cell walls of higher plants, exhibit a high stability upon diagenesis. Thus, their typical pyrolysis products can be considered as specific biomarkers for terrestrial plant input (Saiz-Jimenez & de Leeuw, 1986). The proportion of the three precursor alcohols differ between vascular plant species (e.g. Kirk & Farrell, 1987; van Smeerdijk & Boon, 1987). **Gymnosperm lignin** consists of *trans*-coniferyl alcohol units, **angiosperm lignin** is made up by *trans*-coniferyl and *trans*-sinapyl alcohol units. **Grass and moss lignin** contains all three alcohols as building blocks but it was found that significant amounts of elements that contain *p*-hydroxyphenyl units are always present (Fig. 5.27). High contributions of *p*-vinylphenol were reported to result from the decarboxylation of *p*-coumaric acid (Boon *et al.*, 1987), and previously detected in pyrolysates of grass lignin (Saiz-Jimenez & de Leeuw, 1986; Morrison & Mulder, 1994). In contrast, pyrolytic degradation of angiosperm wood yields products such as 2,6-dimethoxyphenol (syringol) and 2-methoxyphenol (guaiacol), whereas gymnosperm lignin yields for example 2-methoxy-4-methylphenol (4-methylguaiacol). Fig. 5.28 indicates that the pyrolysates in lithozone 2 and 3 contain high proportions of grass related lignin derived pyrolysis products, whereas 4-methylguaiacol and a few syringyl moieties suggest that the terrigenous OM in the lithozones 4 and 6 is derived from angiosperms.

The bulk $\delta^{13}\text{C}_{\text{TOC}}$ values show changes of many permil between the different stratigraphic intervals (Fig. 5.22). Such large fluctuations are difficult to explain in terms of diagenesis. A diagenetic influence was reported for carbon isotope values (e.g. Spiker & Hatcher, 1984; Spiker & Hatcher, 1987), although this effect is minor and accounts for only less than 2% of changes in the isotope values (Dean *et al.*, 1986). Thus, the studied record represents the primary isotopic signature of the OM at the time of deposition and reflects paleoenvironmental changes in the lake and its watershed. A varying input of C_3 and C_4 plants and/or a higher contribution of carbon from aquatic sources can modify the carbon isotope value. Microscopy and pyrolysis revealed that the kerogen sample E 48165 from lithozone 6 contains abundant terrigenous OM (Figs. 5.26 B and 5.31) and yields a $\delta^{13}\text{C}_{\text{TOC}}$ of -28.9‰ , typical for OM produced from land plants using the C_3 pathway. In contrast, carbon isotope values of samples from lithozone 3 are on average 10.6‰ heavier. Although other relatively small effects such as a lowered atmospheric $p\text{CO}_2$ during glacial times, the growth temperature and decreased water availability were probably responsible for a small positive increase

(1.5 to 4‰) of the $\delta^{13}\text{C}_{\text{TOC}}$ values of C_3 plants (O'Leary, 1988; Farquhar *et al.*, 1989; Leavitt & Danzer, 1992), this does not explain this large shift. Thus, a contribution of C_4 plants to lithozone 3 must be considered which exhibit typical carbon isotopic values between -9 and -16 ‰ and -13 ‰ on average (Deines, 1980). It was demonstrated previously that some aquatic C_3 plants provide a further possible source of isotopically heavy OM. Palynological analyses revealed that the submerged aquatic macrophyte *Myriophyllum* is more abundant in lithozone 3 (Mingram *et al.*, 2000). Relatively enriched $\delta^{13}\text{C}_{\text{TOC}}$ values up to -20 ‰ were reported for some submerged macrophytes using the C_3 pathway (Fry & Sherr, 1984; Ficken *et al.*, 2000) but especially heavy values up to -17 ‰ are possible for *Myriophyllum* (A. Lücke, pers. comm.). However, the relative contribution of macrophytes to the total pollen assemblage is low. Thus, it can be assumed that they have only little influence on the $\delta^{13}\text{C}_{\text{TOC}}$ values in lithozone 3.

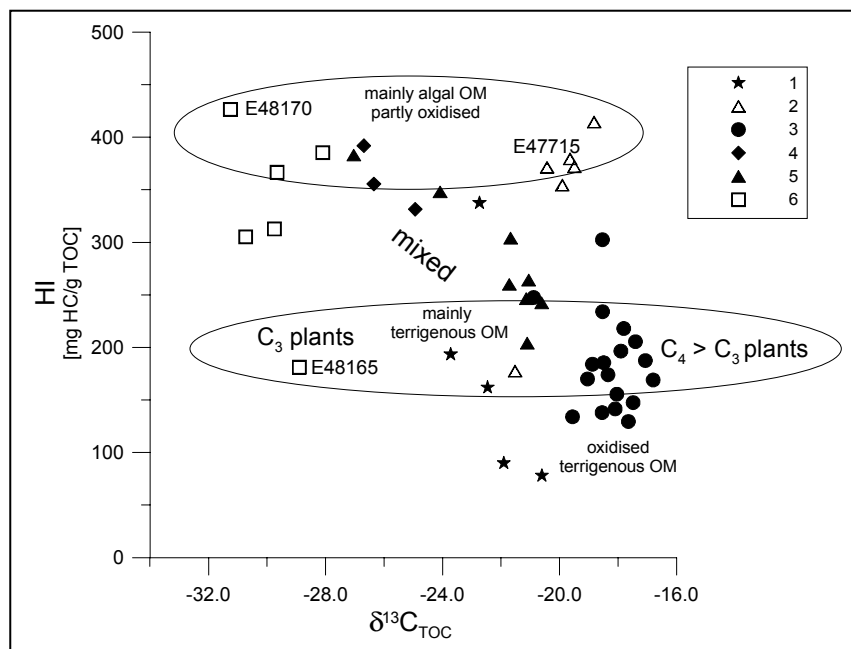


Fig. 5.34. HI and carbon isotopic compositions of sedimentary OM from HM.

Lacustrine phytoplankton normally exhibits carbon isotopic compositions between -30 and -20 ‰. C_3 algae commonly produce OM that has $\delta^{13}\text{C}$ values of -29 to -27 ‰. A bulk $\delta^{13}\text{C}_{\text{TOC}}$ value of -16 ‰ was previously determined for an algal culture of the B race of *B. braunii* which was only slightly heavier compared to the compound-specific isotope values of the *botryococcene* hydrocarbons synthesised by the same alga (Huang *et al.*, 1995). The amount of these lipids can account for up to 75% of the total dry weight of *Botryococcus* (Maxwell *et al.*, 1968; Brown & Knights, 1969). Thus, the varying compound specific $\delta^{13}\text{C}$ values of the *botryococcene* biomarkers suggest varying carbon isotopic compositions of the entire algal biomass. This is substantiated by a HI *versus* $\delta^{13}\text{C}_{\text{TOC}}$ plot in Fig. 5.34, which illustrates that high HI values, typical for relatively more algal derived hydrogen-rich OM are

associated with varying carbon isotopic compositions. Thus, the bulk $\delta^{13}\text{C}_{\text{TOC}}$ in the HM sediments reflect temporal variations of environmental conditions affecting the primary producers in the lake and vegetation changes in the lake watershed.

Biomarker constituents of the epicuticular plant waxes are predominant in the sediments, whereas the contribution of lipids characteristic of algal OM is relatively low. Long-chain *n*-alkanes ($\text{C}_{27}\text{--}\text{C}_{33}$) as well as *n*-fatty acids ($\text{C}_{26:0}, \text{C}_{28:0}$) dominate the aliphatic and fatty acid fraction, respectively (Fig. 5.31). This signals that a significant proportion of the lipids is of allochthonous origin and related to the surrounding vegetation. However, it could also in part reflect the lower degree of terrestrial over aquatic OM degradation in the lacustrine environment (Meyers & Ishiwatari, 1993). For example, diagenesis can selectively alter the *n*-fatty acid distribution by the preferential removal of short-chain compounds (Matsuda & Koyama, 1977; Haddad *et al.*, 1992; Canuel & Martens, 1996). Such a diagenetic influence can lead to an overestimation of the terrigenous input as observed for Lake Ontario by Bourbonniere & Meyers (1996). Although the presence of long-chain *n*-alkanes from *Botryococcus* cannot be fully excluded, their contribution is unlikely because no C_{23} to C_{31} alkadienes or alkatrienes were detected (cf. Lichtfouse *et al.*, 1994). The fatty acid distribution of eutrophic and mesotrophic lakes is commonly dominated by shorter-chain compounds due to the important contribution of planktonic short chain lipids (Robinson *et al.*, 1984; Cranwell *et al.*, 1987). Only in lithozone 5 a higher ATR_{FA} (Tab. 5.11) was observed which could be indicative for a higher primary productivity. Mid-chain *n*-alkanes are thought to mirror inputs from submerged or floating aquatic plants (Ficken *et al.*, 1998; Ficken *et al.*, 2000). Thus, the higher P_{aq} ratio in the lower lithozone 3 reflects a higher contribution of OM derived from aquatic macrophytes as corroborated by pollen analysis (cf. Mingram *et al.*, 2000).

The isotopic compositions of the long-chain *n*-alkanes specifically reflect the CO_2 fixation mechanism employed by the contributing plants. The isotopic compositions of individual *n*-alkanes from C_4 plant species are generally in the range between -18.5 and -26‰ (on average -23‰) whereas values between -28.0 and -43.0‰ (on average -34‰) for C_3 plants were reported in the literature (Deines, 1980; Collister *et al.*, 1994; Freeman & Colarusso, 2001). One should keep in mind that *n*-alkanes extracted from modern plants are always depleted in ^{13}C compared to the bulk TOC (Rieley *et al.*, 1991; Lockheart *et al.*, 1997). Only the average isotopic composition of the *n*-alkanes in lithozone 6 (-32.3‰) falls in the typical range for C_3 plants. While no data are available for lithozone 4 the relatively positive $\delta^{13}\text{C}$ values from the other lithozones suggest a C_3/C_4 mixed origin. In particular, the

$\delta^{13}\text{C}$ value of the C_{29} *n*-alkane is consistent with a C_3 source, whereas heavier ratios were determined for most of the other *n*-alkanes (e.g. *n*- C_{33} in Fig. 5.32).

The varying carbon isotopic compositions of the higher plant and *Botryococcus* derived lipid biomarkers indicate that: (1) isotopic variations of the *n*-alkanes in the different lithozones are related to a varying C_3/C_4 plant input, and (2) that *Botryococcus* changed its carbon isotope discrimination in response to specific paleoenvironmental and paleoclimatic variations. These variations were probably induced by a major change of the carbon source, the atmospheric $p\text{CO}_2$ concentration or changes in the dissolved CO_2 concentration and lake primary productivity. These influences are specified in more detail below.

Terrigenous OM as a Paleoclimatic Indicator

Organic-geochemical results from the present study and pollen data (cf. Mingram *et al.*, 2000) show that the local vegetation experienced three major changes during the last 68,000 years BP. The first of these changes occurred at the transition from lithozone 6 to 5 around 60,000 years BP. The $\delta^{13}\text{C}_{\text{TOC}}$ ratios as well as the compound specific carbon isotopes of the long-chain *n*-alkanes exhibit a typical C_3 higher plant leaf wax fingerprint suggesting a dominant C_3 biomass input during lithozone 6. The ratio B (Fig. 5.35) is proposed as a parameter to estimate the relative contribution of higher plant lignin *versus* grass lignin. This ratio is high in lithozone 6 implying a dominant angiosperm and/or gymnosperm source. Arboreal pollen (AP; trees and shrubs) clearly predominate over non-arboreal pollen (NAP; grasses and herbs) with many elements (e.g. *Altingia*) typical of a warm and humid tropical climate (Fig. 5.35). No indications for such a tropical event were given in other studies. Plant-wax *n*-alkanes as well as bulk isotopic compositions are more enriched in ^{13}C in lithozone 5 suggesting a higher contribution of C_4 plant derived OM. The lignin and pollen analysis suggest that grasses were far more important in the vegetation compared to lithozone 6 and that tropical pollen vanished. This points to a significantly drier and cooler climate than during deposition of lithozone 6. Palynological data from a maar lake in the southern part of the Leizhou Peninsula revealed a cooling for the same time period (Zheng & Lei, 1999).

A high angiosperm derived lignin content from tropical plants such as *Elaeocarpus* and the reduction of grasses is typical for lithozone 4. The $\delta^{13}\text{C}_{\text{TOC}}$ ratios show that mainly organic remains of C_3 plants reached the lake bottom. Results of $\delta^{18}\text{O}$ based temperature reconstructions of an ice-core from Tibet (Guliya ice core) suggest that the temperature during this stage was approx. 4°C higher than today (Shi *et al.*, 2001). A relatively warm

period in the same time interval (50,000 to 41,000 yrs BP) was inferred based on lake sediment studies from south-west China (Hodell *et al.*, 1999). An extremely high tropical precipitation and productivity event was recorded between approx. 43,000 and 37,000 yrs BP in oxygen and carbon isotopic curves from the South China Sea (Pelejero *et al.*, 1999). In addition, the authors detected higher concentrations of the terrigenous biomarkers *n*-nanocosane and *n*-hexacosan-1-ol in the marine sediments which were interpreted as a consequence of surface runoff during wetter conditions caused by an enhanced summer monsoon activity.

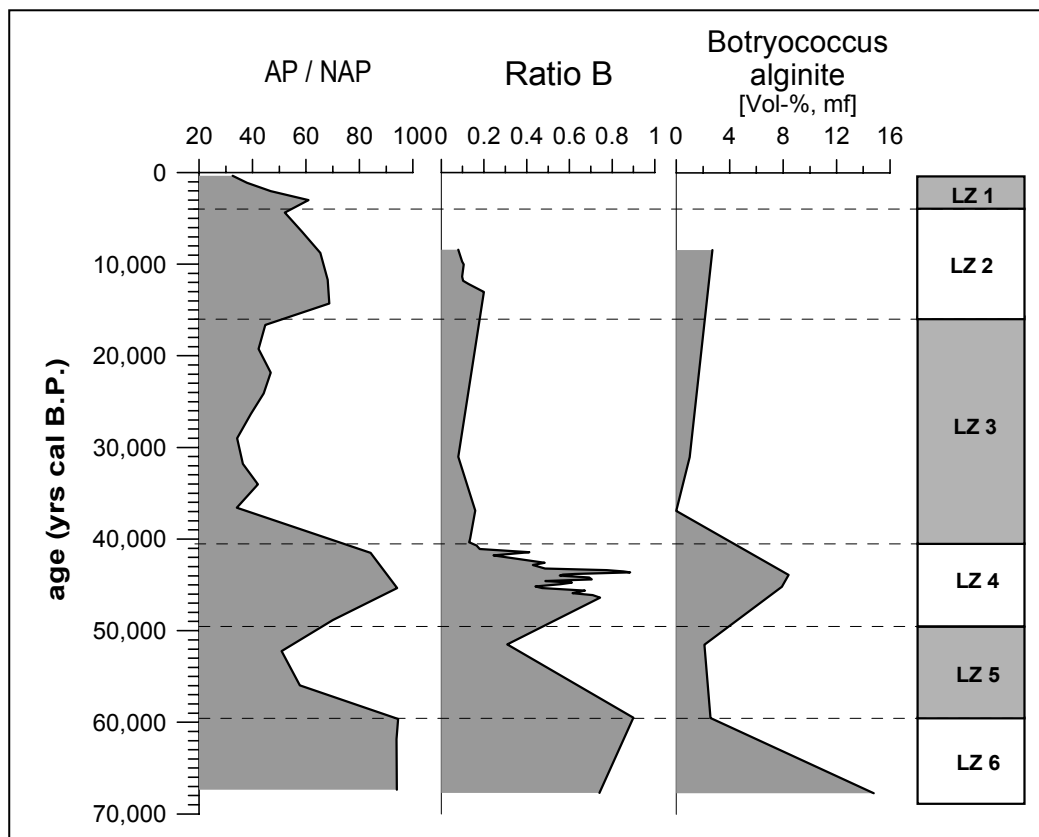


Fig. 5.35. Lake Huguang Maar. Comparison between pollen data (Mingram *et al.*, 2000), pyrolysis and organic petrological results. AP, arboreal pollen (trees and shrubs); NAP, non-arboreal pollen (herbs and grasses); Ratio B, 4-methylguaiaicol/(4-methylguaiaicol+p-vinylphenol). The column on the right displays the studied lithozones.

The second fundamental change took place around 40,000 yrs BP (lithozone 4/3). A remarkably increase of the NAP, together with a decrease of the Ratio A (Fig. 5.35) reflects a higher grass derived contribution during the deposition of lithozone 3 which is associated with a characteristic isotopic enrichment ($\delta^{13}\text{C}_{\text{TOC}}$) from lithozone 4 to 3 (Fig. 5.22 A). This trend is exactly that what was observed for the $\delta^{13}\text{C}$ values of the *n*-alkanes. On average values of -25.8‰ imply a higher contribution of C_4 plants to lithozone 3. These observations are in good agreement with previous results indicating that the regional

climate was cooler and drier during this time and a grassland and savannah vegetation developed (Winkler & Wang, 1993; Huang *et al.*, 1997; Zheng & Lei, 1999). It was suggested that these extremely dry conditions were caused by an increased continentality due to a significant drop of the south China Sea of about 120 m and lowering of the sea-surface temperature in the last glacial period (Wang *et al.*, 1995; Shyu *et al.*, 2001). A cooling of around 5°C was estimated from oxygen isotope studies on foraminifers. These variations were attributed to a weakening of the wet summer monsoon and strongly intensified dry winter monsoon activity, leading to an increased aridity as a consequence of the reduced summer precipitation (Wang *et al.*, 1999; Jian *et al.*, 2001). Palynological and organic petrological data from the Huguang area confirm this aridity. Firstly, increased amounts of *Artemisia*, characteristic for enhanced dryness, were determined in lithozone 3. Secondly, the relatively low TOC and HI values compared to lithozone 4 reflect a high minerogenic contribution and input of terrigenous OM as well as OM oxidation. Thirdly, the oxidised nature of the terrigenous biogenic particles in lithozone 3 compared to lithozone 6 (Fig. 5.30) points to a large fraction of wind transported, primary oxidised and recycled compounds from dust-source areas. They are probably a result of extended savannah fires, high wind intensities and greater erosion rates supported by the enhanced aridity during glacial time (cf. Pokras & Mix, 1985).

Such dry conditions generally favour the evolution of C₄ grasses in the tropics (Street-Perrott *et al.*, 1997). It is also very likely that the reduced atmospheric pCO₂ to about 190-200 µatm during the last glacial period (Barnola *et al.*, 1987), changed the balance between C₃ and C₄ plants. The C₄ plants possess a carbon concentration mechanism and are thus insensitive to a changing CO₂ partial pressure and more efficient at low CO₂/O₂ (Ehleringer *et al.*, 1997). Thus, C₄ plants have a selective advantage over C₃ plants at dry and low pCO₂ conditions and dominated the local vegetation during the deposition of lithozone 3. Samples from the lower lithozone 2 show no major differences in the lignin type. Grass lignin derived phenols are still predominant. Plant-wax *n*-alkanes from the Younger Dryas and lithozone 2 are isotopically only slightly lighter than those from the lithozone 3, indicating a mixture of C₄ and C₃ biomass reaching the lake. A higher C₃ contribution at the top of lithozone 2 is inferred from more negative δ¹³C_{TOC} ratios and much lower HI values. Finally, it was reported that an open grassland is typical for lithozone 1 which indicates the beginning of the human influence (Mingram *et al.*, 2000).

Climatic Controlled Changes in the Lake Ecosystem

The microscopic examination of the sediments and kerogens revealed that a substantial amount of algal OM was deposited. The presence of abundant *n*-alkane/*n*-alk-1-ene doublets in the pyrolysates and *botryococcenes* in the SOM point to a major contribution of the B race of this algal species. Samples with the highest HI values are those with a dominant *B. braunii* input. Especially in the lithozones 6 and 4 abundant fossil remains of the algae were quantified (Fig. 5.35). They correlate with a high Ratio B pointing to a high release of nutrients to the lake by surface runoff and an enhanced algal growth in a favourable tropical climate.

Dissolved molecular CO₂ and dissolved inorganic carbon, such as bicarbonate are possible carbon sources for aquatic organisms to carry out photosynthesis. Dissolved CO₂ is the common substrate for floating planktonic algae such as *Botryococcus*. If an unlimited supply is available due to equilibration with the atmosphere, a shift of about -20.0‰ between the source and the algal photosynthetic fixed carbon occurs, with resulting δ¹³C values of around -28.0‰. Therefore, we would expect no significant isotopic differences between the carbon fixed by the algae and the carbon fixed by terrestrial C₃ plants because of the negligible fractionation between the atmospheric and the dissolved CO₂ (Mook *et al.*, 1974). Consequently the most depleted δ¹³C values of the algal lipid biomarkers, i.e. in lithozone 4 (-31.7‰ on average) reflect the photosynthetic uptake of unlimited dissolved CO₂ in equilibrium with the atmosphere and is thus isotopically indistinguishable from C₃ derived plant-wax lipids. Typical values for C₃ plant derived *n*-alkanes in lithozone 6 are exactly in the same range (-32.3‰).

An exceptional heavy C₃₄ *botryococcene* was detected in lithozone 3 (-6.2‰) with a δ¹³C value that is even less negative than the ambient CO₂ of -7.0‰ during glacial times (Marino *et al.*, 1992). The large shift of the algal δ¹³C biomarker composition between lithozone 4 and lithozone 3 of about -30‰ is difficult to explain with environmental changes such as temperature, salinity or productivity differences which either cause only small shifts or shifts in the wrong direction (Farquhar *et al.*, 1989). Boreham *et al.* (1994) suggested that the thick outer cell walls of *Botryococcus* retards the CO₂ diffusion rate which would lead to a lower isotopic fractionation. However, this does not explain the large isotopic variations in the present study. Highly enriched botryococcene derived biomarkers (-10 to -13‰) were also identified in extracts from hypersaline sediments from the Dead Sea (Grice *et al.*, 1998). The authors favoured different bloom conditions to explain differences in the δ¹³C values of the

L and B race, probably associated with varying water salinities. However, there are no indications of salinity differences within the Huguang maar lake through time. Thus, it is very likely that the $\delta^{13}\text{C}$ variations of the *botryococenes* record differences in the carbon source uptake. The concentration of dissolved CO_2 depends strongly on the atmospheric $p\text{CO}_2$. Thus, a lowered $p\text{CO}_2$ during the last glacial of about 30% compared to present times significantly reduces the CO_2 concentrations in lake waters. To fulfil its demand at low dissolved CO_2 concentrations, phytoplankton starts to incorporate actively bicarbonate (Burns & Beardell, 1987). Bicarbonate is enriched by up to 12‰ with respect to the related CO_2 (Mook *et al.*, 1974) and this in turn decreases the carbon isotope fractionation. In many alkaline lakes it is an additional resource of inorganic carbon available for photosynthesis (e.g. McKenzie, 1985). The ability of *Botryococcus* to use bicarbonate was proposed to lead to isotopically highly enriched botryococenes up to -5.1‰ in Sacred Lake, Kenya (Huang *et al.*, 1999). An alternative explanation for the very heavy lipids within lithozone 3 is that a genetically different strain of *Botryococcus* replaced the previous one, due to the lower atmospheric $p\text{CO}_2$, drier conditions and the ability to use bicarbonate as the dominant carbon source. This may also explain the relative sudden change from monocyclic to acyclic botryococcene structures. The occurrence of both structure types and the intermediate $\delta^{13}\text{C}$ values of the botryococenes in lithozone 2 suggest either the continuous demand of bicarbonate ions by one strain due to an enhanced primary productivity in the lake (McKenzie, 1985; Krishnamurthy *et al.*, 1999), or the presence of both strains.

At the begin of lithozone 2 the TOC and HI values increase which implies a higher primary productivity. This occurs synchronously with abundant fluvial input to the South China Sea which was interpreted to result from a sudden increase in summer monsoon rains (Wang *et al.*, 1999). A similar early Holocene monsoon maximum was reported from countries bordering the Arabian Sea (Sirocko *et al.*, 1993).

6 Summary and Conclusions

The present investigation on lacustrine sediments provides important insights in the paleoenvironmental evolution of lakes from different climatic settings. The paleodepositional history of the Eocene Es4 member in the Liaohe Basin was reconstructed using an approach based on organic and inorganic sediment data. Three major depositional environments were distinguished, each characterised by certain litho- and organofacies successions as well as hydrocarbon generation characteristics.

The **playa and shallow lake facies** is the preferred setting for the formation of an organic-rich facies in the GS sub-unit as well as in the DJT sub-unit of the Lei area. Algal- and fluoramorphinite-rich laminated shales of this facies type (type D and E) have the best source rock quality and were deposited in an alkaline lake system under anoxic/fermentative, relatively high saline and eutrophic conditions within an at least partly stratified water column. This is indicated by different biological markers such as β - and γ -carotane, $\alpha\alpha\alpha$ C₂₈-sterane a relatively high gammacerane index and a low pr/ph ratio. The unusual occurrence of monoaromatic carotenoids in the lipid OM as well as alkylbenzenes in the pyrolysates point to photic zone anoxia in the Lei-Gao area. The microscopic visible OM is a residue of cyanobacterial or microbial mats which is supported by the presence of branched alkanes as well as specific sterols and stanols. High concentrations of phytanic acid and high ph/n-C18 ratios in some samples suggest an additional source for phytane probably from methanogenic archaea. The facies type generates high-wax paraffinic crude oil rich in long-alkyl chains with a very narrow distribution of activation energies. Dolomite and analcime are the dominant minerals both formed mainly by evaporative concentration in shallow waters or on exposed mudflats. However, abundant calcite precipitation in the GS of the Shu-Du and Gao area as well as in the upper DJT of the Lei area suggests more diluted lake waters. In contrast, the lower DJT in the Lei area represents an ecologically stressed, highly alkaline and saline environment with a low-diversity biota (type A) where oxidation and destruction of the OM frequently have occurred.

Shales deposited in the **freshwater environment** (Shale I, Shale II, Es 3) are dominated by *Botryococcus* alginite (type B). The hydrocarbon generative potential was determined to be lower than for the playa and shallow lake facies based on TOC and HI data. Although this facies type can also generate high-wax oils, higher proportions of gas-generating compounds can be expected. The Py-GC-FID pattern with shorter alkyl-chain lengths than for the GS reflects the different source OM input and a broader distribution of activation energies points

to more heterogeneous OM. Organic geochemical parameters suggest an oxic environment with a relatively low salinity. A high input of clay minerals dominated by mixed layer clays is indicative for a warm and humid climate in the catchment area, the occurrence of siderite implies that meromictic conditions were partly present. Strong variations of the HI values within samples of identical OM composition can be related to variable degrees of oxidation due to lake level fluctuations and desiccation.

Only very few samples rich in quartz, feldspars and clay minerals were available which describe a marginal **fan-delta environment**, typical for the DJT sub-unit in the Shu-Du area. The sediment filling reflects the mineralogy of metamorphic rocks in the surrounding areas. The coarse-grained facies is organic-poor and consists of a mixed type II/III OM type. As a result kerogens from this facies type have the highest aromaticities and proportions of phenols. The petroleum generating potential is very low. Highest buddingtonite contents are associated with migrated hydrocarbons in well A. Thus, changes in fixed ammonium in feldspars may serve as an indicator for the presence of hydrocarbons and/or migration pathways.

Organic petrology revealed the presence of predominantly aquatic OM and only few terrigenous particles, restricted to the marginal fan-delta facies type. In addition, oleanane indices are very low indicating that angiosperm input was minor. Consequently, vitrinites are scarce in the investigated area and the reflectance is often suppressed. The best maturity trends were determined for aromatic and non-aromatic hopanoids as well as methylphenanthrenes. Extremely high levels of thermal stress would be necessary to generate petroleum from these source rocks in nature. Maximum oil generation is predicted to occur at 148 to 159°C at a heating rate of 5.3 K/Ma with highest stabilities determined for samples from the GS sub-unit.

The study of geochemical and textural properties of macromolecular OM in **Recent lake sediments** in combination with lipid OM analysis, carbon isotopic compositions and palynological data allows a determination of organic matter sources which are in turn the clue to understand the paleoclimatic history.

Compared to the Liaohe sediments terrigenous OM is abundant in the maar lake sediments. Thus, lignin derived pyrolysis products (methoxyphenols) can be used as specific biomarkers to trace higher plant input and vegetation changes. The 4-methylguaiacol to n-C_{11:1} ratio (Ratio A) together with the aromaticity is indicative for the forestation of the landscape around the Eifel Maar lakes after the last glacial retreat as well as forest reduction during the

Younger Dryas. The 4-methylguaiacol to *p*-vinylphenol ratio (Ratio B) is useful to estimate the relative contribution of higher plant lignin *versus* grass lignin input to Lake Huguang Maar. A dominant delivery of angiosperm OM was proposed for the lithozones 6 and 4 deposited in a tropical climate with a strong summer monsoon. Higher proportions of grass-derived lignins are related to drier and cooler climatic conditions reflecting a savannah vegetation and a more intense winter monsoon in lithozone 5 and 3.

The distribution of the *n*-alkane/*n*-alk-1-ene doublets as well as most of the other compound classes in the pyrolysates suggests multiple precursors in agreement with microscopic observations. The phenols in the pyrolysates of the Eifel Maar lakes derive from the lignocellulose of higher plants and from proteinaceous (tyrosine) autochthonous sources (e.g. cyanobacteria).

High reflectance values (>0.6% Rr) determined on terrigenous particles (huminites/vitrinites), indicate allochthonous components that were introduced to the maar lakes by the erosion of soils during run-off periods in an open tree less vegetation. They were frequently observed during cool periods or indicate an anthropogenic influence. In contrast, fresh low-reflecting plant material (<0.6% Rr) is interpreted as a sign for a rich vegetation settled around the maar lakes.

Abundant algal remains (*Botryococcus*, filamentous algae) in lake sediments are related to periods with a high delivery of nutrients. This happened in a favourable warm climate during deposition of lithozone 6 and 4 in Lake Huguang Maar and during the Holocene optimum in the Eifel Maar lakes.

Systematic variations of the carbon isotopic compositions of kerogens and whole sediments reflect changes in the primary signature of the OM. In Lake Huguang Maar, these changes are caused by fluctuations in the relative proportions of C₃ and C₄ plant material and temporal variations of environmental conditions affecting the primary producers in the lake. Variations of compound specific carbon isotopes of individual *n*-alkanes parallel the vegetation changes. *Botryococcus* derived biomarkers (botryococcenes) show extremely large $\delta^{13}\text{C}$ shifts which are probably related to the ability of this alga to use bicarbonate at low dissolved CO₂ concentrations.

7 References

- Abelson**, P.H. and Hoering, T.C. (1961) Carbon isotope fractionation in formation of amino acids by photosynthetic organisms. *Proc. Nat. Acad. Sci. US*, 47, 623-632.
- Alberdi, M. and López, L. (2000) Biomarker 18 α (H)-oleanane: a geochemical tool to assess Venezuelan petroleum systems. *Journal of South American Earth Sciences*, 13(8), 751-759.
- Albro, P.W. (1976) Bacterial waxes. In: *Chemistry and Biochemistry of Natural Waxes* (Ed. by P.E. Kolattukudy), pp. 419-450. Elsevier.
- Alderman, A.R. and Skinner, H.C. (1957) Dolomite sedimentation in the southeast of South Australia. *American Journal of Science*, 225, 561-567.
- Allard, B., Templier, J. and Largeau, C. (1997) Artfactual origin of mycobacterial bacteran. Formation of melanoidin-like artifact macromolecular material during the usual isolation process. *Organic Geochemistry*, 26(11-12), 691-703.
- Aller, R.C. and Rude, P.D. (1988) Complete oxidation of solid phase sulfides by manganese and bacteria in anoxic sediments. *Geochimica et Cosmochimica Acta*, 52, 751-765.
- Alley, R.B., Mayewski, P.A., Sowers, T., Stuiver, M., Taylor, K.C. and Clark, P.U. (1997) Holocene climatic instability: A prominent widespread event 8200 yr ago. *Geology*, 25(6), 483-486.
- Anderson, R.Y. and Dean, W.E. (1988) Lacustrine varve formation through time. *Palaeogeography, Palaeoclimatology, Palaeoecology*, 62, 215-235.
- Ariztegui, D., Hollander, D.J. and McKenzie, J.A. (1996) Algal dominated lacustrine organic matter can be either Type I or Type II: Evidence for biological, chemical and physical controls on organic matter quality. In: *4th Latin American Congress on Organic Geochemistry* (Ed. by M.R. Mello, L.A.F. Trinidade and M.H.R. Hessel); *ALAGO Special Publications*, pp. 12-16, Bucaramanga, Columbia.
- Baas**, M., Briggs, D.E.G., van Heemst, J.D.H., Kear, A.J. and de Leeuw, J.W. (1995) Selective preservation of chitin during the decay of shrimp. *Geochimica et Cosmochimica Acta*, 59(5), 945-951.
- Bakr, M.M.Y. and Wilkes, H. (2002) The influence of facies and depositional environment on the occurrence and distribution of carbazoles and benzocarbazoles in crude oils: a case study from the Gulf of Suez, Egypt. *Organic Geochemistry*, 33(5), 561-580.
- Baldar, N.A. and Whittig, L.D. (1968) Occurrence and synthesis of soil zeolites. *Soil Science Soc. Am. J.*, 32, 235-238.
- Barakat, A.O. and Rullkötter, J. (1997) A comparative study of molecular paleosalinity indicators: chromans, tocopherols and C₂₀ isoprenoid thiophenes in Miocene lake sediments (Nördlinger Ries, Southern Germany). *Aquatic Geochemistry*, 3, 169-190.
- Barnola, J.M., Raynaud, D., Korotkevich, Y.S. and Lorius, C. (1987) Vostok ice core provides 160,000 year record at atmospheric CO₂. *Nature*, 329, 408-414.
- Bartle, K.D., Perry, D.L. and Wallace, S. (1987) The functionality of nitrogen in coal and derived liquids: an XPS study. *Fuel Proc. Technol.*, 15, 351-361.
- Bauld, J. (1981) Geobiological role of cyanobacterial mats in sedimentary environments: production and preservation of organic matter. *BMR J. Aust. Geol. Geophys.*, 6, 307-317.
- Baxby, M., Patience, R.L. and Bartle, K.D. (1994) The origin and diagenesis of sedimentary organic nitrogen. *Journal of Petroleum Geology*, 17(2), 211-230.
- Beadle, L.C. (1981) *The inland waters of tropical Africa*. Longman, London, pp. 365.
- Béhar, F. and Vandenbrouke, M. (1988) Chemical modelling of kerogens. *Organic Geochemistry*, 11(1), 15-24.

- Béhar, F., Derenne, S. and Largeau, C. (1995) Closed pyrolysis of the isoprenoid algaenan of *Botryococcus braunii*, L race: Geochemical implications for derived kerogens. *Geochimica et Cosmochimica Acta*, 59(14), 2983-2997.
- Béhar, F., Vandenbroucke, M., Tang, Y., Marquis, F. and Espitalie, J. (1997) Thermal cracking of kerogen in open and closed systems: determination of kinetic parameters and stoichiometric coefficients for oil and gas generation. *Organic Geochemistry*, 26(5/6), 321-329.
- Behrens, A., Schaeffer, P., Bernasconi, S. and Albrecht, P. (2000) 7,11-cyclobotryococca-5,12,26-triene, a novel botryococcene-related hydrocarbon occurring in natural environments. *Organic Letters*, 2(9), 1271-1274.
- Berner, R.A. (1970) Sedimentary pyrite formation. *American Journal of Science*, 268, 1-23.
- Berner, R.A. (1981) A new geochemical classification of sedimentary environments. *Journal of Sedimentary Petrology*, 51, 359-365.
- Berner, R.A. and Raiswell, R. (1983) Burial of organic carbon and pyrite sulfur in sediments over Phanerozoic time: a new theory. *Geochimica et Cosmochimica Acta*, 47, 855-862.
- Berner, R.A. (1984) Sedimentary pyrite formation. *Geochimica et Cosmochimica Acta*, 48, 605-615.
- Bertelle, M., Leotta, G., Calogero, S. and Oddone, M. (1998) Characterisation of sediments of the Tarn Flat lake (Antarctica). *International Journal of Environmental Analytical Chemistry*, 71(3-4), 227-244.
- Bertrand, P., Brocero, S., Lallier-Verges, E., Tribouvillard, N.-P. and Bonifay, E. (1992) Sedimentation organique lacustres et paleoclimates du Pleistocene aux moyennes latitudes: exemple du Lac du Bouchet, Haute Loire, France. *Bull. Soc. Géol. France*, 163, 427-433.
- Bierstedt, A., Stankiewicz, B.A., Briggs, D.E.G. and Evershed, R.P. (1998) Quantitative and qualitative analysis of chitin in fossil arthropods using a combination of colorimetric assay and pyrolysis-gas chromatography-mass spectrometry. *Analyst*, 123, 139-145.
- Bishop, A.N. and Philp, R.P. (1994) The potential for amorphous kerogen via adsorption of organic material at mineral surfaces. *207th Amer. Chem. Soc. National Meeting*, San Diego, 13-18.
- Björck, S., Kromer, B., Johnsen, S., Bennike, O., Hammarlund, D., Lemdahl, G., Possnert, G., Rasmussen, T.L., Wohlfahrt, B., Hammer, C.U. and Spurk, M. (1996) Synchronized terrestrial atmospheric deglacial records around the North Atlantic. *Science*, 274(5290), 1155-1160.
- Blokker, P., Schouten, S., van den Ende, H., de Leeuw, J.W., Hatcher, P.G. and Sinninghe Damsté, J.S. (1998) Chemical structure of algaenans from the freshwater algae *Tetraedron minimum*, *Scenedesmus communis* and *Pediastrum boryanum*. *Organic Geochemistry*, 29(5-7), 1453-1468.
- Boettcher, A.A. and Targett, N.M. (1993) Role of polyphenolic molecular size in reduction of assimilation efficiency in *Xiphister mucosus*. *Ecology*, 74, 891-903.
- Bohacs, K.M. (1998) Contrasting expressions of depositional sequences in mudrocks from marine to non marine environs. In: *Mudstones and Shales - Characteristics at the basin scale* (Ed. by J. Schreiber, W. Zimmerle and P. Sethi) 1, pp. 32-77. Schweizerbart'sche Verlagsbuchhandlung, Stuttgart.
- Bohacs, K.M., Carroll, A.R., Neal, J.E. and Mankiewicz, P.J. (2000) Lake-basin type, source potential, and hydrocarbon character: an integrated-sequence-stratigraphic-geochemical framework. In: *Lake basins through space and time* (Ed. by E.H. Gierlowski-Kordesch and K. Kelts); *AAPG Studies in Geology*, Vol. 46, pp. 3-34.
- Bolton, B.R. and Frakes, L.A. (1985) Geology and genesis of manganese colite, Chiatara, Georgia, U.S.S.R. *GSA Bulletin*, 96, 1398-1406.
- Boon, J.J., Hines, H., Burlingame, A.L., Klok, J., Rijpstra, W.I.C., de Leeuw, J.W., Edmunds, K.E. and Eglinton, G. (1983) Organic geochemical studies of of Solar Lake cyanobacterial mats. In: *Advances in Organic Geochemistry 1981* (Ed. by M. Bjorøy), pp. 207-227. J. Wiley and Sons, New York.
- Boon, J.J. and de Leeuw, J.W. (1987) Amino acid sequence information in proteins and complex proteinaceous material revealed by pyrolysis-capillary gas chromatography-low and high resolution mass spectrometry. *Journal of Analytical and Applied Pyrolysis*, 11, 313-327.

- Boon, J.J., Pouwels, A.D. and Eijkel, G.B. (1987) Pyrolysis high-resolution gas chromatography-mass spectrometry studies on beech wood: capillary high-resolution mass spectrometry of a beech lignin fraction. *Biochemical Society Transactions*, 15, 170-174.
- Bordowskiy, O.K. (1965a) Sources of organic matter in marine basins. *Marine Geology*, 3, 5-31.
- Bordowskiy, O.K. (1965b) Accumulation of organic matter in bottom sediments. *Marine Geology*, 3, 33-82.
- Boreham, C.J., Summons, R.E., Roksandic, Z., Dowling, L.M. and Hutton, A.C. (1994) Chemical, molecular and isotopic differentiation of organic facies in the Tertiary lacustrine Duaringa oil shale deposit. *Organic Geochemistry*, 21, 685-712.
- Böttcher, M.E. (1998) Manganese(II) partitioning during experimental precipitation of rhodochrosite-calcite solid solutions from aqueous solutions. *Marine Chemistry*, 62(3-4), 287-297.
- Boucsein, B. and Stein, R. (2000) Particulate organic matter in surface sediments of the Laptev Sea (Arctic Ocean: applications of maceral analysis as organic-carbon-source indicator. *Marine Geology*, 162, 573-586.
- Bourbonniere, R.A. and Meyers, P.A. (1996) Sedimentary geolipid records of historical changes in the watersheds and productivities of Lakes Ontario and Erie. *Limnol. Oceanogr.*, 41, 352-359.
- Bourdon, S., Laggoun-Défarge, F., Disnar, J.-R., Maman, O., Guillet, B., Derenne, S. and Largeau, C. (2000) Organic matter sources and early diagenetic degradation in a tropical peaty marsh (Tritrivakely, Madagascar). Implications for environmental reconstruction during the Sub-Atlantic. *Organic Geochemistry*, 31(5), 421-438.
- Boyer, B.W. (1982) Green River laminites: does the playa-lake model really invalidate the stratified-lake model? *Geology*, 10, 321-324.
- Brassell, S.C., Sheng, G., Fu, J. and Eglinton, G. (1988) Biological markers in lacustrine Chinese oil shales. In: *Lacustrine Petroleum Source Rocks* (Ed. by A.J. Fleet, K. Kelts and M.R. Talbot), pp. 299-308. Blackwell.
- Brauer, A., Endres, C., Günter, C., Litt, T., Stebich, M. and Negendank, J.F.W. (1999a) High resolution sediment and vegetation responses to Younger Dryas climate change in varved lake sediments from Meerfelder Maar, Germany. *Quaternary Science Reviews*, 18, 321-329.
- Brauer, A., Endres, C. and Negendank, J.F.W. (1999b) Lateglacial calendar year chronology based on annually laminated sediments from Lake Meerfelder Maar, Germany. *Quaternary International*, 61, 17-25.
- Brauer, A., Günter, C., Johnsen, S.J. and Negendank, J.F.W. (2000) Land-ice teleconnections of cold climatic periods during the last Glacial/Interglacial transition. *Climate Dynamics*, 16, 229-239.
- Brice, S.E. and Pardo, G. (1980) hydrocarbon occurrences in nonmarine, pre-salt sequences of Cabinda, Angola. *AAPG Bulletin*, 64, 680-681.
- Brincat, D., Yamada, K., Ishiwatari, R., Uemura, H. and Naraoka, H. (2000) Molecular-isotopic stratigraphy of long-chain *n*-alkanes in Lake Baikal Holocene and glacial age sediments. *Organic Geochemistry*, 31, 287-294.
- Brink, A.H. (1974) Petroleum Geology of Gabon basin. *AAPG Bulletin*, 58(2), 216-235.
- Briot, D., Poidevin, J.-L. and Huguene, M. (2001) A Sr-Nd isotopic study on rift-related sediments and fossils: Some clues to the rifting in the French Massif Central. *Bulletin de la Societe Geologique de France*, 172(1), 17-24.
- Broecker, W.S. (1994) Massive iceberg discharges as triggers for global climate change. *Nature*, 372, 421-424.
- Brown, A.C. and Knights, B.A. (1969) Hydrocarbon content and its relationship to physiological state in the green alga *Botryococcus braunii*. *Phytochemistry*, 8, 543-547.
- Brown, H., Eakin, P.A., Fallick, A.E. and Creer, K. (1991) Variations in the carbon isotopic composition of organic matter in lacustrine sediments of Meerfelder Maar. In: *Organic Geochemistry, Manchester 1991, Abstracts* (Ed. by D. Manning), pp. 352-354. University Press.

- Büchel, G. and Mertes, H. (1982) Die Eruptionszentren des Westeifeler Vulkanfeldes. *Zeitschrift der deutschen geologischen Gesellschaft*, 133, 409-429.
- Büchel, G. (1993) Maars of the Westeifel (Germany). In: *Paleolimnology of European maar lakes* (Ed. by J.F.W. Negendank and B. Zolitschka) 49; *Lecture Notes in Earth Sciences* 49, pp. 1-14. Springer.
- Buchholz, B., Laczko, E., Pfennig, N., Rohmer, M. and Neunlist, S. (1993) Hopanoids of a Recent sediment from Lake Constance as eutrophication markers. *FEMS Microbiol. Ecol.*, 102, 217-223.
- Buillit, N., Lallier-Vergès, E., Disnar, J.-R. and Loizeau, J.-L. (1997) Changements climatiques et effets anthropiques au cours du dernier millénaire attestés par l'étude pétrographique de la matière organique (Annecy, Le Petit Lac; France). *Bull. Soc. géol. France*, 168(5), 573-583.
- Burkowsky, A. (1903) Neue Kuttenberger Manganmineralien. *Jahrbuch für Mineralogie*, 2, 338.
- Burnham, A.K., Braun, R.L. and Gregg, H.R. (1987) Comparison of methods for measuring kerogen pyrolysis rates and fitting kinetic parameters. *Energy & Fuels*, 1, 452-458.
- Burnham, A.K., Braun, R.L. and Samoun, A.M. (1988) Further comparison of methods for measuring kerogen pyrolysis rates and fitting kinetic parameters. In: *Advances in Organic Geochemistry 1987* (Ed. by L. Mattavelli and L. Novelli); *Organic Geochemistry* 13, pp. 839-845. Pergamon Press, Oxford.
- Burns, B.D. and Beardell, J. (1987) Utilization of inorganic carbon of marine microalgae. *J. exp. mar. Biol. Ecol.*, 107, 75-86.
- Bustin, R.M., Cameron, A.R., Grieve, D.A. and Kalkreuth, W.D. (1985) Coal Petrology: Its Principles, Methods, and Applications, Vol. 3, 2nd edn, pp. 230. Geological Association of Canada.
- Calvert**, S.E. and Pedersen, T.F. (1996) Sedimentary geochemistry of manganese: implications for the environment of formation of manganiferous black shales. *Economic Geology*, 91, 36-47.
- Cane, R.F. (1969) Coorongite and the genesis of oil shale. *Geochimica et Cosmochimica Acta*, 33, 257-265.
- Canuel, E.A. and Martens, C.S. (1996) Reactivity of recently deposited organic matter: degradation of lipid compounds near the sediment-water interface. *Geochimica et Cosmochimica Acta*, 60, 1793-1806.
- Cardellina, J.K., Kirkup, M.P., Moore, R.E., Mynderse, J.S. and Simmons, C.J. (1979) Hyellazole and chlorohyellazole, two novel carbazoles from the bleu-green alga *Hyella caespitosa*. *Tetrahedron Letters*, 51, 4915-4916.
- Carpenter, S.R., Elser, M.M. and Elser, J.J. (1986) Chlorophyll production, degradation, and sedimentation: Implications for paleolimnology. *Limnol. Oceanogr.*, 31, 112-124.
- Carroll, A.R. (1998) Upper Permian lacustrine organic facies evolution, Southern Junggar Basin, NW China. *Organic Geochemistry*, 28(11), 649-667.
- Carroll, A.R. and Bohacs, K.M. (1999) Stratigraphic classification of ancient lakes: balancing tectonic and climatic controls. *Geology*, 27, 99-102.
- Chalansonnet, S., Largeau, C., Casadevall, E., Berkaloff, C., Peniguel, G. and Couderc, R. (1988) Cyanobacterial resistant biopolymers. Geochemical implications of the properties of *Schizothrix* sp. resistant material. In: *Advances in Organic Geochemistry 1987* (Ed. by L. Matavelli and L. Novelli); *Organic Geochemistry* 13(4-6), pp. 1003-1010. Pergamon Press, Oxford.
- Chamley, H. (1989) *Clay Sedimentology*. Springer-Verlag, Berlin, pp. 623.
- Chang, C.-Y. (1991) Geological characteristics and distribution patterns of hydrocarbon deposits in the Bohai Bay Basin, East China. *Marine and Petroleum Geology*, 8, 98-106.
- Chappe, B., Michaelis, W. and Albrecht, P. (1980) Molecular fossils of Archaeobacteria as selective degradation products of kerogen. In: *Advances in Organic Geochemistry 1979* (Ed. by A.G. Douglas and J.R. Maxwell), pp. 265-274. Pergamon.
- Chappe, B., Albrecht, P. and Michaelis, W. (1982) Polar lipids of archaeobacteria in sediments and petroleum. *Science*, 217, 65-66.

- Charles, C. and Fairbanks, R.G. (1992) Evidence from Southern Ocean sediments for the effect of North Atlantic deep-water flux on climate. *Nature*, 355, 416-419.
- Chen, J., Li, S., Xiong, Y. and Bi, Y. (1998) Multiple Petroleum systems in Tertiary extensional basins, east China: a case study of the Gunun-Fulin Basin. *Journal of Petroleum Geology*, 21, 105-118.
- Chen, Z., Yan, H., Li, J., Zhang, G., Zhang, Z. and Liu, B. (1999) Relationship between Tertiary volcanic rocks and hydrocarbons in the Liaohe Basin, People's Republic of China. *AAPG Bulletin*, 83(6), 1004-1014.
- Cho, K.Y. and Salton, M.R.J. (1966) Fatty acid composition of bacterial membrane and wall lipids. *Biochimica et Biophysica Acta*, 116, 73-79.
- Clausing, A. (1998) Mikro-organofazielle Studien an Sedimenten des Enspel-Sees (Oberoligozän, Westerwald, Deutschland). *Hallesches Jahrb. Geowiss.*, B 20, 119-133.
- Clegg, H., Wilkes, H. and Horsfield, B. (1997) Carbazole distributions in carbonate and clastic source rocks. *Geochimica et Cosmochimica Acta*, 61, 5335-5345.
- Clegg, H., Wilkes, H., Oldenburg, T., Santamaria-Orozco, D. and Horsfield, B. (1998) Influence of maturity on carbazole and benzocarbazole distributions in crude oils and source rocks from the Sonda de Campeche, Gulf of Mexico. *Organic Geochemistry*, 29(1-3), 183-194.
- Colling, E.L. and Nolte, D.G. (1992) Method for Isolating Kerogen from a Mineral Sample in a Pressurized Reaction Cell. Texaco Inc., U.S.
- Collins, A.G. (1975) *Geochemistry of Oilfield Waters*. Elsevier, pp. 510.
- Collister, J.W., Rieley, G., Stern, B., Eglinton, T. and Fry, B. (1994) Compound specific $\delta^{13}\text{C}$ analyses of leaf lipids from plants with differing carbon dioxide mechanisms. *Organic Geochemistry*, 21, 619-627.
- Colombo, J.C., Silverberg, N. and Gearing, J.N. (1996) Lipid biogeochemistry in the Laurentian Trough: I. Fatty acids, sterols and aliphatic hydrocarbons in rapidly settling particles. *Organic Geochemistry*, 25, 211-225.
- Connan, J. and Cassou, A.M. (1980) Properties gases and petroleum liquids derived from terrestrial kerogen at various maturation levels. *Geochimica et Cosmochimica Acta*, 44, 1-23.
- Connan, J., Restle, A. and Albrecht, P. (1980) Biodegradation of crude oils in the Aquitaine basin. In: *Advances in Organic Geochemistry 1979* (Ed. by A.G. Douglas and J.R. Maxwell), pp. 1-17. Pergamon, Oxford.
- Connan, J., Bouroulllec, D., Dessort, D. and Albrecht, P. (1986) The microbial input in carbonate-anhydrite facies of a sabkha paleoenvironment from Guatemala: a molecular approach. In: *Advances in Organic Geochemistry 1985* (Ed. by D. Leythaeuser and J. Rullkötter); *Organic Geochemistry* 10, pp. 29-50. Pergamon Press, Oxford.
- Cook, A.C., Hutton, A.C. and Sherwood, N.R. (1981) Classification of oil shales. *Bulletin Centre Recherche Exploration-Production, Elf-Aquitaine*, 5, 353-381.
- Corbet, B., Albrecht, P. and Ourisson, G. (1980) Photochemical or photomimetic fossil triterpenoids in sediments and petroleum. *Journal of the American Chemical Society*, 102(3), 1171-1173.
- Cowie, G.L. and Hedges, J.J. (1984) Carbohydrate sources in a coastal environment. *Geochimica et Cosmochimica Acta*, 48, 2075-1087.
- Cox, R.E., Burlingame, A.L., Wilson, D.M., Eglinton, G. and Maxwell, J.R. (1973) Botryococcene - a tetramethylated acyclic triterpenoid of algal origin. *J. Chem. Soc., Chem. Commun.*, 284-285.
- Cranwell, P.A. (1982) Lipids of aquatic sediments and sedimenting particulates. *Prog. Lipid Res.*, 21, 271-308.
- Cranwell, P.A. (1985) Long-chain unsaturated ketones in recent sediments. *Geochimica et Cosmochimica Acta*, 49, 1545-1551.
- Cranwell, P.A., Eglinton, G. and Robinson, N. (1987) Lipids of aquatic organisms as potential contributors to lacustrine sediments. *Organic Geochemistry*, 11, 513-527.

- Curiale, J.A. and Gibling, M.R. (1994) Productivity control on oil shale formation-Mae Sot Basin, Thailand. *Organic Geochemistry*, 21(1), 67-89.
- Curry, D.J. and Simpler, T.K. (1987) Isoprenoid constituents in kerogens as a function of depositional environment and catagenesis. *Advances in Organic Geochemistry*, 13(4-6), 995-1001.
- Dahl**, B. and Spears, G.C. (1986) Geochemical significance of a tar mat in the Oseberg field Norwegian sector, North Sea. In: *Advances in Organic Geochemistry 1985* (Ed. by D. Leythaeuser and J. Rullkötter); *Organic Geochemistry* 10, pp. 29-50. Pergamon Press, Oxford.
- Danielson, N.D. and Rogers, L.B. (1978) Determination of tryptohan in proteins by pyrolysis gas chromatography. *Analytical Chemistry*, 50, 1680-1683.
- Dansgaard, W., Johnsen, S.J., Clausen, H.B., Dahl-Jensen, D., Gundestrup, N.S., Hammer, C.U., Hvidberg, C.S., Steffensen, J.P., Sveinbjörnsdottir, A.E., Jouzel, J. and Bond, G. (1993) Evidence for general instability of past climate from a 250-kyr ice-core record. *Nature*, 364, 219-220.
- David, M., Metzger, P. and Casadevall, E. (1988) Two cyclobotryococenes from the B race of the green alga *Botryococcus braunii*. *Phytochemistry*, 27(9), 2863-2867.
- de Leeuw, J.W. and Baas, M. (1986) Early-stage diagenesis of steroids. In: *Biological markers in the sedimentary record* (Ed. by R.B. Johns), pp. 101-123. Elsevier, Amsterdam.
- de Leeuw, J.W. and Largeau, C. (1993) A review of macromolecular organic compounds that comprise living organisms and their role in kerogen, coal, and petroleum formation. In: *Organic Geochemistry* (Ed. by H. Engel and S.A. Macko), pp. 23-72. Plenum Press, New York, London.
- de Rosa, M. and Gambacorta, A. (1988) The lipids of archaebacteria. *Prog. Lipid Res.*, 27, 153-175.
- Dean, W.E. (1981) Carbonate minerals and organic matter in sediments of modern north temperate hard water lakes. In: *Recent and Ancient Nonmarine Depositional Environments: Models for Exploration* (Ed. by E.G. Etheridge and R.M. Flores) 31, pp. 213-232. Soc. Econ. Paleontol. Mineral. Spec. Publ.
- Dean, W.E., Arthur, M.A. and Claypool, G.E. (1986) Depletion of ^{13}C in Cretaceous marine organic matter: source, diagenetic or environmental signal? *Marine Geology*, 70, 119-157.
- Dean, W.E. and Anders, D.E. (1991) Effects of source, depositional environment and diagenesis on characteristics of organic matter in oil shale from the Green River Formation, Wyoming, Utah, and Colorado. *Bulletin U.S. Geological Survey*, 1973, F1-F16.
- Deconinck, J.F. and Chamley, H. (1995) Diversity of smectite origins in Late Cretaceous sediments: example of chalks from northern France. *Clay Minerals*, 30, 365-379.
- Deines, P. (1980) The isotopic composition of reduced organic carbon. In: *Handbook of Environmental Isotope Geochemistry, Vol. 1 - The Terrestrial Environment* (Ed. by P. Fritz and J.C. Fontes), pp. 329-406. Elsevier, Amsterdam.
- Delian, F., Tiebing, L. and Le, Y. (1992) The process of formation of manganese carbonate deposits hosted in black shale series. *Economic Geology*, 87, 1419-1420.
- Demaison, G.J. and Moore, G.T. (1980) Anoxic environments and oil source bed genesis. *Organic Geochemistry*, 2, 9-31.
- Derenne, S., Largeau, C., Casadevall, E. and Berkaloff, C. (1989) Occurrence of a resistant biopolymer in the L race of *Botryococcus braunii*. *Phytochemistry*, 28(4), 1137-1142.
- Derenne, S., Largeau, C., Casadevall, E. and Sellier, N. (1990) Direct relationship between the resistant biopolymer and the tetraterpenic hydrocarbon in the lycopadiene race of *Botryococcus braunii*. *Phytochemistry*, 29(7), 2187-2192.
- Derenne, S., Largeau, C. and Casadevall, E. (1991) Occurrence of tightly bound isoprenoid acids in an algal, resistant biomacromolecule: possible geochemical implications. *Organic Geochemistry*, 17(5), 597-602.
- Derenne, S., Le Berre, F., Largeau, C., Hatcher, P., Connan, J. and Raynaud, J.F. (1992) Formation of ultralaminar in marine kerogens via selective preservation of thin resistant outer walls of microalgae. In: *Advances in Organic Geochemistry 1991* (Ed. by C. Eckhardt and J.R. Maxwell); *Organic Geochemistry* 19(4-6), pp. 345-350.

- Derenne, S., Largeau, C. and Behar, F. (1994) Low polarity pyrolysis products of Permian to Recent *Botryococcus*-rich sediments: First evidence for the contribution of an isoprenoid algaenan to kerogen formation. *Geochimica et Cosmochimica Acta*, 58(17), 3703-3711.
- Derenne, S., Largeau, C. and Berkaloff, C. (1996) First example of an algaenan yielding an aromatic-rich pyrolysate. Possible geochemical implications on marine kerogen formation. *Organic Geochemistry*, 24(6/7), 617-627.
- Derenne, S., Largeau, C., Hetényi, M., Bruckner-Wein, A., Connan, J. and Lugardon, B. (1997) Chemical structure of the organic matter in a pliocene maar-type shale: Implicated *Botryococcus* race strains and formation pathways. *Geochimica et Cosmochimica Acta*, 61(9), 1879-1889.
- Derenne, S., Largeau, C., Bruckner-Wein, A., Hetenyi, M., Bardoux, G. and Mariotti, A. (2000) Origin of variations in organic matter abundance and composition in a lithologically homogeneous maar-type oil shale deposit (Gérce, Pliocene, Hungary). *Organic Geochemistry*, 31(9), 787-798.
- Desborough, G.A. and Pitman, J.K. (1974) Significance of applied mineralogy to oil shale in the upper part of the Parachute Creek Member of the Green River Formation, Piceance Creek Basin, Colorado. *25th Field Conference*, Colorado, 81-89.
- di Primio, R. (1995) The generation and migration of sulphur-rich petroleums in a low-maturity carbonate source rock sequence from Italy, pp. 197. *Berichte des Forschungszentrums Juelich* No. 3110, Juelich.
- Didyk, B.M., Simoneit, B.R.T., Brassell, S.C. and Eglinton, G. (1978) Organic geochemical indicators of palaeoenvironmental conditions of sedimentation. *Nature*, 272, 216-222.
- Duan, Y. (2000) Organic geochemistry of recent marine sediments from the Nansha Sea, China. *Organic Geochemistry*, 31, 159-167.
- Dungworth, G., Thijssen, M., Zuurveld, J., van der Velden, V. and Schwartz, A. (1977) Distribution of amino acids, amino sugars, purines and pyrimidines in a Lake Ontario sediment core. *Chemical Geology*, 19, 295-308.
- Durand, B. (1980) Sedimentary organic matter and kerogen. Definition and quantitative importance of kerogen. In: *Kerogen. Insoluble organic matter from sedimentary rocks* (Ed. by B. Durand), pp. 13-34. Editions Technip, Paris.
- Durand, B. and Nicaise, G. (1980) Procedures for kerogen isolation. In: *Kerogen. Insoluble organic matter from sedimentary rocks* (Ed. by B. Durand), pp. 35-53. Editions Technip, Paris.
- Durham, M.J., Burges, P.C. and Bottinga, R. (1999) Geology of the North Falklands Graben and implications for future hydrocarbon exploration. *American Association of Petroleum Geologists, International Conference and Exhibition Extended Abstracts*, Birmingham, England, 159-162.
- Dutkiewicz, A. and von der Borch, C.C. (1995) Lake Greenly, Eyre Peninsula, South Australia: sedimentology, palaeoclimatic and palaeohydrologic cycles. *Palaeogeography, Palaeoclimatology, Palaeoecology*, 113(1), 43-56.
- DVD (1978) Das Klima der Bundesrepublik Deutschland, Lieferung 1: Niederschlag (1931-1960), Offenbach.
- Dyni, J.R. (1976) Trioctahedral smectite in the Green River Formation, Duchesne County, Utah. In: *U.S. Geological Survey Professional Paper*, 967, pp. 14.
- Dyni, J.R. (1985) Clay mineralogy of the Green River Formation. In: *Clays and Clay minerals, Western Colorado & Eastern and Central Utah* (Ed. by R.B. Hall), pp. 5-8. Int. Clay Conf., Denver.

- Eckartz-Nolden**, G. (1992) The phytoplankton of Lake Laacher See: Species composition and seasonal periodicity. In: *Limnology of Eifel maar lakes* (Ed. by B.W. Scharf and S. Björk); *Advances in Limnology* 38, pp. 143-160. Schweizerbart'sche Verlagsbuchhandlung, Stuttgart.
- Edmunds, K.L.H. and Eglinton, G. (1984) Microbial lipids and carotenoids and their early diagenesis in the Solar Lake laminated microbial mat sequence. In: *Microbial Mats: Stromatolites* (Ed. by Y. Cohen), pp. 343-389. Alan R. Liss, Inc.
- Eglinton, G. and Hamilton, R.J. (1967) Leaf epicuticular waxes. *Science*, 156, 1322.
- Eglinton, T.I., Sinninghe Damsté, J.S., Kohnen, E.L. and de Leeuw, J.W. (1990) Rapid estimation of the sulfur content of kerogens, coals and asphaltenes by pyrolysis-gas chromatography. *Fuel*, 69(11), 1394-1404.
- Ehleringer, J.R., Field, C.B., Lin, Z.F. and Kuo, C.Y. (1986) Leaf carbon isotope ratio and mineral composition in subtropical plants along an irradiance cline. *Oecologia*, 70, 520-526.
- Ehleringer, J.R., Lin, Z.F., Field, C.B. and Kuo, C.Y. (1987) Leaf carbon isotope ratios of plants from a subtropical monsoon forest. *Oecologia*, 27, 109-114.
- Ehleringer, J.R., Cerling, T.E. and Helliker, B.R. (1997) C₄ photosynthesis, atmospheric CO₂ and climate. *Oecologia*, 112, 285-299.
- Ehlscheid, T. (1992) Phytoplankton of Lake Meerfelder Maar. In: *Limnology of Eifel maar lakes* (Ed. by B.W. Scharf and S. Björk); *Advances in Limnology* 38, pp. 129-136. Schweizerbart'sche Verlagsbuchhandlung, Stuttgart.
- Einsele, G. (2000) *Sedimentary Basins. Evolution, Facies and Sediment Budget*. Springer-Verlag, Berlin, Heidelberg, New York, pp. 685.
- El Tabakh, M., Riccioni, R.M. and Schreiber, B.C. (1997) Deposition and diagenesis of non-marine rift-basin evaporites: The Passaic Formation (Late Triassic). *Sedimentology*, 44, 767-791.
- Elias, V.O., Cardoso, J.N. and Simoneit, B.R.T. (2000) Acyclic lipids in Amazon shelf waters. *Estuarine, Coastal and Shelf Science*, 2000, 231-243.
- English, P.M. (2001) Formation of analcime and moganite at Lake Lewis, central Australia: significance of groundwater evolution in diagenesis. *Sedimentary Geology*, 143(3-4), 219-244.
- Erd, R.C., White, D.E., Fahey, J.J. and Lee, D.E. (1964) Buddingtonite, an ammonium feldspar with zeolitic water. *American Mineralogist*, 49(7-8), 831-850.
- Espitalié, J., Laporte, J.L., Madec, M. and Marquis, F. (1977) Rapid method for source rock characterization and for evaluating their petroleum potential and their degree of evolution, pp. 19. Istitut Francais du Petrole, Paris.
- Espitalié, J., Madec, M. and Tissot, B. (1980) Role of mineral matrix in kerogen pyrolysis: Influence on petroleum generation and migration. *AAPG Bulletin*, 64(1), 59-66.
- Espitalié, J., Deroo, G. and Marquis, F. (1985) La pyrolyse Rock-Eval et ses applications. Deuxième partie: Interprétation des paramètres. *Rev. Inst. Fr. Pét.*, 40, 755-784.
- Eugster, H.P. (1970) Chemistry and origin of the brines of Lake Magadi, Kenya. In: *Mineralogy and Geochemistry of Non-Marine Evaporites* (Ed. by B.A. Morgan); *Spec. Paper Miner. Soc. Am.*, pp. 215-235.
- Eugster, H.P. and Surdam, R.C. (1973) Depositional environment of the Green River Formation of Wyoming: a preliminary report. *Geological Society of America Bulletin*, 84, 1115-1120.
- Eugster, H.P. and Hardie, Y.A. (1975) Sedimentation in an ancient playa-lake complex: the Wilkins Peak member of the Green River Formation. *Geological Society of America Bulletin*, 86, 319-334.
- Eugster, H.P. (1980) Geochemistry of evaporitic lacustrine deposits. *Annual Review of Earth Planetary Science*, 8, 35-63.
- Eugster, H.P. and Kelts, K. (1983) Lacustrine chemical sediments. In: *Chemical Sediments and Geomorphology* (Ed. by A.S. Goudie and K. Pye), pp. 321-368. Academic Press, London.
- Everlien, G. (1990) Das Verhalten des in Mineralien enthaltenen Stickstoffs während der Diagenese und Metamorphose von Sedimenten. Dissertation, Braunschweig, pp. 154.

- Faix, O., Meier, D. and Grobe, I. (1987) Studies on isolated lignins and lignins in woody materials by pyrolysis-gas chromatography-mass spectrometry and off-line pyrolysis-gas chromatography with flame ionization detection. *Journal of Analytical and Applied Pyrolysis*, 11, 403-416.
- Fan, P., Philp, R.P., Li, Z., Yu, X. and Ying, G. (1991) Biomarker distribution in crude oils and source rocks from different sedimentary environments. *Chemical Geology*, 93, 61-78.
- Farquhar, G.D., Ehleringer, J.R. and Hubick, K.T. (1989) Carbon isotope discrimination and photosynthesis. *Annual Review of Plant Physiology and Plant Molecular Biology*, 40, 503-537.
- Farrimond, P., Head, I.M. and Innes, H.E. (2000) Environmental influence on the biohopanoid composition of recent sediments. *Geochimica et Cosmochimica Acta*, 64(17), 2985-2992.
- Faure, P. and Landais, P. (2001) Rapid contamination screening of river sediments by flash pyrolysis-gas chromatography-mass spectrometry (PyGC-MS) and thermodesorption GC-MS (TdGC-MS). *Journal of Analytical and Applied Pyrolysis*, 57(2), 187-202.
- Ficken, K.J., Street-Perrott, F.A., Perrott, R.A., Swain, D.L., Olago, D.O. and Eglinton, G. (1998) Glacial/Interglacial variations in carbon cycling revealed by molecular and isotope stratigraphy of Lake Nkunga, Mt. Kenya, East Africa. *Organic Geochemistry*, 29(5-7), 1701-1719.
- Ficken, K.J., Li, B., Swain, D.L. and Eglinton, G. (2000) An *n*-alkane proxy for the sedimentary input of submerged/floating freshwater aquatic macrophytes. *Organic Geochemistry*, 31, 745-749.
- Fischer, G.A. and Roberts, L.T. (1991) Cyclicity in the Green River Formation (Lacustrine Eocene) of Wyoming. *J. Sedim. Petrol.*, 61, 1146-1154.
- Fischer, T. (2002) Lipid Biomarkers in Terrestrial Ecosystems as Indicators of Local Environmental and Climatic Conditions. Ph.D. thesis, in prep.
- Folk, R.L. (1974) *Petrology of sedimentary rocks*. Hemphill, Austin, Texas, pp. 182.
- Folk, R.L. and Land, L.S. (1975) Mg/Ca ratio and salinity: two controls on crystallization of dolomite. *AAPG Bulletin*, 59, 60-68.
- Folk, R.L. (1993) SEM imaging of bacteria and nannobacteria in carbonate sediments and rocks. *Journal of Sedimentary Petrology*, 63(5), 990-999.
- Fong, G.R. (1992) Cenozoic basalts in southern China and their relationship with tectonic environment (in Chinese with English abstracts). *Journal of Zhongshan University*, 27, 93-103.
- Force, E.R. and Cannon, W.F. (1988) Depositional model for shallow-marine manganese deposits around black shale basins. *Economic Geology*, 83, 93-117.
- Franks, S.G. (1999) Mineralogy of shales from the Liahoe Basin, China, pp. 12. RockFluid Systems, Inc., Plano, Texas.
- Franks, S.G. (2000) Mineralogy of shales from the Liahoe Basin, China-Part II, pp. 35. RockFluid Systems, Inc., Plano, Texas.
- Freeman, K.H. and Colarusso, L.A. (2001) Molecular and isotopic records of C₄ grassland expansion in the late Miocene. *Geochimica et Cosmochimica Acta*, 65(9), 1439-1454.
- Frondel, C. and Bauer, L.H. (1955) Kutnahorite: A manganese dolomite, CaMn(CO₃)₂. *American Mineralogist*, 40, 748-750.
- Frostick, L.E., Renaut, R.W., Reid, I. and Tiercelin, J.-J. (1986) Sedimentation in the African Rifts, pp. 382. Blackwell, Oxford.
- Fry, B. and Sherr, E.B. (1984) $\delta^{13}\text{C}$ measurements as indicators of carbon flow in marine and freshwater ecosystems. *Contrib. Mar. Sci.*, 27, 13-47.
- Fu, J., Sheng, G., Peng, P., Brassell, S.C., Eglinton, G. and Jiang, J. (1986) Peculiarities of salt lake sediments as potential source rocks in China. In: *Advances in Organic Geochemistry 1985* (Ed. by D. Leythaeuser and J. Rullkötter); *Organic Geochemistry* 10, pp. 119-126. Pergamon Press, Oxford.
- Fu, J. and Sheng, G. (1989) Biological marker composition of typical source rocks and related crude oils of terrestrial origin in the People's Republic of China. *Applied Geochemistry*, 4(1), 13-22.

- Fu, J., Sheng, G., Xu, J., Eglinton, G., Gowar, A.P., Jia, R., Fan, S. and Peng, P. (1990) Application of biological markers in the assessment of paleoenvironments of Chinese non-marine sediments. *Organic Geochemistry*, 16, 769-779.
- Füchtbauer, H. and Richter, D.K. (1988) Karbonatgesteine. In: *Sedimente und Sedimentgesteine* (Ed. by H. Füchtbauer), pp. 233-434. Schweizerbart'sche Verlagsbuchhandlung, Stuttgart.
- Gadel**, F. and Bruchet, A. (1987) Application of pyrolysis-gas chromatography-mass spectrometry to the characterization of humic substances resulting from decay of aquatic plants in sediments and waters. *Wat. Res.*, 21(10), 1195-1206.
- Gallegos, E.J. (1971) Identification of new steranes, terpanes and branched paraffins in Green River Shale by combined capillary gas chromatography. *Analytical Chemistry*, 43, 1151-1160.
- Galletti, G. and Reeves, J.B. (1992) Pyrolysis/gas chromatography/ion-trap detection of polyphenols (vegetable tannins): preliminary results. *Org. Mass Spectrom.*, 27, 226-230.
- Galletti, G.C. and Bocchini, P. (1995) Pyrolysis/gas chromatography/mass spectrometry of lignocellulose. *Rapid communications in mass spectrometry*, 9, 815-826.
- Gebelein, C.D. and Hoffman, P. (1973) Algal origin of dolomite laminations in stromatolithic limestone. *Journal of Sedimentary Petrology*, 43, 603-613.
- Gelin, F., Boogers, I., Noordeloos, A.A.M., Damsté, J.S.S., Riegmann, R. and de Leeuw, J.W. (1997) Resistant biomacromolecules in marine microalgae of the classes Eustigmatophyceae and Chlorophyceae: Geochemical implications. *Organic Geochemistry*, 26(11-12), 659-675.
- Gelin, F., Volkman, J.K., Largeau, C., Derenne, S., Sinninghe Damsté, J.S. and de Leeuw, J.W. (1999) Distribution of aliphatic, nonhydrolyzable biopolymers in marine microalgae. *Organic Geochemistry*, 30(2-3), 147-159.
- Gelpi, E., Schneider, H.J., Mann, J. and Oro, J. (1970) Hydrocarbons of geochemical significance in microscopic algae. *Phytochemistry*, 9, 603-612.
- Gingele, F. (1996) Holocene climatic optimum in southwest Africa - evidence from the marine clay mineral record. *Palaeogeography, Palaeoclimatology, Palaeoecology*, 122, 77-87.
- Given, R.K. and Wilkinson, B. (1985) Kinetic control of morphology, composition and mineralogy of abiotic sedimentary carbonates. *Journal of Sedimentary Petrology*, 55, 109-119.
- Glikson, M., Lindsay, K. and Saxby, J. (1989) Botryococcus-A planctonic green alga, the source of petroleum through the ages: Transmission electron microscopical studies of oil shales and petroleum source rocks. *Organic Geochemistry*, 14(6), 595-608.
- Glombitza, K.W. and Koch, M. (1989) Secondary metabolites of pharmaceutical potential. In: *Algal and Cyanobacterial Biotechnology* (Ed. by R.C.e.a. Cresswell), *Chapter 7*, pp. 161-235. Bath Press.
- Gonçalves, F.T.T. (2002) Organic and isotope geochemistry of the Early Cretaceous rift sequence in the Camamu Basin, Brazil: paleolimnological inferences and source rock models. *Organic Geochemistry*, 33(1), 67-80.
- Goni, M.A., Hartz, D.M., Thunell, R.C. and Tappa, E. (2001) Oceanographic considerations for the application of the alkenone-based paleotemperature U_{37}^K index in the Gulf of California. *Geochimica et Cosmochimica Acta*, 65(4), 545-557.
- Goossens, H., de Leeuw, J.W., Schenck, P.A. and Brassell, S.C. (1984) Tocopherols as likely precursors of pristane in ancient sediments and crude oils. *Nature*, 312, 440-442.
- Gorham, E., Lund, W.G., Sanger, J.E. and Dean, W.E. (1974) Some relationship between algal standing crop, water chemistry and sediment chemistry in the English lakes. *Limnol. Oceanogr.*, 19, 601-617.
- Goslar, T., Arnold, M., Bard, E., Kuc, T., Pazdur, F., Ralska-Jasiewiczowa, M., Rózanski, K., Tisnerat, N., Walanus, A., Wicik, B. and Wieckowski, K. (1995) High concentration of atmospheric ^{14}C during the Younger Dryas cold episode. *Nature*, 377, 414-417.

- Goslar, T., Balaga, K., Arnold, M., Tisnerat, N., Starnawska, E., Kuzniarski, M., Chrost, L., Walanus, A. and Wieckowski, K. (1999) Climate-related variations in the composition of the Lateglacial and Early Holocene sediments of Lake Perespilno (Eastern Poland). *Quaternary Science Reviews*, 18, 899-911.
- Goslar, T., Arnold, M., Tisnerat-Laborde, N., Czernik, J. and Wieckowski, K. (2000) Variations of Younger Dryas atmospheric radiocarbon explicable without ocean circulation changes. *Nature*, 403, 877-880.
- Goth, K., de Leeuw, J.W., Püttmann, W. and Tegelaar, E.W. (1988) Origin of Messel Oil Shale kerogen. *Nature*, 336, 759-761.
- Goth, K. (1990) Der Messeler Ölschiefer - ein Algenlaminit, pp. 143. Cour. Forsch.-Inst. Senckenberg, Vol. 131.
- Gottardi, G. and Galli, E. (1985) *Natural Zeolites*. Springer-Verlag, Berlin, Heidelberg, pp. 549.
- Grantham, P.J. (1986) The occurrence of unusual C₂₇ and C₂₉ sterane predominance in two types of Oman crude oil. *Organic Geochemistry*, 9, 1-10.
- Grice, K., Schaeffer, P., Schwark, L. and Maxwell, J.R. (1996) Molecular indicators of palaeoenvironmental conditions in an immature Permian shale (Kupferschiefer, Lower Rhine Basin, North-West Germany) from free and S-bound lipids. *Organic Geochemistry*, 25(3/4), 131-147.
- Grice, K., Schouten, S., Nissenbaum, A., Charrach, J. and Sinninghe Damsté, J.S. (1998) A remarkable paradox: Sulfurised freshwater algal (*Botryococcus braunii*) lipids in an ancient hypersaline euxinic ecosystem. *Organic Geochemistry*, 28(3/4), 195-216.
- Guilford, W.J., Schneider, D.M., Labovitz, J. and Opella, S.J. (1988) High resolution solid state ¹³C NMR spectroscopy of sporopollenins from different plant taxa. *Plant Physiology*, 86, 134-136.
- Guillet, B. and Maman, O. (1995) Sulfur specification in the Late Glacial and Holocene sediments of the Lac du Bouchet (Haute Loire, France). In: *Organic Matter Accumulation. The Organic Cyclicities of the Kimmeridge Clay Formation (Yorkshire, GB) and the Recent Maar Sediments (Lac du Bouchet, France)* (Ed. by E. Lallier-Vergès, N.P. Tribovillard and P. Bertrand); *Lecture Notes in Earth Sciences*, Vol. 57, pp. 169-182. Springer, Berlin.
- Gulbrandsen, R.A. (1974) Buddingtonite, ammonium feldspar, in the Phosphoria Formation, Southeastern Idaho. *Journal of Research U.S. Geological Survey*, 2, 693-697.
- Gutjahr, C.C.M. (1983) Introduction to incident-light microscopy of oil and gas source rocks. *Geol. en Mijnbouw*, 62, 417-425.
- Guy-Ohlson, D. (1992) *Botryococcus* as an aid in the interpretation of palaeoenvironmental and depositional processes. *Review of Palaeobotany and Palynology*, 71, 1-15.
- Guy-Ohlson, D. (1998) The use of the microalga *Botryococcus* in the interpretation of lacustrine environments at the Jurassic-Cretaceous transition in Sweden. *Palaeogeography, Palaeoclimatology, Palaeoecology*, 140, 347-356.
- Haddad**, R.I., Martens, C.S. and Farrington, J.W. (1992) Quantifying early diagenesis of fatty acids in a rapidly accumulating coastal marine sediment. *Organic Geochemistry*, 19, 205-216.
- Han, J.C.M. (1969) Hydrocarbon distribution of algae and bacteria, and microbiological activity in sediments. *Proceedings of the National Academy of Sciences of the United States*, 64, 436-444.
- Hanson, A.D., Ritts, B.D., Zinniker, D., Moldowan, J.M. and Biffi, U. (2001) Upper Oligocene lacustrine source rocks and petroleum systems of the northern Qaidam basin, northwest China. *AAPG Bulletin*, 85(4), 601-619.
- Hardie, L.A. (1987) Dolomitization; a critical view of some current views. *Journal of Sedimentary Petrology*, 57(1), 166-183.
- Hardy, R.G. and Tucker, M.E. (1988) X-ray powder diffraction of sediments. In: *Techniques in Sedimentology* (Ed. by M.E. Tucker), pp. 191-228. Blackwell, Oxford.

- Harris, N.B., Freeman, K.H. and Burbank, D.W. (1999) Lacustrine sedimentation in the West African Rift Basins: A record of the interplay of tectonics and climate. *The 2nd International Congress of Limnogeology*, Université de Bretagne Occidentale Plouzané, France, Talk, 4-6.
- Hartgers, W.A., Sinninghe Damsté, J.S. and de Leeuw, J.W. (1994a) Geochemical significance of alkylbenzene distributions in flash pyrolysates of kerogens, coals and asphaltenes. *Geochimica et Cosmochimica Acta*, 58(7), 1759-1775.
- Hartgers, W.A., Sinninghe Damsté, J.S., Requejo, A.G., Allan, J., Hayes, J.M. and de Leeuw, J.W. (1994b) Evidence for only minor contribution from bacteria to sedimentary organic carbon. *Nature*, 369, 224-227.
- Hartmann, M. (1964) Zur Geochemie von Mangan und Eisen in der Ostsee. *Meyniana*, 14, 3-20.
- Hatcher, P.G., Simoneit, B.R.T., Mackenzie, F.T., Neumann, A.C., Thorstenson, D.C. and Gerschakov, S.M. (1982) Organic geochemistry and pore water chemistry of sediments from Mangrove Lake, Bermuda. *Organic Geochemistry*, 4, 93-112.
- Hatcher, P.G., Spiker, E.C., Szeverenyi, N.M. and Maciel, G.E. (1983) Selective preservation and origin of petroleum-forming aquatic kerogen. *Nature*, 305, 498-501.
- Hay, R.L. and Moiola, R.J. (1963) Authigenic silicate minerals in Searles Lake, California. *Sedimentology*, 2, 312-332.
- Hay, R.L., Guldman, S.G., Matthews, J.C., Lander, R.H., Duffin, M.E. and Kyser, T.K. (1991) Clay mineral diagenesis in core KM-3 of Searles Lake, California. *Clays and Clay minerals*, 39, 84-96.
- He, W. and Lu, S. (1990) A new maturity parameter based on monoaromatic hopanoids. In: *Advances in Organic Geochemistry 1989* (Ed. by A. Durand and F. Behar); *Organic Geochemistry* 16(4-6), pp. 1007-1013.
- Hedges, J.I., Cowie, G.L. and Ertel, J.R. (1985) Degradation of carbohydrates and lignins in buried woods. *Geochimica et Cosmochimica Acta*, 49, 701-711.
- Hedges, J.I., Clark, W.A., Quay, P.D., Richey, J.E., Devol, A.H. and Santos, U.d.M. (1986) Composition and fluxes of particulate organic material in the Amazon River. *Limnol. Oceanogr.*, 31(4), 717-738.
- Hem, J.D. and Lind, C.J. (1994) Chemistry of manganese precipitation in Pinal Creek, Arizona, USA: a laboratory study. *Geochimica et Cosmochimica Acta*, 58(6), 1601-1613.
- Henrichs, S.M. and Farrington, J.W. (1987) Early diagenesis of amino acids and organic matter in two coastal marine sediments. *Geochimica et Cosmochimica Acta*, 51, 1-15.
- Heras, X., Grimalt, J., Albaiges, J., Julia, R. and Anadon, P. (1989) Origin and diagenesis of the organic matter in Miocene freshwater lacustrine phosphates (Cerandya Basin, Eastern Pyrenco). *Organic Geochemistry*, 14, 667-677.
- Hilde, T.W.C., Uyeda, S. and Kroenke, L. (1977) Evolution of the Western Pacific and its margin. *Tectonophysics*, 38, 145-165.
- Hills, I.R. and Whitehead, E.V. (1966) Triterpanes in optically active petroleum distillates. *Nature*, 209, 977-979.
- Hodell, D.A., Brenner, M., Kanfoush, S.L., Curtis, J.H., Stoner, J.S., Song, X., Wu, Y. and Whitmore, T.J. (1999) Paleoclimate of southwestern China for the past 50,000 yr inferred from lake sediment records. *Quaternary Research*, 52, 369-380.
- Hoefs, M.J.L., van Heemst, J.D.H., Gelin, F., Koopmans, M.P., van Kaam-Peters, H.M.E., Schouten, S., de Leeuw, J.W. and Sinninghe Damsté, J.S. (1995) Alternative biological sources for 1,2,3,4-tetramethylbenzene in flash pyrolysates of kerogen. *Organic Geochemistry*, 23(10), 975-979.
- Höld, I.M., Schouten, S., van der Gaast, S.J. and Sinninghe Damsté, J.S. (2001) Origin of prist-1-ene and prist-2-ene in kerogen pyrolysates. *Chemical Geology*, 172(3-4), 201-212.
- Hollander, D.J. and McKenzie, J.A. (1991) CO₂ control on carbon-isotope fractionation during aqueous photosynthesis: A paleo-pCO₂ barometer. *Geology*, 19, 929-932.

- Hollander, D.J. and Smith, M.A. (2001) Microbially mediated carbon cycling as a control on the $\delta^{13}\text{C}$ of sedimentary carbon in eutrophic Lake Mendota (USA): new models for interpreting isotopic excursions in the sedimentary record. *Geochimica et Cosmochimica Acta*, 65(23), 4321-4337.
- Holloway, P.J. (1984) Cutins and suberins, the polymeric plant lipids. In: *CRC Handbook of Chromatography, Lipids* (Ed. by H.K. Mangold) Vol. 1, pp. 321-346. CRC Press, Boca Raton, Florida.
- Horsfield, B. and Douglas, A.G. (1980) The influences of minerals on the pyrolysis of kerogen. *Geochimica et Cosmochimica Acta*, 44, 1119-1131.
- Horsfield, B. (1989) Practical criteria for classifying kerogens: Some observations from pyrolysis-gas chromatography. *Geochimica et Cosmochimica Acta*, 53, 891-901.
- Horsfield, B., Curry, D.J., Bohacs, K., Littke, R., Rullkötter, J., Schenk, H.J., Radke, M., Schaefer, R.G., Carrol, A.R., Isaksen, G. and Witte, E.G. (1994) Organic geochemistry of freshwater and alkaline lacustrine sediments in the Green River Formation of the Washakie Basin, Wyoming, U.S.A. In: *Advances in Organic Geochemistry 1993* (Ed. by N. Telnaes, G. Van Graas and K. Øygaard); *Organic Geochemistry* 22(3-5), pp. 415-440.
- Horsfield, B. (1997) The bulk composition of first-formed petroleum in source rocks. In: *Petroleum and basin evolution* (Ed. by D.H. Welte, B. Horsfield and D.R. Baker), pp. 335-402. Springer, Berlin.
- Horsfield, B., Clegg, H., Wilkes, H. and Santamaría-Orozco, D. (1998) Effect of maturity on carbazole distributions in petroleum systems: new insights from the Sonda de Campeche, Mexico, and Hils Syncline, Germany. *Naturwissenschaften*, 85, 233-237.
- Hosterman, J.W. and Dyni, J.R. (1972) Clay mineralogy of the Green River Formation, Piceance Creek basin, Colorado - A preliminary study. In: *U.S. Geological Survey Professional Paper*, pp. 159-163.
- Hou, D., Li, M. and Huang, Q. (2000) Marine transgressional events in the gigantic freshwater lake Songliao: paleontological and geochemical evidence. *Organic Geochemistry*, 31(7/8), 763-768.
- Hsü, K.J. (1967) Chemistry of dolomite formation. In: *Carbonate Rocks* (Ed. by G.V. Chilingar, H.J. Bissell and R.W. Fairbridge), pp. 169-192. Elsevier, Amsterdam.
- Hsü, K.J. and Siegenthaler, C. (1969) Preliminary experiments on hydrodynamic movement induced by evaporation and their bearing on the dolomite problem. *Sedimentology*, 12, 11-25.
- Hsü, K.J. and Kelts, K. (1978) Late Neogene chemical sedimentation in the Black Sea. In: *Modern and Ancient Lake Sediments* (Ed. by A. Matter and M. Tucker); *Spec. Publ. Int. Assoc. Sedimentol.*, 2, pp. 129-145.
- Huang, C.-Y., Liew, P.-M., Meixun, Z., Chang, T.-C., Kuo, C.-M., Chen, M.-T., Wang, C.-H. and Zheng, L.-F. (1997) Deep sea and lake records of the Southeast Asian paleomonsoons for the last 25 thousand years. *Earth and Planetary Science Letters*, 146(1-2), 59-72.
- Huang, D., Li, J. and Dajiang, Z. (1990) Maturation sequence of continental crude oils in hydrocarbon basins in China and its significance. In: *Advances in Organic Geochemistry 1989* (Ed. by A. Durand and F. Behar); *Organic Geochemistry* 16(1-3), pp. 521-529.
- Huang, D. (1999) Advances in hydrocarbon generation theory (I) Generation and evolution model for immature oils and hydrocarbons. *Journal of Petroleum Science and Engineering*, 22(1-3), 121-130.
- Huang, H. and Pearson, M.J. (1999) Source rock palaeoenvironments and controls on the distribution of dibenzothiophenes in lacustrine crude oils, Bohai Bay Basin, eastern China. *Organic Geochemistry*, 30, 1455-1470.
- Huang, W.-Y. and Meinschein, W.G. (1979) Sterols as ecological indicators. *Geochimica et Cosmochimica Acta*, 43, 739-745.
- Huang, Y. and Murray, M. (1995) Identification of 1,6,17,21-octahydrobotryococcene in a sediment. *J. Chem. Soc. Chem. Commun.*, 335-336.
- Huang, Y., Murray, M. and Eglinton, G. (1995a) Sacredicene, a novel monocyclic C₃₃ hydrocarbon from sediment of Sacred Lake, a tropical freshwater lake, Mount Kenya. *Tetrahedron Letters*, 36(33), 5973-5976.

- Huang, Y., Street-Perrott, F.A., Perrott, R.A. and Eglinton, G. (1995b) Molecular and carbon isotopic stratigraphy of a glacial/interglacial sediment sequence from a tropical freshwater lake: Sacred Lake, Mt Kenya. In: *Organic Geochemistry, Developments and Applications to Energy, Climate, Environment and Human History* (Ed. by J. Grimalt and C. Dorronsoro), pp. 826-829.
- Huang, Y., Murray, M., Metzger, P. and Eglinton, G. (1996) Novel unsaturated triterpenoid hydrocarbons from sediments of Sacred Lake, Mt. Kenya, Kenya. *Tetrahedron*, 52(20), 6973-6982.
- Huang, Y., Freeman, K.H., Eglinton, T.I. and Street-Perrott, F.A. (1999a) $\delta^{13}\text{C}$ analysis of individual lignin phenols in Quaternary lake sediments: A novel proxy for deciphering past terrestrial vegetation changes. *Geology*, 27(5), 471-474.
- Huang, Y., Street-Perrott, F.A., Perrott, R.A., Metzger, P. and Eglinton, G. (1999b) Glacial-interglacial environmental changes inferred from molecular and compound-specific $\delta^{13}\text{C}$ analyses of sediments from Sacred Lake, Mt. Kenya. *Geochimica et Cosmochimica Acta*, 63(9), 1383-1404.
- Hubert, J.F., Feshbach-Meriney, P.E. and Smith, M.A. (1992) The Triassic-Jurassic Hartford rift basin, Connecticut and Massachusetts: evolution, sandstone diagenesis, and hydrocarbon history. *AAPG Bulletin*, 76, 1710-1734.
- Huckriede, H. and Meischner, D. (1996) Origin and environment of manganese-rich sediments within black-shale basins. *Geochimica et Cosmochimica Acta*, 60(8), 1399-1413.
- Hughen, K.A., Southon, J.R., Lehman, S.J. and Overpeck, J.T. (2000) Synchronous Radiocarbon and Climate Shifts During the Last Deglaciation. *Science*, 290(5498), 1951-1954.
- Hughes, W.B., Holba, A.G. and Dzou, L.I.P. (1995) The ratios of dibenzothiophene to phenanthrene and pristane to phytane as indicators of depositional environment and lithology of petroleum source rocks. *Geochimica et Cosmochimica Acta*, 59(17), 3581-3598.
- Hunt, J.M. (1979) *Petroleum Geochemistry and Geology*. Freeman, San Francisco, pp. 716.
- Hunt, J.M. (1996) *Petroleum Geochemistry and Geology*. W. H. Freeman & Company, New York, pp. 707.
- Hussler, G., Albrecht, P., Ourisson, G., Cesario, M., Guilhem, J. and Pascard, C. (1984a) Benzohopanes, a novel family of hexacyclic geomarkers in sediments and crude oils. *Tetrahedron Letters*, 25, 1179-1182.
- Hussler, G., Connan, J. and Albrecht, P. (1984b) Novel families of tetra- and hexacyclic aromatic hopanoids predominant in carbonate rocks and crude oils. *Organic Geochemistry*, 6, 39-49.
- Hutchinson, D.R., Golmshtok, A.J., Zonenshain, L.P., Moore, T.C., Scholz, C.A. and Klitgord, K.D. (1992) Depositional and tectonic framework of the rift basins of Lake Baikal from multichannel seismic data. *Geology*, 20, 589-592.
- Hutchison, C.S. (1996) *South-East Asian Oil, Gas, Coal and Mineral Deposits*. Clarendon Press, Oxford, pp. 530.
- Hutton, A.C. and Cook, A.C. (1980) Influence of alginite on the reflectance of vitrinite from Joadja, NSW, and some other coals and oil shales containing alginite. *Fuel*, 59, 711-714.
- Hutton, A.C. (1984) Geology of oil shale deposits within the Narrows Graben, Queensland Australia: Discussion. *AAPG Bulletin*, 68, 1055-1057.
- Hutton, A.C. (1987) Petrographic classification of oil shales. *International Journal of Coal Geology*, 8, 203-231.
- Innes**, H.E., Bishop, A.N., Head, I. and Farrimond, P. (1997) Preservation and diagenesis of hopanoids in Recent lacustrine sediments of Priest Pot, England. *Organic Geochemistry*, 26, 565-576.
- Innes, H.E., Bishop, A.N., Fox, P.A., Head, I.M. and Farrimond, P. (1998) Early diagenesis of bacteriohopanoids in Recent sediments of Lake Pollen, Norway. *Organic Geochemistry*, 29(5-7), 1285-1295.
- International Committee for Coal and Organic Petrology (1998) The new vitrinite classification (ICCP System 1994). *Fuel*, 77(5), 349-358.

- International Committee for Coal and Organic Petrology (2001) The new inertinite classification (ICCP System 1994). *Fuel*, 80(4), 459-471.
- Ishiwatari, M., Ishiwatari, R., Sakashita, H. and Tatsumi, T. (1991) Pyrolysis of chlorophyll a after preliminary heating at a moderate temperature: implications for the origin of prist-1-ene on kerogen pyrolysis. *Journal of Analytical and Applied Pyrolysis*, 18, 207-218.
- Ishiwatari, R. and Machihara, T. (1983) Early stage incorporation of biolipids into kerogen in a lacustrine sediment: Evidence from alkaline potassium permanganate oxidation of sedimentary lipids and humic matter. *Organic Geochemistry*, 4(3/4), 179-184.
- Ishiwatari, R., Houtatsu, M. and Okada, H. (2001) Alkenone-sea surface temperatures in the Japan Sea over the past 36 kyr: warm temperatures at the last glacial maximum. *Organic Geochemistry*, 32(1), 57-67.
- Ivarson, K.C., Ross, G.J. and Miles, N.M. (1978) Alterations of micas and feldspars during microbial formation of basic ferric sulfates in the laboratory. *Soil Science Soc. Am. J.*, 42, 518-524.
- Jaffé**, R. and Gardinali, P.R. (1991) Generation and maturation of carboxylic acids in ancient sediments from the Maracaibo Basin, Venezuela. In: *Advances in Organic Geochemistry 1989* (Ed. by A. Durand and F. Behar); *Organic Geochemistry* 16, pp. 211-218. Pergamon Press, Oxford.
- Jankowski, B. (1981) Die Geschichte der Sedimentation in Nördlinger Ries und Randecker Maar. In: *Bochumer Geol. Geotechn. Arb.*, 6, pp. 315, Bochum.
- Jankowski, B. and Littke, R. (1986) Das organische Material der Ölschiefer von Messel. *Geowissenschaften*, 4(3), 73-80.
- Jarvie, D.M. (1991) Factors affecting Rock-Eval derived parameters. *Chemical Geology*, 93, 79-99.
- Jensen, T.E. and Hites, R.A. (1983) Aromatic diesel emissions as a function of engine conditions. *Analytical Chemistry*, 55, 594-599.
- Jian, Z., Huang, B., Kuhnt, W. and Lin, H.-L. (2001) Late Quaternary Upwelling Intensity and East Asian Monsoon Forcing in the South China Sea. *Quaternary Research*, 55(3), 363-370.
- Johnson, T.C. (1996) Sedimentary processes and signals of past climatic change in the large lakes of the East African Rift Valley. In: *The Limnology, Climatology and Paleoclimatology of the East African Lakes* (Ed. by T.C. Johnson and E.O. Odada), pp. 367-412. Gordon & Breach, Amsterdam.
- Jones, B.F., Eugster, H.P. and Rettig, S.L. (1977) Hydrochemistry of the Lake Magadi basin, Kenya. *Geochimica et Cosmochimica Acta*, 41, 53-72.
- Jones, F.G. and Bowser, C.J. (1978) The mineralogy and related chemistry of lake sediments. In: *Lakes: Chemistry, Geology and Physics* (Ed. by A. Lerman), pp. 179-235. Springer-Verlag, Berlin.
- Jones, R.W. (1987) Organic facies. In: *Advances in Petroleum Geochemistry, Vol. 2* (Ed. by J. Brooks), pp. 1-90. Academic Press, London.
- Jüntgen, H. and Klein, J. (1975) Origin of natural gas from coaly sediments. *Erdöl und Kohle*, 28(2), 65-73.
- Kadouri**, A., Derenne, S., Largeau, C., Casadevall, E. and Berkaloff, C. (1988) Resistant biopolymer in the outer walls of *Botryococcus braunii*, B race. *Phytochemistry*, 27(2), 551-557.
- Katz, A. and Kolodny, N. (1989) Hypersaline brine diagenesis and evolution of the Dead Sea-Late Lisan system. *Geochimica et Cosmochimica Acta*, 41, 1609-1626.
- Katz, B.J. (1983) Limitations of Rock-Eval pyrolysis for typing organic matter. *Organic Geochemistry*, 4(3-4), 195-199.
- Katz, B.J. and Elrod, L.W. (1983) Organic geochemistry of DSDP Site 467, offshore California, Middle Miocene to Lower Pliocene strata. *Geochimica et Cosmochimica Acta*, 47, 389-396.
- Katz, B.J. (1990) Lacustrine Basin Exploration - Case Studies and Modern Analogues. In: *AAPG Memoir*, 50, pp. 340.

- Katz, B.J. (1999) Lacustrine basin hydrocarbon exploration. In: *The 2nd International Congress of LimnogeologyTalk*, pp. 6-8. International Association of Limnogeology (IAL), Plouzané, France.
- Kawamura, K. and Ishiwatari, R. (1981) Polyunsaturated fatty acids in a lacustrine sediment as a possible indicator of paleoclimate. *Geochimica et Cosmochimica Acta*, 45, 149-155.
- Kawamura, K., Tannenbaum, E., Huizinga, B.J. and Kaplan, I.R. (1986) Long chain carboxylic acids in pyrolysates of Green River kerogen. In: *Advances in Organic Geochemistry 1985* (Ed. by D. Leythaeuser and J. Rullkötter); *Organic Geochemistry* 10, pp. 1059-1065. Pergamon Press, Oxford.
- Keely, B.J., Blake, S.R., Schaeffer, P. and Maxwell, J.R. (1995) Distributions of pigments in the organic matter of marls from the Vena del Gesso evaporitic sequence. *Organic Geochemistry*, 23(6), 527-539.
- Keigwin, L.D. (1996) The Little Ice Age and Medieval Warm period in the Saragossa Sea. *Science*, 274(5292), 1503-1508.
- Keller, W.D. (1956) Clay minerals as influenced by environments of their formation. *AAPG Bulletin*, 40, 2689-2710.
- Keller, W.D. (1970) Environmental aspects of clay minerals. *Journal of Sedimentary Petrology*, 40, 788-814.
- Kelts, K. and Hsü, K.J. (1978) Freshwater carbonate sedimentation. In: *Lakes: Chemistry, Geology and Physics* (Ed. by A. Lerman), pp. 295-323. Springer-Verlag, Berlin.
- Kelts, K. (1988) Environments of deposition of lacustrine petroleum source rocks: an introduction. In: *Lacustrine Petroleum Source Rocks* (Ed. by A.J. Fleet, K. Kelts and M.R. Talbot); *Geological Society Special Publication, Vol. 40*, pp. 3-26.
- Kendall, C.G.S.C. and Skipwith, P.A. (1969) Holocene shallow-water carbonate and evaporate sediments of Khor al Bazam, Abu Dhabi, southwest Persian Gulf. *AAPG Bulletin*, 53, 841-869.
- Kenig, F., Huc, A.-Y., Pursor, B.H. and Oudin, J.L. (1990) Sedimentation, distribution and diagenesis of organic matter, in a carbonate hypersaline environment, Abu Dhabi (UAE). *Organic Geochemistry*, 16, 735-747.
- Kenig, F. (2000) C₁₆-C₂₉ homologous series of monomethylalkanes in the pyrolysis products of a Holocene microbial mat. *Organic Geochemistry*, 31, 237-241.
- Kienast, M., Steinke, S., Statterger, K. and Calvert, S.E. (2001) Synchronous Tropical South China Sea SST Change and Greenland Warming During Deglaciation. *Science*, 291(5511), 2132-2134.
- Kirk, T.K. and Farrell, R.L. (1987) Enzymatic "combustion": The microbial degradation of lignin. *Annual Review of Microbiology*, 41, 465-505.
- Kitano, Y. (1962) A study of polymorphic formation of calcium carbonate in thermal springs with emphasis of the effects of temperature. *Chemical Society of Japan Bulletin*, 35, 1980-1985.
- Kitano, Y., Park, K. and Hood, D.W. (1962) Pure aragonite synthesis. *Journal of Geophysical Research*, 67, 4873-4874.
- Klett, T.R., Ahlbrandt, T.A., Schmoker, J.W. and Dolton, G.L. (1997) Ranking of the world's oil and gas provinces by known petroleum volumes. U.S. Geological Survey Open-File Report 97-463.
- Köhler, J. and Clausing, A. (2000) Taxonomy and palaeoecology of dinoflagellate cysts from Upper Oligocene freshwater sediments of Lake Enspel, Westerwald area, Germany. *Review of Palaeobotany and Palynology*, 112, 39-49.
- Kohlhase, M. and Pohl, P. (1988) Saturated and unsaturated sterols of nitrogen-fixing blue-green algae (cyanobacteria). *Phytochemistry*, 27, 1735-1740.
- Kokke, W.C.M.C., Fenical, W. and Djerassi, C. (1982) Sterols of the cultured dinoflagellate *pyrocystis lanula*. *Steroids*, 40, 307-317.
- Kolattukudy, P.E. (1980) Cutin, suberin and waxes. In: *The Biochemistry of Plants, Volume 4* (Ed. by P.K. Stumpf), pp. 571-645. Academic Press, New York.

- Koopmans, M.P., Köster, J., van Kaam-Peters, H.M.E., Kenig, F., Schouten, S., Hartgers, W.A., de Leeuw, J.W. and Sinninghe Damsté, J.S. (1996) Diagenetic and catagenetic products of isorenieratene: Molecular indicators for photic zone anoxia. *Geochimica et Cosmochimica Acta*, 60(22), 4467-4496.
- Koopmans, M.P., Rijpstra, W.I.C., Klapwijk, M.M., de Leeuw, J.W., Lewan, M.D. and Sinninghe Damsté, J.S. (1999) A thermal and chemical degradation approach to decipher pristane and phytane precursors in sedimentary organic matter. *Organic Geochemistry*, 30, 1089-1104.
- Koshijima, T., Watanabe, T. and Yaku, F. (1989) Structure and properties of the lignin-carbohydrate complex polymer as an amphiphathic substance. In: *Lignin: properties and material* (Ed. by W.G. Glasser and S. Sarkanen); *ACS Symp Ser 397*, pp. 11-28.
- Köster, J., Volkman, J.K., Rullkötter, J., Scholz-Böttcher, B.M., Rethmeier, J. and Fischer, U. (1999) Mono-, di- and trimethyl-branched alkanes in cultures of the filamentous cyanobacterium *Calothrix scopulorum*. *Organic Geochemistry*, 30, 1367-1379.
- Krishnamurthy, R.V., Syrup, K. and Long, A. (1999) Is selective preservation of nitrogenous organic matter reflected in the $\delta^{13}\text{C}$ signal of lacustrine sediments? *Chemical Geology*, 158, 165-172.
- Kruege, M.A., Mukhopadhyay, P.K. and Lewis, C.F.M. (1998) A molecular evaluation of contaminants and natural organic matter in bottom sediments from western Lake Ontario. *Organic Geochemistry*, 29(5-7), 1797-1812.
- Kulke, H. (1995) *Regionale Erdöl- und Erdgasgeologie der Erde*. Gebrüder Bornträger, Berlin, pp. 942.
- Lallier-Vergès**, E. and Albéric, P. (1990) Optical and geochemical study of organic matter in present oxic sediments (equatorial North Pacific Ocean, NIXO area). *Oceanologica Acta*, 10, 281-291.
- Lallier-Vergès, E., Perrussel, B.P., Disnar, J.-R. and Baltzer, F. (1998) Relationship between environmental conditions and the diagenetic evolution of organic matter derived from higher plants in a modern mangrove swamp system (Guadeloupe, French West Indies). *Organic Geochemistry*, 29(5-7), 1663-1686.
- Langford, F.F. and Blanc-Valleron, M.-M. (1990) Interpreting Rock-Eval pyrolysis data using graphs of pyrolyzable hydrocarbons vs. total organic carbon. *AAPG Bulletin*, 74(6), 799-804.
- Larcher, A.V., Alexander, R. and Kagi, R.I. (1987) Differences in reactivities of sedimentary hopane diastereomers when heated in the presence of clays. *Advances in Organic Geochemistry*, 13(4-6), 665-669.
- Largeau, C., Derenne, S., Casadevall, E., Kadouri, A. and Sellier, N. (1986) Pyrolysis of immature Torbanite and of the resistant biopolymer (PRB A) isolated from extant alga *Botryococcus braunii*. Mechanism of formation and structure of Torbanite. In: *Advances in Organic Geochemistry 1985* (Ed. by D. Leythaeuser and J. Rullkötter); *Organic Geochemistry* 10, pp. 1023-1032. Pergamon Press, Oxford.
- Largeau, C., Derenne, S., Clairay, C., Casadevall, E., Raynaud, J.F., Lugardon, B., Berkaloff, C., Corolleur, M. and Rousseau, B. (1990) Characterization of various kerogens by scanning electron microscopy (SEM) and transmission electron microscopy (TEM) - morphological relationships with resistant outer cell walls in extant micro-organisms. *Meded. Rijks. Geol. Dienst*, 45, 91-101.
- Largeau, C. and Derenne, S. (1993) Relative efficiency of the selective Preservation and Degradation Recondensation pathway in kerogen formation. Source and environment influence on their contributions to type I and II kerogens. *Organic Geochemistry*, 20, 611-615.
- Larter, S.R. and Douglas, A.G. (1980) Melanoidins-kerogen precursors and geochemical lipid sinks: a study using pyrolysis gas chromatography (Py-GC). *Geochimica et Cosmochimica Acta*, 44, 2087-2095.
- Larter, S.R. and Horsfield, B. (1993) Determination of structural components of kerogens by the use of analytical pyrolysis methods. In: *Organic Geochemistry* (Ed. by M.H. Engel and A. Macko), pp. 287. Plenum Press, New York.
- Larter, S.R. and Aplin, A. (1995) Reservoir geochemistry: methods, applications and opportunities. In: *The Geochemistry of Reservoirs* (Ed. by J.M. Cubitt and W.A. England); *Geol. Soc. Spec. Publ. No. 86*, pp. 5-32. Geological Society, London.

- Larter, S.R., Bowler, B.F.J., Li, M., Chen, M., Brincat, D., Bennett, B., Noke, K., Donohoe, P., Simmons, D., Kohnen, M.L., Allan, J., Telnaes, N. and Horstad, I. (1996) Molecular indicators of secondary oil migration distances. *Nature*, 383, 593-597.
- Last, W.M. and de Deckker, P. (1990) Modern and Holocene carbonate sedimentology of two saline volcanic maar lakes, southern Australia. *Sedimentology*, 37(6), 967-981.
- Latham, D.R., Ferrin, C.R. and Ball, J.S. (1962) Identification of fluorenones in Wilmington petroleum by gas-liquid chromatography and spectrometry. *Analytical Chemistry*, 34, 311-313.
- Leavitt, P.R., Carpenter, S.R. and Kitchell, J.F. (1989) Whole lake experiments: The annual record of fossil pigments and zooplankton. *Limnol. Oceanogr.*, 34, 700-717.
- Leavitt, S.W. and Danzer, S.R. (1992) ^{13}C variations in C3 plants over the past 50,000 years. *Radiocarbon*, 34, 783-791.
- Lehman, S.J. and Keigwin, L.D. (1992) Sudden changes in North Atlantic circulation during the last deglaciation. *Nature*, 356, 757-762.
- Leroy, S.A.G., Zolitschka, B., Negendank, J.F.W. and Seret, G. (2000) Palynological analyses in the laminated sediment of Lake Holzmaar (Eifel, Germany): Duration of Lateglacial and Preboreal biozones. *Boreas*, 29, 52-71.
- Lewis, C.F.M., Mayer, L.A., Mukhopadhyay, P.K., Kruge, M.A., Coakley, J.P. and Smith, M.D. (2000) Multibeam sonar backscatter lineaments and anthropogenic organic components in lacustrine silty clay, evidence of shipping in western Lake Ontario. *International Journal of Coal Geology*, 43, 307-324.
- Li, D. (1980) Geological structure and hydrocarbon occurrence of the Bohai Gulf oil and gas basin (China). In: *Petroleum Geology in China* (Ed. by J.F. Mason), pp. 180-192. Penwell Books, Tulsa, OK.
- Li, J., Philp, R.P., Pu, F. and Allen, J. (1996) Long-chain alkenones in Qinghai Lake sediments. *Geochimica et Cosmochimica Acta*, 60(2), 235-241.
- Li, M., Larter, S.R. and Mei, B. (1994) Early generation of 20S-5 α (H),14 α (H),17 α (H)- and 5 α (H),14 β (H),17 β (H)-steranes in low salinity lacustrine shales. *Organic Geochemistry*, 22(6), 893-902.
- Li, M., Larter, S., Mei, B. and Wu, T. (1995a) Maturity assessment of immature oils produced from the Shaheje Formation of the Liaohe Basin, N. E. China. *17th Int. Meeting on Organic Geochemistry*, San Sebastian, 421-423.
- Li, M., Larter, S.R., Stoddart, D. and Bjorøy, M. (1995b) Fractionation of pyrrolic nitrogen compounds in petroleum during migration: derivation of migration-related geochemical parameters. In: *The Geochemistry of Reservoirs* (Ed. by J.M. Cubitt and W.A. England); *Geol. Soc. Spec. Publ. No. 86*, pp. 103-123. Geological Society, London.
- Li, M., Larter, S.R., Taylor, P., Jones, D.M., Bowler, B. and Bjorøy, M. (1995c) Biomarkers or not biomarkers? A new hypothesis for the origin of pristane involving derivation from methyltrimethyltridecylchromans (MTTCs) formed during diagenesis from chlorophyll and alkylphenols. *Organic Geochemistry*, 23(2), 159-167.
- Li, M., Fowler, M.G., Obermajer, M., Stasiuk, L.D. and Snowdon, L.R. (1999) Geochemical characterisation of Middle Devonian oils in NW Alberta, Canada: possible source and maturity effect on pyrrolic nitrogen compounds. *Organic Geochemistry*, 30, 1039-1057.
- Li, S. (1991) Liaohe field becomes China's premier heavy oil producer. *World Oil*, 212(11), 99.
- Lichtfouse, E., Derenne, S., Mariotti, A. and Largeau, C. (1994) Possible algal origin of long chain odd *n*-alkanes in immature sediments as revealed by distribution and carbon isotope ratios. *Organic Geochemistry*, 22, 1023-1027.
- Lichtfouse, E., Berthier, G., Houot, S., Barriuso, E., Bergheaud, V. and Vallaeys, T. (1995) Stable carbon evidence for the microbial origin of C₁₄-C₁₈ *n*-alkanoic acids in soils. *Organic Geochemistry*, 23(9), 849-852.
- Likens, G.E. (1975) Primary production of inland aquatic ecosystems. In: *Primary Productivity of the Biosphere* (Ed. by H. Lieth and R.H. Whittaker), pp. 186-215. Springer-Verlag, New York.

- Litt, T. and Stebich, M. (1999) Bio- and chronostratigraphy of the Lateglacial in the Eifel region, Germany. *Quaternary International*, 61, 5-16.
- Littke, R. (1993) Deposition, diagenesis and weathering of organic matter-rich sediments. *Lect. Notes in Earth Sci.*, 47, pp. 216.
- Littke, R. and Sachsenhofer, R.F. (1994) Organic petrology of deep sea sediments: a compilation of results from the Ocean Drilling Program and the Deep Sea Drilling Project. *Energy & Fuels*, 8, 1498-1512.
- Liu, H. (1986) Geodynamic Scenario and Structural Styles of Mesozoic and Cenozoic Basins in China. *AAPG Bulletin*, 70(4), 377-394.
- Lockheart, M.J., van Bergen, P.F. and Evershed, R.P. (1997) Variations in the stable carbon isotope compositions of individual lipids from the leaves of modern angiosperms: Implications for the study of higher plant-derived sedimentary organic matter. *Organic Geochemistry*, 26, 137-153.
- Lockheart, M.J., van Bergen, P.F. and Evershed, R.P. (2000) Chemotaxonomic classification of fossil leaves from the Miocene Clarkia lake deposit, Idaho, USA based on *n*-alkyl lipid distributions and principal component analyses. *Organic Geochemistry*, 31(11), 1223-1246.
- Lorenz, V. (2000) Formation of maar-diatreme volcanoes. *Spec. Issue of Terra Nostra*, 2000/6(International Maar Conference, Daun), 284-289.
- Loughnan, F.C. and Roberts, F.I. (1983) Buddingtonite (NH₄-feldspar) in the Condor Oilshale deposit, Queensland, Australia. *Mineralogical Magazine*, 47, 327-334.
- Loureiro, M.R. and Cardoso, J.N. (1990) Aromatic hydrocarbons in the Paraiba Valley oil shale. *Organic Geochemistry*, 15, 351-359.
- Lu, S., He, W. and Huang, H. (1990) The geochemical characteristics of heavy oil and its recovery in Liaohe Basin, China. In: *Advances in Organic Geochemistry 1989* (Ed. by A. Durand and F. Behar); *Organic Geochemistry* 16(1-3), pp. 437-449.
- Lücke, A. (1998) Die Sauerstoffisotope der biogenen Silikate des Holzmaares als mögliches Klimaarchiv. Eine limnologisch-hydrochemische, sedimentologische und isotopengeochemische Prozeßstudie. In: *Berichte des Forschungszentrum Jülich* No. 3523, pp. 90.
- Lücke, A., Vos, H., Schleser, G.H., Zolitschka, B. and Negendank, J.F.W. (2000) Carbon isotopes of lacustrine organic matter-an evaluation of variable carbon sources. *Spec. Issue of Terra Nostra*, 2000/6(International Maar Conference, Daun), 292-295.
- Lückge, A. (1997) Ablagerung und Frühdiagenese organischen Materials in marinen Hochproduktivitätsgebieten. Dissertation, RWTH-Aachen, pp. 161.
- Lyons, P.C. (2000) Funginite and secretinite-two new macerals of the inertinite group. *International Journal of Coal Geology*, 44, 95-98.
- Madigan**, M.T., Martinko, J.M. and Parker, J. (1997) *Brock Biology of Microorganisms*. Prentice-Hall, New Jersey, pp. 985.
- Maillard, L.C. (1912) Action des acides amines sur les sucres; formation des melanoidines par voie methodiques. *C.R. Acad. Sci. Paris*, 154, 66-68.
- Marino, B.D., McElroy, M.B., Salawich, R.J. and Spaulding, W.G. (1992) Glacial-to-interglacial variations in the carbon isotopic composition of atmospheric CO₂. *Nature*, 357, 461-466.
- Marynowski, L., Narkiewicz, M. and Grelowski, C. (2000) Biomarkers as environmental indicators in a carbonate complex, example from the Middle to Upper Devonian, Holy Cross Mountains, Poland. *Sedimentary Geology*, 137(3-4), 187-212.
- Matsuda, H. and Koyama, T. (1977) Early diagenesis of fatty acids in lacustrine sediments-I. Identification and distribution of fatty acids in recent sediments from a freshwater lake. *Geochimica et Cosmochimica Acta*, 41, 777-783.
- Matsumoto, G., Torii, T. and Hanya, T. (1982) High abundance of algal 24-ethylcholesterol in Antarctic lake sediments. *Nature*, 299, 52-54.
- Matthes, S. (1987) *Mineralogie*. Springer-Verlag, Berlin, Heidelberg, New York, pp. 444.

- Maxwell, J.R., Douglas, A.G., Eglington, E. and McCormick, A. (1968) The botryococenes - hydrocarbons of novel structure from the alga *Botryococcus braunii* Kützing. *Phytochemistry*, 7, 2157-2171.
- McCaffrey, M.A., Farrington, J.W. and Repeta, D.J. (1991) The organic geochemistry of Peru margin surface sediments: II. Paleoenvironmental implications of hydrocarbon and alcohol profiles. *Geochimica et Cosmochimica Acta*, 55, 483-498.
- McKenzie, J.A. (1985) Carbon isotopes and productivity in the lacustrine and marine environment. In: *Chemical Processes in Lakes* (Ed. by W. Stumm) Chapter 5, pp. 99-118. Wiley.
- McPherson, J.G., Shanmugam, G. and Moiola, R.J. (1987) Fan-deltas and braid deltas: varieties of coarse-grained deltas. *Geological Society of America Bulletin*, 99, 331-340.
- Meier, D. and Faix, O. (1992) Pyrolysis-Gas Chromatography-Mass Spectrometry. In: *Methods in Lignin Chemistry* (Ed. by S.Y. Lin and C.W. Dence); *Springer Series in Wood Science*, pp. 177-199. Springer, Berlin, Heidelberg.
- Mello, M.R., Telnaes, N., Gaglianone, P.C., Chicarelli, M.I., Brassell, S.C. and Maxwell, J.R. (1988) Organic geochemistry characterization of depositional palaeoenvironments in Brazilian marginal basins. *Organic Geochemistry*, 13, 31-46.
- Mello, M.R. and Maxwell, J.R. (1990) Organic geochemical biological marker characterization of source rocks and oils derived from lacustrine environments in the Brazilian continental margin. In: *Lacustrine Basin Exploration - Case Studies and Modern Analogues* (Ed. by B.J. Katz); *AAPG Memoir*, pp. 77-98.
- Merkt, J. and Müller, H. (1999) Varve chronology and palynology of the Lateglacial in Northwest Germany from lacustrine sediments of Hämelsee in Lower Saxony. *Quaternary International*, 61, 41-59.
- Mermoud, F., Gulacar, F.O. and Buchs, A. (1985) $5\alpha(H)$ -Cholestan- 3α -ol in sediments: characterization and geochemical significance. *Geochimica et Cosmochimica Acta*, 49, 450-462.
- Merritt, M.V., Rosenstein, S.P. and Loh, C. (1991) A comparison of the major lipid classes and fatty acids composition of marine unicellular cyanobacteria with freshwater species. *Archives of Microbiology*, 155, 107-113.
- Metzger, P., Casadevall, E., Pouet, M.J. and Pouet, J. (1985) Structures of some botryococenes: Branched hydrocarbons from the B-race of the green alga *Botryococcus braunii*. *Phytochemistry*, 24(12), 2995-3002.
- Metzger, P., Templier, J., Casadevall, E. and Couté, A. (1986) A *n*-alkatriene and some *n*-alkadienes from the A race of the green alga *Botryococcus braunii*. *Phytochemistry*, 25, 1869.
- Metzger, P. and Casadevall, E. (1987) Lycopadiene, a tetraterpenoid hydrocarbon from new strains of the green alga *Botryococcus braunii*. *Tetrahedron Letters*, 28, 3931-3934.
- Metzger, P., Casadevall, E. and Coute, A. (1988) Botryococcene distribution in strains of the green alga *Botryococcus braunii*. *Phytochemistry*, 27(5), 1383-1388.
- Meyer, W. (1994) *Geologie der Eifel*. E. Schweizerbart'sche Verlagsbuchhandlung, Stuttgart, pp. 618.
- Meyers, P.A. (1990) Impacts of regional Late Quaternary climate changes on the deposition of sedimentary organic matter in Walker Lake, Nevada. *Palaeogeography, Palaeoclimatology, Palaeoecology*, 78, 229-240.
- Meyers, P.A. and Ishiwatari, R. (1993) Lacustrine organic geochemistry - an overview of indicators of organic matter sources and diagenesis in lake sediments. *Organic Geochemistry*, 20(7), 867-900.
- Meyers, P.A. (1994) Preservation of elemental and isotopic source identification of sedimentary organic matter. *Chemical Geology*, 114, 289-302.
- Meyers, P.A. (1997) Organic geochemical proxies of paleoceanographic, paleolimnologic, and paleoclimatic processes. *Organic Geochemistry*, 27(5/6), 213-250.
- Meyers, P.A. and Lallier-Vergès, E. (1999) Lacustrine sedimentary organic matter records of late Quaternary paleoclimates. *Journal of Paleolimnology*, 21(3), 345-372.

- Mingram, J., Nowaczyk, N., Schettler, G., Luo, X., Jiaqi, L. and Negendank, J.F.W. (2000) A 78,000 year record of climatic changes from the South China coast-the Huguang maar lake (Huguangyan). *Spec. Issue of Terra Nostra*, 2000/6(International Maar Conference, Daun), 342-352.
- Mojelsky, T.W. and Strausz, O.P. (1986) Detection of methyl fluorenones in Athabasca oil sand bitumens. *Organic Geochemistry*, 9, 31-37.
- Moldowan, J.M., Seifert, W.K. and Gallegos, E.J. (1985) Relationship between petroleum and depositional environment of petroleum source rocks. *AAPG Bulletin*, 69(8), 1255-1268.
- Moldowan, J.M., Dahl, J.E., Huizinga, B.J., Fago, F.J., Hickey, L.J., Peakman, T.M. and Winship Taylor, D. (1994) The molecular fossil record of oleanane and its relation to angiosperms. *Science*, 265, 768-771.
- Moldowan, J.M., Dahl, J.E., Jacobsen, S.R., Huizinga, B.J., Fago, F.J., Shetty, R., Watt, D.S. and Peters, K.E. (1996) Chemostratigraphic reconstruction of biofacies: molecular evidence linking cyst-forming dinoflagellates with pre-Triassic ancestors. *Geology*, 24(2), 159-162.
- Moldowan, J.M., Zinniker, D., Dahl, J.E., Fago, F.J., Li, H. and Winship Taylor, D. (2001) Clues to the evolutionary roots of angiosperms from the molecular fossil oleanane. *20 th International Meeting on Organic Geochemistry*, Nancy, France, Abstracts Vol. 1, 95-96.
- Mook, W.G., Bommerson, J.C. and Staberman, W.H. (1974) Carbon isotope fractionation between dissolved bicarbonate and gaseous carbon dioxide. *Earth and Planetary Science Letters*, 22, 169-176.
- Morad, S., Ketzer, J.M. and de Ros, L.F. (2000) Spatial and temporal distribution of diagenetic alterations in siliciclastic rocks: implications for mass transfer in sedimentary basins. *Sedimentology*, 47(Suppl. 1), 95-120.
- Morrison, W.H. and Mulder, M.M. (1994) Pyrolysis mass spectrometry and pyrolysis gas chromatography-mass spectrometry of ester- and ether-linked phenolic acids in coastal Bermudagrass cell walls. *Phytochemistry*, 35(5), 1143-1151.
- Mukhopadhyay, P.K., Hagemann, H.W. and Gormly, J.R. (1985) Characterization of kerogens as seen under the aspect of maturation and hydrocarbon generation. *Erdöl und Kohle*, 38(1).
- Müller, A. and Mathesius, U. (1999) The palaeoenvironments of coastal lagoons in the southern Baltic Sea, I. The application of sedimentary Corg/N ratios as source indicators of organic matter. *Palaeogeography, Palaeoclimatology, Palaeoecology*, 145, 1-16.
- Müller, G. (1988) Salzgesteine (Evaporite). In: *Sedimente und Sedimentgesteine* (Ed. by H. Füchtbauer), pp. 1141. Schweizerbart'sche Verlagsbuchhandlung, Stuttgart.
- Müller, M.J. (1980) *Handbuch ausgewählter Klimastationen der Erde*. Forschungsstelle Bodenerosion Mertesdorf, Trier, pp. 346.
- Müller, P.J. (1977) C/N ratios in Pacific deep-sea sediments: Effects inorganic ammonium and nitrogen compounds sorbed by clays. *Geochimica et Cosmochimica Acta*, 41, 765-776.
- Muscio, G.P.A. and Horsfield, B. (1996) Neof ormation of inert carbon during the natural maturation of a marine source rock; Bakken Shale, Williston Basin. *Energy & Fuels*, 10, 10-18.
- Navale**, V. (1994) Comparative study of low and high temperature hydrous pyrolysis products of monoglycerol diether lipid from archaebacteria. *Journal of Analytical and Applied Pyrolysis*, 29, 33-43.
- Neev, D. and Emry, K.O. (1967) The Dead Sea - Depositional processes and environments of evaporites. *Geological Survey of Israel Bulletin*, 41, 1-147.
- Negendank, J.F.W. and Zolitschka, B. (1993) Maars and maar lakes of the Westeifel Volcanic Field. In: *Paleolimnology of European Maar Lakes* (Ed. by J.F.W. Negendank and B. Zolitschka); *Lecture Notes in Earth Sciences* 49, pp. 61-80. Springer, Berlin.
- Nemeth, K., Martin, U. and Philippe, M. (1999) Eroded porous-media aquifer controlled hydrovolcanic centers in the South Lake Balaton Region, Hungary: The Boglar Volcano. *Acta Geologica Hungarica*, 42(3), 251-266.

- Nip, M., Tegelaar, E.W., Brinkhuis, H., de Leeuw, J.W., Schenck, P.A. and Holloway, P.J. (1986a) Analysis of modern and fossil plant cuticles by Curie point Py-GC and Curie point Py-GC-MS: Recognition of a new, highly aliphatic and resistant biopolymer. In: *Advances in Organic Geochemistry 1985* (Ed. by D. Leythaeuser and J. Rullkötter); *Organic Geochemistry* **10**, pp. 769-778. Pergamon Press, Oxford.
- Nip, M., Tegelaar, E.W., de Leeuw, J.W., Schenck, P.A. and Holloway, P.J. (1986b) A new non-saponifiable highly aliphatic and resistant biopolymer in plant cuticles. Evidence from pyrolysis and ^{13}C -NMR analysis of present day and fossil plants. *Naturwissenschaften*, **73**, 579-585.
- Nishimura, M. and Koyama, T. (1976) Stenols and stanols in lake sediments and diatoms. *Chemical Geology*, **17**, 229-239.
- Nishimura, M. (1977) Origin of stanols in young lacustrine sediments. *Nature*, **270**, 711-712.
- Nishimura, M. and Koyama, T. (1977) The occurrence of stanols in various living organisms and the behaviour of sterols in contemporary sediments. *Geochimica et Cosmochimica Acta*, **41**, 379-385.
- Nishimura, M. (1982) 5β -isomers of stanols and stanones as potential markers of sedimentary organic quality and depositional paleoenvironments. *Geochimica et Cosmochimica Acta*, **46**, 423-432.
- Noel, D. and Rouchy, J.M. (1986) Transformations minérales in situ des frustules de diatomées du Miocene d'Egypte. Double voie de la diagenese: silification et argilocinèse. *C.R. Acad. Sci. Paris*, **303**, 1743-1748.
- Noël, H., Garbolino, E., Brauer, A., Lallier-Vergès, E., Beaulieu, J.-L.d. and Disnar, J.-R. (2001) Human impact and soil erosion during the last 5000 yrs as recorded in lacustrine sedimentary organic matter at Lac d'Annecy, the French Alps. *Journal of Paleolimnology*, **25**(2), 229-244.
- Nriagu, J.O. and Soon, Y.K. (1985) Distribution and isotopic composition of sulfur in lake sediments of northern Ontario. *Geochimica et Cosmochimica Acta*, **49**, 823-834.
- O'Leary**, M.H. (1988) Carbon isotopes in photosynthesis. *Bioscience*, **38**(5), 328-336.
- Öborn, I. and Berggren, D. (1995) Characterization of jarosite-natrojarosite in two northern Scandinavian soils. *Geoderma*, **66**(3-4), 213-225.
- Oehms, M. (1995) Zur Limnologie des Holzmaares. In: *Das Holzmaar und seine Sedimente, Tagungsband zum Symposium* (Ed. by GeoForschungsZentrum Potsdam), pp. 8, Scientific Technical Report STR95/16.
- Ogura, K., Machihara, T. and Takada, H. (1989) Diagenesis of biomarkers in Biwa Lake sediments over 1 million years. *Organic Geochemistry*, **16**, 805-813.
- Oliver, J. (1986) Fluids expelled tectonically from orogenic belts: their role in hydrocarbon migration and other geologic phenomena. *Geology*, **14**, 99-102.
- Orr, W.L. (1986) Kerogen/asphaltene/sulphur relationships in sulphur rich Monterey oils. In: *Advances in Organic Geochemistry 1985* (Ed. by D. Leythaeuser and J. Rullkötter); *Organic Geochemistry* **10**, pp. 499-516. Pergamon Press, Oxford.
- Osterkamp, W.R. and Wood, W.W. (1987) Playa-lake basin on the southern high plains of Texas and New Mexico: Part I. Hydrologic, geomorphic, and geologic evidence for their development. *Geological Society of America Bulletin*, **99**, 215-223.
- Otto, A., Walther, H. and Püttmann, W. (1994) Molecular composition of a leaf- and root-bearing Oligocene lake clay in Weissenster Basin, Germany. *Organic Geochemistry*, **22**, 275-286.
- Ourisson, G., Albrecht, P. and Rohmer, M. (1984) The microbial origin of fossil fuels. *Scientific American*, **251**, 44-51.
- Palmisano**, A.C., Summons, R.E., Cronin, S.E. and des Marias, D.J. (1989) Lipophilic pigments from cyanobacterial (blue-green algal) and diatom mats in Hamelin Pool, Shark Bay, Western Australia. *Journal of Phycology*, **25**, 655-661.
- Pastorova, I., Botto, R.E., Arisz, P.W. and Boon, J.J. (1994) Cellulose char structure: a combined analytical Py-GC-MS, FTIR, and NMR study. *Carbohydrate Research*, **262**, 27-47.

- Patience, A.J., Lallier-Vergès, E., Sifeddine, A., Albéric, P. and Guillet, B. (1995) Organic fluxes and early diagenesis in the lacustrine environment: the superficial sediments of the Lac du Bouchet (Haute Loire, France). In: *Organic Matter Accumulation* (Ed. by E. Lallier-Vergès, N.P. Tribouillard and P. Bertrand); *Lecture Notes in Earth Sciences, Vol. 57*, pp. 145-156. Springer-Verlag, Heidelberg.
- Patience, R.L., Clayton, C.J., Kearsley, A.T., Rowland, S.J., Bishop, A.N., Rees, A.G.W., Bibby, K.G. and Hopper, A.C. (1990) An integrated biochemical, geochemical and sedimentological study of organic diagenesis in sediments from ODP Leg 112. *Proc. ODP Sci. Results*, 112, 135-153.
- Patience, R.L., Baxby, M., Bartle, K.D., Perry, D.L., Rees, A.G.W. and Rowland, S.J. (1992) The functionality of nitrogen in some recent sediments from the Peru upwelling region. *Organic Geochemistry*, 18(2), 161-169.
- Patino, F., Salinas, E., Cruells, M. and Roca, A. (1998) Alkaline decomposition-cyanidation kinetics of argentinean natrojarosite. *Hydrometallurgy*, 49(3), 323-336.
- Peakman, T.M., ten Haven, H.L., Rechka, J.R., de Leeuw, J.W. and Maxwell, J.R. (1989) Occurrence of (20R)- and (20S)- $\Delta^{8(14)}$ and Δ^{14} 5 α (H),14 β (H),14 β (H)-steranes in an immature sediment. *Geochimica et Cosmochimica Acta*, 53, 2001-2009.
- Pelejero, C., Grimalt, J.O., Sarnthein, M., Wang, L. and Flores, J.-A. (1999) Molecular biomarker record of sea surface temperature and climatic change in the South China Sea during the last 140,000 years. *Marine Geology*, 156, 109-121.
- Pepper, A.S. and Corvi, P.J. (1995) Simple kinetic models of petroleum formation. Part I: oil and gas generation from kerogen. *Marine and Petroleum Geology*, 12(3), 291-319.
- Perry, E. and Hower, J. (1970) Burial diagenesis in Gulf Coast pelitic sediments. *Clays and Clay minerals*, 18, 165-177.
- Peters, K.E., Rohrback, B.G. and Kaplan, I.R. (1981) Geochemistry of artificially heated humic and sapropelic sediments - I: protokerogen. *AAPG Bulletin*, 65, 688-705.
- Peters, K.E. and Moldowan, J.M. (1991) Effects of source, thermal maturity, and biodegradation on the distribution and isomerization of homohopane in petroleum. *Organic Geochemistry*, 17, 47-61.
- Peters, K.E. and Moldowan, J.M. (1993) *The Biomarker Guide: Interpreting Molecular Fossils in Petroleum and Ancient Sediments*. Prentice Hall, New Jersey, pp. 363.
- Peters, K.E., Cunningham, A.E., Walters, C.C., Jiang, J. and Fan, Z. (1996) Petroleum systems in the Jiangling-Dangyang area, Jiangnan Basin, China. *Organic Geochemistry*, 24(10/11), 1035-1060.
- Peters, K.E., Snedden, J.W., Sulaeman, A., Sarg, J.F. and Enrico, R.J. (2000) New geochemical-sequence stratigraphic model for the Mahakam Delta and Makassar Slope, Kalimantan. *AAPG Bulletin*, 84(1), 12-44.
- Peulvé, S., de Leeuw, J.W., Sicre, M.-A., Baas, M. and Saliot, A. (1996) Characterization of macromolecular organic matter in sediment traps from the northwestern Mediterranean Sea. *Geochimica et Cosmochimica Acta*, 60(7), 1239-1259.
- Philp, R.P. and Fan, Z.F. (1987) Geochemical investigation of oils and source rocks from Qianjiang Depression of Jiangnan Basin, a terrigenous saline basin, China. *Organic Geochemistry*, 11, 549-562.
- Picard, M.D. and High, L.R. (1981) Physical stratigraphy of ancient lacustrine deposits. In: *Recent and Ancient Nonmarine Depositional Environments: Models for Exploration* (Ed. by E.G. Etheridge and R.M. Flores) 31, pp. 233-259. Soc. Econ. Paleontol. Mineral. Spec. Publ.
- Pokras, E.M. and Mix, A.C. (1985) Eolian evidence for spatial variability of Late Quaternary climates in tropical Africa. *Quaternary Research*, 24, 137-149.
- Pontér, C., Ingri, J., Burman, J.O. and Boström, K. (1990) Temporal variations in dissolved and suspended iron and manganese in the Kalix River, northern Sweden. *Chemical Geology*, 81, 121-131.
- Posthumus, M.A., Nibbering, N.M., Boerboom, A.J.H. and Schulen, H.R. (1974) Pyrolysis mass spectrometric studies on nucleic acids. *Biomedical Mass Spectrometry*, 1, 352-357.

- Pouwels, A.D., Tom, A., Eijkel, G.B. and Boon, J.J. (1987) Characterization of beech wood and its holocellulose and xylan fractions by pyrolysis-gas chromatography-mass spectrometry. *Journal of Analytical and Applied Pyrolysis*, 11, 417-436.
- Pouwels, A.D., Eijkel, G.B. and Boon, J.J. (1989) Curie-point pyrolysis-capillary gas chromatographie-high resolution mass spectrometry of microcrystalline cellulose. *Journal of Analytical and Applied Pyrolysis*, 14, 237-280.
- Powell, T.G. and McKirdy, D.M. (1973) Relationship between ratio of pristane to phytane, crude oil composition and geological environment in Australia. *Nature*, 243, 37-39.
- Powell, T.G. (1986) Petroleum geochemistry and depositional setting of lacustrine source rocks. *Marine and Petroleum Geology*, 3, 200-219.
- Powell, T.G. (1987) Pristane/phytane ratio as environmental indicator. *Nature*, 333, 604.
- Radke**, M., Sittardt, H.G. and Welte, D.H. (1978) Removal of soluble organic matter from source rock samples with a flow through extraction cell. *Analytical Chemistry*, 50, 663-665.
- Radke, M., Willsch, H. and Welte, D.H. (1980) Preparative hydrocarbon group type determination by automated medium pressure liquid chromatography. *Analytical Chemistry*, 52, 406-411.
- Radke, M. and Welte, D.H. (1981) The Methylphenanthrene Index (MPI): A maturity parameter based on aromatic hydrocarbons. *Advances in Organic Geochemistry 1981*, 504-512.
- Radke, M., Welte, D.H. and Willsch, H. (1982) Geochemical study on a well in the Western Canada Basin: relation of the aromatic distribution pattern to maturity of organic matter. *Geochimica et Cosmochimica Acta*, 46, 1-10.
- Radke, M., Welte, D.H. and Willsch, H. (1991) Distribution of alkylated aromatic hydrocarbons and dibenzothiophenes in rocks of the Upper Rhine Graben. *Chemical Geology*, 93, 325-341.
- Radke, M. and Willsch, H. (1993) Generation of alkylbenzenes and benzo[b]thiophenes by artificial thermal maturation of sulfur-rich coal. *Fuel*, 72(8), 1103-1108.
- Radke, M. and Willsch, H. (1994) Extractable alkyldibenzothiophenes in Posidonia Shale (Toarcian) source rocks. *Geochimica et Cosmochimica Acta*, 58, 5223-5244.
- Ragan, M.A. and Jensen, A. (1978) Quantitative studies on brown algal phenols. II. Seasonal variation in polyphenol content of *Ascophyllum nodosum* (L.) Le Jol. and *Fucus vesiculosus*. *J. exp. mar. Biol. Ecol.*, 34, 245-258.
- Ragan, M.A. and Glombitza, K.W. (1986) Plorotannins brown algal polyphenols. *Progress in Phycology Research*, 4, 129-241.
- Ramdahl, T. and Becher, G. (1982) Characterisation of polynuclear aromatic hydrocarbon derivatives in emissions from wood and cereal straw combustion. *Analytica Chimica Acta*, 144, 83-91.
- Ramseyer, K., Diamond, L.W. and Boles, J.R. (1993) Authigenic K-NH₄-feldspar in sandstones: a fingerprint of the diagenesis of organic matter. *Journal of Sedimentary Research*, 63, 1092-1099.
- Ratledge, C. and Wilkinson, S.G. (1988) Structures of Lipids. Terpenoid lipids. In: *Microbial Lipids* (Ed. by C. Ratledge and S.G. Wilkinson) 1, pp. 72. Academic Press, London.
- Reed, W.E. (1977) Biogeochemistry of Mono Lake, California. *Geochimica et Cosmochimica Acta*, 41, 1231-1245.
- Remy, R.R. and Ferrell, R.E. (1989) Distribution and origin of analcime in marginal lacustrine mudstones of the Green River Formation, south-central Uinta Basin, Utah. *Clays and Clay minerals*, 37, 419-432.
- Renaut, R.W. (1993) Zeolitic diagenesis of late Quaternary fluviolacustrine sediments and associated calcrete formation in the Lake Bogoria Basin, Kenya Rift Valley. *Sedimentology*, 40, 271-301.
- Renaut, R.W. and Tiercelin, J.-J. (1994) Lake Bogoria, Kenya rift valley - a sedimentological overview. In: *Sedimentology and Geochemistry of Modern and Ancient Saline Lakes* (Ed. by R.W. Renaut and W.M. Last), pp. 101-123. Spec. Pub. Soc. econ. Paleont. Miner., Vol. 50.
- Requejo, A.G., Allan, J., Creaney, S., Gray, N.R. and Cole, K.S. (1992) Aryl isoprenoids and diaromatic carotenoids in Paleozoic source rocks and oils from the Western Canada and Williston

- Basins. In: *Advances in Organic Geochemistry 1991* (Ed. by C. Eckhardt and J.R. Maxwell); *Organic Geochemistry* **19**(1-3), pp. 245-264.
- Requejo, A.G., Sassen, R., McDonald, T., Denoux, G., II, M.C.K. and Brooks, J.M. (1996) Polynuclear aromatic hydrocarbons (PAH) as indicators of the source and maturity of marine crude oils. *Organic Geochemistry*, **24**(10-11), 1017-1033.
- Riding, R. (2000) Microbial carbonates: the geological record of calcified bacterial-algal mats and biofilms. *Sedimentology*, **47**(Suppl. 1), 179-214.
- Rieley, G., Collier, R.J., Jones, D.M. and Eglinton, G. (1991a) The biogeochemistry of Ellesmere Lake, U.K. - I. Source correlation of leaf wax inputs to the sedimentary record. *Organic Geochemistry*, **17**, 901-912.
- Rieley, G., Collister, J.W., Jones, D.M., Eglinton, G., Eakin, P.A. and Fallick, A.E. (1991b) Sources of sedimentary lipids deduced from stable isotope analyses of individual compounds. *Nature*, **352**, 425-427.
- Ritts, B.D., Hanson, A.D., Zinniker, D. and Moldowan, J.M. (1999) Lower-Middle Jurassic nonmarine source rocks and petroleum systems of the northern Qaidam basin, Northwest China. *AAPG Bulletin*, **83**(12), 1980-2005.
- Robert, P. (1981) Classification of organic matter by means of fluorescence, applications to hydrocarbon source rocks. *International Journal of Coal Geology*, **1**, 101-137.
- Robinson, N., Cranwell, P.A., Finlay, B.J. and Eglinton, G. (1984) Lipids of aquatic organisms as potential contributors to lacustrine sediments. *Organic Geochemistry*, **6**, 143-152.
- Robinson, N., Cranwell, P.A., Eglinton, G., Brassell, S.C., Sharp, C.L., Gophen, M. and Pollinger, U. (1986) Lipid geochemistry of Lake Kinneret. *Organic Geochemistry*, **10**, 733-742.
- Rohmer, M., Bouvier-Nave, P. and Ourisson, G. (1984) Distribution of hopanoid triterpenes in prokaryotes. *J. Gen. Microbiol.*, **130**, 1137-1150.
- Rohmer, M. (1993) The biosynthesis of triterpenoids of hopane series in eubacteria: a mime of enzyme reactions. *Pure Applied Chemistry*, **65**, 1293-1298.
- Rohrback, B.G., Peters, K.E., Sweeney, R.E. and Kaplan, I.R. (1983) Ammonia formation in laboratory-simulated thermal maturation: implications related to the origin of nitrogen in natural gas. In: *Advances in Organic Geochemistry 1981* (Ed. by M. Bjorøy), pp. 819-823. J. Wiley and Sons, New York.
- Rosendahl, B.R. (1987) Architecture of continental rifts with special reference to East Africa. *Annual Review of Earth Planetary Science*, **15**, 445-503.
- Rouchy, J.M., Noel, D., Wali, A.M.A. and Aref, M.A.M. (1995) Evaporitic and biosiliceous cyclic sedimentation in the Miocene of the Gulf of Suez - depositional and diagenetic aspects. *Sedimentary Geology*, **94**(3-4), 277-297.
- Rowland, S.J. (1990) Production of acyclic isoprenoid hydrocarbons by laboratory maturation of methanogenic bacteria. *Organic Geochemistry*, **15**, 9-16.
- Roy, S. (1992) Environments and processes of manganese deposition. *Economic Geology*, **87**, 1213-1236.
- Rubinsztain, Y., Ioselis, P., Ikan, R. and Aizenshtat, Z. (1984) Investigations on the structural units of melanoidins. *Organic Geochemistry*, **6**, 791-804.
- Rudd, J.W.M., Kelly, C.A. and Furutani, A. (1986) The role of sulfate reduction in long term accumulation of organic and inorganic sulfur in lake sediments. *Limnol. Oceanogr.*, **31**(6), 1281-1291.
- Rullkötter, J., Spiro, B. and Nissenbaum, A. (1985) Biological marker characteristics of oils and asphalts from carbonate source rocks in a rapidly subsiding graben, Dead Sea, Israel. *Geochimica et Cosmochimica Acta*, **49**, 1357-1370.
- Rullkötter, J. and Marzi, R. (1988) Natural and artificial maturation of biological markers in a Toarcian shale from northern Germany. *Organic Geochemistry*, **13**, 639-645.

- Rullkötter, J., Littke, R. and Schaefer, R.G. (1990) Characterization of organic matter in sulfur-rich lacustrine sediments of Miocene age (Nördlinger Ries, Southern Germany). In: *Geochemistry of sulfur in fossil fuels* (Ed. by W.L. Orr and C.M. White), pp. 149-169. American Chemical Society, Washington.
- Ryder, R.T., Fouch, T.D. and Elison, J.H. (1976) Early Tertiary sedimentation in the western Uinta Basin, Utah. *Geological Society of America Bulletin*, 87, 496-512.
- Sachsenhofer**, R.F., Curry, D.J., Horsfield, B., Rantitsch, G. and Wilkes, H. (1995) Characterization of organic matter in late Cretaceous black shales of the Eastern Alps (Kainach Gosau Group, Austria). *Organic Geochemistry*, 23(10), 915-929.
- Saiz-Jimenez, C. and de Leeuw, J.W. (1984) Pyrolysis-gas chromatography-mass spectrometry of isolated, synthetic and degraded lignins. In: *Advances in Organic Geochemistry 1983* (Ed. by P.A. Schenck, J.W. de Leeuw and G.W.M. Lijubach); *Organic Geochemistry* 6, pp. 417-422. Pergamon Press, Oxford.
- Saiz-Jimenez, C. and de Leeuw, J.W. (1986a) Chemical characterization of soil organic matter fractions by analytical pyrolysis-gas chromatography-mass spectrometry. *Journal of Analytical and Applied Pyrolysis*, 9, 99-119.
- Saiz-Jimenez, C. and de Leeuw, J.W. (1986b) Lignin pyrolysis products: Their structures and their significance as biomarkers. In: *Advances in Organic Geochemistry 1985* (Ed. by D. Leythaeuser and J. Rullkötter); *Organic Geochemistry* 10, pp. 869-876. Pergamon Press, Oxford.
- Sanger, J.E. (1988) Fossil Pigments in paleoecology and paleolimnology. *Palaeogeography, Palaeoclimatology, Palaeoecology*, 62, 343-359.
- Santamaría-Orozco, D., Horsfield, B., Primio, R.d. and Welte, D.H. (1998) Influence of maturity on distributions of benzo- and dibenzothiophenes in Tithonian source rocks and crude oils, Sonda de Campeche, Mexico. *Organic Geochemistry*, 28(7-8), 423-439.
- Schaefer, R.G., Schenk, H.J., Hardelauf, H. and Harms, R. (1990) Determination of gross kinetic parameters for petroleum formation from Jurassic source rocks of different maturity levels by means of laboratory experiments. In: *Advances in Organic Geochemistry 1989* (Ed. by A. Durand and F. Behar) *Organic Geochemistry*, 16(1-3), pp. 115-120. Pergamon Press, Oxford.
- Schaeffer, P., Adam, P., Trendel, J.-M., Albrecht, P. and Connan, J. (1995) A novel series of benzohopanes widespread in sediments. *Organic Geochemistry*, 23, 87-89.
- Schaeffer, P., Adam, P., Wehrung, P. and Albrecht, P. (1997) Novel aromatic carotenoids derivatives from sulfur photosynthetic bacteria in sediments. *Tetrahedron Letters*, 38(48), 8413-8416.
- Scharf, B.W. and Ehlscheid, T. (1992) Summary of paleolimnological investigations with special reference to Late Quaternary trophic variations. In: *Limnology of Eifel maar lakes* (Ed. by B.W. Scharf and S. Björk); *Advances in Limnology* 38, pp. 33-41. Schweizerbart'sche Verlagsbuchhandlung, Stuttgart.
- Scharf, B.W. and Menn, U. (1992) Hydrology and morphometry. In: *Limnology of Eifel maar lakes* (Ed. by B.W. Scharf and S. Björk); *Advances in Limnology* 38, pp. 43-62. Schweizerbart'sche Verlagsbuchhandlung, Stuttgart.
- Scharf, B.W. and Oehms, M. (1992) Physical and chemical characteristics. In: *Limnology of Eifel maar lakes* (Ed. by B.W. Scharf and S. Björk); *Advances in Limnology* 38, pp. 63-83. Schweizerbart'sche Verlagsbuchhandlung, Stuttgart.
- Schenk, H.J., di Primio, R. and Horsfield, B. (1997) The conversion of oil into gas in petroleum reservoirs. Part 1: Comparative kinetic investigation of gas generation from crude oils of lacustrine, marine and fluviodeltaic origin by programmed-temperature closed-system pyrolysis. *Organic Geochemistry*, 26(7/8), 467-481.
- Schenk, H.J. and Horsfield, B. (1998) Using natural maturation series to evaluate the utilization of parallel reaction kinetic models: an investigation of Toarcian shales and Carboniferous Coals. *Organic Geochemistry*, 29(1/3), 137-154.
- Schettler, G. and Romer, R.L. (1998) Anthropogenic influences on Pb/Al and lead isotope signature in annually layered Holocene Maar lake sediments. *Applied Geochemistry*, 13(6), 787-797.

- Schmidt, K. (1978) Biosynthesis of carotenoids. In: *Photosynthetic Bacteria* (Ed. by R.K. Clayton and W.R. Siström), pp. 729-750. Plenum Press, New York.
- Schmitter, J.M., Arpino, P.J. and Guiochon, G. (1981) Isolation of degraded pentacyclic triterpenoid acids in a Nigerian crude oil and their identification as tetracyclic carboxylic acids resulting from ring A cleavage. *Geochimica et Cosmochimica Acta*, 45, 1951-1955.
- Schnitzer, M. (1977) Recent findings on the characterization of humic substances extracted from soils from widely differing climatic zones. *IAEA-SM-211/7*, 117-132.
- Schoell, M., Teschner, M., Wehner, M., Durand, B. and Oudin, J.L. (1983) Maturity related biomarker and stable isotope variations and their application to oil/source rock correlation in the Mahakam Delta, Kalimantan. In: *Advances in Organic Geochemistry 1981* (Ed. by M. Bjorøy), pp. 156-163. J. Wiley and Sons, New York.
- Schreiber, B.C. and El Tabakh, M. (2000) Deposition and early alteration of evaporites. *Sedimentology*, 47(Suppl. 1), 215-238.
- Schubert, C.J., Ferdelman, T.G. and Strotmann, B. (2000) Organic matter composition and sulfate reduction rates in sediments off Chile. *Organic Geochemistry*, 31(5), 351-361.
- Schwark, L., Schulz, U., Vliex, M., Spitthoff, B. and Leythaeuser, D. (1996) Impact of Volcanic Ash Flows on the Biological Communities in an Oligocene Lacustrine Environment - An Organic Geochemical Approach. *Goldschmidt Conference, Abstracts*, Vol. 1, 554.
- Schwertmann, U. (1961) Über das Vorkommen und die Entstehung von Jarosit in Marschböden (Maibolt). *Naturwissenschaften*, 45, 159-160.
- Schwoerbel, J. (1993) *Einführung in die Limnologie*. Gustav Fischer Verlag, Stuttgart, Jena, pp. 387.
- Seifert, W.K. and Moldowan, J.M. (1978) Applications of steranes, terpanes and monoaromatics to the maturation, migration and source of crude oils. *Geochimica et Cosmochimica Acta*, 42, 77-95.
- Seifert, W.K. and Moldowan, J.M. (1980) The effect of thermal stress on source-rock quality as measured by hopane stereochemistry. In: *Advances in Organic Geochemistry 1979* (Ed. by A.G. Douglas and J.R. Maxwell), pp. 229-237. Pergamon, Oxford.
- Seifert, W.K., Carlson, R.M.K. and Moldowan, J.M. (1983) Geomimetic synthesis, structure assignment, and geochemical correlation application of monoaromatized petroleum steranes. In: *Advances in Organic Geochemistry 1981* (Ed. by M. Bjorøy), pp. 710-724. J. Wiley and Sons, New York.
- Seifert, W.K. and Moldowan, J.M. (1986) Use of biological markers in petroleum exploration. In: *Biological markers in the sedimentary record* (Ed. by R.B. Johns), pp. 261-290. Elsevier.
- Senftle, J.T., Brown, J.H. and Larter, S.R. (1987) Refinement of organic petrographic methods for kerogen characterization. *Int. Journal of Coal Geology*, 7, 105-117.
- Severinghaus, J.P. and Brook, E.J. (1999) Abrupt climate change at the end of the last glacial period inferred from trapped air in polar ice. *Science*, 286(29 October), 930-934.
- Sheng, G., Cai, K., Yang, X., Lu, J., Jia, G., Peng, P. and Fu, J. (1999) Long-chain alkenones in Hotong Qagan Nur Lake sediments and its paleoclimatic implications. *Chinese Science Bulletin*, 44(3), 259-263.
- Sherwood, N.R., Cook, A.C., Gibling, M. and Tantisukrit, C. (1984) Petrology of a suite of sedimentary rocks associated with some coal-bearing basins in northwestern Thailand. *International Journal of Coal Geology*, 4, 45-71.
- Shi, Y., Yu, G., Liu, X., Li, B. and Yao, T. (2001) Reconstruction of the 30-40 ka BP enhanced Indian monsoon climate based on geological records from the Tibetan Plateau. *Palaeogeography, Palaeoclimatology, Palaeoecology*, 169(1-2), 69-83.
- Shyu, J.-P., Chen, M.-P., Shieh, Y.-T. and Huang, C.-K. (2001) A Pleistocene paleoceanographic record from the north slope of the Spratly Islands, southern South China Sea. *Marine Micropaleontology*, 42(1-2), 61-93.

- Sicre, M.-A., Peulve, S., Saliot, A., de Leeuw, J.W. and Baas, M. (1994) Molecular characterisation of the organic fraction of suspended matter in the surface waters and bottom nepheloid layer of the Rhone delta using analytical pyrolysis. *Organic Geochemistry*, 21(1), 11-26.
- Sifeddine, A., Bertrand, P., Lallier-Vergès, E. and Patience, A.J. (1996) Lacustrine organic fluxes and paleoclimatic variations during the last 15 ka: Lac du Bouchet (Massif Central, France). *Quaternary Science Reviews*, 15, 203-211.
- Sigleo, A.C., Hoering, T.C. and Helz, G.R. (1982) Composition of estuarine colloidal material: organic components. *Geochimica et Cosmochimica Acta*, 46, 1619-1626.
- Singer, A. and Stoffers, P. (1980) Clay mineral diagenesis in two East African lake sediments. *Clay Minerals*, 15, 291-307.
- Sinninghe Damsté, J.S., Kock-van Dalen, A.C., de Leeuw, J.W., Schenck, P.A., Sheng, G. and Brassell (1987) The identification of mono-, di- and trimethyl 2-methyl-2(4,8,12-trimethyltridecyl)chromans and their occurrence in the geosphere. *Geochimica et Cosmochimica Acta*, 51, 2393-2400.
- Sinninghe Damsté, J.S., Rijpstra, W.I.C., Kock-van Dalen, A.C., de Leeuw, J.W. and Schenck, P.A. (1989) Quenching of labile functionalised lipids by inorganic sulphur species: Evidence for the formation of sedimentary organic sulphur compounds at the early stages of diagenesis. *Geochimica et Cosmochimica Acta*, 53, 1343-1355.
- Sinninghe Damsté, J.S. and de Leeuw, J.W. (1990) Analysis, structure and geochemical significance of organically-bound sulphur in the geosphere: State of the art and future research. In: *Advances in Organic Geochemistry 1989* (Ed. by A. Durand and F. Behar); *Organic Geochemistry* 16(4-6), pp. 1077-1101.
- Sinninghe Damsté, J.S., Eglinton, T.I. and de Leeuw, J.W. (1992) Alkylpyrroles in a kerogen pyrolysate: Evidence for abundant tetrapyrrole pigments. *Geochimica et Cosmochimica Acta*, 56, 1743-1751.
- Sinninghe Damsté, J.S., Keely, B.J., Betts, S.E., Baas, M., Maxwell, J.R. and de-Leeuw, J.W. (1993a) Variations in abundances and distributions of isoprenoid chromans and long-chain alkylbenzenes in sediments of the Mulhouse Basin; a molecular sedimentary record of palaeosalinity. *Organic Geochemistry*, 20(8), 1201-1215.
- Sinninghe Damsté, J.S., Xavier, F., de Las Heras, C., van Bergen, P.F. and de Leeuw, J.W. (1993b) Characterization of Tertiary Catalan lacustrine oil shales: Discovery of extremely organic sulphur-rich Type I kerogens. *Geochimica et Cosmochimica Acta*, 57, 389-415.
- Sinninghe Damsté, J.S., Kenig, F., Koopmans, M.P., Köster, J., Schouten, S., Hayes, J.M. and de Leeuw, J.W. (1995) Evidence for gammacerane as an indicator of water column stratification. *Geochimica et Cosmochimica Acta*, 59(9), 1895-1900.
- Sinninghe Damsté, J.S., Schouten, S. and van Duin, A.C.T. (2001) Isorenieratene derivatives in sediments: possible controls on their distribution. *Geochimica et Cosmochimica Acta*, 65(10), 1557-1571.
- Sirocko, F., Sarnthein, M., Erlenkeuser, H., Lange, H., Aarnold, M. and Duplessy, J.C. (1993) Century-scale events in monsoonal climate over the past 24,000 years. *Nature*, 364, 322-324.
- Skinner, H.C. (1963) Precipitation of calcian dolomites and magnesian calcites in the southeast of South Australia. *American Journal of Science*, 261, 449-472.
- Smith, W.D. and Gibling, M.R. (1987) Oilshale composition related to depositional setting: a case study from the Albert Formation, New Brunswick, Canada. *Bull. Can. Pet. Geol.*, 35, 469-487.
- Snyder, L.R. (1965) Distribution of benzocarbazole isomers in petroleum as evidence for their biogenic origin. *Nature*, 205, 277.
- Spiker, E.C. and Hatcher, P.G. (1984) Carbon isotope fractionation of sapropelic organic matter during early diagenesis. *Organic Geochemistry*, 5, 283-290.
- Spiker, E.C. and Hatcher, P.G. (1987) The effects of early diagenesis on the chemical and stable carbon isotopic composition of wood. *Geochimica et Cosmochimica Acta*, 51, 1385-1391.
- Stafford, H.A. (1988) Proanthocyanidins and the lignin connection. *Phytochemistry*, 27, 1-6.

- Stankiewicz, B.A., Briggs, D.E.G., Evershed, R.P., Flannery, M.B. and Wuttke, M. (1997a) Preservation of chitin in 25-million-year-old fossil. *Science*, 276, 1541-1543.
- Stankiewicz, B.A., Mastalerz, M., Kruger, M.A., Bergen, P.F.v. and Sadowska, A. (1997b) A comparative study of modern and fossil cone scales and seeds of conifers. *New Phytol.*, 135, 375-393.
- Stankiewicz, B.A., Mastalerz, M., Hof, C.H.J., Bierstedt, A., Flannery, M.B., Briggs, D.E.G. and Evershed, R.P. (1998) Biodegradation of the chitin-protein complex in crustacean cuticle. *Organic Geochemistry*, 28(1/2), 67-76.
- Stasiuk, L.D., Osadetz, K.G., Goodarzi, F. and Gentzis, T. (1991) Organic microfacies and basinal tectonic control on source rock accumulation: a microscopic approach with examples from an intracratonic and extensional basin. *International Journal of Coal Geology*, 19, 457-481.
- Stasiuk, L.D. (1993) Algal bloom episodes and the formation of bituminite and micrinite in hydrocarbon source rocks: evidence from the Devonian and Mississippian, northern Williston Basin, Canada. *International Journal of Coal Geology*, 24, 195-210.
- Stasiuk, L.D. (1999) Microscopic studies of sedimentary organic matter: Key to understanding organic-rich strata, with Paleozoic examples from Western Canada Basin. *Geoscience Canada*, 26(4), 149-172.
- Stasiuk, L.D. and Sanei, H. (2001) Characterization of diatom-derived lipids and chlorophyll within Holocene laminites, Saanich Inlet, British Columbia, using conventional and laser scanning fluorescence microscopy. *Organic Geochemistry*, 32(12), 1417-1428.
- Stoffers, P. and Hecky, R.E. (1978) Late Pleistocene-Holocene evolution of the Kivu-Tanganyika Basin. In: *Modern and Ancient Lake Sediments* (Ed. by A. Matter and M.E. Tucker); *Special Publication 2*, pp. 43-55. International Association of Sedimentologists, Oxford.
- Stoffers, P. and Singer, A. (1979) Clay Minerals in Lake Mobuto Sese Seko (Lake Albert) - their Diagenetic Changes as an Indicator of the Paleoclimate. *Geologische Rundschau*, 68(3), 1009-1024.
- Stout, S.A. and Boon, J.J. (1994) Structural characterization of the organic polymers comprising a lignite's matrix and megafossils. *Organic Geochemistry*, 21(8/9), 953-970.
- Street-Perrott, F.A., Huang, Y., Perrott, R.A., Eglinton, G., Barker, P., Khelifa, L.B., Harkness, D.D., Ivanovich, M. and Olago, D.O. (1997) Impact of lower atmospheric carbon dioxide on tropical mountain ecosystems: carbon isotope evidence. *Science*, 278, 1422-1426.
- Suess, E. (1979) Mineral phases formed in anoxic sediments by microbial decomposition of organic matter. *Geochimica et Cosmochimica Acta*, 43, 339-352.
- Sun, Y., Fu, J., Liu, D., Sheng, G., Chen, Z. and Wu, T. (1995a) Effect of volcanism on maturation of sedimentary organic matter and its significance for hydrocarbon generation, a case: the East Sag of Liaohe Basin. *Chinese Science Bulletin*, 40(17), 1446-1450.
- Sun, Y., Wu, X., Fu, J., Liu, D. and Wu, T. (1995b) Organic facies of Early Tertiary sediments from eastern depression, Liaohe Basin, North-Eastern China. *EAOG Meeting*, San Sebastian.
- Surdam, R.C. and Parker, R.D. (1972) Authigenic aluminosilicate minerals in the tuffaceous rocks of the Green River Formation, Wyoming. *Geological Society of America Bulletin*, 83, 689-700.
- Surdam, R.C. and Wolfbauer, C.A. (1975) The Green River Formation - A playa-lake complex. *Geological Society of America Bulletin*, 86, 335-345.
- Surdam, R.C. and Eugster, H.P. (1976) Mineral reactions in the sedimentary deposits of the Lake Magadi region, Kenya. *Geological Society of America Bulletin*, 87, 1739-1752.
- Surdam, R.C. and Sheppard, R.A. (1978) Zeolites in saline, alkaline-lake deposits. In: *Natural Zeolites: Occurrence, Properties, Use* (Ed. by L.B. Sand and F.A. Mumpton), pp. 145-174. Pergamon Press, Elmsford, New York.
- Surdam, R.C. and Stanley, K.O. (1979) Lacustrine sedimentation during the culminating phase of Eocene Lake Gosiute, Wyoming (Green River Formation). *Geological Society of America Bulletin*, 90, 93-110.

- Talbot, M.R. and Livingstone, D.A. (1989) Hydrogen index and carbon isotopes of lacustrine organic matter as lake level indicators. *Palaeogeography, Palaeoclimatology, Palaeoecology*, 70, 121-137.
- Talbot, M.R. and Johannessen, T. (1992) A high resolution paleoclimatic record for the last 27,500 years in tropical West Africa from the carbon and nitrogen isotopic composition of lacustrine organic matter. *Earth and Planetary Science Letters*, 110, 23-37.
- Talbot, M.R. and Allen, P.A. (1996) Lakes. In: *Sedimentary Environments: Processes, Facies and Stratigraphy* (Ed. by H.G. Reading), pp. 83-124. Blackwell Science.
- Talbot, M.R. and Laerdal, T. (2000) The Late Pleistocene-Holocene palaeolimnology of Lake Victoria, East Africa, Based upon elemental and isotopic analysis of sedimentary organic matter. *Journal of Paleolimnology*, 23, 141-164.
- Tang, Z. (1982) Tectonic features of oil and gas basins in eastern part of China. *AAPG Bulletin*, 66(5), 509-521.
- Taylor, G.H., Teichmüller, M., Davis, A., Diessel, C.F.K., Littke, R. and Robert, P. (1998) *Organic Petrology*. Borntraeger, Berlin, Stuttgart, pp. 704.
- Tegelaar, E.W., de Leeuw, J.W., Derenne, S. and Largeau, C. (1989a) A reappraisal of kerogen formation. *Geochimica et Cosmochimica Acta*, 53, 3103-3106.
- Tegelaar, E.W., de Leeuw, J.W., Largeau, C., Derenne, S., Schulten, H.-R., Müller, R., Boon, J.J., Nip, M. and Sprenkels, J.C.M. (1989b) Scope and limitations of several pyrolysis methods in the structural elucidation of a macromolecular plant constituent in the leaf cuticle of *Agave americana* L. *Journal of Analytical and Applied Pyrolysis*, 15, 29-54.
- Tegelaar, E.W. and Noble, R.A. (1993) Kinetics of hydrocarbon generation as a function of the molecular structure of kerogen as revealed by pyrolysis-gas chromatography. *Organic Geochemistry*, 22(3-5), 543-574.
- Tegelaar, E.W., Hollman, G., van der Vegt, P., de Leeuw, J.W. and Holloway, P.J. (1995) Chemical characterization of the periderm tissue of some angiosperm species: recognition of an insoluble, non-hydrolyzable, aliphatic biomacromolecule (Suberan). *Organic Geochemistry*, 23(3), 239-251.
- Teichmüller, M. (1974) Entstehung und Veränderung bituminöser Substanzen in Kohlen in Beziehung zur Entstehung und Umwandlung des Erdöls. *Fortschr. Geol. Rheinld. u. Westf.*, 24, 65-112.
- Teichmüller, M. and Ottenjann, K. (1977) Liptinite und lipoide Stoffe in einem Erdölmuttergestein. *Erdöl und Kohle*, 30, 387-398.
- ten Haven, H.L., de Leeuw, J.W. and Peakman, T.M. (1986) Anomalies in steroid and hopanoid maturity indices. *Geochimica et Cosmochimica Acta*, 50, 853-855.
- ten Haven, H.L., de Leeuw, J.W., Sinninghe Damsté, J.S., Schenck, P.A., Palmer, S.E. and Zumberge, J.E. (1988) Application of biological markers in recognition of palaeo hypersaline environments. In: *Lacustrine Petroleum Source Rocks* (Ed. by A.J. Fleet) 40, pp. 309-325. Geol. Soc. Special Pub.
- ten Haven, H.L. and Rullkötter, J. (1988) The diagenetic fate of taraxer-14-ene and oleanane isomers. *Geochimica et Cosmochimica Acta*, 52, 2543-2548.
- ten Haven, H.L., Rohmer, M., Rullkötter, J. and Bisseret, P. (1989) Tetrahymanol, the most likely precursor of gammacerane occurs ubiquitously in marine sediments. *Geochimica et Cosmochimica Acta*, 53, 3073-3079.
- ten Haven, H.L. and Schiefelbein, C. (1995) The petroleum systems of Indonesia. Proceedings Indonesian Petroleum Association; 24th Annual Convention, 443-459.
- Thamdrup, B., Finster, K., Hansen, J.W. and Bak, F. (1993) Bacterial disproportionation of elemental sulfur coupled to chemical reduction of iron and manganese. *Appl. Environ. Microbiol.*, 59, 101-108.
- Thiry, M. and Jaquin, T. (1993) Clay mineral distribution related to rift activity, sea-level changes and paleoceanography in the Cretaceous of the Atlantic Ocean. *Clay Minerals*, 28, 61-84.

- Thompson, C.L. and Dembicki, H. (1986) Optical characteristics of amorphous kerogens and the hydrocarbon-generating potential of source rocks. *International Journal of Coal Geology*, 6, 229-249.
- Tian, Z. (1990) The formation and distribution of Mesozoic-Cenozoic basins in China. *Journal of Petroleum Geology*, 13(1), 19-34.
- Tissot, B.P. and Welte, D.H. (1984) *Petroleum formation and occurrence*. Springer-Verlag, Berlin, pp. 699.
- Tissot, B.P., Pelet, R. and Ungerer, P. (1987) Thermal history of sedimentary basins, maturation indices, and kinetics of oil and gas generation. *AAPG Bulletin*, 71(12), 1445-1466.
- Trichet, J., Defarge, C., Tribble, J., Tribble, G. and Sansone, F. (2001) Christmas Island lagoonal lakes, models for the deposition of carbonate-evaporite-organic laminated sediments. *Sedimentary Geology*, 140(1-2), 177-189.
- Tsuge, S. and Matsubara, H. (1985) High-resolution pyrolysis-gas chromatography of proteins and related materials. *Journal of Analytical and Applied Pyrolysis*, 8, 49-64.
- Tsusue, A. (1967) Magnesian kutnahorite from Ryujima mine, Japan. *American Mineralogist*, 52, 1751-1761.
- Tulloch, A.P. (1976) Chemistry of waxes of higher plants. In: *Chemistry and Biochemistry of Natural Waxes* (Ed. by P.E. Kolattukudy), pp. 349-418. Elsevier, Amsterdam.
- Tyson, R.V. (1995) *Sedimentary organic matter: Organic facies and palynofacies*. Chapman & Hall, London, pp. 615.
- Urban**, N.R., Ernst, K. and Bernasconi, S. (1999) Addition of sulfur to organic matter during early diagenesis of lake sediments. *Geochimica et Cosmochimica Acta*, 63(6), 837-853.
- Uyeda, S. and Miyashiro, A. (1974) Plate tectonics and the Japanese Islands. *Geological Society of America Bulletin*, 85, 1159-1170.
- van Bergen**, P.F., Collinson, M.E., Damsté, J.S.S. and Leeuw, J.W.d. (1994) Chemical and microscopical characterization of inner seed coats of fossil water plants. *Geochimica et Cosmochimica Acta*, 58, 231-239.
- van de Kamp, P.C. and Leake, B.E. (1996) Petrology, geochemistry, and Na metasomatism of Triassic-Jurassic non-marine clastic sediments in the Newark, Hartford, and Deerfield rift basins, northeastern USA. *Chemical Geology*, 133(1-4), 89-124.
- van der Heijden, E. and Boon, J.J. (1994) A combined pyrolysis mass spectrometric and light microscopic study of peatified *Calluna* wood isolated from raised bog peat deposits. *Organic Geochemistry*, 22(6), 903-919.
- van der Kaaden, A., Haverkamp, J., Boon, J.J. and de Leeuw, J.W. (1983) Analytical pyrolysis of carbohydrates. I. Chemical interpretation of matrix influences on pyrolysis-mass spectra of amylose using pyrolysis-gas chromatography-mass spectrometry. *Journal of Analytical and Applied Pyrolysis*, 5, 199-220.
- van der Kaaden, A., Boon, J.J., de Leeuw, J.W., de Lange, F., Wijnand Schuyl, P.J., Schulten, H.-R. and Bahr, U. (1984a) Comparison of analytical pyrolysis techniques in the characterization of Chitin. *Analytical Chemistry*, 56(12), 2160-2164.
- van der Kaaden, A., Boon, J.J. and Haverkamp, J. (1984b) The analytical pyrolysis of carbohydrates. *Biomedical Mass Spectrometry*, 11(9), 486-492.
- van Heemst, J.D.H., Peulvé, S. and de Leeuw, J.W. (1996) Novel algal polyphenolic biomacromolecules as significant contributors to resistant fractions of marine dissolved and particulate organic matter. *Organic Geochemistry*, 24(6/7), 629-640.
- van Heemst, J.D.H., van Bergen, P.F., Stankiewicz, B.A. and de Leeuw, J.W. (1999) Multiple sources of alkylphenols produced upon pyrolysis of DOM, POM and recent sediments. *Journal of Analytical and Applied Pyrolysis*, 52, 239-256.

- van Heemst, J.D.H., Megens, L., Hatcher, P.G. and de Leeuw, J.W. (2000) Nature, origin and average age of estuarine ultrafiltered dissolved organic matter as determined by molecular and carbon isotope characterization. *Organic Geochemistry*, 31(9), 847-857.
- van Smeerdijk, D.G. and Boon, J.J. (1987) Characterisation of subfossil sphagnum leaves, rootlets of *Ericaceae* and their peat by pyrolysis high-resolution gas chromatography-mass spectrometry. *Journal of Analytical and Applied Pyrolysis*, 11, 377-402.
- Vasconcelos, C., McKenzie, J.A., Bernasconi, S., Grujic, D. and Tien, A. (1995) Microbial mediation as a possible mechanism for natural dolomite formation at low temperatures. *Nature*, 377, 220-222.
- Vasconcelos, C. and McKenzie, J.A. (1997) Microbial mediation of modern dolomite precipitation and diagenesis under anoxic conditions (Lagoa Vermelha, Rio de Janeiro, Brazil). *Journal of Sedimentary Petrology*, 67, 378-390.
- Velde, B. (1985) *Clay Minerals - A physico-chemical explanation of their occurrence*. Elsevier, Amsterdam, pp. 427.
- Venkatesan, M.I. (1989) Tetrahymanol: its widespread occurrence and geochemical significance. *Geochimica et Cosmochimica Acta*, 53, 3095-3101.
- Vogt, C. (1997) Zeitliche und räumliche Verteilung von Mineralvergesellschaftungen in spätquartären Sedimenten des Arktischen Ozeans und ihre Nützlichkeit als Klimaindikatoren während der Glazial/Interglazial-Wechsel. 251, pp. 309. Alfred-Wegener-Institut für Polar- und Meeresforschung, Bremerhaven.
- Volkman, J.K., Gillan, F.T., Johns, R.B. and Eglinton, G. (1981) Sources of neutral lipids in a temperate intertidal sediment. *Geochimica et Cosmochimica Acta*, 45, 1817-1828.
- Volkman, J.K. (1986) A review of sterol markers for marine and terrigenous organic matter. *Organic Geochemistry*, 9, 83-99.
- von der Borch, C.C. (1965) Source of ions for Coorong dolomite formation. *American Journal of Science*, 233, 684-688.
- von der Borch, C.C. (1976) Stratigraphy and formation of Holocene dolomitic carbonate deposits of the Coorong area, South Australia. *Journal of Sedimentary Petrology*, 46(4), 952-966.
- Wagner**, T. (1999) Petrology of organic matter in modern and late Quaternary deposits of the Equatorial Atlantic: climatic and oceanographic links. *International Journal of Coal Geology*, 39, 155-184.
- Wake, L.V. and Hillen, L.W. (1981) Nature and hydrocarbon content of blooms of the alga *Botryococcus braunii* occurring in Australian freshwater lakes. *Aust. J. Mar. Freshwater Res.*, 32, 353-367.
- Wakeham, S.G., Schaffner, C. and Giger, W. (1980) Polycyclic aromatic hydrocarbons in recent lake sediments. II. Compounds derived from biogenic precursors during early diagenesis. *Geochimica et Cosmochimica Acta*, 44(13), 415-429.
- Wallace, S. (1986) The analysis of high molecular weight nitrogen compounds in fossil fuels. Ph.D. thesis, University of Leeds,
- Wang, J.Y. and Wang, J.A. (1988) Thermal structure of the crust and upper mantle of the Liaohe rift basin, North China. *Tectonophysics*, 145(3-4), 293-304.
- Wang, L., Sarnthein, M., Erlenkeuser, H., Grimalt, J., Grootes, P., Heilig, S., Ivanova, E., Kienast, M., Pelejero, C. and Pflaumann, U. (1999) East Asian monsoon climate during the Late Pleistocene: high-resolution sediment records from the South China Sea. *Marine Geology*, 156(1-4), 245-284.
- Wang, P.X., Wang, L.J., Bian, Y.H. and Jian, Z.M. (1995) Late Quaternary paleoceanography of the South China Sea: surface circulation and carbonate cycles. *Marine Geology*, 127, 145-165.
- Wang, S. (1998) Polar lipids in Green River Oil Shale as facies indicators. Dissertation, Carl von Ossietzky Universität, Oldenburg, pp. 231.
- Wang, T., Zhong, N., Hou, D., Huang, G., Bao, J. and Li, X. (1997) Genetic mechanism and occurrence of immature hydrocarbon, pp. 219. Petroleum Industry Press, Beijing.

- Waples, D.W. and Machihara, T. (1991) Biomarkers for geologists. A practical guide to the application of steranes and triterpanes in petroleum geology. In: *AAPG Methods in Exploration, No. 9*. The American Association of Petroleum Geologists, Tulsa, Oklahoma.
- Watanabe, T., Winter, A. and Oba, T. (2001) Seasonal changes in sea surface temperature and salinity during the Little Ice Age in the Caribbean Sea deduced from Mg/Ca and $^{18}\text{O}/^{16}\text{O}$ ratios in corals. *Marine Geology*, 172(1-4), 21-35.
- Weber, J. (1991) Untersuchungen zur Tonmineralführung der Messel-Formation in der Fundstätte Messel (Mittel-Eozän). *Cour. Forsch.-Inst. Senckenberg*, 139, 71-81.
- Weete, J.D. (1976) Algal and fungal waxes. In: *Chemistry and Biochemistry of Natural Waxes* (Ed. by P.E. Kolattukudy), pp. 349-418. Elsevier, Amsterdam.
- Wetzel, R.G. (1983) *Limnology*. W. B. Saunders, Philadelphia, pp. 767.
- Whelan, J.K. and Thompson-Rizer, C.L. (1993) Chemical methods for assessing kerogen and protokerogen types and maturity. In: *Organic Geochemistry* (Ed. by M.H. Engel and S.A. Macko), pp. 289-353. Plenum Press, New York.
- Wilkes, H., Clegg, H., Disko, U., Willsch, H. and Horsfield, B. (1998) Fluoren-9-ones and carbazoles in the Posidonia Shale, Hils Syncline, northwest Germany. *Fuel*, 77(7), 657-668.
- Wilkes, H., Ramrath, A. and Negendank, J.F.W. (1999) Organic geochemical evidence for environmental changes since 34,000 yrs BP from Lago di Mezzano, central Italy. *Journal of Paleolimnology*, 22, 349-365.
- Williams, L.A. and Crerar, D.A. (1985) Silica diagenesis, II. General mechanisms. *Journal of Sedimentary Petrology*, 55(3), 312-321.
- Williams, L.B., Ferrell, R.E., Chinn, E.W. and Sassen, R. (1989) Fixed-ammonium in clays associated with crude oils. *Applied Geochemistry*, 4, 605-616.
- Williams, L.B., Wilcoxon, B.R., Ferrell, R.E. and Sassen, R. (1992) Diagenesis of ammonium during hydrocarbon maturation and migration, Wilcox Group, Louisiana, U.S.A. *Applied Geochemistry*, 7, 123-134.
- Willsch, H., Clegg, H., Horsfield, B., Radke, M. and Wilkes, H. (1997) Liquid chromatographic separation of sediment, rock, and coal extracts and crude oil into compound classes. *Analytical Chemistry*, 69(20), 4203-4209.
- Winkler, M.G. and Wang, P.K. (1993) The Late-Quaternary vegetation and climate of China. In: *Global Climates since the Last Glacial Maximum* (Ed. by H.E. Wright, J.E. Kutzbach, T. Webb, W.F. Ruddiman, F.A. Street-Perrott and P.J. Bartlein), pp. 221-261. University of Minnesota Press, Minneapolis.
- Wolfbauer, C.A. and Surdam, R.C. (1974) Origin of nonmarine dolomite in Eocene Lake Gosiute, Green River Basin, Wyoming. *Geological Society of America Bulletin*, 85, 1733-1740.
- Wright, D.T. (1999) The role of sulfate-reducing bacteria and cyanobacteria in dolomite formation in distal ephemeral lakes of the Coorong region, South Australia. *Sedimentary Geology*, 126, 147-157.
- Yan**, H. (1990) The alluvial fan, fan-delta and sublacustrine fan of Paleogene age within Liaohe Rift, Liaoning Province, China. *Sedimentary Geology*, 68, 75-85.
- Yang, W. (1985) Daqing oil field, People's Republic of China: A giant field with oil of non-marine origin. *AAPG Bulletin*, 69, 1101-1111.
- Yang, W., Li, Y. and Gao, R. (1985) Formation and evolution of non-marine petroleum in Songliao Basin, China. *AAPG Bulletin*, 69, 1112-1122.
- Yuretich, R., Melles, M., Sarata, B. and Grobe, H. (1999) Clay minerals in the sediments of Lake Baikal: A useful climate proxy. *Journal of Sedimentary Research*, 69(3), 588-596.

- Zegouagh, Y., Derenne, S., Largeau, C. and Saliot, A. (1996) Organic matter sources and diagenetic alterations in arctic surface sediments (Lena River delta and Laptev sea, Eastern Siberia). I. Analysis of the carboxylic acids released *via* sequential treatments. *Organic Geochemistry*, 24, 841-849.
- Zegouagh, Y., Derenne, S., Largeau, C., Bertrand, P., Sicre, M.-A., Saliot, A. and Rousseau, B. (1999) Refractory organic matter in sediments from the north-west African upwelling system: Abundance, chemical structure and origin. *Organic Geochemistry*, 30, 83-99.
- Zhang, X., Wang, Y. and Lei, H. (1996) Authigenic mineralogy, depositional environments and evolution of fault-bounded lakes of the Yunnan Plateau. *Sedimentology*, 43(2), 367-380.
- Zhao, M., Eglinton, G., Read, G. and Schimmelmann, A. (2000) An alkenone (U37K') quasi-annual sea surface temperature record (A.D. 1440 to 1940) using varved sediments from the Santa Barbara Basin. *Organic Geochemistry*, 31(9), 903-917.
- Zheng, C. (1988) A new exploration method for buried-hill oil fields, the Liaohe Depression, China. In: *Petroleum resources of China and related subjects* (Ed. by H.C. Wagner, L.C. Wagner, F.F.H. Wang and F.L. Wong) 10; *Circum-Pacific Council for Energy and Mineral Resources, Earth Science Series*, pp. 251-262.
- Zheng, Z. and Lei, Z.-Q. (1999) A 400,000 year record of vegetational and climatic changes from a volcanic basin, Leizhou Peninsula, southern China. *Palaeogeography, Palaeoclimatology, Palaeoecology*, 145, 339-362.
- Zhou, Y. and Littke, R. (1999) Numerical simulation of the thermal maturation, oil generation and migration in the Songliao Basin, Northeastern China. *Marine and Petroleum Geology*, 16, 771-792.
- Zink, K.-G., Leythaeuser, D., Melkonian, M. and Schwark, L. (2001) Temperature dependency of long-chain alkenone distributions in recent to fossil limnic sediments and in lake waters. *Geochimica et Cosmochimica Acta*, 65(2), 253-265.
- Zolitschka, B. (1990) Spätquartäre jahreszeitlich geschichtete Seesedimente ausgewählter Eifelmaare-Paläolimnologische Untersuchungen als Beitrag zur spät- und postglazialen Klima- und Besiedlungsgeschichte. Dissertation, Trier, pp. 226.
- Zolitschka, B. (1991) Absolute dating of late-Quaternary lacustrine sediments by high-resolution varve chronology. *Hydrobiologia*, 214, 59-61.
- Zolitschka, B. (1998a) Paläoklimatische Bedeutung laminierter Sedimente - Holzmaar (Eifel, Deutschland), Lake C2 (Nordwest-Territorien, Kanada) und Lago Grande di Monticchio (Basilikata, Italien). In: *Relief Boden Paläoklima*, 13 (Ed. by H. Bremer, K. Brunnacker, K. Heine and W. Lauer), pp. 176. Gebrüder Borntraeger, Berlin, Stuttgart.
- Zolitschka, B. (1998b) A 14,000 year sediment yield record from western Germany based on annually laminated lake sediments. *Geomorphology*, 22, 1-17.
- Zolitschka, B. and Negendank, J.F.W. (1998) A high resolution record of Holocene palaeohydrological changes from Lake Holzmaar, Germany. *Paläoklimaforschung*, 25, 33-48.
- Zolitschka, B., Brauer, A., Negendank, J.F.W., Stockhausen, H. and Lang, A. (2000) Annually dated late Weichselian continental paleoclimate record from the Eifel, Germany. *Geology*, 28(9), 783-786.

Appendix

I. Liaohe Basin

- A. Mineralogy
- B. Py-GC-FID, gross composition and individual components (Liaohe)
- C. Tentative structures and Mass spectra
- D. Definition of geochemical parameters
- E. Thermovaporisation-gas chromatography, quantitative analysis
- F. Ternary distribution of steranes
- G. Carbazoles and fluoren-9-ones, quantitative analysis and ratios

II. Maar Lake Sediments

- H. Py-GC-FID, gross composition and individual components (HZM, MFM)
- I. Maceral analysis and vitrinite reflectance data (HZM, MFM)
- J. Screening Data (HM)
- K. Py-GC-FID, gross composition and individual components (HM)
- L. Maceral analysis and vitrinite reflectance data (HM)
- M. Yields of individual *n*-alkanes, *n*-fatty acids and selected isoprenoids
- N. Abbreviations
- O. Index of Figures
- P. Index of Tables

E. nr.	Depth [m]	Well	Area	Member	Sub-unit	Expandable Clays [%]	Illite & Mica [%]	Kaolinite & Chlorite [%]	Clay Minerals Total [%]	Quartz [%]	Buddingtonite [%]	Plagioclase [%]	Feldspars Total [%]	Quartz/Feldspar Ratio	Detrital Minerals Total [%]
48479	2556.0	O	Leng	Es3	?	28.8	9.4	3.7	41.8	20.9	5.0	16.8	21.8	1.0	42.6
48494	1455.0	K	Gao	Es3	?	42.2	4.3	1.0	47.5	22.4	5.5	5.4	10.9	2.0	33.3
48499	2060.0	F	Lei	Es3	?	32.5	4.9	2.8	40.2	26.7	6.2	16.5	22.7	1.2	49.4
48451	2590.5	D	Lei	Es4	DJT	26.9	1.9	0.5	29.4	18.1	19.5	8.9	28.4	0.6	46.5
48452	2593.5	D	Lei	Es4	DJT	25.1	2.5	0.6	28.2	24.3	3.6	6.5	10.1	2.4	34.5
48453	2595.0	D	Lei	Es4	DJT	35.2	2.6	0.0	37.8	23.0	12.3	13.2	25.5	0.9	48.5
48455	2638.0	D	Lei	Es4	DJT	1.8	3.0	0.0	4.8	0.0	21.0	15.4	36.3	0.0	36.3
48459	2424.0	B	Lei	Es4	Shale II	23.0	7.9	6.9	37.8	28.4	13.1	14.9	28.0	1.0	56.4
48462	2446.0	B	Lei	Es4	Shale II	26.3	6.8	2.8	35.8	39.3	4.7	4.9	9.6	4.1	48.9
48463	2512.0	B	Lei	Es4	DJT	24.3	3.0	0.3	27.6	13.0	6.8	24.6	31.4	0.4	44.4
48464	2524.0	B	Lei	Es4	DJT	25.4	6.4	0.6	32.4	12.5	16.4	6.8	32.2	0.5	35.7
48465	2526.0	B	Lei	Es4	DJT	20.6	5.8	0.7	27.1	14.2	9.3	5.7	15.0	0.9	29.2
48466	2580.0	B	Lei	Es4	DJT	0.0	2.4	0.0	2.4	5.8	5.3	8.5	13.8	0.4	19.5
48467	2687.5	B	Lei	Es4	GS	6.4	2.7	0.0	9.0	22.6	3.5	10.6	14.1	1.6	36.7
48469	2579.5	B	Lei	Es4	DJT	0.0	2.0	0.0	2.0	0.0	36.3	30.2	66.5	0.0	66.5
48473	1488.0	J	Gao	Es4	Shale I	58.5	5.5	0.0	64.0	24.6	5.4	3.5	8.9	2.8	33.4
48475	1492.0	J	Gao	Es4	Shale I	40.0	4.7	0.9	45.5	15.5	3.5	1.5	5.0	3.1	20.4
48480	2735.0	E	Lei	Es4	Shale II	25.3	4.6	2.0	32.0	28.7	0.7	15.1	15.8	1.8	44.5
48481	2796.0	E	Lei	Es4	DJT	20.9	1.4	0.0	22.3	31.4	1.4	13.5	14.9	2.1	46.3
48482	2792.0	E	Lei	Es4	DJT	17.7	2.5	0.0	20.2	24.6	1.0	18.6	19.6	1.3	44.3
48484	2335.0	C	Lei	Es4	DJT	9.5	4.5	1.6	15.5	40.3	17.5	14.7	32.1	1.3	72.4
48485	2342.0	C	Lei	Es4	DJT	15.7	0.7	0.0	16.3	12.7	10.8	9.8	20.6	0.6	33.3
48486	2360.0	C	Lei	Es4	DJT	23.9	3.7	0.0	27.6	16.5	7.1	4.6	11.7	1.4	28.1
48487	2385.0	C	Lei	Es4	DJT	0.0	8.2	0.0	8.2	8.3	9.1	3.6	12.7	0.7	21.0
48488	2392.0	C	Lei	Es4	DJT	32.4	5.5	0.0	38.0	17.1	6.4	3.8	10.1	1.7	27.2
48492	2818.0	G	Lei	Es4	?	22.2	4.5	0.0	26.7	22.1	5.8	3.7	9.4	2.3	31.6
48498	2722.0	H	Lei	Es4	?	23.5	6.4	0.0	29.9	17.3	2.7	5.8	8.5	2.0	25.8
48501	2186.0	I	Lei	Es4	?	5.6	3.6	0.0	9.2	8.0	18.9	6.3	25.2	0.3	33.2
48502	1357.0	L	Gao	Es4	?	54.3	4.7	0.0	59.0	27.3	2.9	1.6	4.6	6.0	31.8
48504	2116.0	P	Shu-Du	Es4	?	20.4	3.5	0.9	24.8	38.2	2.5	2.2	4.7	8.1	42.9
48505	1847.0	M	Gao	Es4	GS	28.0	5.7	2.0	35.7	10.9	3.1	2.7	5.8	1.9	16.7
48506	2301.0	N	Gao	Es4	?	29.6	7.5	3.9	41.1	18.3	3.1	4.0	7.2	2.5	25.5
48507	2512.0	N	Gao	Es4	?	16.9	6.0	1.4	24.3	16.2	3.0	12.1	15.1	1.1	31.3
48509	2570.0	T	Tuo	Es4	?	38.2	8.6	5.8	52.7	26.5	4.7	13.1	17.8	1.5	44.3
48511	1818.0	R	Tuo	Es4	?	20.8	6.7	1.1	28.7	7.7	3.2	15.6	18.8	0.4	26.5
48513	2490.0	S	Tuo	Es4	NXT	18.5	4.7	1.0	24.2	17.0	12.6	3.9	16.5	1.0	33.6
48514	2312.0	S	Tuo	Es4	GS	54.4	5.3	2.2	61.8	23.1	3.9	5.7	9.7	2.4	32.8
48515	1160.0	Q	Tuo	Es4	?	45.0	7.8	1.8	54.7	18.4	6.0	18.8	24.8	0.7	43.1
48517	1252.0	A	Shu-Du	Es4	DJT	9.5	4.5	1.6	15.5	40.3	17.5	14.7	32.1	1.3	72.4
48518	1288.0	A	Shu-Du	Es4	DJT	0.0	1.8	1.8	3.6	58.1	18.5	16.6	35.1	1.7	93.3
48519	1306.0	A	Shu-Du	Es4	Shale I	44.5	3.8	0.7	49.0	16.9	4.2	4.6	8.8	1.9	25.7
48520	1309.0	A	Shu-Du	Es4	Shale I	45.0	6.4	2.5	53.9	14.0	4.8	3.6	8.3	1.7	22.4
48522	1318.0	A	Shu-Du	Es4	Shale I	53.2	8.1	2.4	63.7	20.9	4.0	5.0	9.0	2.3	29.9
48525	1329.0	A	Shu-Du	Es4	Shale I	54.1	7.3	0.0	61.4	14.9	2.8	3.3	6.2	2.4	21.1
48527	1340.0	A	Shu-Du	Es4	Shale I	16.6	1.8	0.3	18.6	14.7	2.0	2.6	4.6	3.2	19.3
48529	1346.0	A	Shu-Du	Es4	GS	19.1	2.8	0.0	21.9	12.9	2.7	1.9	4.6	2.8	17.5
48532	1348.0	A	Shu-Du	Es4	GS	26.1	4.0	0.0	30.1	23.6	2.0	2.8	4.8	4.9	28.3
48537	1375.0	A	Shu-Du	Es4	GS	33.4	10.4	0.0	43.8	24.2	4.2	2.1	6.3	3.8	30.5
48539	1405.0	A	Shu-Du	Es4	basement	43.5	0.0	0.0	43.5	0.5	0.0	33.2	33.2	0.0	33.7

E. nr.	Opal-C or CT [%]	Analime [%]	Amphibole [%]	Calcite [%]	Dolomite [%]	Aragonite [%]	Kutnahorite [%]	Rhodochrosite [%]	Siderite [%]	Carbonate Minerals Total [%]	Carbonate Facies	Gypsum [%]	Pyrite [%]	Natrojarosite [%]	I/S Ordering
48479	0.0	0.0	0.0	2.3	0.0	0.0	0.0	2.8	4.8	9.8	Rhodochrosite	0.0	5.7	0.0	0.0
48494	0.0	0.0	0.0	1.1	1.8	5.1	0.0	0.0	4.5	12.4	Calcite	0.2	6.7	0.0	0.0
48499	0.0	0.0	0.0	0.7	0.6	0.0	0.0	0.0	7.8	9.1	Siderite	0.0	1.2	0.0	0.0
48451	0.0	0.0	0.0	2.8	0.0	0.0	6.1	0.0	11.6	20.5	Siderite	1.3	2.4	0.0	1.0
48452	0.0	0.0	0.0	1.4	1.3	19.6	1.3	0.0	11.5	35.0	Arag./Sid.	0.8	1.6	0.0	1.0
48453	0.0	0.0	0.0	1.6	0.8	0.0	1.8	0.0	8.0	12.1	Siderite	0.0	1.6	0.0	1.0
48455	0.0	20.6	0.0	4.4	2.5	0.0	23.3	0.0	6.4	36.7	Kutnahorite	0.5	1.1	0.0	1.0
48459	0.0	0.0	0.0	1.3	0.0	0.0	0.0	0.0	1.5	2.8	Low-Carbonate	0.0	3.0	0.0	1.0
48462	0.0	0.0	0.0	7.4	0.0	0.0	0.0	0.0	0.7	8.0	Low-Carbonate	0.0	7.2	0.0	1.0
48463	0.0	0.0	0.0	2.1	0.0	9.6	0.0	0.0	14.7	26.4	Siderite	0.9	0.9	0.0	1.0
48464	0.0	0.0	0.0	1.9	9.2	15.0	0.0	0.0	3.2	29.3	Aragonite	1.3	1.4	0.0	1.0
48465	0.0	2.3	0.0	10.5	17.7	9.9	0.0	0.0	1.5	39.6	Dolomite	0.8	1.0	0.0	1.0
48466	0.0	25.3	0.0	0.0	45.5	0.0	0.0	0.0	7.3	52.8	Dolo/Sid	0.0	0.0	0.0	-
48467	0.0	0.0	0.0	16.6	16.0	0.0	18.3	0.0	0.6	51.4	Kut./Dol./Calc.	1.8	1.0	0.0	1.0
48469	0.0	0.0	0.0	0.0	26.6	0.0	0.0	0.0	3.8	30.3	Dolomite	0.7	0.5	0.0	-
48473	0.0	0.0	0.0	0.6	0.0	0.0	0.0	0.0	0.0	0.6	Low-Carbonate	0.4	1.5	0.0	0.0
48475	0.0	0.0	0.0	7.2	0.9	0.0	24.3	0.0	1.0	33.4	Kutnahorite	0.0	0.6	0.0	0.0
48480	0.0	0.0	0.0	14.8	0.0	0.0	0.0	0.0	3.1	17.9	Calcite	0.9	4.7	0.0	1.0
48481	0.0	0.0	0.0	14.6	9.3	0.0	0.0	0.0	4.4	28.2	Calcite/Dol.	1.0	2.2	0.0	1.0
48482	0.0	0.0	0.0	3.8	8.2	0.0	17.1	0.0	5.0	34.0	Kutnahorite	0.7	0.8	0.0	1.0
48484	0.0	0.0	0.0	0.0	9.4	0.0	0.0	0.0	0.9	10.3	Calc./Sid./Arag.	0.6	1.1	0.0	1.0
48485	0.0	4.4	0.0	4.3	0.0	22.5	12.9	0.0	4.2	43.9	Aragonite	0.5	1.5	0.0	1.0
48486	0.0	4.9	0.0	5.6	0.0	20.0	8.3	0.0	3.1	37.0	Aragonite	0.0	2.4	0.0	1.0
48487	0.0	24.1	0.0	5.0	29.4	0.0	9.2	0.0	1.2	44.9	Dolomite	0.7	1.2	0.0	-
48488	0.0	17.5	0.0	4.1	0.0	0.0	1.9	0.0	8.4	14.3	Siderite	1.6	1.4	0.0	1.0
48492	0.0	1.5	0.0	0.0	0.0	0.0	35.7	0.0	0.7	36.4	Kutnahorite	2.1	1.8	0.0	1.0
48498	0.0	0.0	0.0	1.7	0.0	0.0	38.8	0.0	0.0	40.5	Kutnahorite	2.1	1.7	0.0	1.0
48501	0.0	22.2	0.0	0.0	21.8	0.0	0.0	0.0	12.4	34.2	Dol./Sid.	0.0	1.2	0.0	1.0
48502	0.0	0.0	0.0	0.0	0.0	0.0	0.0	0.0	0.6	0.6	Low-Carbonate	2.2	0.0	6.3	0.0
48504	0.0	0.0	0.0	1.3	18.9	6.1	2.8	0.0	1.6	30.7	Dolomite	0.0	1.6	0.0	0.0
48505	0.0	0.0	0.0	8.5	1.6	34.1	2.2	0.0	0.0	46.4	Aragonite	0.0	1.2	0.0	0.0
48506	0.0	0.0	0.0	5.1	1.2	24.6	0.9	0.0	0.0	31.8	Aragonite	0.0	1.7	0.0	0.0
48507	0.0	0.0	0.0	11.9	31.6	0.0	0.0	0.0	0.0	43.6	Dol./Calc.	0.0	0.8	0.0	1.0
48509	0.0	0.0	0.0	0.6	0.0	0.0	0.0	0.0	1.9	2.4	Low-Carbonate	0.0	0.6	0.0	1.0
48511	0.0	20.1	8.3	0.0	15.8	0.0	0.0	0.0	0.0	15.8	Dolomite	0.0	0.7	0.0	0 S
48513	0.0	17.9	0.0	0.0	23.7	0.0	0.0	0.0	0.0	23.7	Dolomite	0.0	0.6	0.0	0 S
48514	0.0	0.0	0.0	1.2	1.2	0.0	0.0	0.0	1.0	3.3	Low-Carbonate	0.1	1.9	0.0	0.0
48515	0.0	0.0	0.0	0.0	0.0	0.0	0.0	0.0	2.2	2.2	Low-Carbonate	0.0	0.0	0.0	0.0
48517	0.0	0.0	0.0	0.0	9.4	0.0	0.0	0.0	0.9	10.3	Dolomite	0.6	1.1	0.0	1.0
48518	0.0	0.0	0.0	0.8	1.6	0.0	0.0	0.0	0.8	3.1	Low-Carbonate	0.0	0.0	0.0	-
48519	0.0	0.0	0.0	0.0	0.0	0.0	0.0	0.0	23.1	23.1	Siderite	0.0	2.1	0.0	0.0
48520	6.7	0.0	0.0	0.0	0.0	0.0	0.0	0.0	15.7	15.7	Siderite	0.0	1.4	0.0	0.0
48522	6.4	0.0	0.0	0.0	0.0	0.0	0.0	0.0	0.0	0.0	Low-Carbonate	0.0	0.0	0.0	0.0
48525	14.1	0.0	0.0	0.0	0.0	0.0	0.0	0.0	1.3	1.3	Low-Carbonate	1.3	0.8	0.0	0.0
48527	57.1	0.0	0.0	0.0	0.5	0.0	0.0	0.0	0.6	1.1	Low-Carbonate	2.0	1.8	0.0	0.0
48529	0.0	0.0	0.0	0.6	0.0	0.0	59.1	0.0	0.0	59.7	Kutnahorite	0.9	0.0	0.0	0.0
48532	0.0	0.0	0.0	37.2	0.0	0.0	0.0	0.0	0.0	37.2	Calcite	1.4	3.0	0.0	0.0
48537	0.0	0.0	0.0	20.0	1.5	0.0	0.0	0.0	0.0	21.5	Calcite	2.6	1.6	0.0	1.0
48539	0.0	1.7	0.0	16.6	0.9	0.0	1.2	0.0	0.0	18.8	Calcite	0.0	2.2	0.0	0 S

Code #	E48465-MK1-S2 R:2**6	E48467-MK1-S2 R:2**6	E48480-MK1-S2 R:2**6	E48485-MK1-S2 R:2**6	E48494-MK1-S2 R:2**6
MCM #	P497A, 6	P497A, 7	P497A, 8	P497A, 9	P497A
Amount (mg)	2.52	1.61	3.01	2.31	2.48
TOC [%]	47.2	76.2	46.7	56.7	52.3
	(µg/g TOC)	(µg/g TOC)	(µg/g TOC)	(µg/g TOC)	(µg/g TOC)
C1	28525	22916	28424	28955	23967
C02-05 Total	64631	67854	64120	67171	61921
C06-14 Total	162743	173341	158332	176026	166501
C15-32 Total	251269	319264	274097	318362	295981
C01-05 Total	93156	90770	92544	96126	85888
C06-14 Total	162743	173341	158332	176026	166501
C15-32 Total (corr)	225206	293995	252043	294694	272080
C01-32 Total	481105	558106	502919	566846	524469
C06-14 Resolved	110572	128572	104266	119308	108634
C15-32 Resolved	68566	11432	67671	91219	46000
C01-32 Resolved	272294	230774	264481	306653	240522
n6:1	3131	4831	3189	3997	2989
n6	2248	3531	2572	2823	2324
Benzene	1627	1743	1960	1899	1919
n7:1	2341	3985	2480	3089	2010
n7	2689	4134	2954	3243	2527
Toluene	1699	1431	1927	1800	2059
2-M-Thiophene	666	637	763	742	942
n8:1	2094	3514	2074	2701	1738
n8	2249	3741	2426	2877	2013
Ethylbenzene	676	536	789	697	698
Ethylthiop.	737	519	523	699	382
m,p-X + 2,5-DM-Thiop.	3197	1930	2254	3112	2682
2,4-DM-Thiop.	390	148	279	248	464
2,3-DM-Thiop.	346	189	271	245	503
Styrene	658	583	915	639	689
o-Xylene	689	787	789	782	966
n9:1	1870	3271	1880	2377	1321
n9	1995	3688	2249	2579	1782
Ethyl-Methylbenzene	1582	343	217	461	293
Ethyl-Methylbenzene (2)	669	357	419	415	572
1,3,5 Trimethylbenzene	941	695	656	1082	596
Phenole	809	518	1608	2387	4295
1,2,4 Trimethylbenzene	616	705	718	855	1100
n10:1	1773	3492	1940	2577	1426
n10	1876	3593	2132	2476	1581
1,2,3 Trimethylbenzene	686	671	713	962	577
o-Cresol	519	420	953	812	1361
m,p-Cresol	867	608	1129	1032	1043
n11:1	1837	3469	2042	2373	1377
n11	2299	4071	2401	2553	1732

Code #	E48465-MK1-S2 R:2**6 (µg/g TOC)	E48467-MK1-S2 R:2**6 (µg/g TOC)	E48480-MK1-S2 R:2**6 (µg/g TOC)	E48485-MK1-S2 R:2**6 (µg/g TOC)	E48494-MK1-S2 R:2**6 (µg/g TOC)
C2-Phenoles	986	1011	1754	1454	1632
Naphthalene	293	236	366	202	602
n12:1	1920	3131	1814	2119	1076
n12	2248	3919	2477	2491	1471
IP-13	724	526	480	624	596
IP-13:1	201	128	90	193	253
2-M-Naphthalene	208	210	262	304	677
IP-14	521	409	343	377	603
1-M-Naphthalene	270	336	318	388	2433
n13:1	1835	3204	1824	2105	1265
IP-14:1	802	631	477	699	468
n13	2536	3854	2357	2594	1504
IP-15:1	614	606	403	585	412
n14:1	2025	3384	1608	1952	889
IP-15	238	169	195	338	236
n14	2132	3870	2262	2367	1371
IP-16:1	574	373	325	578	288
IP-16	869	539	536	782	405
n15:1	1463	3100	1661	1863	974
n15	2403	3911	2558	2706	1691
n16:1	1387	2956	1610	1990	996
n16	1800	3516	2110	2516	1104
IP-18	990	949	677	980	439
n17:1	1463	2830	1595	2052	819
n17	1932	3580	2119	2675	992
Prist-1-ene	1856	782	760	1594	631
Prist-2-ene	268	136	109	252	150
n18:1	1499	2701	1497	2040	669
n18	1813	3293	1931	2699	707
IP-20	400	327	305	385	180
n19:1	1352	2549	1332	1991	580
n19	2106	3400	1934	2987	697
n20:1	1590	2463	1207	2147	395
n20	1970	3197	1831	3075	706
n21:1	1302	2290	1095	2077	398
n21	2098	3265	1738	3236	571
n22:1	1274	2441	1171	2146	445
n22	1740	3081	1540	3024	551
n23:1	996	2242	1030	1874	343
n23	1552	3185	1482	2734	503
n24:1	847	2355	912	1562	341
n24	1175	2939	1259	2084	449
n25:1	658	2006	788	1256	304
n25	1109	3036	1323	1967	450
n26:1	699	2027	812	1039	327
n26	819	2500	1025	1370	429
n27:1	433	1548	631	663	237
n27	723	2251	903	1123	387
n28:1	365	1178	420	462	186
n28	563	1790	693	807	311
n29:1	363	1090	393	458	159
n29	578	1557	629	718	282
n30:1	299	772	246	280	143
n30	408	1092	419	438	178
n31:1	193	589	254	268	3
n31	497	894	547	509	383
n32:1	270	469	215	553	365
n32	157	639	229	266	118

Code #	E48502-MK1-S2 R:2**6	E48505-MK1-S2 R:2**6	E48514-MK1-S2 R:2**6	E48517-MK1-S2 R:2**6	E48519-MK1-S2 R:2**6
MCM #	P497A	P497A, 12	P497A, 13	P497A, 14	P497A, 15
Amount (mg)	2.11	1.98	2.03	2.83	2.49
TOC [%]	59.6	70.5	66.6	50.1	50.6
	(µg/g TOC)	(µg/g TOC)	(µg/g TOC)	(µg/g TOC)	(µg/g TOC)
C1	27680	30733	27925	21817	19643
C02-05 Total	68096	65001	68096	42627	55711
C06-14 Total	180071	193074	172069	127735	148257
C15-32 Total	344738	373693	340689	201938	260966
C01-05 Total	95776	95734	96021	64444	75354
C06-14 Total	180071	193074	172069	127735	148257
C15-32 Total (corr)	320087	351485	317760	180074	236362
C01-32 Total	595934	640293	585850	372253	459973
C06-14 Resolved	120010	122543	121382	94686	101699
C15-32 Resolved	91279	68388	128650	74997	79090
C01-32 Resolved	307065	286665	346053	234127	256143
n6:1	3312	3070	4172	2414	3420
n6	2928	2395	3470	1677	2377
Benzene	1920	1434	1783	1601	1851
n7:1	2756	2112	3311	1928	2705
n7	3290	2971	3950	1988	2705
Toluene	1948	1511	1884	1586	1722
2-M-Thiophene	934	713	741	533	717
n8:1	2458	1785	2864	1700	2239
n8	2941	2355	3453	1761	2301
Ethylbenzene	740	687	733	576	589
Ethylthiop.	407	1007	447	460	386
m,p-X + 2,5-DM-Thiop.	2346	5491	2091	1918	1799
2,4-DM-Thiop.	485	422	291	174	263
2,3-DM-Thiop.	382	303	261	174	284
Styrene	686	574	545	419	593
o-Xylene	826	880	785	697	764
n9:1	2135	1597	2616	1634	2003
n9	2571	2056	3266	1569	2030
Ethyl-Methylbenzene	255	785	345	317	201
Ethyl-Methylbenzene (2)	409	676	438	400	343
1,3,5 Trimethylbenzene	597	1494	601	619	435
Phenole	1492	1519	1139	7972	2875
1,2,4 Trimethylbenzene	884	1252	712	679	683
n10:1	2377	1258	2849	1847	2287
n10	2463	1688	3231	1517	2018
1,2,3 Trimethylbenzene	759	1931	804	374	526
o-Cresol	979	764	850	1024	976
m,p-Cresol	1590	838	949	1411	1346
n11:1	2261	1731	2933	1689	2173
n11	2768	1897	3868	1670	2139

Code #	E48502-MK1-S2 R:2**6 (µg/g TOC)	E48505-MK1-S2 R:2**6 (µg/g TOC)	E48514-MK1-S2 R:2**6 (µg/g TOC)	E48517-MK1-S2 R:2**6 (µg/g TOC)	E48519-MK1-S2 R:2**6 (µg/g TOC)
C2-Phenoles	1898	1252	1476	1292	1653
Naphthalene	354	287	218	193	262
n12:1	2029	1257	2746	1538	1923
n12	2672	1455	3794	1678	2146
IP-13	554	876	485	490	515
IP-13:1	105	1064	139	170	121
2-M-Naphthalene	535	519	243	213	439
IP-14	429	882	346	232	377
1-M-Naphthalene	411	410	334	320	430
n13:1	2060	1366	2730	1757	2026
IP-14:1	427	926	592	543	387
n13	2702	1797	3612	1891	2148
IP-15:1	330	920	508	407	340
n14:1	1832	1007	2631	1521	1718
IP-15	173	894	179	172	115
n14	2652	1312	3622	1745	2117
IP-16:1	456	894	408	334	381
IP-16	566	1060	607	478	440
n15:1	1904	912	2736	1489	1748
n15	3064	1868	3973	1975	2351
n16:1	1961	1009	2596	1543	1711
n16	2550	1351	3653	1761	1912
IP-18	573	975	660	581	507
n17:1	1910	1199	2610	1542	1673
n17	2690	1507	3548	1905	2025
Prist-1-ene	861	1829	1496	872	752
Prist-2-ene	110	367	359	236	140
n18:1	1822	1072	2409	1548	1633
n18	2562	1487	3207	1838	1975
IP-20	279	420	344	238	219
n19:1	1698	1053	2198	1532	1662
n19	2559	1984	3266	2046	2141
n20:1	1547	1313	2124	1654	1525
n20	2425	1965	3136	2012	2063
n21:1	1433	1065	2138	1472	1413
n21	2281	2361	3258	2079	2033
n22:1	1483	1127	2331	1618	1487
n22	2034	1810	3367	1881	1803
n23:1	1369	918	2316	1447	1330
n23	1995	1640	3558	1834	1739
n24:1	1298	633	2220	1351	1225
n24	1811	935	3534	1615	1505
n25:1	1214	504	2377	1119	1126
n25	1926	840	3781	1638	1492
n26:1	1417	541	2174	1179	1205
n26	1849	698	3655	1398	1366
n27:1	979	322	1473	977	958
n27	1827	666	4584	1324	1367
n28:1	782	244	1314	753	807
n28	1325	508	2730	1043	1124
n29:1	676	251	1170	639	921
n29	1313	637	2726	974	1162
n30:1	539	246	996	566	655
n30	874	424	1943	754	837
n31:1	406	177	777	491	605
n31	1038	620	1929	707	875
n32:1	724	589	1020	481	526
n32	495	176	1077	486	628

APPENDIX B

PY-GC-FID (LIAOHE)

Code #	E48520-MK1-S2 R:2**6	E48525-MK1-S2 R:2**6	E48527-MK1-S2 R:2**6	E48529-MK1-S2 R:2**6	E48532-MK1-S2 R:2**6	E48537-MK1-S2 R:2**6
MCM #	P497A, 16	P497A, 17	P497A, 18	P497A, 19	P497A, 20	P497A, 23
Amount (mg)	2.02	2.13	1.81	1.30	1.31	1.30
TOC [%]	58.6	63.7	63.3	72.5	65.8	70
	(µg/g TOC)	(µg/g TOC)	(µg/g TOC)	(µg/g TOC)	(µg/g TOC)	(µg/g TOC)
C1	23406	23523	20187	18389	18171	13836
C02-05 Total	62489	60778	64655	66707	64368	65113
C06-14 Total	164953	157260	181688	183827	176294	185456
C15-32 Total	313825	294925	359295	387531	378439	441268
C01-05 Total	85895	84301	84842	85096	82539	78949
C06-14 Total	164953	157260	181688	183827	176294	185456
C15-32 Total (corr)	287636	272077	332238	354640	342475	407202
C01-32 Total	538484	513638	598768	623563	601308	671607
C06-14 Resolved	112262	106168	127210	125819	123283	134269
C15-32 Resolved	94067	80542	139122	143193	134214	198757
C01-32 Resolved	292224	271011	351174	354108	340036	411975
n6:1	3522	3126	4061	4783	4127	5080
n6	2983	2690	3178	3305	2945	3107
Benzene	1852	1727	2128	2082	1874	1899
n7:1	2745	2622	3353	3926	3245	3870
n7	3356	3007	3481	3817	3215	3686
Toluene	1934	1850	2055	1635	1612	1244
2-M-Thiophene	779	868	861	894	846	1359
n8:1	2399	2252	2918	3301	2784	3405
n8	2867	2550	3296	3412	2936	3307
Ethylbenzene	664	620	684	561	587	437
Ethylthiop.	405	438	488	408	470	726
m,p-X + 2,5-DM-Thiop.	1876	2004	2179	2041	2238	2127
2,4-DM-Thiop.	374	543	382	322	340	289
2,3-DM-Thiop.	348	329	344	325	329	349
Styrene	598	584	642	596	572	530
o-Xylene	841	788	889	838	850	868
n9:1	2064	1891	2638	2965	2445	3266
n9	2506	2293	2980	3117	2636	3188
Ethyl-Methylbenzene	184	220	287	189	258	324
Ethyl-Methylbenzene (2)	407	381	349	265	335	379
1,3,5 Trimethylbenzene	394	459	544	457	522	565
Phenole	2282	997	1736	804	1480	812
1,2,4 Trimethylbenzene	760	773	742	713	804	741
n10:1	2196	2071	2873	3387	2737	3680
n10	2419	2239	2867	3095	2535	3207
1,2,3 Trimethylbenzene	458	525	579	516	621	483
o-Cresol	976	754	746	846	842	1000
m,p-Cresol	1627	1430	962	956	1453	478
n11:1	2156	2038	2893	3310	2739	3476
n11	2612	2435	3206	3492	2867	3490

Code #	E48520-MK1-S2 R:2**6 (µg/g TOC)	E48525-MK1-S2 R:2**6 (µg/g TOC)	E48527-MK1-S2 R:2**6 (µg/g TOC)	E48529-MK1-S2 R:2**6 (µg/g TOC)	E48532-MK1-S2 R:2**6 (µg/g TOC)	E48537-MK1-S2 R:2**6 (µg/g TOC)
C2-Phenoles	1979	1801	1619	1416	1631	1634
Naphthalene	508	393	311	242	221	218
n12:1	1913	1768	2759	3095	2514	3262
n12	2509	2330	3346	3564	2863	3634
IP-13	724	670	615	496	601	768
IP-13:1	111	104	181	90	171	162
2-M-Naphthalene	548	486	493	427	479	326
IP-14	542	443	497	246	546	499
1-M-Naphthalene	607	297	587	304	343	345
n13:1	2002	1882	2849	3186	2555	3265
IP-14:1	577	575	562	488	597	682
n13	2436	2391	3341	3623	2936	3638
IP-15:1	491	514	529	491	603	830
n14:1	1726	1725	2750	3150	2481	3570
IP-15	141	127	136	137	197	198
n14	2466	2450	3497	3833	3094	3919
IP-16:1	520	494	467	540	613	776
IP-16	648	692	573	591	719	858
n15:1	1824	1795	2773	3173	2557	3411
n15	2684	2745	3802	4222	3465	4235
n16:1	1811	1805	2282	3047	2621	3344
n16	2267	2323	2752	3642	3192	3859
IP-18	699	768	689	812	767	1224
n17:1	1737	1710	2266	2985	2622	3425
n17	2386	2406	2818	3887	3511	4315
Prist-1-ene	1009	1082	1395	1471	1700	2195
Prist-2-ene	173	191	350	168	91	265
n18:1	1683	1568	2215	2982	2503	3653
n18	2311	2169	2806	3719	3138	4234
IP-20	263	263	313	351	335	671
n19:1	1649	1478	2087	2754	2342	3333
n19	2444	2177	2921	3876	3408	4538
n20:1	1532	1375	2024	2677	2326	3266
n20	2413	2120	2820	3669	3246	4390
n21:1	1491	1208	1942	2465	2185	3195
n21	2487	2014	3000	3767	3724	4600
n22:1	1623	1201	2134	2622	3094	3749
n22	2431	1693	2968	3375	3484	4750
n23:1	1617	1104	2115	2454	2412	3633
n23	2746	1640	3418	3468	4022	5548
n24:1	2030	1035	2554	2297	2146	4253
n24	2615	1450	3527	3205	2920	5616
n25:1	1550	941	2395	2317	2008	3831
n25	2781	1459	4537	3517	3054	6979
n26:1	1642	1085	2660	2532	2149	3866
n26	2136	1394	3905	3498	2710	5837
n27:1	1078	815	2023	2167	1768	2254
n27	2000	1421	4321	3691	2939	7912
n28:1	724	575	1776	1571	1425	2877
n28	1283	996	3142	2747	2333	4683
n29:1	701	532	1310	1335	1425	2431
n29	1084	1002	4243	2860	2543	6574
n30:1	462	395	1247	1290	1243	2198
n30	769	694	3223	2163	2005	4535
n31:1	378	350	1072	1054	1125	1765
n31	785	814	2296	2020	2111	4637
n32:1	280	304	1082	799	775	1172
n32	399	429	1492	1343	1599	2843

SPEC: ei48525a1#2.dat (31-Mar-00 21:56:57)

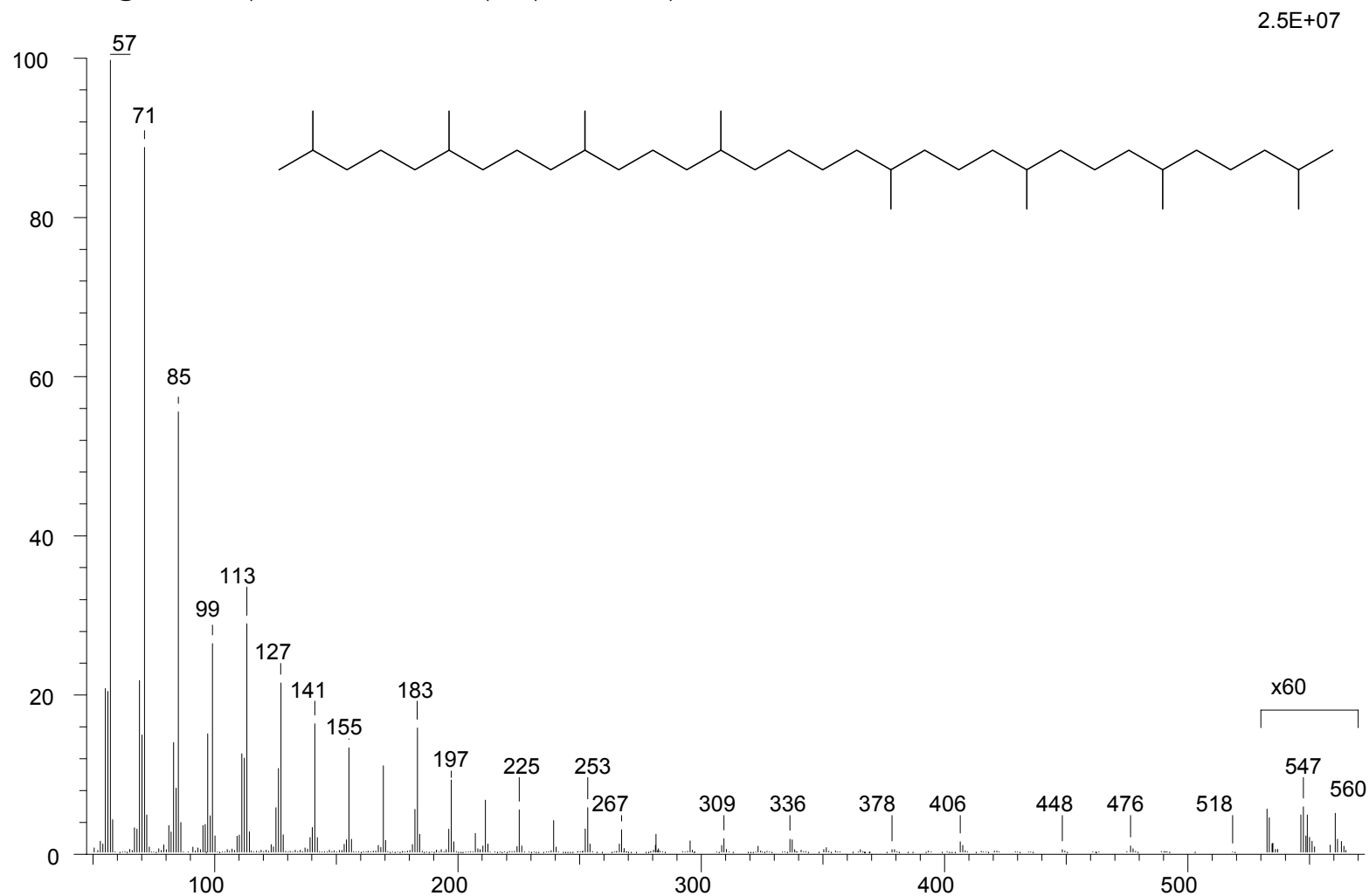
Scans: 1 > 7169

Base: 57.07

Masses: 50.00 > 600.00

#Peaks: 454

Scan 5209 @ 87.41 min (EI +VE +LMR BSCAN (EXP) UP LR NRM)



SPEC: ei48910a1#2.dat (01-Apr-00 00:02:56)

Scans: 1 > 7168

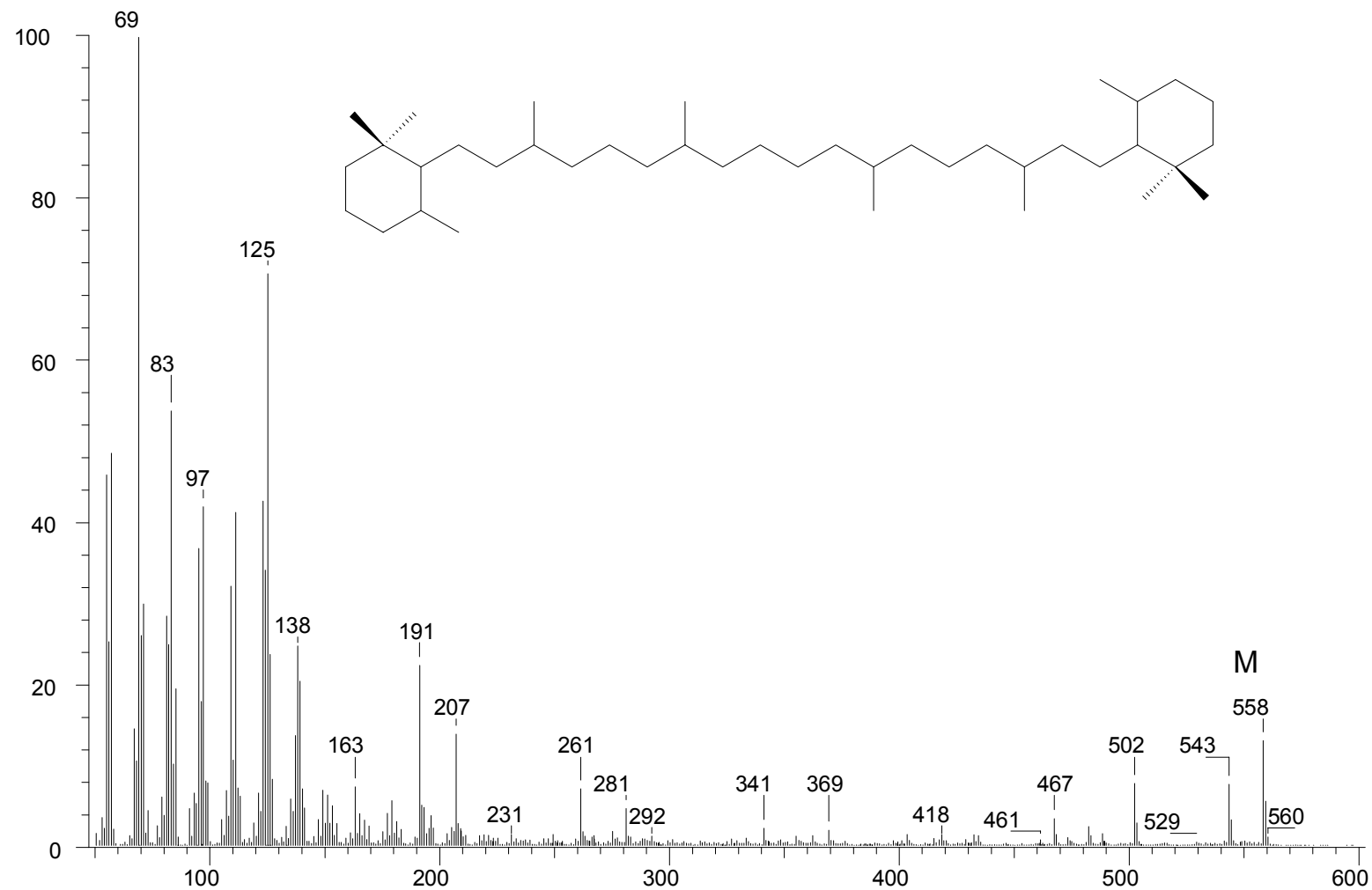
Base: 69.07

Masses: 50.00 > 600.00

#Peaks: 578

Scan 5510 @ 92.47 min (EI +VE +LMR BSCAN (EXP) UP LR NRM)

9.7E+06

Electron impact mass spectrum and structure of β -carotene; after Lopez (unpublished).

SPEC: ei48520al#1.dat (03-Apr-00 08:49:03)

Scans: 1 > 7170

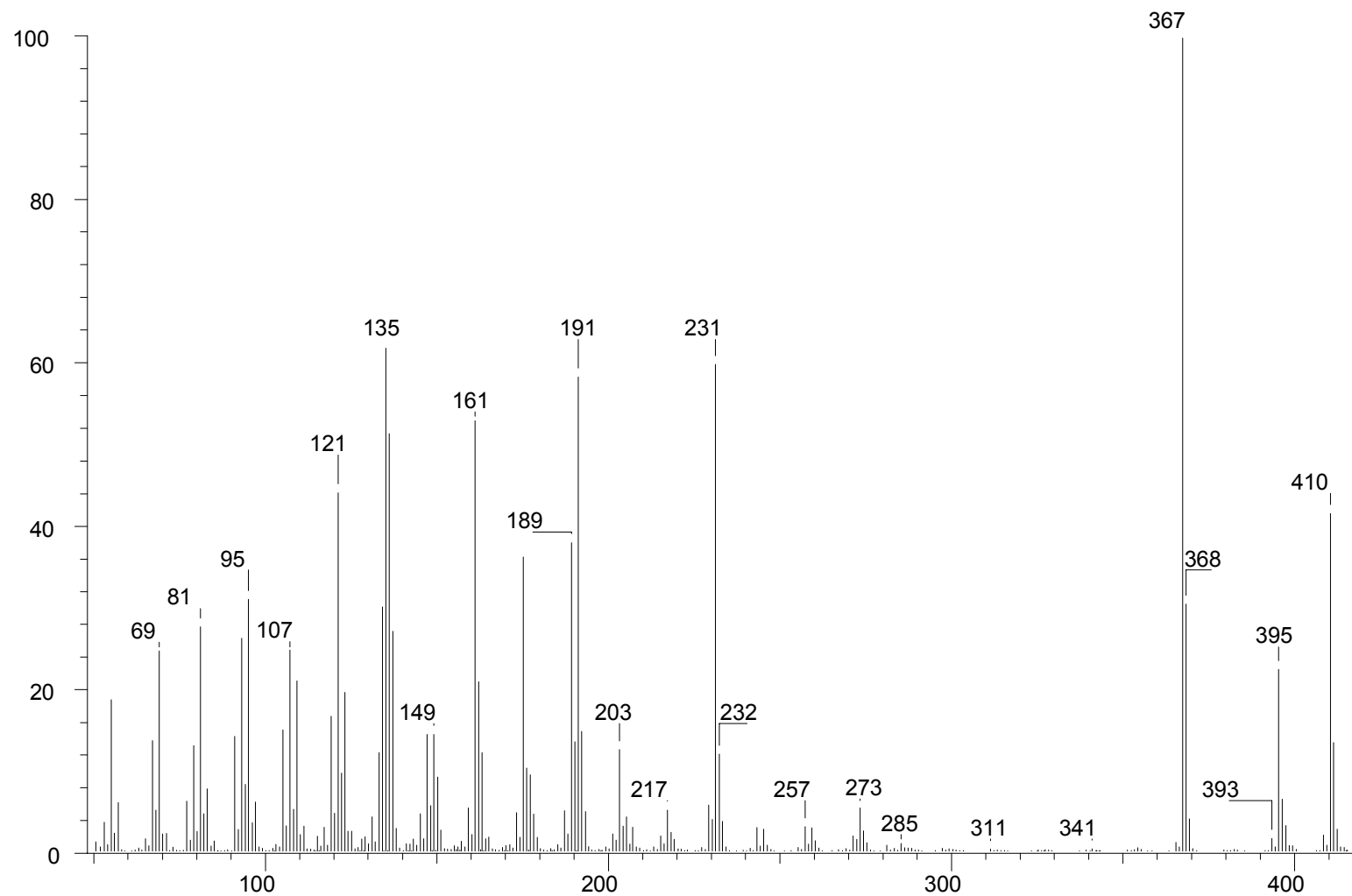
Base: 367.34

Masses: 50.00 > 600.00

#Peaks: 327

Scan 4848 @ 81.36 min (EI +VE +LMR BSCAN (EXP) UP LR NRM)

4.3E+06

Electron impact mass spectrum of a C₃₀ hopene; after Lopez (unpublished).

SPEC: ei48479ar#1.dat (06-Apr-00 15:48:39)

Base: 324.27

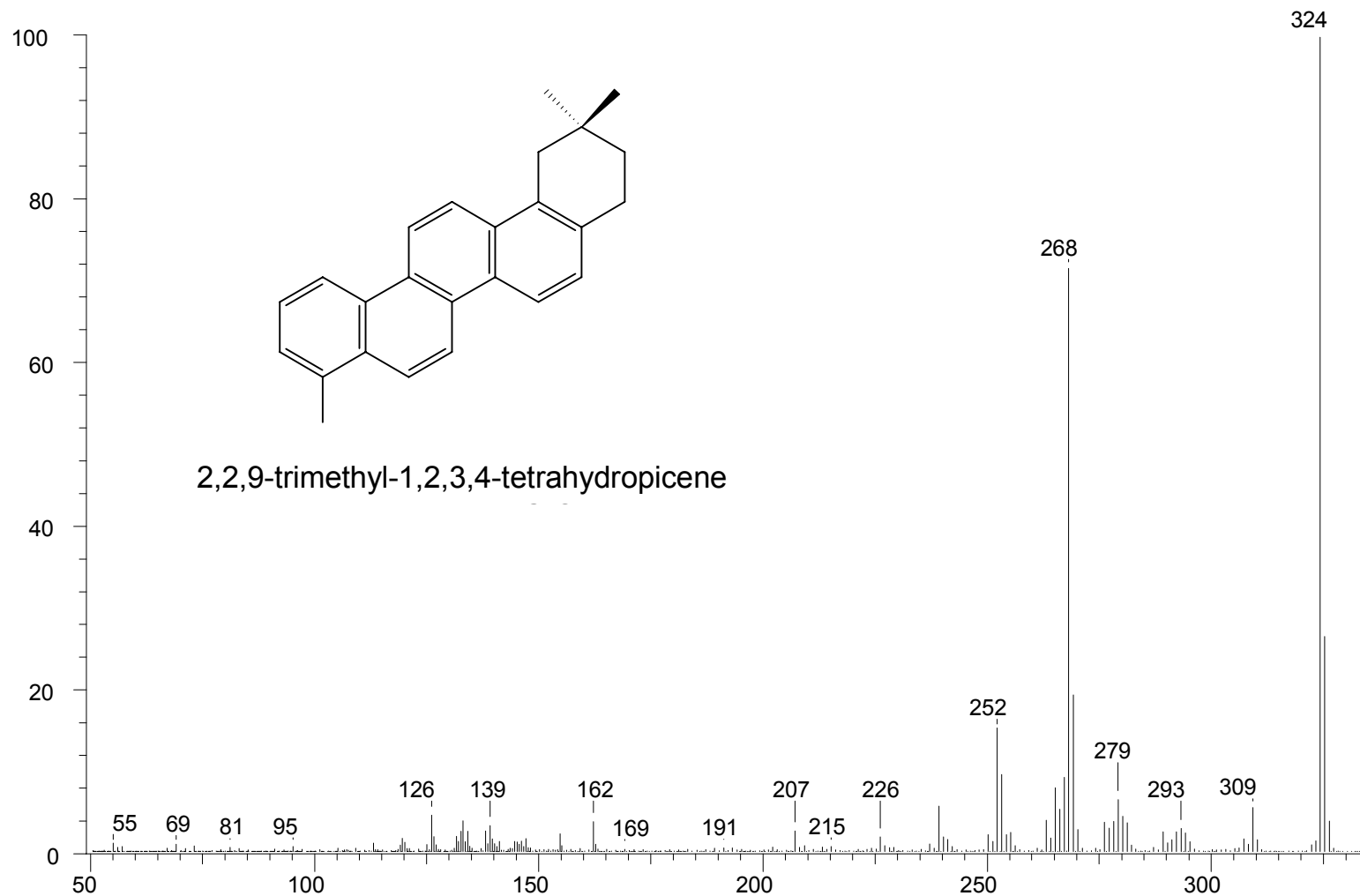
Masses: 50.00 > 600.00

Scans: 1 > 5582

#Peaks: 1378

Scan 4857 @ 88.28 min (EI +VE +LMR BSCAN (EXP) UP LR NRM)

1.6E+07



Electron impact mass spectrum and structure of an aromatic terpenoid; after Lopez (unpublished).

SPEC: ei48520ar#1.dat (11-Apr-00 10:40:21)

Scans: 1 > 6038

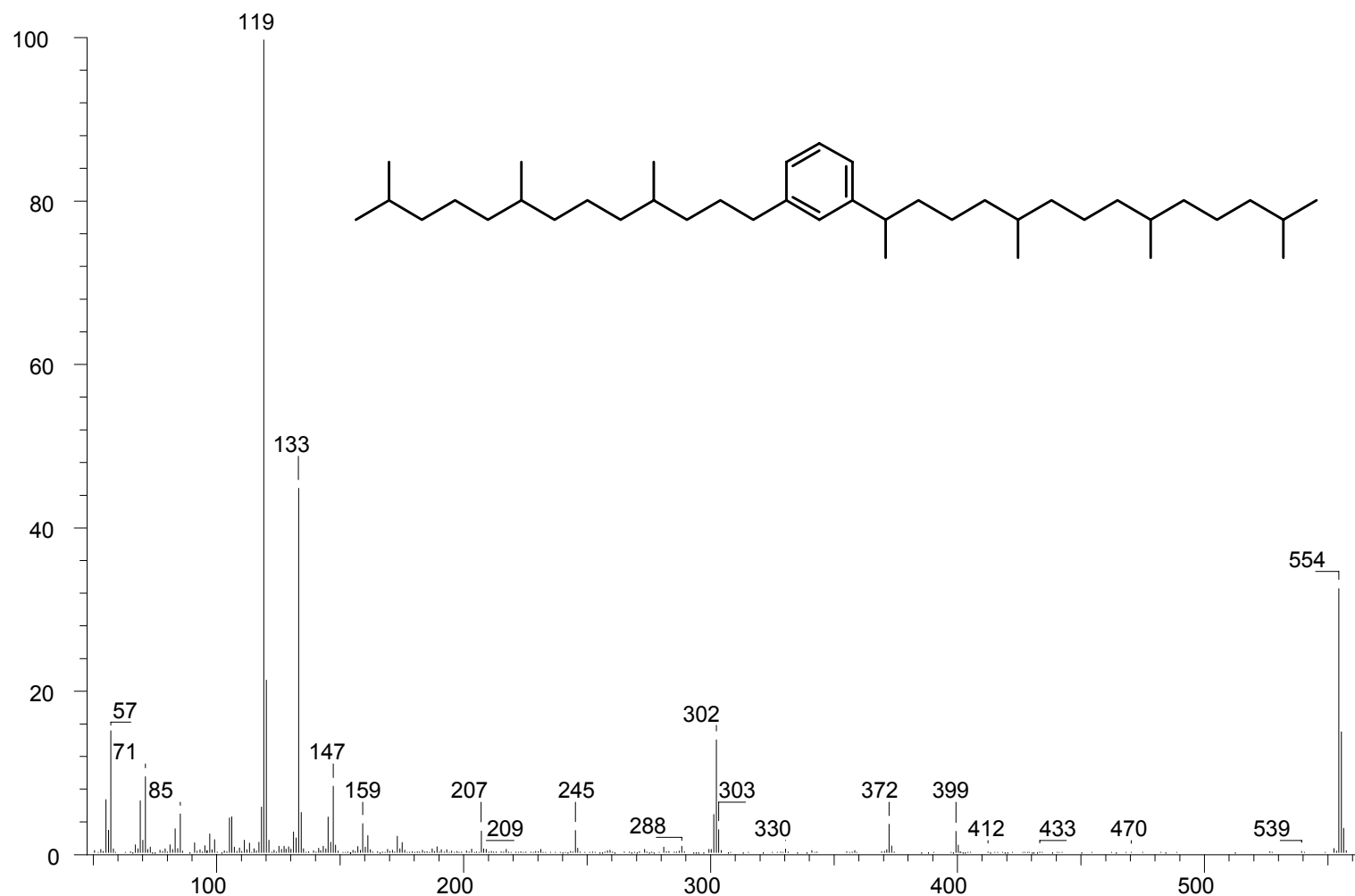
Base: 119.12

Masses: 50.00 > 600.00

#Peaks: 304

Scan 5162 @ 86.62 min (EI +VE +LMR BSCAN (EXP) UP LR NRM)

4.0E+06



Electron impact mass spectrum and tentative structure of an aromatised lycopane; after Lopez (unpublished).

SPEC: ei48505ar#1.dat (11-Apr-00 07:06:02)

Scans: 1 > 6038

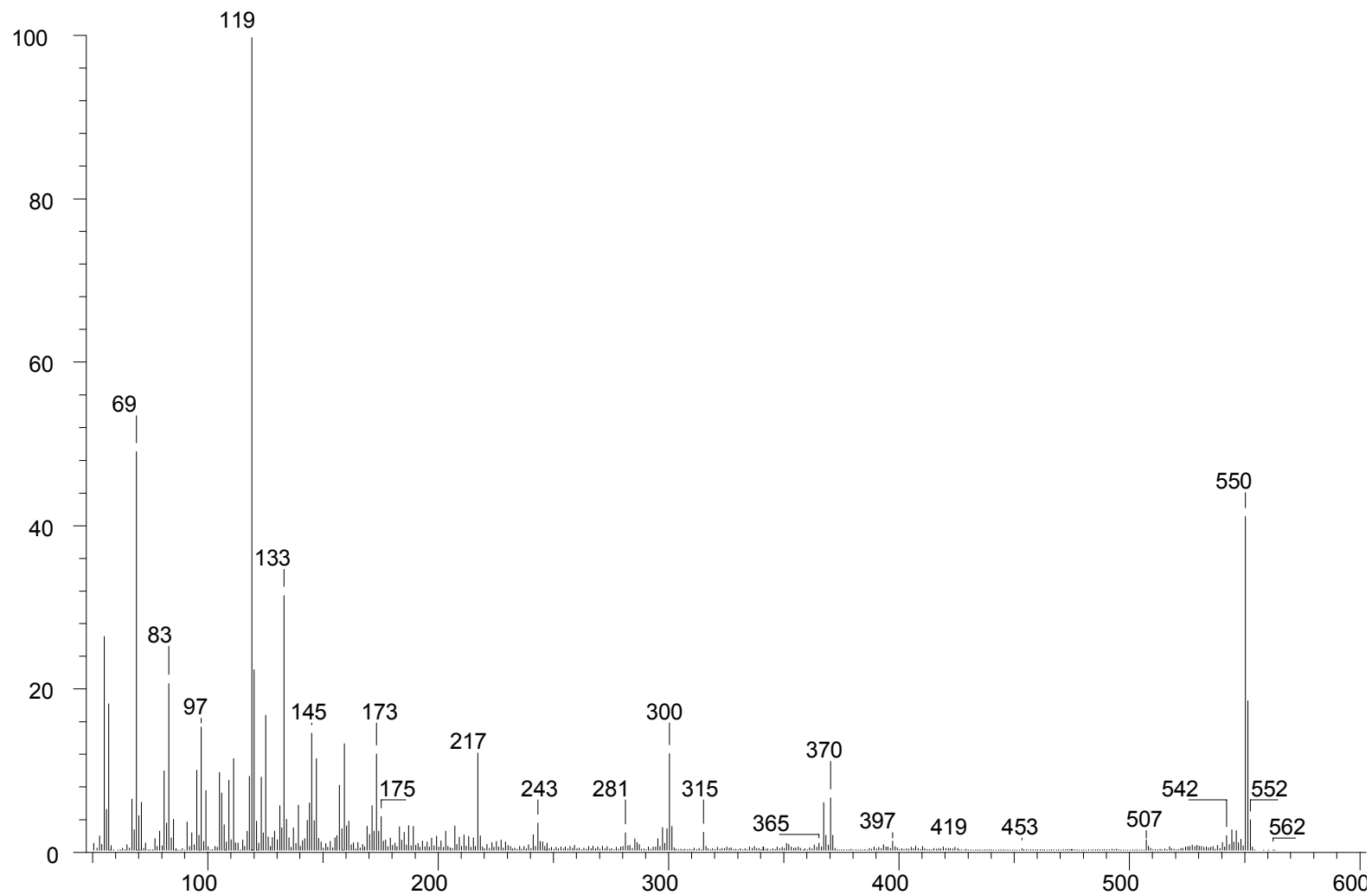
Base: 119.10

Masses: 50.00 > 600.00

#Peaks: 523

Scan 5452 @ 91.48 min (EI +VE +LMR BSCAN (EXP) UP LR NRM)

8.7E+06

Electron impact mass spectrum and tentative structure of a monoaromatic C₄₀ carotenoid; after Lopez (unpublished).

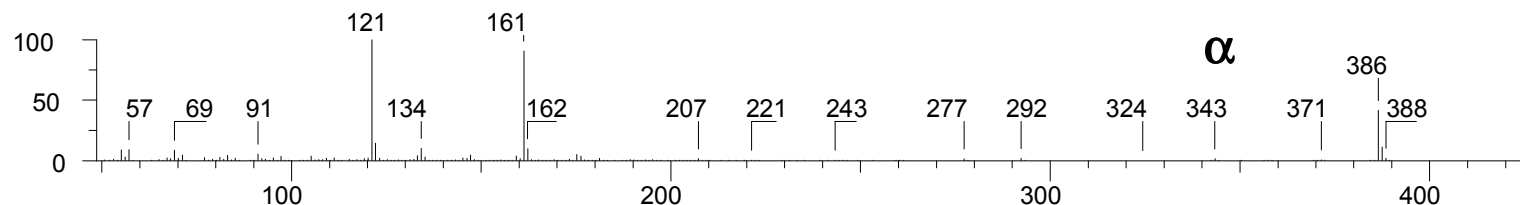
SPEC: ei48487ar#1.dat (07-Apr-00 02:29:10)

Scans: 1 > 5666

Masses: 50.00 > 600.00

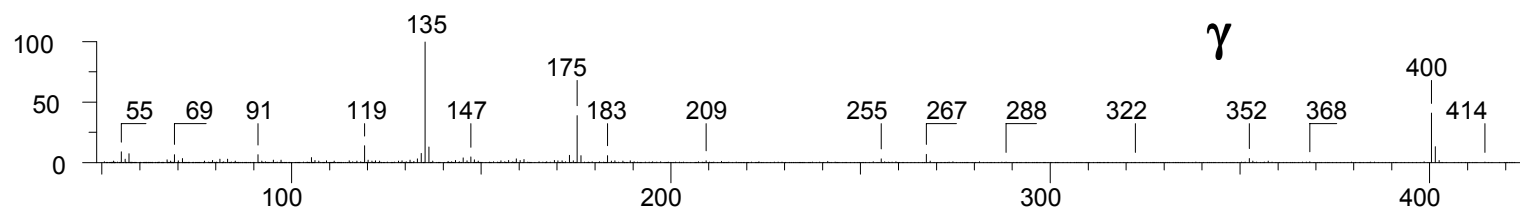
Scan 3916 @ 70.59 min (EI +VE +LMR BSCAN (EXP) UP LR NRM)

5.0E+07



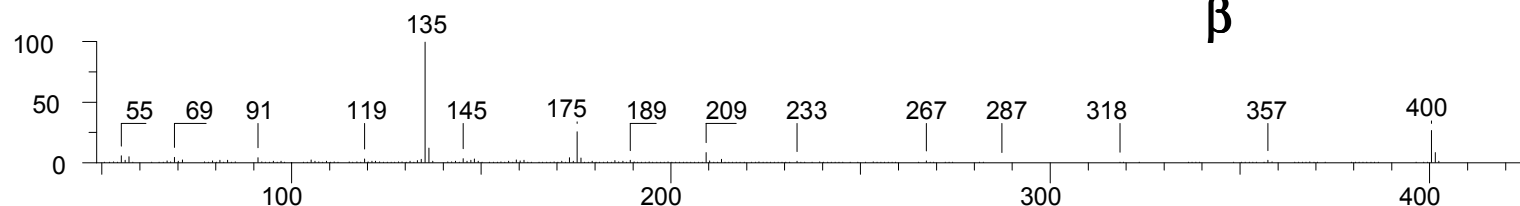
Scan 4056 @ 73.04 min (EI +VE +LMR BSCAN (EXP) UP LR NRM)

8.4E+06



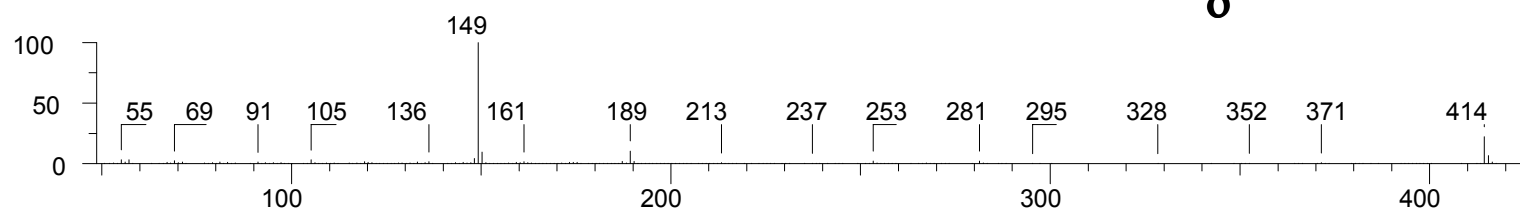
Scan 4070 @ 73.28 min (EI +VE +LMR BSCAN (EXP) UP LR NRM)

1.7E+07



Scan 4195 @ 75.46 min (EI +VE +LMR BSCAN (EXP) UP LR NRM)

6.1E+07



Electron impact mass spectrum of the methyl substituted 2-methyl-2-(4,8,12-trimethyltridecyl) chromans. 5,7,8 Trimethyl (α), 7,8-dimethyl (γ), 5,8-Dimethyl (β) and 8-methyl (δ); after Lopez (unpublished).

SPEC: ei48922ar#1.dat (05-Apr-00 16:17:10)

Base: 365.39

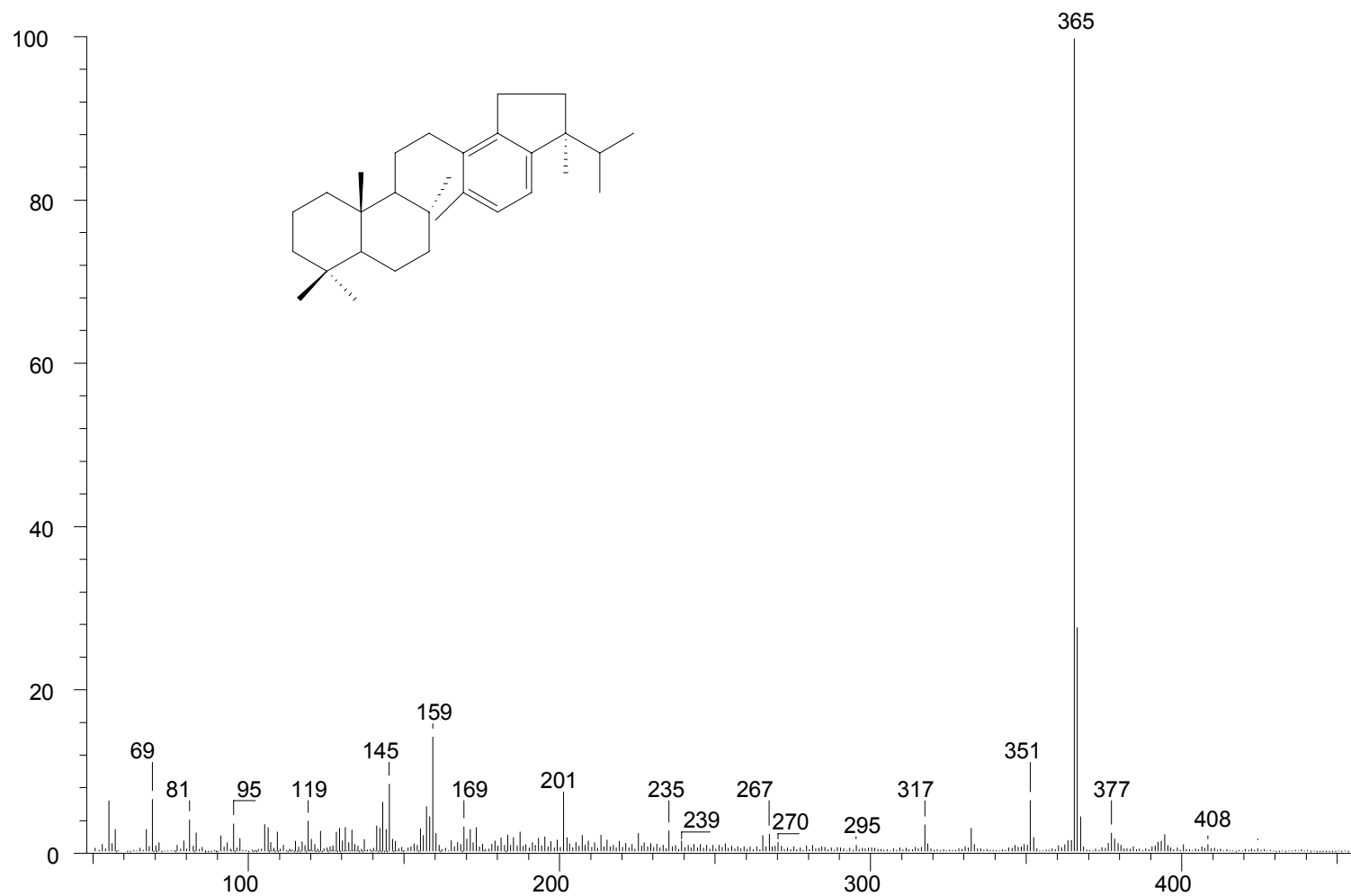
Masses: 50.00 > 600.00

Scans: 1 > 6032

#Peaks: 499

Scan 4693 @ 78.74 min (EI +VE +LMR BSCAN (EXP) UP LR NRM)

4.2E+07

Electron impact mass spectrum of a C₂₉ ring D aromatised 8,14-secohopanoid; after Lopez (unpublished).

SPEC: ei48514ar#2.dat (01-Sep-00 15:48:30)

Base: 28.01

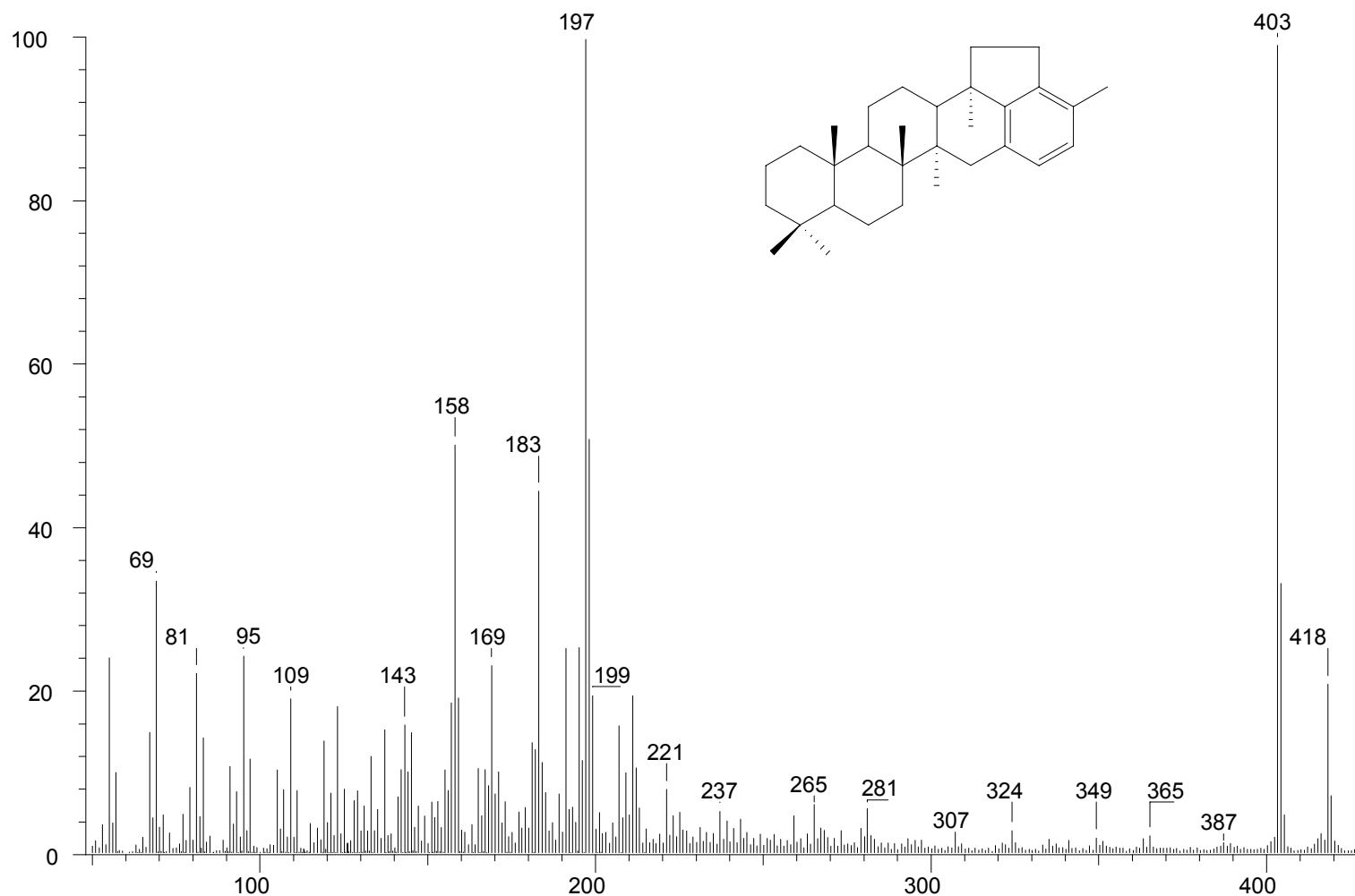
Masses: 20.00 > 800.00

Scans: 1 > 3696

#Peaks: 670

Scan 3233 @ 88.64 min (EI +VE +LMR BSCAN (EXP) UP LR NRM)

2.1E+06



Electron impact mass spectrum and structure of the 4'-methylbenzo[16,17,21]-22,29,30-trinorhop-16-ene.; after Lopez (unpublished).

SPEC: ei48514a#2.dat (01-Sep-00 15:48:30)

Base: 28.01

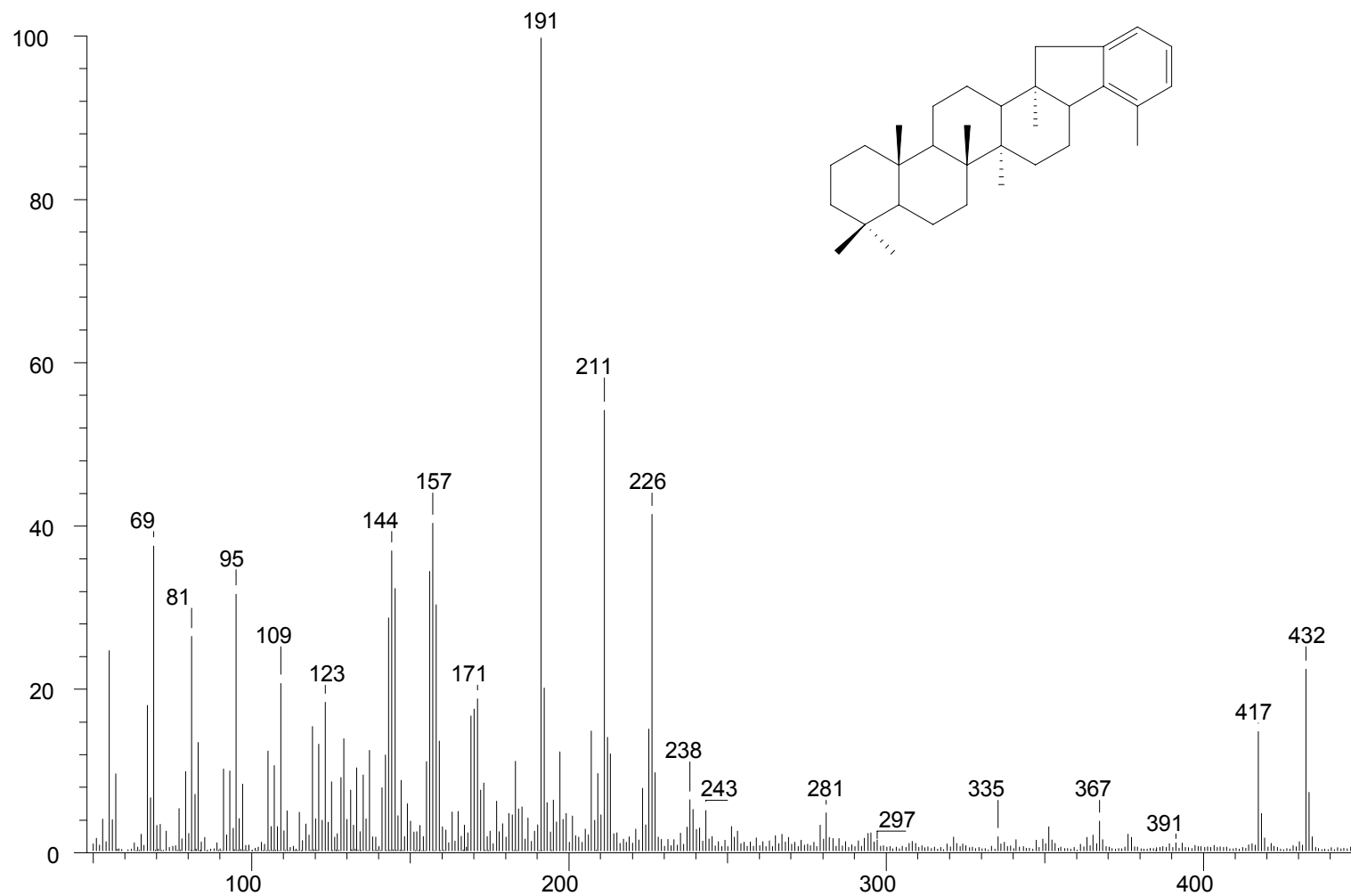
Masses: 20.00 > 800.00

Scans: 1 > 3696

#Peaks: 668

Scan 3273 @ 89.73 min (EI +VE +LMR BSCAN (EXP) UP LR NRM)

2.6E+06



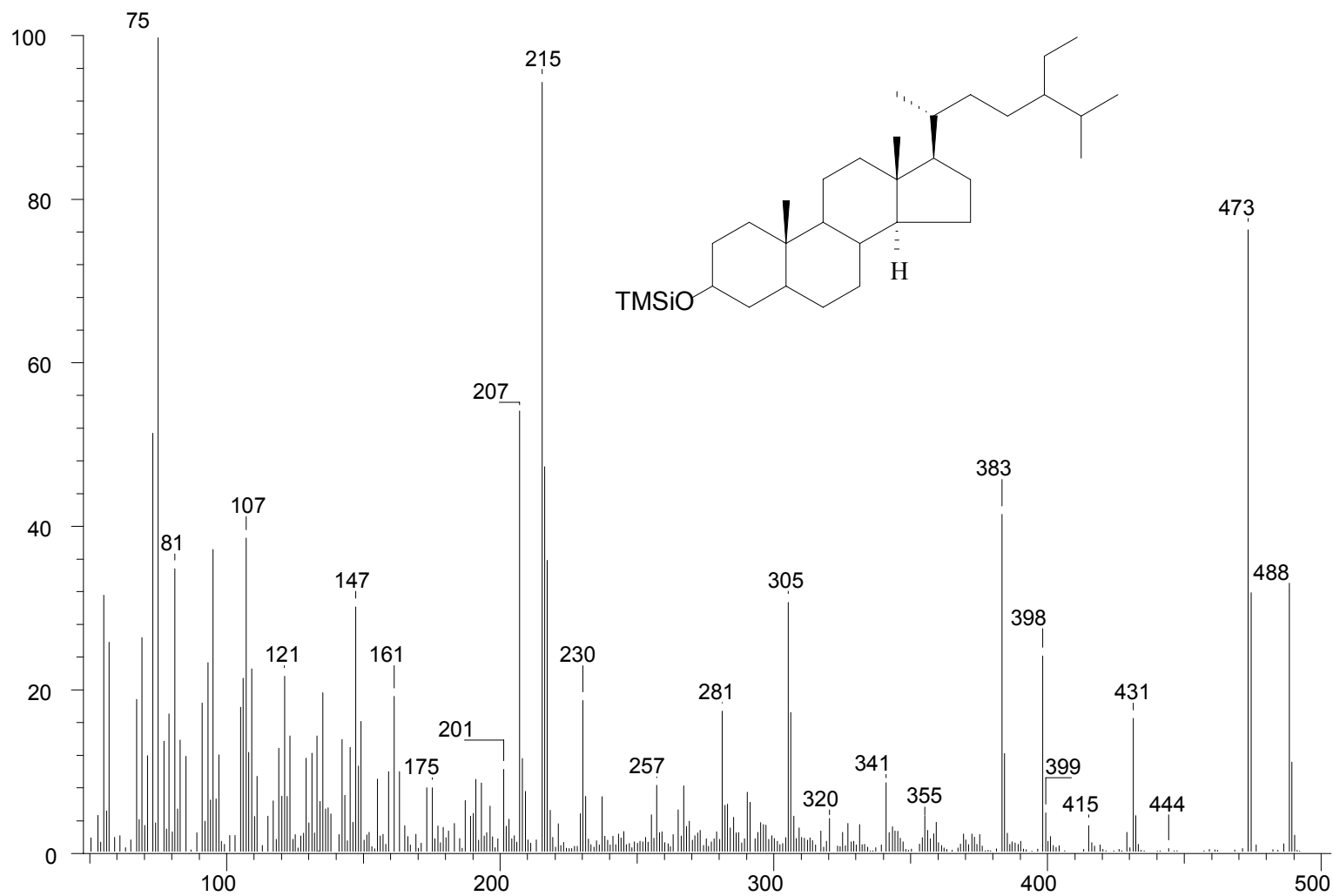
Electron impact mass spectrum and structure of the 3'-methylbenzo[20,21]-22,29,30-trinorhop-20-ene; after Lopez (unpublished).

SPEC: ei48455da#2 (27-Mar-00 15:31:34)

Scans: 1 > 7172

REG #9 @ 85.60 min (+5102>5115 - 5118>5124 , 5070>5073) (EI +VE +LMR*)

2.4E+06



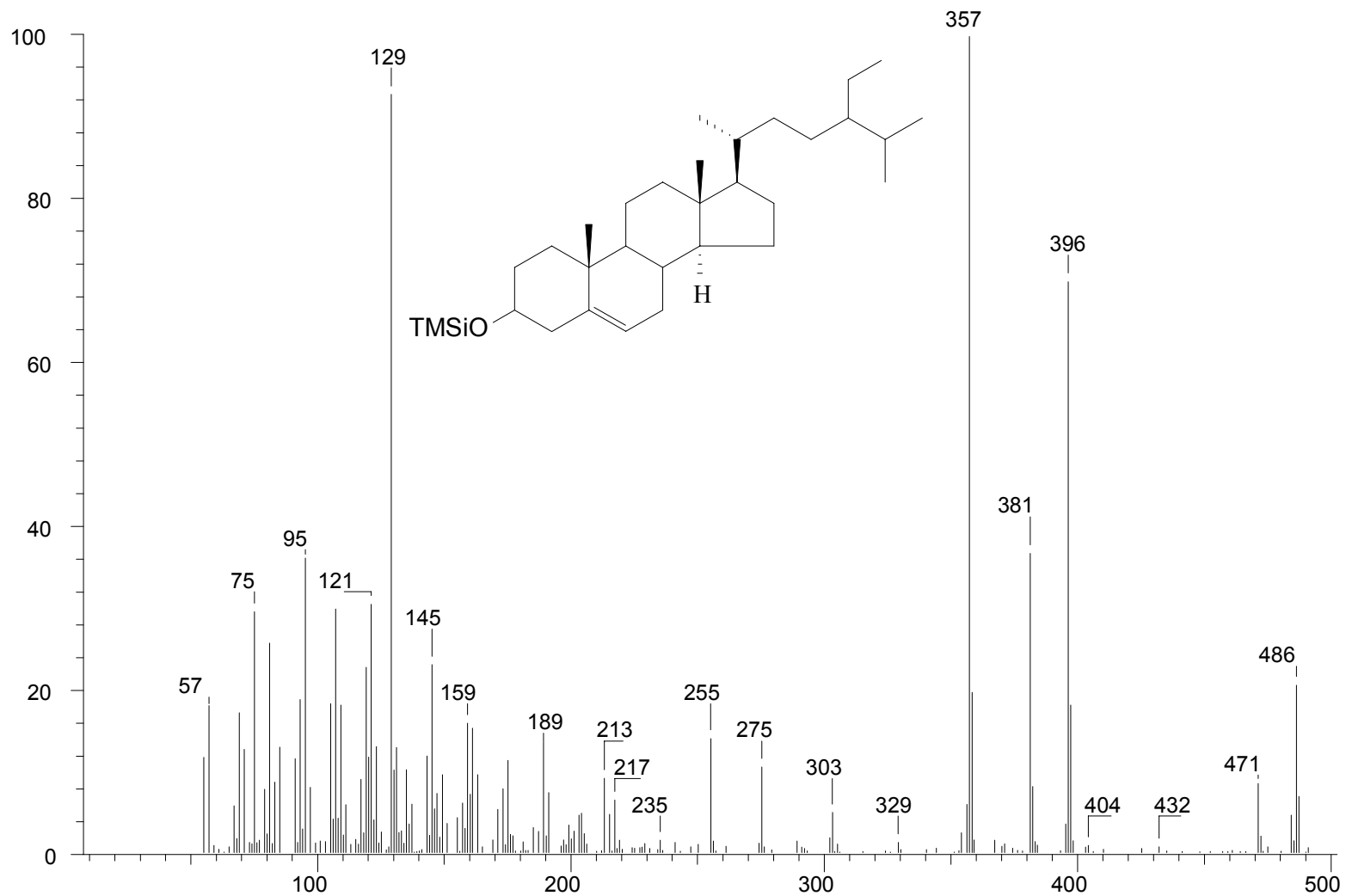
Electron impact mass spectrum and structure of the trimethylsilyl derivative of 24-ethylcholestan-3-ol; after Lopez (unpublished).

SPEC: ei48455da#2 (27-Mar-00 15:31:34)

Scans: 1 > 7172

REG #9 @ 85.38 min (+5089>5094 - 5070>5073 , 5122>5125) (EI +VE +LMR*)

4.9E+05



Electron impact mass spectrum and structure of the trimethylsilyl derivative of 24-ethylcholest-5-en-3β-ol; after Lopez (unpublished).

SPEC: ei48502da#1 (30-Mar-00 14:42:32)

Base: 191.23

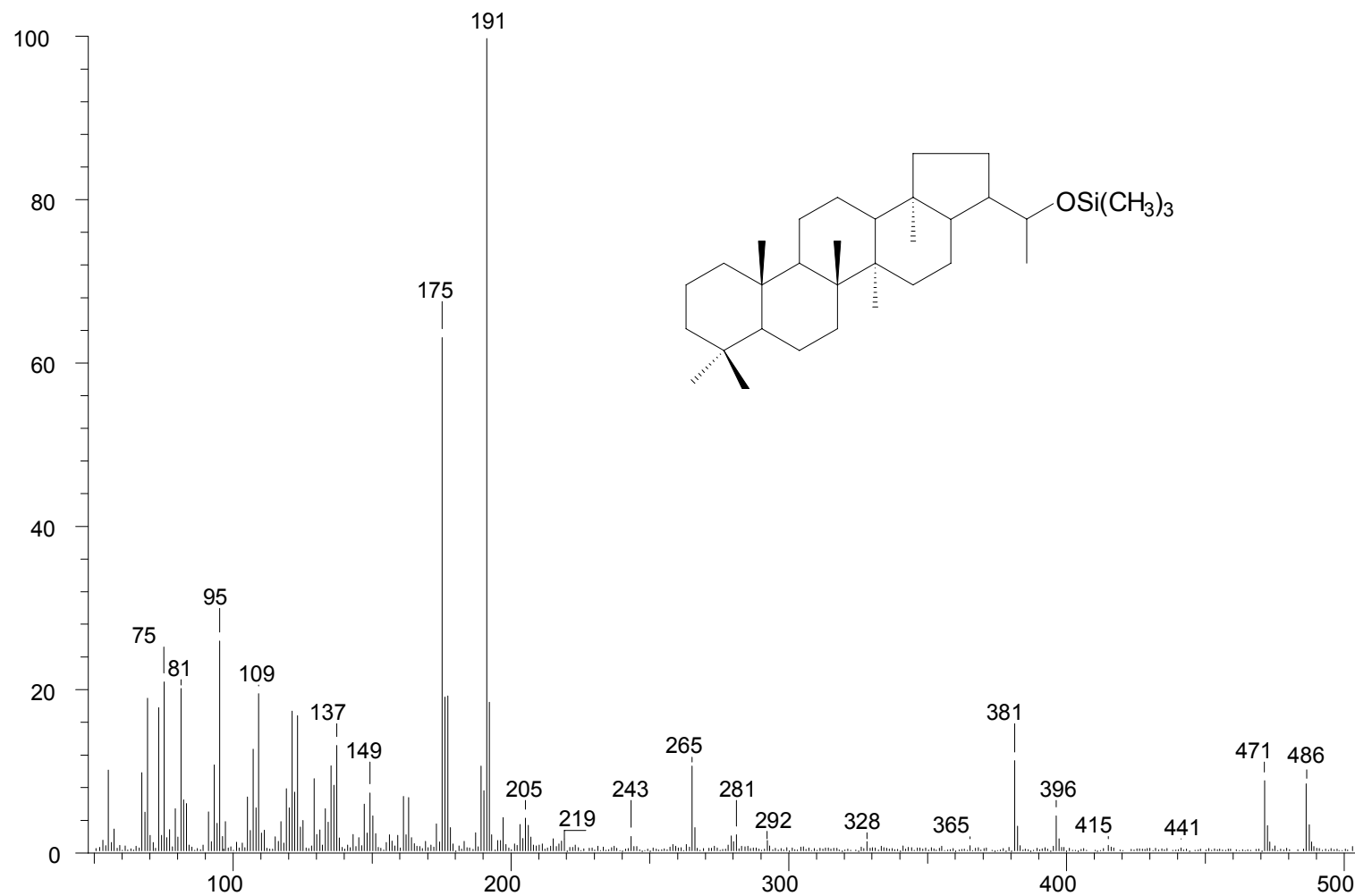
Masses: 50.00 > 600.00

Scans: 1 > 7171

#Peaks: 461

REG #9 @ 89.68 min (!5345) (EI +VE +LMR BSCAN (EXP) UP LR NRM)

9.0E+05



Electron impact mass spectrum and structure of the trimethylsilyl derivative of 30-norhopan-22-ol; after Lopez (unpublished).

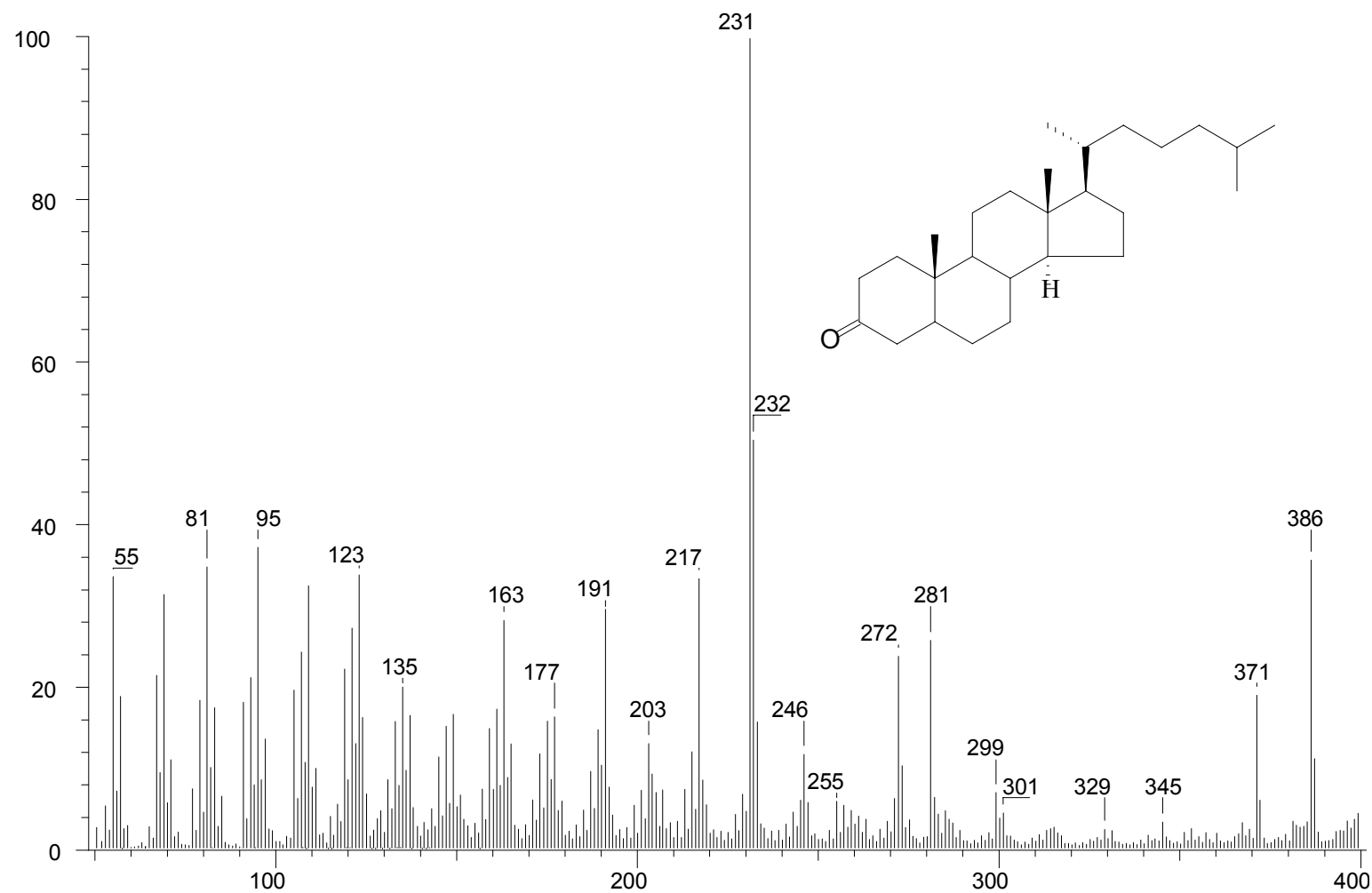
SPEC: ei48532ek#1.dat (20-Feb-00 20:21:36)

Scans: 1 > 6036

Comm: GC-MS-ASAMP-KAS-Inj. SGE-50m, ID 0.22mm, FT 0.25um, EPC=1.0ml/min

Scan 4993 @ 83.78 min (EI +VE +LMR BSCAN (EXP) UP LR NRM)

4.0E+06



Electron impact mass spectrum and structure of cholestan-3-one; after Lopez (unpublished).

SPEC: ei48455ek#1a.dat (21-Feb-00 09:30:15)

Base: 167.03

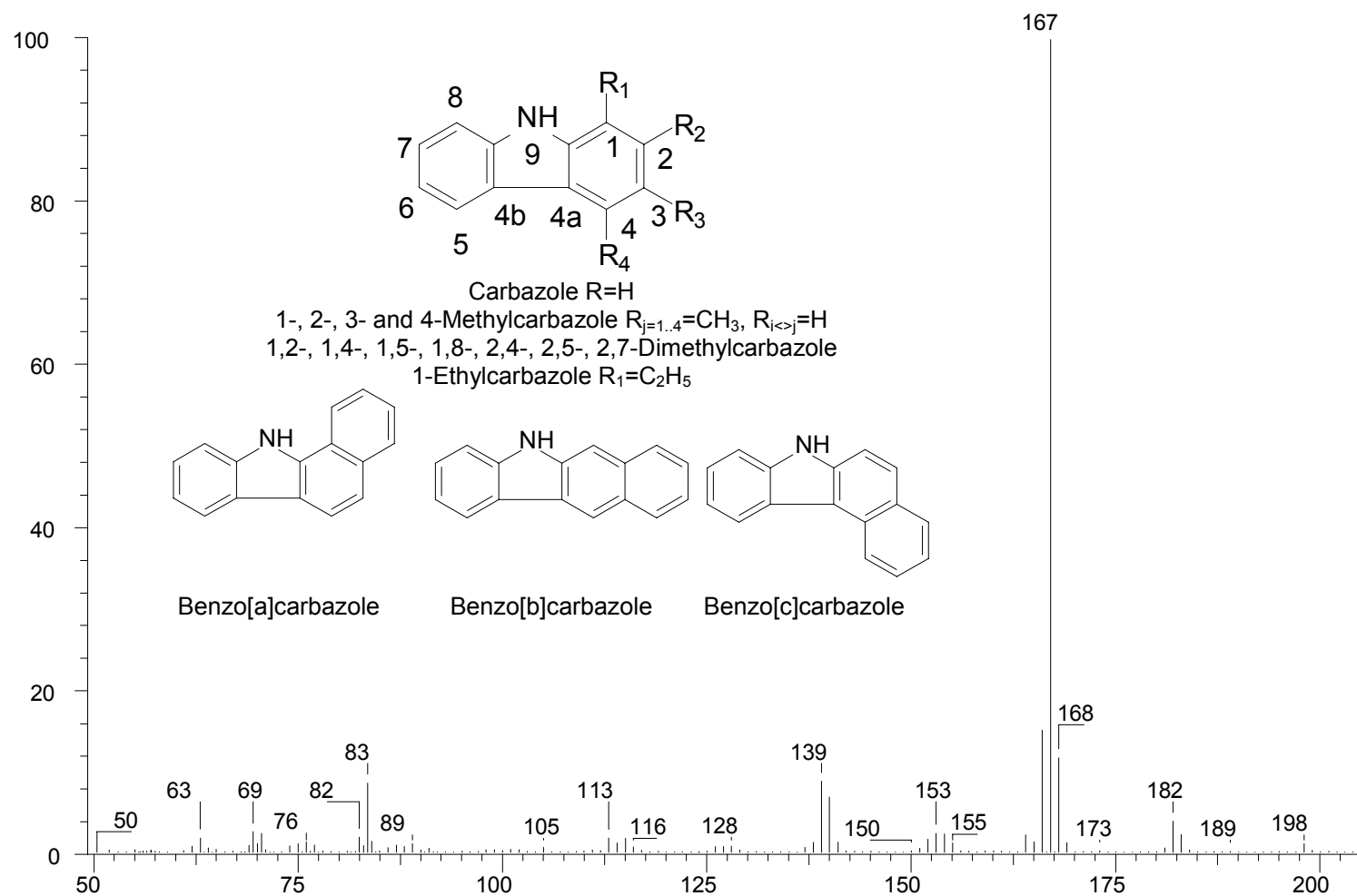
Masses: 50.00 > 600.00

Scans: 1 > 6038

#Peaks: 236

Scan 2959 @ 49.66 min (EI +VE +LMR BSCAN (EXP) UP LR NRM)

3.9E+07



Electron impact mass spectrum of carbazole and carbazole structures; after Lopez (unpublished).

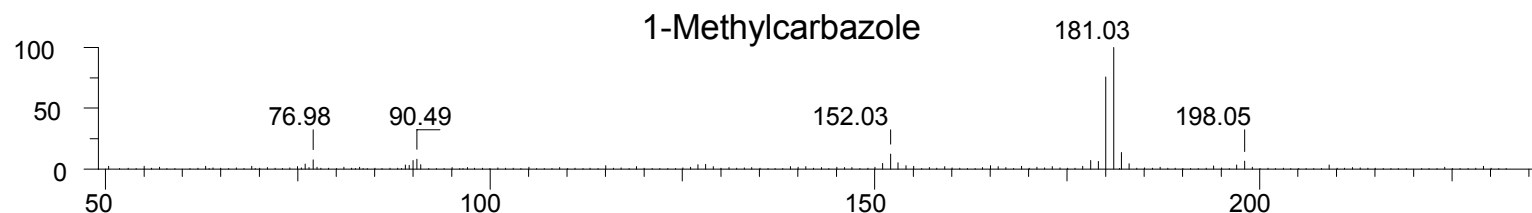
SPEC: ei48467ek#1.dat (19-Feb-00 12:20:26)

Scans: 1 > 6027

Masses: 50.00 > 600.00

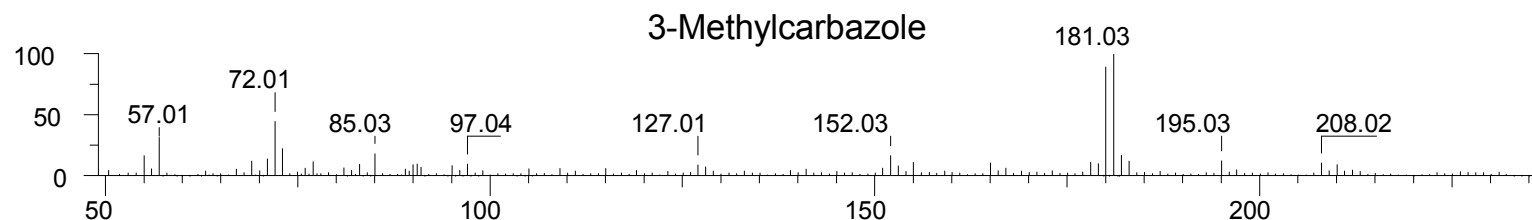
Scan 3097 @ 51.97 min (EI +VE +LMR BSCAN (EXP) UP LR NRM)

1.5E+07



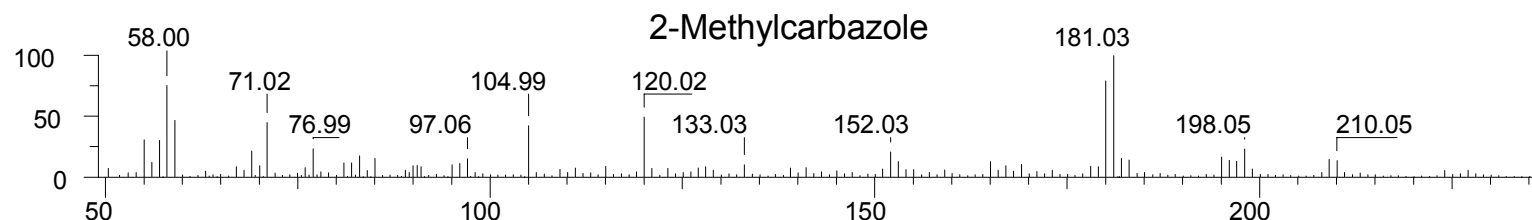
Scan 3176 @ 53.30 min (EI +VE +LMR BSCAN (EXP) UP LR NRM)

6.6E+06



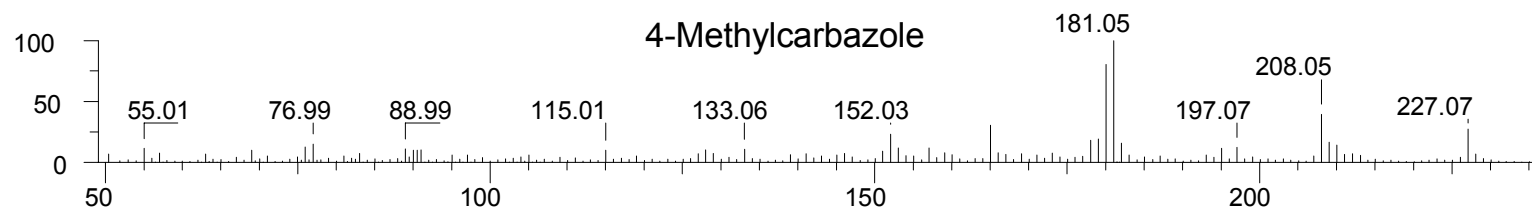
Scan 3189 @ 53.51 min (EI +VE +LMR BSCAN (EXP) UP LR NRM)

6.9E+06



Scan 3215 @ 53.95 min (EI +VE +LMR BSCAN (EXP) UP LR NRM)

3.7E+06



Electron impact mass spectra of methylcarbazoles; after Lopez (unpublished).

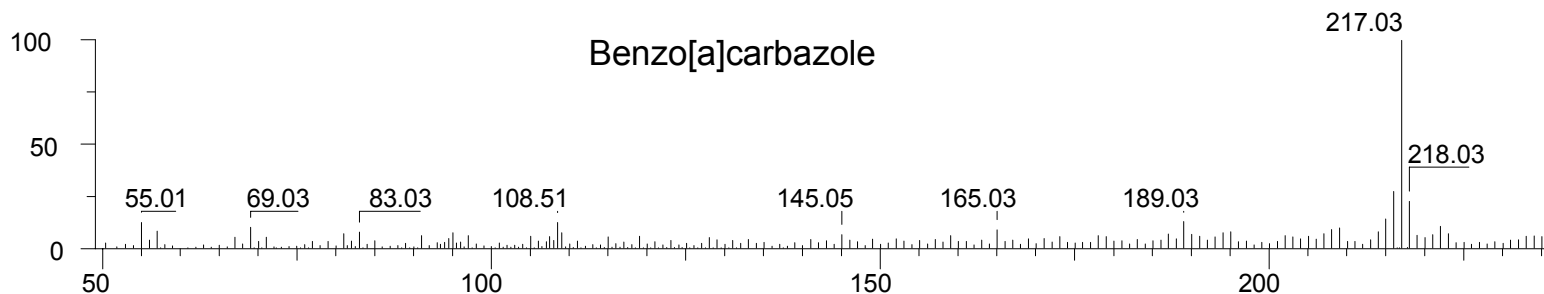
SPEC: ei48467ek#1.dat (19-Feb-00 12:20:26)

Scans: 1 > 6027

Masses: 50.00 > 600.00

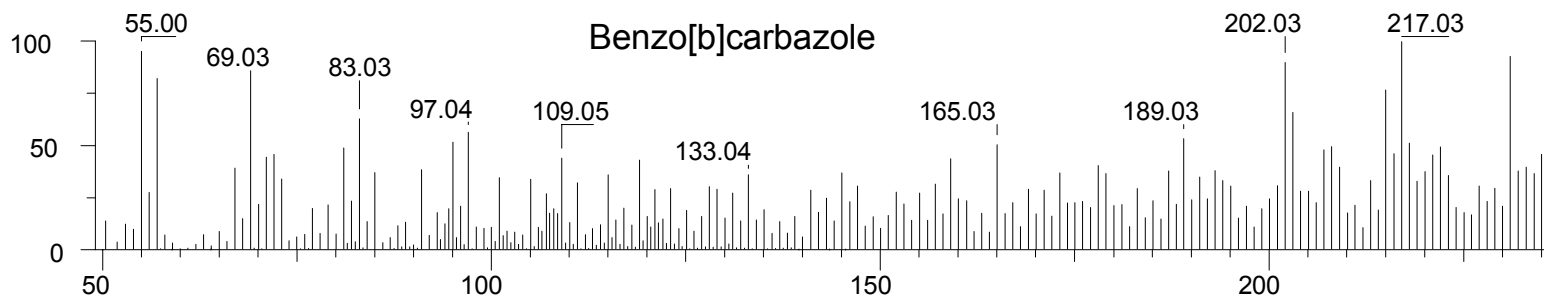
Scan 4094 @ 68.69 min (EI +VE +LMR BSCAN (EXP) UP LR NRM)

4.6E+06



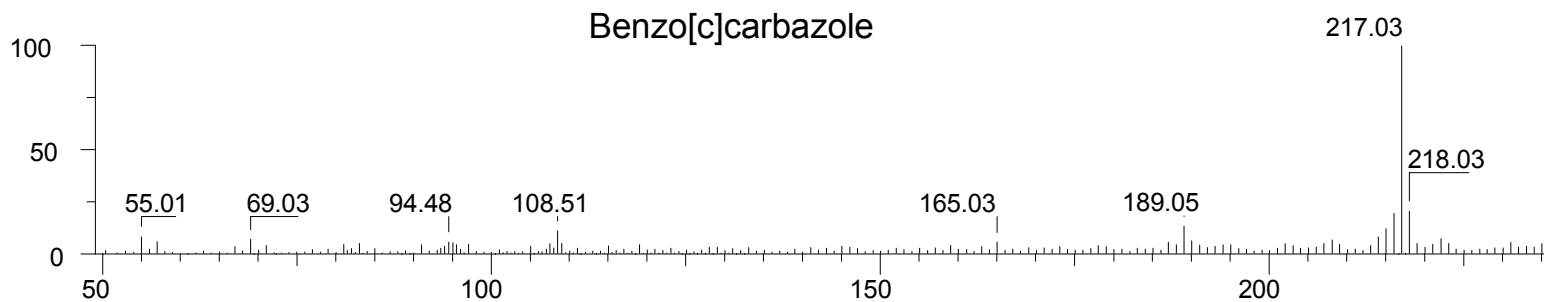
Scan 4189 @ 70.29 min (EI +VE +LMR BSCAN (EXP) UP LR NRM)

7.1E+05



Scan 4207 @ 70.59 min (EI +VE +LMR BSCAN (EXP) UP LR NRM)

7.6E+06



Electron impact mass spectra of benzocarbazoles; after Lopez (unpublished)

SPEC: ei48467ek#1.dat (19-Feb-00 12:20:26)

Base: 180.01

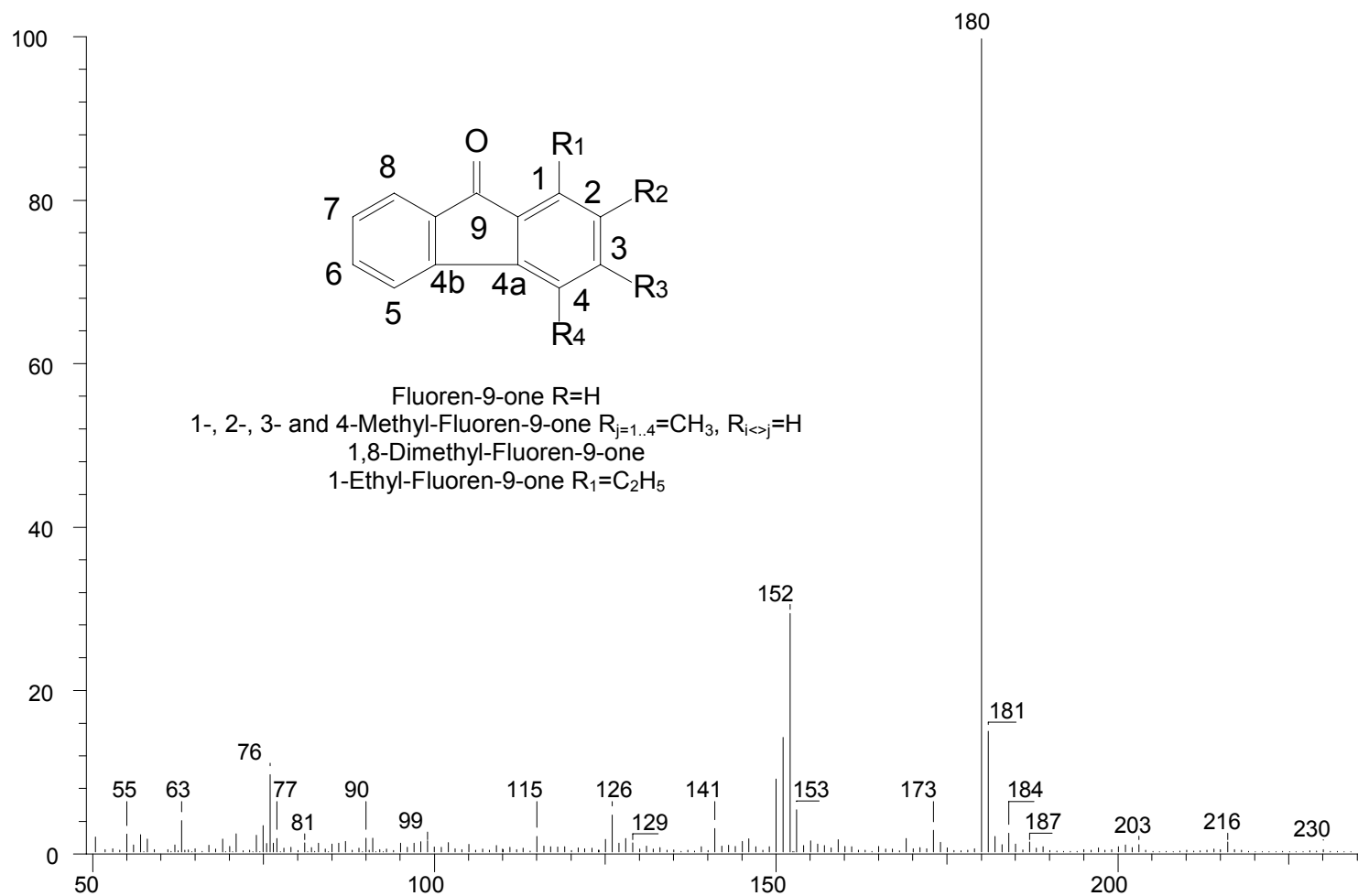
Masses: 50.00 > 600.00

Scans: 1 > 6027

#Peaks: 233

Scan 2743 @ 46.03 min (EI +VE +LMR BSCAN (EXP) UP LR NRM)

1.6E+07



Electron impact mass spectrum of fluoren-9-one and fluoren-9-one structures; after Lopez (unpublished).

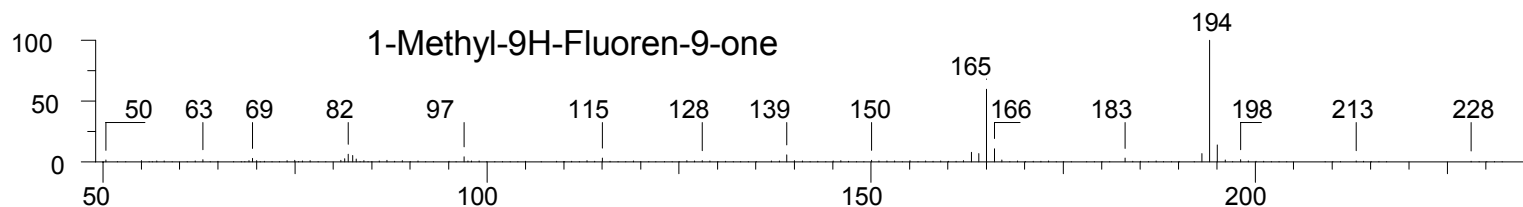
SPEC: ei48467ek#1.dat (19-Feb-00 12:20:26)

Scans: 1 > 6027

Masses: 50.00 > 600.00

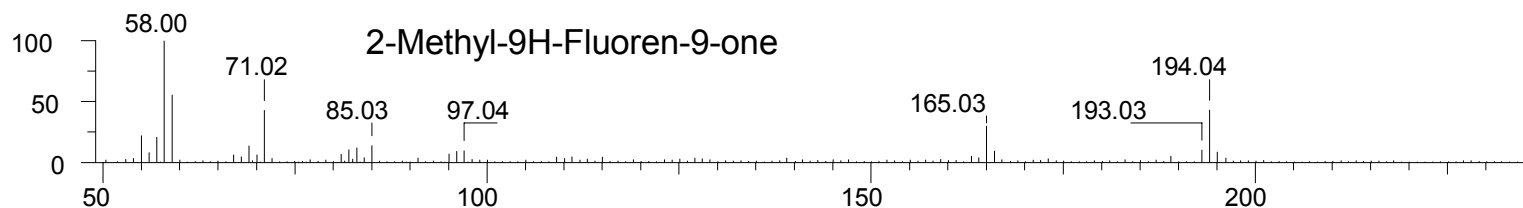
Scan 2919 @ 48.98 min (EI +VE +LMR BSCAN (EXP) UP LR NRM)

4.1E+07



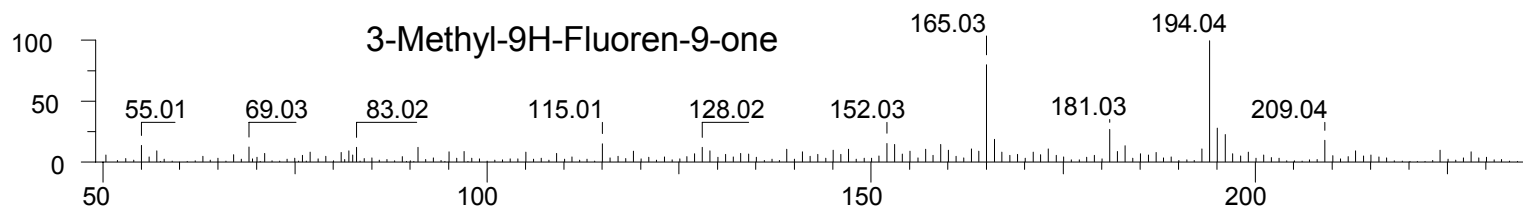
Scan 2993 @ 50.22 min (EI +VE +LMR BSCAN (EXP) UP LR NRM)

1.0E+07



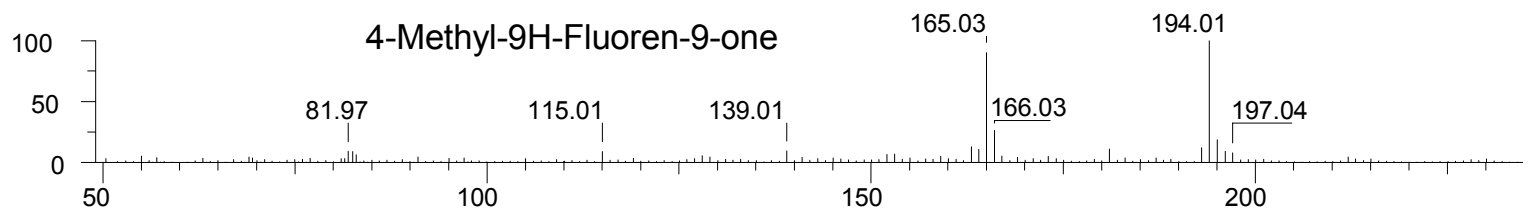
Scan 3019 @ 50.66 min (EI +VE +LMR BSCAN (EXP) UP LR NRM)

2.1E+06



Scan 3049 @ 51.16 min (EI +VE +LMR BSCAN (EXP) UP LR NRM)

5.8E+06



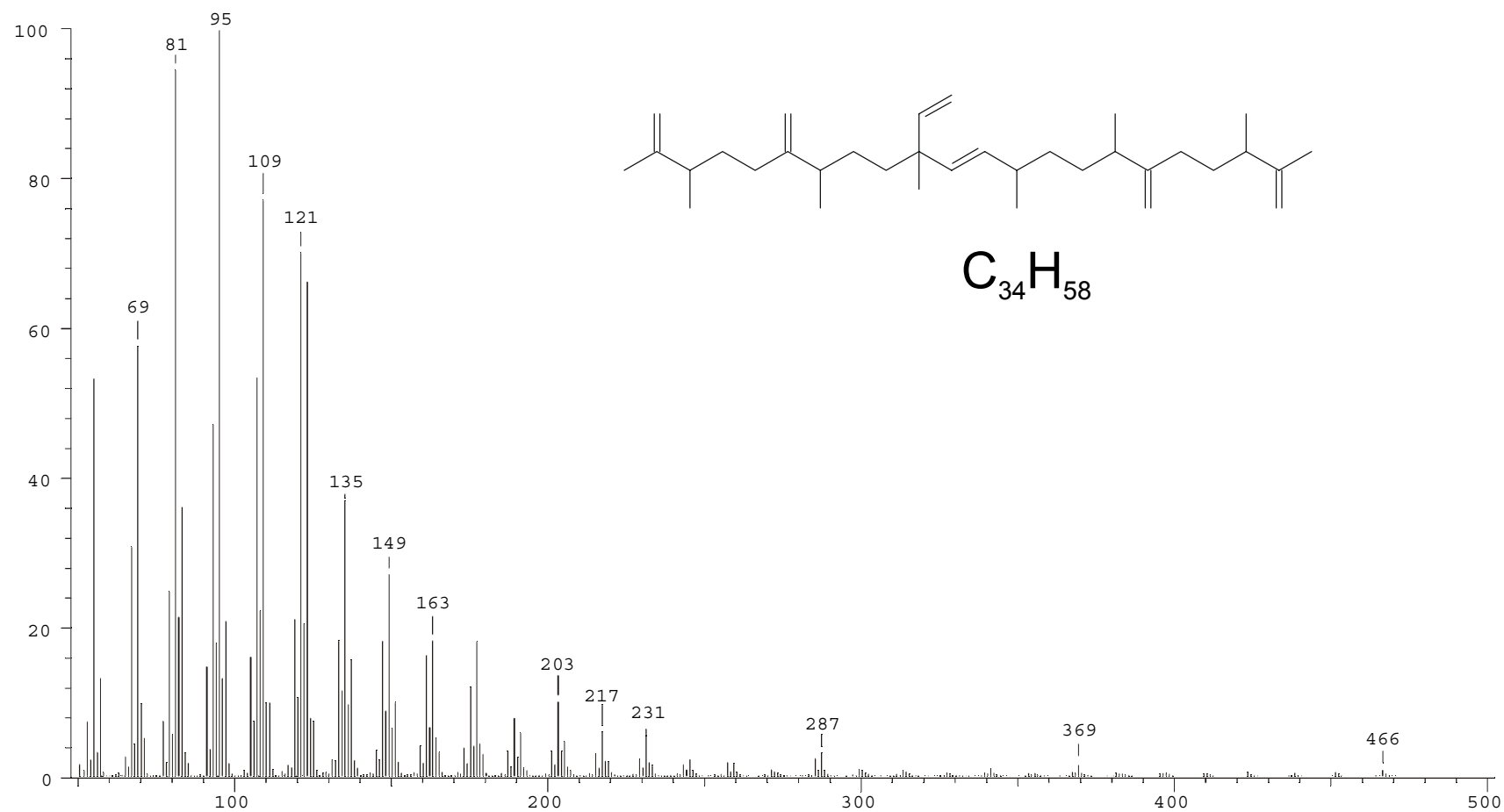
Electron impact mass spectra of methylfluoren-9-ones; after Lopez (unpublished).

SPEC: ei47716ar#2 (06-Oct-00 13:56:26)
Samp: Vial 1 E47716-2 (FS-LR, Fm50, Lm600,)
Comm: GC-MS-ASAMP-KAS-Inj. SGE-50m, ID 0.22mm, FT 0.25um, EPC=1.0ml/min
Oper: ud Study: p481
Base: 95.13 Masses: 50.00 > 600.00
Peak: 1000.0 mmu Intensity: 12045520
REG #9 @ 51.15 min (! 3041) (EI +VE +LMR BSCAN (EXP) UP LR NRM)

Scans: 1 > 7137

Client: A.Fuhrmann
#Peaks: 349
RIC: 170199734

1.2E+07



Mass spectrum and tentative structure of a C₃₄H₅₈ botryococcene; after Cox et al. (1973) and Huang et al. (1999)

SPEC: ei47739al#1.dat (09-Apr-99 13:29:01)

Scans: 1 > 6034

Samp: Vial 2 E47739-1 (FS-LR)

Comm: GC-MS-ASAMP-KAS-Inj. SGE-50m, ID 0.22mm, FT 0.25um, EPC=1.0ml/min

Oper: fjk,cts=583

Study: P481-H.Fuhrmann

Client: He5.6=Fl.

Base: 80.97

Masses: 50.00 > 600.00

#Peaks: 319

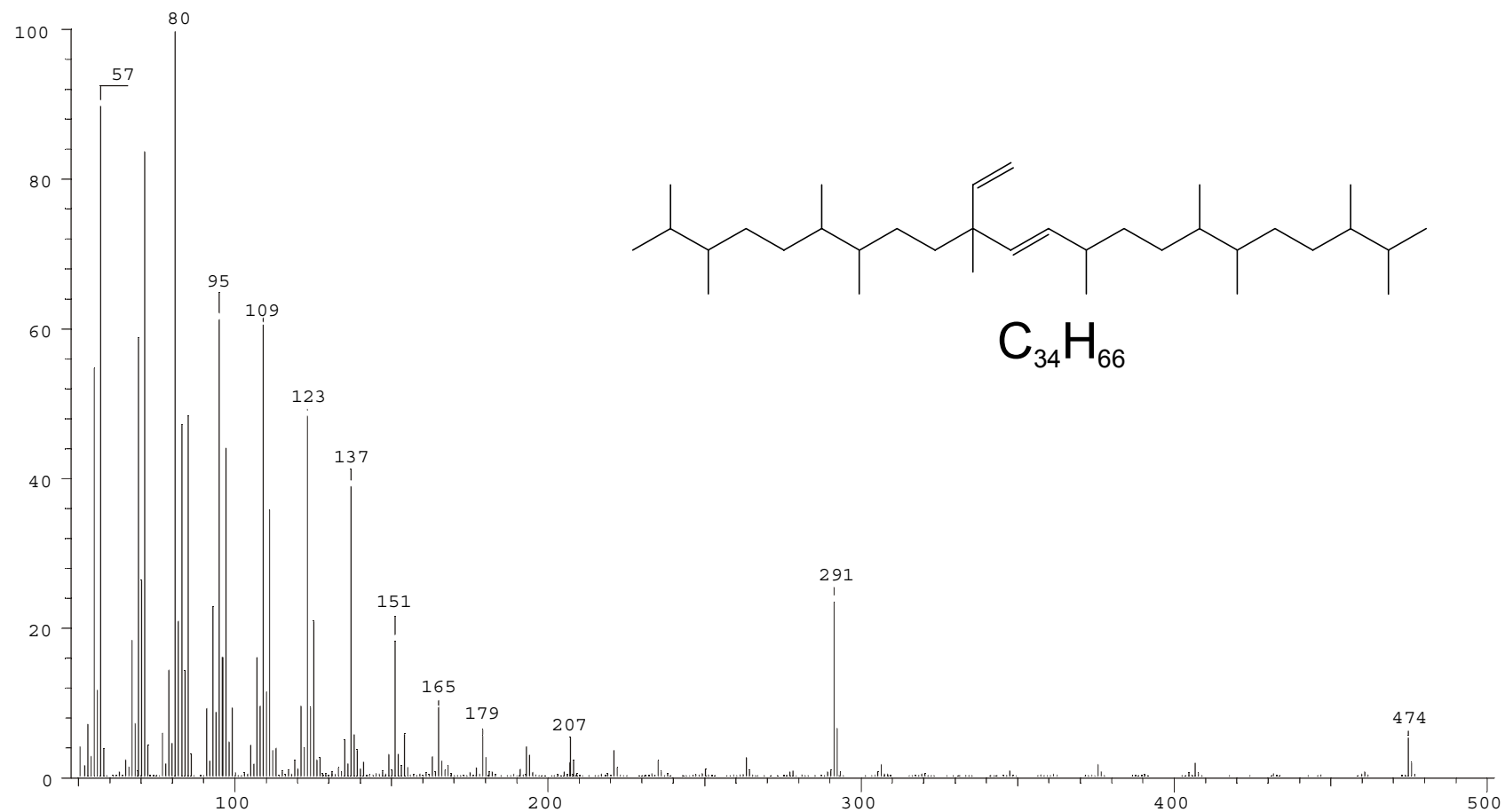
Peak: 1000.0 mmu

Intensity: 4059070

RIC: 51983904

Scan 4344 @ 72.98 min (EI +VE +LMR BSCAN (EXP) UP LR NRM)

4.1E+06



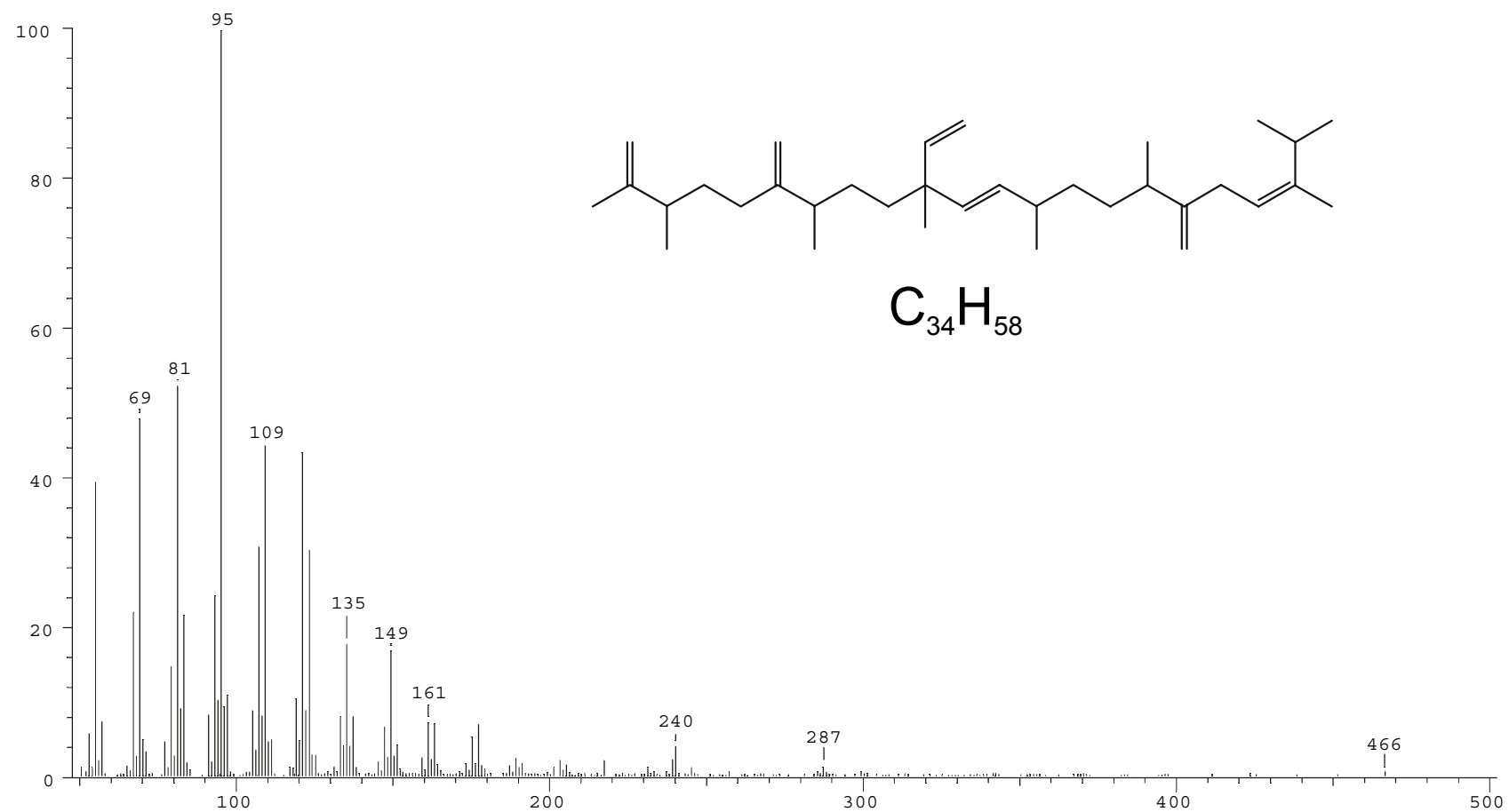
Mass spectrum and structure of 1,6,17,21-octahydrobotryococcene; after Huang & Murray (1995)

SPEC: ei47716ar#2 (06-Oct-00 13:56:26)
Samp: Vial 1 E47716-2 (FS-LR, Fm50, Lm600,)
Comm: GC-MS-ASAMP-KAS-Inj. SGE-50m, ID 0.22mm, FT 0.25um, EPC=1.0ml/min
Oper: ud Study: p481
Base: 95.13 Masses: 50.00 > 600.00
Peak: 1000.0 mmu Intensity: 986107
REG #9 @ 51.30 min (!3050) (EI +VE +LMR BSCAN (EXP) UP LR NRM)

Scans: 1 > 7137

Client: A.Fuhrmann
#Peaks: 259
RIC: 7861228

9.9E+05



Mass spectrum and structure isobutyrococene; after Wake & Hillen (1981)

SPEC: ei47739a1#1.dat (09-Apr-99 13:29:01)
Samp: Vial 2 E47739-1 (FS-LR)
Comm: GC-MS-ASAMP-KAS-Inj. SGE-50m, ID 0.22mm, FT 0.25um, EPC=1.0ml/min
Oper: fjk,cts=583 Study: P481-H.Fuhrmann
Base: 80.97 Masses: 50.00 > 600.00
Peak: 1000.0 mmu Intensity: 49432576
Scan 4365 @ 73.34 min (EI +VE +LMR BSCAN (EXP) UP LR NRM)

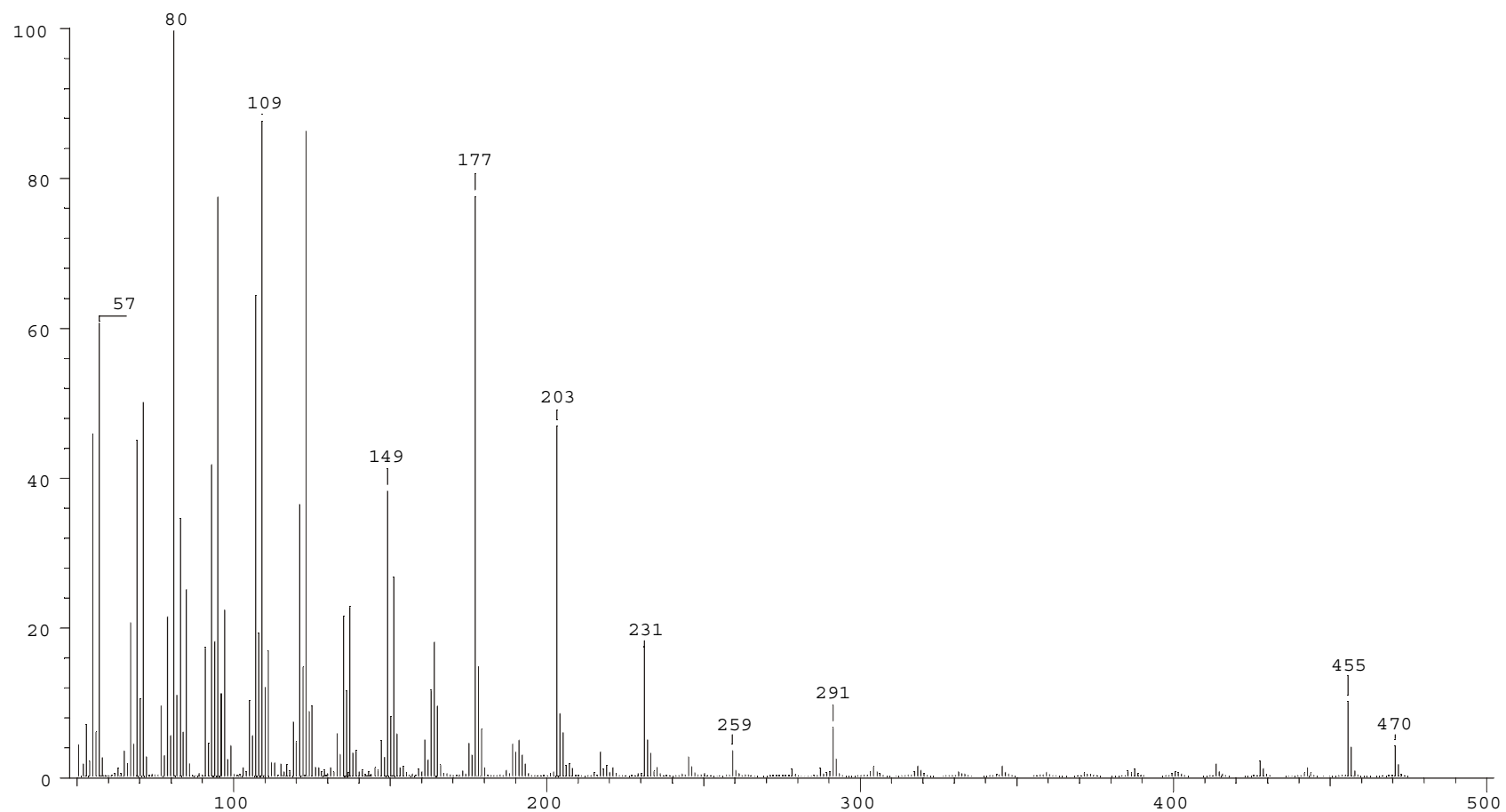
Scans: 1 > 6034

Client: He5.6=Fl.

#Peaks: 474

RIC: 791250503

4.9E+07



Mass spectrum of a novel $C_{34}H_{62}$ botryococcene

SPEC: ei47739a1#1.dat (09-Apr-99 13:29:01)
Samp: Vial 2 E47739-1 (FS-LR)
Comm: GC-MS-ASAMP-KAS-Inj. SGE-50m, ID 0.22mm, FT 0.25um, EPC=1.0ml/min
Oper: fjk,cts=583 Study: P481-H.Fuhrmann
Base: 80.97 Masses: 50.00 > 600.00
Peak: 1000.0 mmu Intensity: 45090304
Scan 4406 @ 74.02 min (EI +VE +LMR BSCAN (EXP) UP LR NRM)

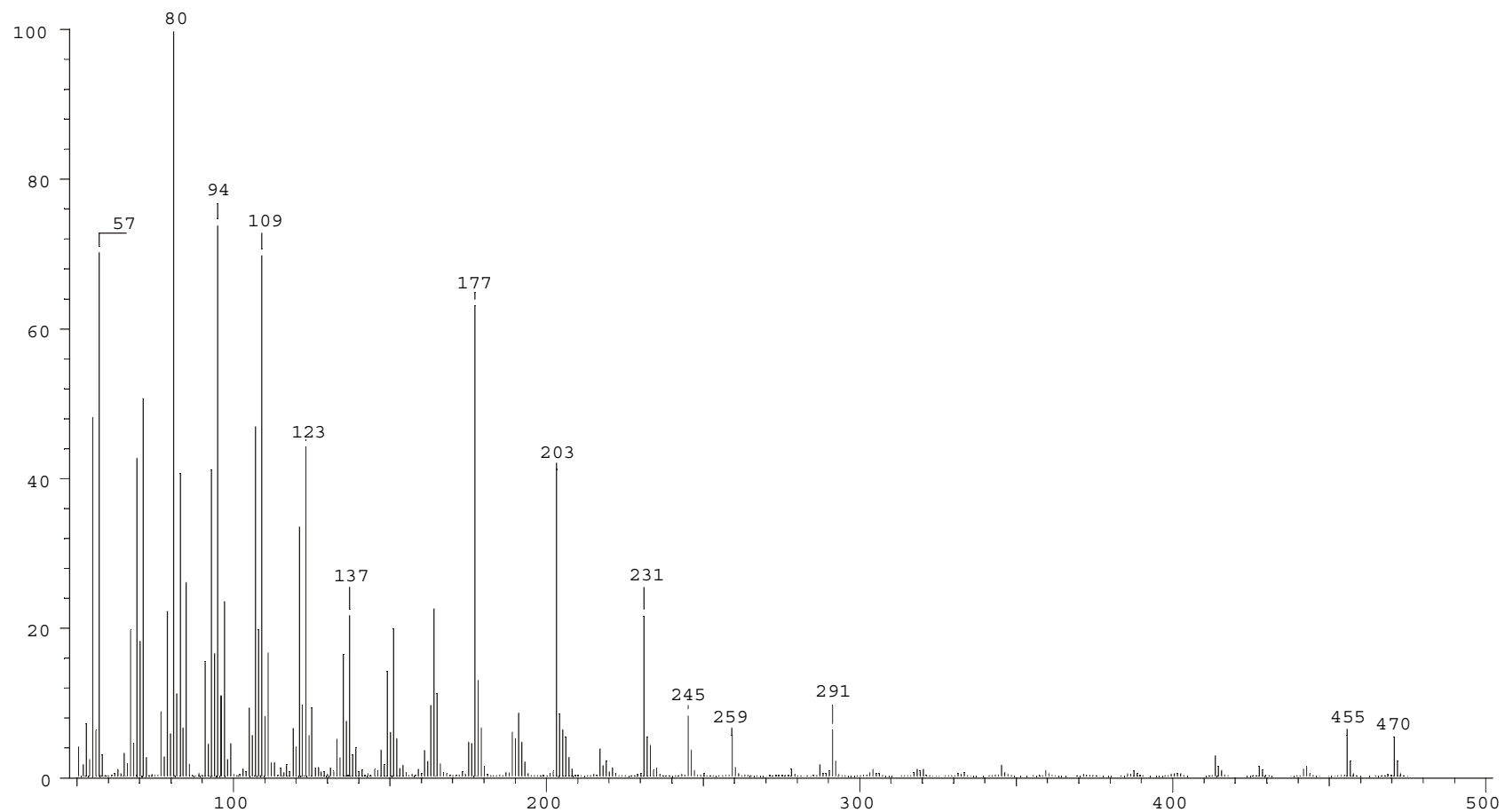
Scans: 1 > 6034

Client: He5.6=Fl.

#Peaks: 453

RIC: 668208408

4.5E+07



Mass spectrum of a novel $C_{34}H_{62}$ botryococcene

Sample Screening

PI S1/(S1+S2) from Rock-Eval pyrolysis **production index**

Py-GC-FID

AbR C₀-C₃ alkylbenzenes/
(C₀-C₃ alkylbenzenes+C₆-C₃₂[*n*-alkanes+*n*-alk-1-enes]) **alkylbenzene ratio**

Aromaticity C₀-C₂ alkylbenzenes + C₀-C₁ alkylphenols + C₀-C₁ alkyl-naphthalenes/
(aromatics+*n*-alkanes and *n*-alk-1-enes $\sum C_5+$)

Phr phenol/(phenol+*n*-C_{11:0}+*n*-C_{11:1}) **phenol ratio**

IpR 1 C₁₃-C₂₀ isoprenoids/
(*n*-alkanes+*n*-alk-1-enes $\sum C_5+$) **isoprenoid ratio 1**

IpR 2 prist-1-ene/(*n*-C_{11:0}+*n*-C_{11:1}) **isoprenoid ratio 2**

WI (*n*-alkanes and *n*-alk-1-enes $\sum C_{20+}$)/
(*n*-alkanes and *n*-alk-1-enes $\sum C_5+$) **wax-index**

GC and GC-MS (aliphatic fraction)

CPI_{HC} $[(n-C_{25}+n-C_{27}+n-C_{29}+n-C_{31})/(n-C_{24}+n-C_{26}+n-C_{28}+n-C_{30}) + (n-C_{25}+n-C_{27}+n-C_{29}+n-C_{31})/(n-C_{26}+n-C_{28}+n-C_{30}+n-C_{32})]/2$ **Carbon Preference Index for hydrocarbons**

GI gammacerane/
(gammacerane+17 α (H), 21 β (H)-hopane) **gammacerane-index**

OLI oleanane/17 α (H), 21 β (H)-hopane **oleanane-index**

HHI (C₃₅ homohopane S+R)/
(C₃₁ to C₃₅ homohopanes S+R) **homohopane-index**

DIAR C₂₉ diasteranes/
(C₂₉diasteranes+C₂₉regular steranes) **diasterane-ratio**

HISO C₃₁-22S/(C₃₁-22S+C₃₁-22R) **homohopane-isomerisation**

Ts/(Ts+Tm) 18 α (H)-22,29,30-trisnorneohopane/
(18 α (H)-22,29,30-trisnorneohopane+ 17 α (H)-22,29,30-trisnorhopane)

H/(H+M) 17 α (H), 21 β (H)-hopane/
(17 β (H), 21 α (H)-hopane+17 α (H), 21 β (H)-hopane) **hopane to moretane ratio**

$\beta\beta/(\beta\beta+\alpha\alpha)$	$\alpha\beta\beta C_{29}-(20S+20R)/$ $(\alpha\beta\beta C_{29}-(20S+20R)+\alpha\alpha\alpha C_{29}-(20S+20R))$	sterane- isomerisation
$20S/(20S+20R)$	$\alpha\alpha\alpha C_{29}-20S/(\alpha\alpha\alpha C_{29}-20S+\alpha\alpha\alpha C_{29}-20R)$	sterane- isomerisation
ATR_{HC}	$(C_{15}+C_{17}+C_{19})/(C_{15}+C_{17}+C_{19}+C_{27}+C_{29}+C_{31})$	aquatic/ terrigenous ratio for hydrocar- bons; after Wilkes et al. (1999)
P_{aq}	$(C_{23}+C_{25})/(C_{23}+C_{25}+C_{29}+C_{31})$	macrophyte input; after Ficken et al. (2000)

GC and GC-MS (aromatic fraction)

chromane	Trimethyl MTTC/ (Dimethyl MTTC+Methyl MTTC)	chromane index; after Sinninghe Damsté <i>et al.</i> (1987)
dbt/phen	dibenzothiophene/phenanthrene	after Hughes <i>et al.</i> (1995)
mpi1	$1.5*(2\text{-}+3\text{-methylphenanthrene})/$ (phenanthrene+9-methylph.+1-methylph.)	methylphenanthrene- index, after Radke <i>et al.</i> (1982)
%Rc	$0.6*mpi1+0.4$	
mpr1	1-methylphenanthrene/phenanthrene	methylphenanthrene- ratio
mpr2	2-methylphenanthrene/phenanthrene	methylphenanthrene- ratio
mdr1	1-methyldibenzothiophene/ dibenzothiophene	after Santamaría-Orozco <i>et al.</i> (1998)
mdr4	4-methyldibenzothiophene/ dibenzothiophene	after Santamaría-Orozco <i>et al.</i> (1998)
edr	4,6-dimethyldibenzothiophene/ ethyldibenzothiophene	
mah	secohopanes/ (secohopanes+benzohopanes)	after He & Lu (1990)
bhp	$C_{32}H_{48}$ benzohopanoids (C20-series)/ $(C_{32}H_{48}$ benzohopanoids (C20-series)+ $C_{31}H_{46}$ benzohopanoids (C16-series))	

GC and GC-MS (heterocompounds)

$$\text{CPI}_{\text{FA}} \frac{[(n\text{-C}_{22}+n\text{-C}_{24}+n\text{-C}_{26}+n\text{-C}_{28})/(n\text{-C}_{21}+n\text{-C}_{23}+n\text{-C}_{25}+n\text{-C}_{27}) + (n\text{-C}_{22}+n\text{-C}_{24}+n\text{-C}_{26}+n\text{-C}_{28})/(n\text{-C}_{23}+n\text{-C}_{25}+n\text{-C}_{27}+n\text{-C}_{29})]/2}$$

Carbon Preference Index for fatty-acids (C₂₂-C₂₈)

$$\text{CPI}_{\text{ALK}} \frac{[(n\text{-C}_{22}+n\text{-C}_{24}+n\text{-C}_{26}+n\text{-C}_{28})/(n\text{-C}_{21}+n\text{-C}_{23}+n\text{-C}_{25}+n\text{-C}_{27}) + (n\text{-C}_{22}+n\text{-C}_{24}+n\text{-C}_{26}+n\text{-C}_{28})/(n\text{-C}_{23}+n\text{-C}_{25}+n\text{-C}_{27}+n\text{-C}_{29})]/2}$$

Carbon Preference Index for *n*-alkan-1- and 2-ols (C₂₂-C₂₈)

$$\text{ATR}_{\text{FA}} \quad (C_{14}+C_{16}+C_{18})/(C_{14}+C_{16}+C_{18}+C_{24}+C_{26}+C_{28})$$

aquatic/terrigenous ratio for fatty acids; after Wilkes et al. (1999)

samples #	E48455-D1-S1	E48463-D1-S1	E48464-D1-S1	E48465-D1-S1	E48466-D1-S1	E48467-D1-S1	E48469-D1-S1	E48475-D1-S1	E48480-D1-S1	E48481-D1-S1
	P497D,5	P497D,6	P497D,7	P497D,8	P497D,9	P497D,10	P497D,11	P497D,17	P497D,14	P497D,15
amount (mg)	49.3	46.9	44.3	52.5	50.0	47.5	52.5	42.0	52.4	44.4
	(µg/g sample)	(µg/g sample)	(µg/g sample)	(µg/g sample)	(µg/g sample)	(µg/g sample)	(µg/g sample)	(µg/g sample)	(µg/g sample)	(µg/g sample)
n-C12	32.16	7.17	20.88	19.16	11.32	24.46	17.23	6.87	9.64	21.29
n-C13	36.18	15.43	31.63	35.28	24.42	33.60	43.88	16.71	18.90	33.65
IP-15	14.35	9.60	14.71	15.43	14.67	12.32	22.23	10.61	6.34	15.42
n-C14	34.35	21.98	31.41	39.59	36.79	37.72	63.57	15.77	22.58	38.82
IP-16	13.22	23.86	24.75	33.07	38.81	16.53	51.19	5.92	13.81	25.49
n-C15	35.60	44.08	49.15	64.18	81.74	42.81	97.62	21.51	39.47	58.08
n-C16	25.62	40.50	32.83	42.30	70.46	32.65	81.05	11.50	37.46	53.06
IP-18	7.71	34.59	24.00	31.47	51.24	12.78	65.29	6.50	15.68	25.88
n-C17	24.96	122.82	95.25	136.94	226.01	35.99	268.84	45.60	48.11	56.21
IP-19	8.13	58.91	28.61	45.41	65.76	17.27	82.03	14.35	25.85	45.89
P-1 ?	2.29	6.13	4.33	4.18	0.00	2.82	0.00	6.48	1.29	1.55
P-2 ?	5.13	20.24	11.70	11.99	0.00	3.84	0.00	18.43	4.76	9.73
n-C18:1	1.37	0.00	7.82	0.00	0.00	0.00	0.00	13.21	0.00	0.00
n-C18	16.02	46.39	32.94	41.03	71.04	25.90	79.09	28.34	29.97	44.58
IP-20	9.98	148.49	73.78	124.99	210.46	27.47	251.88	53.76	55.79	73.15
n-C19:1	1.34	0.00	7.24	0.00	0.00	0.00	0.00	8.44	0.00	0.00
n-C19	17.30	69.49	43.34	56.59	106.69	26.23	115.47	19.38	34.78	52.01
n-C20:1	2.78	0.00	11.64	0.00	0.00	0.00	0.00	7.77	0.00	0.00
n-C20	17.93	63.20	33.34	42.23	69.82	20.15	73.04	24.63	40.04	45.47
n-C21:1	2.04	0.00	6.85	0.00	0.00	0.00	0.00	5.84	0.00	0.00
n-C21	14.15	74.48	35.01	46.45	76.19	16.07	78.07	21.05	40.27	50.99
n-C22:1	1.32	0.00	5.45	0.00	0.00	0.00	0.00	5.97	0.00	0.00
n-C22	11.33	74.71	30.81	44.86	76.36	13.69	77.80	17.12	28.94	52.57
n-C23:1	1.47	0.00	5.02	0.00	0.00	0.00	0.00	5.31	0.00	0.00
n-C23	9.38	88.77	33.13	52.60	90.06	13.01	91.75	25.73	34.57	71.68
n-C24:1	0.75	0.00	3.96	0.00	0.00	0.00	0.00	5.98	0.00	0.00
n-C24	6.53	68.55	23.62	39.63	70.66	10.64	74.07	17.62	27.22	63.06
n-C25:1	0.90	0.00	3.86	0.00	0.00	0.00	0.00	6.18	0.00	0.00
n-C25	5.34	74.52	22.90	42.12	75.87	10.68	79.44	24.43	31.57	80.12
n-C26:1	0.68	0.00	3.28	0.00	0.00	0.00	0.00	3.70	0.00	0.00
n-C26	4.04	48.37	16.10	27.10	51.45	8.78	54.76	16.32	22.66	68.24
n-C27:1	0.00	0.00	2.33	0.00	0.00	0.00	0.00	3.35	0.00	0.00
n-C27	4.58	48.02	15.26	27.08	52.67	7.57	58.43	24.22	23.05	80.98
n-C28:1	0.12	0.00	1.08	0.00	0.00	0.00	0.00	1.27	0.00	0.00
n-C28	3.26	34.66	10.78	19.30	38.35	5.44	42.70	11.61	16.90	68.23
n-C29	3.12	42.31	12.42	23.55	47.27	3.98	56.62	15.69	18.38	73.97
n-C30	1.66	26.58	6.54	13.55	29.31	2.19	36.98	9.38	9.23	47.75
n-C31	1.84	40.48	11.11	20.23	36.88	1.86	48.90	10.18	16.60	56.80
n-C32	0.65	15.34	3.08	6.53	15.73	0.66	19.51	4.40	5.05	26.59

samples #	E48482-D1-S1	E48484-D1-S1	E48485-D1-S1	E48494-D1-S1	E48502-D1-S1	E48505-D1-S1	E48514-D1-S1	E48517-D1-S1	E48519-D1-S1
	P497D,16	P497D,18	P497D,19	P497D,20	P497D,22	P497D,23	P497D,24	P497D,25	P497D,26
amount (mg)	43.5	55.0	55.0	37.0	40.0	41.5	47.5	46.5	43.5
	(µg/g sample)	(µg/g sample)	(µg/g sample)	(µg/g sample)	(µg/g sample)	(µg/g sample)	(µg/g sample)	(µg/g sample)	(µg/g sample)
n-C12	12.99	4.87	3.27	4.14	4.95	3.27	3.69	0.00	1.36
n-C13	24.35	7.42	7.37	5.64	7.48	6.52	6.50	0.00	2.04
IP-15	11.92	3.86	5.06	4.78	3.89	7.62	2.21	0.00	0.78
n-C14	31.53	7.31	9.95	7.26	9.81	6.52	5.52	0.00	2.15
IP-16	22.86	6.39	11.76	5.61	6.73	14.66	4.20	0.00	1.19
n-C15	51.63	11.33	21.60	8.47	9.50	7.28	10.82	3.11	1.96
n-C16	49.75	10.44	20.61	5.43	8.71	4.99	6.36	2.65	1.23
IP-18	26.23	8.79	17.86	3.92	4.15	5.92	3.73	3.20	0.60
n-C17	58.93	34.14	75.62	6.78	13.80	99.01	12.56	5.75	1.29
IP-19	50.61	15.40	30.85	8.94	11.47	18.03	12.65	13.09	0.76
P-1 ?	0.00	2.63	3.87	10.82	8.30	15.00	1.02	1.79	0.14
P-2 ?	0.00	7.36	12.21	23.19	18.46	15.06	3.47	7.33	1.06
n-C18:1	0.00	1.27	0.00	3.37	3.91	2.52	0.00	0.00	0.39
n-C18	46.44	9.72	21.65	5.16	9.12	7.31	7.28	8.11	1.01
IP-20	82.25	26.86	73.17	21.74	19.40	80.79	39.64	52.19	1.29
n-C19:1	0.00	0.46	0.00	1.83	3.17	2.93	0.00	0.00	0.26
n-C19	57.15	10.24	28.64	3.79	8.85	12.15	5.63	24.96	1.19
n-C20:1	0.00	1.29	0.00	1.20	3.86	3.36	0.00	0.00	0.37
n-C20	50.00	9.84	29.30	3.07	11.66	11.42	3.58	46.78	1.18
n-C21:1	0.00	0.60	0.00	1.16	2.61	3.68	0.00	0.00	0.19
n-C21	57.63	9.97	33.25	4.16	13.91	20.30	4.44	61.92	1.39
n-C22:1	0.00	1.09	0.00	3.51	2.46	4.81	0.00	0.00	0.24
n-C22	62.29	10.50	36.08	3.20	7.62	14.27	2.92	78.84	1.72
n-C23:1	0.00	0.78	0.00	2.07	4.14	6.15	0.00	0.00	0.21
n-C23	87.46	12.78	45.87	4.52	15.92	19.34	8.05	100.89	2.36
n-C24:1	0.00	1.16	0.00	1.74	3.69	5.41	0.00	0.00	0.23
n-C24	78.46	9.64	36.70	2.92	7.40	6.84	2.91	108.71	2.13
n-C25:1	0.00	0.71	0.00	1.85	6.18	4.03	0.00	0.00	0.20
n-C25	102.18	10.47	41.82	6.01	17.55	13.42	5.09	138.97	2.06
n-C26:1	0.00	0.43	0.00	1.75	4.66	4.77	0.00	0.00	0.27
n-C26	90.15	7.85	26.82	3.01	9.15	6.12	2.18	123.78	1.67
n-C27:1	0.00	0.52	0.00	3.08	9.19	1.72	0.00	0.00	0.25
n-C27	107.89	7.33	27.46	6.71	30.55	10.65	6.43	149.41	1.73
n-C28:1	0.00	0.49	0.00	0.00	1.81	2.18	0.00	0.00	0.25
n-C28	93.52	5.33	18.71	3.98	8.21	3.53	1.48	161.63	1.49
n-C29	98.22	5.22	22.35	9.16	20.28	17.14	1.78	180.64	1.23
n-C30	63.03	2.95	11.68	1.70	4.96	9.20	0.68	142.63	0.88
n-C31	54.54	5.56	18.54	4.41	13.98	17.93	0.00	142.49	0.90
n-C32	32.84	1.38	10.41	0.99	2.08	10.90	0.00	99.48	0.57

samples #	E48520-D1-S1	E48525-D1-S1	E48527-D1-S1	E48529-D1-S1	E48532-D1-S1	E48537-D1-S1
	P497D,27	P497D,28	P497D,29	P497D,30	P497D,31	P497D,32
amount (mg)	48.5	41.5	38.5	38.5	33.5	37.5
	(µg/g sample)	(µg/g sample)	(µg/g sample)	(µg/g sample)	(µg/g sample)	(µg/g sample)
n-C12	2.34	3.52	2.18	2.75	2.57	3.61
n-C13	4.25	5.54	3.98	4.41	3.84	7.79
IP-15	2.78	3.33	3.01	3.61	5.06	7.04
n-C14	5.90	5.63	6.37	6.09	4.73	8.74
IP-16	4.54	5.79	5.32	5.58	11.54	14.92
n-C15	6.83	5.66	8.64	6.70	6.45	13.90
n-C16	5.59	6.11	5.79	4.75	7.12	10.33
IP-18	4.04	6.01	4.96	3.69	7.27	15.50
n-C17	5.72	14.24	7.35	7.09	15.04	50.96
IP-19	6.67	7.34	12.62	9.22	13.78	48.47
P-1 ?	1.13	3.86	12.75	16.92	34.46	37.29
P-2 ?	5.66	10.65	31.80	15.31	14.09	55.80
n-C18:1	0.00	4.42	3.48	3.55	16.51	19.71
n-C18	3.18	10.69	5.01	6.18	23.38	24.00
IP-20	3.45	9.46	31.01	22.72	55.27	281.85
n-C19:1	0.00	3.19	1.84	2.59	17.23	5.78
n-C19	2.96	9.44	4.61	7.33	32.37	25.71
n-C20:1	0.00	2.15	1.93	3.18	18.54	9.75
n-C20	2.36	9.59	3.87	8.34	30.77	25.11
n-C21:1	0.00	1.62	1.48	3.43	16.63	3.43
n-C21	3.12	9.70	10.14	8.98	35.27	18.48
n-C22:1	0.00	1.49	1.84	4.31	23.83	9.68
n-C22	2.28	7.50	4.36	7.90	31.56	21.77
n-C23:1	0.00	1.51	3.06	7.09	26.97	6.36
n-C23	4.61	10.68	22.90	11.10	47.01	38.77
n-C24:1	0.00	1.91	4.10	6.71	24.16	6.87
n-C24	2.48	7.90	7.78	7.78	30.17	16.13
n-C25:1	0.00	1.49	4.42	8.41	30.96	10.69
n-C25	3.76	8.94	25.19	13.69	44.04	43.27
n-C26:1	0.00	0.63	3.48	6.54	28.61	6.60
n-C26	1.58	5.28	9.37	10.04	36.58	15.32
n-C27:1	0.00	0.53	5.58	7.46	29.44	12.97
n-C27	3.21	6.29	25.16	31.53	63.60	64.17
n-C28:1	0.00	0.40	2.20	2.50	11.79	3.75
n-C28	0.79	2.14	7.33	8.55	23.54	14.02
n-C29	0.62	1.64	13.76	20.35	65.76	42.58
n-C30	0.32	0.49	9.25	9.07	22.83	10.19
n-C31	0.35	1.66	11.33	19.75	71.13	17.23
n-C32	0.09	0.00	1.75	2.75	12.46	3.94

E. nr.	depth [m]	well	area	sub-unit	Steranes		
					% C ₂₇	% C ₂₈	% C ₂₉
48494	1455.0	K	Gao	Es3	32.8	37.3	29.8
48455	2638.0	D	Lei	DJT	22.3	33.4	44.2
48963	2512.0	B	Lei	DJT	16.0	28.3	55.7
48464	2524.0	B	Lei	DJT	18.8	36.4	44.7
48465	2526.0	B	Lei	DJT	14.6	35.2	50.2
48467	2687.5	B	Lei	GS	23.9	42.1	34.0
48475	1492.0	J	Gao	Shale I	23.7	28.1	48.2
48480	2735.0	E	Lei	Shale II	48.6	31.2	20.1
48481	2796.0	E	Lei	DJT	26.8	35.9	37.2
48482	2792.0	E	Lei	DJT	40.4	36.7	22.9
48484	2335.0	C	Lei	DJT	19.2	36.6	44.3
48485	2342.0	C	Lei	DJT	14.4	40.0	45.6
48487	2385.0	C	Lei	DJT	22.4	37.6	40.0
48502	1357.0	L	Gao	Es4/?	28.4	19.4	52.3
48505	1847.0	M	Gao	GS	10.1	50.0	39.9
48514	2312.0	S	Tuo	GS	16.3	29.8	53.8
48520	1309.0	A	Shu-Du	Shale I	27.2	28.6	44.2
48525	1329.0	A	Shu-Du	Shale I	20.7	19.6	59.7
48527	1340.0	A	Shu-Du	Shale I	14.5	20.5	65.0
48529	1346.0	A	Shu-Du	GS	26.3	34.7	38.9
48532	1348.0	A	Shu-Du	GS	24.4	27.7	47.9
48537	1375.0	A	Shu-Du	GS	22.3	36.4	41.3

E.nr.	Well	Stratigraphy	Total methylcarbazoles ($\mu\text{g/g}$ bitumen)	Total C ₂ -carbazoles ($\mu\text{g/g}$ bitumen)	Total benzocarbazoles ($\mu\text{g/g}$ bitumen)	3-MC/(3-MC+2MC)
48494	K	Es3	371.3	385.3	36.3	0.44
48455	D	DJT	4119.0	3713.1	1058.8	0.44
48463	B	DJT	392.8	476.7	64.9	0.50
48464	B	DJT	1950.0	1995.1	255.9	0.51
48465	B	DJT	827.0	856.9	115.1	0.51
48467	B	GS	560.7	742.8	207.9	0.44
48475	J	Shale I	158.3	180.4	20.9	0.54
48480	E	Shale II	1503.6	1689.9	328.1	0.48
48481	E	DJT	751.7	914.9	188.2	0.47
48482	E	DJT	372.7	545.9	103.8	0.45
48484	C	DJT	512.1	585.7	77.1	0.49
48485	C	DJT	495.5	554.6	57.9	0.50
48502	L	Es4/?	99.0	78.1	14.3	0.31
48505	M	GS	84.5	148.8	15.8	0.54
48514	S	GS	320.9	427.6	60.4	0.48
48520	A	Shale I	253.4	208.6	24.7	0.33
48525	A	Shale I	30.3	17.3	3.0	0.22
48527	A	Shale I	34.7	21.8	5.0	0.27
48529	A	GS	66.0	75.5	4.7	0.41
48532	A	GS	77.5	88.9	10.0	0.00
48537	A	GS	598.7	1153.4	292.4	0.42

E.nr.	BaC/(BaC+BcC)	1,8-DMC/(1,8-DMC+1-EtC)	1-MC/(1-MC+1-EtC)	(3-MC+2-MC)/(3-MC+2-MC+C)
48494	0.38	0.43	0.93	0.59
48455	0.49	0.86	0.97	0.55
48463	0.50	0.77	0.94	0.65
48464	0.43	0.77	0.95	0.63
48465	0.39	0.77	0.95	0.63
48467	0.45	0.80	0.94	0.64
48475	0.53	0.61	0.93	0.56
48480	0.56	0.80	0.95	0.63
48481	0.51	0.80	0.95	0.67
48482	0.53	0.81	0.95	0.68
48484	0.58	0.66	0.94	0.67
48485	0.55	0.76	0.94	0.64
48502	n.d.	0.67	0.94	0.45
48505	0.38	0.84	0.91	0.69
48514	0.57	0.74	0.94	0.70
48520	0.38	0.64	0.92	0.49
48525	0.47	0.64	0.94	0.44
48527	0.49	0.59	0.93	0.44
48529	n.d.	0.67	0.92	0.51
48532	0.58	0.71	0.92	0.60
48537	0.61	0.88	0.95	0.57

E.nr.	4-MC/(4-MC+2MC)	vitritite reflectance Rc[%] from mpi 1	fluoren-9-one (µg/g bitumen)	1-methylfluoren-9-one (µg/g bitumen)	1-EF/(1-EF+1,8-DMF)
48494	0.56	0.66	359.7	240.9	0.23
48455	0.54	0.88	968.0	1642.6	0.16
48463	0.44	0.68	131.0	107.1	0.31
48464	0.47	0.83	195.7	221.2	0.34
48465	0.48	0.73	164.9	136.9	0.32
48467	0.46	0.87	515.8	910.6	0.25
48475	0.54	0.50	133.9	70.0	0.12
48480	0.44	0.75	536.9	544.4	0.40
48481	0.42	0.74	342.9	405.0	0.37
48482	0.44	0.72	271.9	343.4	0.33
48484	0.41	0.72	109.6	89.9	0.28
48485	0.39	0.58	257.1	125.9	0.22
48502	0.54	0.61	126.5	57.5	0.18
48505	0.49	0.65	129.8	151.3	0.25
48514	0.48	0.67	216.4	202.6	0.34
48520	0.49	0.49	848.4	216.2	0.25
48525	0.47	0.45	41.1	13.0	0.16
48527	0.45	0.45	149.5	46.5	0.19
48529	0.54	0.49	214.4	70.4	0.13
48532	0.56	0.57	71.3	47.4	0.11
48537	0.62	0.62	290.8	518.7	0.20

APPENDIX H

PY-GC-FID (HZM, MFM)

Code #	E48175-MK1-S2 R:2**6	E48180-MK1-S2 R:2**6	E48184-MK1-S2 R:2**6	E48187-MK1-S2 R:2**6	E48188-MK1-S2 R:2**6	E48189-MK1-S2 R:2**6
Amount (mg)	4.90	6.10	6.40	3.50	3.90	4.20
TOC [%]	43.7	49.1	48.9	49.2	59.6	49
	(µg/g TOC)	(µg/g TOC)	(µg/g TOC)	(µg/g TOC)	(µg/g TOC)	(µg/g TOC)
C1	16800	20821	17395	17891	17054	19530
C02-05 Total	45476	44423	35393	40461	44787	34145
C06-14 Total	120215	116902	91057	119049	140655	104088
C15-32 Total	183982	168703	105292	172090	271407	118226
C01-05 Total	62276	65244	52788	58352	61841	53675
C06-14 Total	120215	116902	91057	119049	140655	104088
C15-32 Total (corr)	182581	167701	104333	170348	270116	116768
C01-32 Total	365072	349847	248178	347749	472612	274531
C06-14 Resolved	84967	80318	63556	79270	96365	71100
C15-32 Resolved	59981	44260	26362	41024	77142	37015
C01-32 Resolved	207224	189822	142706	178646	235348	161790
n6:1	2817	1752	1214	1647	2467	1218
n6:0	1885	1590	1025	1379	2191	1158
benzene	1949	1663	1345	1415	1073	1372
n7:1	2016	1611	1063	1329	2131	1117
n7:0	1779	1615	1080	1499	2272	911
pyridine	425	536	597	555	325	465
pyrrole	614	831	759	847	661	762
toluene	3547	4215	3487	3548	4262	3630
n8:1	1667	1253	788	1226	1920	714
2-methylpyridin	331	556	487	596	360	941
n8:0	1369	1274	738	1043	2024	599
2-methylpyrrole	327	605	499	577	586	352
3-methylpyrrole	380	306	380	420	564	276
3-methylpyridin	339	165	362	418	145	133
ethylbenzene	852	997	881	705	894	734
m+p-xylenes	1243	1354	1274	1356	1473	1040
styrene	735	533	467	619	726	545
o-xylene	780	741	558	615	748	532
n9:1	1156	934	550	841	1621	332
n9:0	1202	1175	747	1034	1977	458
phenol	3922	4033	3877	3563	2064	4239
1,2,4-trimethylbenzene	581	376	915	424	633	351
n10:1	1150	978	526	904	1923	321
n10:0	1117	915	552	1046	1996	394
1,2,3-trimethylbenzene	451	470	372	569	679	472
indene	361	294	335	254	288	296
2-methylphenol	1571	1561	1448	1503	980	1694
3- and 4-methylphenol	2840	3827	3860	4369	3445	4791
n11:1	1415	1010	680	1107	1789	533
n11:0	1262	1050	639	895	2152	398

Code #	E48175-MK1-S2 R:2**6 (µg/g TOC)	E48180-MK1-S2 R:2**6 (µg/g TOC)	E48184-MK1-S2 R:2**6 (µg/g TOC)	E48187-MK1-S2 R:2**6 (µg/g TOC)	E48188-MK1-S2 R:2**6 (µg/g TOC)	E48189-MK1-S2 R:2**6 (µg/g TOC)
2-ethylphenol	186	200	155	148	270	319
C2-phenol (1)	1802	1667	1686	1900	1919	1650
methylindene	300	461	233	215	394	534
C2-phenol (2)	1592	883	1792	1733	1092	3167
naphthalene	272	1081	188	285	544	235
4-methylguaiacol	67	270	57	287	179	439
n12:1	1334	1011	594	922	1947	508
n12:0	1040	1000	563	1182	2183	910
4-ethylguaiacol	267	225	259	353	186	369
2-methylnaphthalene	331	327	279	242	187	348
1-methylnaphthalene	387	240	223	307	122	600
n13:1	1122	845	610	1100	1598	595
n13:0	1071	1158	697	988	2145	315
2,6-dimethoxyphenol	70	80	75	135	184	0
methylindol	186	208	220	330	355	221
n14:1	986	817	576	826	1555	296
n14:0	1071	1034	693	939	2046	339
2,6 dimethoxy-4-methylphenol	312	200	277	396	310	237
trans-isoeugenol	63	34	86	226	132	109
n15:1	1137	883	638	1051	1712	546
n15:0	1107	1021	628	881	2012	464
n16:1	1174	842	640	884	1476	246
n16:0	1039	1065	655	856	1972	204
4-allyl-2,6-dimethoxyphenol	486	163	538	632	467	551
n17:1	961	744	501	679	1397	259
n17:0	1125	989	551	771	1980	216
prist-1-ene	571	819	649	812	891	876
n18:1	981	760	467	639	1459	175
n18:0	976	928	486	640	1939	166
n19:1	829	652	345	514	1250	122
n19:0	1090	1018	495	715	2009	821
n20:1	899	702	366	534	1360	296
n20:0	1014	966	441	613	2033	261
n21:1	892	594	330	514	1146	201
n21:0	1155	1043	447	654	2226	371
n22:1	1432	746	412	683	1580	789
n22:0	1161	923	367	615	1853	425
n23:1	779	623	277	455	1209	175
n23:0	1162	1016	360	609	2053	236
n24:1	1044	977	324	594	1686	321
n24:0	840	850	294	532	1682	235
n25:1	874	831	361	480	1350	205
n25:0	811	1055	299	573	1981	212
n26:1	777	551	275	423	1153	275
n26:0	672	585	256	469	1253	229
n27:1	738	364	292	400	622	182
n27:0	788	747	309	637	1734	278
n28:1	508	273	173	387	888	333
n28:0	572	332	216	442	826	165
n29:1	238	0	100	251	0	77
n29:0	942	970	411	954	2069	158
n30:1	236	156	106	106	429	147
n30:0	375	232	145	207	469	76

APPENDIX H

PY-GC-FID (HZM, MFM)

Code #	E48194-MK1-S2 R:2**6	E48195-MK1-S2 R:2**6	E48198-MK1-S2 R:2**6	E48200-MK1-S2 R:2**6	E48207-MK1-S2 R:2**6	E48210-MK1-S2 R:2**6
Amount (mg)	3.80	3.80	2.80	4.30	5.10	6.20
TOC [%]	51.3	52.3	54.3	43	47.4	41.5
	(µg/g TOC)	(µg/g TOC)	(µg/g TOC)	(µg/g TOC)	(µg/g TOC)	(µg/g TOC)
C1	18221	20400	15568	16930	20027	14560
C02-05 Total	38801	41798	44906	49080	40507	34013
C06-14 Total	110712	121494	139565	133859	108519	96271
C15-32 Total	159502	169940	242726	187038	134635	100426
C01-05 Total	57022	62198	60474	66010	60534	48573
C06-14 Total	110712	121494	139565	133859	108519	96271
C15-32 Total (corr)	157963	168430	240753	185416	133394	99260
C01-32 Total	325697	352122	440792	385285	302447	244104
C06-14 Resolved	73030	77289	91768	92160	75934	69998
C15-32 Resolved	36725	35568	59508	48699	41623	26691
C01-32 Resolved	166777	175055	211750	206869	178091	145262
n6:1	1719	1738	2425	2341	1611	1320
n6:0	1374	1410	1960	1929	1303	1123
benzene	1399	1136	1271	1745	1609	2050
n7:1	1550	1509	2106	1991	1482	967
n7:0	1452	1563	2175	2155	1432	1131
pyridine	482	458	399	751	618	1028
pyrrole	827	778	700	960	721	1001
toluene	3503	3891	3825	4878	3734	3822
n8:1	1276	1221	1801	1626	1057	888
2-methylpyridin	352	546	326	492	505	326
n8:0	1221	1245	1773	1607	1032	811
2-methylpyrrole	596	551	594	691	501	575
3-methylpyrrole	477	485	510	319	370	394
3-methylpyridin	413	363	326	473	318	471
ethylbenzene	798	910	891	1095	897	928
m+p-xylenes	1264	1454	1586	1620	1333	1305
styrene	491	574	738	676	552	492
o-xylene	633	678	739	903	714	622
n9:1	865	770	1322	1143	767	609
n9:0	1076	981	1507	1333	986	850
phenol	2852	3727	3137	3395	5248	5238
1,2,4-trimethylbenzene	477	504	879	1028	374	295
n10:1	957	755	1435	1217	788	570
n10:0	1026	864	1459	1171	877	647
1,2,3-trimethylbenzene	558	749	711	730	520	477
indene	355	344	388	351	269	254
2-methylphenol	1149	1490	1277	1537	1733	1541
3- and 4-methylphenol	3371	3561	3172	3150	3822	3618
n11:1	969	921	1547	1311	967	724
n11:0	968	897	1510	1271	895	665

Code #	E48194-MK1-S2 R:2**6 (µg/g TOC)	E48195-MK1-S2 R:2**6 (µg/g TOC)	E48198-MK1-S2 R:2**6 (µg/g TOC)	E48200-MK1-S2 R:2**6 (µg/g TOC)	E48207-MK1-S2 R:2**6 (µg/g TOC)	E48210-MK1-S2 R:2**6 (µg/g TOC)
2-ethylphenol	154	192	290	291	246	222
C2-phenol (1)	1745	2122	2102	2345	1796	1708
metylindene	203	309	293	367	244	202
C2-phenol (2)	1336	1332	1325	1616	1705	1796
naphthalene	256	495	434	596	248	259
4-methylguaiaicol	213	282	195	192	104	65
n12:1	857	806	1504	1331	818	642
n12:0	1192	727	1289	1033	956	694
4-ethylguaiaicol	246	393	123	207	248	243
2-methylnaphthalene	250	246	221	306	330	292
1-methylnaphthalene	274	309	314	271	282	297
n13:1	1121	825	1287	991	918	706
n13:0	1069	974	1421	1180	969	753
2,6-dimethoxyphenol	99	72	111	87	117	76
methylindol	374	254	434	221	326	304
n14:1	834	690	1203	999	822	644
n14:0	1023	867	1346	1113	993	774
2,6 dimethoxy-4-methylphenol	217	421	212	295	348	176
trans-isoeugenol	99	156	90	105	134	88
n15:1	1007	871	1354	1127	930	709
n15:0	932	778	1387	1146	914	685
n16:1	899	714	1195	1105	862	668
n16:0	901	760	1324	1086	856	633
4-allyl-2,6-dimethoxyphenol	537	474	582	569	434	450
n17:1	770	618	1062	892	708	534
n17:0	889	727	1322	1051	929	624
prist-1-ene	736	807	894	767	629	554
n18:1	738	629	1039	835	661	509
n18:0	751	663	1123	873	759	519
n19:1	545	450	869	711	568	363
n19:0	751	671	1151	877	862	527
n20:1	610	532	952	737	678	407
n20:0	690	639	1107	889	839	502
n21:1	497	427	747	688	578	334
n21:0	679	584	1034	876	887	491
n22:1	528	437	748	701	659	358
n22:0	582	524	878	773	797	405
n23:1	454	366	644	610	619	343
n23:0	608	525	866	841	906	451
n24:1	592	449	662	703	773	392
n24:0	495	412	699	642	799	375
n25:1	470	396	655	645	821	414
n25:0	530	442	764	710	958	435
n26:1	379	376	523	526	613	296
n26:0	372	372	609	572	668	301
n27:1	280	336	409	493	569	280
n27:0	413	459	685	664	813	345
n28:1	197	231	296	302	332	140
n28:0	227	296	443	410	454	189
n29:1	0	163	0	316	0	0
n29:0	692	758	1527	868	1332	595
n30:1	94	128	206	232	195	86
n30:0	135	216	376	297	296	131

APPENDIX H

PY-GC-FID (HZM, MFM)

Code #	E48339-MK1-S2 R:2**6	E48343-MK1-S2 R:2**6	E48347-MK1-S2 R:2**6	E48348-MK1-S2 R:2**6	E48353-MK1-S2 R:2**6	E48357-MK1-S2 R:2**6
Amount (mg)	6.70	3.20	4.00	3.90	4.20	4.00
TOC [%]	45.3	52.6	51.3	51.9	51.8	47.4
	(µg/g TOC)	(µg/g TOC)	(µg/g TOC)	(µg/g TOC)	(µg/g TOC)	(µg/g TOC)
C1	18500	17249	19279	18755	18097	17886
C02-05 Total	41600	47715	40261	44391	38526	57177
C06-14 Total	120900	146377	116981	129266	111079	171779
C15-32 Total	208900	239959	172050	203299	164154	258414
C01-05 Total	60100	64964	59540	63146	56623	75063
C06-14 Total	120900	146377	116981	129266	111079	171779
C15-32 Total (corr)	207912	238177	170588	201817	162775	256832
C01-32 Total	388912	449518	347109	394229	330477	503674
C06-14 Resolved	78569	99311	78206	88459	75323	118603
C15-32 Resolved	51855	70276	47836	60755	43126	81540
C01-32 Resolved	190524	234551	185582	212360	175072	275206
n6:1	1583	2439	1755	2260	1621	3116
n6:0	1469	1944	1387	1768	1353	2511
benzene	1250	1788	1618	1459	1470	2209
n7:1	1536	2116	1402	1900	1590	2540
n7:0	1497	2147	1548	1862	1487	2713
pyridine	405	544	502	570	499	840
pyrrole	643	904	876	1041	858	1031
toluene	4054	4845	3687	4256	3551	5851
n8:1	1124	1967	1253	1751	1334	2404
2-methylpyridin	381	458	443	495	414	604
n8:0	1145	1776	1163	1609	1349	2142
2-methylpyrrole	559	651	473	685	606	610
3-methylpyrrole	290	480	378	523	484	612
3-methylpyridin	163	439	446	454	444	564
ethylbenzene	955	942	788	862	758	1367
m+p-xylenes	1618	1611	1371	1256	1261	2013
styrene	555	952	658	774	498	940
o-xylene	633	760	646	689	636	969
n9:1	875	1572	959	1399	888	1896
n9:0	1088	1852	1166	1668	1141	2171
phenol	4148	2836	3687	3171	2798	3420
1,2,4-trimethylbenzene	248	511	532	460	431	721
n10:1	907	1721	1074	1539	939	2155
n10:0	968	1955	1086	1518	1010	2089
1,2,3-trimethylbenzene	651	619	521	469	449	702
indene	391	362	270	357	275	467
2-methylphenol	1316	1147	1406	1238	1132	1300
3- and 4-methylphenol	3408	3624	4409	3026	3319	3249
n11:1	940	2072	1313	1670	1147	2588
n11:0	1017	2053	1088	1692	1106	2320

Code #	E48339-MK1-S2 R:2**6 (µg/g TOC)	E48343-MK1-S2 R:2**6 (µg/g TOC)	E48347-MK1-S2 R:2**6 (µg/g TOC)	E48348-MK1-S2 R:2**6 (µg/g TOC)	E48353-MK1-S2 R:2**6 (µg/g TOC)	E48357-MK1-S2 R:2**6 (µg/g TOC)
2-ethylphenol	206	211	360	235	146	333
C2-phenol (1)	1418	2087	1979	1956	1622	2585
metylindene	320	327	224	295	192	395
C2-phenol (2)	1018	1638	1881	947	1269	1937
naphthalene	771	546	282	977	232	746
4-methylguaiaicol	384	299	267	280	317	251
n12:1	899	1837	1024	1590	855	2328
n12:0	1190	1977	1431	1629	1483	2290
4-ethylguaiaicol	346	365	382	269	440	361
2-methylnaphthalene	206	273	279	213	233	339
1-methylnaphthalene	224	358	351	305	412	349
n13:1	951	1678	1173	1382	1248	1908
n13:0	1111	1966	1153	1670	1194	2179
2,6-dimethoxyphenol	60	126	233	142	123	135
methylindol	223	479	361	367	378	519
n14:1	769	1534	1009	1266	949	1867
n14:0	1050	1816	1134	1454	1097	1996
2,6 dimethoxy-4-methylphenol	191	510	340	341	370	391
trans-isoeugenol	42	178	192	103	169	131
n15:1	1028	1934	1126	1426	1083	2216
n15:0	1096	1939	1103	1490	1013	2230
n16:1	826	1562	1051	1319	910	1777
n16:0	1031	1620	1078	1423	1018	1861
4-allyl-2,6-dimethoxyphenol	378	639	599	690	557	669
n17:1	714	1327	895	1219	841	1654
n17:0	946	1665	1146	1476	1070	2017
prist-1-ene	1119	667	790	668	798	906
n18:1	684	1658	953	1452	933	1752
n18:0	840	1780	1052	1621	1013	1934
n19:1	628	1118	749	1089	744	1425
n19:0	830	1726	1130	1567	1146	2148
n20:1	534	1240	868	1207	825	1692
n20:0	798	1690	1053	1524	993	1968
n21:1	488	961	802	955	686	1307
n21:0	739	1484	1155	1579	1082	2011
n22:1	648	890	915	1109	722	1134
n22:0	792	1221	942	1278	823	1444
n23:1	490	796	708	907	617	1077
n23:0	713	1132	1012	1336	884	1511
n24:1	632	1089	809	1111	836	1363
n24:0	612	929	753	1029	717	1210
n25:1	657	988	748	1169	669	1373
n25:0	707	974	798	1153	840	1458
n26:1	557	720	571	752	552	868
n26:0	600	616	556	754	499	808
n27:1	388	592	588	669	376	623
n27:0	988	864	655	798	562	971
n28:1	248	378	332	403	242	358
n28:0	572	414	386	543	294	545
n29:1	0	0	259	300	87	0
n29:0	1572	1593	772	904	808	1915
n30:1	190	190	245	192	150	208
n30:0	315	264	259	294	179	360

Code #	E48360-MK1-S2 R:2**6	E48365-MK1-S2 R:2**6	E48370-MK1-S2 R:2**6	E48376-MK1-S2 R:2**6	E48380-MK1-S2 R:2**6
Amount (mg)	4.00	5.50	2.90	5.50	7.70
TOC [%]	53.4	44	54.2	40.7	31
	(µg/g TOC)	(µg/g TOC)	(µg/g TOC)	(µg/g TOC)	(µg/g TOC)
C1	17237	17436	15942	16664	10013
C02-05 Total	37216	42517	43242	32872	32991
C06-14 Total	115760	122379	134317	86102	97853
C15-32 Total	190032	176757	212662	79924	130405
C01-05 Total	54453	59953	59184	49536	43004
C06-14 Total	115760	122379	134317	86102	97853
C15-32 Total (corr)	188628	175517	210753	78584	129148
C01-32 Total	358841	357849	404254	214222	270005
C06-14 Resolved	74825	87823	88245	60206	70683
C15-32 Resolved	42382	50231	57513	18897	39713
C01-32 Resolved	171660	198007	204942	128639	153400
n6:1	1532	1898	2102	1103	1709
n6:0	1314	1583	1782	844	1233
benzene	1013	1471	1544	1641	1320
n7:1	1249	1719	1822	792	1389
n7:0	1416	1703	1797	881	1411
pyridine	415	515	521	651	533
pyrrole	880	737	973	617	605
toluene	3709	3722	4058	3168	3062
n8:1	1256	1534	1705	649	1220
2-methylpyridin	428	449	370	309	209
n8:0	1116	1429	1459	620	1007
2-methylpyrrole	622	565	521	406	495
3-methylpyrrole	494	289	459	185	215
3-methylpyridin	407	320	424	288	270
ethylbenzene	610	996	765	763	813
m+p-xylenes	1321	1415	1273	949	959
styrene	683	769	806	436	580
o-xylene	548	786	676	544	670
n9:1	871	1185	1304	402	954
n9:0	1161	1354	1564	447	954
phenol	3874	5761	3560	6165	6251
1,2,4-trimethylbenzene	428	161	456	212	284
n10:1	835	1249	1388	425	1038
n10:0	1040	1109	1589	329	813
1,2,3-trimethylbenzene	610	534	460	283	343
indene	410	343	326	274	318
2-methylphenol	1093	1727	1263	1736	1348
3- and 4-methylphenol	3913	2966	4692	3664	2325
n11:1	1016	1305	1706	497	1090
n11:0	1052	1309	1625	401	895

Code #	E48360-MK1-S2 R:2**6 (µg/g TOC)	E48365-MK1-S2 R:2**6 (µg/g TOC)	E48370-MK1-S2 R:2**6 (µg/g TOC)	E48376-MK1-S2 R:2**6 (µg/g TOC)	E48380-MK1-S2 R:2**6 (µg/g TOC)
2-ethylphenol	165	245	192	118	194
C2-phenol (1)	1801	1909	2038	1516	1267
metyllindene	273	363	245	476	330
C2-phenol (2)	1058	1234	1908	1627	1332
naphthalene	566	671	216	200	290
4-methylguaiaicol	326	170	291	189	51
n12:1	900	1284	1379	497	1123
n12:0	1026	1260	1554	367	849
4-ethylguaiaicol	316	192	248	208	112
2-methylnaphthalene	126	247	223	243	235
1-methylnaphthalene	172	364	368	209	238
n13:1	991	1248	1480	499	1344
n13:0	1245	1340	1528	476	977
2,6-dimethoxyphenol	166	109	91	36	76
methylindol	319	218	422	157	241
n14:1	914	995	1302	449	871
n14:0	1196	1201	1476	464	926
2,6 dimethoxy-4-methylphenol	208	283	339	250	225
trans-iso Eugenol	158	20	178	119	46
n15:1	1064	1098	1476	541	897
n15:0	1096	1260	1515	10	939
n16:1	901	1119	1314	527	930
n16:0	1060	1233	1426	440	880
4-allyl-2,6-dimethoxyphenol	498	459	584	342	353
n17:1	767	987	1229	376	810
n17:0	1074	1283	1464	378	941
prist-1-ene	732	734	622	346	499
n18:1	745	1001	1293	322	807
n18:0	934	1135	1434	316	825
n19:1	599	883	1075	279	713
n19:0	944	1328	1527	389	999
n20:1	663	1039	1309	306	856
n20:0	894	1214	1504	358	955
n21:1	530	820	1011	275	730
n21:0	887	1337	1494	370	1068
n22:1	548	924	918	318	0
n22:0	739	1041	1118	321	933
n23:1	491	714	851	246	643
n23:0	767	1085	1145	324	961
n24:1	648	840	783	276	496
n24:0	624	767	854	265	510
n25:1	499	789	752	267	528
n25:0	710	892	876	275	493
n26:1	452	564	661	232	408
n26:0	428	550	640	220	394
n27:1	306	342	546	207	533
n27:0	456	725	745	240	470
n28:1	207	223	346	119	207
n28:0	234	358	438	157	363
n29:1	59	0	368	127	205
n29:0	1101	1131	1019	253	618
n30:1	95	136	250	83	117
n30:0	131	286	332	115	222

E.nr.	Lake	Huminite/Vitrinite [%]	Liptinite (total) [%]	Sporinite [%]	Alginite [%]	other Lipt. [%]	Inertinite [%]	total AOM [%]	fluoramorphinite [%]	hebamorphinite [%]
48175	HZM	6.7	16.0	12.0	0.0	4.0	4.0	73.3	50.6	22.7
48180	HZM	12.0	23.0	17.0	1.0	5.0	1.0	64.0	41.0	23.0
48184	HZM	11.5	17.3	9.6	7.7	0.0	0.0	71.2	30.8	40.4
48187	HZM	5.2	10.4	6.3	1.0	3.1	2.1	82.3	40.6	41.7
48188	HZM	8.4	16.9	2.4	13.3	1.2	0.0	74.7	60.2	14.5
48189	HZM	46.7	33.3	3.3	0.0	30.0	0.0	20.0	6.7	13.3
48194	HZM	5.2	16.7	10.4	2.1	4.2	1.0	77.1	32.3	44.8
48195	HZM	4.5	24.7	5.6	14.6	4.5	2.2	68.6	55.1	13.5
48198	HZM	4.1	26.5	4.1	16.3	6.1	2.0	67.4	49.0	18.4
48200	HZM	5.1	16.6	1.3	12.8	2.6	1.3	77.0	51.3	25.7
48205	HZM	15.6	23.4	18.8	1.6	3.1	1.6	59.4	40.6	18.8
48207	HZM	12.2	14.3	10.2	2.0	2.0	10.2	63.3	24.5	38.8
48210	HZM	15.4	17.3	15.4	0.0	1.9	13.5	53.8	15.4	38.4
48339	MFM	15.1	12.2	6.1	6.1	0.0	15.1	57.6	33.3	24.3
48343	MFM	5.3	4.3	3.2	1.1	0.0	2.1	88.3	72.3	16.0
48347	MFM	15.9	10.6	7.4	3.2	0.0	3.2	70.2	44.7	25.5
48348	MFM	5.3	7.8	2.6	2.6	2.6	0.0	86.9	76.4	10.5
48349	MFM	13.3	4.1	4.1	0.0	0.0	2.0	80.6	54.1	26.5
48353	MFM	9.7	6.4	3.2	0.0	3.2	4.3	79.5	36.5	43.0
48357	MFM	5.2	11.5	10.4	1.0	0.0	1.0	82.3	56.3	26.0
48360	MFM	10.3	20.7	10.3	10.3	0.0	3.4	65.5	51.7	13.8
48365	MFM	3.8	5.0	2.5	1.3	1.3	25.3	65.9	36.8	29.1
48370	MFM	9.4	17.1	10.9	1.6	4.7	4.7	68.8	59.4	9.4
48376	MFM	11.5	5.8	3.5	2.3	0.0	12.7	70.0	33.4	36.6
48380	MFM	2.3	0.0	0.0	0.0	0.0	18.2	79.5	27.3	52.2

E.nr.	Lake	vitrinite reflectance Rr(%) counts				total counts
		from 0.00 to 0.30	from 0.30 to 0.60	from 0.60 to 1.00	>1.00	
48175	HZM	0	4	7	7	18
48180	HZM	23	7	0	2	32
48184	HZM	16	5	8	2	31
48187	HZM	8	10	2	2	22
48188	HZM	-	-	-	-	-
48189	HZM	17	6	1	3	27
48194	HZM	17	12	3	2	34
48195	HZM	18	19	2	2	41
48198	HZM	9	1	0	0	10
48200	HZM	14	5	2	1	22
48205	HZM	10	3	3	1	17
48207	HZM	19	6	7	0	32
48210	HZM	18	4	4	5	31
48339	MFM	4	9	10	1	24
48343	MFM	3	22	3	3	31
48347	MFM	10	24	2	2	38
48348	MFM	20	2	0	1	23
48349	MFM	30	8	2	0	40
48353	MFM	30	6	3	1	40
48357	MFM	9	3	2	0	14
48360	MFM	14	5	3	2	24
48365	MFM	9	8	16	35	68
48370	MFM	2	12	2	0	16
48376	MFM	26	10	16	40	92
48380	MFM	1	2	17	22	42

E.-nr. (Jülich)	E.-nr. (GFZ)	Lithozone	Depth [cm]	TC %	TOC %	TIC %	CaCO ₃ %	TS %	TOC/TS	TN %	TOC/TN	S1 (mg HC/g)	S2 (mg HC/g)	S3 (mg CO ₂ /g)	HI (mg HC/g TOC)	OI (mg CO ₂ /g TOC)	δ ¹³ C _{TOC}
47709	D 1-o-r	1	50	2.06	1.93	0.13	1.04	0.06	32.17	0.24	8.04	0.58	1.75	5.46	90	282	-21.91
47710	D 1-u-l	1	150	2.19	1.78	0.41	3.41	0.05	34.23	0.17	10.47	0.40	1.40	7.01	78	394	-20.60
47711	F 1-o-l	1	250	4.40	3.80	0.60	5.00	0.10	38.14	0.40	9.49	1.44	6.16	8.01	162	211	-22.46
47712	F 1-u-l	1	345	5.50	3.18	2.33	19.36	0.08	41.50	0.30	10.58	1.24	6.18	23.27	194	731	-23.72
47713	F 2-o-l	1	450	5.96	4.65	1.31	10.87	0.13	35.09	0.48	9.69	3.04	15.72	11.17	338	240	-22.74
47714	F 2-u-l	2	552	11.00	9.93	1.07	8.91	0.29	33.89	0.96	10.34	15.24	35.26	12.24	355	123	-19.90
47715	F 3-o-r	2	650	9.28	8.74	0.55	4.54	0.31	28.04	0.92	9.49	10.25	36.29	9.70	415	111	-18.82
47716	F 3-u-l	2	749	11.60	10.60	1.00	8.33	0.37	28.84	0.96	11.04	12.18	40.31	11.47	380	108	-19.64
47717	F 4-o-r	2	850	6.23	4.40	1.83	15.24	0.11	40.51	0.37	11.88	1.51	7.83	19.89	178	452	-21.52
47718	F 4-u-r	2	950	10.25	7.94	2.32	19.28	0.32	24.91	0.87	9.12	10.60	29.52	12.36	372	155	-19.50
47719	F 5-o-l	2	1050	11.45	8.59	2.86	23.81	0.27	32.35	0.77	11.16	11.04	31.99	12.91	372	150	-20.43
47720	F 5-u-r	3	1150	7.01	5.17	1.84	15.32	0.19	27.11	0.51	10.13	2.26	12.81	14.19	248	274	-20.88
47721	F 6-o-r	3	1250	6.63	5.06	1.57	13.07	0.12	40.93	0.50	10.11	2.15	11.88	12.09	234	239	-18.53
47722	F 6-u-r	3	1350	6.88	5.45	1.44	11.95	0.14	38.62	0.50	10.89	2.44	16.52	10.19	303	186	-18.53
47723	F 7-o-r	3	1450	5.48	3.92	1.56	12.95	0.12	33.22	0.42	9.33	1.02	6.83	10.70	174	273	-18.34
47724	F 7-u-r	3	1550	6.09	4.48	1.61	13.36	0.14	31.44	0.42	10.67	1.63	9.78	11.49	218	256	-17.81
47725	F 8-o-l	3	1650	5.96	4.41	1.55	12.91	0.11	39.16	0.41	10.74	1.27	9.27	12.81	206	290	-17.41
47726	F 8-u-l	3	1750	5.81	4.28	1.54	12.78	0.17	25.68	0.42	10.18	1.32	8.05	11.87	188	277	-17.07
47727	F 9-o-l	3	1850	5.67	4.24	1.43	11.91	0.15	28.84	0.40	10.60	1.20	7.89	12.01	186	283	-18.49
47728	F 9-u-r	3	1950	4.97	3.19	1.78	14.82	0.08	37.95	0.36	8.86	0.66	4.15	16.58	130	520	-17.65
47729	F 10-o-r	3	2050	4.99	3.47	1.53	12.70	0.09	40.50	0.36	9.63	0.82	5.14	12.90	148	371	-17.49
47730	F 10-u-r	3	2150	6.21	3.73	2.48	20.61	0.09	40.13	0.40	9.33	0.82	5.30	19.05	142	510	-18.10
47731	F 11-o-l	3	2250	6.00	4.70	1.30	10.78	0.12	39.50	0.51	9.22	1.29	9.28	10.79	197	229	-17.91
47732	F 11-u-l	3	2350	5.80	4.62	1.19	9.87	0.11	43.54	0.48	9.61	1.22	7.85	11.72	169	254	-16.80
47733	F 12-o-r	3	2450	5.43	4.00	1.43	11.91	0.09	42.69	0.44	9.09	0.92	6.24	13.30	156	332	-18.04
47734	F 12-u-r	3	2550	5.41	3.62	1.79	14.86	0.10	37.95	0.44	8.23	0.76	5.11	15.43	138	426	-18.55
47735	F 13-o-r	3	2648	6.68	4.93	1.75	14.57	0.17	28.66	0.46	10.72	1.22	8.43	14.50	170	293	-19.05
47736	F 13-u-l	3	2752	4.68	3.43	1.25	10.37	0.29	11.81	0.41	8.37	0.69	4.61	13.71	134	399	-19.56
47737	F 14-o-l	3	2850	6.70	5.09	1.61	13.41	0.18	28.57	0.55	9.25	1.42	9.39	10.97	184	215	-18.88
47738	F 14-u-r	4	2940	10.70	9.23	1.47	12.24	0.38	24.42	0.74	12.47	6.22	30.64	11.07	332	120	-24.93
47739	F 15-o-r	4	3048	15.15	13.30	1.85	15.40	0.47	28.42	0.93	14.30	11.65	52.19	15.09	392	113	-26.69
47740	F 15-u-l	4	3140	9.11	7.45	1.66	13.82	0.20	36.77	0.70	10.64	4.20	26.50	13.23	356	177	-26.35
47741	F 16-u-r	5	3250	7.76	6.50	1.26	10.49	0.20	32.23	0.68	9.55	3.57	22.65	9.71	348	149	-24.08
47742	F 17-o-l	5	3350	7.46	6.42	1.04	8.66	0.11	57.58	0.69	9.30	2.62	19.52	9.47	304	147	-21.67
47743	F 17-u-r	5	3441	6.48	5.07	1.42	11.78	0.09	55.32	0.61	8.30	1.98	13.37	12.08	264	238	-21.06
47744	F 18-u-l	5	3550	6.47	5.34	1.14	9.45	0.16	32.63	0.56	9.53	1.90	13.08	9.30	243	172	-20.61
47745	F 19-o-l	5	3650	4.90	4.16	0.75	6.20	0.16	25.34	0.52	7.99	1.26	10.15	5.73	247	138	-21.14
47746	F 20-o-l	5	3750	6.01	5.12	0.89	7.41	0.21	24.18	0.56	9.13	1.82	13.31	6.22	260	121	-21.71
47747	F 21-o-l	5	3870	6.00	4.32	1.68	13.99	0.15	29.66	0.52	8.30	1.46	8.83	10.02	204	231	-21.10
47748	F 21-o-l	5	3950	9.16	8.47	0.68	5.70	0.21	39.86	0.57	14.86	3.65	32.46	8.22	383	97	-27.03
48165	F 21-u-r	6	4050	21.55	20.30	1.25	10.41	0.36	56.31	0.58	35.00	8.20	36.78	19.20	181	95	-28.90
48166	F 22-o-l	6	4150	13.45	12.65	0.80	6.66	0.34	37.48	0.57	22.19	7.91	39.55	11.95	313	94	-29.75
48167	F 22-u-l	6	4250	13.45	13.05	0.40	3.33	0.59	22.19	0.49	26.63	12.29	50.29	10.71	385	82	-28.10
48168	F 23-o-l	6	4360	12.45	11.85	0.60	5.00	0.74	6.12	0.40	29.63	8.87	43.44	9.92	367	84	-29.66
48169	F 24-u-l	6	4450	13.85	13.50	0.35	2.91	1.00	5.03	0.38	35.53	10.91	41.20	9.86	305	73	-30.73
48170	F 25-u-r	6	4540	14.80	13.45	1.35	11.24	0.97	5.43	0.41	32.80	15.96	57.34	9.06	426	67	-31.25

E. nr. (Jülich)	E. nr. (GFZ)	Depth in E [cm]	Depth in F [cm]	lithozone	TC [%]	TOC [%]	CaCO ₃ [%]	TS [%]	TOC/TS	TN [%]	TOC/TN	S1 [mg HC/g sample]	S2 [mg HC/g sample]	S3 [mg CO ₂ /g sample]	HI [mg HC/g TOC]	OI [mg CO ₂ /g TOC]
49996	HUG E 4-o	715	707	2	9.0	8.6	3.0	0.4	24.1	0.9	9.9	8.0	27.6	11.2	320	130
49997	HUG E 4-o	740	730	2	10.4	10.2	2.1	0.4	23.7	-	-	11.6	31.3	11.7	308	115
49998	HUG E 4-o	765	757	2	11.6	10.9	5.8	0.5	24.2	1.1	9.8	16.0	39.0	12.0	358	110
49999	HUG E 4-o	790	778	2	9.9	8.7	10.4	0.3	29.3	-	-	11.6	26.9	11.9	311	137
50000	HUG E 4-u	815	800	2	8.6	7.2	11.9	0.2	32.1	0.8	9.0	9.2	23.9	13.2	331	183
50001	HUG E 4-u	840	823	2	7.6	7.1	3.8	0.2	33.2	0.7	10.1	5.3	16.5	10.5	232	148
50002	HUG E 4-u	865	850	2	6.1	4.3	14.5	0.2	26.1	0.5	8.3	1.9	7.6	14.8	175	342
50003	HUG E 4-u	890	879	2	6.3	5.6	5.3	0.2	27.1	0.6	9.0	2.7	10.1	12.1	179	215
50004	HUG E 5-o	915	911	2	8.6	8.0	4.9	0.2	33.5	0.8	10.0	8.5	19.6	12.0	243	149
50005	HUG E 15-o	2960	2867	3	6.6	5.4	9.8	0.2	27.2	0.6	8.9	1.5	8.8	10.5	162	193
50006	HUG E 15-o	2975	2882	3	7.9	7.6	1.9	0.3	24.8	0.7	10.9	3.5	16.9	8.7	222	114
50007	HUG E 15-o	2990	2896	3	7.2	6.1	9.3	0.3	17.9	0.7	9.4	2.2	11.8	9.3	192	151
50008	HUG E 15-o	3006	2910	3	7.8	6.8	8.3	0.3	19.5	0.7	10.2	4.1	16.0	11.8	237	174
50009	HUG E 15-u	3018	2924	4	9.4	9.0	3.4	0.4	25.1	0.8	11.8	6.0	23.5	10.7	262	119
50010	HUG E 15-u	3033	2938	4	9.9	9.8	0.7	0.4	23.1	0.8	12.1	8.3	29.3	10.0	299	102
50011	HUG E 15-u	3048	2969	4	13.3	13.2	0.8	0.4	32.5	0.9	14.2	20.2	43.3	12.1	328	92
50012	HUG E 15-u	3063	2978	4	11.6	11.4	1.7	0.4	26.5	0.9	13.1	10.9	35.0	10.8	307	95
50013	HUG E 15-u	3078	2993	4	10.1	9.6	3.9	0.3	28.9	0.8	12.4	5.6	29.8	10.0	309	104
50014	HUG E 15-u	3093	3008	4	14.6	14.0	5.4	0.4	39.8	0.9	15.3	12.3	40.4	12.9	289	92
50015	HUG E 15-u	3104	3019	4	21.4	20.7	5.4	0.4	55.9	1.0	20.3	16.2	42.1	18.7	204	90
50016	HUG E 16-o	3120	3028	4	20.1	20.0	0.8	0.5	41.2	1.1	18.1	21.3	66.2	19.2	331	96
50017	HUG E 16-o	3135	3042	4	17.1	16.9	2.1	0.4	40.0	1.0	16.4	20.8	61.4	15.8	364	94
50018	HUG E 16-o	3150	3056	4	14.2	13.7	4.2	0.4	38.1	0.9	15.0	21.8	61.0	13.8	445	101
50019	HUG E 16-o	3165	3071	4	15.4	15.2	1.7	0.4	40.2	0.9	16.6	12.1	46.5	12.9	307	85
50020	HUG E 16-o	3180	3088	4	14.9	14.3	5.0	0.4	36.1	0.9	15.4	15.0	53.7	12.8	377	90
50021	HUG E 16-o	3195	3101	4	13.0	12.9	0.4	0.4	32.2	0.9	14.6	11.3	50.0	11.9	387	92
50022	HUG E 16-u	3210	3114	4	9.9	8.2	13.8	0.3	26.7	0.7	11.9	5.6	27.8	13.2	337	160
50023	HUG E 16-u	3225	3128	4	13.4	12.7	5.8	0.4	31.4	0.9	14.7	12.6	51.9	12.1	410	96
50024	HUG E 16-u	3240	3143	4	8.9	7.5	10.9	0.2	34.0	0.6	11.8	4.5	24.2	11.6	320	153
50025	HUG E 17-o	3253	3154	4	11.0	11.0	0.0	0.3	34.5	0.8	13.7	9.1	40.7	10.5	372	96
50026	HUG E 17-o	3268	3169	4	11.1	10.9	2.1	0.4	30.0	0.8	13.5	6.9	35.6	11.1	328	102
50027	HUG E 17-o	3283	3184	4	14.8	14.7	0.8	0.4	34.3	0.9	15.9	9.3	45.9	16.2	313	110
50028	HUG E 17-o	3298	3198	4	15.3	13.6	14.6	0.3	41.0	0.9	15.4	11.4	51.3	14.3	378	105
50029	HUG E 17-o	3313	3213	4	14.3	13.6	6.3	0.4	30.9	1.0	13.9	11.7	47.7	13.9	352	103

Code #	E47716-MK1-S2 R:2**6	E47730-MK1-S2 R:2**6	E47736-MK1-S2 R:2**6	E47739-MK1-S2 R:2**6	E47744-MK1-S2 R:2**6	E48165-MK1-S2 R:2**6	E48170-MK1-S2 R:2**6
Amount (mg)	3.20	5.20	5.00	4.10	4.00	6.90	3.90
TOC (%)	54.0	57.1	49.4	54.1	54.4	50.0	52.4
	(µg/g TOC)	(µg/g TOC)	(µg/g TOC)	(µg/g TOC)	(µg/g TOC)	(µg/g TOC)	(µg/g TOC)
C1	7081	4977	4896	9657	7188	19519	22551
C02-05 Total	15777	10447	10083	14835	13506	20197	64457
C06-14 Total	45850	30317	30350	45929	39253	64891	184142
C15-32 Total	61278	34391	33537	54419	53251	50312	296834
C01-05 Total	22858	15424	14979	24492	20674	39716	87008
C06-14 Total	45850	30317	30350	45929	39253	64891	184142
C15-32 Total (corr)	59542	33381	32322	53066	51872	49442	295366
C01-32 Total	128250	79122	77651	123487	111799	154049	566516
C06-14 Resolved	30849	22178	21024	31458	26710	47304	125434
C15-32 Resolved	18272	13050	10961	15163	16087	14561	94047
C01-32 Resolved	71979	50652	46964	71113	63471	101581	306489
n6:1	787	587	483	687	710	665	3732
n6:0	588	449	368	515	518	659	2807
Benzene	610	587	488	530	579	1167	2428
n7:1	604	456	376	554	566	506	3142
n7:0	564	460	381	499	522	584	2831
Pyridine	171	79	152	135	135	443	764
Pyrrrole	345	204	274	386	309	333	1309
Toluene	2125	1169	1199	1398	1505	1759	4832
n8:1	543	391	347	509	497	345	2702
2-Methylpyridin	153	70	125	124	116	399	559
n8:0	494	437	319	440	442	416	2422
2-Methylpyrrol	185	82	123	211	168	153	238
3-Methylpyrrol	187	69	95	158	142	152	570
3-Methylpyridin	112	85	69	64	58	137	412
Ethylbenzene	331	303	255	273	281	342	1121
m+p-Xylenes	534	364	356	503	426	633	2065
Styrene	359	190	228	273	271	350	966
o-Xylene	248	310	233	291	253	369	1204
n9:1	453	325	264	390	395	243	2169
n9:0	464	333	287	444	432	358	2406
Ethyl-Methylbenzene	140	133	109	150	128	n.a.	n.a.
1,3,5 Trimethylbenzene	80	54	52	76	73	n.a.	n.a.
1-Ethyl-2-Methylbenzene	98	147	100	97	96	n.a.	n.a.
Phenol	764	590	637	988	648	2952	3883
1,2,4 Trimethylbenzene	243	200	186	241	203	225	886
n10:1	484	325	283	423	413	259	2318
n10:0	434	311	251	378	369	291	2098
1,2,3 Trimethylbenzene	219	174	129	164	199	228	806
Indene	72	91	80	143	112	187	398
Cresol	280	226	231	392	231	1083	1558
n-Butylbenzene	123	112	34	118	92	n.a.	n.a.

Code #	E47716-MK1-S2 R:2**6 (µg/g TOC)	E47730-MK1-S2 R:2**6 (µg/g TOC)	E47736-MK1-S2 R:2**6 (µg/g TOC)	E47739-MK1-S2 R:2**6 (µg/g TOC)	E47744-MK1-S2 R:2**6 (µg/g TOC)	E48165-MK1-S2 R:2**6 (µg/g TOC)	E48170-MK1-S2 R:2**6 (µg/g TOC)
Cresol	1097	477	706	1310	925	2549	4032
Guaiacol	176	31	24	245	56	1846	200
n11:1	552	353	319	435	460	338	2692
n11:0	483	336	267	386	409	299	2285
2-Ethylphenol	111	45	46	70	67	119	535
C2-Phenol (1)	382	219	205	377	276	1028	2899
Methylindene	122	83	83	99	96	87	358
C2-Phenol (2)	433	213	236	389	308	968	2239
Naphtalene	133	158	134	132	133	401	436
4-Methylguaiacol	134	59	106	442	207	1823	412
n12:1	508	344	294	767	424	903	2302
n12:0	536	410	310	628	454	527	2392
4-Ethylguaiacol	125	83	93	296	182	940	302
Indol	48	32	24	52	32	60	0
2-Methylnaphtalene	95	152	108	154	120	161	501
1-Methylnaphtalene	102	106	92	194	97	341	413
n13:1	516	365	314	536	458	468	2181
n13:0	519	378	316	510	476	381	2166
2,6-Dimethoxyphenol	81	44	75	243	111	61	314
Eugenol	62	44	50	79	75	100	0
Methylindol	148	135	118	108	115	171	451
n14:1	449	327	289	394	434	298	2046
n14:0	470	348	288	406	426	400	2148
2,6 Dimethoxy-4-Methylphenol	155	115	108	159	144	158	543
trans-Isoeugenol	80	15	49	122	91	341	230
Acetovanillone	67	51	42	86	64	30	160
n15:1	432	282	237	346	371	491	2183
n15:0	461	327	260	362	417	353	2172
n16:1	361	250	211	321	325	311	1994
n16:0	382	300	231	342	356	312	2003
4-Allyl-2,6-Dimethoxyphenol	120	62	110	183	148	162	772
n17:1	360	259	211	295	325	202	1802
n17:0	411	302	250	376	392	295	2175
Prist-1-ene	170	68	98	176	143	264	1291
n18:1	306	236	186	277	282	183	1632
n18:0	343	284	227	330	338	249	1924
n19:1	290	210	169	259	262	153	1544
n19:0	370	285	239	353	352	277	2083
n20:1	277	202	177	266	274	169	1651
n20:0	343	272	227	320	338	262	1999
n21:1	265	169	149	222	234	155	1481
n21:0	347	256	220	309	326	264	2031
n22:1	274	171	157	218	239	159	1533
n22:0	322	221	186	252	289	259	1781
n23:1	261	174	145	210	239	171	1445
n23:0	321	217	186	252	294	265	1822
n24:1	275	194	167	222	248	201	1494
n24:0	298	199	160	213	258	237	1624
n25:1	238	163	139	210	248	203	1594
n25:0	328	211	169	220	261	255	1783
n26:1	259	146	126	202	219	158	1452
n26:0	280	182	142	207	225	233	1586
n27:1	202	124	109	161	171	173	1283
n27:0	276	185	140	206	234	314	2249
n28:1	186	102	92	157	146	129	969
n28:0	228	130	106	159	171	184	1328
n29:1	131	77	71	116	115	112	778
n29:0	359	156	152	245	253	349	2054
n30:1	146	80	67	133	133	103.96	887.478
n30:0	166	99	79	114	129	125.248	1124.826

Code #	E49996-PA1-Extr.-S2 R:**6	E49998-PA1-Extr.-S2 R:**6	E49999-PA1-Extr.-S2 R:**6	E50001-PA1-Extr.-S2 R:**6	E50002-PA1-Extr.-S2 R:**6	E50003-PA1-Extr.-S2 R:**6
Amount (mg)	17.30	11.30	17.30	28.20	40.00	33.00
TOC [%]	8.615	10.9	8.665	7.11	4.315	5.635
	(µg/g TOC)	(µg/g TOC)	(µg/g TOC)	(µg/g TOC)	(µg/g TOC)	(µg/g TOC)
C1	14443	12837	11353	11658	15666	17795
C02-05 Total	47712	44351	39116	36094	46859	41384
C06-14 Total	119922	105894	93865	102134	101399	91508
C15-32 Total	80583	79262	53886	61198	34326	34316
C01-05 Total	62155	57188	50469	47752	62525	59179
C06-14 Total	119922	105894	93865	102134	101399	91508
C15-32 Total (corr)	78570	76826	51885	59702	32588	32703
C01-32 Total	260647	239908	196219	209588	196512	183390
2-propanone	2068	2474	2983	2439	4768	1682
Furan	1596	1525	1268	445	1774	1134
cyclopentadiene	1020	912	993	1155	223	750
butadiene and cyclopentene	1967	1597	1574	1411	2689	2299
2,3-butanedione	391	359	461	349	305	347
2-butanone	880	728	1234	1113	2367	1463
n-C6:1	1366	1256	957	1074	779	725
2-methylfuran	700	725	727	801	736	740
n-C6:0	1213	955	895	724	1514	1206
3-methylfuran	548	419	432	453	610	533
1,4-cyclohexadiene	638	543	641	662	889	523
1,3-cyclohexadiene	684	572	641	731	788	488
Methylcyclopentene,Metylbutanal	914	715	657	682	778	642
Benzene	1874	1724	2045	1720	3494	2364
Thiophene	340	488	286	509	287	298
cyclohexene	374	307	263	298	248	228
n-C7:1	995	940	669	766	407	421
n-C7:0	1108	899	742	695	802	755
alkene (4)	277	223	247	328	260	244
pyridine	1373	1123	1146	1002	2493	1925
pyrrole	1607	1326	1551	1742	2170	1695
Toluene	4791	4830	4368	3509	5071	4502
2-methylthiophene	216	251	211	220	198	191
furan-2-one	633	564	474	551	614	610
n-C8:1	831	826	600	972	525	546
methylpyridine (1)	944	569	552	760	1273	1050
2-Cyclopenten-1-one	457	702	687	295	360	305
n-C8:0	1059	1013	855	823	685	652
n-alkene (1)	290	282	255	276	255	245
2-Methylpyrrole	896	790	809	1053	1068	923
3-Methylpyrrole	502	414	419	601	544	484

Code #	E49996-PA1-Extr.-S2 R:**6 (µg/g TOC)	E49998-PA1-Extr.-S2 R:**6 (µg/g TOC)	E49999-PA1-Extr.-S2 R:**6 (µg/g TOC)	E50001-PA1-Extr.-S2 R:**6 (µg/g TOC)	E50002-PA1-Extr.-S2 R:**6 (µg/g TOC)	E50003-PA1-Extr.-S2 R:**6 (µg/g TOC)
methylpyridine (2)	840	716	182	704	1165	1104
Ethylbenzene	1065	980	908	658	1082	1025
m+p-Xylenes	1273	1072	1069	943	1368	1275
Dimethylpyridine	74	59	84	65	117	94
Styrene+methylcyclopentenone	1646	1663	1340	1977	1397	1472
o-Xylene	823	754	775	646	890	825
n-C9:1	657	662	470	510	259	276
2,5-dimethylpyrrole	340	313	305	368	391	332
n-C9:0	757	678	557	490	453	458
alkene (3)	736	623	575	620	674	567
2,4-dimethylpyrrole	74	0	50	106	116	80
dimethylpyridine	348	269	249	0	567	321
2,3-dimethylpyrrole	496	411	427	472	556	494
methylfuranaldehyde	255	217	196	298	378	365
3-methyl-2-cyclopentenone	588	514	390	488	251	292
n-propylbenzene	287	258	267	244	321	299
1-ethyl-3-methylbenzene-cybenz	717	547	693	585	1157	934
1-ethyl-4-methylbenzene	182	141	146	151	216	179
1,3,5-trimethylbenzene	119	74	82	539	493	513
phenol	2915	1943	1926	2740	3075	2866
1-ethyl-2-methylbenzene	504	375	496	455	584	585
Benzofuran	213	164	167	204	306	283
1,2,4-trimethylbenzene	932	749	683	780	786	845
n-C10:1	695	738	482	529	231	287
2,3,5-trimethylpyrrole	223	302	312	384	453	377
n-C10:0	776	670	550	491	468	471
1,2,3-trimethylbenzene	581	487	461	380	527	581
dimethylcyclopentenone	255	236	202	290	210	158
1-isopropyl-3-methylbenzene	196	114	108	99	89	104
3-ethyl-4-methylpyrrole	78	44	61	90	30	30
1-propenylbenzene	202	157	163	152	246	203
indene	378	280	314	446	458	316
o-Cresol	961	919	591	906	791	873
1,3-diethylbenzene	332	214	282	466	503	372
1-methyl-3-propylbenzene	147	118	117	162	165	155
alkylbenzenes	388	353	310	326	372	346
1,2-diethylbenzene	91	65	68	75	80	75
1-ethyl-3,5-dimethylbenzene	207	143	114	196	277	284
m+p-Cresol	2582	2013	1537	2224	1881	1977
2-methoxyphenol	48	57	45	99	20	75
2-ethyl-1,4-dimethylbenzene	180	170	100	75	117	131
1-ethyl-2,4-dimethylbenzene	221	185	173	248	199	202
ethylidimethylpyrrole (1)	204	224	225	261	175	167
1-ethyl-3,4-dimethylbenzene	351	280	221	165	270	258
2,6-dimethylphenol	121	91	67	99	72	91
n-C11:1	744	757	497	546	256	302
methylbenzofuran	355	285	245	323	358	365
cyanomethylbenzene	405	340	318	411	311	312
n-C11:0	734	708	526	449	398	412
1-ethyl-2,3-dimethylbenzene	221	186	155	190	128	138
1,2,4,5-tetramethylbenzene	74	66	66	79	61	61
1,2,3,5-tetramethylbenzene	298	241	234	275	225	228
2-ethylphenol	149	98	95	122	131	145
C2-Phenoles (A+B)	699	542	433	641	529	551

Code #	E49996-PA1-Extr.-S2 R:**6 (µg/g TOC)	E49998-PA1-Extr.-S2 R:**6 (µg/g TOC)	E49999-PA1-Extr.-S2 R:**6 (µg/g TOC)	E50001-PA1-Extr.-S2 R:**6 (µg/g TOC)	E50002-PA1-Extr.-S2 R:**6 (µg/g TOC)	E50003-PA1-Extr.-S2 R:**6 (µg/g TOC)
methylindene	893	665	746	784	927	748
1,2,3,4-tetramethylbenzene	366	255	239	340	360	305
C2-Phenoles (C+D)	1113	804	675	855	771	789
2,3-dimethylphenol	412	274	289	328	234	329
Naphthalene	477	364	456	452	803	618
4-methylguaiacol	35	37	36	30	28	40
n-C12:1	803	804	540	568	360	377
vinylphenol	408	342	307	278	244	273
n-C12:0	890	813	637	570	497	522
dimethylindene	870	699	435	804	700	468
4-ethylguaiacol	299	228	233	265	340	278
indole	312	340	281	325	198	207
2-M-Naphthalene	490	364	395	422	609	498
4-vinylguaiacol	207	153	152	174	211	183
n-C13:1	650	621	415	491	205	237
alkene (1)	771	644	567	597	952	835
1-M-Naphthalene	606	450	429	471	539	491
n-C13:0	924	809	655	603	490	511
alkene (2)	1331	1051	1170	1236	1581	1405
alkene (3)	201	140	145	144	117	102
methylindole	890	795	719	738	875	783
2,6-dimethoxyphenol	71	37	50	46	50	31
2-ethylnaphthalene	136	118	128	119	156	141
n-C14:1	624	642	434	475	210	229
n-C14:0	895	810	640	569	438	454
1,3-DMN	218	150	159	155	240	206
1,7-and 1,6-DMN	421	356	300	342	296	288
eugenol	65	50	68	82	59	46
n-C15:1	608	590	412	462	240	245
n-C15:0	1008	744	744	682	640	603
1,6,7-and 1,2,6-TMN	100	72	81	79	66	80
fluorene	156	115	140	157	320	194
n-C16:1	602	554	386	525	315	293
n-C16:0	684	588	499	508	403	391
alkene	596	374	413	393	555	395
biphenol	221	179	136	178	112	120
n-C17:1	398	403	275	340	185	146
n-C17:0	508	496	384	404	343	321
Prist-1-ene	152	135	90	92	51	54
prist-2-ene	278	201	163	174	76	104
phenanthrene	196	173	131	111	97	124
n-C18:1	300	342	218	221	108	110
n-C18:0	423	440	334	282	211	212
unknown	1821	1366	1196	1115	1134	1238
n-C19:1	315	331	214	216	121	126
n-C19:0	455	445	333	284	205	202
n-C20:1	272	290	181	205	83	84
n-C20:0	426	414	312	280	194	178
n-C21:1	291	292	196	240	104	99
n-C21:0	398	407	288	277	173	149
n-C22:1	243	270	181	207	84	78
n-C22:0	332	335	247	245	145	124
n-C23:1	132	168	92	114	25	24
n-C23:0	317	328	240	236	126	99
n-C24:1	255	264	143	204	64	65
n-C24:0	296	310	218	229	107	84
n-C25:1	347	323	177	271	68	95
n-C25:0	257	283	191	204	88	66
n-C26:1	98	134	57	71	13	54
n-C26:0	293	295	169	202	60	15
n-C27:1	96	119	54	73	12	51
n-C27:0	297	317	182	237	58	6
n-C28:1	70	107	43	50	9	24
n-C28:0	186	217	112	129	27	4
n-C29:1	106	123	30	75	13	13
n-C29:0	131	161	72	91	24	12
n-C30:1	19	62	17	17	2	0
n-C30:0	143	171	86	90	17	17

Code #	E50004-PA1-Extr.-S2 R:**6	E50005-PA1-Extr.-S2 R:**6	E50006-PA1-Extr.-S2 R:**6	E50007-PA1-Extr.-S2 R:**6	E50008-PA1-Extr.-S2 R:**6	E50009-PA1-Extr.-S2 R:**6
Amount (mg)	18.00	52.00	23.50	41.50	26.80	19.50
	8.03	5.405	7.625	6.13	6.765	8.985
	(µg/g TOC)	(µg/g TOC)	(µg/g TOC)	(µg/g TOC)	(µg/g TOC)	(µg/g TOC)
C1	11418	18534	16112	18505	17909	14184
C02-05 Total	38608	41670	38529	45529	48452	42111
C06-14 Total	99560	92180	101704	94863	116718	109898
C15-32 Total	68635	31177	66309	35488	60873	84425
C01-05 Total	50026	60204	54641	64034	66361	56295
C06-14 Total	99560	92180	101704	94863	116718	109898
C15-32 Total (corr)	66559	30110	64635	34309	59218	82713
C01-32 Total	216145	182494	220980	193206	242297	248906
2-propanone	2485	2044	2322	1201	3196	2480
Furan	1800	1017	1538	718	1431	1827
cyclopentadiene	1268	371	1239	828	1244	1330
butadiene and cyclopentene	1311	2391	1403	2229	2303	1303
2,3-butanedione	523	293	427	271	419	407
2-butanone	1026	1415	982	1306	1624	903
n-C6:1	1128	547	931	669	981	1302
2-methylfuran	769	597	612	625	881	627
n-C6:0	722	1102	777	1063	1347	842
3-methylfuran	376	651	530	664	924	496
1,4-cyclohexadiene	682	556	778	532	816	775
1,3-cyclohexadiene	646	501	696	474	727	689
Methylcyclopentene,Metylbutanal	547	724	622	677	839	686
Benzene	2304	2338	1994	2428	2843	1826
Thiophene	531	258	483	288	379	608
cyclohexene	305	198	261	241	351	338
n-C7:1	783	282	659	378	601	971
n-C7:0	594	1206	767	1059	1099	861
alkene (4)	293	187	249	282	306	231
pyridine	1182	1712	1164	1454	1503	1098
pyrrole	1939	1331	1624	1515	1838	1492
Toluene	3829	4208	3141	4098	4362	3258
2-methylthiophene	228	196	221	242	257	293
furan-2-one	565	350	667	528	752	620
n-C8:1	737	365	607	482	554	834
methylpyridine (1)	1003	1029	1109	745	1092	1203
2-Cyclopenten-1-one	678	309	582	309	614	541
n-C8:0	688	645	685	707	837	814
n-alkene (1)	225	226	261	255	310	262
2-Methylpyrrole	907	843	947	909	1100	911
3-Methylpyrrole	550	398	528	481	527	530

Code #	E50004-PA1-Extr.-S2 R:**6 (µg/g TOC)	E50005-PA1-Extr.-S2 R:**6 (µg/g TOC)	E50006-PA1-Extr.-S2 R:**6 (µg/g TOC)	E50007-PA1-Extr.-S2 R:**6 (µg/g TOC)	E50008-PA1-Extr.-S2 R:**6 (µg/g TOC)	E50009-PA1-Extr.-S2 R:**6 (µg/g TOC)
methylpyridine (2)	728	1025	783	999	938	735
Ethylbenzene	718	1023	658	1025	934	655
m+p-Xylenes	926	1426	1032	1411	1376	1069
Dimethylpyridine	0	71	53	82	106	67
Styrene+methylcyclopentenone	1905	983	1839	1259	1679	1824
o-Xylene	644	867	675	851	910	707
n-C9:1	570	183	399	260	348	604
2,5-dimethylpyrrole	307	318	397	375	378	390
n-C9:0	448	520	464	572	688	538
alkene (3)	473	583	637	726	796	627
2,4-dimethylpyrrole	96	156	93	220	126	90
dimethylpyridine	283	184	276	66	361	243
2,3-dimethylpyrrole	382	416	476	552	582	454
methylfurancarboxaldehyde	222	208	226	151	242	217
3-methyl-2-cyclopentenone	474	93	463	69	171	571
n-propylbenzene	214	318	228	343	343	237
1-ethyl-3-methylbenzene-cybenz	643	994	696	917	1086	561
1-ethyl-4-methylbenzene	117	226	127	223	184	134
1,3,5-trimethylbenzene	108	635	141	547	123	118
phenol	2901	2593	2780	2881	3442	3286
1-ethyl-2-methylbenzene	323	580	376	668	547	403
Benzofuran	177	308	192	216	280	216
1,2,4-trimethylbenzene	679	886	843	841	800	782
n-C10:1	579	150	409	241	377	642
2,3,5-trimethylpyrrole	356	516	450	483	691	410
n-C10:0	437	478	480	484	610	596
1,2,3-trimethylbenzene	477	480	474	506	539	378
dimethylcyclopentenone	155	207	257	229	314	346
1-isopropyl-3-methylbenzene	80	118	119	126	162	117
3-ethyl-4-methylpyrrole	96	40	65	34	49	87
1-propenylbenzene	155	273	217	242	274	221
indene	407	347	459	315	447	438
o-Cresol	866	847	950	950	1082	1052
1,3-diethylbenzene	416	389	417	403	509	414
1-methyl-3-propylbenzene	109	187	128	176	153	189
alkylbenzenes	318	407	369	388	454	393
1,2-diethylbenzene	67	89	80	86	94	80
1-ethyl-3,5-dimethylbenzene	79	398	152	367	218	134
m+p-Cresol	2245	1862	2193	2198	2562	2689
2-methoxyphenol	86	39	96	44	115	190
2-ethyl-1,4-dimethylbenzene	78	114	97	107	128	127
1-ethyl-2,4-dimethylbenzene	185	225	190	223	162	117
ethylidimethylpyrrole (1)	80	175	82	177	191	216
1-ethyl-3,4-dimethylbenzene	173	260	208	239	347	221
2,6-dimethylphenol	105	97	175	109	136	183
n-C11:1	601	208	462	257	456	738
methylbenzofuran	272	411	308	394	381	233
cyanomethylbenzene	391	315	327	321	382	317
n-C11:0	417	413	407	416	527	529
1-ethyl-2,3-dimethylbenzene	174	132	209	146	211	213
1,2,4,5-tetramethylbenzene	84	72	111	64	85	118
1,2,3,5-tetramethylbenzene	262	215	279	216	280	312
2-ethylphenol	145	150	154	147	186	166
C2-Phenoles (A+B)	620	610	666	664	782	760

Code #	E50004-PA1-Extr.-S2 R:**6 (µg/g TOC)	E50005-PA1-Extr.-S2 R:**6 (µg/g TOC)	E50006-PA1-Extr.-S2 R:**6 (µg/g TOC)	E50007-PA1-Extr.-S2 R:**6 (µg/g TOC)	E50008-PA1-Extr.-S2 R:**6 (µg/g TOC)	E50009-PA1-Extr.-S2 R:**6 (µg/g TOC)
methyindene	779	863	862	764	969	883
1,2,3,4-tetramethylbenzene	303	326	309	347	357	297
C2-Phenoles (C+D)	990	803	1076	986	1219	998
2,3-dimethylphenol	332	366	393	344	464	389
Naphthalene	465	695	511	631	682	474
4-methylguaiaicol	70	36	40	50	65	120
n-C12:1	580	323	472	342	514	671
vinylphenol	281	229	267	252	294	171
n-C12:0	536	518	535	555	713	676
dimethylindene	921	813	1027	873	1130	1117
4-ethylguaiaicol	240	424	429	432	500	435
indole	352	193	283	226	281	295
2-M-Naphthalene	387	676	484	581	613	504
4-vinylguaiaicol	147	242	207	224	240	162
n-C13:1	490	175	400	228	377	653
alkene (1)	611	903	793	817	892	642
1-M-Naphthalene	389	577	493	527	627	546
n-C13:0	480	518	637	551	728	724
alkene (2)	802	1683	1162	1051	1414	1058
alkene (3)	103	116	171	111	143	173
methyindole	788	825	866	855	999	835
2,6-dimethoxyphenol	50	42	81	60	68	132
2-ethylnaphthalene	121	152	121	158	164	132
n-C14:1	539	314	413	218	436	641
n-C14:0	512	440	594	475	682	672
1,3-DMN	140	277	188	249	244	173
1,7-and 1,6-DMN	339	310	395	329	437	431
eugenol	71	45	103	184	215	118
n-C15:1	485	167	411	233	411	559
n-C15:0	618	638	694	665	835	758
1,6,7-and 1,2,6-TMN	71	68	80	83	102	69
fluorene	153	215	174	176	198	165
n-C16:1	559	182	388	195	327	620
n-C16:0	458	367	482	397	565	571
alkene	415	261	494	269	577	493
biphenol	168	66	141	85	123	167
n-C17:1	344	174	353	133	189	335
n-C17:0	377	281	412	332	460	493
Prist-1-ene	105	33	96	46	103	137
prist-2-ene	224	55	241	114	252	313
phenanthrene	119	92	148	119	160	143
n-C18:1	280	93	255	106	221	359
n-C18:0	290	189	370	233	398	445
unknown	1013	851	1158	1073	1331	1051
n-C19:1	284	114	260	130	242	360
n-C19:0	308	209	383	237	408	472
n-C20:1	249	55	222	88	203	331
n-C20:0	291	194	350	210	378	439
n-C21:1	263	83	225	98	219	332
n-C21:0	255	158	291	168	318	396
n-C22:1	244	23	186	78	187	338
n-C22:0	225	131	246	139	286	354
n-C23:1	136	34	97	31	82	231
n-C23:0	217	108	235	119	260	337
n-C24:1	208	63	209	77	198	312
n-C24:0	214	85	233	105	260	338
n-C25:1	236	69	262	93	235	362
n-C25:0	200	69	185	72	200	299
n-C26:1	110	15	63	17	60	144
n-C26:0	196	49	172	57	175	287
n-C27:1	64	9	13	3	21	79
n-C27:0	215	46	179	54	185	322
n-C28:1	71	5	40	6	37	106
n-C28:0	134	23	109	30	116	217
n-C29:1	87	13	62	14	80	147
n-C29:0	79	12	96	17	73	151
n-C30:1	49	17	18	0	16	171
n-C30:0	120	5	93	25	102	50

Code #	E50010-PA1-Extr.-S2 R:**6	E50011-PA1-Extr.-S2 R:**6	E50012-PA1-Extr.-S2 R:**6	E50013-PA1-Extr.-S2 R:**6	E50014-PA1-Extr.-S2 R:**6	E50015-PA1-Extr.-S2 R:**6
Amount (mg)	16.50	9.20	10.80	13.30	9.40	9.20
	9.8	13.2	11.4	9.635	13.95	20.7
	(µg/g TOC)	(µg/g TOC)	(µg/g TOC)	(µg/g TOC)	(µg/g TOC)	(µg/g TOC)
C1	17327	11670	12360	14062	14627	12196
C02-05 Total	48892	4317	25894	37992	31300	27616
C06-14 Total	106655	108645	99363	114734	96499	81927
C15-32 Total	72217	111329	172050	107987	88137	78006
C01-05 Total	66219	15987	38254	52054	45927	39812
C06-14 Total	106655	108645	99363	114734	96499	81927
C15-32 Total (corr)	70362	108859	169613	105646	85849	76431
C01-32 Total	243236	233491	307230	272434	228275	198170
2-propanone	4737	1844	1747	2104	2076	2104
Furan	1694	1892	1717	1962	1500	1580
cyclopentadiene	943	1195	1038	1287	958	754
butadiene and cyclopentene	1463	897	814	956	701	618
2,3-butanedione	382	398	355	409	308	295
2-butanone	861	554	576	751	671	648
n-C6:1	1278	1540	1328	1548	1176	904
2-methylfuran	635	551	449	513	453	546
n-C6:0	1176	811	682	931	637	508
3-methylfuran	582	391	348	434	306	252
1,4-cyclohexadiene	556	655	596	738	529	416
1,3-cyclohexadiene	488	580	512	645	471	372
Methylcyclopentene,Metylbutanal	638	658	560	534	493	355
Benzene	2078	2425	2086	1712	2393	2112
Thiophene	356	516	443	436	469	443
cyclohexene	326	379	318	390	285	213
n-C7:1	868	1174	1047	1131	913	710
n-C7:0	985	848	709	806	647	536
alkene (4)	273	177	158	204	134	114
pyridine	954	707	695	748	673	656
pyrrole	1294	1122	1137	1510	1125	1064
Toluene	4057	2930	2672	3062	2764	2418
2-methylthiophene	288	319	294	336	277	213
furan-2-one	523	388	343	451	330	293
n-C8:1	780	1009	929	995	786	643
methylpyridine (1)	544	322	320	340	289	212
2-Cyclopenten-1-one	820	983	1106	1247	918	605
n-C8:0	957	879	785	898	691	506
n-alkene (1)	304	217	213	260	186	155
2-Methylpyrrole	780	592	603	749	562	444
3-Methylpyrrole	415	338	356	436	325	240

Code #	E50010-PA1-Extr.-S2 R:**6 (µg/g TOC)	E50011-PA1-Extr.-S2 R:**6 (µg/g TOC)	E50012-PA1-Extr.-S2 R:**6 (µg/g TOC)	E50013-PA1-Extr.-S2 R:**6 (µg/g TOC)	E50014-PA1-Extr.-S2 R:**6 (µg/g TOC)	E50015-PA1-Extr.-S2 R:**6 (µg/g TOC)
methylpyridine (2)	699	381	396	475	336	285
Ethylbenzene	974	613	507	645	512	433
m+p-Xylenes	1329	1007	947	1109	962	828
Dimethylpyridine	83	54	69	134	43	37
Styrene+methylcyclopentenone	1924	1362	1373	1489	1155	713
o-Xylene	915	599	568	656	507	395
n-C9:1	602	831	768	815	629	525
2,5-dimethylpyrrole	328	233	238	276	214	153
n-C9:0	724	628	563	636	479	386
alkene (3)	699	498	480	585	418	301
2,4-dimethylpyrrole	68	0	0	0	0	0
dimethylpyridine	269	160	178	198	159	119
2,3-dimethylpyrrole	447	298	291	387	272	153
methylfuranaldehyde	192	60	134	160	128	114
3-methyl-2-cyclopentenone	384	552	522	797	367	164
n-propylbenzene	296	184	174	201	156	136
1-ethyl-3-methylbenzene-cybenz	721	527	468	486	498	409
1-ethyl-4-methylbenzene	187	127	121	135	121	90
1,3,5-trimethylbenzene	126	89	104	112	83	68
phenol	2584	2209	2215	2900	3294	2715
1-ethyl-2-methylbenzene	531	319	315	387	332	278
Benzofuran	226	155	148	208	173	185
1,2,4-trimethylbenzene	815	669	639	647	547	492
n-C10:1	649	838	811	845	669	548
2,3,5-trimethylpyrrole	357	273	286	386	356	215
n-C10:0	702	700	626	646	613	577
1,2,3-trimethylbenzene	327	485	476	242	187	201
dimethylcyclopentenone	407	75	74	381	346	233
1-isopropyl-3-methylbenzene	133	97	64	148	79	67
3-ethyl-4-methylpyrrole	46	94	101	119	114	94
1-propenylbenzene	246	163	158	185	160	103
indene	329	355	375	429	356	256
o-Cresol	875	883	913	953	1016	745
1,3-diethylbenzene	402	284	222	405	335	296
1-methyl-3-propylbenzene	146	106	101	110	165	67
alkylbenzenes	382	461	335	374	293	302
1,2-diethylbenzene	90	95	84	88	78	147
1-ethyl-3,5-dimethylbenzene	195	74	70	86	87	153
m+p-Cresol	2186	2066	1981	2588	2966	2532
2-methoxyphenol	113	238	202	285	487	844
2-ethyl-1,4-dimethylbenzene	120	107	94	105	96	92
1-ethyl-2,4-dimethylbenzene	135	123	109	84	75	138
ethyl dimethylpyrrole (1)	143	89	72	123	97	0
1-ethyl-3,4-dimethylbenzene	318	198	231	232	158	138
2,6-dimethylphenol	125	118	112	135	122	369
n-C11:1	744	864	874	904	711	608
methylbenzofuran	224	174	146	191	179	135
cyanomethylbenzene	273	197	189	273	179	183
n-C11:0	665	583	526	548	433	399
1-ethyl-2,3-dimethylbenzene	216	191	176	215	139	106
1,2,4,5-tetramethylbenzene	109	40	59	110	51	111
1,2,3,5-tetramethylbenzene	286	242	247	171	132	162
2-ethylphenol	142	119	111	152	111	82
C2-Phenols (A+B)	652	580	589	726	766	560

Code #	E50010-PA1-Extr.-S2 R:**6 (µg/g TOC)	E50011-PA1-Extr.-S2 R:**6 (µg/g TOC)	E50012-PA1-Extr.-S2 R:**6 (µg/g TOC)	E50013-PA1-Extr.-S2 R:**6 (µg/g TOC)	E50014-PA1-Extr.-S2 R:**6 (µg/g TOC)	E50015-PA1-Extr.-S2 R:**6 (µg/g TOC)
methylindene	788	763	742	863	636	650
1,2,3,4-tetramethylbenzene	328	253	259	308	241	257
C2-Phenoles (C+D)	1120	908	880	1239	1107	815
2,3-dimethylphenol	393	389	430	393	416	297
Naphthalene	535	405	346	448	387	338
4-methylguaiacol	76	286	199	271	765	1336
n-C12:1	759	839	875	911	703	635
vinylphenol	234	304	264	286	221	231
n-C12:0	782	688	641	696	577	538
dimethylindene	144	429	853	1133	874	656
4-ethylguaiacol	476	423	351	434	482	514
indole	239	313	287	324	245	180
2-M-Naphthalene	526	414	400	493	419	347
4-vinylguaiacol	208	243	191	265	415	1346
n-C13:1	767	768	726	753	620	0
alkene (1)	570	528	397	633	426	333
1-M-Naphthalene	569	451	361	533	375	291
n-C13:0	912	672	634	689	543	435
alkene (2)	1172	612	677	744	626	518
alkene (3)	173	95	111	120	80	59
methylindole	856	757	754	852	672	525
2,6-dimethoxyphenol	87	106	97	120	160	143
2-ethylnaphthalene	135	116	117	112	118	208
n-C14:1	609	813	755	835	697	515
n-C14:0	799	655	615	709	526	404
1,3-DMN	193	118	132	169	129	81
1,7-and 1,6-DMN	422	363	361	466	395	414
eugenol	169	128	119	177	250	620
n-C15:1	537	732	707	760	695	493
n-C15:0	855	692	672	761	598	527
1,6,7-and 1,2,6-TMN	92	0	0	0	0	38
fluorene	127	189	193	233	212	166
n-C16:1	530	695	641	695	551	454
n-C16:0	610	572	513	572	440	391
alkene	421	290	222	364	276	204
biphenol	165	176	160	185	169	167
n-C17:1	323	508	464	476	410	464
n-C17:0	645	521	480	548	419	375
Prist-1-ene	119	223	172	204	186	223
prist-2-ene	270	273	255	398	275	191
phenanthrene	174	123	122	155	112	78
n-C18:1	315	465	426	463	384	356
n-C18:0	506	433	400	461	346	336
unknown	1185	835	842	1057	822	698
n-C19:1	406	465	424	460	377	345
n-C19:0	497	468	416	504	385	372
n-C20:1	272	445	386	422	346	352
n-C20:0	450	436	383	455	352	361
n-C21:1	282	432	386	414	354	397
n-C21:0	405	394	346	395	316	370
n-C22:1	278	418	358	398	337	403
n-C22:0	349	340	297	359	288	331
n-C23:1	185	317	277	303	278	331
n-C23:0	335	352	310	360	305	399
n-C24:1	257	353	307	337	315	369
n-C24:0	314	333	290	347	306	386
n-C25:1	333	321	291	356	292	342
n-C25:0	260	297	265	316	286	388
n-C26:1	96	239	192	197	198	308
n-C26:0	256	278	237	297	240	288
n-C27:1	43	142	105	115	146	202
n-C27:0	295	293	242	319	287	359
n-C28:1	93	224	153	164	173	197
n-C28:0	217	260	193	239	223	203
n-C29:1	135	158	143	164	167	141
n-C29:0	149	189	111	140	117	167
n-C30:1	50	159	98	96	100	124
n-C30:0	155	225	174	205	195	222

Code #	E50016-PA1-Extr.-S2 R:**6	E50017-PA1-Extr.-S2 R:**6	E50018-PA1-Extr.-S2 R:**6	E50019-PA1-Extr.-S2 R:**6	E50020-PA1-Extr.-S2 R:**6	E50021-PA1-Extr.-S2 R:**6	E50022-PA1-Extr.-S2 R:**7
Amount (mg)	11.50	7.30	7.10	9.20	8.10	8.00	19.50
	20	16.85	13.7	15.15	14.25	12.9	8.245
	(µg/g TOC)	(µg/g TOC)	(µg/g TOC)	(µg/g TOC)	(µg/g TOC)		
C1	13841	11440	13156	13826	13812	13358	17294
C02-05 Total	33211	36960	42852	39559	41268	45488	36600
C06-14 Total	79995	104909	113994	112233	112822	124330	148160
C15-32 Total	58319	124105	130628	118431	129987	144788	139671
C01-05 Total	47052	48400	56008	53385	55080	58846	53894
C06-14 Total	79995	104909	113994	112233	112822	124330	148160
C15-32 Total (corr)	57015	121666	127544	116279	127388	141881	137805
C01-32 Total	184062	274975	297546	281897	295290	325057	339859
2-propanone	2130	1682	1971	2035	1902	2183	3914
Furan	949	1862	2025	1942	2058	2226	2161
cyclopentadiene	591	1143	1297	1206	1266	1411	1727
butadiene and cyclopentene	686	726	864	862	878	990	1331
2,3-butanedione	319	307	410	427	382	472	424
2-butanone	582	536	588	690	610	677	1585
n-C6:1	873	1646	1965	1640	1897	2150	1969
2-methylfuran	582	564	543	617	564	635	694
n-C6:0	633	835	980	923	963	1115	1319
3-methylfuran	277	320	409	408	406	509	602
1,4-cyclohexadiene	406	677	854	681	769	861	1035
1,3-cyclohexadiene	472	601	813	574	659	747	915
Methylcyclopentene,Metylbutanal	345	649	511	576	702	791	775
Benzene	1637	1895	1861	1937	2059	2637	2428
Thiophene	295	304	295	516	318	342	532
cyclohexene	231	428	527	437	528	528	486
n-C7:1	661	1296	1503	1248	1457	1588	1470
n-C7:0	638	855	987	840	964	1075	1141
alkene (4)	171	201	220	169	226	317	261
pyridine	521	542	489	660	587	691	1358
pyrrole	746	1051	955	1274	1127	1249	2032
Toluene	2748	2483	2865	2670	2772	2984	3981
2-methylthiophene	259	311	358	304	339	374	372
furan-2-one	319	325	377	419	363	470	733
n-C8:1	617	1081	1292	1049	1239	1344	1312
methylpyridine (1)	229	269	289	234	301	334	1204
2-Cyclopenten-1-one	437	876	970	1224	1022	1298	741
n-C8:0	688	896	1014	916	1000	1122	1154
n-alkene (1)	219	189	251	255	230	258	332
2-Methylpyrrole	358	487	513	602	551	639	1076
3-Methylpyrrole	171	276	316	317	318	366	616

Code #	E50016-PA1-Extr.-S2 R:**6 (µg/g TOC)	E50017-PA1-Extr.-S2 R:**6 (µg/g TOC)	E50018-PA1-Extr.-S2 R:**6 (µg/g TOC)	E50019-PA1-Extr.-S2 R:**6 (µg/g TOC)	E50020-PA1-Extr.-S2 R:**6 (µg/g TOC)	E50021-PA1-Extr.-S2 R:**6	E50022-PA1-Extr.-S2 R:**7
methylpyridine (2)	433	306	353	380	400	431	839
Ethylbenzene	617	595	611	552	593	634	856
m+p-Xylenes	991	949	1099	984	1033	1112	1434
Dimethylpyridine	58	74	104	59	87	101	133
Styrene+methylcyclopentenone	798	1005	1268	1291	1178	1419	1855
o-Xylene	518	555	698	595	634	716	964
n-C9:1	426	871	1024	876	992	1100	979
2,5-dimethylpyrrole	125	174	201	222	211	257	488
n-C9:0	470	639	759	641	730	827	791
alkene (3)	387	449	557	472	507	608	746
2,4-dimethylpyrrole	0	0	0	28	37	52	120
dimethylpyridine	116	161	174	121	183	208	261
2,3-dimethylpyrrole	213	211	288	281	260	335	507
methylfurancarboxaldehyde	72	107	124	63	120	150	182
3-methyl-2-cyclopentenone	319	594	674	584	647	822	666
n-propylbenzene	179	154	183	171	167	197	265
1-ethyl-3-methylbenzene-cybenz	389	391	443	434	468	588	633
1-ethyl-4-methylbenzene	123	107	126	114	117	135	143
1,3,5-trimethylbenzene	83	81	126	103	105	122	97
phenol	3615	2124	1856	2612	2248	2115	3232
1-ethyl-2-methylbenzene	330	288	383	369	327	362	617
Benzofuran	176	140	143	263	150	165	200
1,2,4-trimethylbenzene	483	770	754	776	689	906	1004
n-C10:1	536	962	1160	929	1093	1209	1076
2,3,5-trimethylpyrrole	454	189	213	266	225	267	525
n-C10:0	537	682	724	866	781	771	945
1,2,3-trimethylbenzene	363	393	444	226	450	506	466
dimethylcyclopentenone	125	81	127	341	83	123	399
1-isopropyl-3-methylbenzene	79	124	136	92	93	110	173
3-ethyl-4-methylpyrrole	66	113	136	130	140	144	129
1-propenylbenzene	122	144	170	171	174	198	274
indene	238	337	412	398	406	442	592
o-Cresol	1074	835	886	916	948	977	1183
1,3-diethylbenzene	212	232	219	357	243	289	524
1-methyl-3-propylbenzene	89	98	135	144	104	130	230
alkylbenzenes	225	460	364	542	409	477	589
1,2-diethylbenzene	61	80	124	108	85	107	122
1-ethyl-3,5-dimethylbenzene	82	43	17	156	50	62	134
m+p-Cresol	2959	2081	1882	2616	2243	2119	3265
2-methoxyphenol	530	321	225	422	342	212	342
2-ethyl-1,4-dimethylbenzene	77	108	118	110	121	132	147
1-ethyl-2,4-dimethylbenzene	90	134	144	100	124	150	126
ethylidimethylpyrrole (1)	141	84	0	128	97	107	214
1-ethyl-3,4-dimethylbenzene	190	202	327	227	229	275	400
2,6-dimethylphenol	121	126	147	148	143	144	330
n-C11:1	488	920	1087	920	1058	1199	1156
methylbenzofuran	251	183	153	200	175	187	252
cyanomethylbenzene	148	179	159	227	187	209	373
n-C11:0	471	585	677	601	647	749	848
1-ethyl-2,3-dimethylbenzene	100	165	153	177	176	209	291
1,2,4,5-tetramethylbenzene	45	40	59	77	44	68	146
1,2,3,5-tetramethylbenzene	140	272	280	288	283	322	421
2-ethylphenol	126	107	110	128	120	133	175
C2-Phenoles (A+B)	777	614	594	724	671	623	899

Code #	E50016-PA1-Extr.-S2 R:**6 (µg/g TOC)	E50017-PA1-Extr.-S2 R:**6 (µg/g TOC)	E50018-PA1-Extr.-S2 R:**6 (µg/g TOC)	E50019-PA1-Extr.-S2 R:**6 (µg/g TOC)	E50020-PA1-Extr.-S2 R:**6 (µg/g TOC)	E50021-PA1-Extr.-S2 R:**6	E50022-PA1-Extr.-S2 R:**7
methyindene	549	760	871	828	879	962	1197
1,2,3,4-tetramethylbenzene	240	236	280	263	235	288	401
C2-Phenoles (C+D)	1078	860	848	1126	948	981	1708
2,3-dimethylphenol	271	385	423	387	435	490	513
Naphthalene	447	349	366	394	366	380	635
4-methylguaiacol	984	474	308	515	609	262	308
n-C12:1	516	894	1021	878	1001	1115	1115
vinylphenol	128	282	248	228	255	276	196
n-C12:0	584	683	841	748	786	874	1079
dimethylindene	569	920	784	962	949	1034	1557
4-ethylguaiacol	572	401	395	497	488	455	581
indole	78	262	291	270	279	306	393
2-M-Naphthalene	411	411	472	463	466	483	683
4-vinylguaiacol	252	363	235	0	332	257	174
n-C13:1	514	782	930	1179	938	982	1187
alkene (1)	381	396	648	488	463	611	761
1-M-Naphthalene	362	565	525	429	458	493	746
n-C13:0	552	653	768	700	772	851	1045
alkene (2)	476	647	708	737	706	838	1124
alkene (3)	79	90	115	96	117	135	181
methyindole	309	775	779	620	756	892	1097
2,6-dimethoxyphenol	70	125	82	132	125	108	120
2-ethylnaphthalene	148	107	119	147	124	122	178
n-C14:1	538	845	1021	918	1000	1055	1051
n-C14:0	548	659	757	715	774	842	992
1,3-DMN	151	113	145	146	139	143	186
1,7-and 1,6-DMN	293	365	403	431	414	414	513
eugenol	207	188	118	232	171	147	183
n-C15:1	486	732	856	807	868	923	881
n-C15:0	567	634	728	777	753	823	1027
1,6,7-and 1,2,6-TMN	49	0	0	0	0	0	0
fluorene	120	203	258	228	214	233	325
n-C16:1	411	676	769	777	819	902	940
n-C16:0	425	503	578	588	606	687	802
alkene	94	344	373	306	383	442	486
biphenol	167	196	184	184	185	210	213
n-C17:1	356	560	654	568	658	716	648
n-C17:0	416	511	589	561	622	684	770
Prist-1-ene	153	331	240	180	225	248	229
prist-2-ene	131	239	251	262	248	300	424
phenanthrene	100	124	138	123	132	159	207
n-C18:1	310	555	595	551	607	685	648
n-C18:0	377	463	512	496	534	612	715
unknown	579	772	868	892	840	992	1187
n-C19:1	276	518	560	530	576	659	640
n-C19:0	388	515	531	532	563	654	764
n-C20:1	269	546	534	516	568	655	633
n-C20:0	367	465	468	479	510	596	708
n-C21:1	264	481	497	474	524	597	620
n-C21:0	399	413	417	425	459	526	621
n-C22:1	269	464	486	469	520	585	629
n-C22:0	317	357	363	367	401	463	567
n-C23:1	193	368	373	367	409	455	466
n-C23:0	326	358	357	377	407	459	557
n-C24:1	252	385	384	405	442	494	524
n-C24:0	315	341	333	350	376	425	537
n-C25:1	242	344	350	376	383	449	532
n-C25:0	307	319	310	323	356	394	466
n-C26:1	166	262	259	260	322	331	312
n-C26:0	273	267	274	295	327	368	466
n-C27:1	162	180	197	197	237	254	210
n-C27:0	330	294	291	340	367	430	531
n-C28:1	142	267	229	243	284	305	275
n-C28:0	219	258	237	257	280	325	379
n-C29:1	108	191	160	164	195	227	192
n-C29:0	183	207	167	187	208	230	279
n-C30:1	83	157	130	141	162	177	172
n-C30:0	224	215	181	203	214	246	285

Code #	E50023-PA1-Extr.-S2 R:**6	E50024-PA1-Extr.-S2 R:**6	E50025-PA1-Extr.-S2 R:**6	E50026-PA1-Extr.-S2 R:**6	E50027-PA1-Extr.-S2 R:**6	E50028-PA1-Extr.-S2 R:**6	E50029-PA1-Extr.-S2 R:**6
Amount (mg)	8.80	18.00	9.30	11.20	8.20	7.30	7.70
	12.65	7.54	10.95	10.85	14.7	13.55	13.55
C1	12729	18310	12483	17942	16517	13146	13773
C02-05 Total	45894	46938	44523	51728	44356	44163	46765
C06-14 Total	128762	146695	117515	131975	114276	116264	127957
C15-32 Total	146940	116208	124960	118977	120866	133507	141732
C01-05 Total	58623	65248	57006	69670	60873	57309	60538
C06-14 Total	128762	146695	117515	131975	114276	116264	127957
C15-32 Total (corr)	146245	113998	122014	116508	118377	130474	138857
C01-32 Total	333630	325941	296535	318153	293526	304047	327352
2-propanone	2067	3197	2069	2584	2448	2047	2257
Furan	2298	1839	2076	3041	1990	1986	2225
cyclopentadiene	1510	1626	1421	1300	1231	1363	1474
butadiene and cyclopentene	1005	1610	953	1281	1029	817	1011
2,3-butanedione	414	407	469	550	349	375	498
2-butanone	674	1716	689	974	803	656	737
n-C6:1	2210	1713	1993	1763	1944	2048	1991
2-methylfuran	620	719	576	772	522	554	704
n-C6:0	1087	1441	1018	1174	1065	994	988
3-methylfuran	489	765	464	584	528	457	468
1,4-cyclohexadiene	837	1031	847	764	765	803	795
1,3-cyclohexadiene	714	912	730	714	654	734	740
Methylcyclopentene,Metylbutanal	777	1017	637	702	561	517	799
Benzene	2334	2990	1765	2774	2236	2082	2446
Thiophene	309	399	350	543	339	328	392
cyclohexene	562	496	520	503	534	577	493
n-C7:1	1667	1244	1495	1374	1476	1563	1534
n-C7:0	1097	1234	1034	1086	1095	1000	1055
alkene (4)	217	339	217	291	269	243	212
pyridine	736	1397	678	985	613	519	840
pyrrole	1302	1743	1228	1615	1026	1111	1373
Toluene	2956	4062	2844	3602	3497	2832	3129
2-methylthiophene	406	342	382	377	370	392	403
furan-2-one	460	893	459	646	446	376	447
n-C8:1	1420	1060	1269	1136	1252	1369	1325
methylpyridine (1)	340	1282	351	370	344	292	333
2-Cyclopenten-1-one	1311	680	1141	1405	785	926	1258
n-C8:0	1185	1164	1077	1150	1100	1114	1086
n-alkene (1)	281	393	275	377	280	280	282
2-Methylpyrrole	649	1085	606	813	562	502	673
3-Methylpyrrole	369	573	368	429	331	302	394

Code #	E50023-PA1-Extr.-S2 R:**6	E50024-PA1-Extr.-S2 R:**6	E50025-PA1-Extr.-S2 R:**6	E50026-PA1-Extr.-S2 R:**6	E50027-PA1-Extr.-S2 R:**6	E50028-PA1-Extr.-S2 R:**6	E50029-PA1-Extr.-S2 R:**6
methylindene	1019	1289	943	981	876	903	905
1,2,3,4-tetramethylbenzene	301	385	303	325	276	234	252
C2-Phenoles (C+D)	1043	1708	948	1522	1254	1002	1171
2,3-dimethylphenol	430	558	350	509	389	377	456
Naphthalene	410	683	382	521	548	420	443
4-methylguaiacol	291	152	184	328	320	576	443
n-C12:1	1175	840	951	925	1012	1086	1091
vinylphenol	231	193	206	159	201	237	153
n-C12:0	912	926	739	868	876	825	849
dimethylindene	1161	1416	1025	1228	1034	998	1068
4-ethylguaiacol	480	623	443	625	524	498	509
indole	314	330	269	301	267	255	357
2-M-Naphthalene	536	716	477	561	555	498	501
4-vinylguaiacol	292	286	217	255	231	434	429
n-C13:1	1092	718	819	866	946	1016	999
alkene (1)	605	982	581	729	551	566	574
1-M-Naphthalene	650	711	597	570	484	540	525
n-C13:0	929	957	742	846	897	831	804
alkene (2)	963	1405	917	1046	771	803	888
alkene (3)	148	202	123	143	151	137	127
methylindole	970	1080	833	918	812	377	955
2,6-dimethoxyphenol	115	150	87	158	148	135	149
2-ethylnaphthalene	110	170	97	151	116	133	166
n-C14:1	1168	780	936	885	1004	1092	1062
n-C14:0	934	928	744	837	874	833	808
1,3-DMN	153	252	144	180	150	141	144
1,7-and 1,6-DMN	463	554	423	478	430	448	458
eugenol	166	175	118	329	163	244	260
n-C15:1	1001	667	797	799	895	989	953
n-C15:0	901	1017	733	925	909	837	839
1,6,7-and 1,2,6-TMN	0	0	0	0	0	0	0
fluorene	247	346	234	276	296	262	252
n-C16:1	918	792	726	838	910	937	911
n-C16:0	724	787	603	795	777	803	660
alkene	408	467	431	353	408	363	329
biphenol	213	185	198	213	209	214	217
n-C17:1	736	446	599	567	707	745	703
n-C17:0	736	785	642	730	804	732	661
Prist-1-ene	291	165	237	159	177	270	263
prist-2-ene	363	420	387	396	294	343	322
phenanthrene	171	167	211	191	172	177	152
n-C18:1	733	477	604	546	666	723	657
n-C18:0	654	675	563	628	703	650	562
unknown	1062	1517	1016	1282	1046	1002	976
n-C19:1	700	477	580	546	632	697	638
n-C19:0	707	696	603	657	711	689	603
n-C20:1	718	432	560	509	591	669	627
n-C20:0	645	635	523	596	666	625	557
n-C21:1	647	441	467	468	580	629	601
n-C21:0	578	540	444	514	597	555	496
n-C22:1	635	448	477	481	606	646	621
n-C22:0	505	479	377	454	555	515	469
n-C23:1	493	309	342	347	486	519	492
n-C23:0	501	439	354	439	569	521	479
n-C24:1	528	359	362	434	536	544	537
n-C24:0	468	412	329	429	545	503	468
n-C25:1	481	423	336	474	504	514	489
n-C25:0	437	343	283	368	543	503	446
n-C26:1	356	139	175	201	418	418	376
n-C26:0	403	315	243	347	535	462	382
n-C27:1	266	94	115	157	337	324	282
n-C27:0	465	386	258	440	645	565	465
n-C28:1	311	132	189	189	330	368	347
n-C28:0	342	246	237	291	435	420	332
n-C29:1	229	164	131	186	245	261	239
n-C29:0	253	145	152	216	320	300	250
n-C30:1	180	47	101	95	190	257	245
n-C30:0	257	182	166	213	279	285	245

E.nr.	Huminite/Vitrinite [%]	Liptinite (total) [%]	Sporinite [%]	Alginite [%]	other Lipt. [%]	Inertinite [%]	total AOM [%]	fluoramorphinite [%]	hebamorphinite [%]	n
47716	5.1	11.4	7.0	2.7	1.7	2.9	80.6	61.1	19.5	120
47730	31.7	2.1	1.1	1.0	0.0	7.3	59.0	19.0	40.0	163
47736	32.1	5.5	5.5	0.0	0.0	5.0	57.5	13.1	44.4	112
47739	1.8	23.3	7.8	8.4	7.1	0.0	74.9	50.7	24.2	178
47744	28.1	7.3	1.0	2.1	4.2	3.1	61.5	43.8	17.7	98
48165	51	2.8	2.6	0.2	0.0	0.0	46.2	16.7	29.5	116
48170	4.5	23.9	6.0	14.9	3.0	0.0	71.6	53.7	17.9	120

E.nr.	vitrinite reflectance Rr(%) counts				total counts
	from 0.00 to 0.30	from 0.30 to 0.60	from 0.60 to 1.00	>1.00	
47716	14	3	17	21	55
47730	1	1	3	8	13
47736	9	5	9	15	38
47739	33	14	2	1	50
47744	12	10	12	6	40
48165	48	12	0	0	60
48170	54	6	0	0	60

E.nr.	47716-1	50002-1	47730-1	47736-1	50006-1	47739-1	50018-1	47744-1	48165-1	48170-1					
Depth [cm]	750	850	2150	2750	2880	3050	3060	3550	4050	4540					
Lithozone	2	2 (Younger Dryas)	3	3	3	4	4	5	6	6					
<i>n</i>-alkanes	Concentrations in µg/g TOC and carbon isotopic compositions of individual <i>n</i>-alkanes														
15	1.07	-	0.95	-	1.17	1.65	0.90	-	1.66	2.01	1.64	-	1.32	-	1.65
16	0.85	-	0.57	-	1.34	1.62	0.92	-	0.61	0.99	1.67	-	1.65	-	0.99
17	1.65	-	1.35	-	3.38	3.39	2.20	-	0.90	1.63	2.63	-	1.36	-	2.37
pristane	0.84	-	0.97	-	1.75	1.71	0.66	-	1.12	1.00	1.87	-	1.33	-	0.59
18	5.37	-	3.25	-	12.36	17.12	6.80	-	3.76	10.46	16.76	-	3.10	-	2.85
phytane	1.46	-	2.21	-	3.63	4.68	1.99	-	2.07	3.26	4.33	-	2.54	-	2.90
19	6.34	-	8.39	-	12.84	20.99	9.11	-	3.84	12.85	23.25	-	0.78	-	0.52
20	13.21	-28.2	7.96	-	10.35	35.44	5.99	-	8.17	16.25	36.78	-28.8	0.85	-	0.41
21	20.09	-26.6	12.97	-	10.66	46.72	18.65	-	15.20	17.85	38.38	-28.2	0.98	-	0.94
22	21.71	-28.0	10.13	-	8.46	47.05	14.32	-	18.52	16.32	28.94	-27.5	1.03	-	0.59
23	23.38	-27.0	13.66	-	15.37	52.43	20.20	-26.7	28.27	36.19	18.35	-27.4	5.50	-34.3	13.04
24	19.34	-28.5	10.24	-	8.13	30.86	16.52	-	19.52	22.12	8.90	-27.1	2.35	-	2.32
25	34.55	-27.1	27.36	-26.9	20.53	36.91	23.70	-25.8	35.63	41.26	17.51	-28.4	28.75	-33.3	23.27
26	17.20	-24.8	12.64	-	10.16	15.96	12.33	-	14.27	20.21	6.42	-28.2	4.23	-	29.40
27	43.29	-26.7	29.89	-26.2	31.58	40.00	27.77	-24.1	48.77	54.07	22.30	-27.6	40.30	-31.1	44.37
28	25.53		12.94	-	10.49	13.35	11.10	-	22.92	18.74	8.69	-	9.02	-	7.52
29	55.32	-29.3	32.75	-28.1	36.56	53.96	34.98	-27.2	108.05	118.13	35.01	-28.5	90.82	-32.8	46.20
30	15.83		13.13	-	10.36	13.53	12.01	-	20.75	18.98	8.91	-28.9	11.15	-33.3	13.29
31	77.09	-27.0	38.99	-26.4	51.22	80.75	35.12	-26.4	99.31	105.74	61.16	-28.4	73.65	-32.9	89.46
32	14.33		10.36	-	8.96	11.57	11.25	-	16.96	17.25	9.29	-	7.77	-30.6	13.69
33	64.71	-25.5	26.89	-24.3	37.91	52.13	28.00	-24.3	56.55	72.59	46.60	-25.1	25.24	-30.2	42.34
34	5.56		2.20	-	3.29	4.09	2.10	-	3.26	8.98	3.92	-	2.65	-	4.99
35	20.61		4.10	-	14.26	16.69	6.90	-	12.01	21.00	18.92	-	16.97	-	18.43
36	0.95		-	-	0.85	0.90	-	-	0.79	0.63	1.08	-	-	-	-
37	3.76		-	-	2.43	2.84	-	-	1.65	1.98	3.15	-	-	-	-
sum	494.03		283.88		328.03	606.32	303.53		544.53	640.49	426.42		333.35		362.11
mean value δ ¹³ C		-27.2		-26.4				-25.8				-27.8		-32.3	

E.nr.	47716	47730	47736	47739	47744	48165	48170
Depth [cm]	750	2150	2750	3050	3550	4050	4540
Lithozone	2	3	3	4	5	6	6
<i>n</i>-fatty acids	Concentrations in µg/g TOC						
14	8.78	7.05	20.10	19.27	15.56	0.29	2.20
15	7.39	5.33	16.65	21.03	9.76	0.23	1.91
16	45.15	26.01	129.03	124.32	75.91	0.97	7.54
17	9.26	5.83	15.51	16.44	9.57	0.36	3.20
18	28.95	23.55	101.77	80.92	59.64	0.85	5.81
19	4.30	2.82	6.09	3.91	2.32	0.26	2.28
20	12.56	16.20	30.39	45.23	20.45	1.30	13.47
21	9.74	11.33	23.21	34.70	13.18	0.72	8.66
22	46.23	50.62	104.78	143.24	45.76	3.48	48.87
23	10.29	10.89	23.80	39.91	12.34	0.54	6.16
24	35.99	56.98	108.50	206.09	40.49	4.96	32.92
25	12.91	20.08	30.74	49.96	11.83	1.21	7.35
26	126.56	163.03	238.61	464.87	95.91	35.33	92.17
27	28.46	29.40	35.89	69.68	14.74	2.06	18.22
28	123.36	200.97	272.76	415.33	98.96	27.17	316.60
29	23.63	20.76	31.53	61.33	14.27	2.12	15.72
30	57.21	66.53	103.98	213.90	46.86	13.31	62.26
31	12.57	14.51	22.33	40.13	10.80	0.00	13.45
32	30.37	50.53	78.65	148.81	37.14	0.00	56.30
sum <i>n</i> -fatty acids	633.69	782.40	1394.32	2199.05	635.49	95.17	715.10

Abbreviations

approx.	approximately
AbR	Alkylbenzene Ratio (definition in Appx. D)
ALK	Alkanols
Appx.	Appendix
aq	aquatic
ATR	Aquatic Terrigenous Ratio
<i>B. braunii</i>	Botryococcus braunii
bbl.	imperial barrel (1.636 hl)
BP	Before Present
BPX-5	5% phenyl polysilphenylene-siloxane non-polar stationary phase
Ca	Calcium
CAM	Crassulacean Acid Metabolism
C/N	Total carbon/ total nitrogen ratio
Chromane	Chromane-Index (definition in Appx. D)
CO	Carbon Monoxide
CO ₂	Carbon Dioxide
CPI	Carbon Preference Index (definition in Appx. D)
CuO	copper (II) oxide
dbt	dibenzothiophene
DIAR	Diasterane Ratio (definition in Appx. D)
DJT	Duijatai sub-unit
E	East
EI	Electron impact
Es	Eocene Shahejie Formation
F	Feldspar
FA	Fatty Acids
Fe	iron
FID	Flame Ionisation Detector
Fig.	Figure
FZ Jülich	Forschungszentrum Jülich GmbH
gal.	Gallon
GC	Gas Chromatography
GC-irmMS	Gas Chromatography Isotope-Ratio Mass Spectrometry
GC-MS	Gas Chromatography - Mass Spectrometry
GI	Gammacerane Index (definition in Appx. D)

GS	Gaosheng sub-unit
H	17 α (H),21 β (H)-Hopane
HARC	Houston Advanced Research Centre
HC	Hydrocarbons
H/C	atomic hydrogen/carbon ratio
HCl	Hydrochloric Acid
HCO ₃ ⁻	Bicarbonate
HF	Hydrofluoric Acid
HHI	Homohopane Index (definition in Appx. D)
HI	Hydrogen Index (mg HC/g TOC)
HM	Lake Huguang Maar
HZM	Lake Holzmaar
i.d.	internal diameter
IFP	Institut Francais du Petrole
IpR (1+2)	Isoprenoid Ratio (definition in Appx. D)
I/S	mixed-layer illite smectite
KOH	Potassium Hydroxide
LGM	Last Glacial Maximum
LPEB	Liaohu Petroleum Exploration Bureau
LSR	Liaohu Source Rocks
M	17 β (H),21 α (H)-Hopane
<i>m/z</i>	mass/charge
<i>mf</i>	mineral free basis
MFM	Lake Meerfelder Maar
Mg	Magnesium
Mio	Million years
MRM	Reaction Monitoring mode
mpi-1	Methylphenanthrene Index 1 (definition in Appx. D)
MPLC	Medium Pressure Liquid Chromatography
mpr	Methylphenanthrene Ratio (definition in Appx. D)
N	North
Na	Sodium
NE	North-east
NSO	Heterocompounds with nitrogen, sulphur and oxygen
NW	North-west
O/C	atomic oxygen/carbon ratio

OI	Oxygen Index (mg CO ₂ /g TOC)
OLI	Oleanane Index (definition in Appx. D)
OM	Organic Matter
PDB	Isotopic Standard, based on a rostrum of <i>Belemnitella americana</i> from the Cretaceous Peedee Formation
ph	phytane
pH	the negative logarithm of the hydrogen ion (H ⁺) concentration (in moles per l)
phen	phenanthrene
PhR	Phenol Ratio (definition in Appx. D)
PI	Production Index
ppb	parts per billion
pr	pristane
Q	Quartz
Py-GC	Pyrolysis - Gas Chromatography
Py-GC-MS	Pyrolysis - Gas Chromatography - Mass Spectrometry
%Rc	Calculated vitrinite reflectance (definition in Appx. D)
RIR	Reference Intensity Ratio
%Ro	Measured mean random vitrinite reflectance in oil
S	South
SE	South-east
SW	South-west
Tab.	Table
TCD	Thermal Conductivity Detection
TC	Total Carbon
TOC	Total Organic Carbon
Tm	17 α (H)-22,29,30-trisnorhopane
Ts	18 α (H)-22,29,30-trisnorneohopane
U.S.	United States
vol.-%	volume percent
W	West
WI	Wax-Index (definition in Appx. D)
wt.-%	weight percent
XRD	X-ray diffraction
ZCH	Central Department of Analytical Chemistry

Index of Figures

- Fig. 1.1.** Temperature profile and penetration of solar radiation in a lake (page 2).
- Fig. 1.2.** Organic matter sources in lake environments (page 6).
- Fig. 1.3.** Kerogen type and facies relationship in the Quingshankou Formation, Songliao Basin (page 9).
- Fig. 3.1.** Schematic sketch of the liquid chromatographic separation (page 25).
- Fig. 4.1.** Location and structural subdivision of the Liaohe Basin (page 28).
- Fig. 4.2.** Cross section showing the different structural and producing areas of the Western Depression (page 29).
- Fig. 4.3.** Generalised stratigraphic column for the Western Depression (page 31).
- Fig. 4.4.** Sketch map of the Western Depression with location of the studied wells and major producing areas (page 35).
- Fig. 4.5.** Lithology and related lithostratigraphic subdivision of two representative key wells (page 36).
- Fig. 4.6.** Detailed mineralogy of the Es4 member in well A (page 40).
- Fig. 4.7.** Detailed mineralogy of the Es4 member in well B (page 41).
- Fig. 4.8.** Cluster analysis of samples based on carbonate mineralogy (page 42).
- Fig. 4.9.** Formation of manganese-rich sediments (page 47).
- Fig. 4.10.** Expandable clays versus dolomite for the different stratigraphic units in the Western Depression (page 50).
- Fig. 4.11.** Expandable clays versus depth for samples from the Western Depression (page 51).
- Fig. 4.12.** Microscopic characteristics of non-laminated and laminated sediment samples from the Western Depression of the Liaohe Basin (page 65).
- Fig. 4.13.** Hydrogen Index versus Oxygen Index values for the Liaohe sample set (page 67).
- Fig. 4.14.** Hydrogen Index versus Tmax for samples from the Liaohe Basin (page 70).
- Fig. 4.15.** Van Krevelen diagram for the analysed Liaohe kerogen concentrates (page 72).
- Fig. 4.16.** Carbon isotope values of the Liaohe kerogens and other lacustrine sediments and oil shales (page 74).
- Fig. 4.17.** Kerogen typing according to the chain length distribution from Py-GC-FID (page 76).
- Fig. 4.18.** Kerogen typing on the basis of sulphur-containing, aromatic and alkyl groups from Py-GC-FID (page 76).

- Fig. 4.19.** Pyrolysis gas-chromatograms of typical representative kerogens from the Western Depression (page 81).
- Fig. 4.20.** Activation energy distributions as derived from pyrolysis experiments of selected source rock samples from the Western Depression (page 83).
- Fig. 4.21.** Compound class distribution. Variation of NSO compounds, aromatics and saturates in source rock extracts from the Western Depression (page 86).
- Fig. 4.22.** Biomarker parameters and stratigraphy for well A (page 88).
- Fig. 4.23.** Biomarker parameters and stratigraphy for well B (page 88).
- Fig. 4.24.** GC-MS total ion chromatograms of the aliphatic hydrocarbons in sample E 48537 (A), well A and E 48467 (B), well B (page 89).
- Fig. 4.25.** Plot of pristane/*n*-C₁₇ versus phytane/*n*-C₁₈ for source rock bitumens from the Es4 and Es3 member (page 91)
- Fig. 4.26.** Hopane distribution patterns (m/z 191) in samples E 48532 (A), well A and E 48467 (B), well B (page 92).
- Fig. 4.27.** Sterane distribution patterns (m/z: 217) in well A. Samples E 48525 (A), Shale I sub-unit and E 48529 (B), GS sub-unit (page 93).
- Fig. 4.28.** Ternary distribution of $\alpha\alpha\alpha$ -20R steranes in bitumens from the Es4 and Es3 member (page 94).
- Fig. 4.29.** Hopane isomerisation versus depth for bitumens from the GS sub-unit (page 96).
- Fig. 4.30.** Pr/ph versus Ts/(Ts+Tm) for bitumens from the DJT sub-unit (page 96).
- Fig. 4.31.** GC-MS total ion chromatogram of the aromatic fraction from sample E 48463 (page 99).
- Fig. 4.32.** Pr/ph versus dbt/phen ratio for bitumens from the Es3 and Es4 member (page 101).
- Fig. 4.33.** Mpr 2 versus depth for samples from the GS sub-unit (page 101).
- Fig. 4.34.** Aromatic hopanoids ratio versus depth for bitumens from the DJT sub-unit (page 103).
- Fig. 4.35.** GC-MS total ion chromatograms of the carboxylic acid fraction in sample E 48537 (A), well A and E 48480 (B), well E (page 105).
- Fig. 4.36.** Concentration of methylcarbazoles versus calculated vitrinite reflectance from mpi 1 for source rock bitumens from the Es4 and Es3 member (page 109).
- Fig. 4.37.** Distribution patterns of fluoren-9-ones and alkylated derivatives (page 110).
- Fig. 4.38.** Fan-delta depositional environment with facies associations (page 113).
- Fig. 4.39.** Facies summary for well A (page 115).
- Fig. 4.40.** Fluctuating-profunda facies association, typical for the freshwater facies in the Western Depression of the Liaohé Basin (page 117)
- Fig. 4.41.** Mineral precipitation in a playa-lake/mudflat environment (page 119)

- Fig. 5.1.** Lake Holzmaar and Lake Meerfelder Maar in the Westeifel volcanic field (page 124)
- Fig. 5.2.** Stratigraphy of the Lateglacial (page 125).
- Fig. 5.3.** Lithological profile of Lake Meerfelder Maar (MFM) (page 126)
- Fig. 5.4.** Lithological profile of Lake Holzmaar (HZM) (page 127)
- Fig. 5.5.** Location of Lake Huguang Maar (HM) and the Tianyang crater (page 128).
- Fig. 5.6.** Monsoon influence in south-east Asia (page 129)
- Fig. 5.7.** Sample screening for the sediment profile from HZM (page 132).
- Fig. 5.8.** Sample screening for the sediment profile from MFM (page 135).
- Fig. 5.9.** S2 versus TOC of sedimentary OM from selected stratigraphic intervals in HZM and MFM (page 136).
- Fig. 5.10.** Pyrolysis gas-chromatograms of selected representative maar lake kerogens from HZM (page 138)
- Fig. 5.11.** Total ion current (TIC) traces of the pyrolysate and characteristic pyrolysis products (page 139)
- Fig. 5.12.** Structures of three common amino acids (page 141)
- Fig. 5.13.** Partial summed mass chromatograms of m/z 94+107+108+120+121+122 revealing the distributions of the C_1 - C_2 alkylated phenols of the kerogens (page 142)
- Fig. 5.14.** Microphotographs of OM in sediment samples and kerogens from HZM and MFM (page 150-151).
- Fig. 5.15.** Proportions of amorphous organic matter (AOM), terrigenous OM (huminite/vitrinite+sporinite+inertinite) and aquatic OM (alginite) versus depth for (A) HZM and (B) MFM (page 151).
- Fig. 5.16.** Petrographic composition of kerogen concentrates from Lateglacial and Holocene sediments of HZM and MFM (page 152).
- Fig. 5.17.** Histograms of reflectance, measured on huminite, vitrinite and inertinite particles in sediment samples and kerogens from MFM (page 153).
- Fig. 5.18.** TOC/TN versus $\delta^{13}C_{TOC}$ of sediments from HZM and MFM and collected reference samples; *Oscillatoria*, macrophytes and alder leave (page 155).
- Fig. 5.19.** Carbon isotopic compositions of the HCl demineralised sediments ($\delta^{13}C_{TOC}$) versus kerogen concentrates ($\delta^{13}C_{conc}$) from HZM and MFM (page 157).
- Fig. 5.20.** Temporal variations of macromolecular parameters based on maceral analysis and analytical pyrolysis for MFM (page 159).
- Fig. 5.21.** Temporal variations of macromolecular parameters based on maceral analysis and analytical pyrolysis for HZM (page 161)

- Fig. 5.22A.** Sample screening for the HM profile (core D and F; page 162)
- Fig. 5.22B.** Sample screening for the HM high resolution profile (core E) lithozone 2 (page 163)
- Fig. 5.22C.** Sample screening for the HM high resolution profile (core E) lithozone 3 and 4 (page 164)
- Fig. 5.23.** S2 versus TOC of sedimentary OM from Lake Huguang Maar (page 165).
- Fig. 5.24.** (A) HI versus TOC/TN and (B) HI versus TN in sediment samples from HM (page 166)
- Fig. 5.25.** Stratigraphic origin of the kerogen concentrates (conc) and bulk samples for Py-GC-FID and Py-GC-MS (page 168).
- Fig. 5.26.** Pyrolysis gas-chromatograms of selected representative HM kerogens (page 169).
- Fig. 5.27.** Structures of lignin precursor alcohols (page 170)
- Fig. 5.28.** Distribution of lignin pyrolysis products in lithozones of core E and F (page 171)
- Fig. 5.29.** Microphotographs of OM in sediment samples and kerogens from Lake Huguang Maar (page 174).
- Fig. 5.30.** Histograms of reflectance, measured on huminite, vitrinite and inertinite particles in two kerogens from HM (page 175).
- Fig. 5.31.** Distributions and concentrations of *n*-alkanes and *n*-fatty acids in the analysed samples from HM (page 179).
- Fig. 5.32.** $\delta^{13}\text{C}$ ratios of individual *n*-alkanes in HM sediment samples (page 182).
- Fig. 5.33.** Distributions and stable carbon isotope values ($\delta^{13}\text{C}$) of botryococenes extracted from HM sediments deposited during (A) lithozone 2 (E 47716, aliphatic fraction), (B) lithozone 3 (E 50006, aromatic fraction) and (C) lithozone 4 (E 50016, aliphatic fraction) (page 183).
- Fig. 5.34.** HI and carbon isotopic compositions of sedimentary OM from HM (page 185).
- Fig. 5.35.** Lake Huguang Maar. Comparison between pollen data, pyrolysis and organic petrological results (page 188).

Index of Tables

- Tab. 3.1.** Methods employed to Liaohe source rocks and maar lake sediments (page 18).
- Tab. 3.2.** List of identified and quantified pyrolysis products (page 23).
- Tab. 4.1.** Sample set for the Liaohe project (page 37).
- Tab. 4.2.** Bulk mineralogy and carbonate facies of samples from the Liaohe Basin determined by XRD analysis (page 39).
- Tab. 4.3.** Maceral classification applied in this study (page 61).
- Tab. 4.4.** Organic microfacies classification of the studied samples (page 62).
- Tab. 4.5.** Organic carbon, sulphur and Rock-Eval data of all Liaohe samples analysed (page 68-69).
- Tab. 4.6.** Organic carbon, sulphur, elemental and Rock-Eval data of the Liaohe kerogen concentrates (page 71).
- Tab. 4.7.** Kerogen typing according to chain length distribution and organic sulphur compounds (page 77).
- Tab. 4.8.** Parameters applied for kerogen characterisation from Py-GC-FID (page 78).
- Tab. 4.9.** Extract yields and proportions of saturates, aromatics and NSO compounds in source rock bitumens from the Es3 and Es4 member (page 85).
- Tab. 4.10.** Facies parameters calculated from thermovaporisation-GC and GC-MS (page 87).
- Tab. 4.11.** Hopane and sterane maturity parameters calculated from GC-MS (page 97).
- Tab. 4.12.** Aromatic maturity parameters calculated from GC-MS (page 102).
- Tab. 4.13.** Facies parameters based on heterocompounds (page 104).
- Tab. 4.14.** Development of the Liaohe lake through time and space (page 112).
- Tab. 5.1.** Maar lake sample set for the project (page 131).
- Tab. 5.2.** Morphometric and limnological data of the investigated maar lakes (page 132).
- Tab. 5.3.** TOC, TS, TN and Rock-Eval data for the sediment profile from HZM (page 133).
- Tab. 5.4.** TOC, TS, TN and Rock-Eval data for the sediment profile from MFM (page 134).
- Tab. 5.5.** Elemental data of selected kerogen concentrates (page 137).
- Tab. 5.6.** Petrographic composition of maar lake kerogen concentrates (page 147).
- Tab. 5.7.** Stable isotopic values of organic carbon measured on carbonate free sediments ($\delta^{13}\text{C}_{\text{TOC}}$), corresponding kerogen concentrates ($\delta^{13}\text{C}_{\text{conc}}$) and reference samples from HZM and MFM (page 156).
- Tab. 5.8.** Bulk organic geochemical parameters of the lithozones (page 162).
- Tab. 5.9.** Elemental data of selected kerogen concentrates (page 167).
- Tab. 5.10.** Bulk petrographic composition of the HM kerogen samples (page 173).

Tab. 5.11. Bulk geochemical parameters, fraction yields, biomarker parameters and compound specific carbon isotopic compositions for sediment samples from HM analysed for lipid distributions (page 177).

Tab. 5.12. Concentrations and carbon isotopic values of individual botryococenes from HM (page 181).